DEVELOPING TARGETED THERANOSTIC AGENTS FOR TUMORS

A Dissertation

by

SYED MUHAMMAD USAMA

Submitted to the Office of Graduate and Professional Studies of
Texas A&M University
in partial fulfillment of the requirements for the degree of

DOCTOR OF PHILOSOPHY

Chair of Committee,	Kevin Burgess
Committee Members,	Frank Raushel
	Robert Burghardt
	Wenshe Liu
	Jonathan Sczepanski
Head of Department,	Simon North

August 2019

Major Subject: Chemistry

ABSTRACT

Optical imaging is most favorable for dyes that absorb in the near-IR region because tissue is more permeable to light >750 nm. A particular set of cyanine dyes localize and persists in almost all solid tumors (e.g. glioblastoma, hepatocellular carcinoma, non-small lung cancer, breast cancer etc) for days, relative to healthy tissue. Remarkably, these tumor seeking dyes also absorb above 750 nm (in near-infrared region, NIR) where penetration of light is at maximum (up to 10 mm).

Early work described in this dissertation focuses on conjugation of a small molecule which targets $TrkC^+$ cancer cells, overexpressed in metastatic breast cancer, with a near-infrared zwitterionic cyanine dye for deep tumor imaging. The newly developed probe maintained the specific targeting to $TrkC^+$ 4T1 metastatic breast tumor cells as well as $TrkC^+$ metastatic breast tumor tissue. However, as the work progressed, we shifted our attention to using tumor seeking dyes as delivery agents, i.e. formation of theranostics for optical imaging and therapy.

This dissertation presents mechanistic work to exploring reactions of these tumor seeking dyes with different nucleophilic amino acids. It was observed that only thiol presenting amino acids (i.e. cysteine) substitute the *meso*-chlorine of these dyes under physiological conditions. Human serum albumin, the most abundant protein in the human body, and other thiol presenting proteins were also labeled by this technique.

This dissertation explores the possibility of covalently binding a fluorophore for *in vivo* optical imaging to a kinase inhibitor (dasatinib) where the particular fluorophore chosen for this study, a heptamethine cyanine (Cy) derivative, tends to accumulate in

tumors. Our preliminary results are promising; we have been able to, (i) enhance the IC_{50} of KI after conjugating with tumor seeking dyes; and, (ii) deliver KI specifically to cancer cells over normal cells.

This dissertation also discusses work on synthesizing a small library of iodine incorporated tumor seeking dyes for PDT with absorbance around 800 nm region and good photophysical properties. The *N*-substituents of these cyanines were varied to adjust their charges and polarities, and to accommodate conjugation to other entities (e.g. biomolecules or fragments to expand their theranostic modalities). Thus, it was possible to optimize their photocytotoxicities without compromising their other desirable characteristics for PDT.

DEDICATION

To

My Family

ACKNOWLEDGEMENTS

I would like to thank my committee chair, Dr. Kevin Burgess for giving me the opportunity to work in his lab and to learn from him. I would also like to thank him for his support, encouragement and motivation through the course of my graduate studies. I would also like to thank my committee members, Dr. Frank Raushel, Dr. Robert Burghardt, Dr. Wenshe Liu and Dr. Jonathan Sczepanski, for their help and guidance.

I would like to thank all the lab members of Burgess Lab for creating a productive lab environment. A special thanks to Dr. Zhengyang Jiang for being an ideal mentor, guiding me through all my projects and ever willing to help me out in and outside lab. Thanks to Dr. Maritess Noelle Victoria Arancillo, Dr. Chen-Ming Lin and Dr. Zhengyang Jiang, for their wonderful friendship; including uncountable lunches, dinners, movies and other extracurricular activities we had that took stress off me and helped me pass most difficult times. Thanks to Dr. Bosheng Zhao and Sopida Thavornpradit for their friendship and fruitful collaborations. I would also like to thank Tye Thompson, Aaron Jacobson, Jonathan Whisenant, Shaon Joy and Rui-Liang Lyu for being wonderful lab and office mates.

Also, I would like to thank Dr. Stanislav Vitha for always patiently teaching and helping me with the confocal imaging. A special thanks to Dr. Rahul A. Sheth at MD Anderson for providing me an opportunity to do *in vivo* work.

Thanks to Andrea Scott and Jill Powers for their assistance with all lab related administrative tasks.

Thanks also go to my friends and colleagues and the department faculty and staff for making my time at Texas A&M University a great experience.

Last but not the least, I would like to thank my family members, for their love, support and encouragement without which I would not have been able to reach this stage. Thanks to all my friends for providing the best support system during my graduate studies. I would also like to thank my professors (particularly of Chemistry Department) at Lahore University of Management Sciences (LUMS) for helping me get to Texas A&M University.

CONTRIBUTORS AND FUNDING SOURCES

Contributors

This work was supervised by a dissertation committee consisting of Dr. Kevin Burgess [advisor], Dr. Frank Raushel, Dr. Wenshe Liu and Jonathan Sczepanski from Department of Chemistry and Dr. Robert Burghardt [Department of Veterinary Integrative Biosciences.

In vivo experiments in Chapter 2 were carried out by Dr. Zhen Yang and Dr. Zheng Li at Center for Bioenergetics, Houston Methodist Research Institute. Experiments and data analysis in Chapter 3 and 4 were carried out in collaboration with Dr. Chen-Ming Lin. Dr. Lawrence J. Dangott (Department of Biochemistry and Biophysics) helped with gel analysis and Dr. David Barondeau (Department of Chemistry) helped with the protein purification. Western Blots and wound healing experiments in Chapter 5 were carried out by Bosheng Zhao. Synthesis of compounds in Chapter 6 was carried out with the help of Sopida Thavornpradit.

All other work conducted for the dissertation was completed by the student independently.

Funding Sources

This work was made possible by Department of Defense – Breast Cancer Research Program Breakthrough Award (BC141561), Cancer Prevention and Research Institute of Texas (RP150559 and RP170144), The Robert A. Welch Foundation (A-1121), Texas A&M University (RP180875) and National Science Foundation (M1603497) for financial support. The NMR instrumentation at Texas A&M University

was supported by a grant from the National Science Foundation (DBI-9970232) and the Texas A&M University System. The use of the Microscopy and Imaging Center facility at Texas A&M University is acknowledged. The Olympus FV1000 confocal microscope acquisition was supported by the Office of the Vice President for Research at Texas A&M University. The use of Chemistry Mass Spectrometry Facility and College of Medicine Cell Analysis Facility (COM-CAF) is acknowledged.

The contents are solely the responsibility of the authors and do not necessarily represent the official views of the National Science Foundation, the Welch Foundation, Department of Defense, Cancer Prevention and Research Institute of Texas or Texas A&M University.

TABLE OF CONTENTS

Page

LIST OF FIGURES

Page

LIST OF TABLES

Page

CHAPTER I

INTRODUCTION

Historically, fluorescence imaging facilitates tracking cellular movement of organelles or protein expression levels.[1] It works by attaching a fluorescence molecule with a protein or target of interest and then irradiating at the absorption wavelength of the fluorophore and observing it under the microscope at optimum fluorescence wavelengths (Figure I-1).[2] Penetration of light through tissue depends on where it lies in the electromagnetic spectrum. As the wavelength of absorbance of light increases from ultraviolet (UV) to near infrared (NIR) region, the less it is reflected from the surface, and instead absorbed and scattered by the organelles.[3] Hence, fluorophores that absorb in the near infrared region are ideal due to maximal penetration of light of those wavelengths through the tissue.

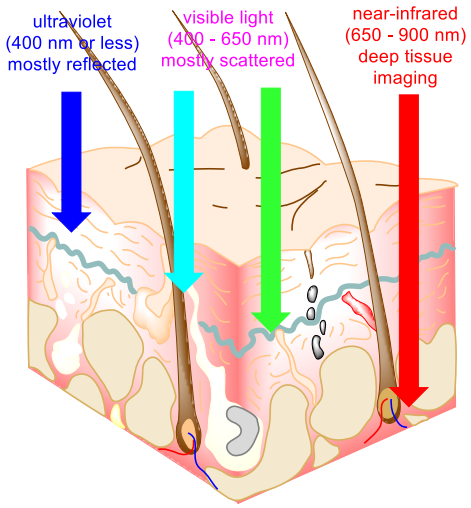

Figure I-1. Penetration of different wavelengths of light through tissue is dictated by where it lies in the electromagnetic spectrum

Fluorescence guided optical imaging in medicine is becoming increasingly important, especially in oncology. Approximately 45% of all cancer patients are cured by surgery.[4] Survival rate is higher for tumor patients after surgery, more than any other technique.[5] Radiative imaging techniques like magnetic resonance imaging (MRI), single photon emission computed tomography (SPECT) and positron emission tomography (PET), computed tomography (CT) are currently used to diagnose cancer patients, but these techniques lack real time diagnosis capability. On the other hand, fluorescence guided surgery (FGS) uses non-invasive and radiation-less technique for intraoperative imaging.[6]

For a fluorophore to be used in FGS, it should have the following characteristics: (i) absorbs in NIR region, (ii) high fluorescence quantum yields and extinction coefficients, (iii) non-toxic to organs in the body, and (iv) selectively localize in tumor cells relative to normal healthy ones. Unfortunately, most common fluorescent dyes (e.g. BODIPY, FITC and DAPI) do not absorb in the NIR region. NIR fluorophores can be organic or inorganic. Inorganic fluorescent quantum dots have potential cytotoxicity issues arising from use of elements like cadmium, tellurium and selenium, and their surface coating complication, costly preparation and difficulties in quantification and reproducibility.[7,8] Amongst organic dyes heptamethine cyanine dyes fulfil the above criteria.

Small Molecule Targeted Fluorescent Imaging

Ideally, active targeting helps deliver drugs or other cytotoxic payloads to tumor sites with minimal consequences to normal healthy tissues.[9] Small molecules and

monoclonal antibodies (mAbs) are mostly exploited for active targeting. Interest in mAbs the most prevalent area of active targeting because antibody development reliably gives products that bind strongly to specific targets overexpressed on cell surface membranes.[10,11] On the other hand, mAbs have significant limitations due to their large size. Firstly, the penetration of mAbs is limited by their size, hence they tend to be unable to penetrate to the core of tumors where the cells are most aggressive.[12,13] Secondly, due to strong binding to their receptors, mAbs are slowly cleared out of the body (half-life in days) and tend to accumulate in liver and kidneys.[14] Thirdly, mAbs can have immunogenic response which might affect their pharmacokinetic properties.[15] Lastly, it is costly to produce mAbs on a large scale, the purity might vary from batch to batch and their shelf life is limited.

In some cases, shortcomings of mAbs in active targeting can be overcome by using small molecules instead. Small molecules targeting receptors overexpressed on cell surface include folic acid,[16,17] RGD peptides,[18,19] biotin[20] and prostrate specific membrane antigen (PSMA) inhibitors[21,22] (Figure I-2). Our group developed a bivalent small peptide molecule which mimics the beta turn of tropomyosin receptor C (TrkC),[23-25] which is overexpressed in several different cancers including metastatic breast cancer,[26-28] melanoma,[29-31] glioblastoma[32-34] and neuroblastoma.[35,36]

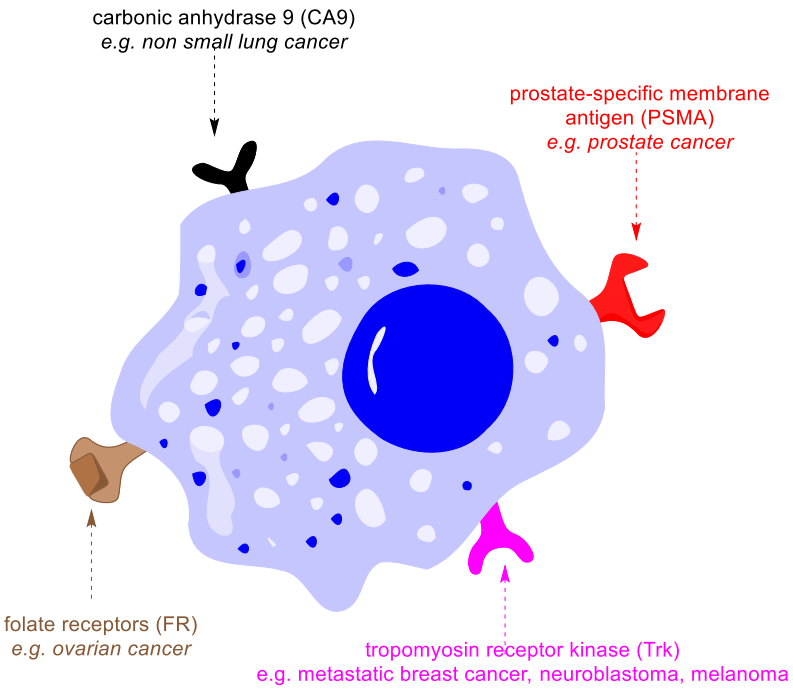

Figure I-2: Various cell surface receptors are expressed on different cancer types that can be targeted by multiple small molecules

Previous work in the group has used BODIPY[37] and aza-BODPIY[38] fluorophores for *in vivo* imaging. As described above, imaging in visible light is hampered by excessive scattering, less penetration and high tissue autofluorescence. In this work, a zwitterionic cyanine dye, with absorption in NIR region (~780 nm) was used for *in vivo* imaging. A zwitterionic dye was chosen because some literature indicates that charge neutral dyes tend to have the lowest binding with normal tissues and organs, and are rapidly cleared from the body.[39,40]

Mode of Uptake Tumor Seeking Cyanine

ICG, the only FDA approved NIR dye, is non-selective to tumors; its main applications are for determining blood flow and liver clearance. However, there are

similar cyanine dyes **A** – **D** (Figure I-3) that *do* accumulate in tumors in preference to normal tissues and organs,[41-43] and do *not* require mAb or small molecule targeting groups.

Cyanines (**A** – **D**) are well suited for *in vivo* imaging because they have absorption and emission maxima in NIR region (700-900 nm) and have high extinction co-efficients.[44-47] They tend to specifically localize solid tumors (*e.g.* prostate,[48] gastric,[49] kidney,[50], hepatocytes,[51] kidney,[50] lung,[52] and glioblastoma[53]) and persist there for long days. Preferential uptake of these dyes in cancer cells over normal cells has been credited to organic anion transporting polypeptides (OATPs)[54,55] which is overexpressed in cancerous cells under hypoxic environment,[49,56] but that hypothesis is tested in work described here. Dye **A** was chosen for case study, and its reactivity was measured with various side chains of amino acids at physiological conditions, and the role of *meso* chlorine of **A** was explored.

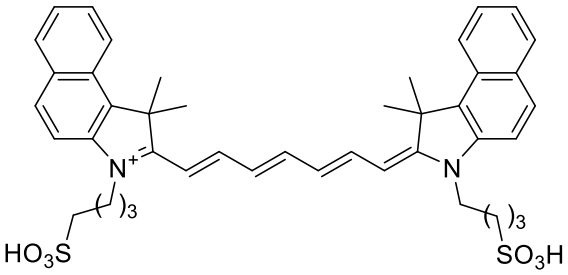

indocyanine green (ICG)

Figure I-3: Structures of ICG, the only FDA approved cyanine and other other tumor-targeted cyanines dyes reported in the literature are shown

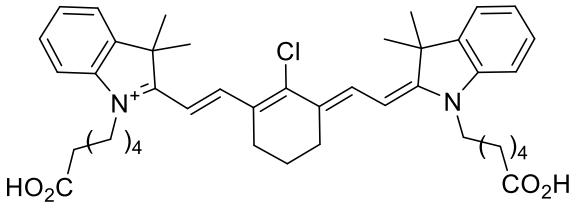

MHI-148, **A**

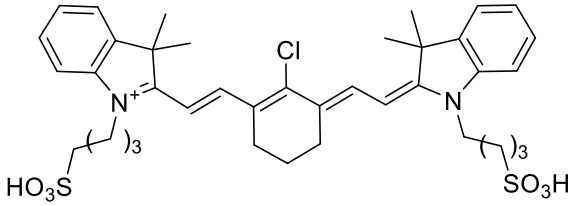

IR-783, **B**

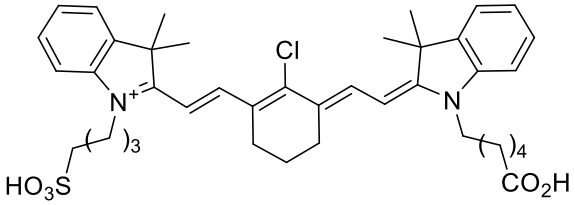

DZ-1, **C**

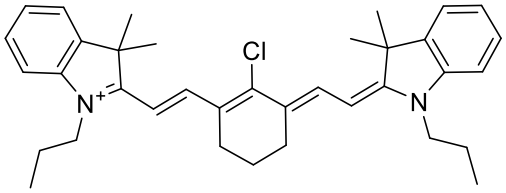

IR-780, **D**

Figure I-3: Continued

Tumor Targeted Cyanines as Drug Carrier

Before our studies, there were only few reports in literature wherein dyes **A** – **D** have been conjugated with cytotoxic drugs (Figure I-4), specifically with monoamine oxidase inhibitors (**Ac**, **Ai**),[57-59] faresnyl transferase inhibitor (**Cf**),[60] a mustard agent (**An**)[61] and gemcitabine (**Cg**).[51,53] Results from these studies suggests conjugation of

cytotoxic drugs tends not to unduly influence the tumor localization properties of the parent dye, implying some active uptake mechanism.

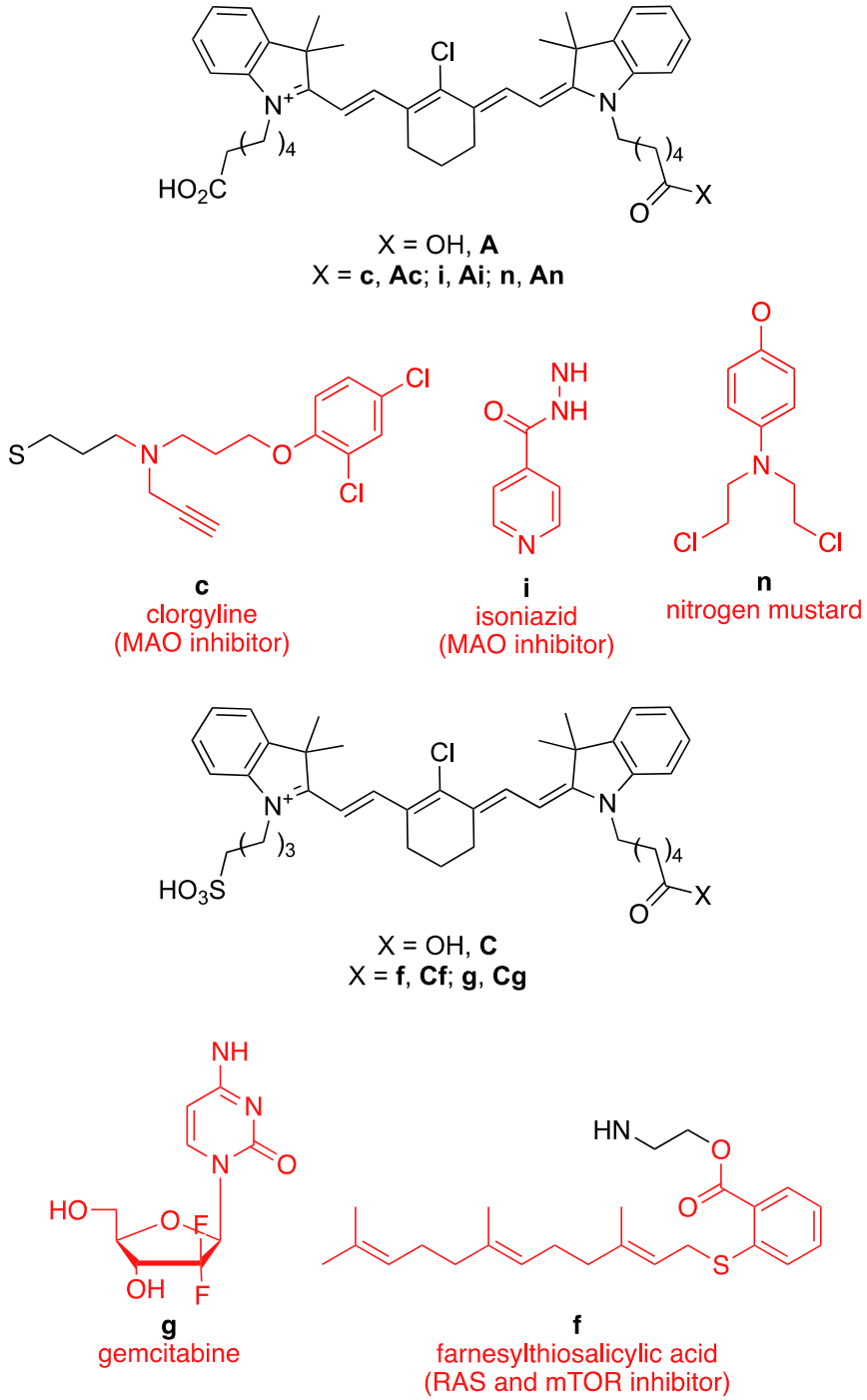

Figure I-4. Structures of the known drug conjugates with **A** and **C**.

We saw opportunities to conjugate *kinase inhibitors* with tumor seeking dyes. Kinases modulates protein function by adding phosphate groups.[62] There are a total of 518 kinases in the human genome but little is known about the majority of them.[63] Recent advances in science have shed light on the importance of kinases in signaling pathways leading to growth, survival and motility of cells. A kinome wide study unraveled the significance of kinase signaling pathways in different diseases including cancer.[64] There is strong evidence linking abnormal kinase activity with carcinogenesis and metastases of various cancer types. Since the approval of first kinase inhibitor (imatinib, Gleevec®) towards CML in 2001, at least 40 kinase inhibitors have been FDA approved.

This dissertation discusses our effort in selecting a kinase inhibitor (dasatinib, SRC promiscuous) with a solvent exposed nucleophilic handle and conjugating it with **A**. Tests were done to determine the binding constant of the conjugate and *in vitro* assay to prove its effectiveness. Preliminary *in vitro* data of other solvent exposed kinase inhibitors (palbociclib, ribocilcib, crizotinib and ceritinib) on multiples cancer cell lines are reported in Appendix G.

Photodynamic Therapy

The first FDA-approved photodynamic therapy (PDT) agent appeared 20 years ago, and since then seven more have been approved.[3] There are three main components in photodynamic therapy: (i) photosensitizer (PS), (ii) light, and (iii) oxygen. After administration in the body, the PS is allowed to accumulate in the cancer region, after which light of a certain wavelength is irradiated on it. Upon irradiation, photosensitizers

are excited from their ground state and through a cascade of processes it transfers the energy to ubiquitous triplet oxygen generating singlet oxygen (Figure I-5).[65] This $^1O_2$ is very reactive and can harm the nearby cell.

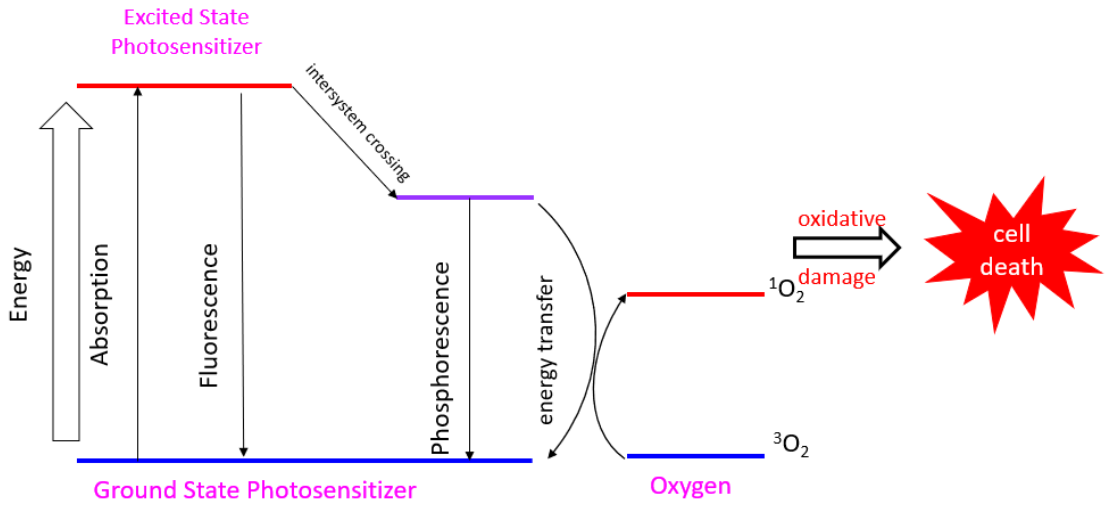

Figure I-5. Mechanism of singlet oxygen generation after irradiation of correct wavelength of light.

Most FDA approved PDT agents are based on porphyrin rings which absorb around 650 nm (Figure I-6).[66] Previously, our lab has worked with PDT active BODIPY[67] cores but, as mentioned above, they usually absorb in visible light region where penetration of light is not optimal. Hence, this dissertation shows our efforts in synthesizing a series of novel heptamethine cyanine dyes with incorporation of a heavy atom. The core of the molecule was structures **A-D**. The photophysical properties and *in vitro* assays were conducted to prove the effectiveness of the new dyes.

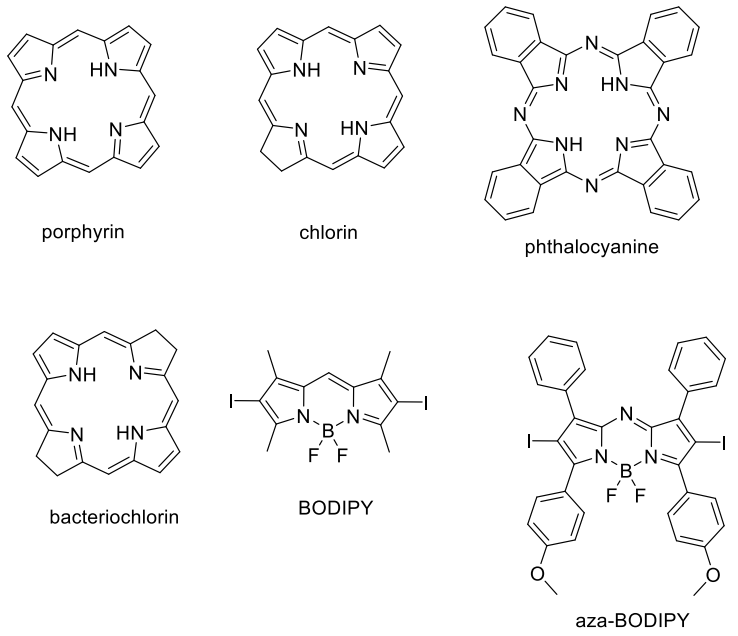

Figure I-6. Commonly used photosensitizers for photodynamic therapy.

CHAPTER II

A ZWITTERIONIC NEAR-INFRARED DYE LINKED TRKC TARGETING AGENT FOR METASTATIC BREAST CANCER

Introduction

Development of imaging probes that selectively associate with metastatic tumor cells expands useful diagnostic tools for the therapeutic assessment of the cancer treatment.[68,69] For the breast cancer, there is an emerging demand for imaging probes that are capable for the recognition of metastatic breast tumor cells not just normal breast tumor, with the increased academic and clinical efforts in the fighting against late-stage breast cancer.[70,71] Tropomyosin kinase receptor C (TrkC) has been identified as a characteristic regulator of breast cancer cell growth and metastasis and tends to be overexpressed in metastatic breast tumor cells.[27,72] Consequently, it is a potential target for active targeting of metastatic breast cancer.

Most often, monoclonal antibodies (mAbs) are used as targeting agents.[73,74] Small-molecule alternatives, however, have advantages with respect to cost, reagent stabilities, immunogenic effects, circulation times in the course of patient imaging, and, most important superior permeation into solid tumors.[68,75] Consequently, the focus of our research is on small molecules for active targeting of TrkC.

---

[76]Reprinted with permission from "A Zwitterionic Near-infrared Dye Linked TrkC Targeting Agent For Imaging Metastatic Breast Cancer" by Zhen Yang, Syed Muhammad Usama, Feng Li, Kevin Burgess and Zheng Li, *Med. Chem. Commun.* 2018, *9*, 1754-1760. DOI: 10.1039/C8MD00190A. Reproduced by permission of The Royal Society of Chemistry.

Targeting TrkC with small molecules has featured a bivalent targeting fragment (IY-IY, blue color throughout diagrams in this paper).[37,67,77] In this work, that fragment, "IY-IY", was covalently linked to a zwitterionic cyanine dye (purple color throughout) to give a near-infrared probe for TrkC targeted imaging. Polar, zwitterionic characteristics of the dye were anticipated to foster the aqueous dissolution for *in vivo* administration, and simultaneously diminish net-charges that might otherwise induce non-specific binding.[39] Since the intrinsic structure of IY-IY fragment was preserved, we hypothesized that final assembly of the probe would maintain its characteristics of TrkC targeting.

Results and Discussion

Probe Design: Motivation for these studies came from positive results obtained in a study of the photodynamic therapy (PDT) agent **A** in mice impregnated with 4T1 mouse breast tumors.[67] In that work, one single dose of 10 mg/Kg followed by illumination for 10 min caused near complete regression of the primary tumor over 28 days *and* inhibited metastatic spread relative to untreated control animals.

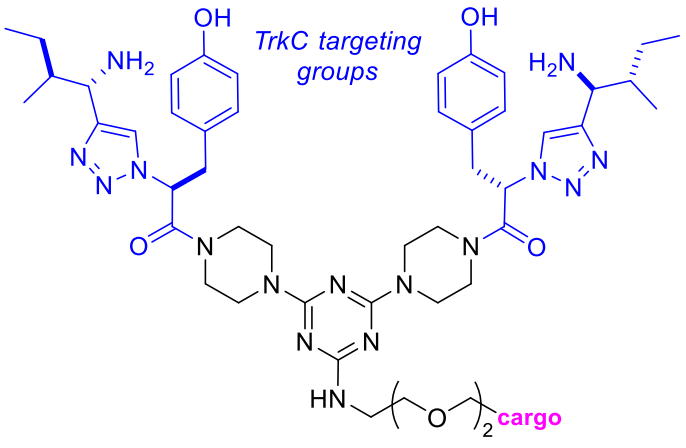

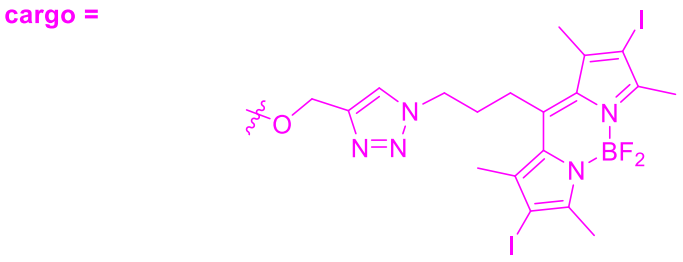

A
PDT agent

The next step in our research has been to develop a TrkC-targeted compound for optical imaging *in vivo*. Agent **A**, and especially its non-iodinated analog, stained 4T1 cells (that are TrkC$^+$) well in culture,[78] but it is unsuitable for *in vivo* imaging because it absorbs light maximally at 530 nm. Dyes that absorb above 700 nm are preferred for *in vivo* imaging because tissue is most permeable to light above that wavelength, hence the fluorophores can be excited in more deeply situated tumors. Consequently, we designed and studied agent **B**.[46,79]

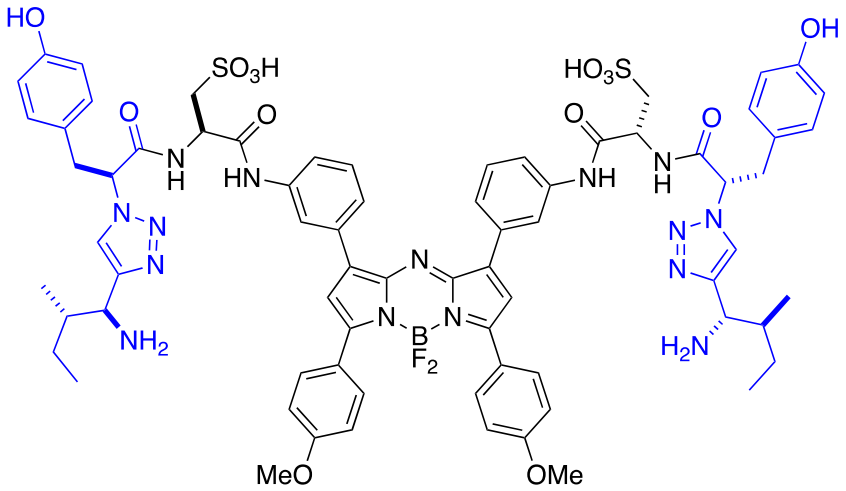

B
in vivo imaging
λ_{max} 633 nm

The outcome of our studies on **B** was a mixed success.[38] Agent **B** selectively accumulated in the TrkC$^+$ 4T1 tumors (relative to an isomeric, non-TrkC targeting,

control similar to that shown below). That observation means that the different linker and spacing of the TrkC-targeting groups in **B** relative to **A** did not perturb its honing ability; other work has shown that is not always the case.[77] On the other hand, a shortcoming was that **B** absorbs at 633 nm which, though more appropriate than 540 nm in **A**, is still not a long enough wavelength. Another shortcoming was that **B** accumulated about three times more in the liver than in the tumor, and it had a long residence time there (still observed after 48 h).

Based on the studies outlined above, the current study was initiated to change the fluorophore completely, to a hydrophilic cyanine dye as in **1**. Structure **1** has the same IY-IY targeting arrangement as our original lead **A**, and a more water-soluble fluorophore than **B** that absorbs light maximally at around 760 nm. Consequently, the visibility of this probe *in vivo* should be superior to **A** and **B**, and we anticipated that it would be less retained in the liver than the lipophilic aza-BODIPY system **B**. The parameter that could not be anticipated was the effect of the targeting groups in **1** offset by the pharmacokinetic influence of the cyanine fragment. Important work, particularly by Henary and co-workers, on distribution of cyanine dyes *in vivo* enables some predictions to be made with more confidence,[39,40,42,43,80,81] but, nevertheless, experimentation is necessary.

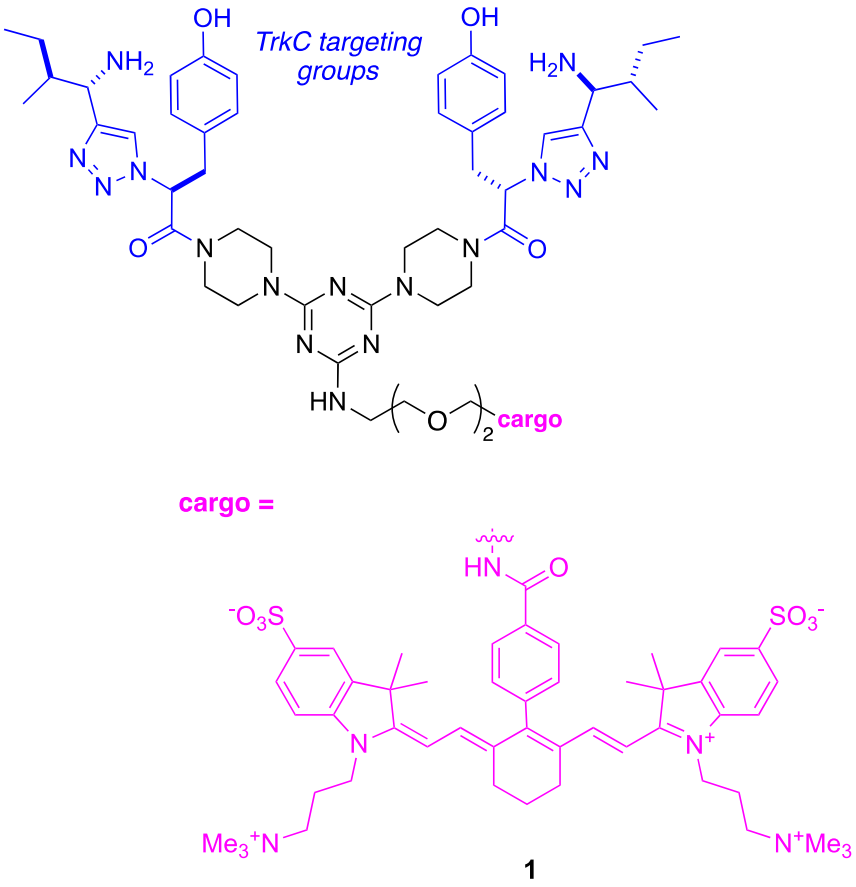

Probe Synthesis and Optical Properties: The IY-IY targeting group has been made many times previously in these labs, but for the current study a modified procedure was developed to facilitate synthesis on a larger scale. Details of the modified route are given in the supporting material, and the concept is outlined in Scheme II-1. The last step involved a coupling of the targeting fragment C with the activated cyanine part D.[82] The innovation in the modification was in the construction of C. Previously IY-piperazine fragments had been added to the triazine, but that step did not scale well. Instead, the current route involves S*N*Ar reaction of tyrosine-derived azide, then click reaction to build up the IY-IY fragment in layers.

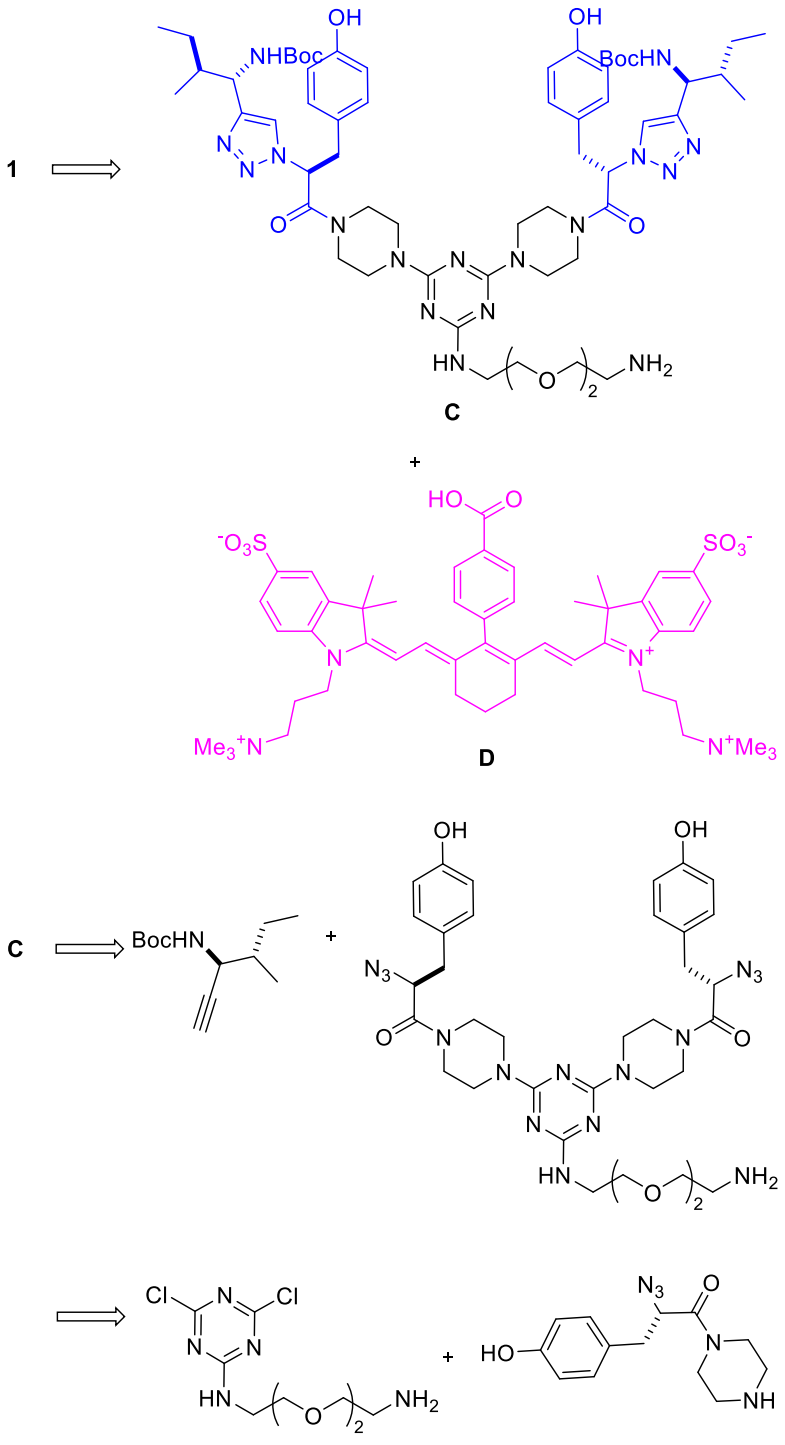

Scheme II-1. Retrosynthetic route to probe **1** illustrating an improved route to the IY-IY fragment.

The following electronic spectral data summarize the key points from the full analysis shown in the supporting. Probe **1** had an extinction coefficient of 140,000 L mol^{-1} cm^{-1} and a quantum yield of 5.6% (in 7.4 PBS buffer); these data are typical of the strong absorption from the cyanine fragment and indicate an excellent overall brightness. Maximal absorption and emission were observed at 760 and 780 nm (in pH 7.4 PBS buffer), ideal for optical imaging.

Compound **2** is an isomer of **1** with the targeting amino acids inverted (YI-YI); this was a useful control in the cellular studies that are now described.

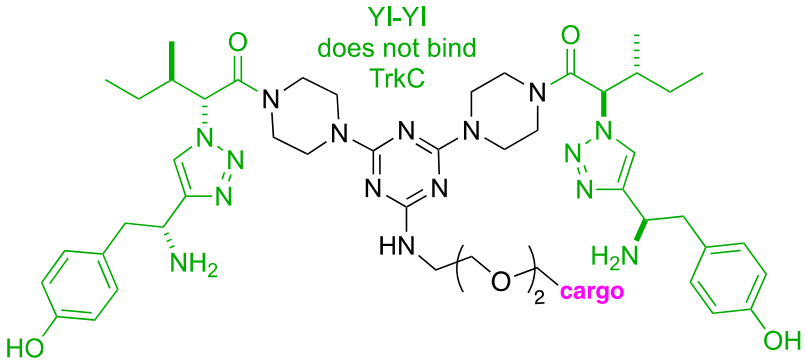

cargo =

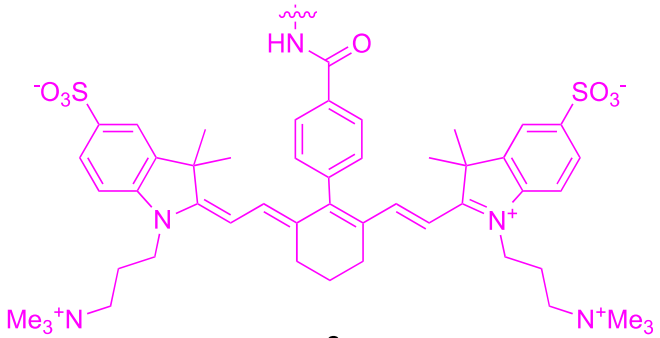

2

Probe Behavior in Live Cell and Tissue Studies: Probe **1** was first tested for binding cells stably transfected with TrkC; data obtained (Figure II-1a, horizontal row) show the cells did bind the probe, whereas the parent NIH 3T3 cells do not express this

receptor (Figure II-1b). Control experiments (Appendix Figure A-S1-3), demonstrated that the control probe 2 did not stain TrkC^{+} or wild type (TrkC^{-}) NIH 3T3 cells, and neither did the parent cyanine dye without the targeting group. Confocal studies at a higher magnification revealed 1 tends to localize in the lysosomes (Figure II-1c and d), just as natural neurotrophins to when they are imported via the TrkC receptor.[83] In histology studies with commercial samples from breast cancer patients, metastatic breast cancer tissue was stained but not normal tissue (Figure II-1e and f).

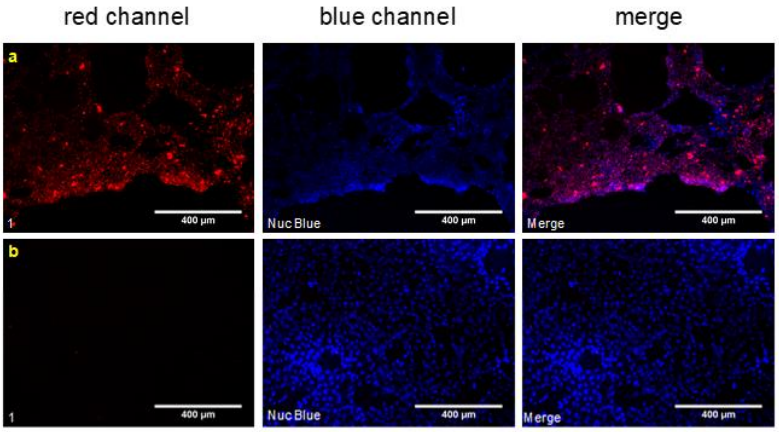

Figure II-1. a Probe **1** binds NIH3T3 TrkC^{+} cells, but not to NIH3T3 WT cells (**b**). Confocal experiments revealed **1** colocalizes: **c** with LysoTracker Green; and, **d** not with MitoTracker Green. Histology study of **1** with: **e** metastatic breast cancer tissue (invasive ductal carcinoma); and, **f** normal breast tissue (adjacent normal breast tissue). Throughout the blue channel is to detect nuclear staining with Nuc Blue.

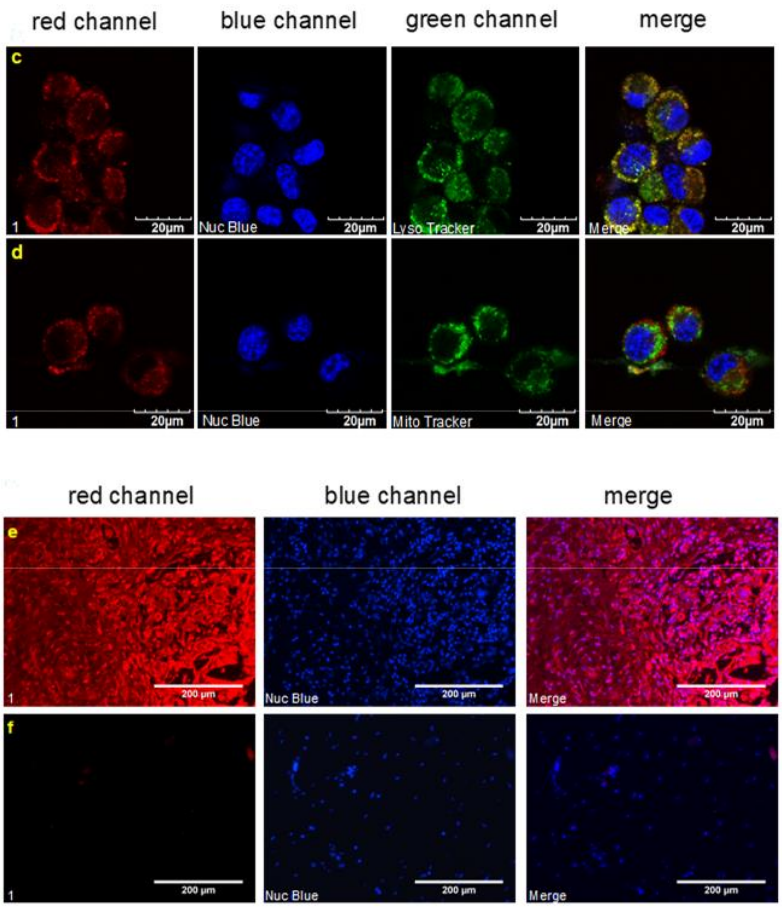

Figure II-1. Continued

In Vivo *Imaging with Probe 1:* Mouse 4T1 breast tumor is a well-established animal model for study of human metastatic breast cancer. [84] In this study, murine 4T1 tumor cells were subcutaneously injected into BALB/c nu/nu mice to create 8-10 mm diameter metastatic breast tumor xenografts. After intravenous injection of the imaging probe, NIR fluorescence images of the tumor-bearing mice were captured at various time points after injection of **1** (Figure II-2). The 4T1 tumors were clearly visualized through the fluorescence differences displayed from tumor to muscle background as early as 15 min post injection of the targeting agent. Moreover, the agent 1 rapidly cleared from the body; fluorescence intensities of the tumor dropped from 15 min to 1 h, and further at 3

h, and almost to background at 24 h. Compared to TrkC targeting agent B, the retention time of the **1** was much shorter, presumably because of the more hydrophilic nature of the zwitterionic dye.

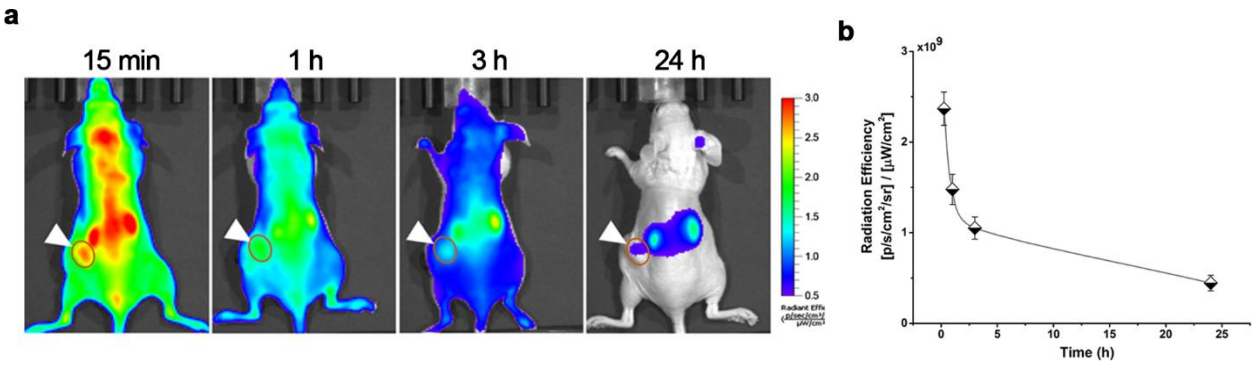

Figure II-2. a *In vivo* NIR fluorescence images of 4T1 tumor-bearing mice at 15 min, 1 h, 3 h, and 24 h post-injection of the targeting agent. White arrows in indicate the tumors, and the circles mark ROI study of tumor for the quantification analysis in **b**. **b** Quantification of fluorescence in the tumors. Data shown represent mean ± SD (n = 3 per group).

To further validate tumor uptake of the targeting agent, internal organs of the imaged mice were collected for *ex vivo* imaging. The relatively higher fluorescence intensities displayed in tumors, compared to muscle background, indicated the selective update of the targeting agent by the tumors (Figure II-3a). Trk receptors play important roles in the mammalian nervous system, and tends to exhibit high expression of TrkC receptor.[85] So far we did not observe uptake in the mice brain and spinal cord, we believe that the charge of the probe make it difficult to penetrate into the central nervous system. A kinetic curve of the tumor uptake extracted from *ex vivo* imaging data corresponded to that from *in vivo* imaging (Figure II-3b). Uptake of the targeting agent in tumor reached its peak half an hour after the injection, then clearance from the body dominated.

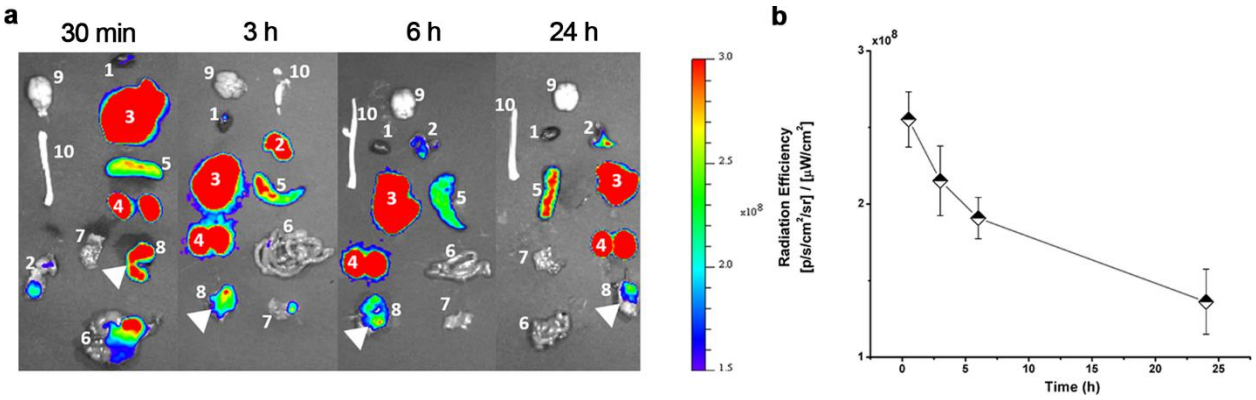

Figure II-3. a Representative *ex vivo* fluorescence images of: 1 heart, 2 lung, 3 liver, 4 kidney, 5 spleen, 6 gastrointestine, 7 muscle, 8 tumor, 9 brain, 10 spinal cord, collected from the mice at 30 min, 3 h, 6 h and 24 h post-injection of the targeting agent. White arrows mark the tumors. **b** Quantification of fluorescence in the tumors. Data shown represent mean ± SD (n = 3 per group).

Probe **1** localized in the TrkC expressing tumors, as anticipated, providing a way to stain them with NIR fluorescence. In retrospect, the observation that the probe was washed out of the system relatively rapidly can be attributed to the polarity of the cyanine dye. However, the observation of the rapid washout from tumors in vivo surprised us, for two reasons. First, the cell imaging data in this paper prove that probe **1** is selectively imported into the $TrkC^+$ cells. Secondly, at least some members of the parent dye system E (particularly where R^1 and R^2 contain carboxylate or sulfonate functionalities) tend to localize in many types of solid tumors.[69,86-88] Further experiments are in progress to try to understand these apparent inconsistences.

Conclusions

In this work, an imaging probe that incorporated with the TrkC targeting agent and zwitterionic NIR dye was reported for imaging metastatic breast cancer. In vitro and in vivo imaging studies showed the specific association of the TrkC targeting probe with

4T1 tumors. This study is helpful for further development of a TrkC targeting agent for theranostics of metastatic breast cancer.

CHAPTER III

SITE-SPECIFIC LABELING OF PROTEINS WITH NEAR-IR HEPTAMETHINE CYANINE DYES

Introduction

Hydrophilic near-infrared (NIR) fluorescent dyes are valued for in-depth imaging in tissues, and heptamethine cyanines, or Cy-7 dyes, which absorb in the NIR region (700–900 nm), are amongst the most widely used [89]. Indocyanine green (ICG, Figure III-1), the only FDA-approved Cy-7 dye, has been widely used in medical and clinical diagnostics. [90-92]

Many applications of Cy-7 dyes require that they be covalently conjugated to, for example, antibodies, cell surface targeting peptides/biomarkers, and small molecule substrates. This is often achieved by modifying Cy-7 derivatives with coupling functionalities such as maleimide, succinimide esters, isocyanates, or sulfonyl halides. The challenge with strategies like this is balancing the demands of experimental convenience with selectivity towards targeted amino acid types. Extensive modifications to Cy-7 dyes can also alter their solubility and photophysical properties.[93]

Figure III-1 shows dyes featured in this study. Probes of this type, i.e., with a 1-chloro-2,6-disubstituted cyclohexane (i.e., MHI-148, IR-780, IR-783, and DZ-1) [81,94,95], are known for their tumor localizing properties.[48-50,96] Therefore, these Cy-7 dyes are potential carriers of cytotoxic payload for combined cancer targeted therapy and

---

[97]Reprinted with permission from "Site-Specific Labeling of Proteins with Near-IR Heptamethine Cyanine Dyes" by Chen-Ming Lin, Syed Muhammad Usama and Kevin Burgess, *Molecules.* 2018, *23*, 2900. DOI:10.3390/molecules23112900.

imaging.[53,57,59,60] conjugation process. Specifically, when investigating *in vitro* reactions and cell lysates featuring MHI-148, it was found to covalently bind to several proteins with high selectivity as evidenced by gel electrophoresis and NIR imaging at around 800 nm.

We hypothesized that the *meso*-Cl of MHI-148 was substituted by nucleophilic functional groups of amino acids (cysteine, serine, tyrosine, and lysine) of proteins. This paper provides data to support this hypothesis and understand the selectivity.

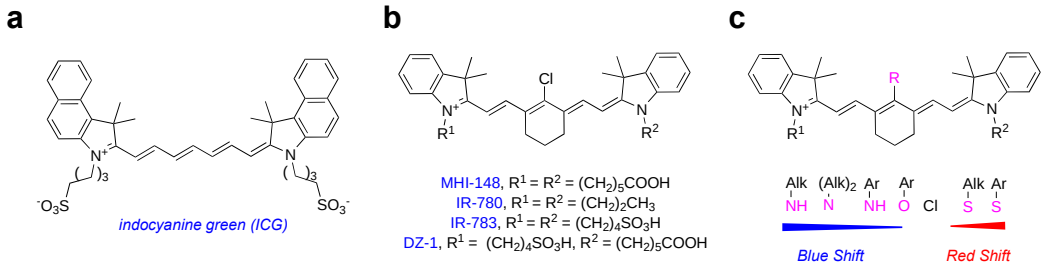

Figure III-1. Structures of: **a** ICG; **b** cancer-tissue-targeting Cy-7 dyes and their *meso*-substituted derivatives; and **c** graphical representation of the effects of *meso*-substitution on electronic spectra.

Results and Discussion

Syntheses of Amino-Acid-Substituted Cy-7 Dyes: Reactions under controlled conditions were used to test if nucleophilic substitution of the chloride of MHI-148 possibly occurred in DMF solvent. Thus, several amino acids with different nucleophilic side-chains (*N*-acetyl-L-cysteine, *N*-acetyl-L-tyrosine, *Nα*-acetyl-L-lysine, *Nε*-acetyl-L-lysine, and L-proline) were reacted with MHI-148 under conditions that were varied to force the reactions to proceed. The corresponding amino-acid-substituted Cy-7 dyes were indeed formed (Scheme III-1); these were isolated, characterized (see supplementary

materials for NMR and mass spectrometry), and later used as standards for comparison of high-performance liquid chromatography (HPLC) retention times. Serine was excluded from these experiments because alcohol hydroxyl groups are known to not substitute the *meso*-Cl without complications.[98-101]

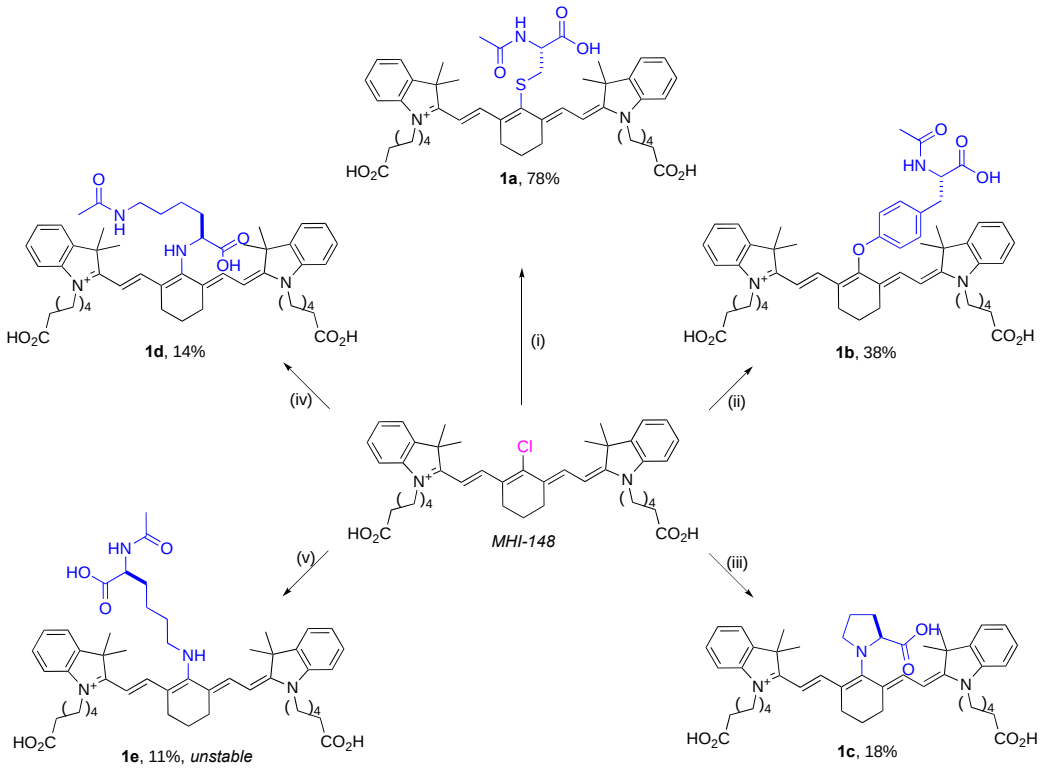

Scheme III-1. Preparation of amino-acid-substituted Cy-7 dyes. (i) *N*-acetyl-L-cysteine (1 eq.), $^{i}Pr_2NEt$ (1.5 eq.), DMF, 25 °C, 1 h (ii) *N*-acetyl-L-tyrosine (1 eq.), NaH, DMF, 25 °C, 18 h (iii) proline (1 eq.), $^{i}Pr_2NEt$ (1 eq.), DMF, 60 °C, 2 h (iv) *Nε*-acetyl-L-lysine (1 eq.), $^{i}Pr_2NEt$ (1 eq.), DMF, 60 °C, 20 h (v) *Nα*-acetyl-L-lysine (1 eq.), $^{i}Pr_2NEt$ (1 eq.), DMF, 60 °C, 20 h.

N-Acetyl-L-cysteine was the most reactive nucleophile of the five amino acids studied. In the presence of Hünig's base, MHI-148 was completely converted to the thiol-substituted product within 1 h at 25 °C in DMF (0.1 M 1:1 dye:Cys-derivative, LC-MS

analyses). Four other amino acid nucleophiles studied required a stronger base (Tyr) and/or elevated temperatures (Pro and Lys), and even then, a significant amount of unreacted MHI-148 was observed after several hours. *N*α-Acetyl-L-lysine reacted faster than those three, giving the substituted product **1e**, which can be isolated by reversed-phase flash chromatography; however, significant decomposition was observed (color change from blue to pink) in organic solvents after only 20 min. The instability caused by delocalization of a lone pair of elections by primary amine at *meso* position is also reported by other groups;[102] Overall, the data indicated the *meso*-Cl substitution reactivity was thiol > phenol > 2° amine > 1° amine, which corresponds to the observations in the literature [103]. At this stage, we did not know if these reactivities would also be observed in aqueous media, but preferential conjugation of MHI-148 to Cys residues seemed more likely.

Optical Properties of Amino-Acid-Substituted Cy-7 Dyes. Figure III-2 shows absorbance and fluorescence of compounds **1a**–**d** in 10 mM PBS buffer. The S- or O-substituted compounds (**1a** and **1b**) had absorbance and fluorescence spectra similar to those of MHI-148. Significant red-shifts of absorbance and fluorescence were observed for both N-substituted Cy-7 dyes (**1c** and **1d**), which have been attributed [42,104] to conjugation of the nitrogen lone pair with the Cy-7 core. Interestingly, the peaks for the N-substituted products are significantly broader, implying more vibrational fine structures than the S- or O-substituted products.[105]

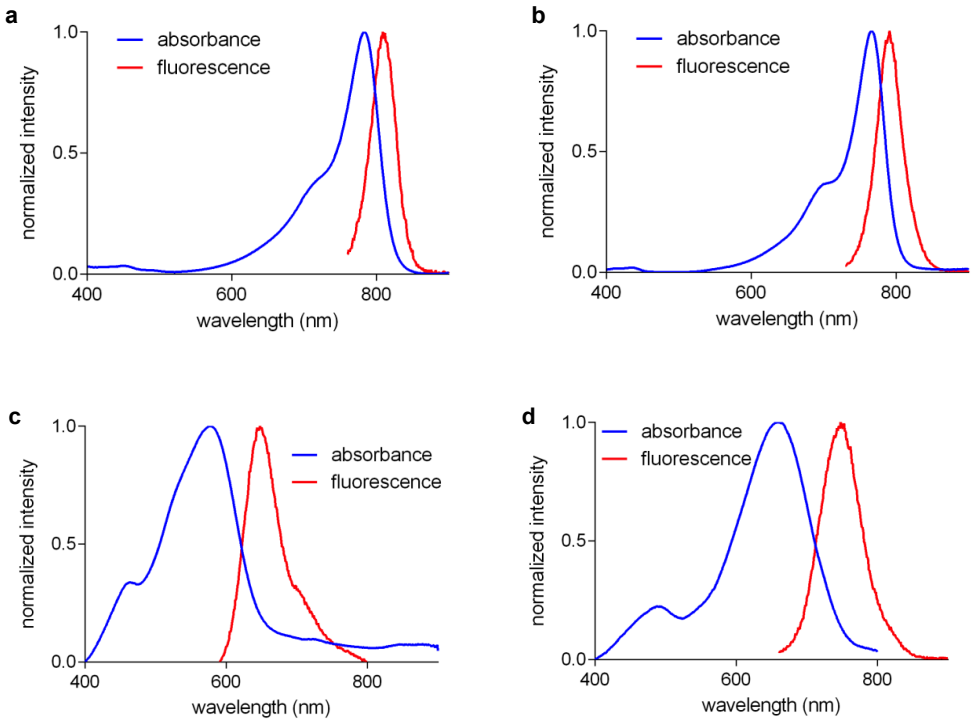

Figure III-2. Normalized absorbance and fluorescence of compounds **1a**–**d** (6 µM, 37 °C) in pH 7.24 10 mM PBS buffer. **a** compound **1a**: $\lambda_{max\ abs}$ 783 nm (blue), $\lambda_{max\ emiss}$ 809 nm (red). **b** compound **1b**: $\lambda_{max\ abs}$ 766 nm (blue), $\lambda_{max\ emiss}$ 791 nm (red). **c** compound **1c**: $\lambda_{max\ abs}$ 578 nm (blue), $\lambda_{max\ emiss}$ 648 nm (red). **d** compound **1d**: $\lambda_{max\ abs}$ 658 nm (blue), $\lambda_{max\ emiss}$ 748 nm (red).

Meso-Cl Functionality of Cy-7 Dyes Is Essential For Cys-Selective Protein Labeling: Vimentin, a structural protein, was chosen for study because it has only one Cys residue (C328). Vimentin (1 µg, 1 µM) was incubated with Cy-7 dyes containing meso-Cl (MHI-148, IR-780, IR-783, and DZ-1; 10 µM) and with Cy-7 dyes without meso-Cl (ICG and 1a) for comparison (throughout, 10 µM in 50 mM pH 7.24 HEPES buffer at 37 °C for up to 24 h). An equal amount of the samples (100 ng) was electrophoresed under reducing conditions, and the gel was analyzed using an NIR imager. Only the Cy-7 dyes containing meso-Cl reacted to give a band observable at 800 nm (Figure III-3).

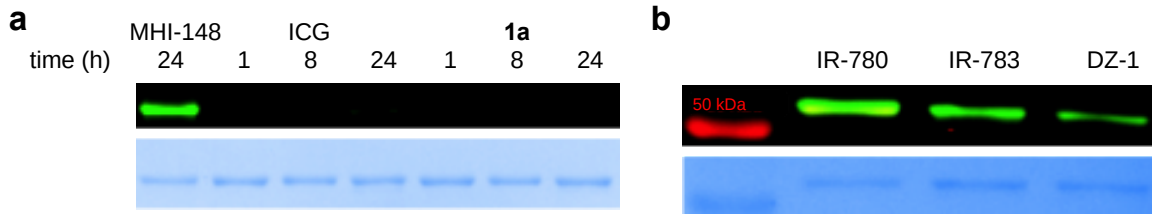

Figure III-3. Near-infrared (NIR) fluorescent gel image of **a** vimentin (1 μM) incubated with different cyanines (10 μM) in 50 mM pH 7.24 HEPES buffer at different incubation times; **b** vimentin (1 μM) incubated with IR-780, IR-783, and DZ-1 in the same buffer as **a** for 24 h. CBB-G250 staining indicated an equal amount of protein (100 ng) was loaded into gel.

Further evidence for the superior reactivities of Cys side-chains over other nucleophilic amino acid residues was obtained via competition experiments. Thus, MHI-148 (200 μM) in 50 mM pH 8.0 HEPES buffer was incubated with equimolecular amounts of five amino acids (Scheme III-2) at 37 °C, and the reaction was monitored by HPLC up to 27 h. Prototypes of this experiment were intended to measure relative rates, however, only formation of the Cys-product **1a** occurred (HPLC spike with the standard from Scheme III-1 (Figure III-4) and LC-MS analyses). Under these conditions, approximately 32% of MHI-148 was substituted and 68% remained after 15 h. The reaction did not go to completion due to equilibrium of the reaction or due to oxidation of cysteines in aqueous conditions. This observation implied amine, alcohol, and phenol side-chains in the protein did not react with the dye.

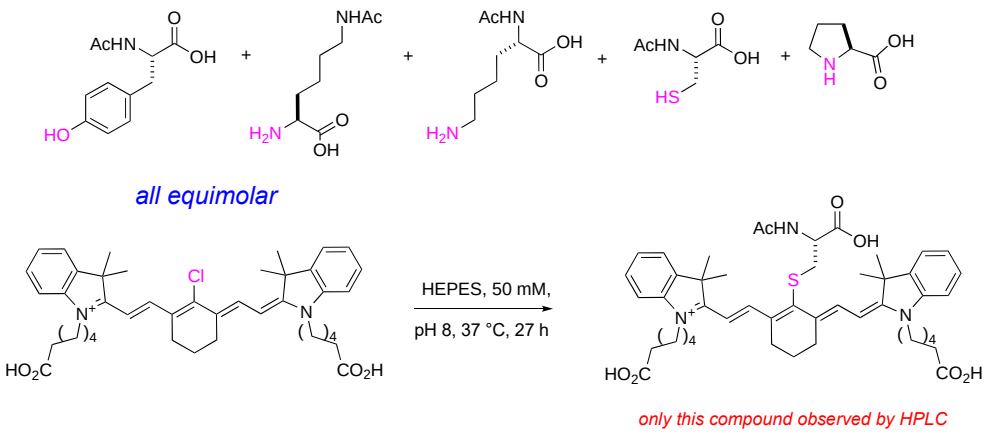

Scheme III-2. Competition study of MHI-148 with amino acids in aqueous buffer.

Blocking experiments were performed to be absolutely sure that the vimentin Cys was the reactive group for coupling to MHI-148 in aqueous buffer at 37 °C. Thus, maleimide-blocked protein [106,107] was formed by incubating vimentin with 6-maleimidohexanoic acid (6-MA; 18 h in 50 mM pH 7.24 HEPES buffer at 37 °C). Vimentin and the thiol-blocked vimentin were incubated with MHI-148 for different incubation times, then analyzed using SDS-PAGE gel electrophoresis. Figure III-4c shows that the concentration of MHI-148 covalently bound to vimentin progressively increased (NIR fluorescence at ~800 nm), whereas no fluorescent band was observed for the thiol-blocked vimentin.

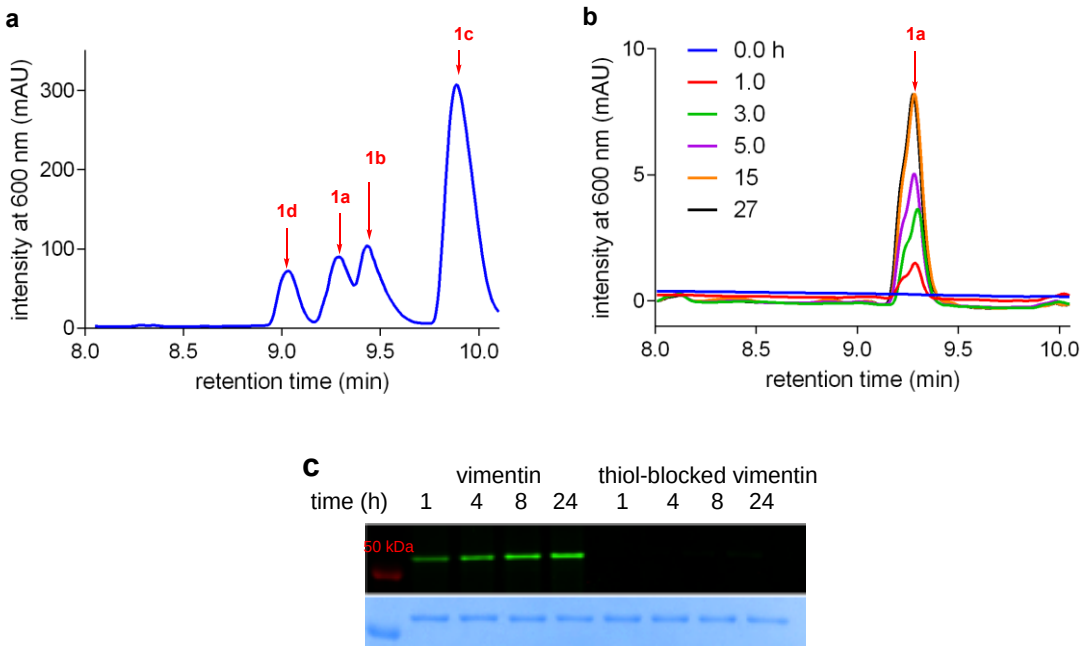

Figure III-4. High-performance liquid chromatography (HPLC) analysis of **a** 200 μM of each amino-acid-conjugate standard **1a**–**d** in 50 mM pH 8.0 HEPES buffer; **b** kinetic study for 200 μM of MHI-148 with 200 μM of each amino acid (*N*-acetyl-L-Cys, *N*-acetyl-L-Tyr, *N*α-acetyl-L-Lys, *N*ε-acetyl-L-Lys, and L-proline) in 50 mM pH 8.0 HEPES buffer incubating at 37 °C; **c** NIR fluorescent gel image of vimentin or 6-MA-blocked vimentin (1 μM) incubated with MHI-148 (1 μM) in 50 mM pH 7.24 HEPES buffer at different incubation times.

Overall, based on all the experiments above, we concluded that MHI-148 selectively bind the only free Cys in vimentin, C328, in aqueous buffer at 37 °C, and went on to calibrate the efficiency of binding. Thus, NIR fluorescence (>800 nm) in gel electrophoresis was quantitative for vimentin (1 μM in 50 mM pH 7.24 HEPES buffer) when incubated with of MHI-148 (0–30 μM, 3 h at 37 °C). Fluorescence intensities of the salient band saturated at 10 μM (Figure III-5a), which means the tested fluorescent compound can quantitatively label the protein at a 10:1 ratio within 3 h when incubated under these conditions in HEPES aqueous buffer. Experiments to test sensitivity revealed

labeled vimentin was detectable at concentrations as low as 1 ng on our gel imaging apparatus (Figure III-5b).

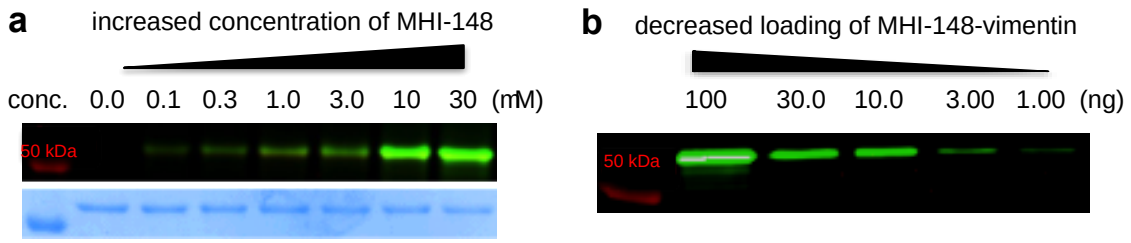

Figure III-5. NIR fluorescent gel image of **a** vimentin (1 μM) incubated with different concentrations of MHI-148 in 50 mM pH 7.24 HEPES buffer for 3 h at 37 °C **b** 10:1 concentration ratio of MHI-148: vimentin sample was loaded into 10% SDS-PAGE gel with different amounts of vimentin sample.

Labeling of Other Proteins Using MHI-148: Several proteins with and without free Cys residues were labeled to test the robustness of the method developed for vimentin. NEDD8-activating enzyme (NAE)[108], Ubc1[109], and PCSK9[110] contain free thiols (reduced Cys residues), whereas NEDD8[108] (no Cys in sequences), truncated suPAR (residues 1-281, 12 disulfides)[111], and EGFR (25 disulfides)[112] have none. Figure III-6 shows that only the proteins containing sulfhydryl groups reacted under the standard conditions. NAE consists of two subunits (APPBP1 and UBA3) which each contain free Cys; hence, two NIR fluorescence bands were observed for that sample.

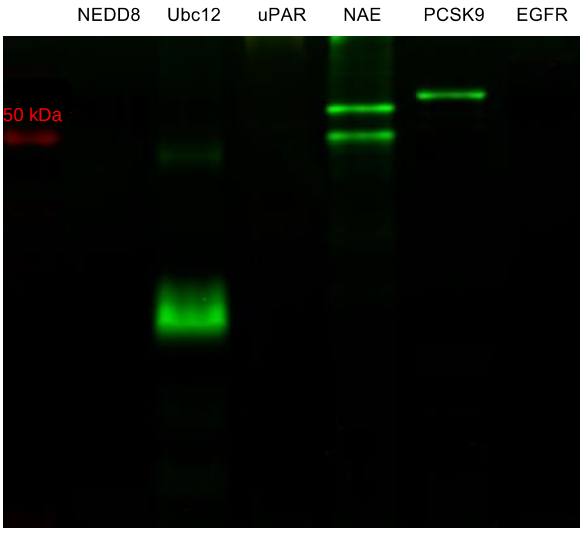

Figure III-6. NIR fluorescent gel image of diverse proteins (4 μM) incubated with MHI-148 (4 μM) for 3 h using 50 mM pH 7.24 HEPES buffer at 37 °C.

Conclusions

MHI-148 can label proteins that have free Cys residues such as serum albumin[113] and vimentin. Other Cy-7 dyes containing *meso*-Cl were only used to label vimentin in this work, but it would be unsurprising if they can be used. It seems clear that this methodology could be applied with a high probability of success to conveniently conjugate *meso*-Cl NIR dyes to antibodies, monobodies, and nanobodies to form selective agents for optical imaging in vivo. Traditional conjugation techniques tend to require modification of the dye to include maleimide or succinimide functionality[107,114,115], but the method developed here circumvents that process.

CHAPTER IV

ON THE MECHANISMS OF UPTAKE OF TUMOR-SEEKING CYANINE DYES

Introduction

Indocyanine green (ICG, **A**), a heptamethine cyanine or "Cy-7" dye, is the only near-IR FDA-approved optical marker for clinical use.[116,117] ICG is used in surgical procedures because of its favorable safety profile,[45,46,118] and because it is fluorescent with an absorbance maximum around 750 nm. Below 750 nm, excitation of dyes obscured by more than a few millimeters of tissue becomes impractical with even the highest laser powers acceptable in surgical settings. To calibrate, penetration of light of wavelength 800 nm is twice that of light of 630 nm.[44]

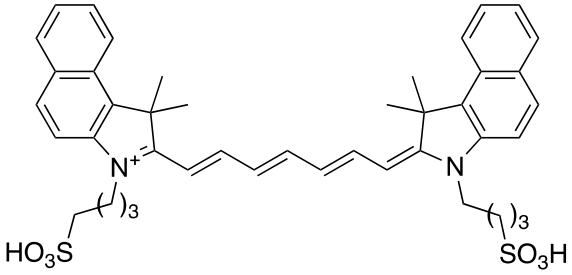

A

indocyanine green (ICG)

Fluorophore **A** can be used in surgery, but it is not disposed to especially accumulate in cancer tissue. In fact, ICG collects in the liver and gastrointestinal tract, and tends to mostly wash out of the body within a few hours.[39] However, at least in animal models, other heptamethine cyanine dyes like **1**-Cl and **B** – **D** *do* accumulate in

[113]Reprinted with permission from "On the Mechanisms of Uptake of Tumor-Seeking Cyanine Dyes" by Syed Muhammad Usama, Chen-Ming Lin and Kevin Burgess, *Bioconjugate Chem.* 2018, *29*, 3886-3895. DOI: 10.1021/acs.bioconjchem.8b00708. Copyright 2018 American Chemical Society.

solid tumors (*e.g.* prostate,[48] gastric,[49] kidney,[50] hepatocytes,[51,96] lung cancer,[52] and glioblastoma[53]) but not in normal cells and tissue.[69,86-88,94] Moreover, fluorophores **B** – **D** tend to persist in those tumors; they can still be observed there after 1 – 2 days. There is an enormous amount of literature on antibody drug conjugates (illustrative reviews[119,120]), and a growing volume on small molecules that target tumor tissue conjugated to cytotoxic species (illustrative reviews[68,121]). Consequently, the potential importance of near-IR dyes that localize in, apparently, *any* solid tumor is immense; they can be used for *in vivo* experiments,[89] have the potential in image guided surgery,[117] and can be conjugated to cytotoxic substances for theranostic approaches (near-IR imaging and chemotherapy,[57-61] in this case). These tumor seeking near-IR dyes at the very least complement targeted approaches, and in some cases could surpass them.

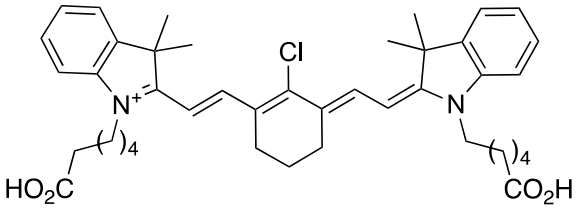

1-Cl
MHI-148, IR-808

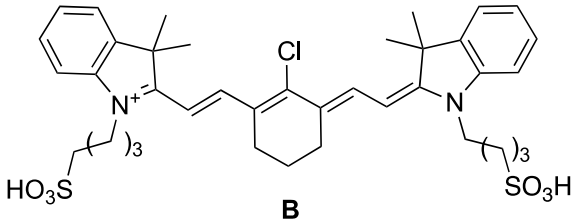

B
IR-783

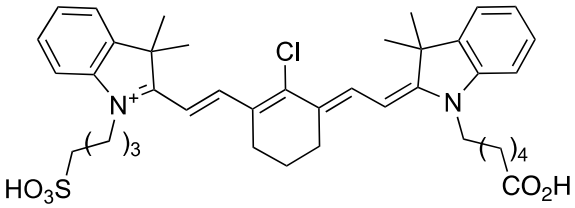

C
DZ-1

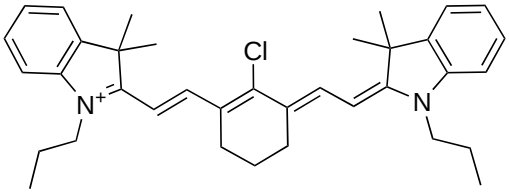

D
IR-780

Many reports (for example[48,50-53,56,86,88,94]) explain the "tumor-seeking" characteristics of fluorophores **1**-Cl and **B** – **D** in terms of uptake via the Organic Anion Transporter Proteins (OATPs).[54,55] Hypoxia (common in compressed solid tumors) triggers activation of HIF1α, and promotes OATPs overexpression in cancer tissue relative to levels found in normal cells.[49,56] The natural role of OATPs is to mediate influx of organic anions and some neutral materials that are important to cells (*e.g.* bile salts, steroids, bilirubin, and thyroid hormones). This diversity of substrates means OATPs are not particularly selective and, coincidentally, these receptors also import some drug structures and fluorophores **1**-Cl, **B** – **D**.[122-124] To balance this ion influx, OATPs efflux intracellular bicarbonate, glutathione, and glutathione adducts. Consequently, OATPs can promote influx of fluorophores **1**-Cl, **B** – **D** into cells, *without pumping the same ones out*.

A discovery by chance in our laboratory led us to question the assumption that import via the OATPs predominantly accounts for the tumor-seeking characteristics of

fluorophores **1**-Cl, **B** – **D**. In the event, data presented in this paper indicates that OATPs *are* a mechanism of import in *ex vivo* cellular experiments, but an alternative mechanism accounts for the persistent fluorescence of tumors in animal experiments featuring fluorophores of this category.

Results and Discussion

*Observation of a Fluorescent Protein in Cell Lysates after Treatment With Fluorophore **1**-Cl*: The following is a typical literature procedure for treatment of cancer cells with fluorophore **1**-Cl. The cells (in our case a leukemia line, K562) are suspended in RPMI-1640 medium with 10 % FBS added, then seeded to 24-well plates. Various concentrations of **1**-Cl in the same medium are added to the cells to give final fluorophore concentrations of 0 - 30 μM. After 20 h incubation at 37 °C, the cells are collected, and washed twice with ice-cold PBS buffer.

In a particular experiment in our laboratory, RIPA lysis buffer containing of 1% of a pan protease inhibitor was added to the cells after the procedure outlined above. The cell samples were gently shaken on ice for 30 min, and the lysates were centrifuged to remove cell debris. Supernatants were collected and the protein concentrations were determined using a colorimetric protein assay kit. Equal total protein amounts were electrophoresed under reducing conditions on 15% SDS-PAGE. The gel was washed with de-ionized water, then *analyzed with an imager designed to detect the near IR fluorescence (>800 nm)*; this gave a conspicuous fluorescent band at over 50 KDa. We were surprised by the selectivity with which this band formed, excited by the prospect of

identifying this fluorescent conjugate (Figure IV-1a), then, later, amused by the result (Figure IV-1b).

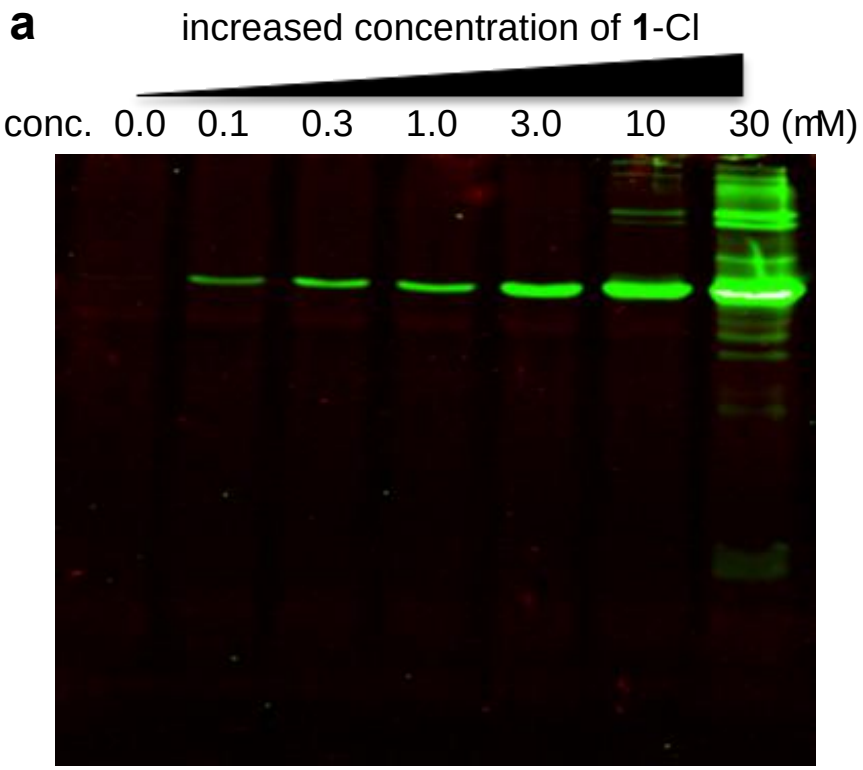

Figure IV-1. **a** NIR-fluorescent gel image (>800 nm) of K562 cell lysate prior treated with different concentrations of **1**-Cl for 20 h in RPMI-1640 medium containing 10% FBS. **b** Lane 1, K562 cell lysates treated with 10 μM of **1**-Cl as in **a**. Lane 2, K562 cell lysates treated with 10 μM of **1**-Cl as in **a** *except* serum-free RPMI-1640 medium was used. Lane 3, 10 μM of **1**-Cl incubated with RPMI-1640 medium containing 10% FBS for 20 h as in **a** but *without cells*. Lane 4, 10 μM of **1**-Cl as in **a**, except no cells were used and 10 μM BSA was added in their place. Staining the gel with Coomassie Blue G250 showed an equal amount of protein was loaded into each well (Fig S10). Electrospray ionization (ESI) mass spectra of: **c** free HSA; and **d** ESI MS of **1**-Cl covalently bound to HSA; formed by reacting the two components in a 2.5:1 ratio (1 M HEPES buffer).

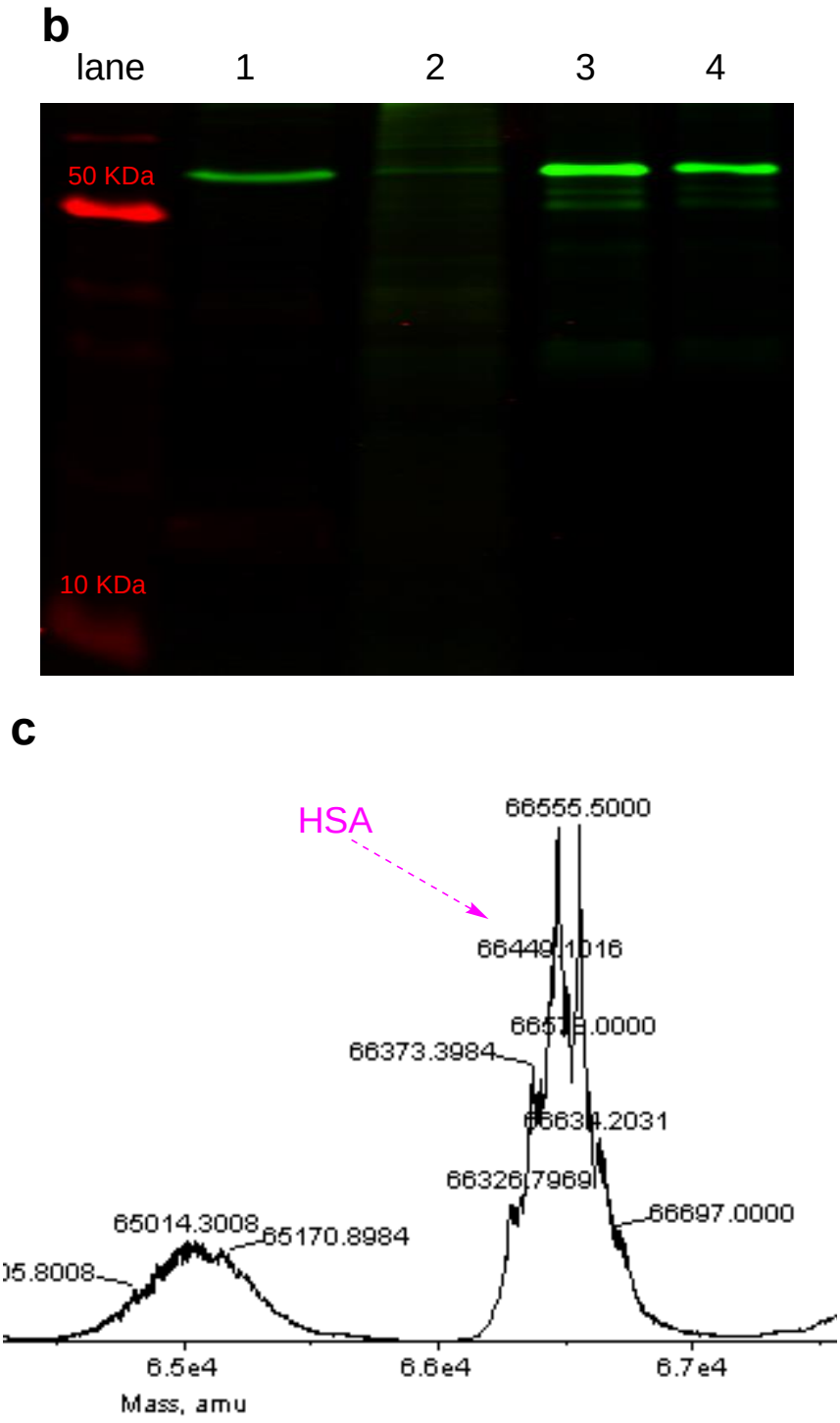

Figure IV-1. Continued.

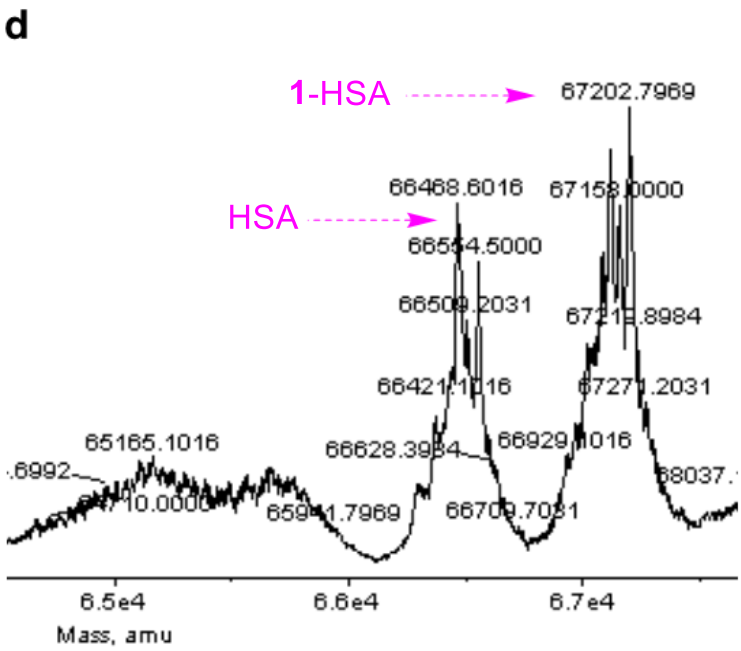

Figure IV-1. Continued.

After a few false starts, we hypothesized the pronounced fluorescent band in the gel shown in Figure IV-1a was derived from bovine serum albumin (BSA) in the FBS medium. Consistent with this assertion, Figure IV-1b shows the band from the lysate was *not* formed when FBS was excluded from the culture medium (lane 2), but it *was* formed when FBS was present without cells, or when only BSA was added (*i.e.* no cells and no FBS; lanes 3 and 4, respectively). Albumin concentrations in FBS vary between 20 – 36 mg/mL;[125-127] assuming a conservative mid-range figure of 25 mg/mL BSA in FBS, this corresponds to 384 μM. Thus, cellular experiments involving 10 μM **1**-Cl would have almost a forty-fold excess of BSA (384 μM) to react with.

In a control experiment, human serum albumin (HSA) was reacted with 2.5 equivalents of **1**-Cl at 37 °C in 1 M HEPES buffer. This **1**-Cl:albumin molar ratio was

selected because it is approximately that used in cell culture experiments to probe uptake of this dye. Figure IV-1c shows the ESI mass spectra of HSA, and 1d shows that a product formed when HSA combined with **1**-Cl; the molecular mass formed correspond to a 1:1 covalent adduct between **1**-Cl (after loss of Cl) and HSA. This is consistent with the fact that HSA has one free Cys residue (and 34, oxidized, i.e. disulfide-linked, Cys residues).

At this stage we hypothesized that the 1:1 covalent adduct is formed by displacement of the *meso*-Cl from **1**-Cl by a nucleophile on HSA, and that nucleophile was probably the free Cys thiol. Three derivatives of **1** (Figure IV-2a) that had *meso*-functionalities that cannot readily be leaving groups were made and reacted with HSA to test a *meso*-leaving group was required for covalent binding. It emerged that ICG (**A**), **1**-H, **1**-Me, and **1**-Ph do *not* react with HSA at 37 °C in aqueous buffer (Figure C-S4 and C-S7), under the conditions that **1**-Cl does combine with HSA (Figure IV-2b); in fact, nearly all the **1**-Cl is consumed after 72 h.

At this stage it seemed probable that **1**-Cl reacts with a free thiol on albumin. To exclude the possibility that other nucleophilic amino acid side-chains might be involved (*e.g.* Lys, Tyr, Ser) experiments were performed using HSA that was first treated with 6-maleimide-hexanoic acid to *selectively* block free thiols.[128,129] Unexpectedly, this experiment still gave a fluorescent band, but we concluded that there was some **1**-Cl *non-covalently* bound to albumin, and this became covalently bound after the protein had been reduced for loading onto the gel. To test this assertion the experimental design was modified in the following way. HSA was first completely reduced with *tris*(2-carboxyethyl)phosphine (TCEP) to break all its disulfide bonds, then the product was

thiol-blocked using 6-maleimidohexanoic acid, and finally this sample was treated with **1**-Cl. This approach is imperfect because it tests the interaction of **1**-Cl with *reduced* albumin, but it is sufficient to prove that *O*- and *N*-based nucleophilic side-chains (specifically those *not* derived from cysteine) of the reduced protein did *not* combine with **1**-Cl. Thus, binding of free Cys to **1**-Cl is implicated in the covalent binding step (Figure IV-2d).

a

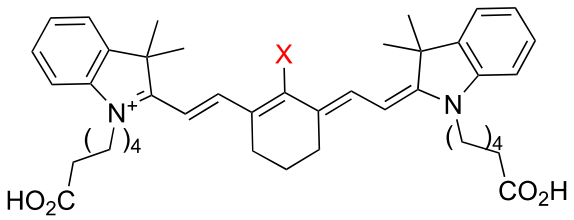

when X = Cl, **1**-Cl; H, **1**-H; Me, **1**-Me; Ph, **1**-Ph

Figure IV-2. **a** Structures of **1**-Cl and *meso*-blocked derivatives. **b** Analytical HPLC analyses for reactions of 0.5 mM HSA with 0.2 mM **1**-Cl (in 1 M HEPES buffer pH 7.4) at 37 °C.

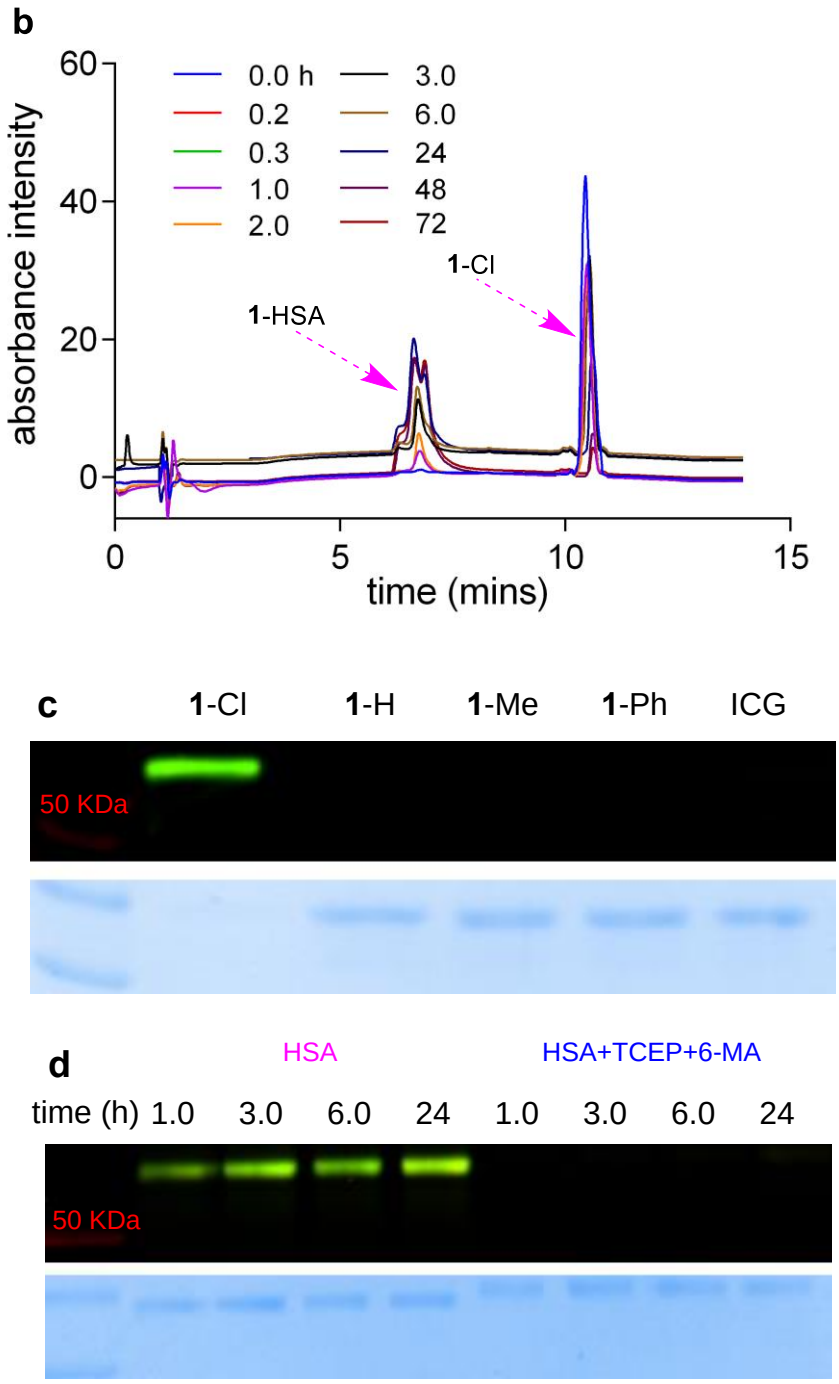

Figure IV-2. Continued.

Non-covalent interactions of the dyes **1** with HSA were also explored. Thus, 10 μM solutions of ICG, **1**-Cl, **1**-H, **1**-Me and **1**-Ph were mixed with varied concentrations

of HSA and the interaction was followed by UV spectroscopy. Absorbance saturation was observed for **1**-Cl at a 1:1 ratio with HSA, but for the other compounds, none of which have a leaving group at the *meso*-position, saturation was achieved at around 1.5 equivalents of HSA (Figure C-S5 and C-S6).

Uptake of Fluorophore 1-Cl and 1-HSA into Cells: Figure IV-2b indicates that albumin and **1**-Cl at approximately the ratio typically used in cell culture experiments (2.5:1.0, see above) react over time periods that are similar to the span of a typical cell culture experiment. Consequently, we set out to test first where the fluorescent signal localizes in cells *if albumin is excluded from the medium*, then to determine if **1**-HSA is imported and, if so, where it localizes.

Figure IV-3 shows confocal images for uptake of **1**-Cl into a human glioblastoma cell line (U87-MG) cultured in a medium without albumin. Under these conditions, the dye was imported into the cells after 30 min incubation, and localized in the mitochondria.

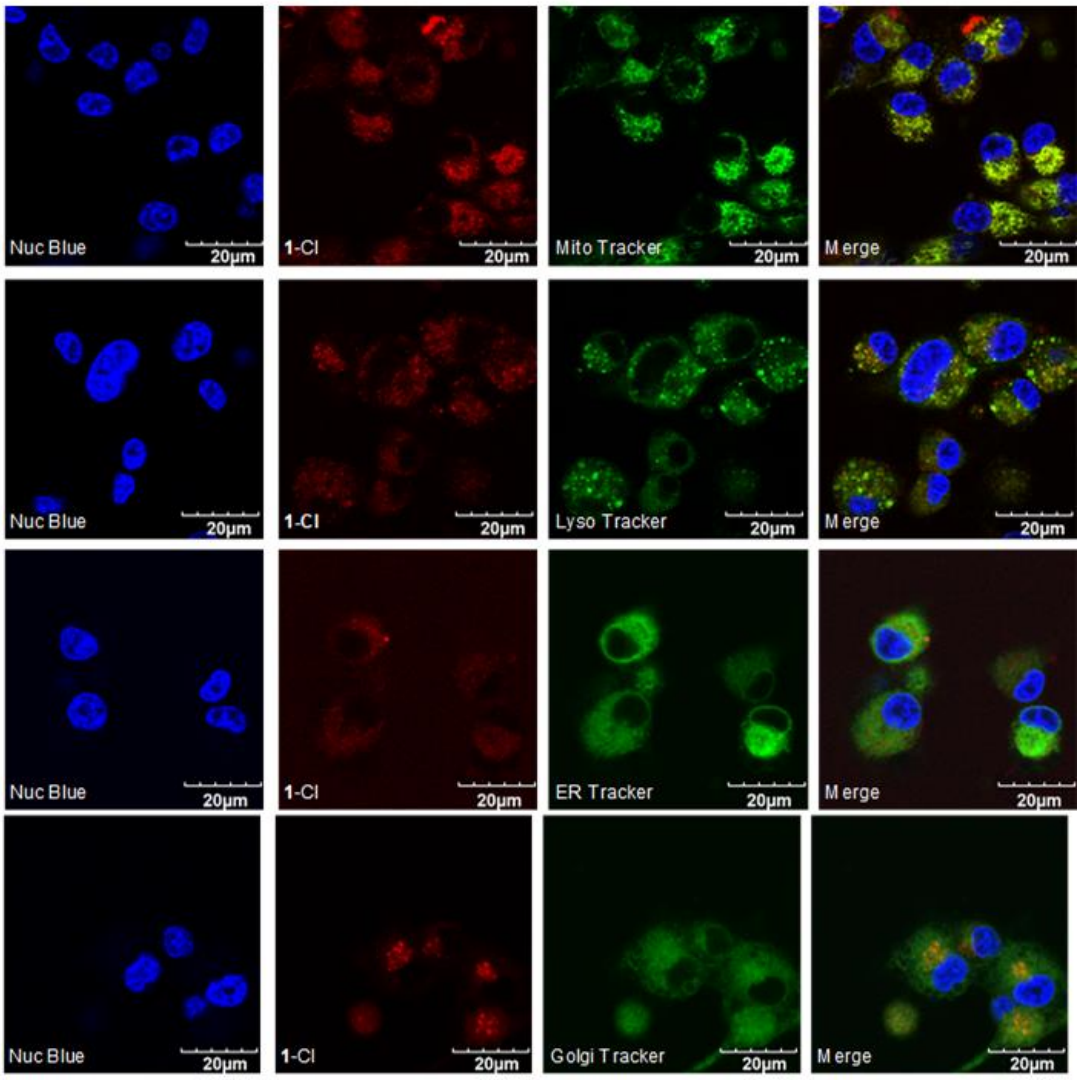

Figure IV-3. Uptake of **1**-Cl (20 μM) into U87-MG cells incubated in serum free medium for 30 min. Colocalization with trackers for mitochondria, lysosome, ER and Golgi are featured. Images were taken using Olympus confocal microscope at 60x/1.2 water immerse objective after 30 min of incubation. Most colocalization was seen with the mitochondria.

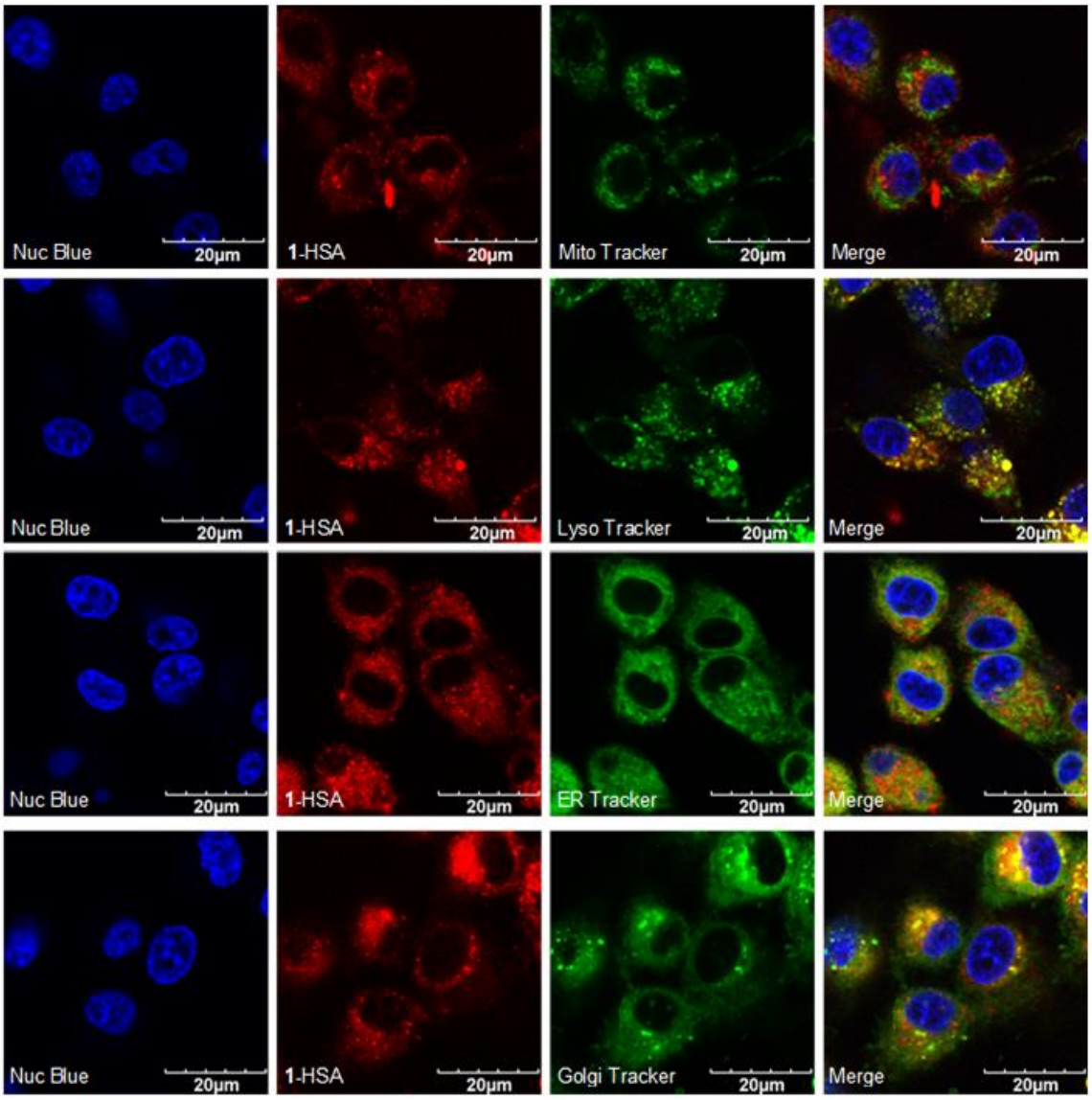

Figure IV-4. Uptake of **1**-HSA (20 μM) into U87-MG cells incubated in serum free medium. Colocalization with trackers for mitochondria, lysosome, ER and Golgi was featured. Images were taken using Olympus confocal microscope at 60x/1.2 water immerse objective after 30 min of incubation. Most colocalization was seen with lysosome and Golgi.

As far as we are aware, without exception, the evidence for OATPs mediated uptake of **1**-Cl in tissue culture is based on the same experimental format. Briefly, cells are allowed to attach to imaging chamber overnight in a medium containing BSA at 37 °C, **1**-Cl is added in the same medium, and after 30 min at 37 °C the cells are collected, and washed twice with ice-cold PBS buffer. Microscopy is then used to qualitatively monitor the uptake. This protocol is performed side-by-side with two similar experiments but where the medium contains the pan-OATP inhibitor BSP (bromosulfophthalein),[130] or in which the cells were treated with an agent to induce hypoxia (DMOG, dimethyloxalylglycine[131,132]). Under these conditions, BSP suppresses the fluorescence observed in the cells (presumably by inhibiting OATP-mediated uptake), whereas under hypoxic conditions for which OATPs are overexpressed, the fluorescence uptake was increased. We were intrigued to explore how **1**-HSA would behave under these conditions because the data above indicates that at least partial conversion of **1**-Cl to **1**-HSA occurs in these types of cellular experiments featuring albumin in the medium. These experiments would reveal if **1**-HSA was imported into the cells and, if so, how its uptake responds to the pan-OATP inhibitor, BSP.

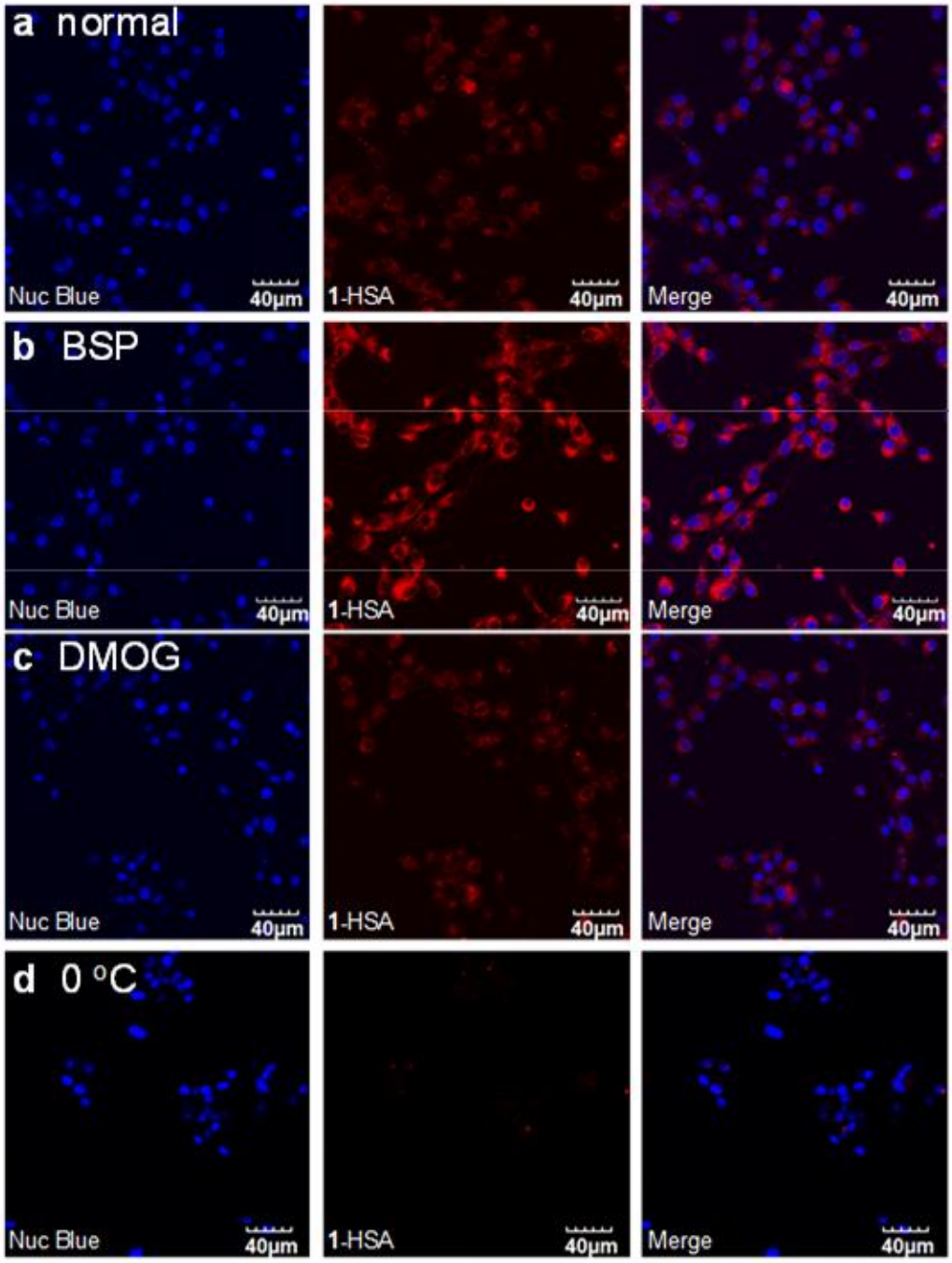

Figure IV-5. Experiments to test *uptake of **1**-HSA* (20 μM) into U87-MG cells (grown in DMEM medium supplemented with 10% FBS, i.e. containing approximately 0.038 mM BSA). **a** Without any blocking agents or abnormal conditions; **b** pre-treated with 250 μM BSP to block OATPs for 10 min; **c** after the cells were pretreated with 1 mM DMOG for 24 h to induce hypoxia; and, **d** when the cells were maintained at 0 °C for 30 min to retard active transport. All images were collected using an Olympus confocal microscope at 20x magnification.

Data in Figure IV-5 shows that **1**-HSA is imported into the glioblastoma cells (first row). Import of **1**-HSA is conspicuously *increased* when the cells are pretreated with pan-OATP inhibitor, BSP. Hypoxic and normoxic cells import about the same amount of fluorescence from **1**-HSA (rows 3 and 1), but cooling the cells to retard active transport mechanisms also diminishes uptake of fluorescence from **1**-HSA. Whereas **1**-Cl uptake in the cell was enhaced in hypoxia condition but reduced in presence of BSP or at low temperatures, implying the uptake was dependent on active transport via OATPs (Figure C-S8). Collectively these data shows uptake of **1**-HSA is enhanced by active transport mechanisms, but not via the OATPs. Figure C-S9 shows data from similar experiments that show **1**-HSA uptake was: (i) not inhibited by an inhibitor of clathrin mediated endocytosis (PitStop2);[133] but it was by, (ii) a micropinocytosis inhibitor (amiloride);[134] and by, (iii) an inhibitor of lipid raft endocytosis (MβCD).[135]

Albumin (Figure IV-6; from PDB 1AO6) has 14 disulfide bonds and one unique, free cysteine residue, Cys34. It is present in high concentrations in the blood where is acts as a carrier for small molecules, many of which non-covalently bind one of the two binding sites indicated. Consequently, electrophilic small molecules might react with Cys34 directly, or possibly associate with one of the binding sites then be relayed to that free thiol. Albumin is known to be imported into cells via several mechanisms[136] and particularly into cancer cells[137,138] though, to the best of our knowledge, this does not include OATP-mediated pathways.

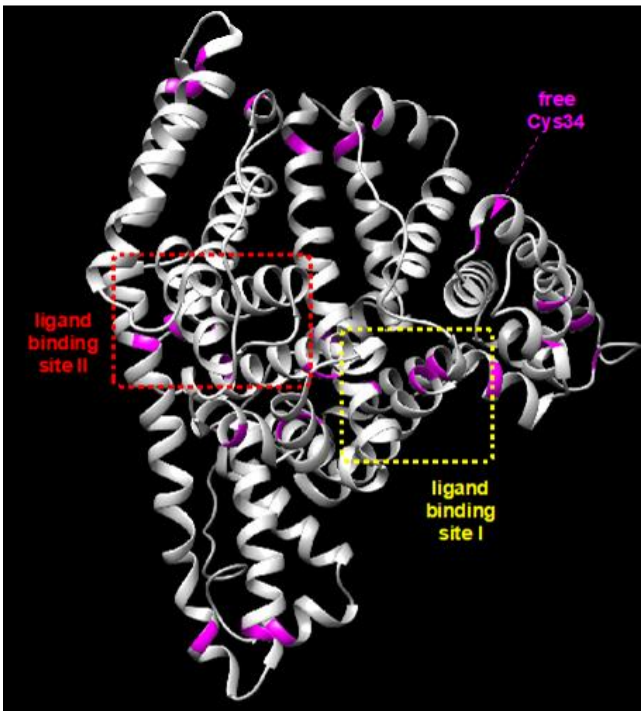

Figure IV-6. HSA structure from PDB 1AO6. Figure S1 depicts the HSA with different helical structures and binding domains whereas Figure C-S2-S4 shows diagrams emphasizing cysteine 34 pointing outside in the solvent.

Both non-covalent and covalent binding to albumin have dramatic effects on the pharmacokinetics of small molecules.[139,140] Some small molecule drugs associate with albumin;[141] this can be problematic if they are not released, but in other situations it is an advantage due to the prolonged half-life of the compound in the blood. Small molecules also have been covalently bound to albumin via Cys34 to improve their pharmacokinetics.[136] This is frequently achieved by attaching a maleimide functionality to the small molecule and either reacting it with HSA[142,143] or simply allowing the drug to combine with HSA *in situ* in a novel prodrug approach.[144-148] Albumin itself has been estimated to have a turn-over rate of over 20 days in humans,[149] so it seems likely that most covalent small molecule-to-albumin adducts would be long-lived *in vivo*.

Albumin is the most abundant protein in the blood, being present at around 35 – 50 g/L or 0.53 – 0.73 mM (human and mouse). We estimate (see supporting) that by injecting **1**-Cl into a 25 g mouse at 10 mg/Kg (a typical dose in an *in vivo* experiment featuring this dye), then the initial concentration in the blood would also be in the same range, ~0.53 mM. After the injection, clearance mechanisms would rapidly decrease the amount of free **1**-Cl in the blood; consequently, *excess albumin is always present.* Our data indicates that **1**-Cl would be converted to **1**-HSA (and presumably to lesser amounts of adducts with other serum proteins like LDL) reasonably quickly.

There does not appear to be published *in vivo* work on the lifetime of **1**-Cl in the blood, but a very careful study of derivative **E** has reported the half-life of this compound in mice to be 36 min. Formation of covalent adducts to albumin and other serum proteins with free thiols[150] must account, at least in part, for the rapidly decreasing **1**-Cl concentration in the blood in that study. Assuming the same half-life for **1**-Cl, and considering that the blood circulates in about one minute, it is reasonable to conclude some **1**-Cl does enter cancer cells *in vivo* shortly after administration *iv*. However, once inside the cells then **1**-Cl encounters high concentrations of other nucleophilic thiols, notably, glutathione. In unpublished work, performed in parallel to this, we have also proved **1**-Cl has a similar reactivity towards Cys as to albumin, so it seems likely that this chloride would be short lived inside cells. However, the fluorescence observed inside tumors *in vivo* persists for *days*.[50,60,94]

Conclusions

The observations outlined above explains why heptamethine cyanine dyes with a *meso*-chloride tend to be much longer-lived in tumors than Cy-7 derivatives without a

meso-chloride, *e.g.* ICG.[89] Thus, the weight of the evidence points to short-term (~30 min) accumulation of **1**-Cl in cancer tissue *in vivo*, but, after this, transformation into covalent adducts with biomolecules possessing free thiols, particularly including serum proteins in the blood. Albumin adducts would be especially favored, because of the abundance of the high blood concentrations of this protein. This accounts for persistent fluorescence from cancer tissue *in vivo* after injection of **1**-Cl. Various factors might contribute to persistent localization of covalent adducts formed *in situ*, *e.g.* **1**-albumin, including slow efflux, and the EPR effect.

The data interpretation outlined above is consistent with many observations in the literature. Our assertion that **1**-Cl and similar Cy7 dyes with *meso*-chlorines (*e.g.* **B** – **D**) probably have parallel pharmacokinetics, is consistent with observations that describe of these types of fluorophores being retained in tumor tissues (*e.g.* kidney, brain, breast, and liver) for many days (*e.g.* 5 – 20 d);[50,51,61,88,96] in fact, for periods that are comparable with the half-life albumin *in vivo* (20 d). Conversely, ICG (no *meso*-chlorine) is cleared *in vivo* in < 24 h,[51,88,96] and a direct analog of **1**, *but substituted at the meso position*, *i.e.* **E**, was not observed to be retained in an embedded prostate tumor.[94] We thank a referee for pointing out that another group has observed an immediate UV λ_{max} red-shift for **1**-Cl when added to albumin *in vitro*, followed by a gradual blue-shift to another λ_{max} after 1.5 h.[151] Those researchers did not attempt to explain that observation, but it is easily interpreted in the light of our work. We suggest under those conditions **1**-Cl rapidly forms a non-covalent adduct with albumin, that is slowly transformed into a covalent one.

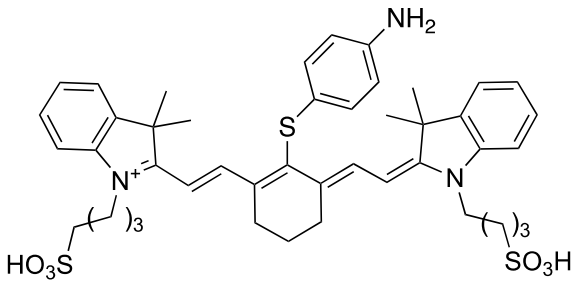

E

Increased uptake of **1**-HSA by the pan-OATP inhibitor BSP (Figure IV-5) surprised us, but, in retrospect, perhaps it should not have. BSP is an old small molecule that rose to fame as a probe for testing liver function; *it binds albumin*[152] as well as inhibiting OATPs.[153] In fact, *molecules like this tend to bind several proteins non-selectively*, so much that they are described by some as a PAIN (Pan Assay Interference compound).[154] BSP is an inexpensive and convenient probe for testing inhibition of OATPs, and in many cases it may be the only logistically feasible option to do so. However, BSP has limitations associated with its interactions with other receptors on cells, and proteins in tissue culture medium, and data from cell uptake experiments using this probe should not be over interpreted.

Small molecules attached to albumin in covalent adducts can be fluorescein derivatives as in the conjugate manufactured by Orpegen Pharma (Heidelberg, Germany) for intraoperative fluorescence staining of brain tumors during surgery.[155,156] Related to this, the prospect of conjugating *near-IR* dyes to albumin for optical imaging has been described in a patent application,[157] but without the realization that **1**-Cl could be combined simply via direct displacement of the *meso*-Cl via Cys34 in that protein. Moreover, there is growing interest in drugs conjugated to **1**-Cl[59-61] (like **F**).[57,58] It is reasonable to assume that these too would combine with albumin *in situ* when injected

into the blood; this might be advantageous insofar as it would generate theranostics for optical imaging and therapy with largely predictable, and extended, blood plasma life-times *in vivo.*

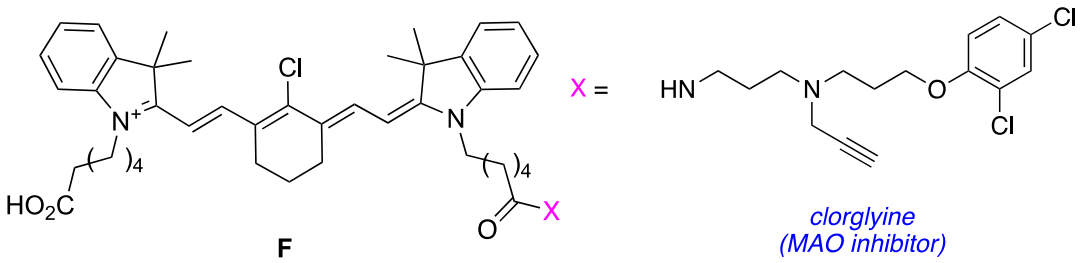

Data presented here also explains some observations in the literature, and some misconceptions to be avoided. For instance, a recent paper noted exceptionally different photophysical properties of a dye related to **1**-Cl in the presence and absence of albumin;[158] it may be that a covalent adduct is implicated. With regards to pitfalls, there are two quite different ways to go about making drug-adducts with the core of cyanine **1**. When peripheral carboxylic acids are used to make amides or esters, *e.g.* **E**, then these will accumulate in tumors and persist there for a long time as albumin and similar adducts. However, conjugation of drugs to **1**-Cl via displacement of the *meso*-chloride[159] is likely to give products that persist for much shorter times in tumor tissue.

CHAPTER V

A NEAR-IR FLUORESCENT DASATINIB DERIVATIVE THAT LOCALIZES IN CANCER CELLS

Introduction

Dasatinib (Sprycel®) is a tyrosine kinase inhibitor (TKI) clinically used to treat Philadelphia chromosome, chronic myeloid leukemia, and acute lymphoblastic leukemia (https://www.cancer.gov/about-cancer/treatment/drugs). According to clinicaltrials.gov, dasatinib (alone or in combination with other chemotherapy agents) features in over 120 clinical trials for different types of cancers, including pancreatic, non-small cell lung carcinoma, and bone metastases of breast cancer. However, dasatinib's efficacy is diminished by cell-efflux,[160-164] and, eventually, acquired resistance via mutations in and around the tyrosine kinase active site.

Dasatinib inhibits multiple kinases, including Bcr-Abl and members of the Src-family. While polypharmacology[165-167] is sometimes desirable, poor selectivity may lead to side-effects. Indeed, dasatinib tends to reduce counts for platelets, red and white blood cells; these physiological effects may account for anemia, pulmonary edema, and heart function complications that are observed in some patients receiving this drug.[168,169]

Two strategies to increase efficacy of KIs are possible. One of these features structural modifications that reduce off-target interactions. The other focuses on conjugating the

---

[170]Reprinted with permission from "A Near-IR Fluorescent Dasatinib Derivative That Localizes In Cancer Cells", Syed Muhammad Usama, Bosheng Zhao and Kevin Burgess, *Bioconjugate Chem.* 2019, *30*, 1175-1181. DOI: 10.1021/acs.bioconjchem.9b00118. Copyright 2019 American Chemical Society.

drug to agents (typically antibodies, but sometimes small molecules) that bind cell-surface receptors and enhance intracellular drug concentrations in cancer cells relative to healthy ones, increasing therapeutic indices. Research described in this paper was initiated to explore the second strategy. Additionally, we wanted to make a derivative of dasatinib that would *target cancer cells and be near-IR fluorescent*. We hypothesized this fluorescence could be used to track the conjugate in cell studies and would have potential in theranostic applications involving optical imaging and tumor suppression *in vivo* with improved localization in cancer cells. One possibility was to conjugate a near-IR dye and a small molecule targeting group to a KI, but more compact molecular designs are preferred. The innovation in this study is to form conjugates with a special sub-set of heptamethine cyanine (Cy7) dyes, **A** – **C**, that are known to enhance delivery of the conjugate into solid tumors and show no systemic toxicity in mice, *i.e.* they are both targeting and fluorescent. [57-59,60,51,53,61]

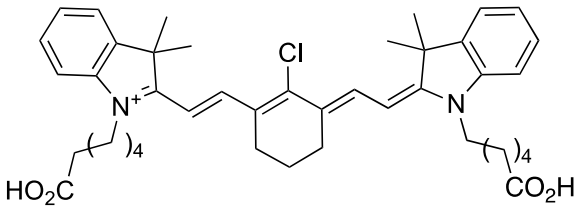

A

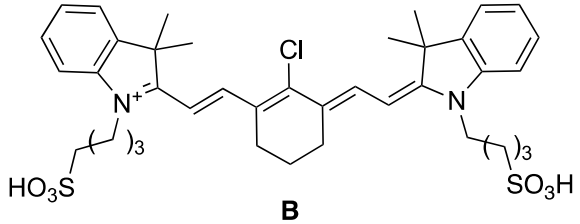

B

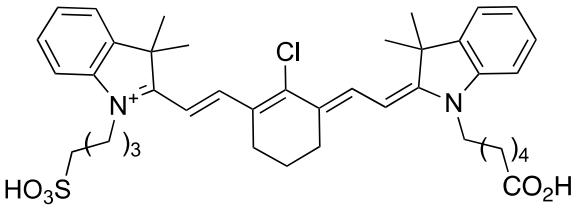

C

The following text outlines some salient literature on dyes **A** – **C**. First these water-soluble fluorophore absorb at around 780 nm with high extinction coefficients, and fluoresce at around 800 nm with acceptable quantum yields, *i.e.* they have excellent characteristics for optical imaging *in vivo*.[44-47] Cellular and *in vivo* studies indicate **A** localizes in many different types of cancer lines and in solid tumors (*e.g.* prostate,[48] gastric,[49] kidney,[50]) but not in normal cells and tissue.[69,86-88,94] Preferential uptake of **A** in cancer cells is mediated by Organic Anion Transporting Polypeptides (OATPs).[54,55] Specifically, hypoxia (common in solid tumors) triggers activation of HIF1α, which promotes OATPs expression,[49,56] and these receptors influx organic anions and some neutral materials that are important to cell metabolism (*e.g.* bile salts, steroids, bilirubin, and thyroid hormones). To balance this ion influx, OATPs efflux intracellular bicarbonate, glutathione, and glutathione-adducts. Consequently, OATPs can promote influx of suitable small molecule organics into cancer cells, including some drug structures and the cyanine dyes **A**, **B**, and **C** shown above, *without pumping them out*.

Our group is interested in the design of small-molecules that bind cell surface receptors and increase the concentration of the drug in cancerous cells, relative to healthy ones.[67,77,171,172] We saw the potential of conjugates formed by tethering cyanine dyes like **A** or **C** to kinase inhibitors (KIs) such as dasatinib. Such conjugates might be

preferentially delivered into cancerous over healthy cells via the OATPs, and their desirable near-IR fluorescence properties would facilitate intracellular imaging so uptake of the conjugate could be tracked. Conversely, it was not clear that conjugate **1** would retain their inhibition activity against SRC kinases, but we estimated the probability that they would retain their activity as high enough to justify syntheses and a series of cell studies. In the event the data collected on these conjugates are interesting, those studies are reported here.

Results and Discussion

Design, Synthesis, and Characteristics of the Conjugate 1: There are crystal structures of dasatinib **D** complexed with the cellular sarcoma kinase (cSrc)[173], Abelson kinase (Abl) [174] and Lck/Yes novel kinase (Lyn).[175] In these structures, the hydroxyl group of the KI projects into solvent, while the heterocyclic scaffold binds the kinase active site (Figure V-1). On the basis of this observation we hypothesized that kinase inhibitors could be added to that hydroxyl group without major perturbations to their efficacy. Consequently, we designed conjugate **1** which conjugates dasatinib to cyanine **A** via the solvent-exposed hydroxyl group. We hypothesized **1** might be selectively imported into cancer cells via the OATPs, and transport the kinase inhibitor fragment with it. Once inside the cell, **1**, being larger and more polar than dasatinib alone, might be less vulnerable to efflux via mechanisms featuring P-glycoprotein and alike.[160-164]

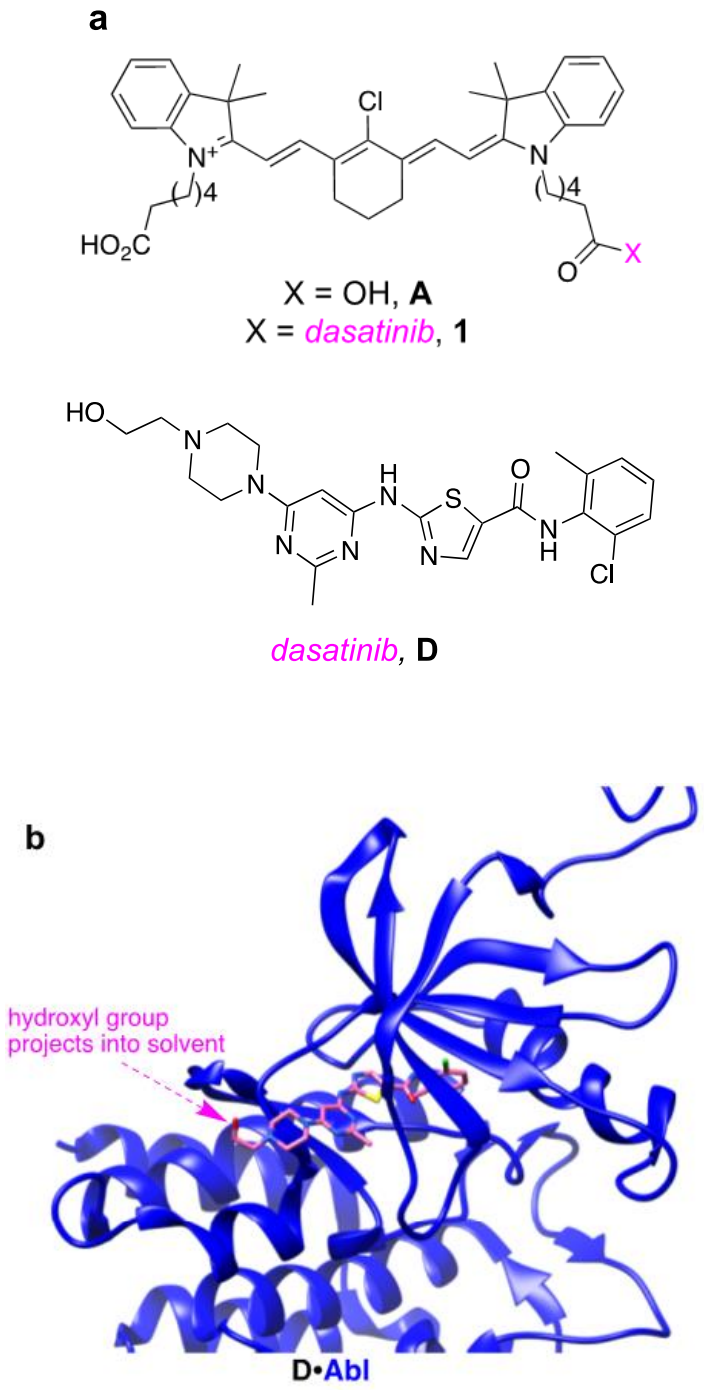

Figure V-1. **a** Structure of dasatinib **D** and the KI-Cy **1**. Crystal structures of **D** bound to three of its target kinases, i.e. **b** to Abl (PDB: 2GQG); **c** to cSrc (3G5D); and, **d** to Lyn (2ZVA). All three structures show the hydroxy group of **D** is solvent exposed.

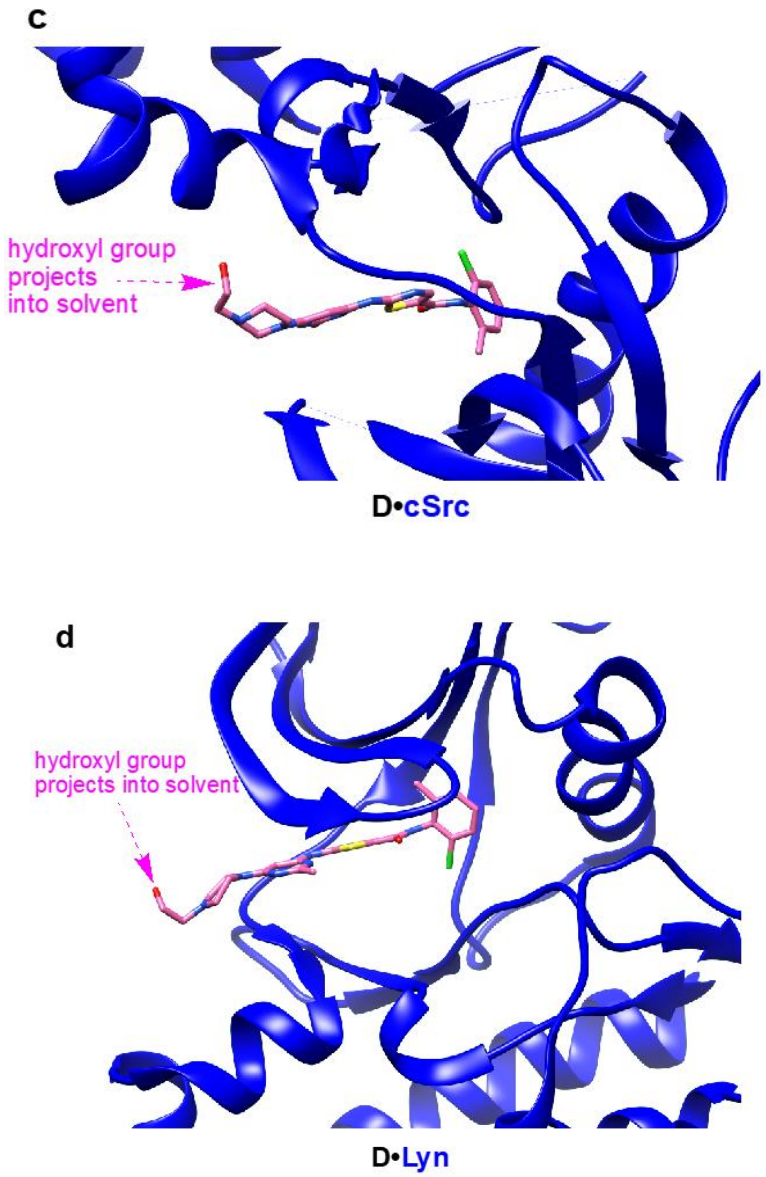

Figure V-1. Continued.

Conjugate **1** was prepared by coupling dasatinib with the parent cyanine dye in a 1:1 stoichiometry as described in the supporting material. In water with 0.1% Kolliphor EL (to prevent aggregation), **1** was observed to have a maximal absorbance at 796 nm, and emission at 815 nm (Figure D-S1). The fluorescence quantum yield of **1** (8 %) and

extinction coefficient of 205,480 $M^{-1}cm^{-1}$ which is typical of near-IR Cy7 dyes, hence the conjugate **1** has brightness (Φ x ε_{max}) similar to parent dye **A**.

Cell Studies: Cell studies were performed on HepG2 human hepatocellular carcinoma (HCC) cell line, for the following reasons. First, even though dasatinib is not approved for treatment of HCC, it is a logical therapeutic to test since signaling via the Src kinases[176] is heavily implicated in this disease.[176,177] Indeed, dasatinib has featured in cellular,[177] preclinical, and clinical trials for HCC (NCT00459108, NCT00835679, NCT00382668). Second, while non-invasive optical imaging of the liver is impractical because it is a deeply imbedded organ, surgical intervention is often practiced for advanced liver cancer, hence development of a theranostic that selectively stains cancerous tissue in a diseased liver could potentially assist excision with negative margins while simultaneously suppress tumor growth and metastases.

KinaseSeeker™ assays were used to determine IC_{50} values of **1** with Src and Lyn. This is a competition binding assay in which change in luminescence signal is measured by displaced of active site displacement probe by inhibitor. Observed IC_{50} values, for **1** were 184 nM (Src) and 556 nM (Lyn), whereas the corresponding values for **D** were 12 nM (Src) and 18 nM (Lyn). Thus, conjugation of dasatinib with **A** perturbed the affinity of the kinase inhibitor part for the parent kinases, but still significant binding was observed (Figure D-S1b and c).

Figure V-2a shows cytotoxicity data for HepG2 cells treated with **1**, **D**, **A**, and a mixture of {**A** + **D**} where the concentrations of **1**, **D**, **A**, **A**-fragment and **D**-fragment were equal throughout. Conjugate **1** (blue line; IC_{50} 5.4 ± 0.4 μM) decreased cell viability by almost an order of magnitude relative to the parent kinase inhibitor **D** (red

line; IC_{50} 34.0 ± 4.95 μM), the cyanine dye **A** (green line; IC_{50} 18.9 ± 1.35 μM), and *relative to a mixture of **A** and **D** unconjugated at the same concentrations* (purple line; IC_{50} 14.9 ± 0.9 μM). A cell proliferation assay was performed to determine effect of 5 μM **1**, **D**, **A**, and **A** + **D** on HepG2 cells. Compound **1** inhibited cell growth more than **D**, **A**, or **A** + **D** (Figure D-S1d). Treatment with **1** caused the cells to change shape in the short term, and most died after 48 h, whereas those treated with the dasatinib **D** alone were largely unperturbed (Figure V-2b). Figure V-2c shows average speed of scratch closure from wound healing experiments to simulate cell migration; DMSO (control) and **A** had comparable effects on the average speed of migration, but rate of recovery was less in the experiments featuring **1** and **D**.

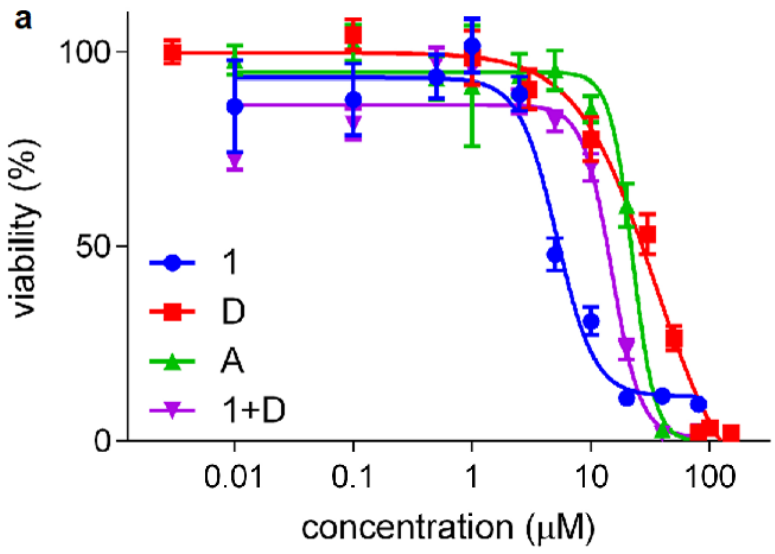

Figure V-2. **a** Viabilities of HepG2 cells induced by **1**, **D**, **A**, and {**A** plus **D**} after incubating with the test compounds for 48 h in the dark, before an AlamarBlue test for cell viability. **b** Morphology of HepG2 cells at 10X/0.4 treated with 5 μM of **A** and **1**. **c** Influence of DMSO (blank), **A**, **1**, **D** at 1μM on a wound healing assay featuring HepG2 cells.

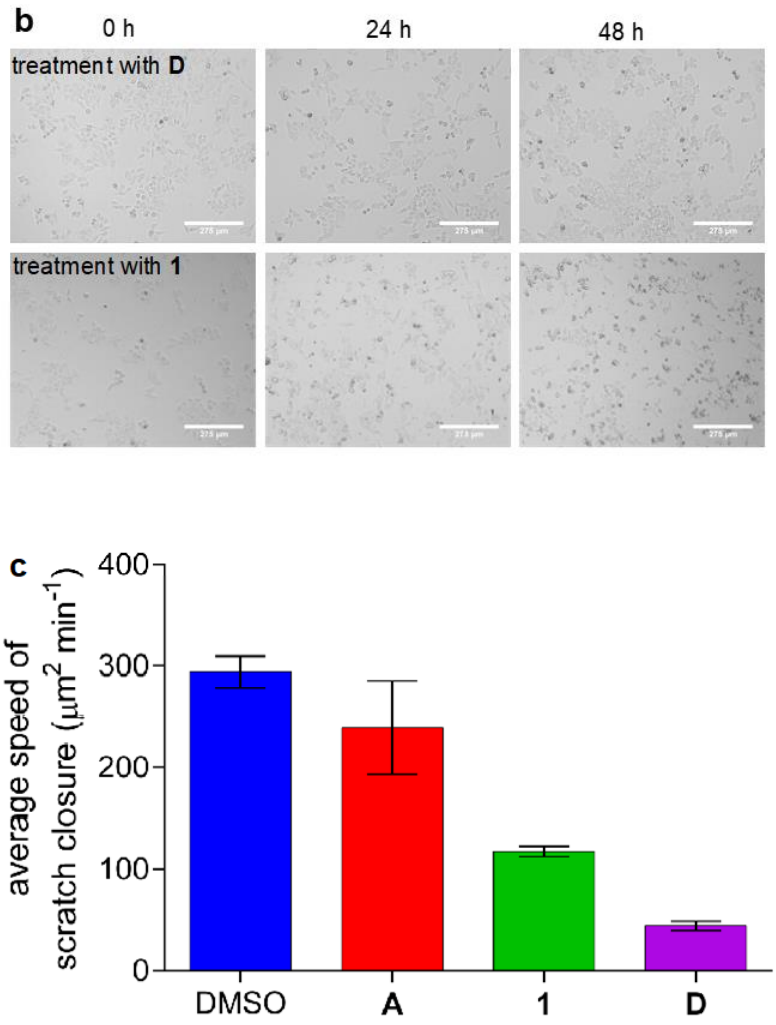

Figure V-2. Continued.

Dasatinib is designed to curb the proliferation of cancer cells, rather than be cytotoxic in the way that early cancer drugs are. In fact, the free dye **A** showed slightly *more* cytotoxicity than dasatinib (Figure V-2a). Thus, beside the attributes of a near-IR labeled kinase inhibitors outlined above, for HepG2 cells there may be some toxicity of the dye itself that synergizes with the effects of the dasatinib component.

Confocal images of HepG2 cells treated with **1** indicated that the conjugate internalized more in mitochondria than lysosomes (Figure V-3). The parent dye **A** also localizes in mitochondria,[48,50,94] hence this data indicates **1** is imported by the same mechanism, or that the link is broken in cells to liberate the free dye. Localization in mitochondria is characteristic of lipophilic, positively charged, organic materials, like **A**. Moreover, import through OATPs receptors is more often associated with localization in the mitochondria than endocytosis.[86]

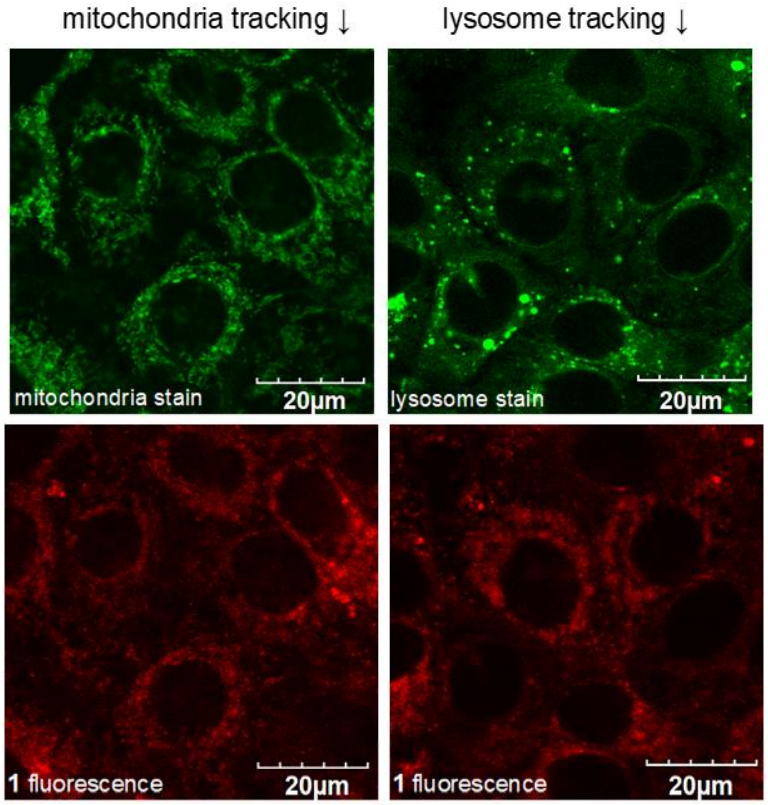

Figure V-3. Confocal imaging of HepG2 cells treated with **1** and MitoTracker Green, Pearson's co efficient 0.72 (left column) or **1** and LysoTracker Green, Pearson's co efficient 0.56 (right). Nuclei stained with NucBlue are included in the merged images in the bottom row. The images were taken at 60x/1.20 water immersed objective.

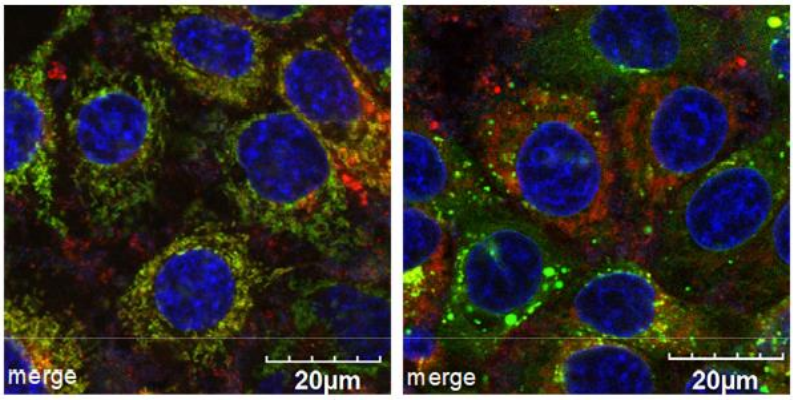

Figure V-3. Continued.

A series of experiments were undertaken to determine the mechanism of uptake of **1** into HepG2 cells. Figure V-4a shows the fluorescence of cells incubated with **1** for 30 min, washed, then visualized under a 775/46 nm filter (710/40 nm excitation); this experiment provides a calibration point for subsequent ones in the same Figure, in which uptake through the OATPs is blocked, or their expression is enhanced. Thus, significantly less fluorescence uptake was observed when the experiments were repeated under exactly same conditions except that a pan-OATP inhibitor (bromosulfophthalein, BSP),[130] was included in the medium (Figure V-4b). Conversely, the near-IR fluorescence of the cells was significantly *increased* if DMOG (dimethyloxalylglycine), [132,131] an inducer of hypoxia, was added to the medium instead. OATP uptake is energy dependent (ATP mediated) hence it shuts down after incubation at low temperatures.[178] Thus, in the light of the data above, it is unsurprising that uptake of the near-IR fluorescence was suppressed when the cells were incubated at 0 °C (Figure D-S3). Figure V-4d shows quantitation of this data via flow cytometry.

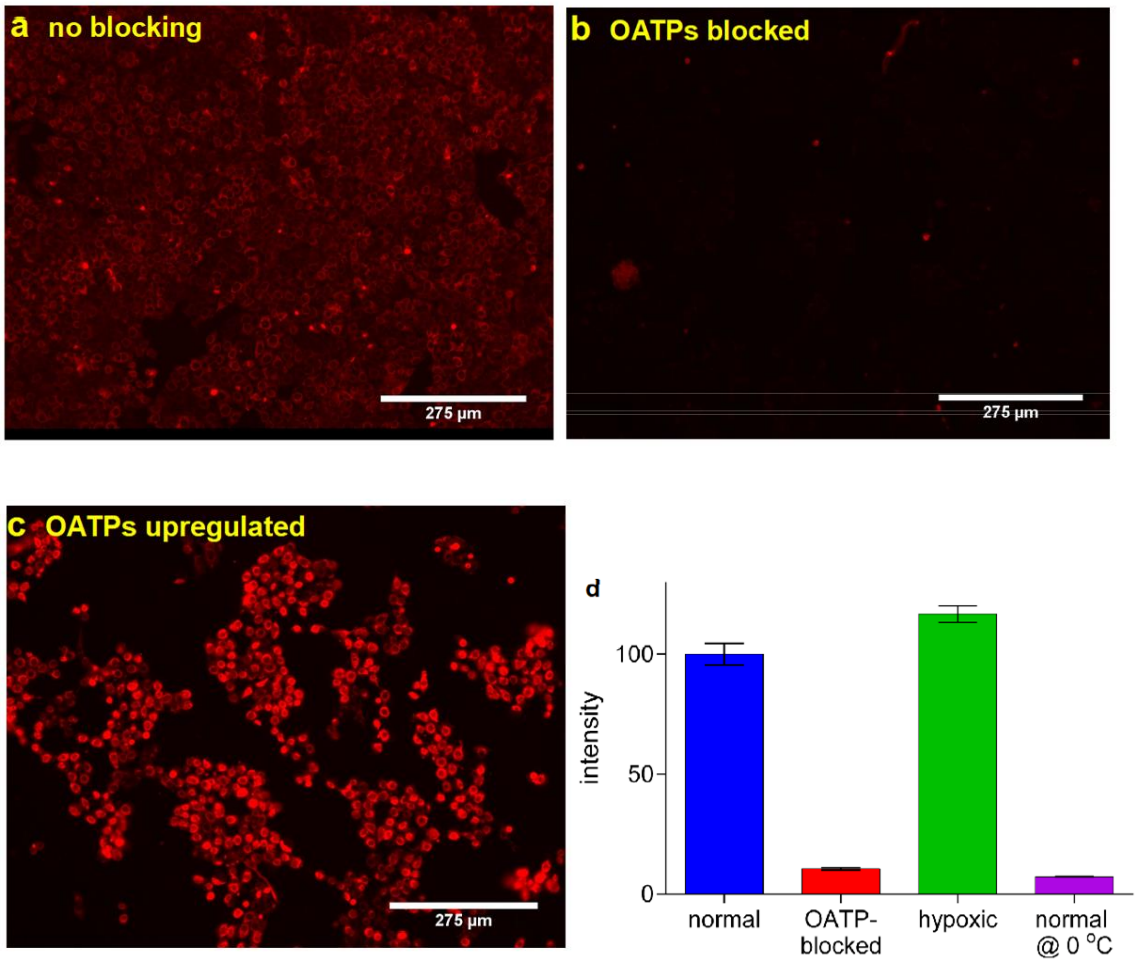

Figure V-4. Uptake of **1** under: **a** normal condition; **b** in the presence of the pan-OATP inhibitor BSP (250 µM); **c** under hypoxia conditions induced by 1 mM DMOG; **d** quantification via flow cytometry, and scale bar 275 µm, throughout.

Finally, induction of intracellular Src phosphorylation was probed in a blotting assay. HepG2 cells were incubated with **1**, **D**, **A** for 24 h before lysis. Total cell lysates were calibrated and subjected to SDS-PAGE followed by blotting with mAbs. **1** was shown to inhibit phosphorylation of Src family kinases in a dose-dependent way, though not as effectively as **D**. Dye **A** does not inhibit Src phosphorylation (Figure V-5).

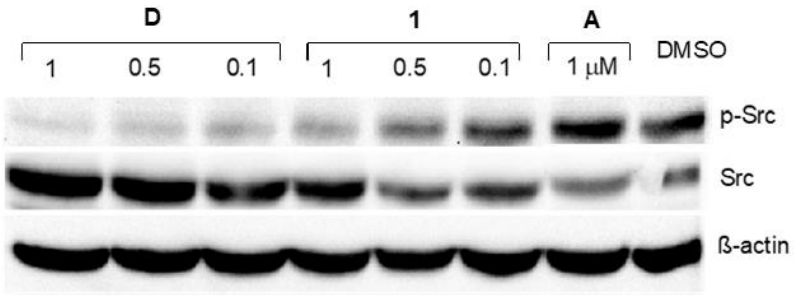

Figure V-5. Western blot analysis of HepG2 cell lysates treated with **1**, **D** and **A**. Total protein calibrated by BCA protein assay.

Conclusions

To date eight papers that feature conjugates of A with cytotoxic materials which preserve the *meso*-chloride functionality. These include two different experimental monoamine oxidase inhibitors,[57-59] an experimental faresnyl transferase inhibitor,[60] a mustard agent[61] and gemicitabine.[51,53] However, there are no reports of conjugation of **A** or relevant analogs *to kinase inhibitors*. The therapeutic window for kinase inhibitors is arguably wider that for conventional cytotoxic drugs. Consequently, the merits of active targeting are perhaps less obvious for kinase inhibitors than for generally cytotoxic materials. However, we believe the prospect of cyanine-drug conjugates binding to albumin, permeating into the tumor, then *being retained there as an albumin complex* is an exciting possibility with respect to potential therapeutic applications.

Kinase inhibitors have problems associated with efflux from cells[179-182] and acquired resistance.[183] Consequently, they may be less susceptible to these undesirable characteristics because they become covalently bound to kinases are now highly topical.[184-187] We see a complementary potential here since conjugate **1** is actively

imported into cells and the fluorescence is retained in cells for at least 24 h. These data indicate that in conjugate **1** either dasatinib must be cleaved to be active, or **1** can inhibit phosphorylation by SRC kinases, but less effectively than dasatinib itself. We think the data in Figure V-5 indicating **1** has a *greater* effect on cell viability may be attributable to the conjugate being retained in cells for longer than the parent inhibitor, perhaps circumventing efflux mechanisms that expel dasatinib form the cells. It is also possible that the inhibitor is more effective because the fluorophore directs it to the mitochondria. An alternative explanation, that the conjugate has a greater effect on other kinases, seems much less likely.

Conjugate **1** is based on near-IR dyes in the series **A** – **C**; these dyes are known to localize in *many* different solid tumors (*e.g.* prostate,[48] gastric,[49] kidney,[50]). Consequently, research described in this paper highlights opportunities for testing conjugates of other kinase inhibitors with tumor-targeting cyanine dyes in models for other types of cancers.

CHAPTER VI

OPTIMIZED HEPTAMETHINE CYANINES FOR PHOTODYNAMIC THERAPY

Introduction

Photodynamic therapy, PDT, relies on illumination of sensitizers absorbed in tissue.[3,188,189] Appropriate sensitizers populate triplet excited states with long half-lives (relative to singlet states), which therefore have time to react with endogenous oxygen. That interaction transforms ubiquitous $^3O_2$ into its extremely reactive singlet state. Singlet oxygen destroys tissues via several oxidative mechanisms and this effect can be used in various ways, including for cancer therapy.[66,190,191]

A significant attribute of PDT is that it is *spatially targeted*. This is because the areas to be illuminated can be controlled, singlet oxygen can only be generated there, and $^1O_2$ is so reactive that tissue damage is effectively confined in those regions (the half-life of singlet oxygen in tissue has been estimated to be 3.5 μs,[192,193] hence its effects in PDT are localized to within about 155 nm of the illuminated area).[194,195] Overall, these combined effects widen the therapeutic window of PDT relative to agents that are not targeted.

The main weakness of PDT is that light must permeate through tissue to excite the sensitizers. At best, light only traverses through about 1 cm in tissue, so PDT is only viable for destruction of cells on or near tissues accessible to surface illumination, or via

---

[196]Reprinted with permission from "Optimized Heptamethine Cyanines For Photodynamic Therapy" by Syed Muhammad Usama, Sopida Thavornpradit and Kevin Burgess, *ACS Appl. Bio Mater.* 2018, *1,* 1195-1205. DOI: 10.1021/acsabm.8b00414. Copyright 2018 American Chemical Society.

fiber-optic devices delivered through needles into deep tissue. In both cases, it is necessary to treat *around* the area targeted in case there are outbreaks, *e.g.* tumor growths, that were undetectable; in other words, to maintain a "negative margin" around the legion. The optimal wavelength range for excitation of sensitizers in PDT is from approximately 750 to around 850 nm. Tissue is relatively opaque to light of <750 nm than to longer wavelengths (penetration of light wavelength 800 nm is twice that of light 630 nm),[44] whereas above 850 nm the quanta do not have enough energy to form singlet oxygen.[197]

Characteristics of ideal PDT sensitizers include: (i) strong absorption in the 750 – 850 nm range; (ii) high quantum yield for singlet oxygen generation; (iii) low dark cytotoxicity for the agent and its metabolites; (iv) photostability; (v) solubility in aqueous media; and, (vi) an intrinsic tendency to localize in cancer cells over healthy ones. In our view, and in the opinion of others,[197-199] the most limiting restriction on the available hydrophilic PDT sensitizers is: (i) strong absorbance in the 750 – 850 nm range combined with (ii) efficient generation of singlet oxygen. This assertion is supported by review of sensitizers for PDT that are either FDA-approved (i.e. in the US; five total, Porfimer sodium, ALA, MAL, HAL, BPD-MA), and/or those approved in other countries (three total, mTHPC, NPe6, AlPcS4; Figure VI-1), all of which have absorption maxima well below the desired 750 – 850 nm range {the aminovulinate derivatives (ALA, MAL, and HAL) are transformed into porphyrins *in situ*, which have absorption maxima below the desired range}. Studies that feature hydrophilic sensitizers that do not absorb strongly in the 750 – 850 nm range are unlikely to improve upon the clinically approved substances, despite the fact that the greatest potential for improvements in the area are associated

with facilitating PDT for non-superficial tissue. There is some interest in modified bacteriochlorins, a few of which do absorb above 750 nm.[44,188,200] However, the efficiency of PDT sensitizers is directly related to the product of their extinction coefficient and quantum yield for singlet oxygen production, and even the most promising bacteriochlorins have lesser values for both these parameters relative to the heptamethine cyanine dyes considered here.

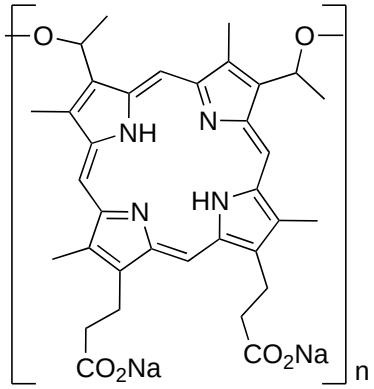

porfimer sodium, Photofrin®
λ_{max} 630 nm, ε_{max} 3000 M^{-1} cm^{-1}

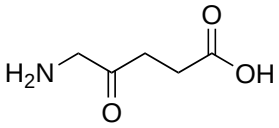

5-aminolevulinic acid (ALA), Levulan®
λ_{max} 635 nm, ε_{max} 5000 M^{-1} cm^{-1}

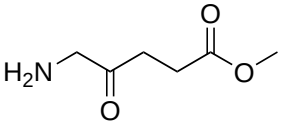

methyl aminolevulinate (MAL), Metvix®
λ_{max} 570-670 nm

Figure VI-1. Photosensitizers clinically approved for PDT treatment.

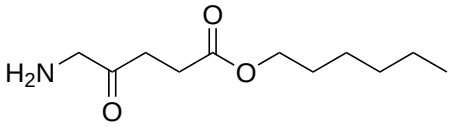

hexaminolevulinate (HAL), Cysview®

λ_{max} 570-670 nm

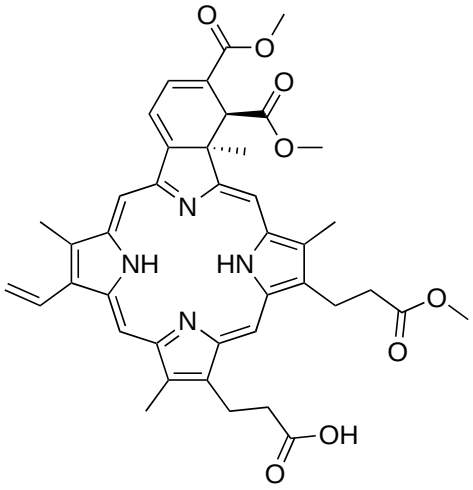

benzoporphyrin derivative monoacid ring A (BPD-MA), Visudine®

λ_{max} 689 nm, ε_{max} 34,000 M^{-1} cm^{-1}

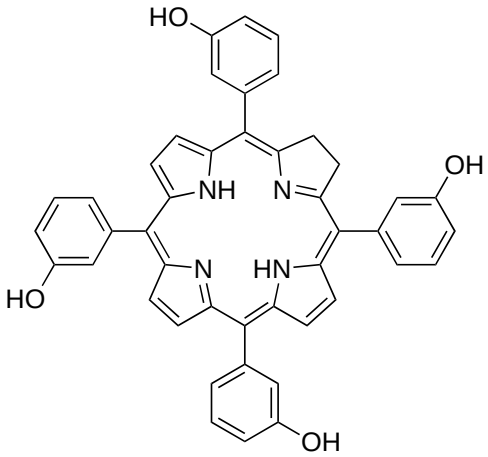

meta-tetra(hydroxyphenyl)chlorin (m-THPC), Foscan®

λ_{max} 652 nm, ε_{max} 35,000 M^{-1} cm^{-1}

Figure VI-1. Continued

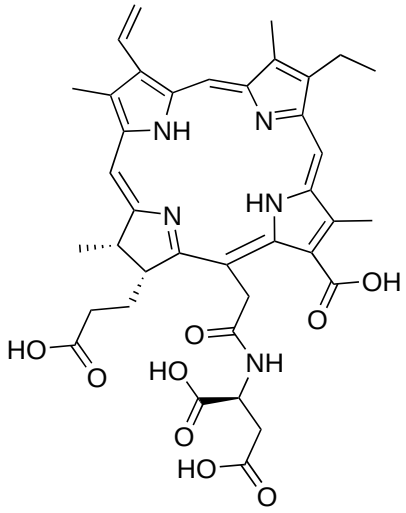

N-aspartyl chlorin e6 (NPe6), Laserphyrin®
λ_{max} 664 nm, ε_{max} 40,000 M^{-1} cm^{-1}

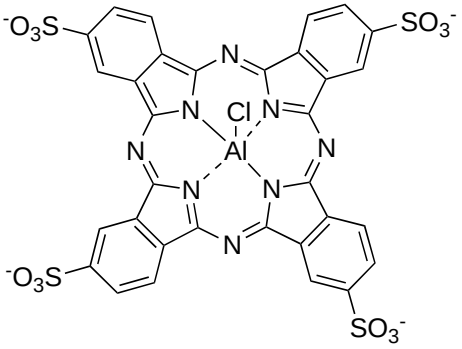

aluminium phthalocyanine tetrasulfonate (AlPcS4), Photosense®
λ_{max} 676 nm, ε_{max} 200,000 M^{-1} cm^{-1}

Figure VI-1. Continued.

Heptamethine cyanine ("Cy7") dyes (**A** Figure VI-2) tend to absorb in the 750 – 850 nm range, but there has been relatively few reported attempts to modify them for use in PDT.[188,201-208] Indocyanine green (ICG) is particularly relevant because it is FDA-approved for optical imaging, but, typical of cyanines for PDT, it has an extremely low quantum yield for singlet oxygen production (0.077).[209] Heptamethine cyanines **B**, with

a six member carbocyclic ring, have increased rigidity, leading to increase in fluorescence quantum yield and decrease in aggregation relative to the parent systems **A**. Some systems containing framework **B** (without heavy atoms) can be photosensitizers, but their quantum yields for singlet oxygen production are also low.[52,86,210,211] In a patent, iodinated systems **B** for PDT have been described, with no evidence that they were actually made. Another patent covered diiodinated indozalines specifically for conversion into class **A** cyanine dyes for PDT, but no examples with type **B** systems were reported. While this work was in progress, Callan and co-workers published on a diiodinated Cy7 derivative that has a significantly higher efficiency for $^1O_2$-production than those mentioned previously (this compound is later numbered **2bb**, see Figure VI-3 below for structure and explanation of numbering scheme in this paper).[212]

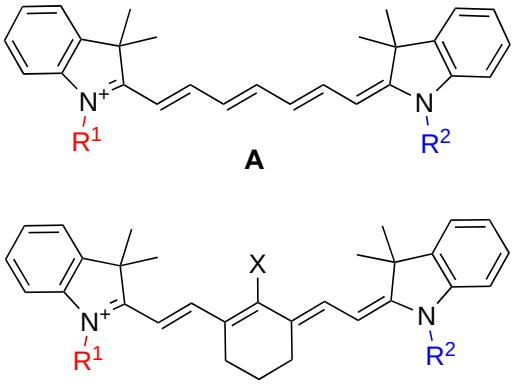

Figure VI-2. Basic structures of heptamethine cyanine dyes. **A** does not have a cyclohexyl ring whereas **B** has it.

Cyanines with different *N*-alkyl substituents are desirable because they facilitate optimization for PDT effects (it is known the *N*-alkyl substituents can have an influence).[52,86,210,211] However, unsymmetrical Cy7 analogs are significantly harder to make than symmetrical ones. In fact, there are only a few experimental procedures for making unsymmetrical cyanine dyes, and they are all small-scale, low-yielding procedures.[60,213] It is therefore unsurprising that unsymmetrical Cy7 analogs for PDT are at least rare, and indeed may not have been reported to date.

This manuscript reports syntheses of 10 new cyanine dyes to test for PDT. Throughout, they retain some near-IR fluorescence properties (emission maxima around 780 nm) hence they are dual mode theranostics (for fluorescence detection of tumor tissue locations, and for therapy). We show that these sensitizers also have properties that are conducive to import into cancer cells. They include compounds that are symmetrical *and* unsymmetrical, containing zero, one or two iodine atoms (hereafter labeled with the numbers **0**, **1**, and **2**). Photophysical properties of these compounds, including quantum yields of singlet oxygen generation, have been measured and compared to the literature standard mentioned above (**2bb**). Two Cy7 derivatives were shown to be significantly more photocytotoxic than the others. These two particular compounds were tracked via confocal microscopy to determine sites of localization in cells, particularly in mitochondria since compounds that accumulate there can be especially effective in cancer therapy.[214] Preferred cell uptake mechanisms for one of these compounds were also established.

Results and Discussion

Syntheses: Symmetrical cyanine dyes are typically prepared by double condensation reactions (Scheme E-S1a), while the few protocols for unsymmetrical ones available describe stepwise, different, conjugation processes (E-S1b). The problem with the stepwise route is that the products tend to be contaminated by symmetrical impurities, hence the yields of the isolated, pure unsymmetrical products tend to be low. Others have noted that this difficulty is accentuated for type **B** cyanine dyes.[215] In this work it was found to be a considerable advantage to perform the first condensation to give the hemi-cyanines at 50 °C (a significantly lower temperature than used in published procedures) then to purify via flash chromatography on silica. Using this modification, it was possible to obtain gram amounts of *pure* (usually >95 % by analytical HPLC) materials after preparative HPLC or MPLC on C18 reverse phase supports. The products prepared are shown in Figure VI-3 where the numbers **0** – **2** denote the number of iodines on the scaffold, and the suffixes describe the *N*-substituents. Of these, the iodinated compounds are new except our "literature standard" **2bb**.[212]

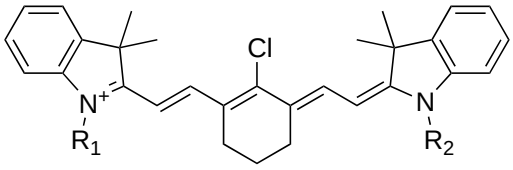

0
aa, **bb**, **cc**

Figure VI-3. Cyanines prepared in this work with zero, one or two iodines with different side chains are notated **0**,**1** and **2** respectively. The synthesis of these compounds is described in Appendix Figure E-S2- S4.

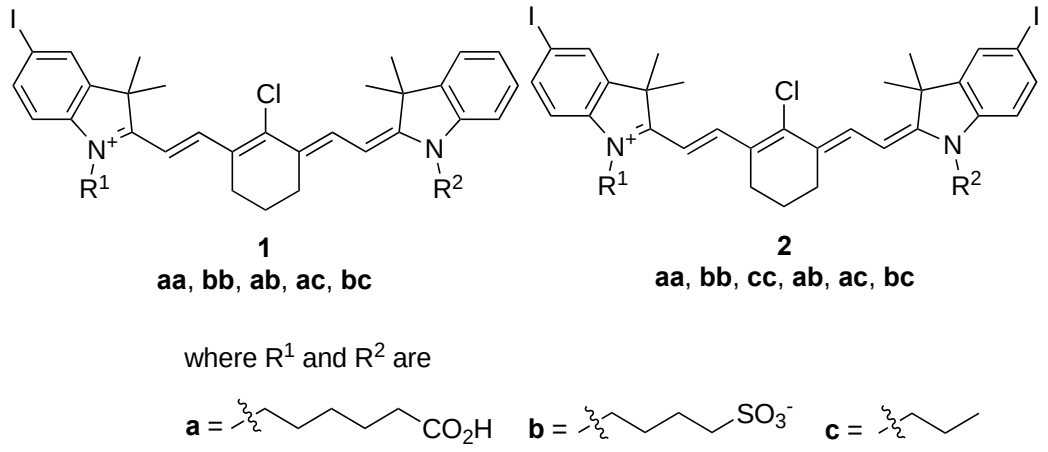

Figure VI-3. Continued.

Photophysical Properties: Rates of singlet oxygen production for the compounds **0** – **2** are shown in Figures E-S1a – c, respectively. There appears to be no correlation between the polarities or acidities of the side-chain (**a**, **b**, and **c**) combinations and the amounts of singlet oxygen produced. Figures E-S2a – c indicate there is a similar lack of correlation for the photostabilities of these dyes, and, in any event, photostabilities did not vary much with *N*-substitution ($t_{1/2}$ between around 12 and 32 min), except compound **2bc** was somewhat more resilient to excitation, especially over the early stages.

Singlet oxygen production and photostability data described above is summarized with other photophysical data in Table VI-1. All the dyes absorb maximally between 794 and 812 nm and fluorescence with maxima in the range 811 – 827 nm. Their fluorescence quantum yields are low (0.044 – 0.095) but their high extinction coefficients (*ca* 100,000 – 340,000) means these dyes are bright (brightness = quantum yield x extinction coefficient, Table E-S2), as expected for Cy7 dyes. The data indicates that compounds with a sulfonic acid in the *N*-substituent tend to have higher extinction

coefficients, presumably due to increased water solubility and less aggregation in aqueous media. Broadly speaking, compounds **2** tend to have higher quantum yields for singlet oxygen production than **1**, than **0**, i.e. the most iodinated fluorophores produce the most singlet oxygen, again as expected from heavy atom effects. The presence of two iodines facilitates transitions between singlet and triplet states that would be forbidden in simpler systems, and less facile in monoiodo-compounds. Singlet oxygen generation increased by approximately four-fold on addition of first iodine and two-fold with the addition of second iodine atom (average for compounds: **0**, 0.091; **1**, 0.370; **2**, 0.689).[216]

compound	R^1	R^2	λ_{abs} (nm)	λ_{em} (nm)	ε_{max} ($M^{-1}cm^{-1}$)	Φ^a	Φ ($^1O_2$)^b
0	**a**	**a**	796	815	235120	0.076	0.058
	b	**b**	812	827	340920	0.095	0.070
	c	**c**	803	818	100080	0.077	0.144
1	**a**	**a**	803	819	209480	0.071	0.379
	b	**b**	796	812	208600	0.072	0.347
	a	**b**	812	823	211800	0.069	0.272
	a	**c**	803	819	199960	0.077	0.403
	b	**c**	812	827	200240	0.071	0.449
2	**a**	**a**	794	811	229200	0.044	0.627
	b	**b**	812	825	252000	0.065	0.686
	c	**c**	813	827	148360	0.047	0.591
	a	**b**	812	825	268560	0.063	0.790
	a	**c**	803	816	180680	0.069	0.675
	b	**c**	803	819	248960	0.062	0.767

Table VI-1. Spectroscopic properties of compound **0**, **1**, and **2** dissolved in PBS buffer (pH 7.4).[a] Fluorescence quantum yields *vs* ICG ($\Phi = 0.13$ in DMSO) as a standard. [b] $^1O_2$ quantum yield measured using ICG ($\Phi = 0.077$) as a reference.

Cell Studies - Light and Dark Toxicities: Throughout, the photocytotoxicity experiments described below were performed using inexpensive LEDs that generate a light flux of only 2.28 J/cm^2. Choice of low-flux light sources was deliberate to emphasize the effectiveness of the featured photosensitizers.

Compounds **2**, *i.e.* the ones that afforded the most singlet oxygen when illuminated, were incubated with HepG2 cells in the absence of light for 48 h to examine viability under those conditions. In the event, there was little difference; all the compounds had IC_{50} values in the 7 – 23 μM range (Figure E-S3). However, differences in the characteristics of the compounds became more prevalent in *photocytotoxicity* experiments. Thus, HepG2 cells were incubated with compounds **2** for 1 h, washed, then illuminated in fresh media at 780 nm (3.8 mW/cm^2 LED) for 10 min, incubated for 24 h, then tested for viability (AlamarBlue). Throughout this paper, the Thor Lab LED780E used has maximum absorbance around 780±10 nm, which covers the maximum wavelengths for most of the synthesized compounds. Figure VI-4 shows data for compounds **2** organized from least to most photocytotoxic. All the compounds were significantly more photocytotoxic (red bars) than dark controls (blue bars) in which the illumination step was omitted. The di-*n*-propyl compound **2cc**, was less photocytotoxic than the known, disulfonic acid, sensitizer **2bb**, but all the others were more so. The following observation is to compare the best (**2ac**) with the standard (**2bb**): more than 50 % of the cells remained in the experiments featuring treatment with **2bb** at 10 μM, but under the same conditions **2ac** (sulfonic acid and propyl *N*-substituents) killed almost all of the cells. At 6 μM, **2ac** killed more than half the cells in this assay.

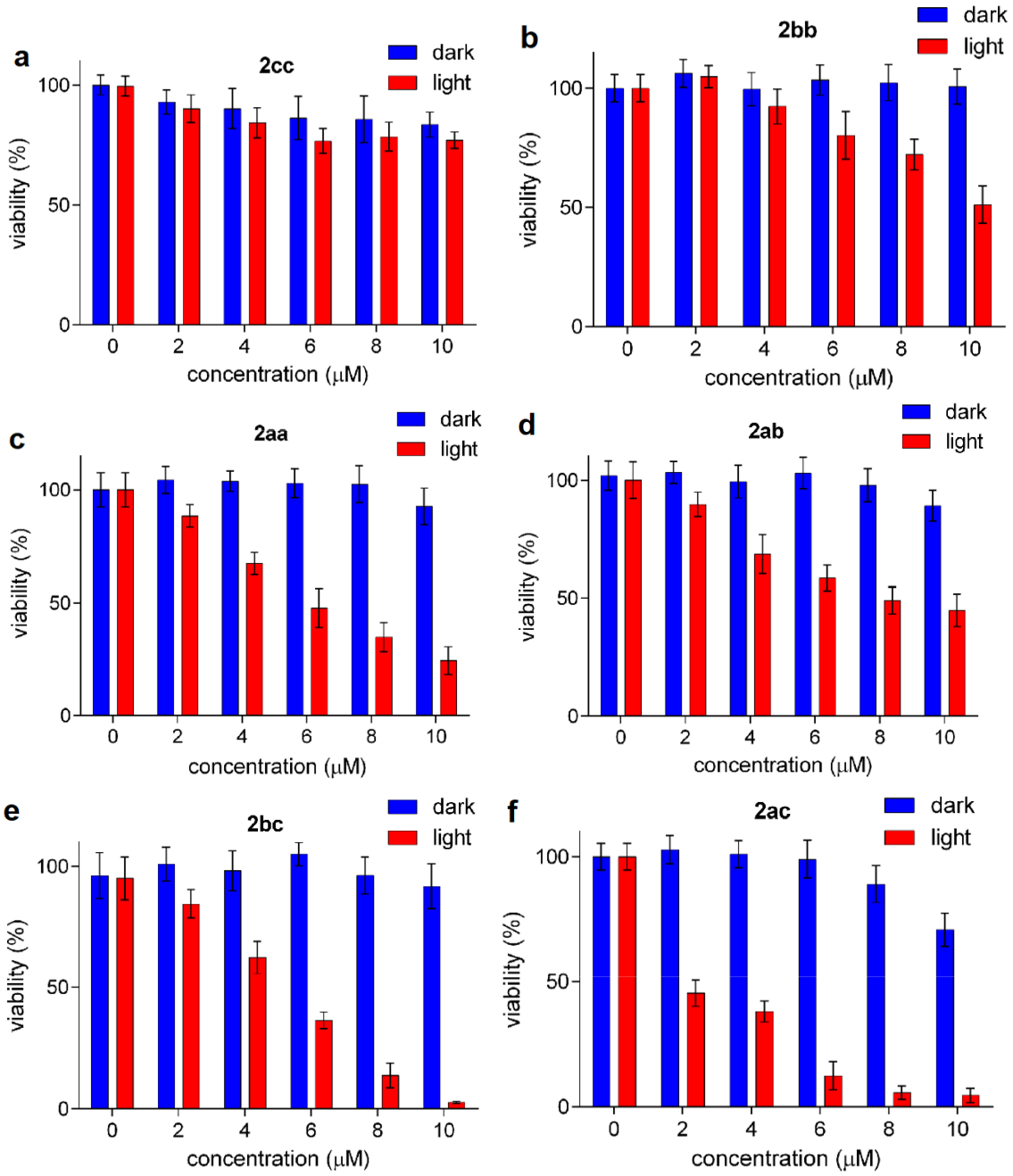

Figure VI-4. Light and dark cytotoxicity of compounds: **a**, **2cc**; **b**, **bb**; **c**, **aa**; **d**, **ab**; **e**, **bc**; and **f**, **ac** determined after irradiation under 780 nm LED or kept in dark as control (see text for details).

Localization of the Sensitizers in Cancer Cell: Confocal microscopy experiments were undertaken to visualize favored organelles for accumulation of the two most

photocytotoxic of the featured sensitizers: *i.e.* **2ac** and **2bc**. Both dyes readily permeated into HepG2 cells. Both **2ac** and **2bc** colocalized to some degree with LysoTracker green, and much more with MitoTracker green (Figures VI-5 and VI-6, respectively). In fact, similar localization studies were performed for all the series **2** compounds reported in this paper. All of them accumulated mostly in the mitochondria and less in the lysosome, with the exception of the control **2bb**, which was found mostly in the lysosome and less in the mitochondria (Figure E-S4). This observation is consistent with the greater positive charges of these particular sensitizers in the series.

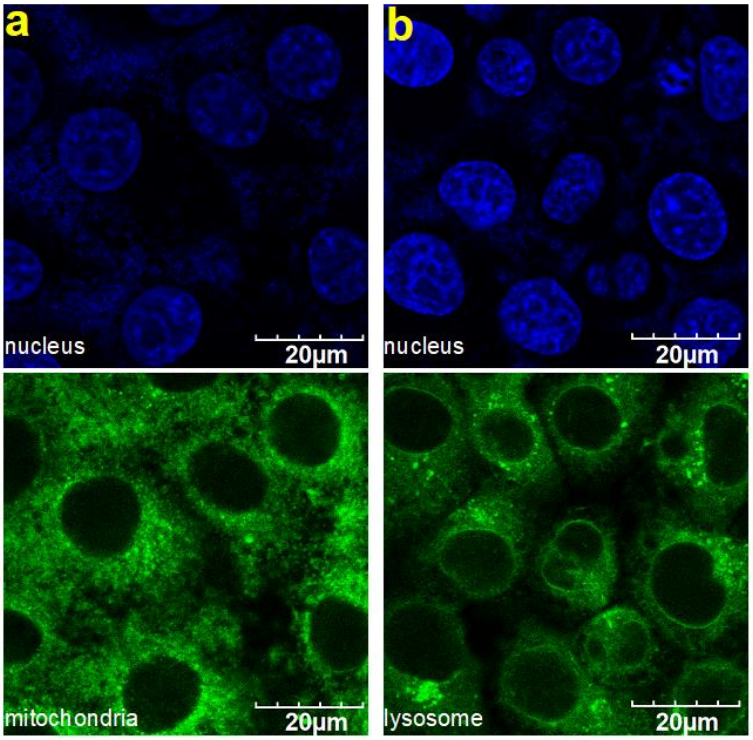

Figure VI-5. Confocal imaging of **2ac** with **a** MitoTracker Green (Pearson's R value: 0.70); and **b** LysoTracker Green (0.68). **2ac** internalized more in mitochondria than lysosome.

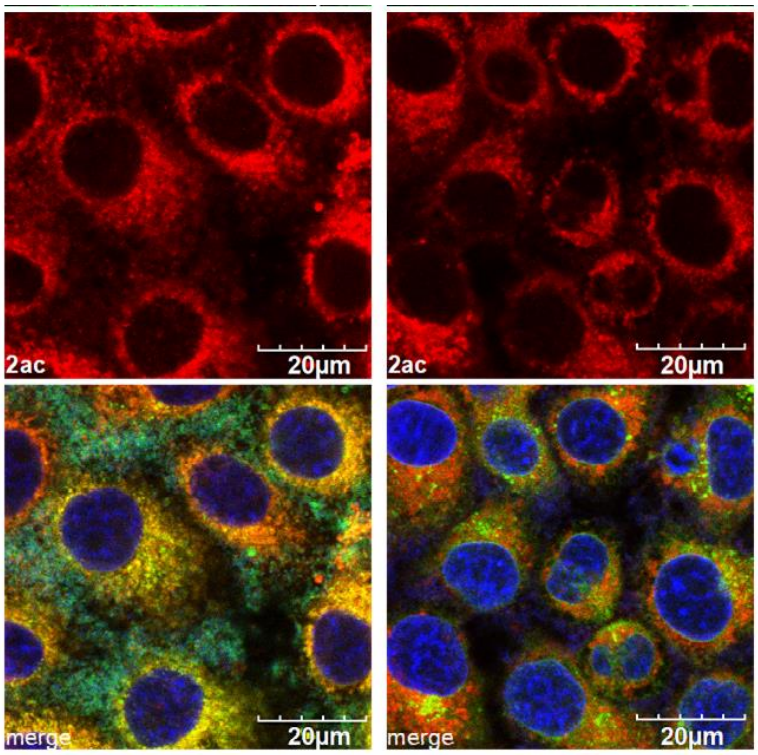

Figure VI-5. Continued

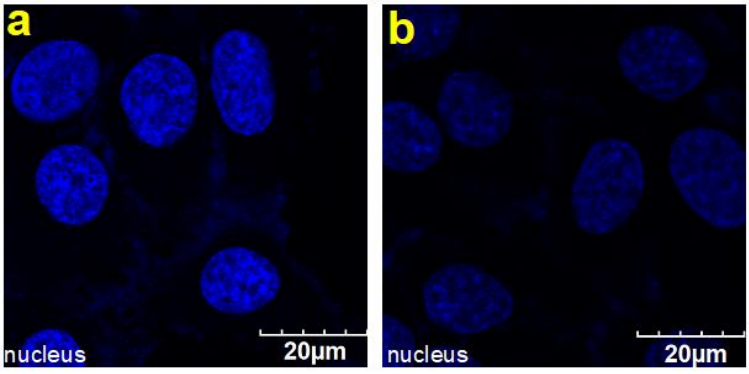

Figure VI-6. Confocal imaging of **2bc** with **a** MitoTracker Green (Pearson's R value: 0.89); and **b** LysoTracker Green (0.54). **2bc** internalized more in mitochondria than lysosome.

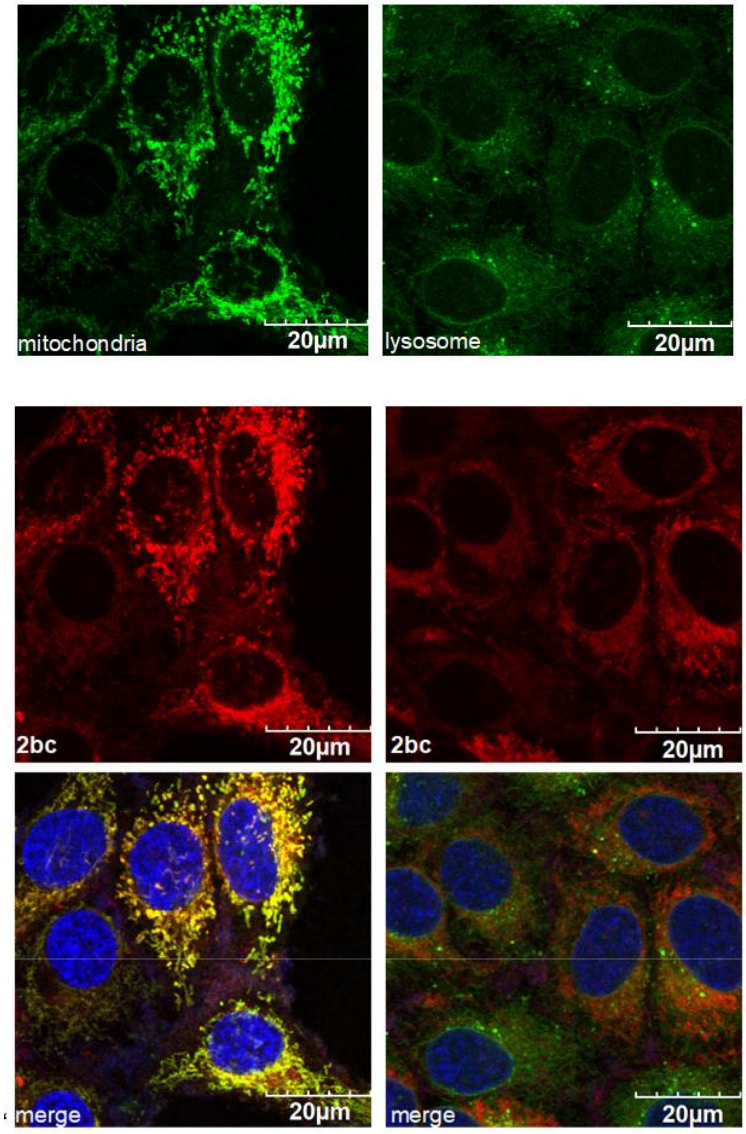

Figure VI-6. Continued.

Some class **B** dyes are known to localize in solid tumor tissue (*e.g.* prostate,[48] gastric,[49] kidney,[50] lung,[52]and glioblastoma,[53,58] *and in liver tumor tissues*[51]) but not in normal cells and tissue.[69,86-88,94]. Evidence from several studies suggest this is because those particular fluorophores are uptaken by the organic anion transporter proteins (OATPs).[54,55] These OATP cell surface receptors are overexpressed on solid tumors;

their natural function is to influx organic anions (and some neutral materials) that are important to cells (*e.g.* bile salts, steroids, bilirubin, and thyroid hormones), and, to balance this ion influx, OATP receptors efflux intracellular bicarbonate, glutathione, and glutathione adducts. We inferred that OATP-mediated uptake of the iodinated dyes in series **2** imparts the potential for enhanced tumor uptake over healthy tissues that do not express these receptors. Consequently, a series of fluorescence studies were undertaken to establish a mechanism of uptake of **2ac** into HepG2 cells (Figure VI-7).

Figure VI-7 compares the fluorescence uptake by HepG2 cells treated with **2ac** alone (*i.e.* no blocking, Figure VI-7a), with the fluorescence when the same cell type but treated first with a pan-inhibitor OATPs (there are several sub-types within this category, but the inhibitor is believed to inhibit all; Figure VI-7b),[54,55] and finally (Figure VI-7c) with HepG2 cells treated with an agent to induce hypoxia and therefore to promote expression of HIF1α leading to enhance expression of OATPs.[49,56] Data in Figure VI-7 shows there is less uptake of **2ac** when the OATPs are inhibited, and more when their overexpression is enhanced (quantification is provided in Appendix Figure E-S5).

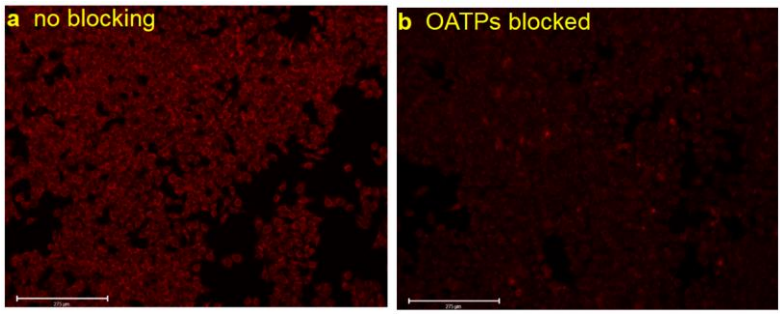

Figure VI-7. Uptake of **2ac** under: **a** normal conditions; **b** blocked by a pan-OATP inhibitor BSP (bromosulfophthalein); and, **c** under hypoxia conditions induced by DMOG (dimethyloxalylglycine). Scale bar 275 μm.

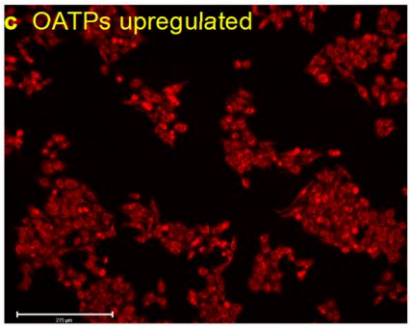

Figure VI-7. Continued

Derivatives of the parent cyanine dyes that are too lipo- or hydrophilic tend not to localize in tumor tissue. Calculations physiochemical properties were performed using Marvin (17.21.0, ChemAxon; supporting Table E-S1) to examine if substitution of iodine atoms on to the cyanine framework impacts these types of properties. Relative to the non-iodinated cyanines **0**, the mono- and di-iodinated ones **1** and **2** had insignificant differences in calculated polar surface areas. Addition of one then another iodines (from **0** to **1** to **2**) somewhat increased the calculated LogP and LogD values for the compounds, but only by around one or two log units, *i.e.* probably not enough to cause significant changes in their pharmacokinetic properties. LogD (and LogP) data are important because others have singled this out as important for biodistribution of Cy7 derivatives.[42] Callan's sensitizer, **2bb**, has no convenient function groups to facilitate its conjugation to biomolecules or other fragments to expand theranostic modalities, except displacement of the *meso* chloride via $S_{RN}1$ or SNAr mechanisms. Consequently, we were curious to probe the effects of substituting that same chloride with nitrogen, oxygen, and sulfur

nucleophiles, hence three test compounds were made (see supporting) giving compounds **3bb**, **4bb**, and **5bb** (Table VI-2).

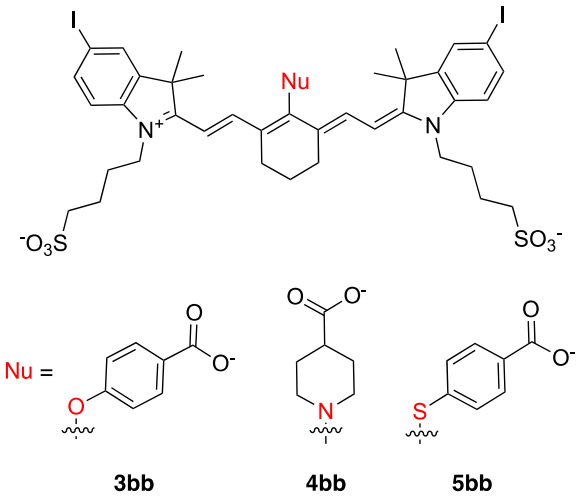

3bb **4bb** **5bb**

compound	λ_{abs} (nm)	λ_{em} (nm)	Φ ($^1O_2$)[b]
2bb	812	825	0.686
3bb	793	816	0.382
4bb	667	800	-
5bb	820	832	0.298

Table VI-2. Absorption and emission maxima of the *meso*-substituted compounds **3bb** – **5bb** (synthesis described in Supporting Figure E-S5), and quantum yields for singlet oxygen generation. [b] $^1O_2$ quantum yield measured using ICG (Φ = 0.077) as a reference.

Table VI-2 shows that the absorption and emission maxima of the *N*-substituted compound **4bb** is blue-shifted relative to **2bb** by 145 nm, whereas the *O*- and *S*-substituted ones were much less affected by this change. These observations are consistent with literature reports on the structurally similar, but non-iodinated, cyanines.[42,81] Unfortunately, we were not able to make a true comparison of quantum

yields for singlet oxygen production because the LED we used (780 nm) was appropriate for excitation of **2bb** and the *O*- and *S*-substituted compounds **3bb** and **5bb**, but gave effectively no excitation of the "blue-shifted sensitizer" **4bb**. However, these experiments do show the quantum yields of singlet oxygen production for *O*- and *S*-substituted compounds **3bb** and **5bb** were approximately half that of **2bb**.

Conclusions

Callan *et al* reported the first near-IR cyanine sensitizer in the open literature; this was a milestone in the area, and the work reported here builds on those studies. Thus, a slight refinement of literature syntheses of unsymmetrical cyanines facilitated preparation and studies of the series **0**, **1**, and **2** molecules, some of which might not have been conveniently accessible otherwise. The only iodinated compound in series **1** and **2** that has been reported in the open literature prior to this work was **2bb**.

Most of the new compounds featured here in series **2** (specifically: **aa**, **ab**, **ac**, and **bc**) were more photocytotoxic than the literature control **2bb**. Moreover, unlike **2bb**, the novel sensitizers *accumulated in the mitochondria*. Mitochondria targeting is particularly important for PDT in cancer, because where sensitizers accumulate is of comparable importance to the number of reactive oxygen species it produces. Targeting mitochondria makes cells particularly sensitive to PDT,[66,214] so this tends to explain why most of the compounds in series **2** were *more* photocytotoxic than **2bb**. The observation that **2bb** localized in the lysosome, in preference to the mitochondria, might correlate with the observation that this compound is uniquely has two sulfonates making it the most hydrophilic member of series **2**. Consistent with this, the parent disulfonate dye with no

iodines, **0bb** also accumulates mostly in the lysosomes. However, mitochondria targeting in not the *only* factor involved. Compound **2cc** also localized at mitochondria, but it was one of the least potent photosensitizers in series **2**. We suggest the explanation for this is that more of this relatively hydrophilic dye is retained in the membrane, and this is not accounted for in *relative* colocalization studies that only consider the dye inside the cell.

Finally, uptake of photosensitizers via over-expressed OATPs is potentially useful for targeting PDT agents, most of which have a dual function, *i.e.* they are theranostics for, imaging and therapy. Parenthetically, we note that **2bb** is less suitable for conjugation to other agents than the novel member of series **2** that have a carboxylic acid side-chain(s) (denoted **a**). In other words, **2bb** is not amenable to the typical mode of conjugation of fluorescent dyes to biomolecules (*e.g.* mAbs) via amide bond coupling, but the compounds developed here are. Data in Table VI-2 shows that conjugation by *meso*-substitution would be possible, but the absorption maxima would be blue-shifted for secondary amine nucleophiles (*c.f.* **4bb**), and if *S*- and *O*-nucleophiles were used (*c.f.* **3bb** and **5bb**) researchers could anticipate that singlet oxygen production would be cut by around 50%.

CHAPTER VII

CONCLUSIONS

This dissertation featured theranostic agents for cancer. A small molecule targeting TrkC receptors on metastatic breast cancer was conjugated with zwitterionic cyanine dye for deep tumor imaging. Zwitterionic cyanine dye was selected because of their net neutral charge which helps clearance out of the body quickly without getting stuck in the organs. Moreover, this dissertation discusses an innovative one step method to specifically label cysteines with near-infrared dyes on proteins. As a proof of concept, this procedure was applied to label several proteins containing free cysteines e.g. human serum albumin (HSA) vimentin, NAE, PCSK9 etc. Thus, proving our methodology is easy, simple, precise and eliminates use of tedious multistep procedures. In addition to this, the work on displacing *meso*-Cl with cysteines helped in deciphering the mechanism behind long tumor retention time associated with tumor-targeted cyanine dyes. It also sheds lights on the importance of meso-Cl of cyanine dyes and its reactivity with HSA. Later on, these dyes were conjugated with dasatinib, SRC promiscuous kinase inhibitor, to specifically deliver dasatinib to cancer cells. This targeted delivery helped in increasing the therapeutic effect of the conjugate. Furthermore, heavy atom (iodine) was incorporated into these targeted cyanines to extract photodynamic therapy (PDT) in near-infrared region. A library of photosensitizers was synthesized that showed good photophysical properties and high singlet oxygen quantum yields. This dye showed *in vitro* photocytotoxicity with negligible dark toxicity.

REFERENCES

(1) Stuker, F.; Ripoll, J.; Rudin, M. *Pharmaceutics* **2011**, *3*, 229.

(2) Konig, K. *J. Microsc.* **2000**, *200*, 83.

(3) Agostinis, P.; Berg, K.; Cengel Keith, A.; Foster Thomas, H.; Girotti Albert, W.; Gollnick Sandra, O.; Hahn Stephen, M.; Hamblin Michael, R.; Juzeniene, A.; Kessel, D.; Korbelik, M.; Moan, J.; Mroz, P.; Nowis, D.; Piette, J.; Wilson Brian, C.; Golab, J. *CA Cancer J Clin* **2011**, *61*, 250.

(4) De Grand, A. M.; Frangioni, J. V. *Technol Cancer Res Treat* **2003**, *2*, 553.

(5) Lim, M. C.; Seo, S.-S.; Kang, S.; Kim, S. K.; Kim, S. H.; Yoo, C. W.; Park, S.-Y. *Quant. Imaging. Med. Surg.* **2012**, *2*, 114.

(6) Willmann, J. K.; van Bruggen, N.; Dinkelborg, L. M.; Gambhir, S. S. *Nat. Rev. Drug Discovery* **2008**, *7*, 591.

(7) Patel, N. J.; Manivannan, E.; Joshi, P.; Ohulchanskyy, T. J.; Nani, R. R.; Schnermann, M. J.; Pandey, R. K. *Photochem. Photobiol.* **2015**, *91*, 1219.

(8) Zang, C.; Long, L.; Shi, C. *Adv. Ther.* **2018**, *1*, 180069.1

(9) Torchilin Vladimir, P. *Handb. Exp. Pharmacol.* **2010**, *197*, 3.

(10) Sievers Eric, L.; Senter Peter, D. *Annu. Rev. Med.* **2013**, *64*, 15.

(11) Alley, S. C.; Okeley, N. M.; Senter, P. D. *Curr. Opin. Chem. Biol.* **2010**, *14*, 529.

(12) Saga, T.; Neumann, R. D.; Heya, T.; Sato, J.; Kinuya, S.; Le, N.; Paik, C. H.; Weinstein, J. N. *Proc. Natl. Acad. Sci.* **1995**, *92*, 8999.

(13) Adams, G. P.; Schier, R.; McCall, A. M.; Simmons, H. H.; Horak, E. M.; Alpaugh, R. K.; Marks, J. D.; Weiner, L. M. *Cancer Res.* **2001**, *61*, 4750.

(14) Borsi, L.; Balza, E.; Bestagno, M.; Castellani, P.; Carnemolla, B.; Biro, A.; Leprini, A.; Sepulveda, J.; Burrone, O.; Neri, D.; Zardi, L. *Int. J. Cancer* **2002**, *102*, 75.

(15) Carrasco-Triguero, M.; Yi, J.-H.; Dere, R.; Qiu, Z. J.; Lei, C.; Li, Y.; Mahood, C.; Wang, B.; Leipold, D.; Poon, K. A.; Kaur, S. *Bioanalysis* **2013**, *5*, 1007.

(16) Lu, Y.; Low Philip, S. *Adv. Drug Deliv. Rev.* **2012**, *64*, 342.

(17) Hilgenbrink, A. R.; Low, P. S. *J. Pharm. Sci.* **2005**, *94*, 2135.

(18) Garanger, E.; Boturyn, D.; Dumy, P. *Anti-Cancer Agents Med. Chem.* **2007**, *7*, 552.

(19) Dunehoo, A. L.; Anderson, M.; Majumdar, S.; Kobayashi, N.; Berkland, C.; Siahaan, T. J. *J. Pharm. Sci.* **2006**, *95*, 1856.

(20) Ojima, I. *Acc. Chem. Res.* **2008**, *41*, 108.

(21) Henne, W. A.; Kularatne, S. A.; Ayala-Lopez, W.; Doorneweerd, D. D.; Stinnette, T. W.; Lu, Y.; Low, P. S. *Bioorg. Med. Chem. Lett.* **2012**, *22*, 709.

(22) Jayaprakash, S.; Wang, X.; Heston, W. D.; Kozikowski, A. P. *ChemMedChem* **2006**, *1*, 299.

(23) Zhang, A. J.; Khare, S.; Gokulan, K.; Linthicum, D. S.; Burgess, K. *Bioorg. Med. Chem. Lett.* **2001**, *11*, 207.

(24) Zaccaro, M. C.; Lee, H. B.; Pattarawarapan, M.; Xia, Z.; Caron, A.; Burgess, K.; Saragovi, H. U. *Nat. Biotech.* **2003**, submitted.

(25) Zaccaro, M. C.; Lee, B. H.; Pattarawarapan, M.; Xia, Z.; Caron, A.; L' Heureux, P.-J.; Bengio, Y.; Burgess, K.; Saragovi, H. U. *Chem. Biol.* **2005**, *12*, 1015.

(26) Stephens, P.; Edkins, S.; Davies, H.; Greenman, C.; Cox, C.; Hunter, C.; Bignell, G.; Teague, J.; Smith, R.; Stevens, C.; O'Meara, S.; Parker, A.; Tarpey, P.; Avis, T.; Barthorpe, A.; Brackenbury, L.; Buck, G.; Butler, A.; Clements, J.; Cole, J.; Dicks, E.; Edwards, K.; Forbes, S.; Gorton, M.; Gray, K.; Halliday, K.; Harrison, R.; Hills, K.; Hinton, J.; Jones, D.; Kosmidou, V.; Laman, R.; Lugg, R.; Menzies, A.; Perry, J.; Petty, R.; Raine, K.; Shepherd, R.; Small, A.; Solomon, H.; Stephens, Y.; Tofts, C.; Varian, J.; Webb, A.; West, S.; Widaa, S.; Yates, A.; Brasseur, F.; Cooper, C. S.; Flanagan, A. M.; Green, A.; Knowles, M.; Leung, S. Y.; Looijenga, L. H. J.; Malkowicz, B.; Pierotti, M. A.; Teh, B.; Yuen, S. T.; Nicholson, A. G.; Lakhani, S.; Easton, D. F.; Weber, B. L.; Stratton, M. R.; Futreal, P. A.; Wooster, R. *Nat. Genet.* **2005**, *37*, 590.

(27) Jin, W.; Kim, G.-M.; Kim, M.-S.; Lim, M.-H.; Yun, C.-H.; Jeong, J.; Nam, J.-S.; Kim, S.-J. *Carcinogenesis* **2010**, *31*, 1939.

(28) Jin, W.; Yun, C.; Kwak, M. K.; Kim, T. A.; Kim, S. J. *Oncogene* **2007**, *26*, 7684.

(29) Marconi, A.; Terracina, M.; Fila, C.; Franchi, J.; Bonte, F.; Romagnoli, G.; Maurelli, R.; Failla, C. M.; Dumas, M.; Pincelli, C. *J. Invest. Dermatol.* **2003**, *121*, 1515.

(30) Marchetti, D.; Murry, B.; Galjour, J.; Wilke-Greiter, A. *J. Cell. Biochem.* **2003**, *88*, 865.

(31) Marconi, A.; Panza, M. C.; Bonnet-Duquennoy, M.; Lazou, K.; Kurfurst, R.; Truzzi, F.; Lotti, R.; De Santis, G.; Dumas, M.; Bonte, F.; Pincelli, C. *Int. J. Cosmet. Sci.* **2006**, *28*, 255.

(32) Dutta, A. K.; Kamada, K.; Ohta, K. *Photochem. Photobiol.* **1996**, *93*, 57.

(33) Wang, Y.; Hagel, C.; Hamel, W.; Muller, S.; Kluwe, L.; Westphal, M. *Acta Neuropathol.* **1998**, *96*, 357.

(34) Assimakopoulou, M.; Kondyli, M.; Gatzounis, G.; Maraziotis, T.; Varakis, J. *BMC Cancer* **2007**, *7*, 202.

(35) Brodeur, G. M.; Nakagawara, A.; Yamashiro, D. J.; Ikegaki, N.; Liu, X. G.; Azar, C. G.; Lee, C. P.; Evans, A. E. *J. Neuro-Oncology* **1997**, *31*, 49.

(36) Encinas, M.; Iglesias, M.; Llecha, N.; Comella, J. X. *J. Neurochem.* **1999**, *73*, 1409.

(37) Kamkaew, A.; Burgess, K. *J. Med. Chem.* **2013**, *56*, 7608.

(38) Kamkaew, A.; Li, F.; Li, Z.; Burgess, K. *MedChemComm* **2017**, *8*, 1946.

(39) Choi, H.-S.; Nasr, K.; Alyabyev, S.; Feith, D.; Lee, J.-H.; Kim, S.-H.; Ashitate, Y.; Hyun, H.; Patonay, G.; Strekowski, L.; Henary, M.; Frangioni, J. V. *Angew. Chem., Int. Ed.* **2011**, *50*, 6258.

(40) Choi, H. S.; Gibbs, S. L.; Lee, J. H.; Kim, S. H.; Ashitate, Y.; Liu, F.; Hyun, H.; Park, G. L.; Xie, Y.; Bae, S.; Henary, M.; Frangioni, J. V. *Nat. Biotechnol.* **2013**, *31*, 148.

(41) Kim, S. H.; Park, G.; Hyun, H.; Lee, J. H.; Ashitate, Y.; Choi, J.; Hong, G. H.; Owens, E. A.; Henary, M.; Choi, H. S. *Biomed. Mater.* **2013**, *8*, 014110.

(42) Njiojob, C. N.; Owens, E. A.; Narayana, L.; Hyun, H.; Choi, H. S.; Henary, M. *J. Med. Chem.* **2015**, *58*, 2845.

(43) Owens, E. A.; Hyun, H.; Tawney, J. G.; Choi, H. S.; Henary, M. *J. Med. Chem.* **2015**, *58*, 4348.

(44) Ethirajan, M.; Chen, Y.; Joshi, P.; Pandey, R. K. *Chem. Soc. Rev.* **2011**, *40*, 340.

(45) Vahrmeijer, A. L.; Hutteman, M.; van der Vorst, J. R.; van de Velde, C. J. H.; Frangioni, J. V. *Nat. Rev. Clin. Oncol.* **2013**, *10*, 507.

(46) Frangioni, J. V. *Curr. Opin. Chem. Biol.* **2003**, *7*, 626.

(47) Hilderbrand, S. A.; Weissleder, R. *Curr. Opin. Chem. Biol.* **2010**, *14*, 71.

(48) Yuan, J.; Yi, X.; Yan, F.; Wang, F.; Qin, W.; Wu, G.; Yang, X.; Shao, C.; Chung, L. W. K. *Mol. Med. Rep.* **2015**, *11*, 821.

(49) Zhao, N.; Zhang, C.; Zhao, Y.; Bai, B.; An, J.; Zhang, H.; Shi, C.; Wu Jason, B. *Oncotarget* **2016**, *7*, 57277.

(50) Yang, X.; Shao, C.; Wang, R.; Chu, C.-Y.; Hu, P.; Master, V.; Osunkoya, A. O.; Kim, H. L.; Zhau, H. E.; Chung, L. W. K. *J. Urol.* **2013**, *189*, 702.

(51) An, J.; Zhao, N.; Zhang, C.; Zhao, Y.; Tan, D.; Zhao, Y.; Bai, B.; Zhang, H.; Shi, C.; An, J.; Wu Boyang, J. *Oncotarget* **2017**, *8*, 56880.

(52) Luo, S.; Tan, X.; Qi, Q.; Guo, Q.; Ran, X.; Zhang, L.; Zhang, E.; Liang, Y.; Weng, L.; Zheng, H.; Cheng, T.; Su, Y.; Shi, C. *Biomaterials* **2013**, *34*, 2244.

(53) Wu, J. B.; Shi, C.; Chu, G. C.-Y.; Xu, Q.; Zhang, Y.; Li, Q.; Yu, J. S.; Zhau, H. E.; Chung, L. W. K. *Biomaterials* **2015**, *67*, 1.

(54) Thakkar, N.; Lockhart, A. C.; Lee, W. *AAPS Journal* **2015**, *17*, 535.

(55) Kotsampasakou, E.; Ecker, G. F. In *Transporters as Drug Targets*; Sitte, H. H., Ecker, G. F., Mannhold, R., Buschmann, H., Clausen, R. P., Eds.; Wiley - VCH Verlag GmbH & Co. KGaA: 2017, p 271

(56) Wu, J. B.; Shao, C.; Li, X.; Shi, C.; Li, Q.; Hu, P.; Chen, Y.-T.; Dou, X.; Sahu, D.; Li, W.; Harada, H.; Zhang, Y.; Wang, R.; Zhau, H. E.; Chung, L. W. K. *Biomaterials* **2014**, *35*, 8175.

(57) Wu, J. B.; Lin, T.-P.; Gallagher, J. D.; Kushal, S.; Chung, L. W. K.; Zhau, H. E.; Olenyuk, B. Z.; Shih, J. C. *J. Am. Chem. Soc.* **2015**, *137*, 2366.

(58) Kushal, S.; Wang, W.; Vaikari, V. P.; Kota, R.; Chen, K.; Yeh, T.-S.; Jhaveri, N.; Groshen, S. L.; Olenyuk, B. Z.; Chen, T. C.; M., H. F.; Shih, J. C. *Oncotarget* **2016**, *7*, 13842.

(59) Lv, Q.; Yang, X.; Wang, M.; Yang, J.; Qin, Z.; Kan, Q.; Zhang, H.; Wang, Y.; Wang, D.; He, Z. *J. Controlled Release* **2018**, *279*, 234.

(60) Guan, Y.; Zhang, Y.; Xiao, L.; Li, J.; Wang, J.-p.; Chordia, M. D.; Liu, Z.-Q.; Chung, L. W. K.; Yue, W.; Pan, D. *Mol. Pharmaceutics* **2017**, *14*, 1.

(61) Zhang, E.; Luo, S.; Tan, X.; Shi, C. *Biomaterials* **2014**, *35*, 771.

(62) Fabbro, D.; Cowan-Jacob, S. W.; Moebitz, H. *Br. J. Pharmacol.* **2015**, *172*, 2675.

(63) Manning, G.; Whyte, D. B.; Martinez, R.; Hunter, T.; Sudarsanam, S. *Science* **2002**, *298*, 1912.

(64) Gross, S.; Rahal, R.; Stransky, N.; Lengauer, C.; Hoeflich Klaus, P. *J. Clin. Invest.* **2015**, *125*, 1780.

(65) Juarranz, A.; Jaen, P.; Sanz-Rodriguez, F.; Cuevas, J.; Gonzalez, S. *Clin. Transl. Oncol.* **2008**, *10*, 148.

(66) Mehraban, N.; Freeman, H. S. *Materials* **2015**, *8*, 4421.

(67) Kue, S. C., Anyanee Kamkaew, Hong Boon Lee, Lip Long Chung, Lik Voon Kiew, and Kevin Burgess *Mol. Pharmacetics* **2015**, *12*, 212.

(68) Kue, C. S.; Kamkaew, A.; Burgess, K.; Kiew, L. V.; Chung, L. Y.; Lee, H. B. *Med. Res. Rev.* **2016**, *36*, 494.

(69) Gao, M.; Yu, F.; Lv, C.; Choo, J.; Chen, L. *Chem. Soc. Rev.* **2017**, *46*, 2237.

(70) Cedolini, C.; Bertozzi, S.; Seriau, L.; Concina, S.; Cattin, F.; Risaliti, A.; Londero, A. P.; Bernardi, S. *Clin. Breast Cancer* **2014**, *14*, 235.

(71) Welch, H. G.; Gorski, D. H.; Albertsen, P. C. *N. Engl. J. Med.* **2015**, *373*, 1685.

(72) Vaishnavi, A.; Le Anh, T.; Doebele Robert, C. *Cancer Discov.* **2015**, *5*, 25.

(73) Slamon, D. J.; Leyland-Jones, B.; Shak, S.; Fuchs, H.; Paton, V.; Bajamonde, A.; Fleming, T.; Eiermann, W.; Wolter, J.; Pegram, M.; Baselga, J.; Norton, L. *N. Engl. J. Med.* **2001**, *344*, 783.

(74) Ogawa, M.; Kosaka, N.; Choyke, P. L.; Kobayashi, H. *Cancer Res.* **2009**, *69*, 1268.

(75) Imai, K.; Takaoka, A. *Nat. Rev. Cancer* **2006**, *6*, 714.

(76) Yang, Z.; Usama, S. M.; Li, F.; Burgess, K.; Li, Z. *Med. Chem. Comm.* **2018**, *9*, 1754.

(77) Kamkaew, A.; Fu, N.; Cai, W.; Burgess, K. *ACS Med. Chem. Lett.* **2017**, *8*, 179.

(78) Kamkaew, A.; Burgess, K. *Chem. Comm.* **2015**, *51*, 10664.

(79) Pysz, M. A.; Gambhir, S. S.; Willmann, J. K. *Clin. Radiol.* **2010**, *65*, 500.

(80) Beckford, G.; Owens, E.; Henary, M.; Patonay, G. *Talanta* **2012**, *92*, 45.

(81) James, N. S.; Chen, Y.; Joshi, P.; Ohulchanskyy, T. Y.; Ethirajan, M.; Henary, M.; Strekowski, L.; Pandey, R. K. *Theranostics* **2013**, *3*, 692.

(82) Su, D.; Teoh, C. L.; Samanta, A.; Kang, N.-Y.; Park, S.-J.; Chang, Y.-T. *Chem. Commun.* **2015**, *51*, 3989.

(83) Butowt, R.; von Bartheld, C. S. *J. Neurosci.* **2001**, *21*, 8915.

(84) Pulaski, B. A.; Ostrand-Rosenberg, S. *Curr. Protoc. Immunol.* **2001**, *Chapter 20*, 20.21.1.

(85) Stoleru, B.; Popescu, A. M.; Tache, D. E.; Neamtu, O. M.; Emami, G.; Tataranu, L. G.; Buteica, A. S.; Dricu, A.; Purcaru, S. O. *Maedica* **2013**, *8*, 43.

(86) Tan, X.; Luo, S.; Wang, D.; Su, Y.; Cheng, T.; Shi, C. *Biomaterials* **2012**, *33*, 2230.

(87) Luo, S.; Yang, X.; Shi, C. *Curr. Med. Chem.* **2016**, *23*, 483.

(88) Zhang, C.; Liu, T.; Su, Y.; Luo, S.; Zhu, Y.; Tan, X.; Fan, S.; Zhang, L.; Zhou, Y.; Cheng, T.; Shi, C. *Biomaterials* **2010**, *31*, 6612.

(89) Shi, C.; Wu Jason, B.; Pan, D. *J. Biomed. Opt.* **2016**, *21*, 50901:1

(90) Schaafsma, B. E.; Mieog, J. S. D.; Hutteman, M.; van der Vorst, J. R.; Kuppen, P. J. K.; Loewik, C. W. G. M.; Frangioni, J. V.; van de Velde, C. J. H.; Vahrmeijer, A. L. *J. Surg. Oncol.* **2011**, *104*, 323.

(91) Alander, J. T.; Kaartinen, I.; Laakso, A.; Patila, T.; Spillmann, T.; Tuchin, V. V.; Venermo, M.; Valisuo, P. *Int. J. Biomed. Imaging* **2012**, 940585:1

(92) Nagahara, R.; Onda, N.; Yamashita, S.; Kojima, M.; Inohana, M.; Eguchi, A.; Nakamura, M.; Matsumoto, S.; Yoshida, T.; Shibutani, M. *Cancer Sci.* **2018**, *109*, 1638.

(93) Luo, S.; Zhang, E.; Su, Y.; Cheng, T.; Shi, C. *Biomaterials* **2011**, *32*, 7127.

(94) Yang, X.; Shi, C.; Tong, R.; Qian, W.; Zhau, H. E.; Wang, R.; Zhu, G.; Cheng, J.; Yang, V. W.; Cheng, T.; Henary, M.; Strekowski, L.; Chung, L. W. K. *Clin. Cancer Res.* **2010**, *16*, 2833.

(95) Henary, M.; Pannu, V.; Owens, E. A.; Aneja, R. *Bioorg. Med. Chem. Lett.* **2012**, *22*, 1242.

(96) Zhang, C.; Zhao, Y.; Zhang, H.; Chen, X.; Zhao, N.; Tan, D.; Zhang, H.; Shi, C. *Int. J. Mol. Sci.* **2017**, *18*, E1332.

(97) Lin, C.-M.; Usama, S. M.; Burgess, K. *Molecules* **2018**, *23*, 2900.

(98) Strekowski, L.; Lipowska, M.; Patonay, G. *Synth. Commun.* **1992**, *22*, 2593.

(99) Strekowski, L.; Lipowska, M.; Patonay, G. *J. Org. Chem.* **1992**, *57*, 4578.

(100) Cha, J.; Nani, R. R.; Luciano, M. P.; Broch, A.; Kim, K.; Namgoong, J.-M.; Kulkarni, R. A.; Meier, J. L.; Kim, P.; Schnermann, M. J. *Bioorg. Med. Chem. Lett.* **2018**, *28*, 2741.

(101) Nani, R. R.; Shaum, J. B.; Gorka, A. P.; Schnermann, M. J. *Org. Lett.* **2015**, *17*, 302.

(102) Samanta, A.; Vendrell, M.; Das, R.; Chang, Y.-T. *Chem. Commun.* **2010**, *46*, 7406.

(103) Pascal, S.; Haefele, A.; Monnereau, C.; Charaf-Eddin, A.; Jacquemin, D.; Le Guennic, B.; Andraud, C.; Maury, O. *J. Phys. Chem. A* **2014**, *118*, 4038.

(104) Guo, Z.; Zhu, W.; Zhu, M.; Wu, X.; Tian, H. *Chem. - Eur. J.* **2010**, *16*, 14424.

(105) Peng, X.; Song, F.; Lu, E.; Wang, Y.; Zhou, W.; Fan, J.; Gao, Y. *J. Am. Chem. Soc.* **2005**, *127*, 4170.

(106) Warnecke, A.; Fichtner, I.; Garmann, D.; Jaehde, U.; Kratz, F. *Bioconjugate Chem.* **2004**, *15*, 1349.

(107) Nanda, J. S.; Lorsch, J. R. In *Methods Enzymol.*; Lorsch, J. R., Ed.; Elsevier: San Diego, CA, 2014; Vol. 536, p 79.

(108) Walden, H.; Podgorski, M. S.; Huang, D. T.; Miller, D. W.; Howard, R. J.; Minor, D. L., Jr.; Holton, J. M.; Schulman, B. A. *Mol. Cell* **2003**, *12*, 1427.

(109) Huang, D. T.; Miller, D. W.; Mathew, R.; Cassell, R.; Holton, J. M.; Roussel, M. F.; Schulman, B. A. *Nat. Struct. Mol. Biol.* **2004**, *11*, 927.

(110) Cunningham, D.; Danley, D. E.; Geoghegan, K. F.; Griffor, M. C.; Hawkins, J. L.; Subashi, T. A.; Varghese, A. H.; Ammirati, M. J.; Culp, J. S.; Hoth, L. R.; Mansour, M. N.; McGrath, K. M.; Seddon, A. P.; Shenolikar, S.; Stutzman-Engwall, K. J.; Warren, L. C.; Xia, D.; Qiu, X. *Nat. Struct. Mol. Biol.* **2007**, *14*, 413.

(111) Llinas, P.; Le Du, M. H.; Gardsvoll, H.; Dano, K.; Ploug, M.; Gilquin, B.; Stura, E. A.; Menez, A. *Embo J.* **2005**, *24*, 1655.

(112) Ogiso, H.; Ishitani, R.; Nureki, O.; Fukai, S.; Yamanaka, M.; Kim, J.-H.; Saito, K.; Sakamoto, A.; Inoue, M.; Shirouzu, M.; Yokoyama, S. *Cell* **2002**, *110*, 775.

(113) Usama, S. M.; Lin, C.-M.; Burgess, K. *Bioconjugate Chem.* **2018**, *29*, 3886.

(114) Sato, K.; Gorka, A. P.; Nagaya, T.; Michie, M. S.; Nakamura, Y.; Nani, R. R.; Coble, V. L.; Vasalatiy, O. V.; Swenson, R. E.; Choyke, P. L.; Schnermann, M. J.; Kobayashi, H. *Mol. BioSyst.* **2016**, *12*, 3046.

(115) Nani, R. R.; Gorka, A. P.; Nagaya, T.; Kobayashi, H.; Schnermann, M. J. *Angew. Chem., Int. Ed.* **2015**, *54*, 13635.

(116) Gibbs, S. L. *Quant. Imaging. Med. Surg.* **2012**, *2*, 177.

(117) Nagaya, T.; Nakamura Yu, A.; Choyke Peter, L.; Kobayashi, H. *Front Oncol* **2017**, *7*, 314.

(118) Gioux, S.; Choi, H. S.; Frangioni, J. V. *Mol. Imaging* **2010**, *9*, 237.

(119) Chari, R. V. J.; Miller, M. L.; Widdison, W. C. *Angew. Chem., Int. Ed.* **2014**, *53*, 3796.

(120) Casi, G.; Neri, D. *J. Med. Chem.* **2015**, *58*, 8751.

(121) Srinivasarao, M.; Low, P. S. *Chem. Rev.* **2017**, *117*, 12133.

(122) Karlgren, M.; Vildhede, A.; Norinder, U.; Wisniewski, J. R.; Kimoto, E.; Lai, Y.; Haglund, U.; Artursson, P. *J. Med. Chem.* **2012**, *55*, 4740.

(123) Obaidat, A.; Roth, M.; Hagenbuch, B. *Annu. Rev. Pharmacol. Toxicol.* **2012**, *52*, 135.

(124) Roth, M.; Obaidat, A.; Hagenbuch, B. *Br. J. Pharmacol.* **2012**, *165*, 1260.

(125) Okamura, K.; Dummer, P.; Kopp, J.; Qiu, L.; Levi, M.; Faubel, S.; Blaine, J. *PLoS One* **2013**, *8*, e54817.

(126) Peters, J. T. *All About Albumin: Biochemistry, Genetics, and Medical Applications*, 1995.

(127) Gonyar, L. A.; Gray, M. C.; Christianson, G. J.; Mehrad, B.; Hewlett, E. L. *Infect. Immun.* **2017**, *85*, e00198/1.

(128) Spicer, C. D.; Davis, B. G. *Nat. Commun.* **2014**, *5*, 4740.

(129) Kim, Y.; Ho, S. O.; Gassman, N. R.; Korlann, Y.; Landorf, E. V.; Collart, F. R.; Weiss, S. *Bioconjugate Chem.* **2008**, *19*, 786.

(130) Kullak-Ublick, G.-A.; Hagenbuch, B.; Stieger, B.; Wolkoff, A. W.; Meier, P. J. *Hepatology* **1994**, *20*, 411.

(131) Milkiewicz, M.; Pugh, C. W.; Egginton, S. *J. Physiol.* **2004**, *560*, 21.

(132) Jaakkola, P.; Mole, D. R.; Tian, Y.-M.; Wilson, M. I.; Gielbert, J.; Gaskell, S. J.; von Kriegsheim, A.; Hebestreit, H. F.; Mukherji, M.; Schofield, C. J.; Maxwell, P. H.; Pugh, C. W.; Ratcliffe, P. J. *Science* **2001**, *292*, 468.

(133) Dutta, D.; Williamson Chad, D.; Cole Nelson, B.; Donaldson Julie, G. *PLoS One* **2012**, *7*, e45799.

(134) Koivusalo, M.; Welch, C.; Hayashi, H.; Scott, C. C.; Kim, M.; Alexander, T.; Touret, N.; Hahn, K. M.; Grinstein, S. *J. Cell Biol.* **2010**, *188*, 547.

(135) Dutta, D.; Donaldson Julie, G. *Cell Logist* **2012**, *2*, 203.

(136) Liu, Z.; Chen, X. *Chem. Soc. Rev.* **2016**, *45*, 1432.

(137) Frei, E. *Diabetol. Metab. Syndr.* **2011**, *3*, 11.

(138) Stehle, G.; Sinn, H.; Wunder, A.; Schrenk, H. H.; Schutt, S.; Maier-Borst, W.; Heene, D. L. *Anti-Cancer Drugs* **1997**, *8*, 677.

(139) Elsadek, B.; Kratz, F. *J. Controlled Release* **2012**, *157*, 4.

(140) Larsen Maja, T.; Kuhlmann, M.; Hvam Michael, L.; Howard Kenneth, A. *Mol Cell Ther* **2016**, *4*, 3.

(141) Yang, F.; Zhang, Y.; Liang, H. *Int. J. Mol. Sci.* **2014**, *15*, 3580.

(142) Stoddart, C. A.; Bales, C. A.; Bare, J. C.; Chkhenkeli, G.; Galkina, S. A.; Kinkade, A. N.; Moreno, M. E.; Rivera, J. M.; Ronquillo, R. E.; Sloan, B.; Black, P. L. *PLoS One* **2007**, *2*, e655.

(143) Stoddart, C. A.; Nault, G.; Galkina, S. A.; Thibaudeau, K.; Bakis, P.; Bousquet-Gagnon, N.; Robitaille, M.; Bellomo, M.; Paradis, V.; Liscourt, P.; Lobach, A.; Rivard, M.-E.; Ptak, R. G.; Mankowski, M. K.; Bridon, D.; Quraishi, O. *J. Biol. Chem.* **2008**, *283*, 34045.

(144) Kratz, F.; Mueller-Driver, R.; Hofmann, I.; Drevs, J.; Unger, C. *J. Med. Chem.* **2000**, *43*, 1253.

(145) Graeser, R.; Esser, N.; Unger, H.; Fichtner, I.; Zhu, A.; Unger, C.; Kratz, F. *Invest. New Drugs* **2010**, *28*, 14.

(146) Kratz, F.; Warnecke, A.; Scheuermann, K.; Stockmar, C.; Schwab, J.; Lazar, P.; Drueckes, P.; Esser, N.; Drevs, J.; Rognan, D.; Bissantz, C.; Hinderling, C.; Folkers, G.; Fichtner, I.; Unger, C. *J. Med. Chem.* **2002**, *45*, 5523.

(147) Baggio, L. L.; Huang, Q.; Cao, X.; Drucker, D. J. *Gastroenterology* **2008**, *134*, 1137.

(148) Kim, J.-G.; Baggio, L. L.; Bridon, D. P.; Castaigne, J.-P.; Robitaille, M. F.; Jette, L.; Benquet, C.; Drucker, D. J. *Diabetes* **2003**, *52*, 751.

(149) Levitt, D. G.; Levitt, M. D. *Int. J. Gen. Med.* **2016**, *9*, 229.

(150) Kratz, F.; Beyer, U. *Drug Delivery* **1998**, *5*, 281.

(151) Awasthi, K.; Nishimura, G. *Photochem Photobiol Sci* **2011**, *10*, 461.

(152) Rosenthal, S. M.; White, E. C. *J. Am. Med. Assoc.* **1925**, *84*, 1112.

(153) Jacquemin, E.; Hagenbuch, B.; Stieger, B.; Wolkoff, A. W.; Meier, P. J. *Proc. Natl. Acad. Sci. U. S. A.* **1994**, *91*, 133.

(154) Baell, J. B.; Holloway, G. A. *J. Med. Chem.* **2010**, *53*, 2719.

(155) Ding, R.; Frei, E.; Fardanesh, M.; Schrenk, H.-H.; Kremer, P.; Haefeli, W. E. *J. Clin. Pharmacol.* **2011**, *51*, 672.

(156) Kremer, P.; Fardanesh, M.; Ding, R.; Pritsch, M.; Zoubaa, S.; Frei, E. *Neurosurgery* **2009**, *64*, 53.

(157) Frangioni, J. V.; Onishi, S.; (Beth Israel Deaconess Medical Center, USA). WO, 2005, p 43 pp.

(158) Li, B.; Lu, L.; Zhao, M.; Lei, Z.; Zhang, F. *Angew. Chem., Int. Ed.* **2018**, *57*, 7483.

(159) De los Reyes-Berbel, E.; Salto-Gonzalez, R.; Ortega-Munoz, M.; Reche-Perez, F. J.; Jodar-Reyes, A. B.; Hernandez-Mateo, F.; Giron-Gonzalez, M. D.; Santoyo-Gonzalez, F. *Bioconjugate Chem.* **2018**, *29*, 2561.

(160) Chen, Y.; Agarwal, S.; Shaik, N. M.; Chen, C.; Yang, Z.; Elmquist, W. F. *J. Pharmacol. Exp. Ther.* **2009**, *330*, 956.

(161) Lagas, J. S.; van Waterschoot, R. A. B.; van Tilburg, V. A. C. J.; Hillebrand, M. J.; Lankheet, N.; Rosing, H.; Beijnen, J. H.; Schinkel, A. H. *Clin. Cancer Res.* **2009**, *15*, 2344.

(162) Agarwal, S.; Mittapalli, R. K.; Zellmer, D. M.; Gallardo, J. L.; Donelson, R.; Seiler, C.; Decker, S. A.; SantaCruz, K. S.; Pokorny, J. L.; Sarkaria, J. N.; Elmquist, W. F.; Ohlfest, J. R. *Mol. Cancer Ther.* **2012**, *11*, 2183.

(163) Schiff, D.; Sarkaria, J. *Neuro Oncol* **2015**, *17*, 910.

(164) De Witt Hamer, P. C. *Neuro-Oncology* **2010**, *12*, 304.

(165) Peters, J.-U. *J. Med. Chem.* **2013**, *56*, 8955.

(166) Reddy, A. S.; Zhang, S. *Expert Rev. Clin. Pharmacol.* **2013**, *6*, 41.

(167) Anighoro, A.; Bajorath, J.; Rastelli, G. *J. Med. Chem.* **2014**, *57*, 7874.

(168) Wong, S.-F. *J. Hematol. Oncol.* **2009**, *2*, No pp given.

(169) Conchon, M.; de Moura Freitas, C. M. B.; Rego, M. A. d. C.; Braga Junior, J. W. R. *Rev. Bras. Hematol. Hemoter.* **2011**, *33*, 131.

(170) Usama, S. M.; Zhao, B.; Burgess, K. *Bioconjugate Chem.* **2019**, accepted.

(171) Kamkaew, A.; Li, F.; Li, Z.; Burgess, K. *MedChemComm* **2017**, *8*, 1946.

(172) Voon, S. H.; Tiew, S. X.; Kue, C. S.; Lee, H. B.; Kiew, L. V.; Misran, M.; Kamkaew, A.; Burgess, K.; Chung, L. Y. *J. Biomed. Nanotech.* **2016**, *12*, 1431.

(173) Getlik, M.; Gruetter, C.; Simard, J. R.; Kluter, S.; Rabiller, M.; Rode, H. B.; Robubi, A.; Rauh, D. *J. Med. Chem.* **2009**, *52*, 3915.

(174) Tokarski, J. S.; Newitt, J. A.; Chang, C. Y. J.; Cheng, J. D.; Wittekind, M.; Kiefer, S. E.; Kish, K.; Lee, F. Y. F.; Borzillerri, R.; Lombardo, L. J.; Xie, D.; Zhang, Y.; Klei, H. E. *Cancer Res.* **2006**, *66*, 5790.

(175) Williams, N. K.; Lucet, I. S.; Klinken, S. P.; Ingley, E.; Rossjohn, J. *J. Biol. Chem.* **2009**, *284*, 284.

(176) Chang, A. Y.; Wang, M. *BMC Cancer* **2013**, *13*, 267.

(177) Finn, R. S.; Aleshin, A.; Dering, J.; Yang, P.; Ginther, C.; Desai, A.; Zhao, D.; von Euw, E.; Busuttil, R. W.; Slamon, D. J. *Hepatology* **2013**, *57*, 1838.

(178) Choy, C. J.; Ling, X.; Geruntho, J. J.; Beyer, S. K.; Latoche, J. D.; Langton-Webster, B.; Anderson, C. J.; Berkman, C. E. *Theranostics* **2017**, *7*, 1928.

(179) Huang, W.-C.; Hsieh, Y.-L.; Hung, C.-M.; Chien, P.-H.; Chien, Y.-F.; Chen, L.-C.; Tu, C.-Y.; Chen, C.-H.; Hsu, S.-C.; Lin, Y.-M.; Chen, Y.-J. *PLoS One* **2013**, *8*, e83627/1.

(180) Shao, J.; Markowitz, J. S.; Bei, D.; An, G. *J. Pharm. Sci.* **2014**, *103*, 3810.

(181) D'Cunha, R.; Bae, S.; Murry, D. J.; An, G. *Biopharm. Drug Dispos.* **2016**, *37*, 397.

(182) Deng, J.; Shao, J.; Markowitz, J. S.; An, G. *Pharm. Res.* **2014**, *31*, 2237.

(183) Engel, J.; Lategahn, J.; Rauh, D. *ACS Med. Chem. Lett.* **2016**, *7*, 2.

(184) Kwarcinski, F. E.; Fox, C. C.; Steffey, M. E.; Soellner, M. B. *ACS Chem. Biol.* **2012**, *7*, 1910.

(185) Gonzalez-Bello, C. *ChemMedChem* **2016**, *11*, 22.

(186) Weisner, J.; Gontla, R.; van der Westhuizen, L.; Oeck, S.; Ketzer, J.; Janning, P.; Richters, A.; Muehlenberg, T.; Fang, Z.; Taher, A.; Jendrossek, V.; Pelly, S. C.; Bauer, S.; van Otterlo, W. A. L.; Rauh, D. *Angew. Chem., Int. Ed.* **2015**, *54*, 10313.

(187) Wu, P.; Clausen, M. H.; Nielsen, T. E. *Pharmacol. Ther.* **2015**, *156*, 59.

(188) Ormond, A. B.; Freeman, H. S. *Materials* **2013**, *6*, 817.

(189) Celli, J. P.; Spring, B. Q.; Rizvi, I.; Evans, C. L.; Samkoe, K. S.; Verma, S.; Pogue, B. W.; Hasan, T. *Chem. Rev.* **2010**, *110*, 2795.

(190) Foote, C. S. *Photochem. Photobiol.* **1991**, *54*, 659.

(191) Plaetzer, K.; Krammer, B.; Berlanda, J.; Berr, F.; Kiesslich, T. *Lasers Med Sci* **2009**, *24*, 259.

(192) Pedersen, B. W.; Sinks, L. E.; Breitenbach, T.; Schack, N. B.; Vinogradov, S. A.; Ogilby, P. R. *Photochem. Photobiol.* **2011**, *87*, 1077.

(193) Ogilby, P. R. *Chem. Soc. Rev.* **2010**, *39*, 3181.

(194) Schweitzer, C.; Schmidt, R. *Chem. Rev.* **2003**, *103*, 1685.

(195) da Silva, E. F. F.; Pedersen, B. W.; Breitenbach, T.; Toftegaard, R.; Kuimova, M. K.; Arnaut, L. G.; Ogilby, P. R. *J. Phys. Chem. B* **2012**, *116*, 445.

(196) Usama, S. M.; Thavornpradit, S.; Burgess, K. *ACS Appl. Bio Mater.* **2018**, *1*, 1195.

(197) Castano, A. P.; Demidova, T. N.; Hamblin, M. R. *Photodiag. Photodyn. Ther.* **2004**, *1*, 279.

(198) Zhu, T. C.; Finlay, J. C. *Med. Phys.* **2008**, *35*, 3127.

(199) Yoon, I.; Li Jia, Z.; Shim Young, K. *Clin. Endosc.* **2013**, *46*, 7.

(200) Patel, N.; Pera, P.; Joshi, P.; Dukh, M.; Tabaczynski, W. A.; Siters, K. E.; Kryman, M.; Cheruku, R. R.; Durrani, F.; Missert, J. R.; Watson, R.; Ohulchanskyy, T. Y.; Tracy, E. C.; Baumann, H.; Pandey, R. K. *J. Med. Chem.* **2016**, *59*, 9774.

(201) Santos, P. F.; Reis, L. V.; Almeida, P.; Oliveira, A. S.; Vieira Ferreira, L. F. *J. Photochem. Photobiol., A* **2003**, *160*, 159.

(202) Wezgowiec, J.; Kotulska, M.; Saczko, J.; Derylo, M. B.; Teissie, J.; Rols, M.-P.; Orio, J.; Garbiec, A.; Kulbacka, J. *Photodiagn. Photodyn. Ther.* **2013**, *10*, 490.

(203) Murakami, L. S.; Ferreira, L. P.; Santos, J. S.; da Silva, R. S.; Nomizo, A.; Kuz'min, V. A.; Borissevitch, I. E. *Biochim. Biophys. Acta, Gen. Subj.* **2015**, *1850*, 1150.

(204) James, N. S.; Ohulchanskyy, T. Y.; Chen, Y.; Joshi, P.; Zheng, X.; Goswami, L. N.; Pandey, R. K. *Theranostics* **2013**, *3*, 703.

(205) Camerin, M.; Jori, G.; Della Ciana, L.; Fabbroni, S.; Bonacchi, S.; Montalti, M.; Prodi, L. *Photochem. Photobiol. Sci.* **2009**, *8*, 1422.

(206) Santos, P. F.; Reis, L. V.; Almeida, P.; Serrano, J. P.; Oliveira, A. S.; Vieira Ferreira, L. F. *J. Photochem. Photobiol., A* **2004**, *163*, 267.

(207) Santos, P. F.; Reis, L. V.; Duarte, I.; Serrano, J. P.; Almeida, P.; Oliveira, A. S.; Ferreira, L. F. V. *Helv. Chim. Acta* **2005**, *88*, 1135.

(208) Pandey, R. K.; James, N.; Chen, Y.; Dobhal, M. P. *Top. Heterocycl. Chem.* **2008**, *14*, 41.

(209) Cardillo, J. A.; Jorge, R.; Costa, R. A.; Nunes, S. M. T.; Lavinsky, D.; Kuppermann, B. D.; Tedesco, A. C.; Farah, M. E. *Br. J. Ophthalmol.* **2008**, *92*, 276.

(210) Luo, S.; Tan, X.; Fang, S.; Wang, Y.; Liu, T.; Wang, X.; Yuan, Y.; Sun, H.; Qi, Q.; Shi, C. *Adv. Funct. Mater.* **2016**, *26*, 2826.

(211) Tan, X.; Luo, S.; Long, L.; Wang, Y.; Wang, D.; Fang, S.; Ouyang, Q.; Su, Y.; Cheng, T.; Shi, C. *Adv. Mater.* **2017**, *29*, 1704196.

(212) Atchison, J.; Kamila, S.; Nesbitt, H.; Logan, K. A.; Micholas, D. M.; Fowley, C.; Davis, J.; Callan, B.; McHale, A. P.; Callan, J. F. *Chem. Comm.* **2017**, *53*, 2009.

(213) Xi, R.; Zhang, J.; Zhang, Y.; Li, S.; Li, Y.; Li, X.; Chen, L.; Li, C. *RSC Adv.* **2016**, *6*, 68220.

(214) van Straten, D.; Mashayekhi, V.; Oliveira, S.; de Bruijn Henriette, S.; Robinson Dominic, J.; Oliveira, S. *Cancers* **2017**, *9*, 19.

(215) Henary, M.; Levitz, A. *Dyes Pigm.* **2013**, *99*, 1107.

(216) Gorman, A.; Killoran, J.; O'Shea, C.; Kenna, T.; Gallagher, W. M.; O'Shea, D. F. *J. Am. Chem. Soc.* **2004**, *126*, 10619.

(217) Flanagan, J. H., Jr.; Khan, S. H.; Menchen, S.; Soper, S. A.; Hammer, R. P. *Bioconjugate Chem.* **1997**, *8*, 751.

(218) Li, X.; Fu, Y.; Ma, L.; Wang, Z.; Zhang, H. *Chem. Res. Chin. Univ.* **2016**, *32*, 343.

(219) Mottram, L. F.; Boonyarattanakalin, S.; Kovel, R. E.; Peterson, B. R. *Org. Lett.* **2006**, *8*, 581.

(220) Tian, J.; Zhou, J.; Shen, Z.; Ding, L.; Yu, J.-S.; Ju, H. *Chem. Sci.* **2015**, *6*, 5969.

(221) Minko, T.; Dharap, S. S.; Pakunlu, R. I.; Wang, Y. *Curr. Drug Targets* **2004**, *5*, 389.

(222) Mrdenovic, S.; Mrdenovic, S.; Wang, R.; Yin, L.; Chu, G. C.-Y.; Yin, L.; Zhau Haiyen, E.; Chung Leland, W. K.; Zhang, Y.; Lewis, M.; Heffer, M. *Cancer* **2019**.

(223) Zhang, C.; Tan, X.; Tan, L.; Liu, T.; Liu, D.; Zhang, L.; Fan, S.; Su, Y.; Cheng, T.; Zhou, Y.; Shi, C. *Cell Transplant* **2011**, *20*, 741.

(224) Tang, Q.; Liu, W.; Zhang, Q.; Huang, J.; Hu, C.; Liu, Y.; Wang, Q.; Zhou, M.; Lai, W.; Sheng, F.; Li, G.; Zhang, R. *J. Cell. Mol. Med.* **2018**, 1.

(225) Lv, Q.; Wang, D.; Yang, Z.; Yang, J.; Zhang, R.; Yang, X.; Wang, M.; Wang, Y. *Biomater. Sci.* **2019**, *7*, 296.

(226) Zhang, C.; Zhao, Y.; Zhao, N.; Tan, D.; Zhang, H.; Chen, X.; Zhang, H.; An, J.; Shi, C.; Li, M. *Contrast Media Mol. Imaging* **2018**, 4979746/1.

(227) Xiao, L.; Zhang, Y.; Yue, W.; Xie, X.; Wang, J.-p.; Chordia, M. D.; Chung, L. W. K.; Pan, D. *Nucl. Med. Biol.* **2013**, 351.

(228) Shi, C.; Wu, J. B.; Chu, G. C. Y.; Li, Q.; Wang, R.; Zhau, H. E.; Chung, L. W. K.; Zhang, C.; Zhang, Y.; Pan, D.; Kim, H. L.; Wang, J. *Oncotarget* **2014**, 10114.

(229) Canovas, C.; Bellaye, P.-S.; Moreau, M.; Romieu, A.; Denat, F.; Goncalves, V. *Org. Biomol. Chem.* **2018**, *16*, 8831.

(230) Thavornpradit, S.; Usama, S. M.; Shrestha, J.; Park, G. K.; Choi, H. S.; Burgess, K. *Theranostics* **2019**, *9*, 2856.

(231) Harrison, V. S. R.; Carney, C. E.; MacRenaris, K. W.; Waters, E. A.; Meade, T. J. *J. Am. Chem. Soc.* **2015**, *137*, 9108.

(232) Baker, K. J.; Bradley, S. E. *J. Clin. Invest.* **1966**, *43*, 281.

(233) Wolkoff, A. W. *Hepatology* **1987**, *7*, 777.

(234) Pfaff, E.; Schwenk, M.; Burr, R.; Remmer, H. *Mol. Pharmacol.* **1975**, *11*, 144.

(235) Onoe, S.; Temma, T.; Shimizu, Y.; Ono, M.; Saji, H. *Cancer Med.* **2014**, *3*, 775.

(236) Poor, M.; Kunsagi-Mate, S.; Czibulya, Z.; Li, Y.; Peles-Lemli, B.; Petrik, J.; Vladimir-Knezevic, S.; Koszegi, T. *Luminescence* **2013**, *28*, 726.

(237) Lee, H.; Mason, J. C.; Achilefu, S. *J. Org. Chem.* **2006**, *71*, 7862.

APPENDIX A

SUPPORTING INFORMATION FOR CHAPTER II

General Experimental Procedures: All reactions were carried out under an inert atmosphere (nitrogen or argon where stated) with dry solvents under anhydrous conditions. Glassware for anhydrous reactions was dried in an oven at 140 ºC for minimum 6 h prior to use. Dry solvents were obtained by passing the previously degassed solvents through activated alumina columns. Yields refer to chromatographically and spectroscopically (1H-NMR) homogeneous materials, unless otherwise stated. Reagents were purchased at a high commercial quality (typically 97 % or higher) and used without further purification, unless otherwise stated. Analytical thin layer chromatography (TLC) was carried out on Merck silica gel plates with QF-254 indicator and visualized by UV. Flash column chromatography was performed using silica gel 60 (Silicycle, 230-400 mesh). ^{1}H and ^{13}C spectra were recorded on a 400 MHz spectrometer and were calibrated using residual non-deuterated solvent as an internal reference. Detailed synthesis information is provided in supporting materials. The abbreviations or combinations in the supporting materials thereof were used to explain the multiplicities: s = singlet, d = doublet, t = triplet, q = quartet, m = multiplet, dd = doublet of doublet, ddd = doublet of doublet of doublets.

In-Vitro Assays: NIH3T3-WT cells (from American Type Culture Collection) were cultured on 75 cm^2 culture flasks in Dulbecco's Modified Eagle Medium/nutrient mixture F-12 (DMEM/F12, Sigma Chemical, St. Louis, MO) supplemented with 10 % FBS. NIH3T3-TrkC cells were obtained and cultured. Cells were cultured in a humidified incubator at 37 °C with 5 % CO2 and 95 % air.

Fluorescence Microscopy: Intracellular localization of the NIH3T3 cells was measured using Olympus Fluoview FV1000. The images were taken at 60x/1.20 water immersed objective. Lysosome, Mitochondria and Nucleus were stained using Lysotracker Green DND 26, Mitotracker Green FM and, NucBlue respectively were bought from Life Technologies. 488 nm laser was used for green channel, 405 nm laser was used for nucleus and 633 nm laser was used for compound 1 and 2. Rest of the fluorescence images were taken using Evos FL Imaging System (Thermofisher) at 10x/0.4.

Intracellular localization: Briefly, 50,000 cells were seeded on 4 well chambers (Nunc Lab-Tek) and allowed to adhere overnight. The cells were incubated with 20 μM of compound 1 and 2 for 30 mins, washed twice with PBS, incubated with organelle stains according to manufacturer's instructions. The cells were washed twice again and stained with NucBlue for 10 mins

Histology on patient's tissues: Slide of human malignant melanoma tissue microarray (BR243w) was purchased from US Biomax, Inc., the array includes 13 cases of malignant melanoma and 12 cases of adjacent normal cells. The slide was transferred to a xylene bath for 10 min and then rehydrated in two changes of fresh absolute ethanol for 7 min each. Excess liquid was shaken off and the slide was incubated in fresh 90%, 70 % ethanol then water for 7 min each. The slide was washed in two changed of PBS for 5 min each, then incubated with PBS containing 4 % BSA for 30 min. The tissues were rinsed with PBS and incubated again in two changed of PBS for 5 min each. Compound 1 solution in 4 % PBS/BSA was added to the slide and incubated overnight at 4 ^{o}C. The slide was rinsed twice in PBS, then in water (10 min each). Then the slide contained 1 was mounted in permanent mounting media with DAPI (Vector) and incubated at 4 ^{o}C for 4 h. The tissues were imaged with an Evos FL Imaging System. Throughout, digital images were captured with a 20x/ 0.45 excitation at 730 nm for 1 and 405 nm for DAPI.

Animal model: Murine breast cancer 4T1 cells were obtained from American Type Culture Collection and cultured as protocol suggested, *i.e.* in Dulbecco's modified Eagle medium (DMEM) supplemented with 10% fetal bovine serum (FBS) at 37 ^{o}C in humidified atmosphere with 5% CO_2. Upon 80% confluence, cells were collected and suspended into PBS, and then subcutaneously injected into 6 weeks BALB/c nu/nu mouse (Charles River) at 2 x 10^6 cells per 100 µL per mouse. Then mice were fed for two weeks to allow tumor growth reaching to 8-10 mm for the imaging study. Animals were handled according to a protocol approved by Houston Methodist Research Institute Animal Care and Use Committee.

***In vivo* and *ex vivo* fluorescence imaging:** The fluorescence imaging was performed using IVIS200 imaging system, and quantified the ROI study by Living Imaging software (Xenogen, CA). Excitation and emission filters were set at 745 nm and 800 nm, respectively, for imaging acquisition. For injection, the synthesized agent was firstly prepared as 1 mM stock solution in DMSO, and then diluted into 10 nmol per 100 μL in PBS for each mouse. Upon intravenous injection via tail vein, the mice (3 per group) were anesthetized to allow imaging acquisition accomplished. As to *ex vivo* imaging, mice (3 per group) were euthanized as animal protocol described at various time points after injection of the targeting agent, and internal organs (*i.e.* heart, lung, liver, kidney, spleen, gestrointestine, tumor, muscle, brain, spinal cord) were collected for *ex vivo* imaging acquisition. Upon the imaging acquisition, ROI analysis and quantification of the fluorescence signals were performed with Living Imaging software.

All reactions were carried out under an argon atmosphere. Reagents were purchased at a high commercial quality (typically 97 % or higher) and used without further purification, unless otherwise stated. High field NMR spectra were recorded with Bruker Avance III at 400 MHz for ^{1}H, and 100 MHz for ^{13}C and were calibrated using residual non-deuterated solvent as an internal reference ($CDCl_3$: ^{1}H NMR = 7.24, ^{13}C NMR = 77.0, MeOD: ^{1}H NMR = 3.30, ^{13}C NMR = 49.0, DMSO-d_6: ^{1}H NMR = 2.50, ^{13}C NMR = 39.5). The following abbreviations were used to explain the multiplicities: s = singlet, d = doublet, t = triplet, q = quartet, quint = quintet, dd = double doublet, dt = double triplet, dq = double quartet, m = multiplet, br = broad. Electrospray ionization mass spectrometry (ESI-MS) data were collected on triple-stage quadrupole instrument in a positive mode. Flash chromatography was performed using silica gel (230-400 mesh).

LC-MS analyses were collected from Agilent 1260 Infinity Quaternary LC and Agilent 6120 Quadrupole LC/MS modules using Poroshell 120 EC-C18 2.7 µM (4.6 x 50 mm) column in 5-95% CH_3CN/water gradient with 0.1% formic acid over 10 minutes. Prep HPLC was performed on Agilent 1260 Infinity in 50-90 CH_3CN/water gradient with 0.1% TFA over 20 mins. All statistical analyses were carried out by Graphpad Prism version 6.0 (Graphpad Software

General Experimental Procedures

Synthesis of 1 and 2

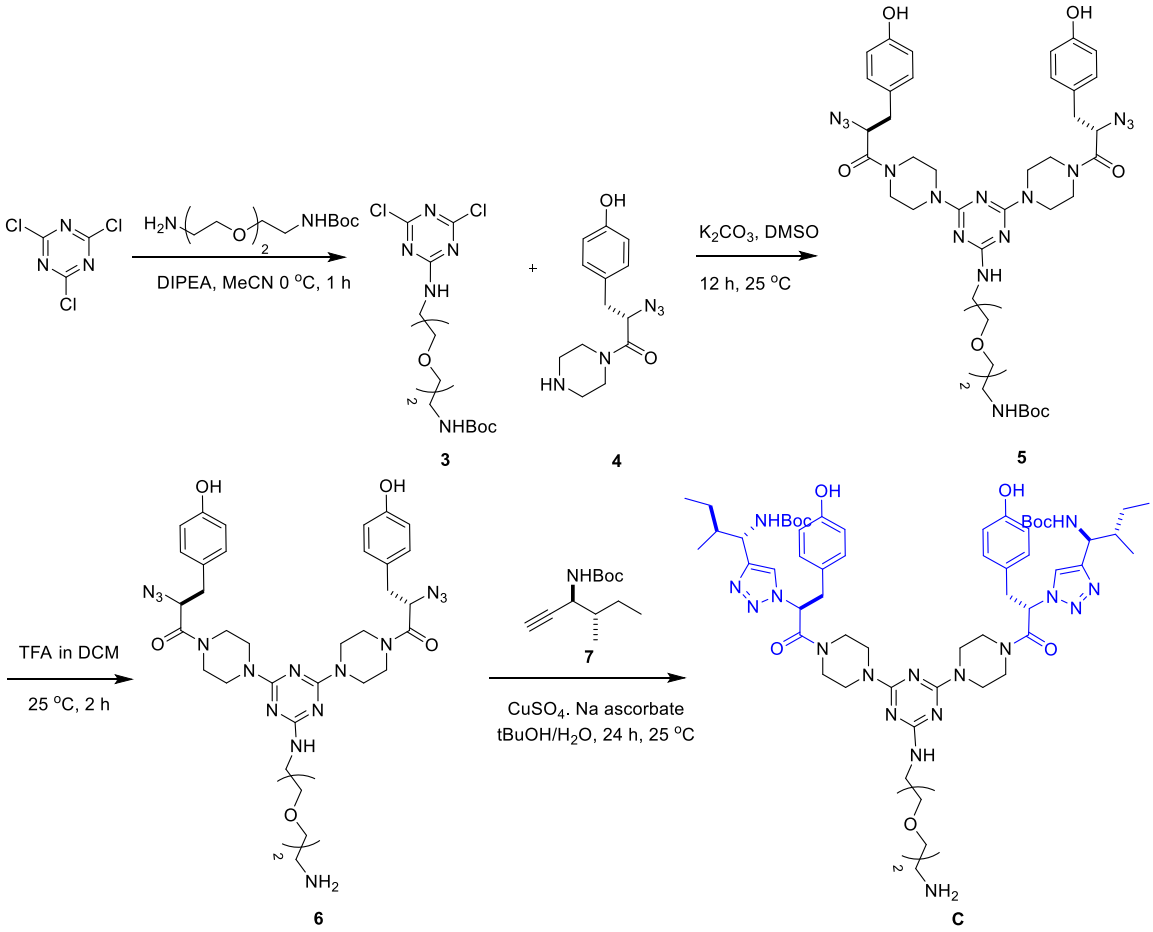

Scheme A-S1. Synthesis of IY-IY Fragment (**C**)

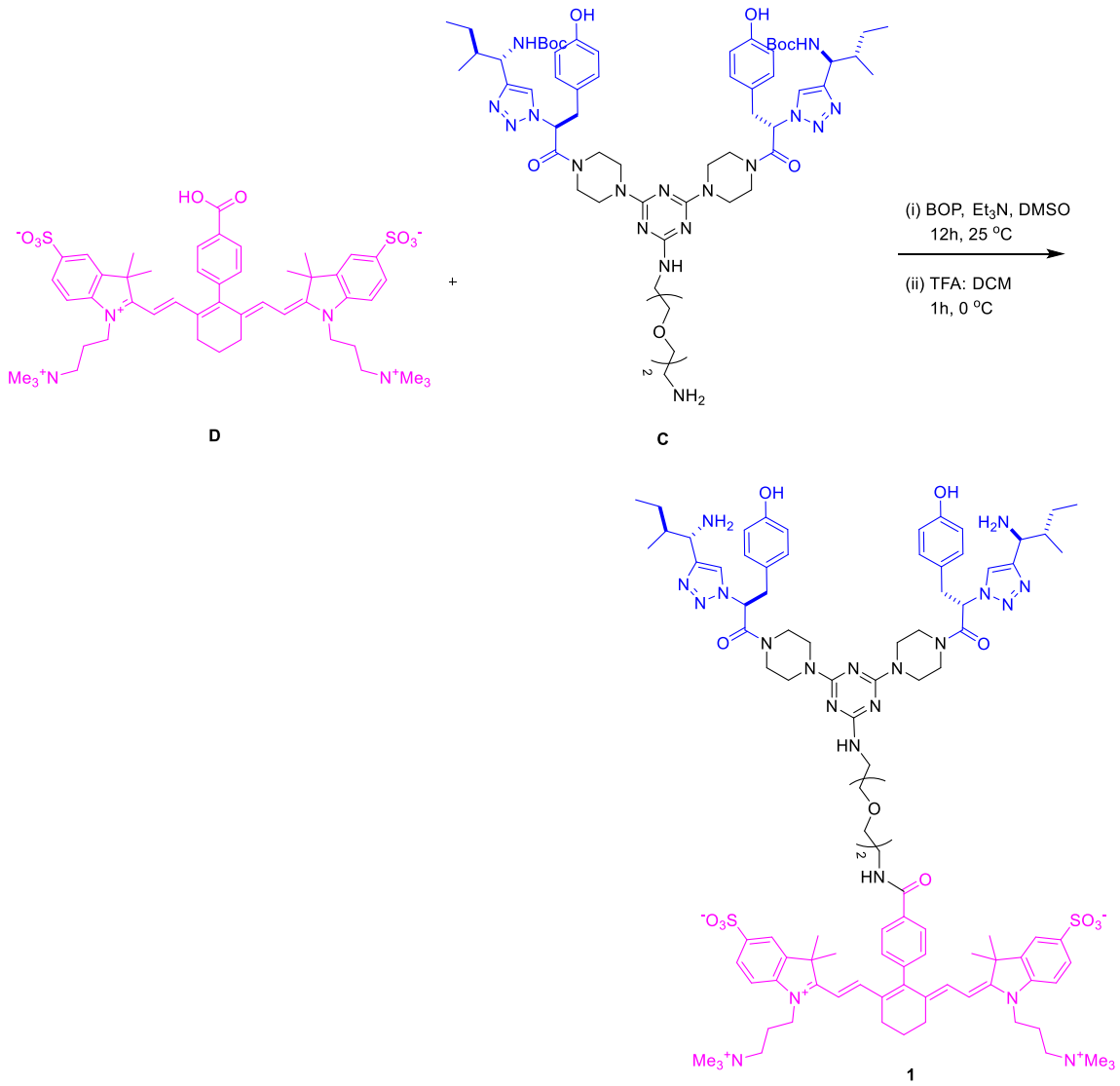

Scheme A-S2. Synthesis of **1**

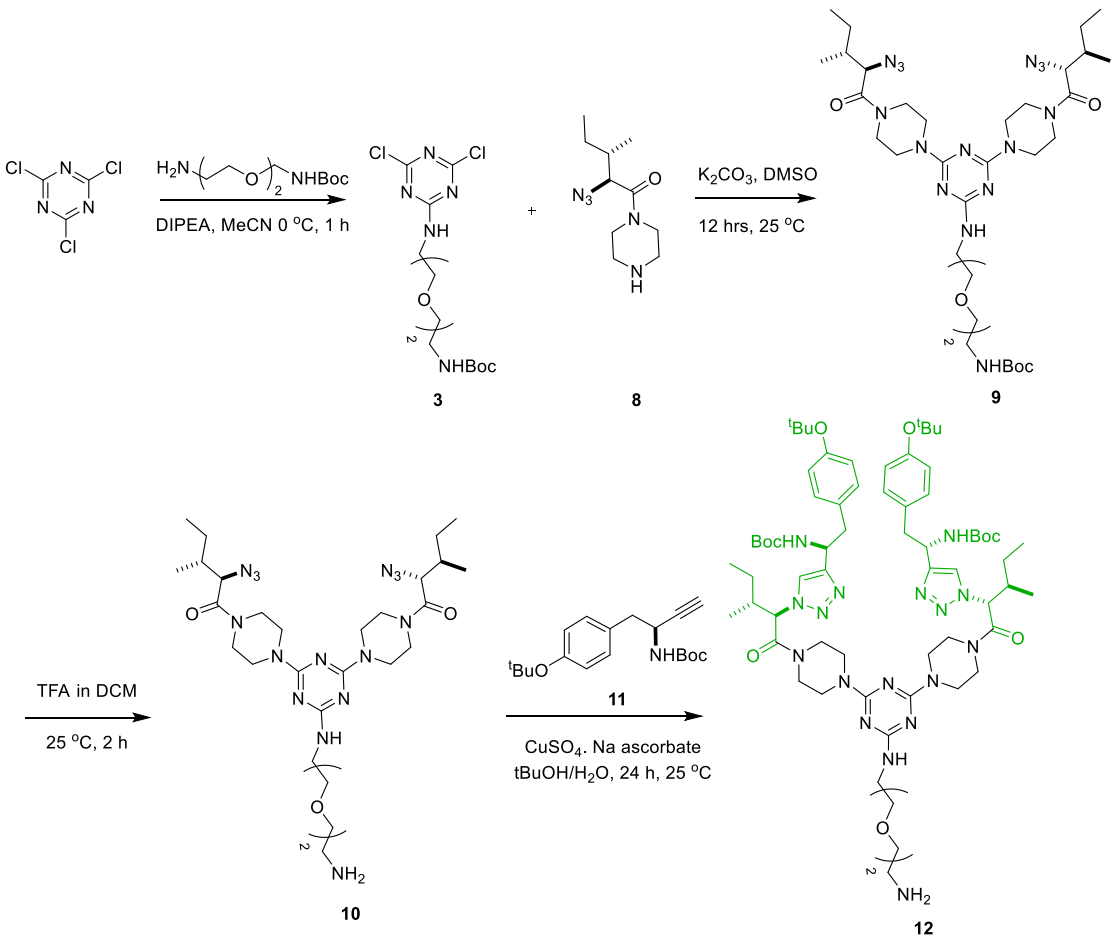

Scheme A-S3. Synthesis of YI-YI Fragment (**12**)

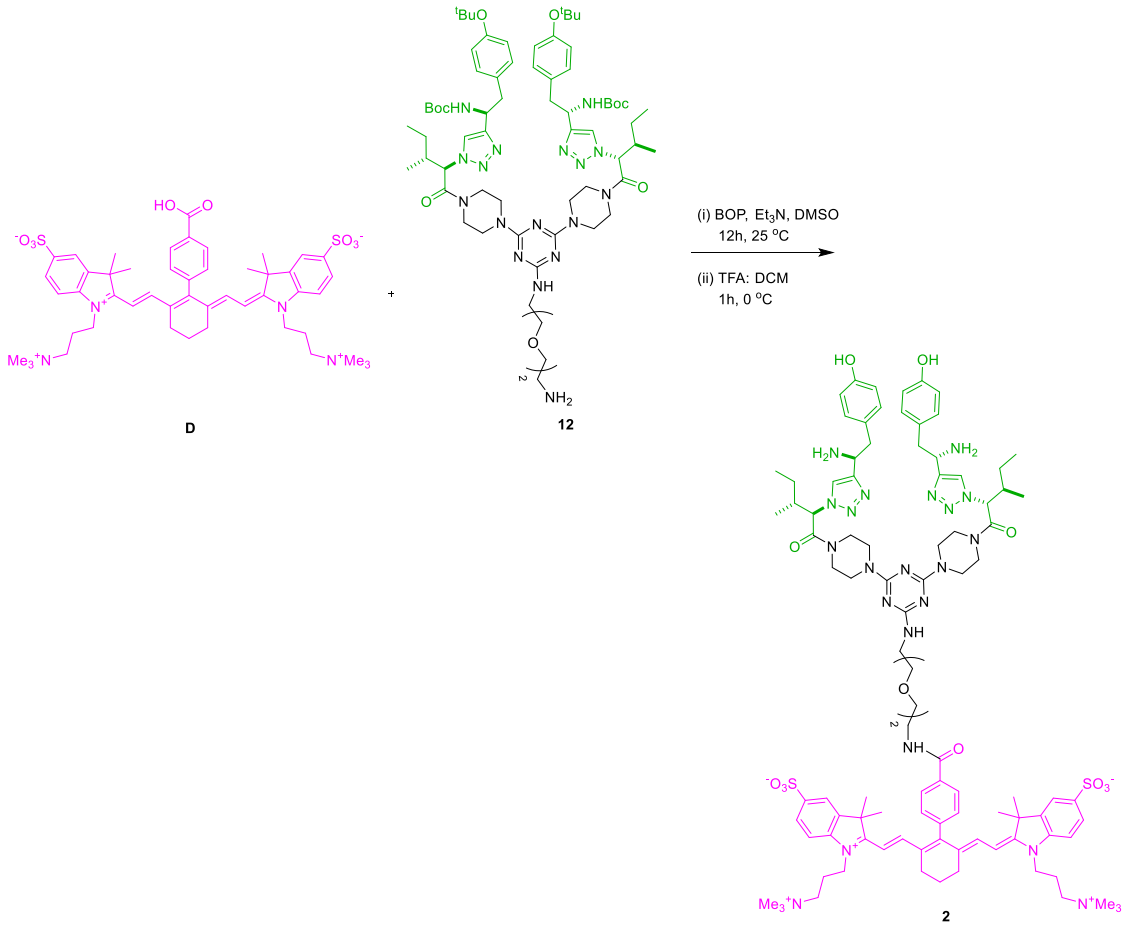

Scheme A-S4. Synthesis of **2**

Synthesis Procedure

Synthesis of C:

Compound **4, 7 8, 11** were synthesized according to previous procedure[1].

Synthesis of *tert-butyl (2-(2-(2-((4,6-dichloro-1,3,5-triazin-2-yl)amino)ethoxy)ethoxy)ethyl)carbamate* (**3**)

At 0 ^{o}C, N-Boc- 2,2′-(ethylenedioxy)diethylamine (218.5 mg) and cynuric chloride (162.1 mg) were added together followed by DIPEA (306.5 uL) and stirred for 1 hr. Progress of reaction was monitored by TLC. After completion of reaction, the solvent was revomed under vacuum. The crude was taken to next step without further purification.

LRMS (ESI-) m/z calcd for $C_{14}H_{23}Cl_2N_5O_4$ $(M+H)^+$ 396.1; found 396.7

Synthesis of *tert-butyl (2-(2-(2-((4,6-bis(4-((S)-2-azido-3-(4-hydroxyphenyl)propanoyl)piperazin-1-yl)-1,3,5-triazin-2-yl)amino)ethoxy)ethoxy)ethyl)carbamate* (5)

3 (0.88, 348.48), **4** (586.1 mg) and K_2CO_3 (364.8 mg) were add together in DMSO (10mL) and stirred at room temperature for 24 h. . Progress of reaction was monitored by TLC. After completion of reaction, the solvent was removed. The crude was taken to next step without further purification.

LRMS (ESI+) m/z calcd for $C_{40}H_{55}N_{15}O_8$ $(M+H)^+$ 874.4; found 874.4

Synthesis of (2S,2'S)-1,1'-((6-((2-(2-(2-aminoethoxy)ethoxy)ethyl)amino)-1,3,5-triazine-2,4-diyl)bis(piperazine-4,1-diyl))bis(2-azido-3-(4-hydroxyphenyl)propan-1-one) (6)

TFA:DCM (1:1, 10 mL) was added to crude **5** and stirred for 1.5 h. Progress of reaction was monitored by TLC. After completion of reaction, the solvent was removed.

LRMS (ESI+) m/z calcd for $C_{35}H_{47}N_{15}O_6$ $(M+H)^+$ 774.3; found 774.4.

Synthesis of di-tert-butyl ((1S,1'S,2S,2'S)-(((2S,2'S)-((6-((2-(2-(2-aminoethoxy)ethoxy)ethyl)amino)-1,3,5-triazine-2,4-diyl)bis(piperazine-4,1-diyl))bis(3-(4-hydroxyphenyl)-1-oxopropane-1,2-diyl))bis(1H-1,2,3-triazole-1,4-diyl))bis(2-methylbutane-1,1-diyl))dicarbamate (C)

Under inert atmosphere **6** (680.24 mg) and **7** (223.1 mg) were dissolved in tBuOH:H_2O (1:1, 5 mL), followed by $CuSO_4$ (44 mg) and Na ascorbate (139.46 mg). The reaction was stirred for 24 hrs at room temperature. The solvent was removed and the crude was purified by prep HPLC (280 mg, 32%).

^{1}H NMR (400 MHz, MeOD) δ 8.00 (s, 2H), 7.03 (d, *J* = 8.4 Hz, 4H), 6.70 (dd, *J* = 8.4, 3.7 Hz, 4H), 6.07 (t, *J* = 7.7 Hz, 2H), 3.69 (qd, *J* = 10.5, 4.5 Hz, 18H), 3.56 – 3.38 (m, 7H), 3.14 (d, *J* = 4.9 Hz, 2H), 1.90 – 1.77 (m, 2H), 1.44 (d, *J* = 4.3 Hz, 18H), 1.10 (ddd, *J* = 35.2, 14.8, 7.4 Hz, 2H), 0.96 – 0.85 (m, 7H), 0.81 (d, *J* = 6.8 Hz, 5H).

^{13}C NMR (101 MHz, MeOD) δ 167.03, 156.74, 156.52, 156.39, 148.46, 130.19, 125.67, 121.69, 117.68, 115.15, 114.79, 78.99, 69.96, 69.95, 68.54, 66.50, 60.55, 51.88, 44.90, 43.30, 41.69, 40.38, 39.26, 39.08, 37.61, 27.79, 27.38, 25.72, 24.87, 14.57, 13.75, 10.40, 10.23.

HRMS (ESI+) m/z calcd for $C_{59}H_{89}N_{17}O_{10}$ $(M+H)^+$ 1196.6978; found 1196.6959.

Synthesis of 10

Synthesis of *tert-butyl (2-(2-(2-((4,6-bis(4-((2R,3R)-2-azido-3-methylpentanoyl)piperazin-1-yl)-1,3,5-triazin-2-yl)amino)ethoxy)ethoxy)ethyl)carbamate* (9)

1 (645.48 mg), **8** (881.35 mg) and K_2CO_3 (675.79 mg) were add together in DMSO (10 mL)and stirred at room temperature for 24h. . Progress of reaction was monitored by TLC. After completion of reaction, the solvent was removed. The crude was taken to next step without further purification.

LRMS (ESI+) m/z calcd for $C_{34}H_{59}N_{15}O_6$ $(M+H)^+$ 774.4; found 774.4

Synthesis of (2R,2'R,3R,3'R)-1,1'-((6-((2-(2-(2-aminoethoxy)ethoxy)ethyl)amino)-1,3,5-triazine-2,4-diyl)bis(piperazine-4,1-diyl))bis(2-azido-3-methylpentan-1-one) (10)

TFA:DCM (1:1, 10 mL) was added to crude **9** and stirred for 1.5 h. Progress of reaction was monitored by TLC. After completion of reaction, the solvent was removed.

LRMS (ESI+) m/z calcd for $C_{29}H_{51}N_{15}O_4$ $(M+H)^+$ 674.4; found 674.4.

Synthesis of di-tert-butyl ((1S,1'S)-(((2R,2'R,3R,3'R)-((6-((2-(2-(2-aminoethoxy)ethoxy)ethyl)amino)-1,3,5-triazine-2,4-diyl)bis(piperazine-4,1-diyl))bis(3-methyl-1-oxopentane-1,2-diyl))bis(1H-1,2,3-triazole-1,4-diyl))bis(2-(4-(tert-butoxy)phenyl)ethane-1,1-diyl))dicarbamate (12)

Under inert atmosphere **10** (771.73 mg) and **11** (452.3 mg) were dissolved in tBuOH:H_2O (1:1, 5 mL), followed by $CuSO_4$ (57.5 mg) and Na ascorbate (184.24 mg). The reaction was stirred for 24 hrs at room temperature. The solvent was removed and the crude was purified by prep HPLC (560 mg, 55%).

^{1}H-NMR (400 MHz, D_2O:CD_3CN (7:3)) δ 7.88 (s, 2H), 7.08 (d, *J* = 8.4 Hz, 4H), 6.85 (d, *J* = 8.4 Hz, 4H), 5.62 (d, *J* = 10.2 Hz, 2H), 5.02 (t, *J* = 7.3 Hz, 3H), 4.06 (s, 3H), 3.89 (s, 7H), 3.72 – 3.59 (m, 10H), 3.56 (s, 4H), 3.33 (dt, *J* = 3.3, 1.6 Hz, 4H), 3.21 – 3.09 (m, 4H), 3.08 – 2.98 (m, 1H), 2.40 (d, *J* = 3.6 Hz, 2H), 1.38 (s, 20H), 1.29 (s, 18H), 1.04 (d, *J* = 6.6 Hz, 10H), 0.88 (d, *J* = 7.0 Hz, 5H).

^{13}C-NMR (101 MHz, D_2O:CD_3CN (7:3)) 7.88, 7.09, 7.07, 6.86, 6.84, 5.63, 5.60, 5.04, 5.02, 5.00, 4.06, 3.89, 3.74, 3.73, 3.71, 3.70, 3.68, 3.56, 3.34, 3.33, 3.33, 3.33, 3.32, 3.20, 3.19, 3.17, 3.15, 3.15, 3.13, 3.09, 3.07, 3.06, 3.04, 1.38, 1.29, 1.05, 1.03, 0.89, 0.87.

HRMS (ESI+) m/z calcd for $C_{67}H_{105}N_{17}O_{10}$ $(M+H)^+$ 1308.8230; found 1308.8259

Synthesis of 1 and 2:

Synthesis of **D** was done as reported in literature[2].

^{1}H NMR (400 MHz, D_2O) δ 8.52 (d, *J* = 7.8 Hz, 2H), 8.30 (d, *J* = 8.2 Hz, 1H), 8.17 (d, *J* = 8.2 Hz, 1H), 8.00 (d, *J* = 8.2 Hz, 3H), 7.94 (s, 2H), 7.49 (s, 1H), 7.35 (s, 3H), 6.43 (s, 1H), 4.19 (s, 4H), 3.71 – 3.62 (m, 4H), 3.35 (s, 21H), 2.99 (d, *J* = 19.6 Hz, 3H), 2.50 – 2.33 (m, 6H), 1.32 (s, 12H)

^{13}C NMR (101 MHz, D_2O) δ 172.78, 169.04, 149.06, 143.47, 140.99, 134.31, 133.45, 130.90, 130.42, 129.89, 129.11, 127.29, 120.08, 119.28, 110.87, 101.17, 63.35, 53.40, 48.78, 40.84, 27.22, 24.61, 21.08

LRMS (ESI+) m/z calcd for $C_{49}H_{63}N_4O_8S_2^+$ 899.4; found 900.6.

Synthesis of 2-((E)-2-((E)-4'-((2-(2-(2-((4,6-bis(4-((S)-2-(4-((1S,2S)-1-amino-2-methylbutyl)-1H-1,2,3-triazol-1-yl)-3-(4-hydroxyphenyl)propanoyl)piperazin-1-yl)-1,3,5-triazin-2-yl)amino)ethoxy)ethoxy)ethyl)carbamoyl)-6-(2-((E)-3,3-dimethyl-5-sulfonato-1-(3-(trimethylammonio)propyl)indolin-2-ylidene)ethylidene)-3,4,5,6-tetrahydro-[1,1'-biphenyl]-2-yl)vinyl)-3,3-dimethyl-1-(3-(trimethylammonio)propyl)-3H-indol-1-ium-5-sulfonate (1)

BOP (22 mg), **C** (38 mg)**, D** (30 mg) Et_3N were added in 1 mL DMSO and stirred for 12 hr. After removal of DMSO. The crude was cooled on ice for 10 mins. TFA:DCM (1:1, 1 mL) was added to the mixture and stirred for 1 hr. Solvent was removed on vacuum and purified by reverse phase prep HPLC. (40 mg, 60%).

^{1}H-NMR (400 MHz, D_2O:CD_3CN (7:3)) δ 8.43 (d, *J* = 15.4 Hz, 3H), 8.28 (d, *J* = 8.7 Hz, 2H), 8.15 – 8.03 (m, 3H), 7.90 – 7.82 (m, 3H), 7.62 – 7.39 (m, 6H), 7.29 (d, *J* = 8.2 Hz, 6H), 6.97 (s, 5H), 6.37 (d, *J* = 44.0 Hz, 5H), 3.72 (tdd, *J* = 31.9, 20.7, 11.9 Hz, 34H), 3.31 (s, 18H), 2.91 (s, 3H), 2.66 (s, 2H), 2.42 (s, 4H), 2.28 – 2.17 (m, 7H), 2.05 – 1.80 (m, 6H), 1.68 (s, 3H), 1.54 (dt, *J* = 19.4, 7.8 Hz, 10H), 1.34 (s, 12H), 1.13 (s, 7H), 1.04 (d, *J* = 6.2 Hz, 10H).

^{13}C-NMR (101 MHz, D_2O:CD_3CN (7:3)) δ 185.11, 168.45, 167.65, 162.80, 162.46, 162.11, 161.76, 155.88, 155.46, 153.79, 146.04, 144.08, 142.16, 141.98, 130.93, 129.71, 127.81, 127.19, 126.14, 124.39, 121.18, 118.27, 115.86, 115.36, 114.84, 112.78, 112.46, 110.79, 63.41, 62.75, 61.21, 53.51, 53.34, 51.76, 48.80, 43.33, 40.86, 39.91, 39.20, 37.53, 37.39, 28.88, 27.22, 26.12, 25.81, 25.45, 24.67, 22.33, 21.06, 14.60, 13.65, 10.59, 10.32.

HRMS (ESI+) m/z calcd for $C_{67}H_{105}N_{17}O_{10}$ $(M+H)^+$ 1876.9906; found (M/2+H)+ 938.9998

Synthesis of 2-((E)-2-((E)-4'-((2-(2-(2-((4,6-bis(4-((2R,3R)-2-(4-((S)-1-amino-2-(4-hydroxyphenyl)ethyl)-1H-1,2,3-triazol-1-yl)-3-methylpentanoyl)piperazin-1-yl)-1,3,5-triazin-2-yl)amino)ethoxy)ethoxy)ethyl)carbamoyl)-6-(2-((E)-3,3-dimethyl-5-sulfonato-1-(3-(trimethylammonio)propyl)indolin-2-ylidene)ethylidene)-3,4,5,6-tetrahydro-[1,1'-biphenyl]-2-yl)vinyl)-3,3-dimethyl-1-(3-(trimethylammonio)propyl)-3H-indol-1-ium-5-sulfonate (2)

BOP (21.67 mg) , **12** (86.32 mg)**, D** (30 mg) Et_3N (6.83 uL) were added in 1 mL DMSO and stirred for 12 hr. After removal of DMSO. The crude was cooled on ice for 10 mins. TFA:DCM (1:1, 1 mL) was added to the mixture and stirred for 1 hr. Solvent was removed on vacuum and purified by reverse phase prep HPLC (35 mg, 56%).

^{1}H NMR (400 MHz, D_2O:CD_3CN (7:3)) δ 8.51 – 8.32 (m, 5H), 8.15 (dd, *J* = 33.1, 12.0 Hz, 3H), 8.03 (d, *J* = 16.6 Hz, 2H), 7.87 (s, 1H), 7.81 – 7.71 (m, 2H), 7.67 (s, 1H), 7.50 (s, 2H), 6.98 (d, *J* = 8.2 Hz, 5H), 6.72 (d, *J* = 14.7 Hz, 1H), 6.52 (d, *J* = 13.8 Hz, 1H), 5.89 (s, 2H), 5.12 (dd, *J* = 10.2, 5.5 Hz, 3H), 4.45 (d, *J* = 7.1 Hz, 2H), 4.25 (s, 3H), 4.14 – 3.81 (m, 30H), 3.83 – 3.68 (m, 6H), 3.66 (dd, *J* = 13.6, 5.4 Hz, 4H), 3.49 (dd, *J* = 25.1, 12.0 Hz, 5H), 3.47 – 3.37 (m, 18H), 3.35 – 3.25 (m, 4H), 3.28 (d, *J* = 6.3 Hz, 2H), 3.14 (s, 1H), 3.02 (s, 2H), 2.74 – 2.43 (m, 7H), 2.39 – 2.27 (m, 6H), 1.67 (d, *J* = 19.9 Hz, 2H), 1.64 – 1.57 (m, 3H), 1.54 (dd, *J* = 20.1, 10.0 Hz, 3H), 1.46 (d, *J* = 5.9 Hz, 6H), 1.36 (d, *J* = 17.5 Hz, 2H), 1.24 (dd, *J* = 19.6, 6.9 Hz, 13H), 1.11 – 1.01 (m, 5H).

^{13}C NMR (101 MHz, D_2O:CD_3CN (7:3)) δ 168.84, 167.56, 162.53, 162.18, 161.83, 161.48, 155.98, 155.66, 143.41, 141.92, 130.92, 129.60, 129.39, 128.02, 127.31, 126.56, 124.12, 121.21, 120.22, 115.75, 115.40, 112.49, 107.09, 70.10, 69.46, 68.78, 64.09,

63.50, 53.57, 53.44, 50.12, 49.43, 48.73, 44.04, 43.56, 40.60, 40.05, 37.92, 37.76, 27.37, 27.27, 27.03, 26.38, 24.44, 22.75, 21.19, 17.50, 14.95, 12.37, 10.26.

HRMS (ESI+) m/z calcd for $C_{67}H_{105}N_{17}O_{10}$ $(M+H)^+$ 1876.9906; found (M/2+H)+ 938.9980

Compound Characterization

2-((E)-2-((E)-4'-carboxy-6-(2-((E)-3,3-dimethyl-5-sulfonato-1-(3-(trimethylammonio)propyl)indolin-2-ylidene)ethylidene)-3,4,5,6-tetrahydro-[1,1'-biphenyl]-2-yl)vinyl)-3,3-dimethyl-1-(3-(trimethylammonio)propyl)-3H-indol-1-ium-5-sulfonate (D)

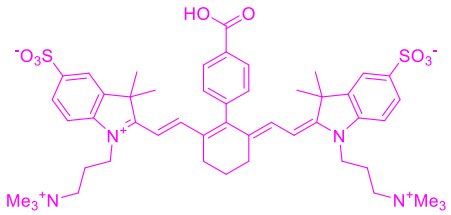

^{1}H NMR (deuterium oxide:acetonitrile-d$_3$)

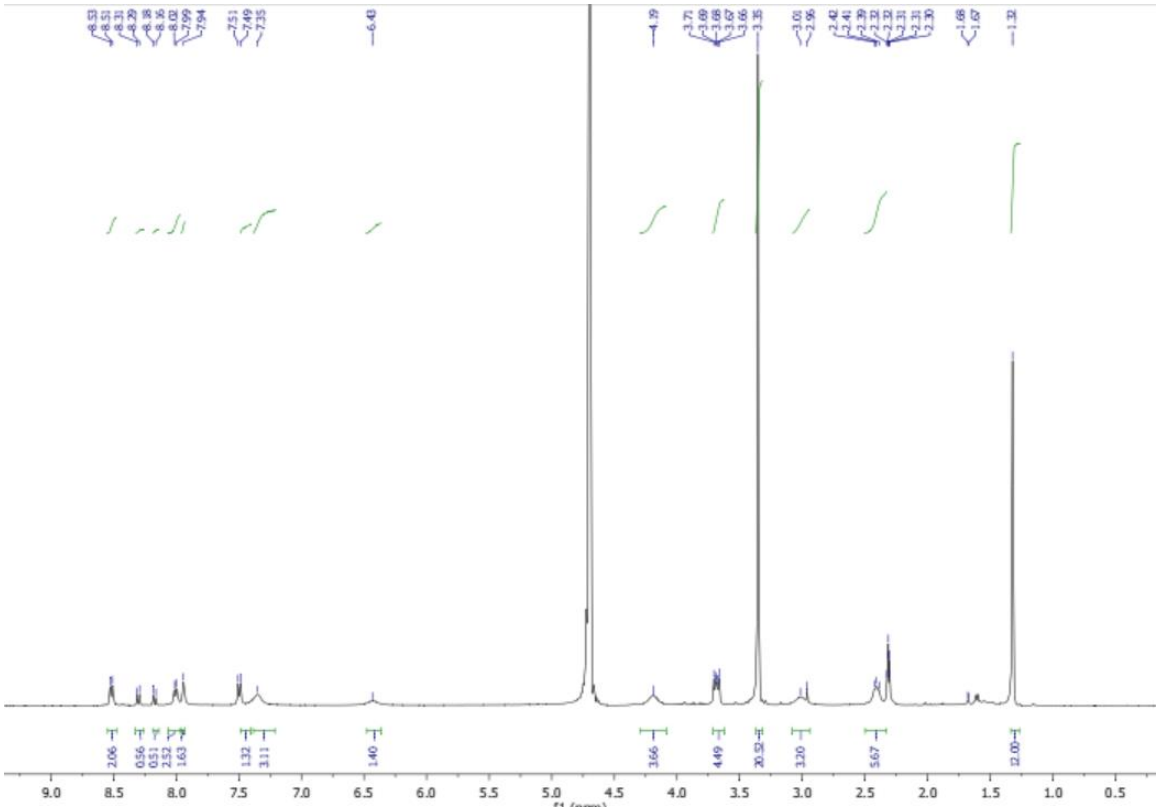

^{13}C (deuterium oxide:acetonitrile-d_3)

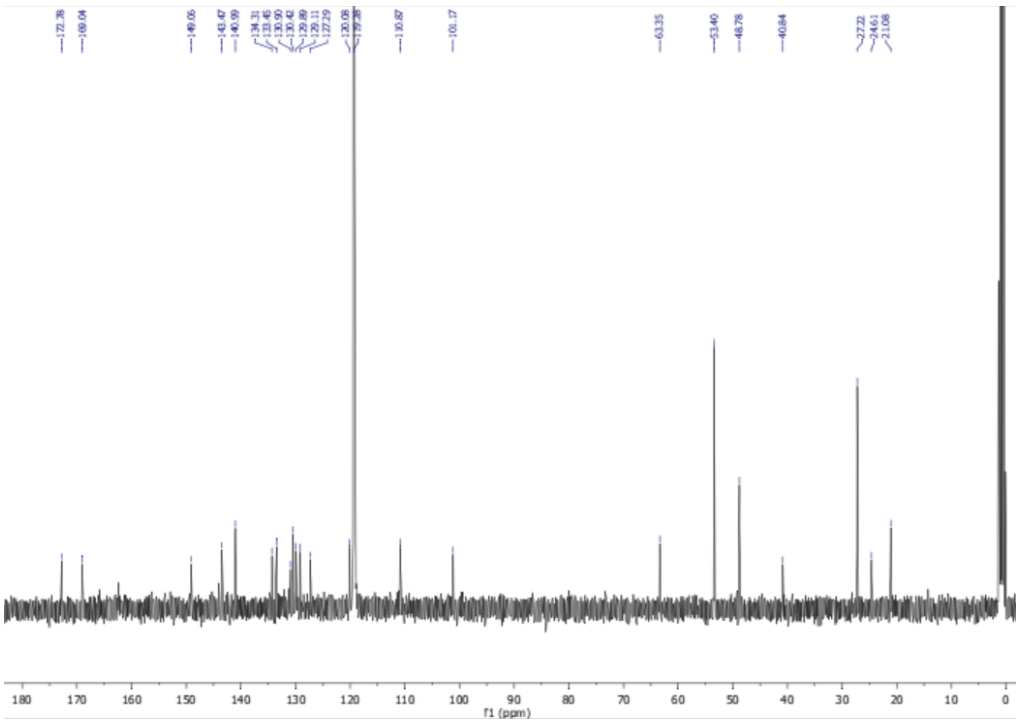

LC/MS at 600 nm

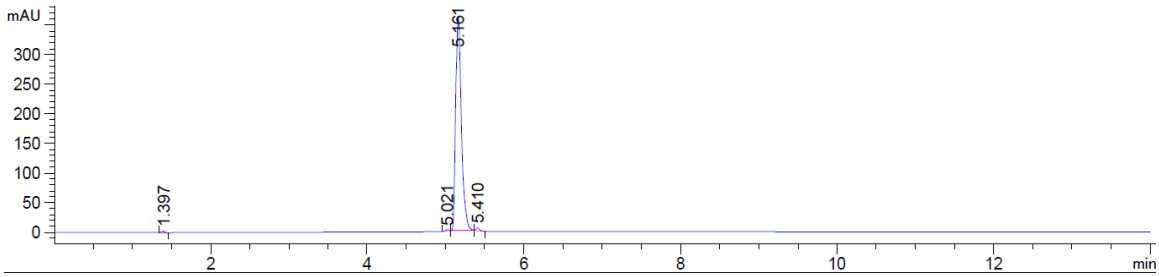

HRMS

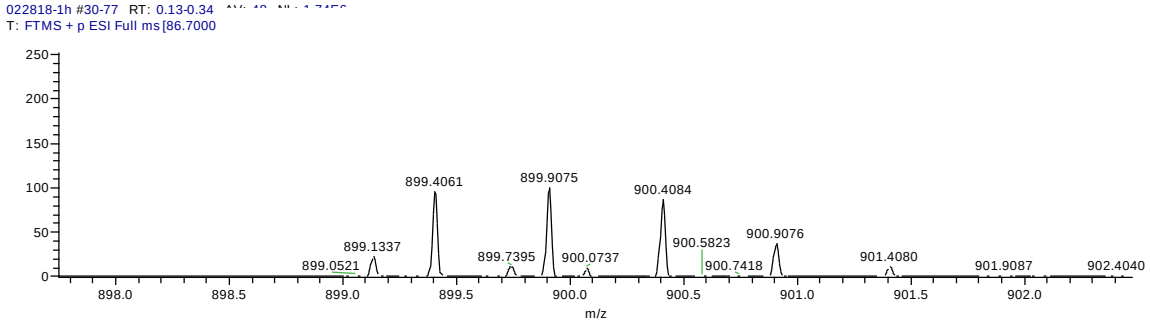

di-tert-butyl ((1S,1'S,2S,2'S)-(((2S,2'S)-((6-((2-(2-(2-aminoethoxy)ethoxy)ethyl)amino)-1,3,5-triazine-2,4-diyl)bis(piperazine-4,1-diyl))bis(3-(4-hydroxyphenyl)-1-oxopropane-1,2-diyl))bis(1H-1,2,3-triazole-1,4-diyl))bis(2-methylbutane-1,1-diyl))dicarbamate (C)

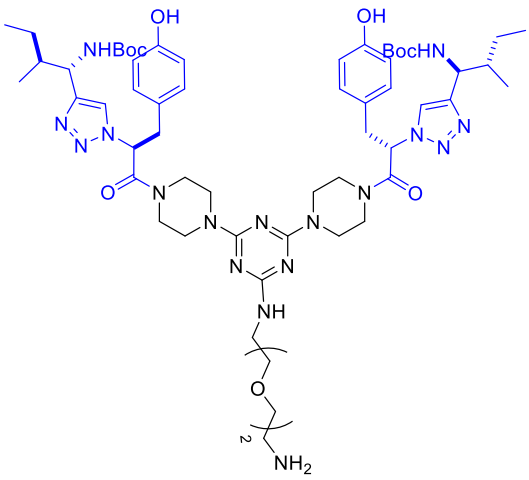

^{1}H NMR (methanol-d$_4$)

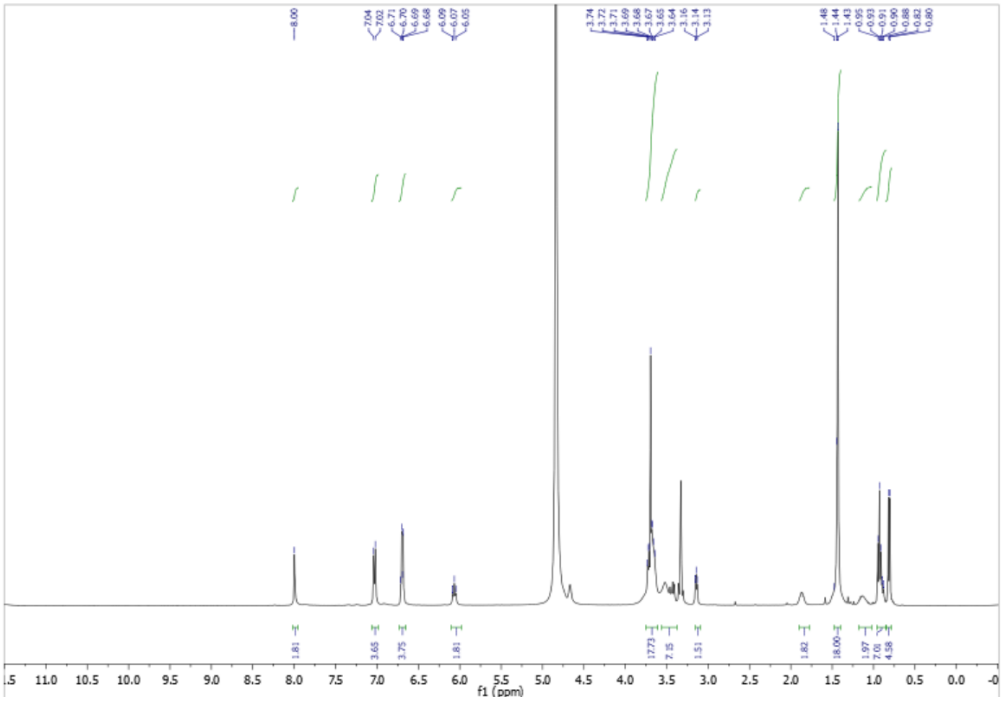

^{13}C NMR (methanol-d$_4$)

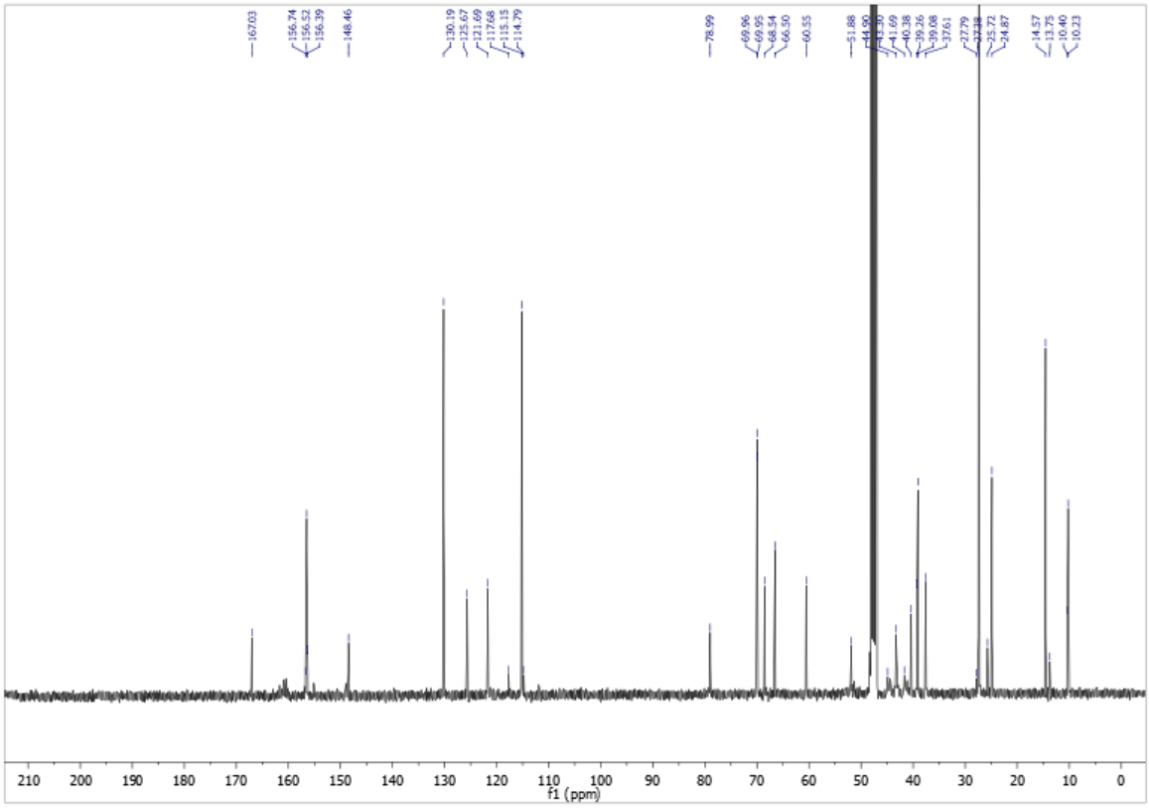

135 DEPT (methanol-d_4)

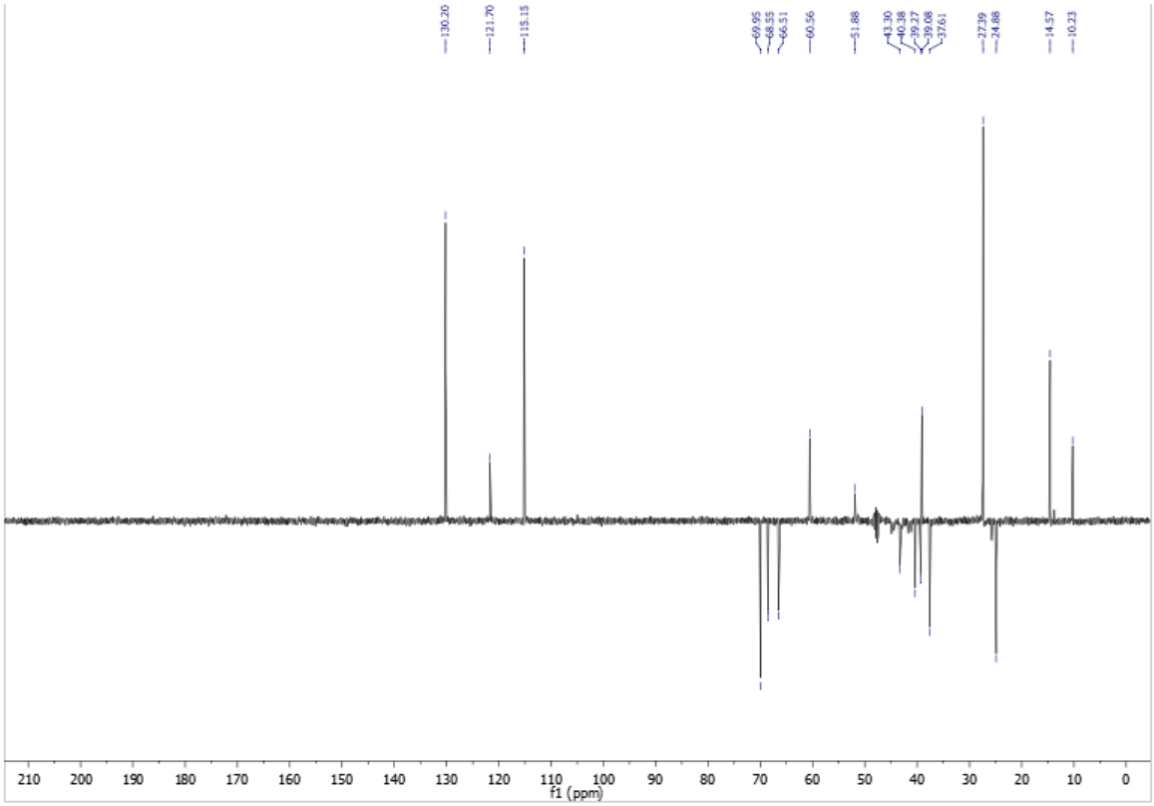

LC/MS at 254 nm

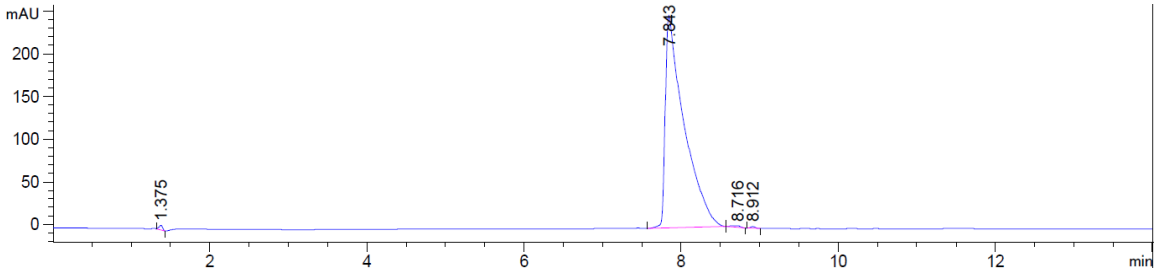

HRMS

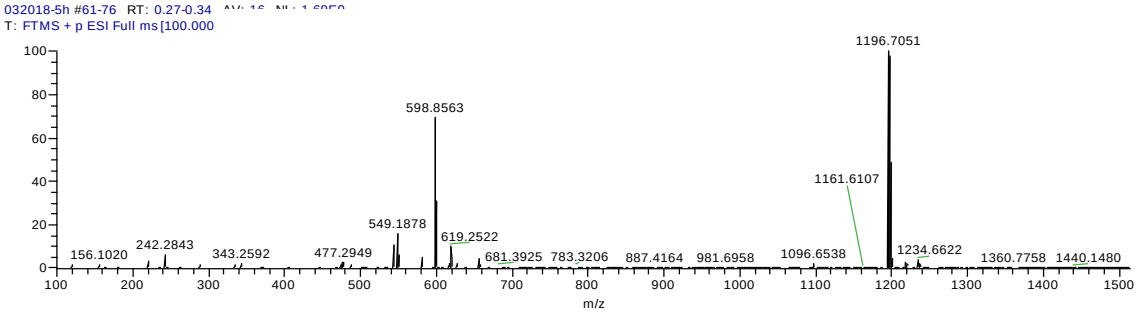

2-((E)-2-((E)-4'-((2-(2-(2-((4,6-bis(4-((S)-2-(4-((1S,2S)-1-amino-2-methylbutyl)-1H-1,2,3-triazol-1-yl)-3-(4-hydroxyphenyl)propanoyl)piperazin-1-yl)-1,3,5-triazin-2-yl)amino)ethoxy)ethoxy)ethyl)carbamoyl)-6-(2-((E)-3,3-dimethyl-5-sulfonato-1-(3-(trimethylammonio)propyl)indolin-2-ylidene)ethylidene)-3,4,5,6-tetrahydro-[1,1'-biphenyl]-2-yl)vinyl)-3,3-dimethyl-1-(3-(trimethylammonio)propyl)-3H-indol-1-ium-5-sulfonate (1)

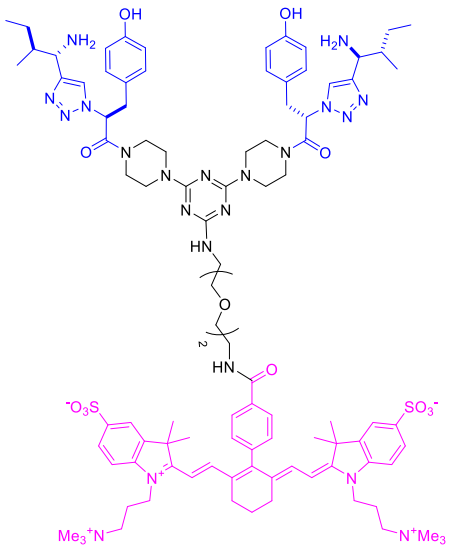

^{1}H NMR – (deuterium oxide:acetonitrile-d_3)

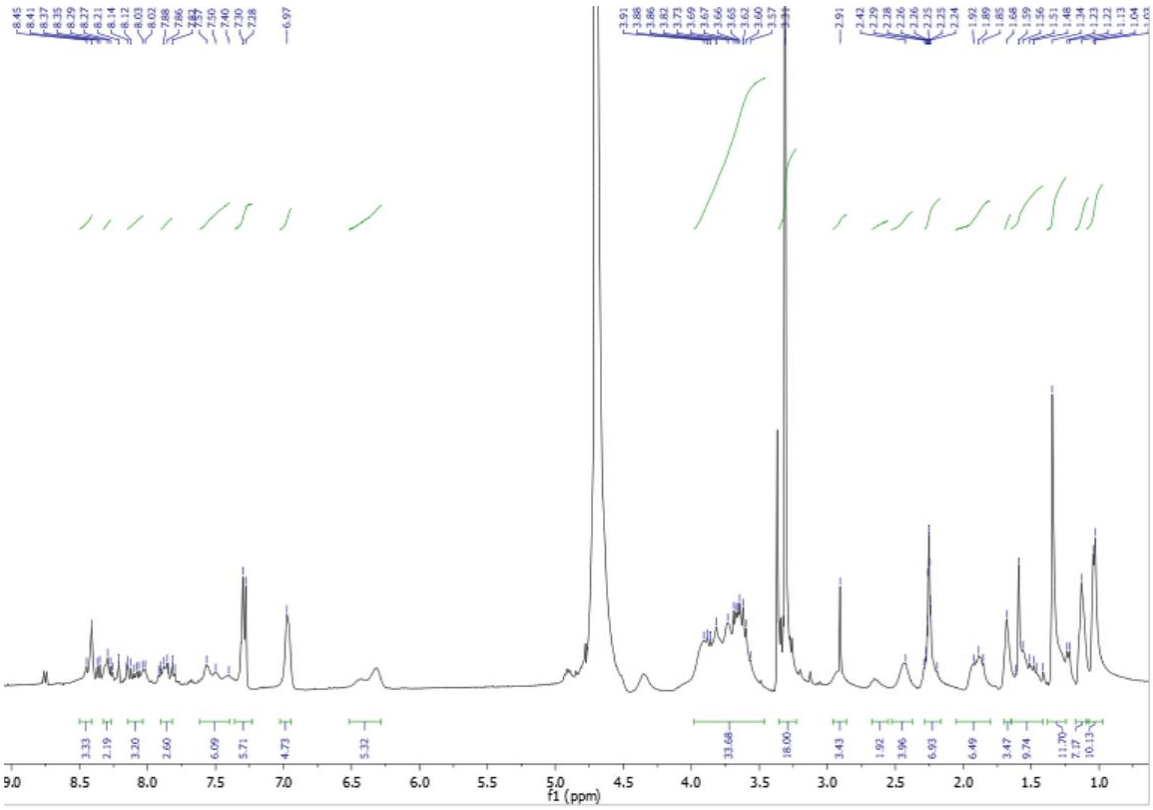

^{13}C NMR (deuterium oxide:acetonitrile-d_3)

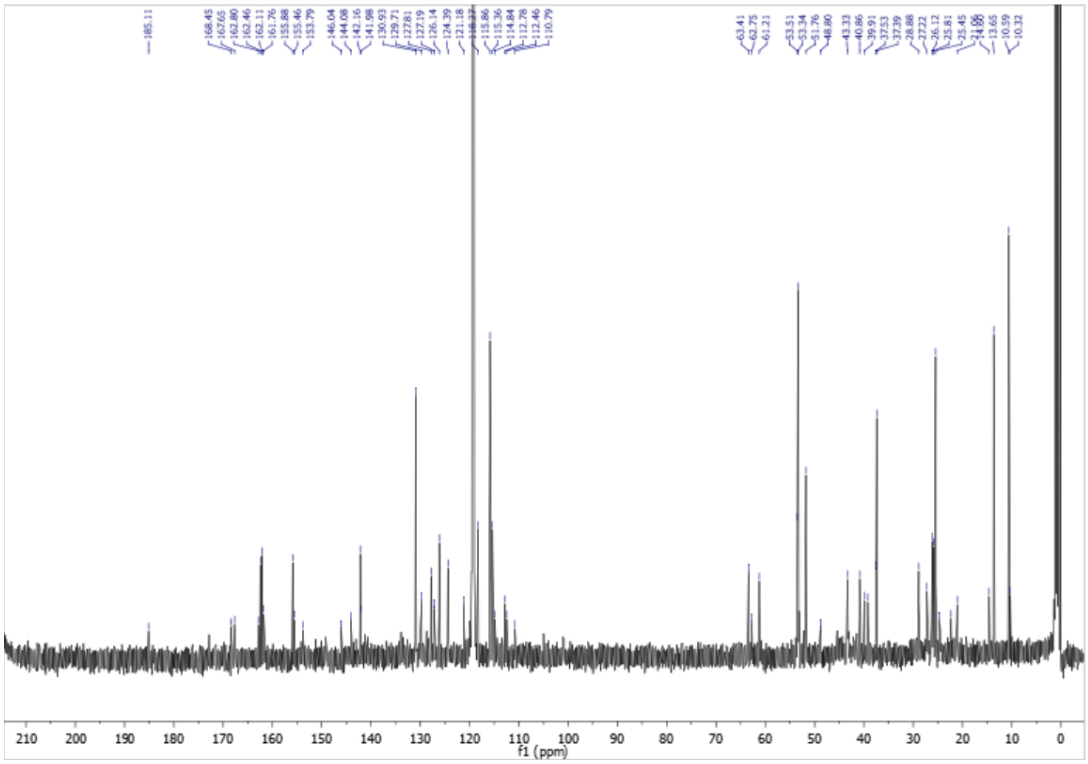

LC/MS at 600 nm

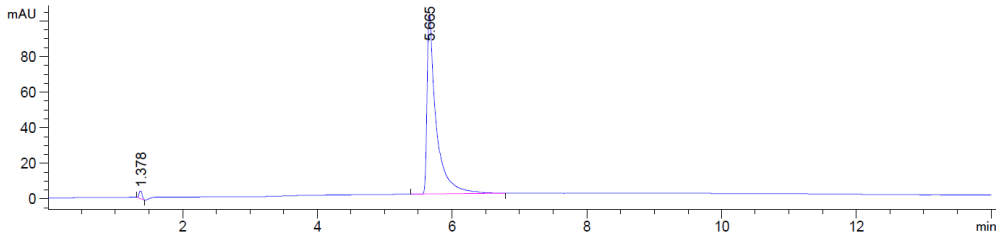

HRMS

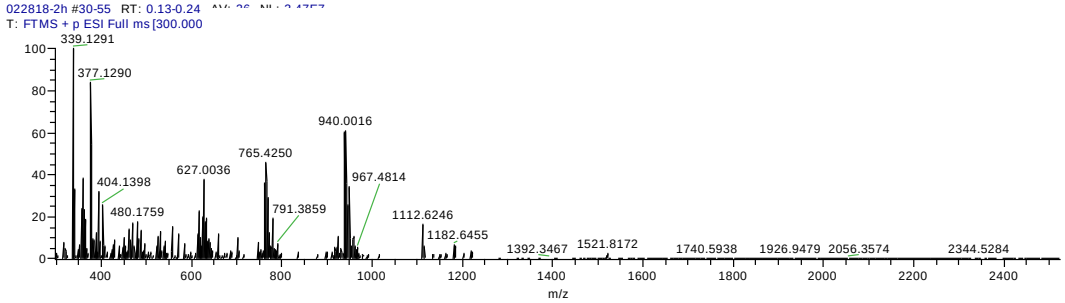

di-tert-butyl ((1S,1'S)-(((2R,2'R,3R,3'R)-((6-((2-(2-(2-aminoethoxy)ethoxy)ethyl)amino)-1,3,5-triazine-2,4-diyl)bis(piperazine-4,1-diyl))bis(3-methyl-1-oxopentane-1,2-diyl))bis(1H-1,2,3-triazole-1,4-diyl))bis(2-(4-(tert-butoxy)phenyl)ethane-1,1-diyl))dicarbamate (12)

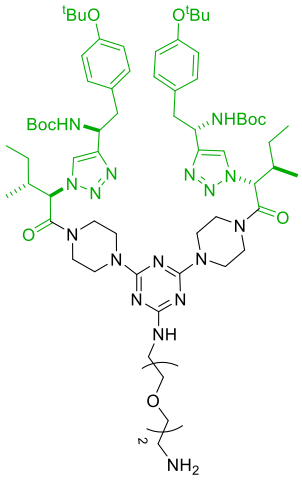

^{1}H (methanol-d$_4$)

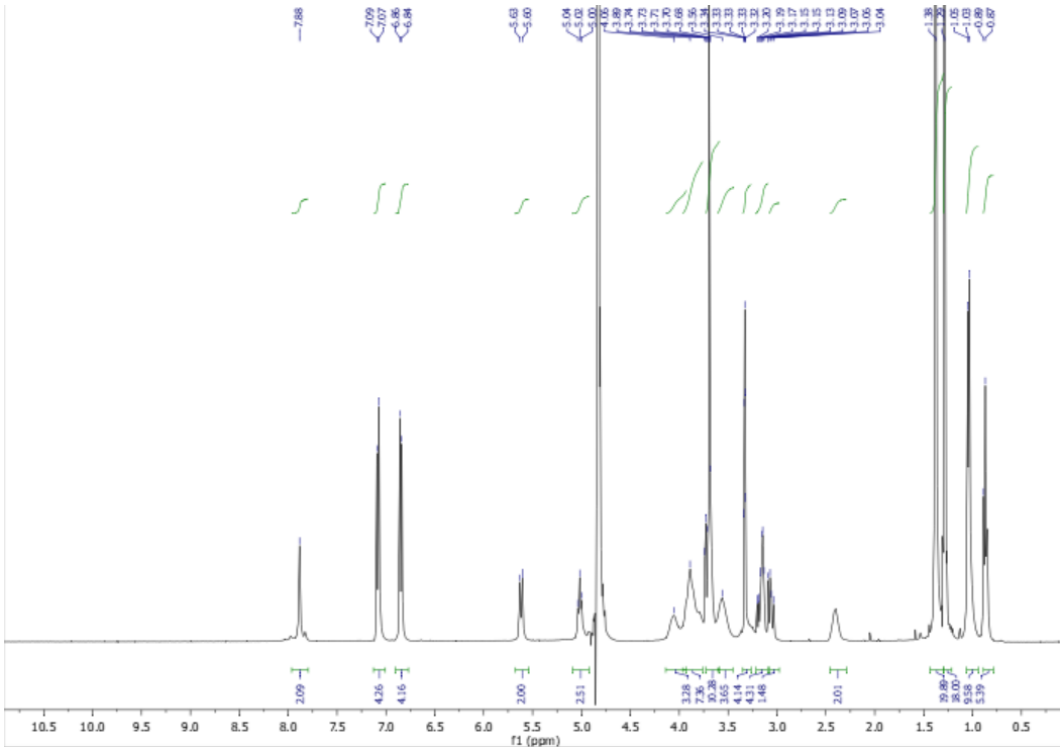

^{13}C (methanol-d$_4$)

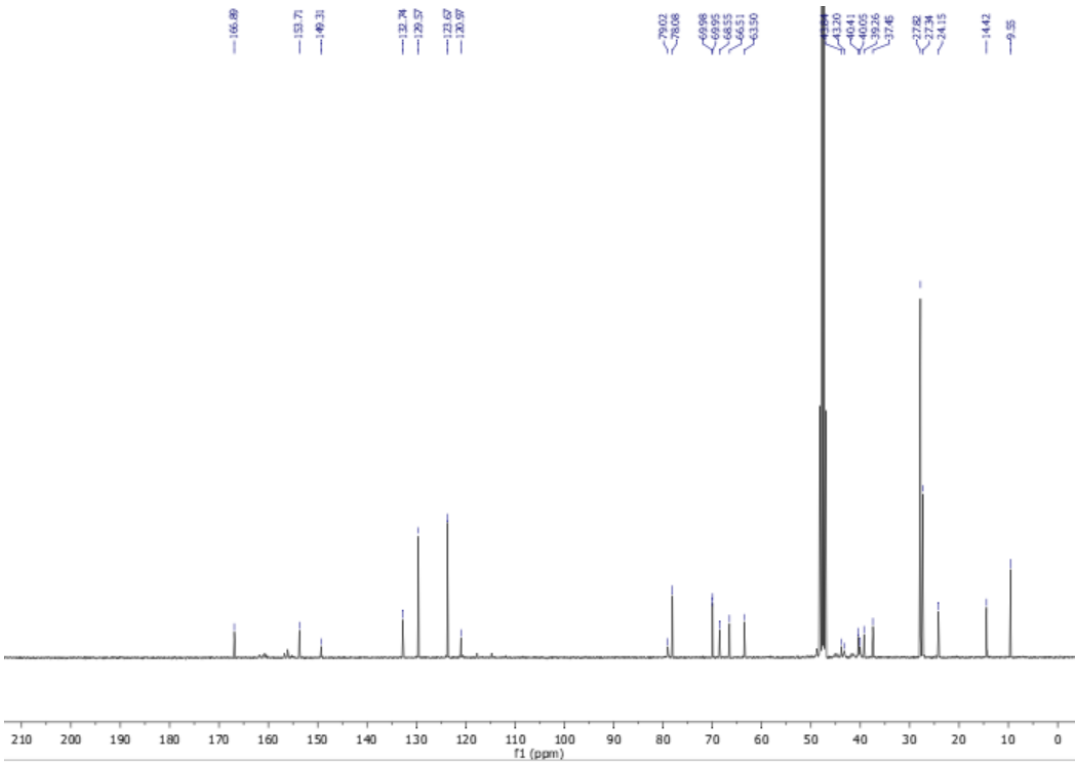

135 DEPT (methanol-d4)

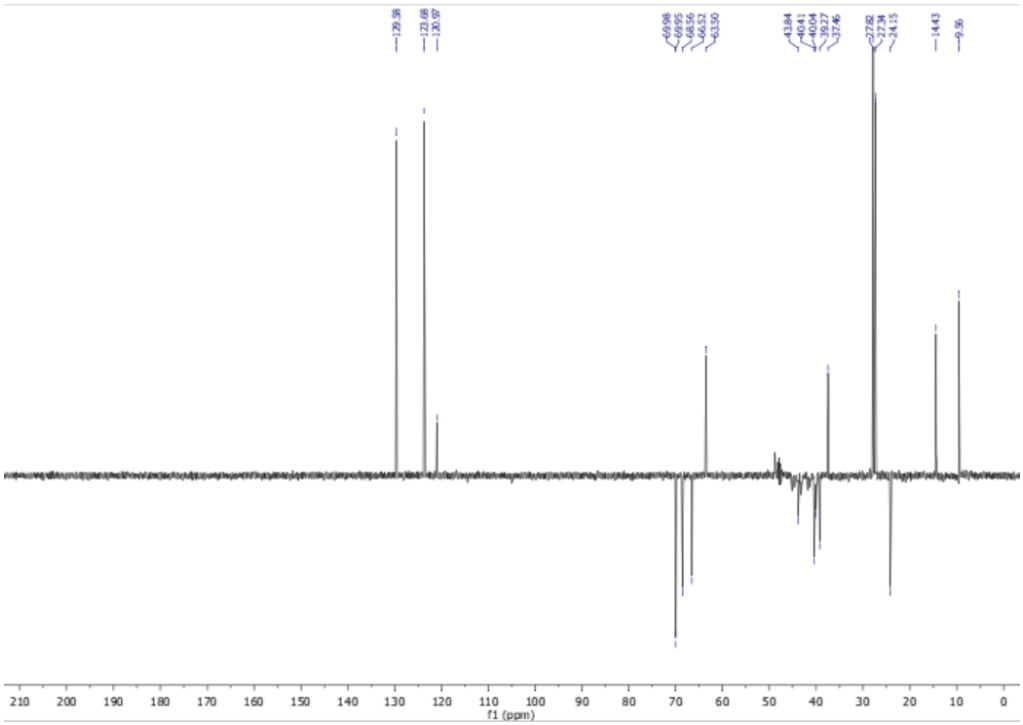

LC/MS at 254 nm

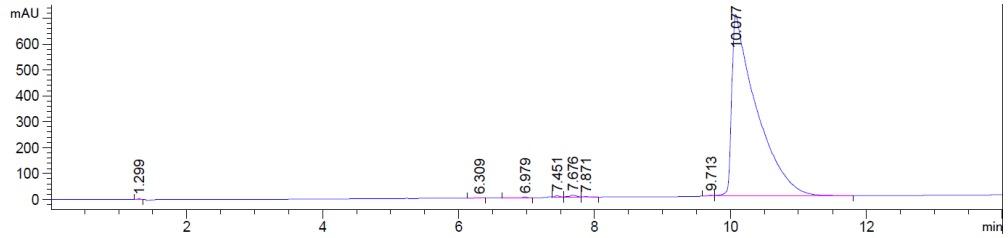

HRMS

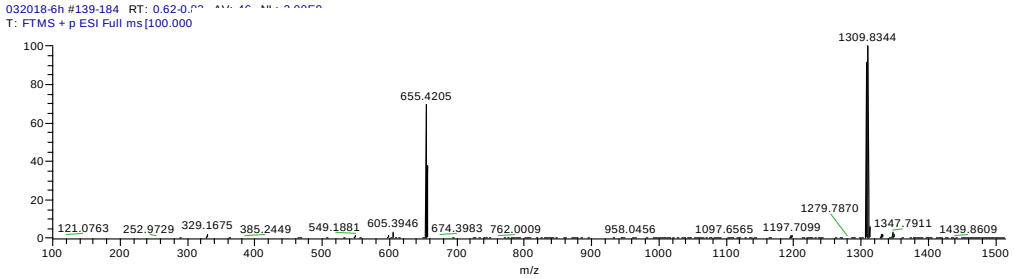

2-((E)-2-((E)-4'-((2-(2-(2-((4,6-bis(4-((2R,3R)-2-(4-((S)-1-amino-2-(4-hydroxyphenyl)ethyl)-1H-1,2,3-triazol-1-yl)-3-methylpentanoyl)piperazin-1-yl)-1,3,5-triazin-2-yl)amino)ethoxy)ethoxy)ethyl)carbamoyl)-6-(2-((E)-3,3-dimethyl-5-sulfonato-1-(3-(trimethylammonio)propyl)indolin-2-ylidene)ethylidene)-3,4,5,6-tetrahydro-[1,1'-biphenyl]-2-yl)vinyl)-3,3-dimethyl-1-(3-(trimethylammonio)propyl)-3H-indol-1-ium-5-sulfonate (2)

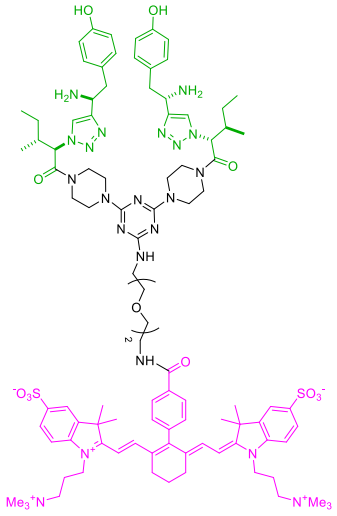

^{1}H NMR – (deuterium oxide:acetonitrile-d_3)

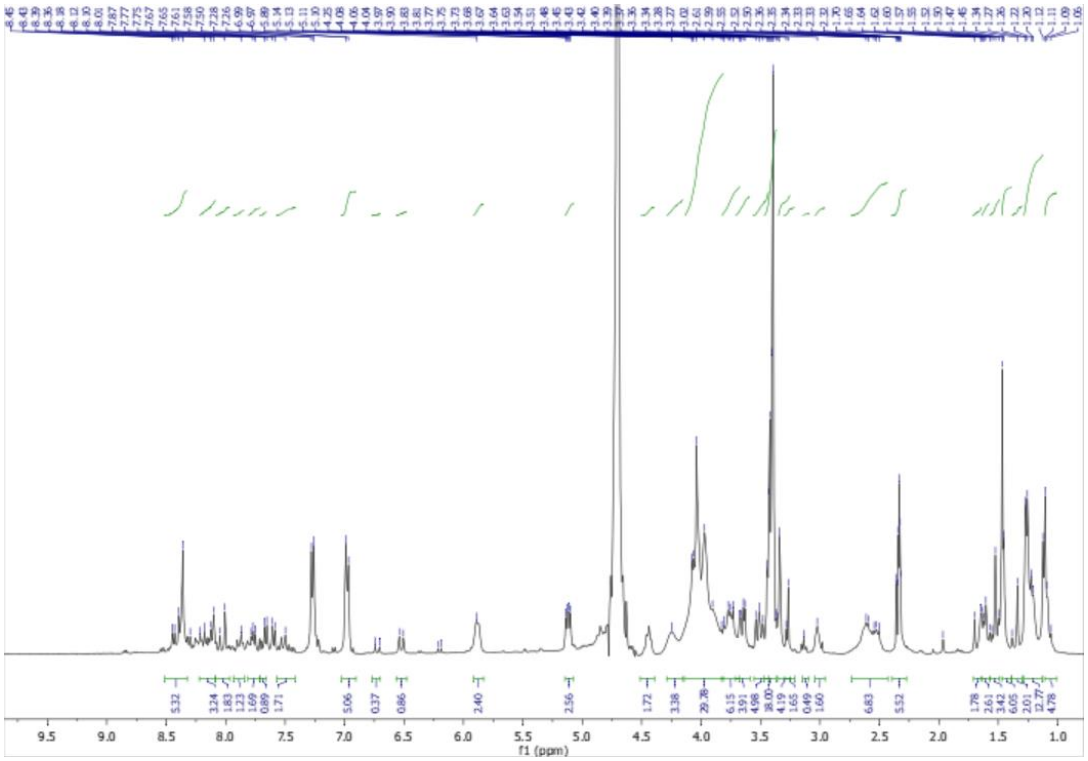

^{13}C NMR – (deuterium oxide:acetonitrile-d_3)

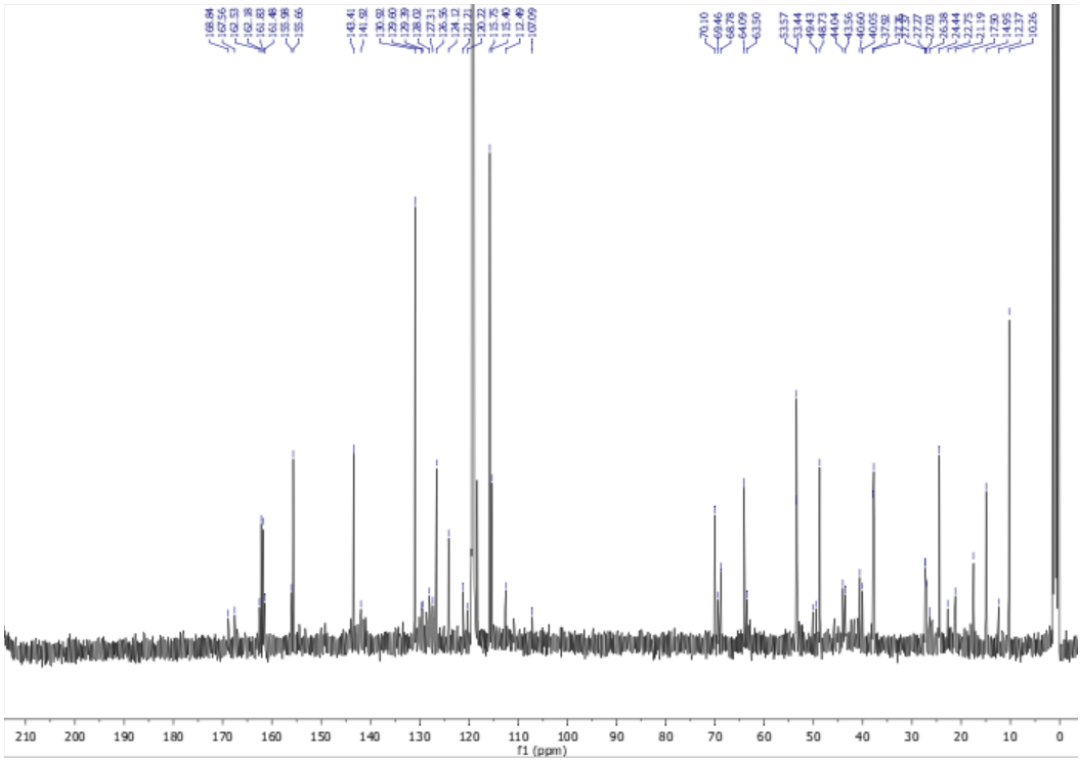

LC/MS at 600 nm

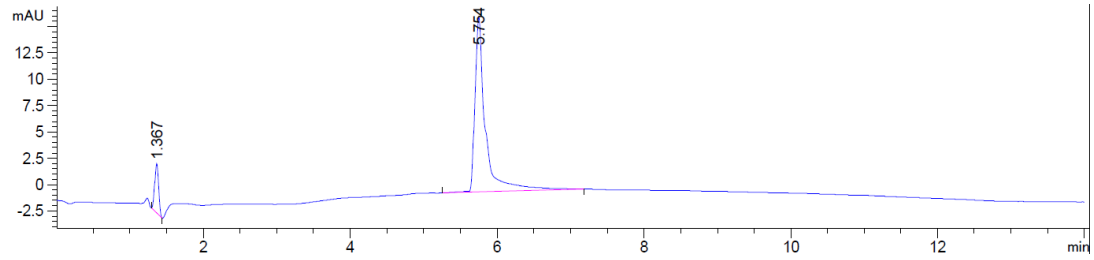

HRMS

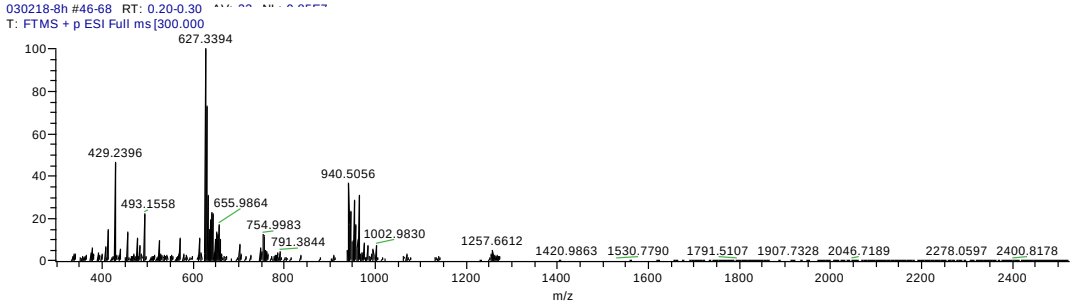

Supporting Figures

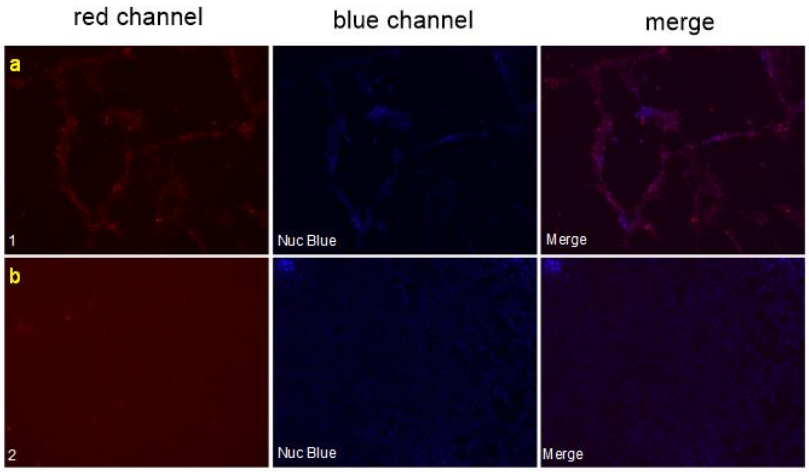

Figure A-S1: **a**. **1** binds to NIH3T3 TrkC cells stronger than **2** (**b**)

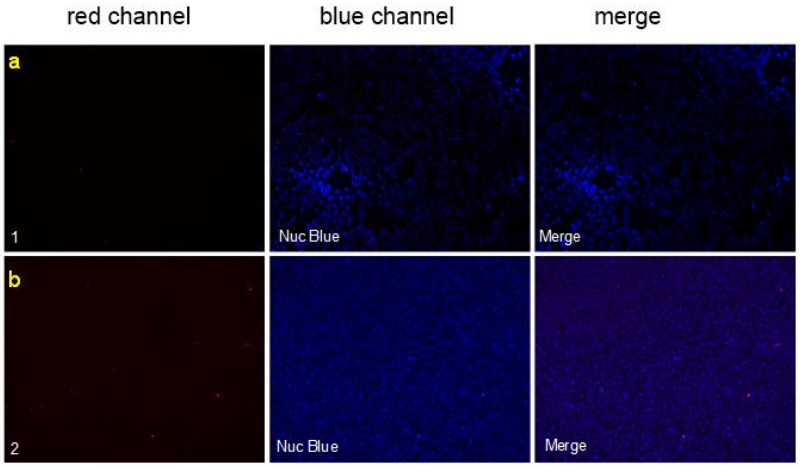

Figure A-S2: **a**. **1** and **b. 2** does not bind to NIH3T3 WT cells.

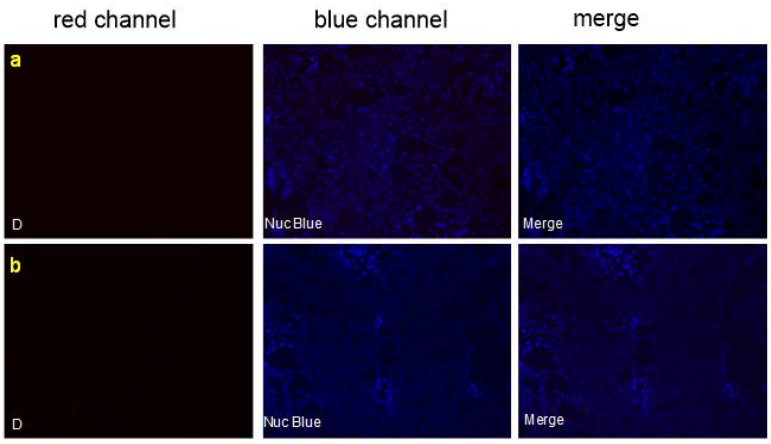

Figure A-S3. Free zwitterionic cyanine (**D**) does not bind to **a.** NIH3T3 TrkC or **b.** NIH3T3 WT cells.

APPENDIX B

SUPPORTING INFORMATION FOR CHAPTER III

General Information

All reactions were carried out with dry solvents under anhydrous conditions under an inert atmosphere (argon). Glassware was dried in an oven at 140 °C for a minimum of 6 h prior to use for all reactions. IR-783 and IR-780 were purchased from Sigma Aldrich (Atlanta, GA, USA) and abcr GmBH (Karlsruhe, Germany), respectively, and DZ-1 and MHI-148 were synthesized according to literature protocol [53,94,96,196]. All other reagents were purchased at a high commercial quality (typically 97% or higher) and used without further purification, unless otherwise stated. Products were purified using a reverse-phase column on a preparative high-performance liquid chromatography (prep HPLC) (Agilent, Santa Clara, CA, USA-) obtained from solid-phase synthesis in 10%–95% MeCN/water with 0.05% trifluoroacetic acid over 20 min. High-field NMR spectra were recorded with Bruker Avance III (Billerica, MA, USA) at 400 MHz for ^{1}H, and 100 MHz for ^{13}C for all compounds. All spectra were calibrated using residual nondeuterated solvent as an internal reference (MeOD-d_4: ^{1}H-NMR = 3.30, ^{13}C-NMR = 49.0, DMSO-d_6: ^{1}H-NMR = 2.50, ^{13}C-NMR = 39.5). The following abbreviations were used to explain the multiplicities: s = singlet, d = doublet, t = triplet, q = quartet, quint = quintet, dd = double doublet, dt = double triplet, dq = double quartet, and m = multiplet. Electrospray ionization mass spectrometry (ESI-MS) data were collected on a triple-stage quadrupole instrument (Thermo Scientific, Waltham, MA, USA) in a positive mode. All statistical analyses were carried out by GraphPad Prism version 6.0 (GraphPad Software, La Jolla, CA, USA).

Synthesis and Characterization

2-((E.)-2-((E)-2-(((R)-2-acetamido-2-carboxyethyl)thio)-3-(2-((E)-1-(5-carboxypentyl)-3,3-dimethylindolin-2-ylidene)ethylidene)cyclohex-1-en-1-yl)vinyl)-1-(5-carboxypentyl)-3,3-dimethyl-3H-indol-1-ium (1a)

To a solution of MHI-148 (25.0 mg, 0.04 mmol) in DMF (1.00 mL), *N*-acetyl-L-cysteine (5.98 mg, 0.04 mmol) and $^{i}Pr_2NEt$ (9.41 μL, 0.06 mmol) were added and the reaction was stirred at 25 °C for 1 h. Solvent was removed under a stream of nitrogen gas and purified by preparative reversed-phase HPLC (10%–95% CH_3CN/water containing 0.05% TFA). Compound was lyophilized to obtain green solid (23.4 mg, 78%).

^{1}H-NMR (400 MHz, MeOD) δ 8.77 (d, *J* = 13.9 Hz, 2H), 7.49 (d, *J* = 7.3 Hz, 2H), 7.45–7.36 (m, 2H), 7.27 (dd, *J* = 14.9, 7.6 Hz, 4H), 6.28 (d, *J* = 13.8 Hz, 2H), 4.55 (dd, *J* = 7.5, 5.3 Hz, 1H), 4.15 (t, *J* = 6.9 Hz, 4H), 3.40 (dd, *J* = 13.4, 5.3 Hz, 1H), 3.12 (dd, *J* = 13.4, 7.5 Hz, 1H), 2.75–2.54 (m, 4H), 2.31 (t, *J* = 7.3 Hz, 4H), 1.98–1.92 (m, 2H), 1.95 (s, 3H), 1.90–1.80 (m, 4H), 1.74 (s, 12H), 1.72–1.64 (m, 4H), 1.55–1.45 (m, 4H).

^{13}C-NMR (100 MHz, MeOD) δ 177.23, 173.86, 173.21, 172.93, 157.83, 146.46, 143.72, 142.48, 134.54, 129.83, 126.27, 123.46, 112.00, 102.20, 54.36, 50.51, 50.49, 49.85, 44.97, 39.51, 34.61, 28.44, 28.02, 27.38, 25.65, 22.75, 22.03.

HRMS calculated for $C_{47}H_{60}N_3O_7S^+$ $(M)^+$: 810.4146; found 810.4166.

6-((E.)-2-((E)-2-(2-(4-(2-acetamido-2-carboxyethyl)phenoxy)-3-((E)-2-(1-(5-carboxypentyl)-3,3-dimethyl-3H-indol-1-ium-2-yl)vinyl)cyclohex-2-en-1-ylidene)ethylidene)-3,3-dimethylindolin-1-yl)hexanoate (1b)

NaH (0.89 mg, 0.04 mmol) was added to a solution of *N*-acetyl-L-tyrosine (8.25 mg, 0.04 mmol) in DMF (1.00 mL) and the reaction was stirred at 25 °C for 30 min. MHI-148 (25.0 mg, 0.04 mmol) was then added to the above reaction and the reaction was stirred for an additional 18 h at 25 °C. Solvent was removed under a stream of nitrogen gas and purified by preparative reversed-phase HPLC (10%–95% CH_3CN/water containing 0.05% TFA). Compound was lyophilized to obtain green solid (12.2 mg, 38%).

^{1}H-NMR (400 MHz, MeOD) δ 8.01–7.92 (m, 2H), 7.36 (t, *J* = 7.8 Hz, 4H), 7.31–7.15 (m, 6H), 7.05 (d, *J* = 8.7 Hz, 2H), 6.13 (d, *J* = 14.2 Hz, 2H), 4.54 (dd, *J* = 9.1, 5.2 Hz, 1H), 4.09 (t, *J* = 7.3 Hz, 4H), 3.14 (dd, *J* = 14.0, 5.2 Hz, 1H), 2.84 (dd, *J* = 14.2, 9.2 Hz, 1H), 2.73 (t, *J* = 5.8 Hz, 4H), 2.30 (t, *J* = 7.3 Hz, 4H), 2.04 (t, *J* = 7.3 Hz, 2H), 1.84 (s, 3H), 1.83–1.73 (m, 4H), 1.67 (dd, *J* = 15.1, 7.5 Hz, 4H), 1.46 (t, *J* = 7.7 Hz, 4H), 1.33 (s, 12H).

^{13}C-NMR (100 MHz, MeOD) δ 177.20, 174.59, 173.75, 173.05, 165.43, 160.25, 143.57, 143.34, 142.51, 132.96, 132.16, 129.76, 126.19, 123.40, 123.20, 115.75, 111.94, 100.93, 55.48, 50.27, 44.85, 37.62, 34.59, 28.25, 27.96, 27.33, 25.63, 25.21, 22.48, 22.39.

HRMS calculated for $C_{53}H_{64}N_3O_8^+$ $(M)^+$: 870.4688; found 870.4675.

1-(5-C.arboxypentyl)-2-((E)-2-((E)-3-(2-((E)-1-(5-carboxypentyl)-3,3-dimethylindolin-2-ylidene) ethylidene)-2-((S)-2-carboxypyrrolidin-1-yl)cyclohex-1-en-1-yl)vinyl)-3,3-dimethyl-3H-indol-1-ium (1c)

To a solution of MHI-148 (25.0 mg, 0.04 mmol) in DMF (1.00 mL), L-proline (4.26 mg, 0.04 mmol) and $^iPr_2NEt$ (6.27 μL, 0.04 mmol) were added and the reaction was stirred at 60 °C monitored by Agilent LC-MS. The reaction reached equilibrium after 2 h

and the solvent was removed under a stream of nitrogen gas and purified by preparative reversed-phase HPLC (10%–95% CH_3CN/water containing 0.05% TFA). Compound was lyophilized to obtain blue solid (5.18 mg, 18%). ^{1}H-NMR (400 MHz, DMSO) δ 7.42 (d, *J* = 7.3 Hz, 2H), 7.28 (t, *J* = 7.7 Hz, 2H), 7.11 (d, *J* = 7.7 Hz, 2H), 7.04 (t, *J* = 7.2 Hz, 2H), 5.68 (d, *J* = 12.4 Hz, 2H), 4.96 (d, *J* = 7.3 Hz, 2H), 4.02–3.97 (m, 1H), 3.90–3.87 (m, 4H), 2.76–2.57 (m, 3H), 2.46–2.29 (m, 3H), 2.28–2.18 (m, 1H), 2.20 (t, *J* = 7.3 Hz, 4H), 2.09–1.98 (m, 3H), 1.79–1.70 (m, 2H), 1.70–1.62 (m, 4H), 1.57 (s, 6H), 1.61–1.48 (m, 4H), 1.54 (s, 6H), 1.45–1.30 (m, 4H). ^{13}C-NMR (100 MHz, DMSO) δ 174.29, 172.71, 166.02, 158.00, 142.99, 139.74, 136.52, 128.11, 123.13, 122.28, 122.00, 109.00, 94.22, 64.69, 56.49, 46.93, 42.26, 33.52, 30.04, 29.59, 28.65, 28.11, 26.70, 25.81, 24.22, 20.65. HRMS calculated for $C_{47}H_{60}N_3O_6^+$ $(M)^+$: 762.4477; found 762.4457.

2-((E.)-2-((E)-2-(((S)-5-acetamido-1-carboxypentyl)amino)-3-(2-((E)-1-(5-carboxypentyl)-3,3-dimethylindolin-2-ylidene)ethylidene)cyclohex-1-en-1-yl)vinyl)-1-(5-carboxypentyl)-3,3-dimethyl-3H-indol-1-ium (1d)

To a solution of MHI-148 (25.0 mg, 0.04 mmol) in DMF/H_2O (1:1; 1.00 mL), *N*ε-acetyl-L-lysine (6.96 mg, 0.04 mmol) and ^{i}Pr$_2$NEt (6.27 μL, 0.04 mmol) were added and the reaction was stirred at 60 °C monitored by Agilent LC-MS. The reaction reached equilibrium after 20 h and the solvent was removed under a stream of nitrogen gas and purified by preparative reversed-phase HPLC (10%–95% CH_3CN/water containing 0.05% TFA). Compound was lyophilized to obtain blue solid (4.33 mg, 18%).

^{1}H-NMR (400 MHz, DMSO) δ 8.02 (d, *J* = 9.4 Hz, 1H), 7.78 (d, *J* = 12.9 Hz, 2H), 7.45 (d, *J* = 7.2 Hz, 2H), 7.35–7.28 (m, 2H), 7.24 (dd, *J* = 11.6, 3.9 Hz, 1H), 7.17 (d, *J* = 8.0 Hz, 2H), 7.09 (t, *J* = 7.4 Hz, 2H), 7.05–7.00 (m, 1H), 5.85 (d, *J* = 13.2 Hz, 2H), 4.43 (dd, *J* = 13.9, 8.8 Hz, 1H), 4.00–3.95 (m, 4jH), 3.68–3.61 (m, 4H), 3.01 (t, *J* = 5.4 Hz, 2H), 2.56 (dd, *J* = 13.9, 7.2 Hz, 2H), 2.42–2.33 (m, 2H), 2.20 (dd, *J* = 13.4, 6.3 Hz, 4H), 1.75 (s, 3H), 1.72–1.63 (m, 6H), 1.60 (s, 12H), 1.52 (dd, *J* = 14.8, 7.4 Hz, 6H), 1.43–1.34 (m, 8H).

^{13}C-NMR (100 MHz, DMSO) δ 174.22, 173.25, 168.88, 167.91, 142.71, 140.05, 128.12, 127.58, 122.74, 122.42, 121.96, 120.58, 109.39, 108.49, 95.36, 47.32, 43.24, 42.35, 38.21, 33.47, 28.99, 28.01, 27.60, 25.94, 25.77, 25.62, 24.45, 24.18, 24.11, 24.05, 22.53.

HRMS calculated for $C_{50}H_{67}N_4O_7^+$ $(M)^+$: 835.5004; found 835.4972.

UV-Vis and Fluorescence Analysis

Here, 6 μM of compounds **1a**–**d** samples in 10 mM PBS buffer was prepared by diluting their corresponding stock solution (20 mM) in DMSO using pH 7.24 10 mM PBS buffer. The absorbance and fluorescence of these samples were analyzed using a Varian Cary 100 UV-Vis spectrometer and Varian Cary Eclipse fluorescence spectrophotometer, respectively. The excitation wavelength for compounds **1a**–**d** was set as 740, 720, 580, and 650 nm, respectively. The normalized absorbance and fluorescence data were plotted using GraphPad Prism version 6.0 (GraphPad Software).

NIR Gel Image Protocol

Different cyanines (10 μM; 20 mM stock in DMSO) were incubated with vimentin (1 μM; 1 μg) in pH 7.24 HEPES buffer (50 mM) at 37 °C monitored up to 24 h. For this, 100 ng of each cyanine-vimentin conjugate samples was treated under reducing condition with heating at 95 °C for 10 min and loaded into 15% SDS-PAGE for electrophoresis. The gel was washed with deionized water (10 min × 3 times), and the gel was analyzed by an Odyssey imager to detect the NIR fluorescence.

Preparation of Thiol-Blocked Vimentin

Using pH 7.24 HEPES buffer (50 mM), thiol-blocked vimentin was prepared by incubating 6-maleimide-hexanoic acid (6-MA, 10 μM) with vimentin (1 μg, 1 μM) for 18 h at 37 °C. The thiol-blocked vimentin solution was directly used to incubate with MHI-148 (1 μM) without further purifications.

Kinetic Study of MHI-148 with Amino Acids in Aqueous Buffer

To a solution of MHI-148 (400 μM) in pH 8.00 HEPES buffer (500 μL), 100 μL of each amino acid solution (2.00 mM) in pH 8.00 HEPES buffer was added to make a final concentration of 200 μM of each reagent. The reaction was incubated and shaken at 37 °C and was monitored using HPLC at 600 nm from 0 to 27 h to reach reaction equilibrium. The data was plotted using GraphPad Prism version 6.0 (GraphPad Software).

NIR Gel Image of MHI-148 with Different Proteins

Different proteins, including NEDD8, Ubc12, truncated suPAR (residues 1-281), NAE, PCSK9, and EGFR (4 μM; 1 μg), were incubated with MHI-148 (4 μM) in pH 7.24 HEPES buffer (50 mM) at 37 °C for 3 h. For this, 500 ng of each protein samples were treated under nonreducing condition with heating at 95 °C for 10 min and loaded into 10% SDS-PAGE for electrophoresis. The gel was washed with deionized water (10 min × 3 times), and the gel was analyzed by an Odyssey imager to detect the NIR fluorescence.

Characterization Spectra of Compound 1a

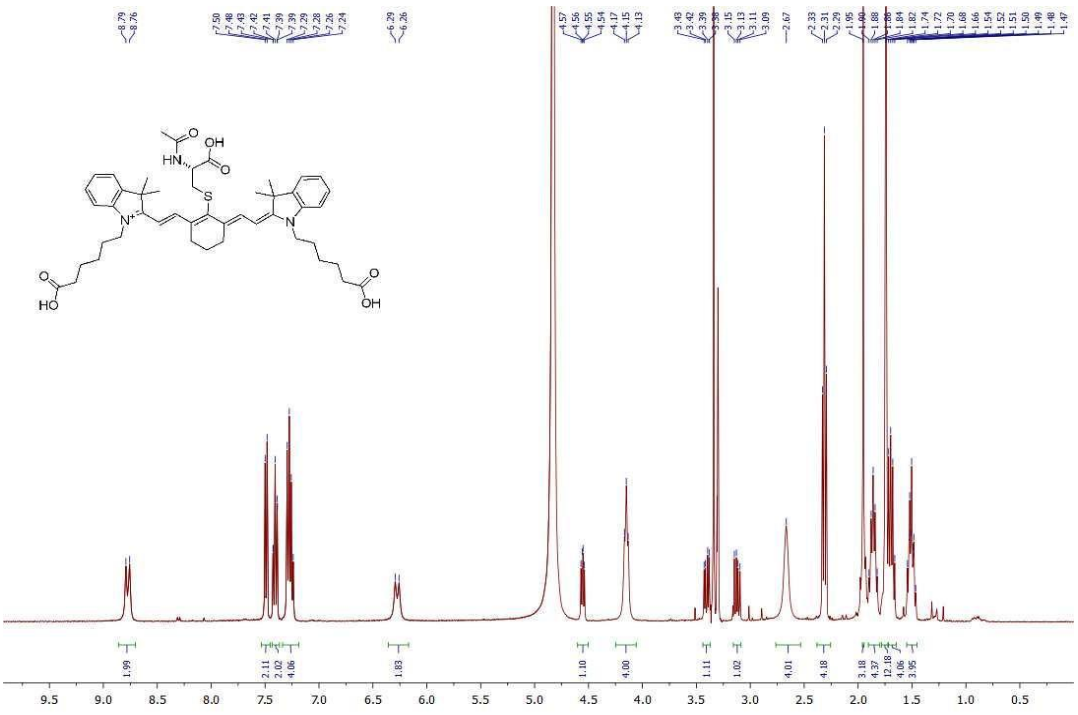

Figure B-S1. ^{1}H NMR of compound **1a** in Methanol-d4

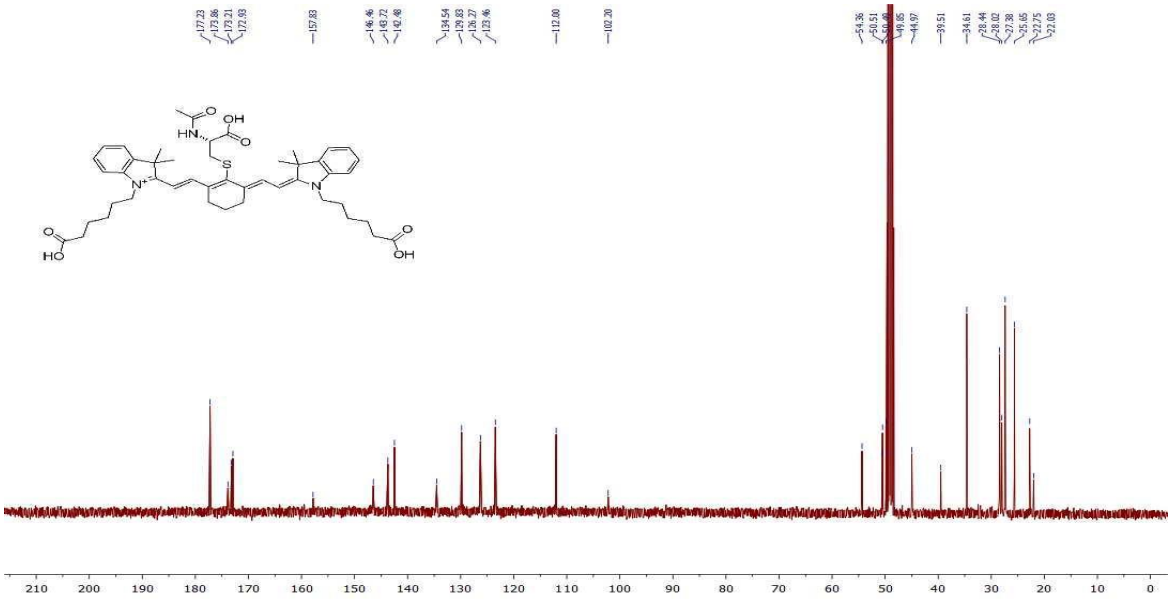

Figure B-S2. ^{13}C NMR of compound **1a** in Methanol-d4

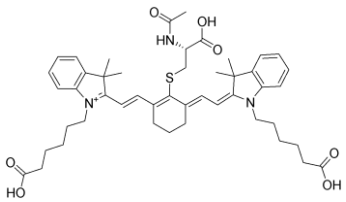

Chemical Formula: $C_{47}H_{60}N_3O_7S^+$

Exact Mass: 810.4146

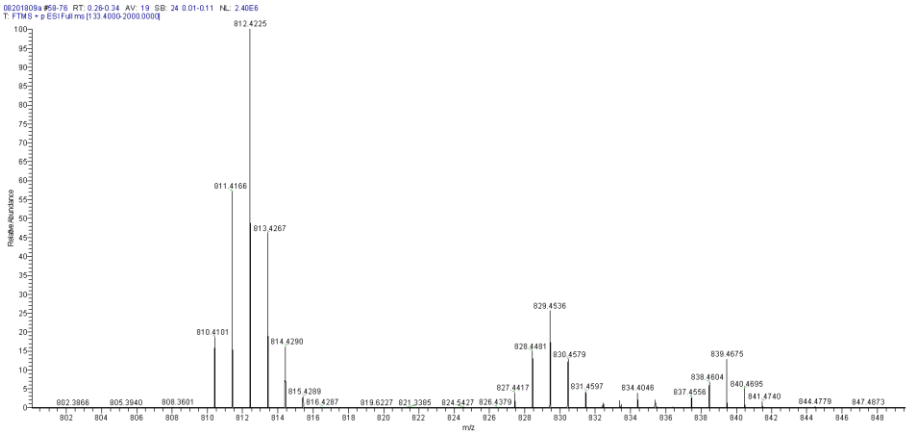

Figure B-S3. HRMS of compound **1a**

Characterization Spectra of Compound 1b

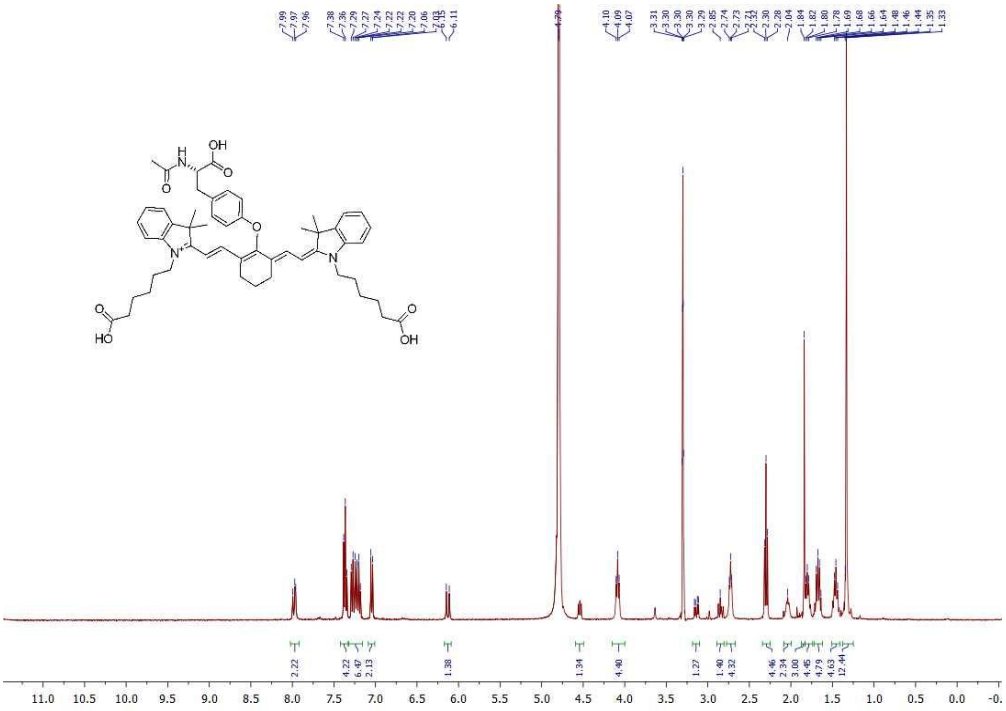

Figure B-S4. ^{1}H NMR of compound **1b** in Methanol-d4

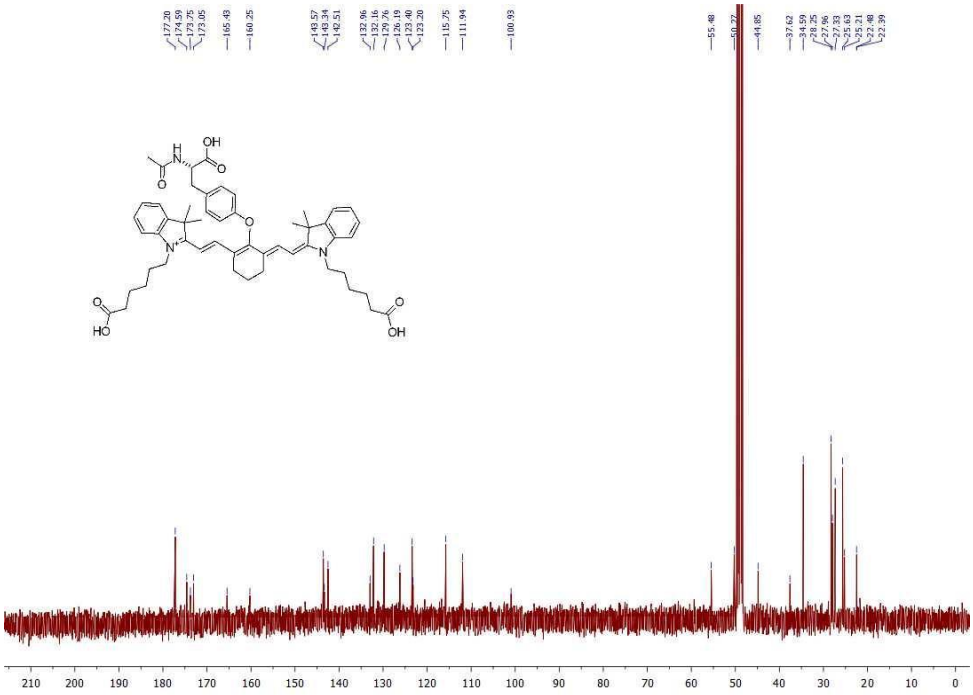

Figure B-S5. ^{13}C NMR of compound **1b** in Methanol-d4

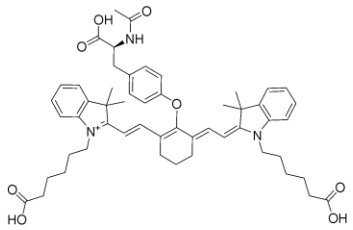

Chemical Formula: $C_{53}H_{64}N_3O_8^+$

Exact Mass: 870.4688

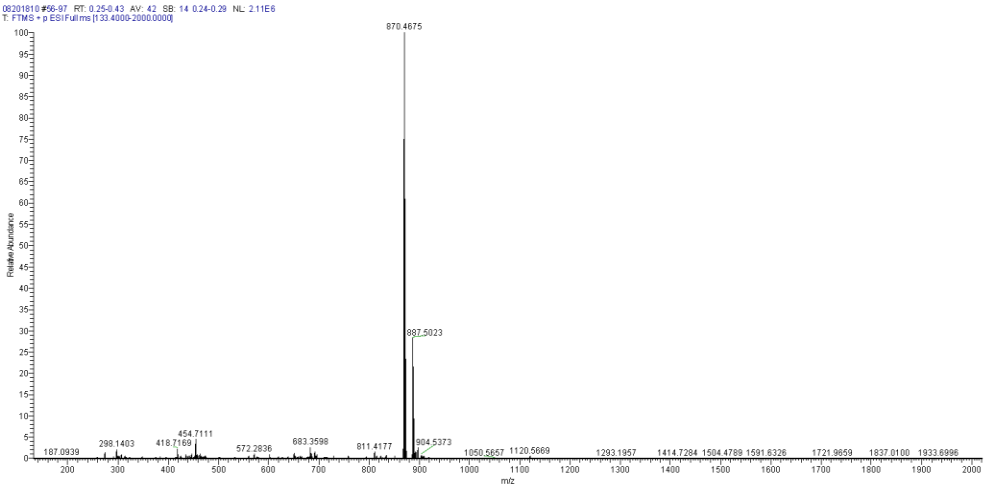

Figure B-S6. ^{1}H NMR of compound **1b**

Characterization Spectra of Compound 1c

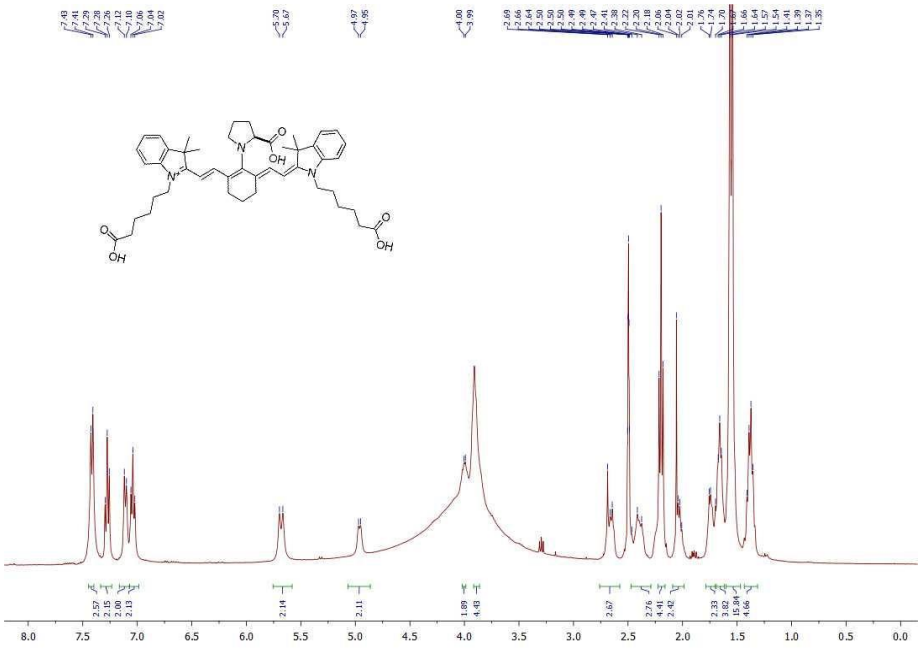

Figure B-S7. ^{1}H NMR of compound **1c** in Methanol-d4

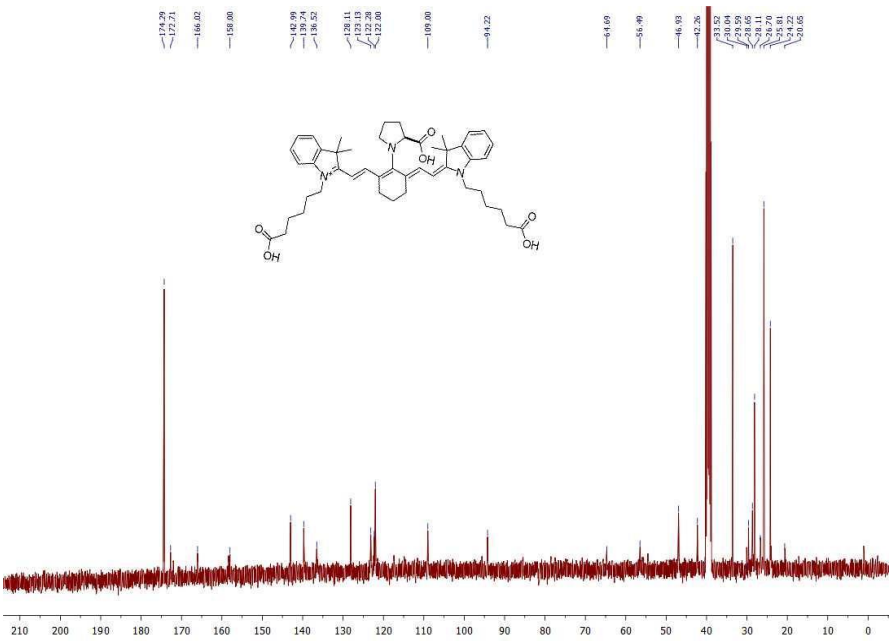

Figure B-S8. ^{13}C NMR of compound **1c** in Methanol-d4

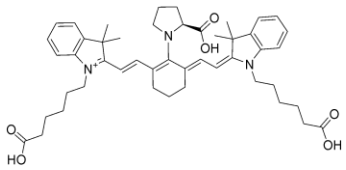

Chemical Formula: $C_{47}H_{60}N_3O_6^+$

Exact Mass: 762.4477

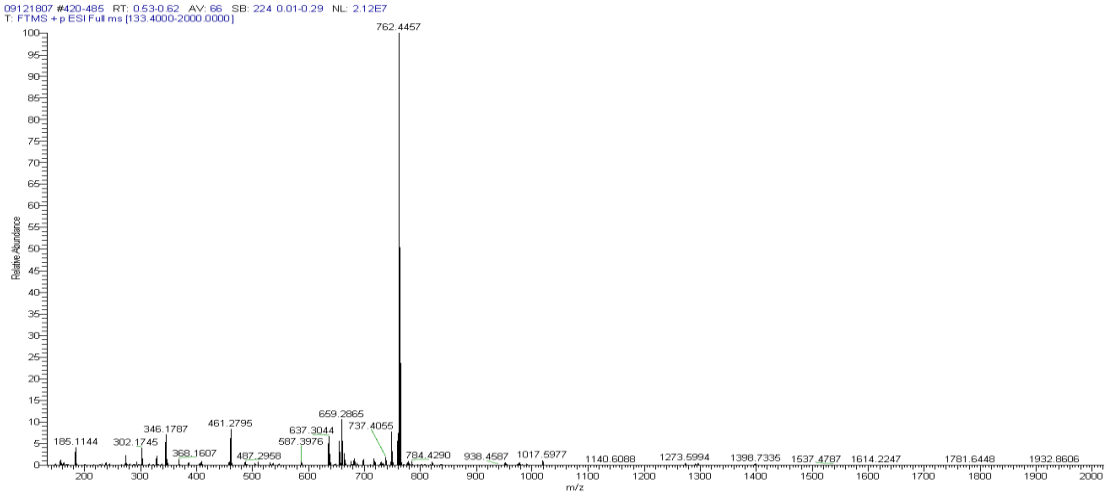

Figure B-S9. HRMS of compound **1c**

Characterization Spectra of Compound 1d

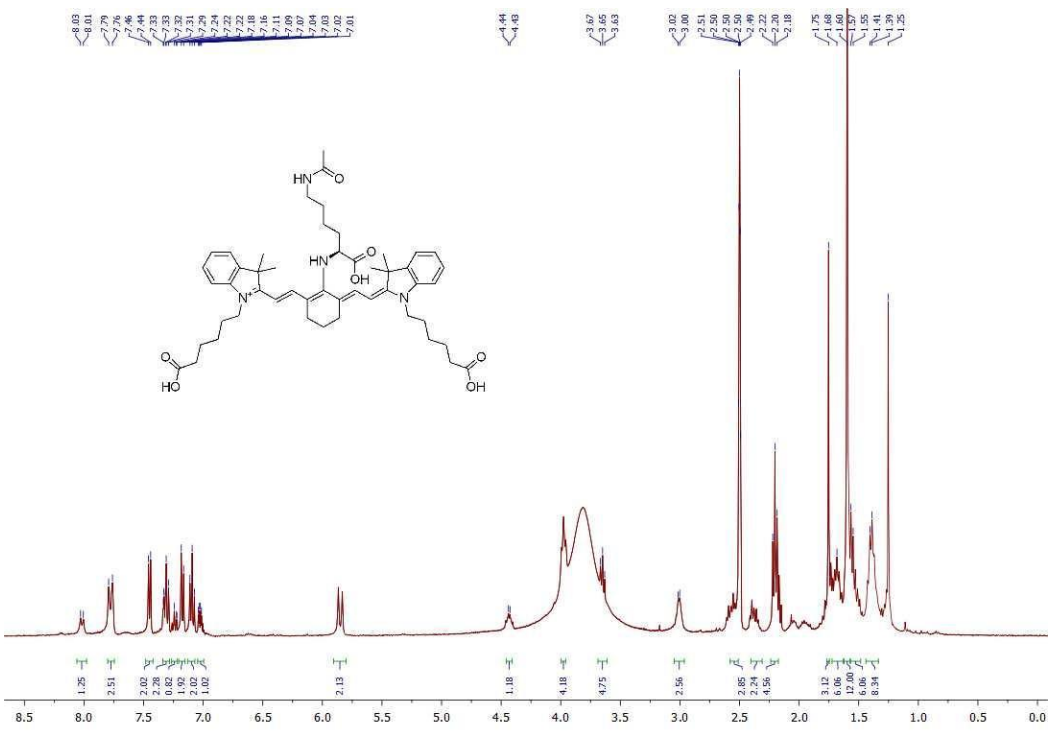

Figure B-S10. ^{1}H NMR of compound **1d** in Methanol-d4

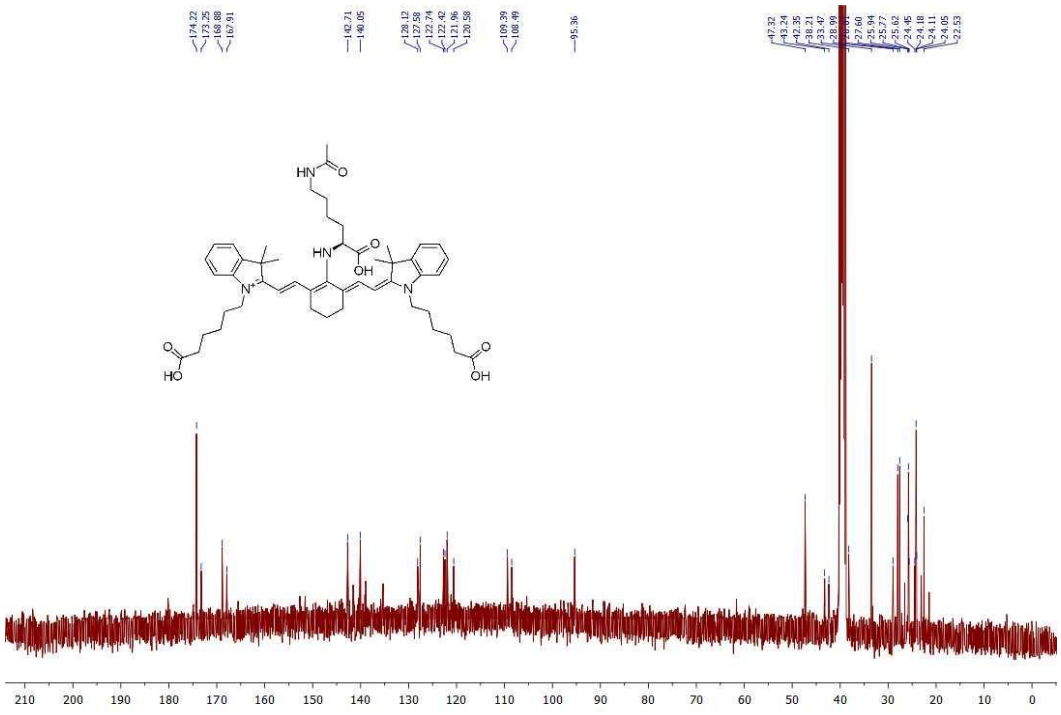

Figure B-S11. ^{13}C NMR of compound **1d** in Methanol-d4

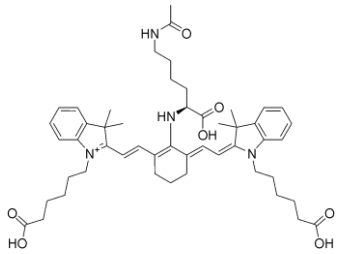

Chemical Formula: $C_{50}H_{67}N_4O_7^+$

Exact Mass: 835.5004

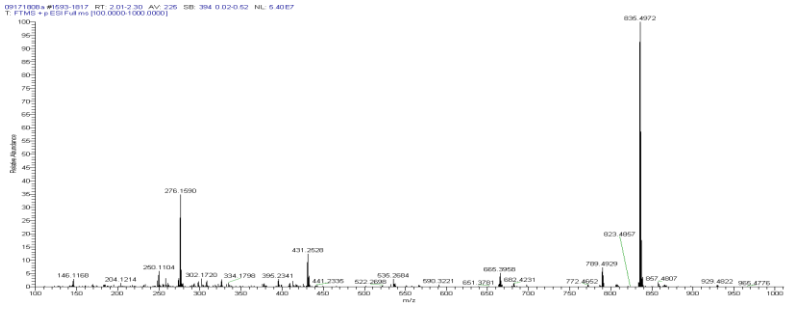

Figure B-S12. HRMS of compound **1d**

Coomassie Blue Staining of Diverse Proteins Gel

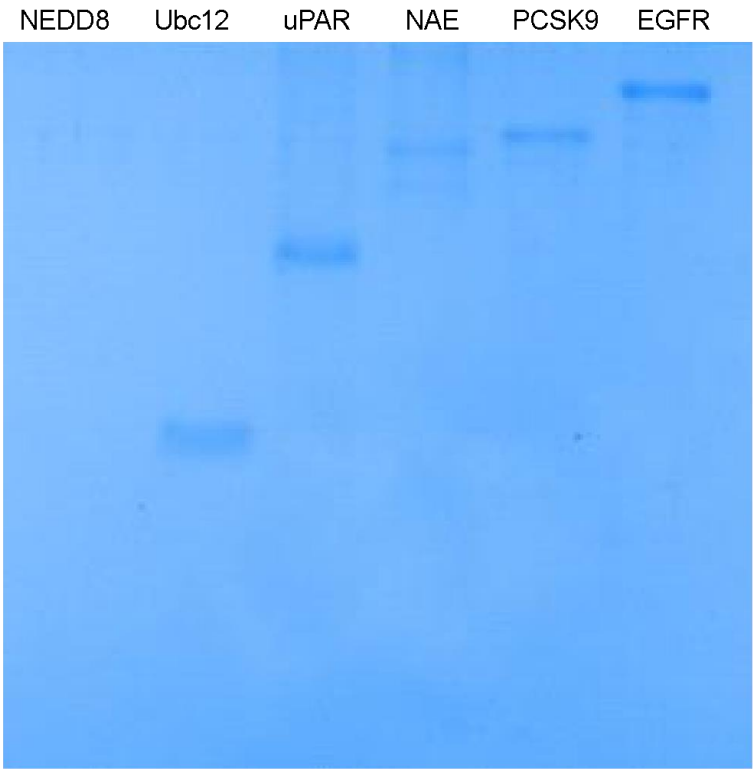

Figure B-S13. CBB-G250 staining of SDS-PAGE gel referred to Figure 6.

APPENDIX C

SUPPORTING INFORMATION FOR CHAPTER IV

General Experimental Procedures

All reactions were carried out under an argon atmosphere. Reagents were purchased at a high commercial quality (typically 97 % or higher) and used without further purification, unless otherwise stated. High field NMR spectra were recorded with Bruker Avance III at 400 MHz for ^{1}H, and 100 MHz for ^{13}C and were calibrated using residual non-deuterated solvent as an internal reference ($CDCl_3$: ^{1}H NMR = 7.24, ^{13}C NMR = 77.0, MeOD: ^{1}H NMR = 3.30, ^{13}C NMR = 49.0, DMSO-d_6: ^{1}H NMR = 2.50, ^{13}C NMR = 39.5). The following abbreviations were used to explain the multiplicities: s = singlet, d = doublet, t = triplet, q = quartet, quint = quintet, dd = double doublet, dt = double triplet, dq = double quartet, m = multiplet, br = broad. Electrospray ionization mass spectrometry (ESI-MS) data were collected on triple-stage quadrupole instrument in a positive mode. Flash chromatography was performed using silica gel (230-400 mesh). LC-MS analyses were collected from Agilent 1260 Infinity Quaternary LC and Agilent 6120 Quadrupole LC/MS modules using Poroshell 120 EC-C18 2.7 µM (4.6 x 50 mm) column in 5-95% CH_3CN/water gradient with 0.1% formic acid over 10 minutes. Prep HPLC was performed on Agilent 1260 Infinity in 50-90% CH_3CN/water gradient with 0.1% TFA over 20 mins. All statistical analyses were carried out by Graphpad Prism version 6.0 (Graphpad Software).

Synthetic Scheme

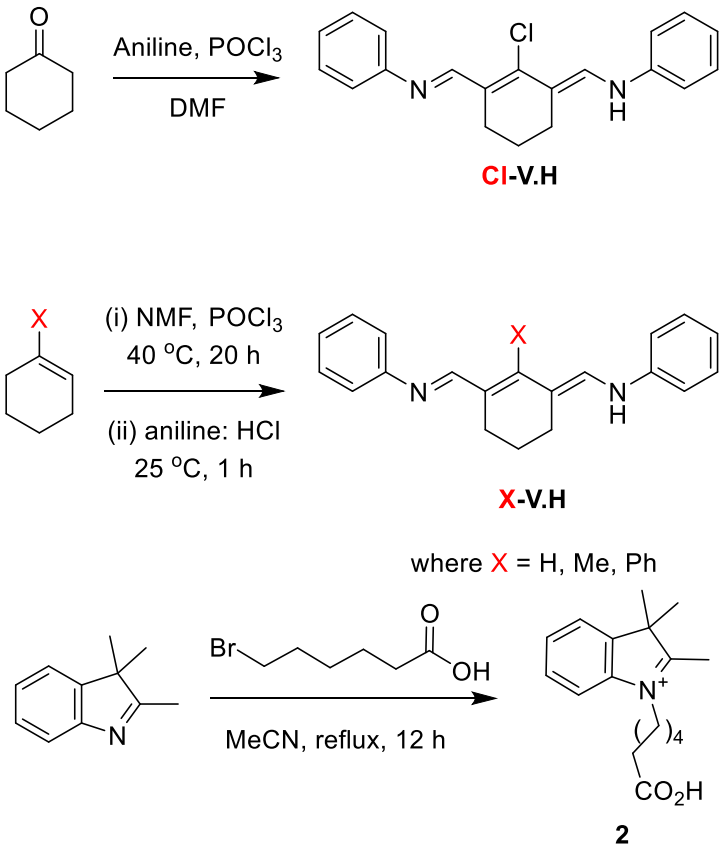

Scheme C-S1: Preparation of different substituted Vilsmeier Haack and substituted indole (**2**)

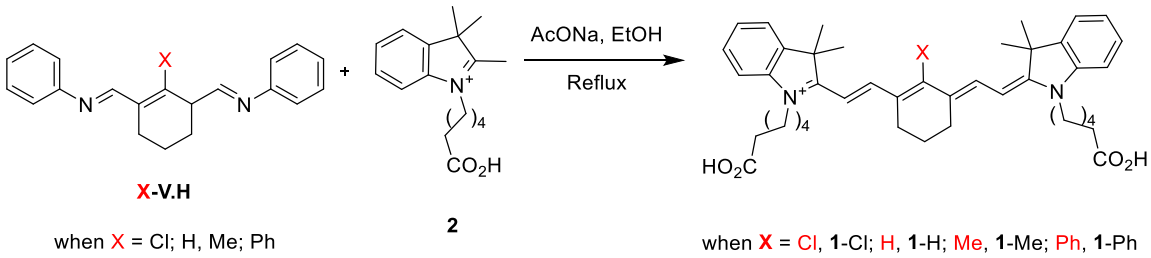

Scheme C-S2: Preparation of **1**-Cl, **1**-H, **1**-Me and **1**-Ph

Materials and Methods

Photophysical Properties: ICG was bought from Ark Pharm where as human serum albumin (HSA) was bought from Sigma Aldrich. HSA was stored in -20 ^{o}C and fresh 0.5 mM (33 mg in 1 mL) solution was prepared for experiments.

UV Absorbance with HSA: 10 μM of **1**-Cl, **1**-H, **1**-Me, **1**-Ph and ICG was dissolved in PBS pH 7.4 and different concentrations of HSA were added and stirred for 90 mins in dark. After which absorbance was determined using Cary-Varian 100 UV-Vis NIR spectrophotometer.

Kinetics Experiment: 200 μM of **1**-Cl, **1**-H, **1**-Me, **1**-Ph and ICG was dissolved in 500 μM of PBS pH 7.4 containing HSA. The reaction mixture was kept in incubator at 37 ^{o}C for up to 72 h and it was observed at different time points using C18 column on Agilent 1200 LC/MS. The detection wavelength was set up at 600 nm to observe ICG, **1**-Cl, **1**-H, **1**-Me, and **1**-Ph and their respective conjugate with HSA.

Mass Spec Analysis: 200 μM of **1**-Cl, **1**-H, **1**-Me, **1**-Ph and ICG was dissolved in 500 μM of HSA in PBS pH 7.4 for 3 h at 37 ^{o}C in an incubator set to shake at 90 rpm. Afterwards, the mixture was concentrated using 10 kDa (GE Health) cut off filter and washed thrice with 50 mM ammonium carbonate to replace the solvent.

In-Vitro Assays: U87-MG cells were grown in Dulbecco's Modified Eagle's medium (DMEM) containing 10% fetal bovine serum (FBS). Cells were grown in an incubator at 37°C, humidified atmosphere containing 5% CO_2. Cells were grown in T-75 culture flask till 70% confluency before splitting into next passage.

Live Cell Staining: Intracellular localization of dyes with the U87-MG cells was measured using Olympus Fluoview FV1000. The images were taken at 60x/1.20 water immersed objective. Lysosome, Mitochondria and Nucleus were stained using Lysotracker Green DND 26, Mitotracker Green FM and, NucBlue respectively were bought from Life Technologies. 488 nm laser was used for green channel, 405 nm laser was used for nucleus and 633 nm laser was used for compound **1**-Cl and **1**-HSA.

Blocking Experiment: Briefly, 50,000 cells were seeded on 4 well chambers (Nunc Lab-Tek) and allowed to adhere overnight. The cells were incubated with 20 μM of compound **2** for 30 mins, washed twice with PBS, and incubated with organelle stains according to manufacturer's instructions. The cells were washed twice again and stained with Nuc Blue for 10 mins.

Mode of uptake of **1**-Cl and **1**-HSA was determined on using Olympus FV1000 confocal microscope at 20x/0.75 Briefly, cells were either pre-blocked with 250 μM BSP for 10 mins or treated with 1 mM DMOG for 24 h before treating with the dye. After 30 mins incubation with **1**-Cl and **1**-HSA, cells were washed twice with PBS and stained with NucBlue for 10 mins and taken for imaging.

For endocytosis inhibitors, cells were starved for 20 h and different routes of endocytosis were blocked using Pitstop (20 μM), Amiloride (1 mM) and MβCD (15 μM) for 15 mins. After 30 mins incubation with **1**-Cl and **1**-HSA, cells were washed twice with PBS and stained with NucBlue for 10 mins and were imaged under confocal microscope as mentioned above.

NIR Gel Image Protocol

Incubation of 1-Cl with K562 cells: RPMI-1640 with 10 % FBS medium was used for K562 cell suspensions which were seeded to 24-well plates with 3 x 10^5 cells/well (500 µL). Various concentrations of **1**-Cl (20 mM stock in DMSO) were prepared in the same medium and added to 24-well plate containing cells (500 µL/well) to make final concentrations from 0 to 30 µM. After 20 h incubation, the cells were collected, washed twice with ice-cold PBS buffer, and RIPA lysis buffer (60 µL) containing 1% protease inhibitor was added to each cell sample. Each cell sample was gently shaken on ice for 30 min, and the lysate samples were centrifuged at 19000 rcf for 25 min at 4 ˚C to remove cell debris. The supernatant was collected and the protein concentration was determined using Pierce BSA protein assay kit (cat. #23225). Equal total protein amounts (30 µg) were electrophoresed in a 15% SDS-PAGE. The gel was washed with de-ionized water (10 min × 3 times), and the gel was analysized by an Odyssey imager to detect the Near IR fluorescence. The preparation of K562 lysate sample (10 µM of **1**-Cl used) from serum free medium is the same except serum free RPMI-1640 medium was used.

Incubation of 1-Cl, 1-H, 1-Me, and 1-Ph with HSA: Different cyanines (10 µM; 20 mM stock in DMSO) were incubated with HSA (1 µM; 1 µg) in pH 7.4 HEPES buffer (50 mM) for 3 h at 37 ^{o}C. 30 ng of **1**-HSA and 100 ng of other cyanine-HSA conjugates were treated with reducing condition and loaded into 10 % SDS-PAGE for electrophoresis. The gel was washed with de-ionized water (10 min × 3 times), and the gel was analysized by an Odyssey imager to detect the Near IR fluorescence**.**

Preparation of Thiol-blocked HSA: Using pH 7.4 HEPES buffer (50 mM), thiol-blocked HSA was prepared by reducing disulfide bonds of HSA (15 μM) with incubation of tris(2-carboxyethyl)phosphine) (TCEP, 1.5 mM, 100 fold) for 2 h at 25 ^{o}C, and followed by addition and incubation of 6-maleimide-hexanoic acid (6-MA, 6 mM) for another 18 h at 37 ^{o}C.

Synthetic Procedure

Synthesis of (1*E*,1'*E*)-1,1'-(2-chlorocyclohex-1-ene-1,3-diyl)bis(*N*-phenylmethanimine) (Cl-V.H) [217]

DMF (65 mL, 0.85 mol) was added to a 500 mL round bottom flask and cooled in an ice bath. $POCl_3$ (55 mL, 0.6 mol) was added dropwise over 10 min and the mixture was stirred for 30 min. Cyclohexanone (27.5 mL, 0.265 mol) was added and the solution was refluxed at 100 ^{o}C for 1 h. Subsequently, the heating was stopped and the reaction was cooled down to 0 ^{o}C by placing on ice bath. While the mixture was cooling, aniline/EtOH (1:1 v/v, 90 mL) was added, then the mixture was stirred for 1 h. The solution was poured to cold H_2O:conc. HCl (10:1, 110 mL) and allowed to stand for 2 h. The dark purple solid was collected by filtration and dissolved with methanol. The product was recrystallized using methyl *tert*-butyl ether:hexane (1:1) to give purple crystals (45.78 g, 86%).

^{1}H NMR (400 MHz, MeOD) δ 8.66 (s, 2H), 7.50 (s, 3H), 7.49 (d, *J* = 2.0 Hz, 3H), 7.31 (ddd, *J* = 8.4, 5.6, 3.0 Hz, 2H), 2.74 (t, *J* = 6.2 Hz, 4H), 2.00 (s, 2H).

^{13}C NMR (100 MHz, MeOD) δ 157.52, 149.00, 139.25, 129.70, 126.59, 118.47, 114.99, 24.19, 19.66.

General Procedure for X-V.H synthesis: Chloroform (20 mL) was cooled down to 0 ^{o}C and *N*-methyl-*N*-phenylformide (NMF) (48.6 mL, 0.36 mol, 3eq) was added to it. $POCl_3$ (33.5 mL, 0.36 mol, 3 eq) was added dropwise over 30 mins and stirred for 1 h at 0 ^{o}C. Afterwards, either cyclohexene (12.34 mL, 0.12 mol, 1 eq), 1-methyl-1-cyclohexene (12.3 mL, 0.10 mmol, 1 eq) or 1-phenyl-1-cyclohexene (10.0 mL, 0.06 mmol, 1 eq) was added and heated at 45 ^{o}C for 20 h. The reaction was cooled down at ice to 0 ^{o}C, distilled water (100 mL) was added gently to the reaction mixture, followed by 8 g of K_2CO_3 and stirred for 10 mins at room temperature. This was followed by addition of aniline:conc HCl (15:3) in water 8 mL and reaction mixture was stirred for additional 30 mins. After cooling the reaction mixture K_2CO_3 was added dropwise over 15 mins. The reaction was left at 0 ^{o}C for 15 mins for precipitates to form which were filtered and washed with cold water. To get pure compounds, the products were precipitated from different solutions as mentioned below.

Synthesis of *N*-((*E*)-(3-((*E*)-(phenylimino)methyl)cyclohex-2-en-1-ylidene)methyl)aniline (H-V.H)

Pure compound was precipitated from dissolving the crude material in acetone and stirred vigorously for 10 mins to give the product. (8 g, 24%)

^{1}H NMR (400 MHz, MeOD) δ 8.13 (s, 2H), 7.79 (s, 1H), 7.50 – 7.39 (m, 8H), 7.28 (dd, *J* = 7.6, 6.1 Hz, 2H), 2.60 (t, *J* = 6.2 Hz, 4H), 2.03 – 1.93 (m, 2H).

^{13}C NMR (101 MHz, MeOD) δ 191.23, 162.19, 151.82, 139.30, 129.81, 129.57, 125.79, 119.16, 118.57, 117.80, 117.49, 21.53, 20.16.

HRMS calculated for $C_{20}H_{20}N_2^+$ calculated $(M+H)^+$: 289.3940; found 289.1694

Synthesis of *N*-((*E*)-(2-methyl-3-((*E*)-(phenylimino)methyl)cyclohex-2-en-1-ylidene)methyl)aniline (Me-V.H)

Pure compound was precipitated by dissolving the crude precipitate in acetonitrile and stirring vigorously for 10 mins to give pure compound. (13 g, 38%)

^{1}H NMR (400 MHz, MeOD) δ 8.48 (s, 1H), 7.75 (s, 1H), 7.71 – 7.61 (m, 1H), 7.56 (ddd, *J* = 15.3, 10.5, 6.7 Hz, 2H), 7.51 – 7.39 (m, 5H), 7.31 – 7.25 (m, 1H), 2.63 – 2.57 (m, 4H), 2.54 – 2.42 (m, 2H), 2.02 – 1.88 (m, 1H), 1.84 (t, *J* = 6.3 Hz, 1H).

^{13}C NMR (101 MHz, MeOD) δ 162.26, 157.09, 139.75, 129.73, 129.53, 125.76, 122.84, 122.69, 121.64, 120.29, 118.25, 117.79, 23.14, 21.50, 20.03, 13.07.

HRMS calculated for $C_{21}H_{22}N_2^+$ calculated $(M+H)^+$: 303.4285; found 303.1852

Synthesis of *N*-((*E*)-(6-((*E*)-(phenylimino)methyl)-4,5-dihydro-[1,1'-biphenyl]-2(3H)-ylidene)methyl)aniline (Ph-V.H)

Pure compound was precipitated from dissolving the crude precipitate in acetonitrile and stirred vigorously for 10 mins to give pure compound. (16 g, 47%)

^{1}H NMR (400 MHz, MeOD) δ 8.97 (s, 1H), 7.54 – 7.43 (m, 3H), 7.43 – 7.38 (m, 1H), 7.37 – 7.26 (m, 2H), 7.26 – 7.19 (m, 1H), 7.16 (t, *J* = 7.9 Hz, 3H), 6.88 (t, *J* = 7.4 Hz,

1H), 6.72 (d, *J* = 8.1 Hz, 2H), 6.60 (s, 1H), 2.59 (t, *J* = 6.0 Hz, 2H), 2.46 (t, *J* = 6.1 Hz, 3H), 1.91 – 1.81 (m, 2H).

^{13}C NMR (101 MHz, MeOD) δ 191.90, 160.72, 141.84, 136.56, 136.41, 130.20, 130.00, 129.05, 128.16, 127.74, 127.62, 127.53, 121.44, 114.65, 113.80, 23.47, 21.64, 20.70.

HRMS calculated for $C_{26}H_{24}N_2^+$ calculated $(M+H)^+$: 365.4920; found 365.2008

Synthesis of 1-(5-carboxypentyl)-2,3,3-trimethyl-3H-indol-1-ium (2) [95]

In 500 mL round bottom flask, 2,3,3-trimethylindolenine (5.00 g, 31.4 mol) and 6-bromohexanoic acid (12.3 g, 62.8 mmol) were added to 200 mL of acetonitrile. The mixture was refluxed for 12 h. Subsequently, the mixture was cooled to room temperature and acetonitrile was removed under reduced pressure. Subsequently, the flask was placed in an ice bath, the solid residue was dissolved in 100 mL dichloromethane, then 300 mL diethyl ether was added to precipitate the product. That product was collected by filtration and washed with diethyl ether to afford pink crystals (6.4 g, 72%).

^{1}H NMR (400 MHz, MeOD) δ 7.91 – 7.84 (m, 1H), 7.79 (dt, *J* = 7.5, 3.8 Hz, 1H), 7.71 – 7.61 (m, 3H), 4.58 – 4.49 (m, 3H), 2.36 (t, *J* = 7.2 Hz, 3H), 2.05 – 1.96 (m, 3H), 1.77 – 1.67 (m, 3H), 1.63 (s, 8H), 1.62 – 1.49 (m, 3H).

^{13}C NMR (100 MHz, MeOD) δ 196.51, 175.75, 142.02, 141.08, 129.83, 129.14, 123.26, 115.13, 54.56, 32.98, 27.15, 25.66, 23.99, 21.40.

HRMS calculated for $C_{42}H_{51}ClIN_2O_4^+$ calculated: 809.2577; found 809.2508

General synthesis for 1 and 1-analogues: Vilsmeier Haack Reagent **X-V.H** (1 eq, 3.64 mmol), **2** (2 eq, 7.28 mmol) and NaOAc (1 eq, 7.28 mmol) were dissolved in 100 mL of absolute ethanol in 250 mL round bottom flask. The mixture was refluxed for 6 h. The final product was either purified by normal silica column or prep column as mentioned below.

Synthesis of 1-(5-carboxypentyl)-2-((E)-2-((E)-3-(2-((E)-1-(5-carboxypentyl)-3,3-dimethylindolin-2-ylidene)ethylidene)-2-chlorocyclohex-1-en-1-yl)vinyl)-3,3-dimethyl-3H-indol-1-ium (1-Cl) [86]

Crude product was purified by normal phase flash chromatography with MeOH:CH_2Cl_2 (1:25 v/v) to obtain green solid (0.98 g, 48%).

^{1}H NMR (400 MHz, MeOD) δ 8.47 (d, *J* = 14.1 Hz, 2H), 7.54 (d, *J* = 7.3 Hz, 2H), 7.48 – 7.42 (m, 2H), 7.37 – 7.28 (m, 4H), 6.31 (d, *J* = 14.1 Hz, 2H), 4.20 (t, *J* = 7.3 Hz, 3H), 2.75 (d, *J* = 5.5 Hz, 4H), 2.34 (t, *J* = 7.2 Hz, 4H), 2.04 – 1.96 (m, 2H), 1.95 – 1.84 (m, 4H), 1.76 (s, 12H), 1.74 – 1.68 (m, 3H), 1.59 – 1.49 (m, 4H).

^{13}C NMR (100 MHz, MeOD) δ 175.78, 172.93, 149.82, 144.17, 142.21, 141.23, 128.51, 126.64, 125.18, 122.12, 110.88, 100.91, 49.27, 43.70, 33.19, 26.92, 26.68, 25.96, 24.24, 20.71.

Synthesis of 1-(5-carboxypentyl)-2-((*E*)-2-((*E*)-3-(2-((*E*)-1-(5-carboxypentyl)-3,3-dimethylindolin-2-ylidene)ethylidene)cyclohex-1-en-1-yl)vinyl)-3,3-dimethyl-3H-indol-1-ium (1-H)

Crude product was purified by reverse phase column on prep-HPLC {10% MeCN/90%H_2O – 90%MeCN/10%H_2O (containing 0.1% TFA) in 20 mins} to get the desired product as amorphous green solid (1.06 g, 41%).

^{1}H NMR (400 MHz, MeOD) δ 7.78 (s, 2H), 7.48 (d, *J* = 7.3 Hz, 2H), 7.41 (t, *J* = 7.6 Hz, 2H), 7.26 (s, 4H), 6.19 (s, 1H), 4.13 (s, 3H), 2.59 (s, 3H), 2.34 (t, *J* = 7.3 Hz, 4H), 2.04 – 1.89 (m, 3H), 1.87 (dt, *J* = 15.0, 7.4 Hz, 5H), 1.75 (d, *J* = 7.4 Hz, 2H), 1.72 (d, *J* = 6.8 Hz, 12H), 1.70 (d, *J* = 7.4 Hz, 1H), 1.53 (dd, *J* = 15.4, 8.4 Hz, 4H).

^{13}C NMR (100 MHz, MeOD) δ 175.79, 148.39, 142.38, 140.99, 128.32, 124.52, 121.95, 110.30, 48.85, 43.28, 33.20, 26.60, 25.98, 24.25, 23.58, 21.29.

HRMS calculated for $C_{42}H_{53}N_2O_4^+$calculated: 649.4000; found 649.3991

Synthesis of 1-(5-carboxypentyl)-2-((*E*)-2-((*E*)-3-(2-((*E*)-1-(5-carboxypentyl)-3,3-dimethylindolin-2-ylidene)ethylidene)-2-methylcyclohex-1-en-1-yl)vinyl)-3,3-dimethyl-3H-indol-1-ium (1-Me)

Crude product was purified by reverse phase column on prep-HPLC {10% MeCN/90%H_2O – 90%MeCN/10%H_2O (containing 0.1% TFA) in 20 mins} to get the desired product as amorphous green solid (1.56 g, 57%).

^{1}H NMR (400 MHz, MeOD) δ 8.19 (s, 2H), 7.50 (d, *J* = 7.4 Hz, 2H), 7.42 (t, *J* = 7.3 Hz, 2H), 7.27 (dd, *J* = 12.3, 7.7 Hz, 4H), 6.25 (d, *J* = 13.0 Hz, 1H), 4.14 (d, *J* = 6.6 Hz, 4H), 2.62 (s, 3H), 2.48 (s, 3H), 2.34 (t, *J* = 7.3 Hz, 4H), 1.97 – 1.83 (m, 6H), 1.77 (d, *J* = 3.1 Hz, 1H), 1.74 (s, 12H), 1.73 – 1.68 (m, 3H), 1.58 – 1.45 (m, 4H).

^{13}C NMR (101 MHz, MeOD) δ 175.79, 171.45, 156.14, 142.56, 142.42, 140.92, 130.99, 128.39, 124.52, 121.99, 110.32, 99.84, 48.77, 43.38, 33.19, 27.14, 26.50, 26.01, 25.05, 24.26, 21.03, 13.69.

HRMS calculated for $C_{43}H_{55}N_2O_4^+$ calculated: 663.4156; found 663.4145

Synthesis of 1-(5-carboxypentyl)-2-((E)-2-((E)-6-(2-((E)-1-(5-carboxypentyl)-3,3-dimethylindolin-2-ylidene)ethylidene)-3,4,5,6-tetrahydro-[1,1'-biphenyl]-2-yl)vinyl)-3,3-dimethyl-3H-indol-1-ium (1-Ph)

Crude product was purified by reverse phase column on prep-HPLC {10% MeCN/90%H_2O – 90%MeCN/10%H_2O (containing 0.1% TFA) in 20 mins} to get the desired product as amorphous green solid (2.0 g, 68%).

^{1}H NMR (400 MHz, MeOD) δ 7.70 – 7.56 (m, 3H), 7.42 – 7.32 (m, 5H), 7.24 (ddd, *J* = 25.5, 12.5, 6.7 Hz, 8H), 6.20 (d, *J* = 13.6 Hz, 2H), 4.09 (t, *J* = 6.7 Hz, 4H), 2.74 (s, 4H), 2.33 (t, *J* = 7.3 Hz, 4H), 2.15 – 2.03 (m, 2H), 1.87 – 1.75 (m, 4H), 1.75 – 1.64 (m, 5H), 1.53 – 1.44 (m, 4H), 1.21 (d, *J* = 9.5 Hz, 12H).

^{13}C NMR (100 MHz, MeOD) δ 175.78, 171.92, 148.21, 142.24, 140.75, 139.06, 131.24, 129.38, 128.49, 128.32, 128.01, 124.57, 121.93, 110.33, 99.45, 48.50, 43.34, 33.20, 26.59, 26.52, 25.94, 24.25, 21.16.

HRMS calculated for $C_{48}H_{57}N_2O_4^+$ calculated: 725.4313; found 725.4306

NMR Spectra

(1E,1'E)-1,1'-(2-chlorocyclohex-1-ene-1,3-diyl)bis(N-phenylmethanimine) (Cl-V.H)

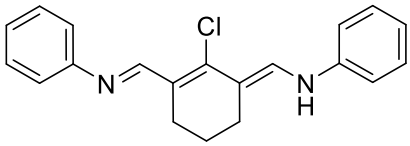

^{1}H

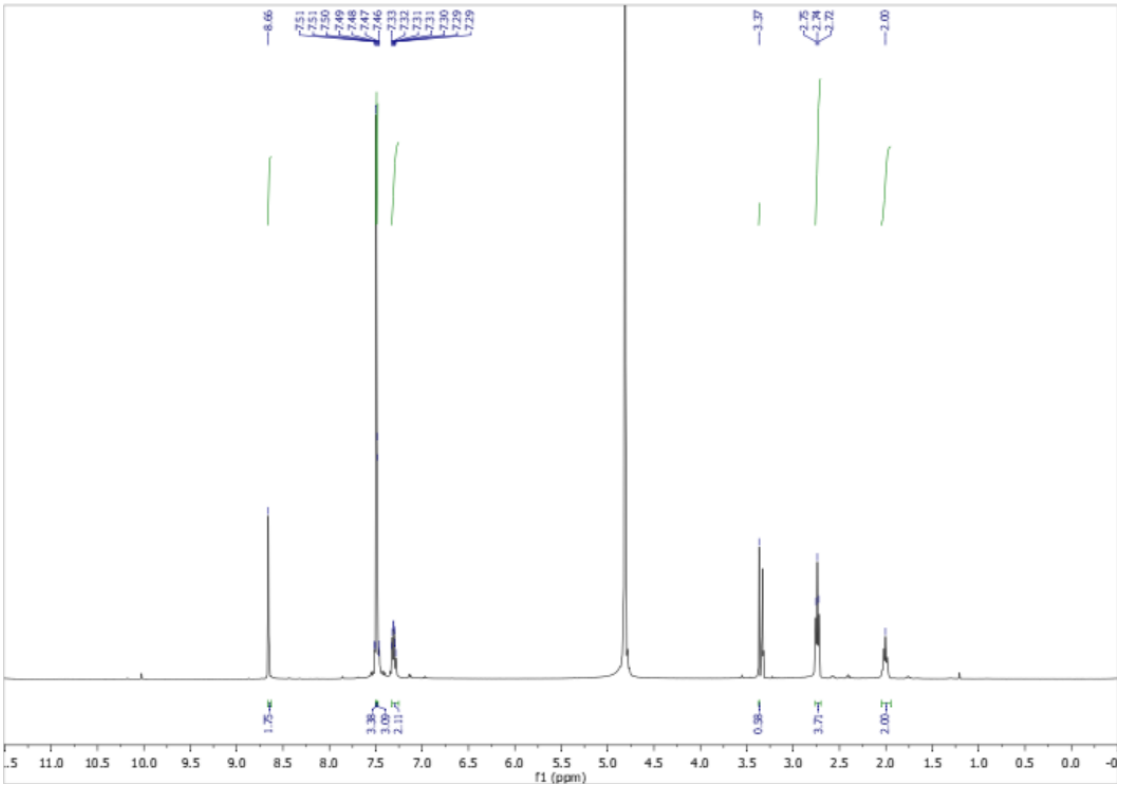

^{13}C

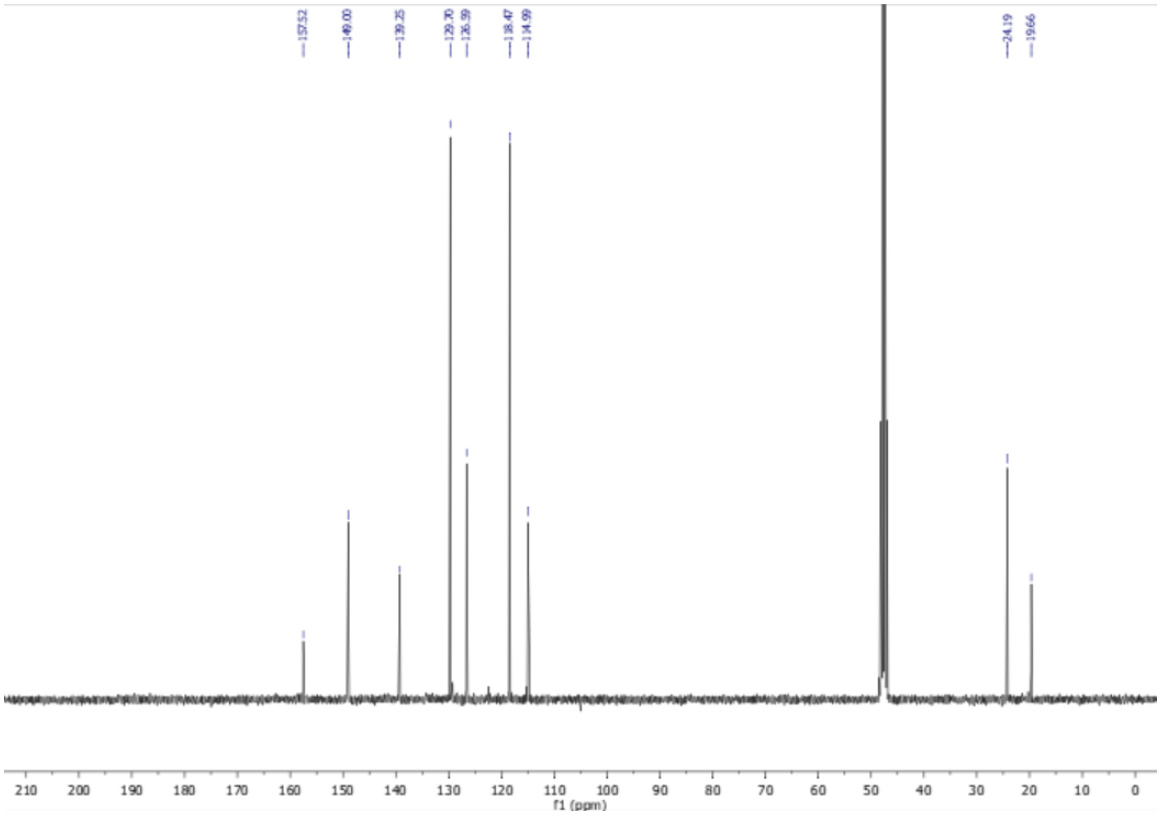
157.52
149.00
139.25
129.70
126.99
118.47
114.99
34.19
19.66
210 200 190 180 170 160 150 140 130 120 110 100 90 80 70 60 50 40 30 20 10 0
f1 (ppm)

N-((E)-(3-((E)-(phenylimino)methyl)cyclohex-2-en-1-ylidene)methyl)aniline (H-V.H)

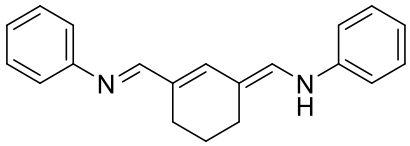

^{1}H

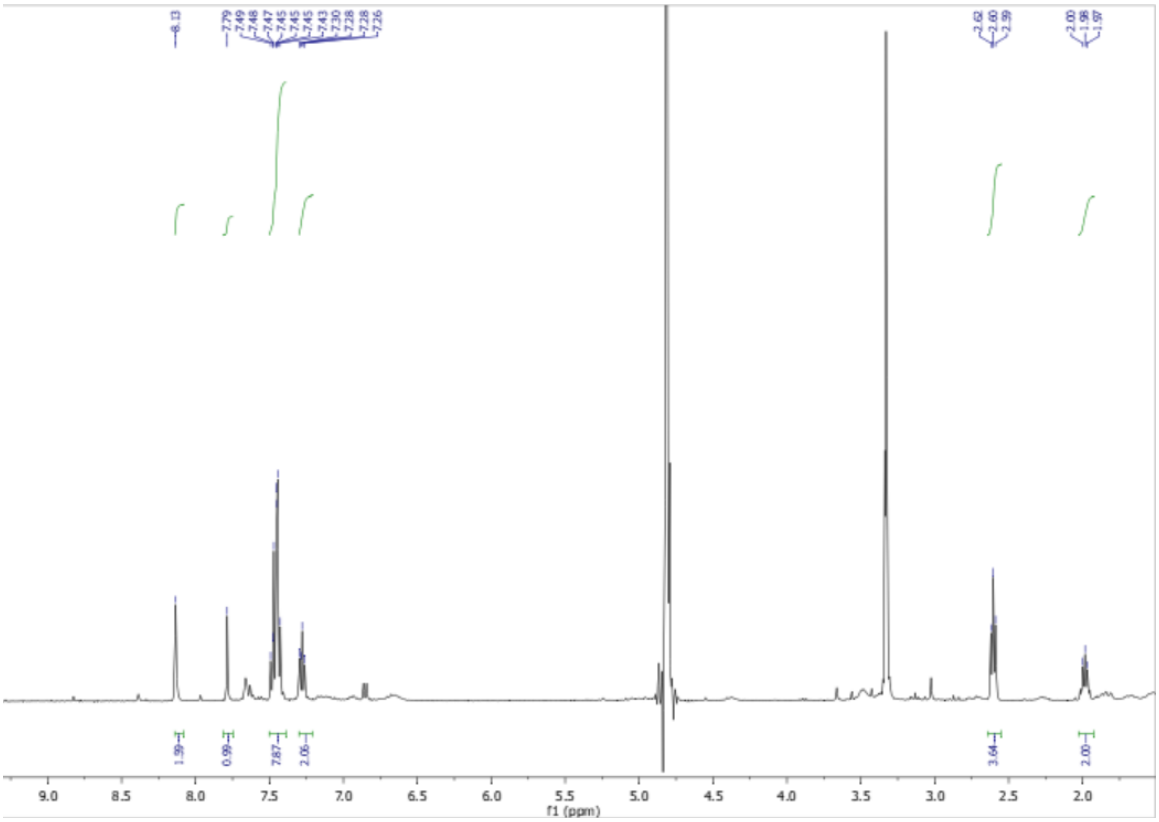

^{13}C

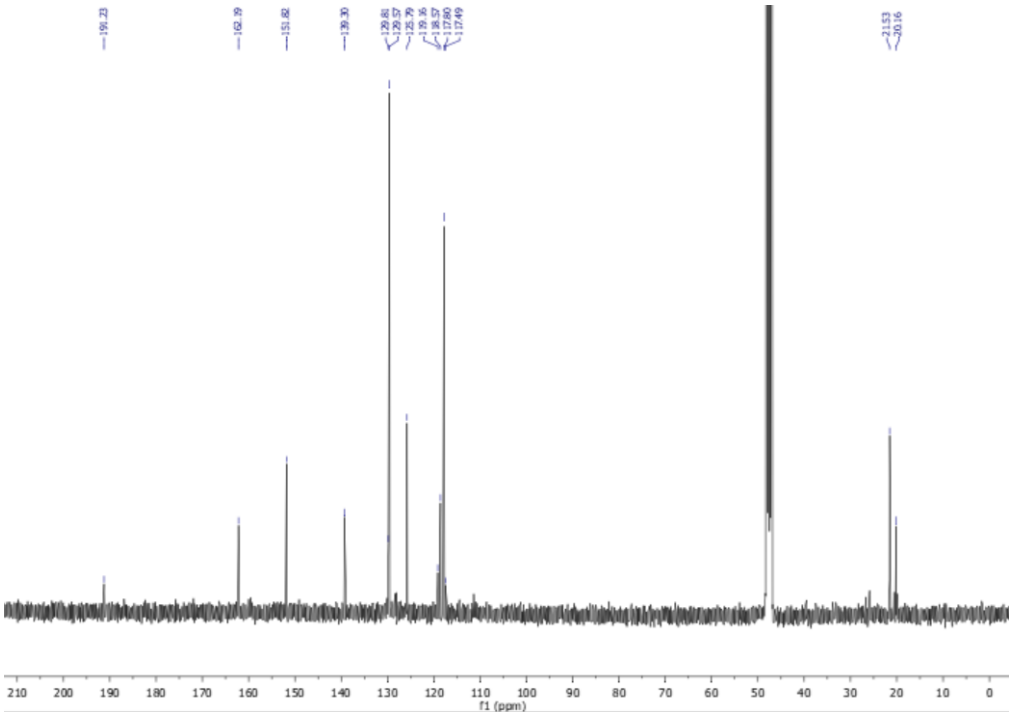
196.23
162.39
151.82
139.30
129.81
129.57
125.79
119.36
118.57
117.80
117.49
21.53
20.16
210 200 190 180 170 160 150 140 130 120 110 100 90 80 70 60 50 40 30 20 10 0
f1 (ppm)

HRMS

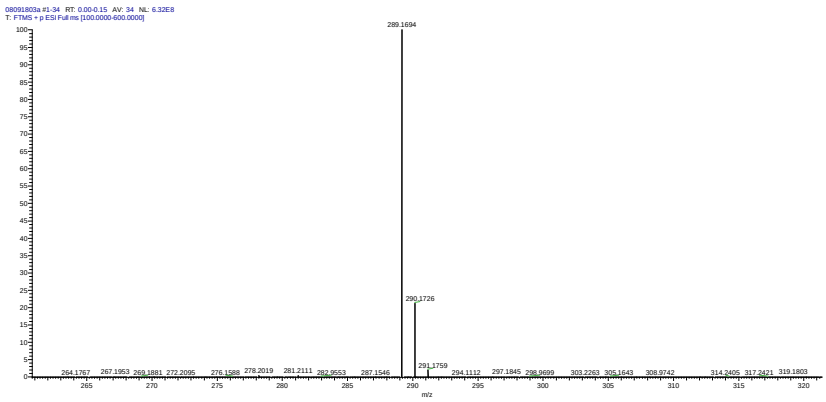
08091803a #1-34 RT: 0.00-0.15 AV: 34 NL: 6.32E8
T: FTMS + p ESI Full ms [100.0000-600.0000]
289.1694
290.1726
291.1759
264.1767
267.1953
269.1881
272.2095
276.1588
278.2019
281.2111
282.9553
287.1546
294.1112
297.1845
298.9699
303.2263
305.1643
308.9742
314.2405
317.2421
319.1803
m/z

N-((E)-(2-methyl-3-((E)-(phenylimino)methyl)cyclohex-2-en-1-ylidene)methyl)aniline (Me-V.H)

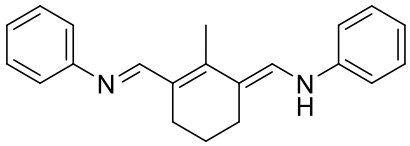

^{1}H

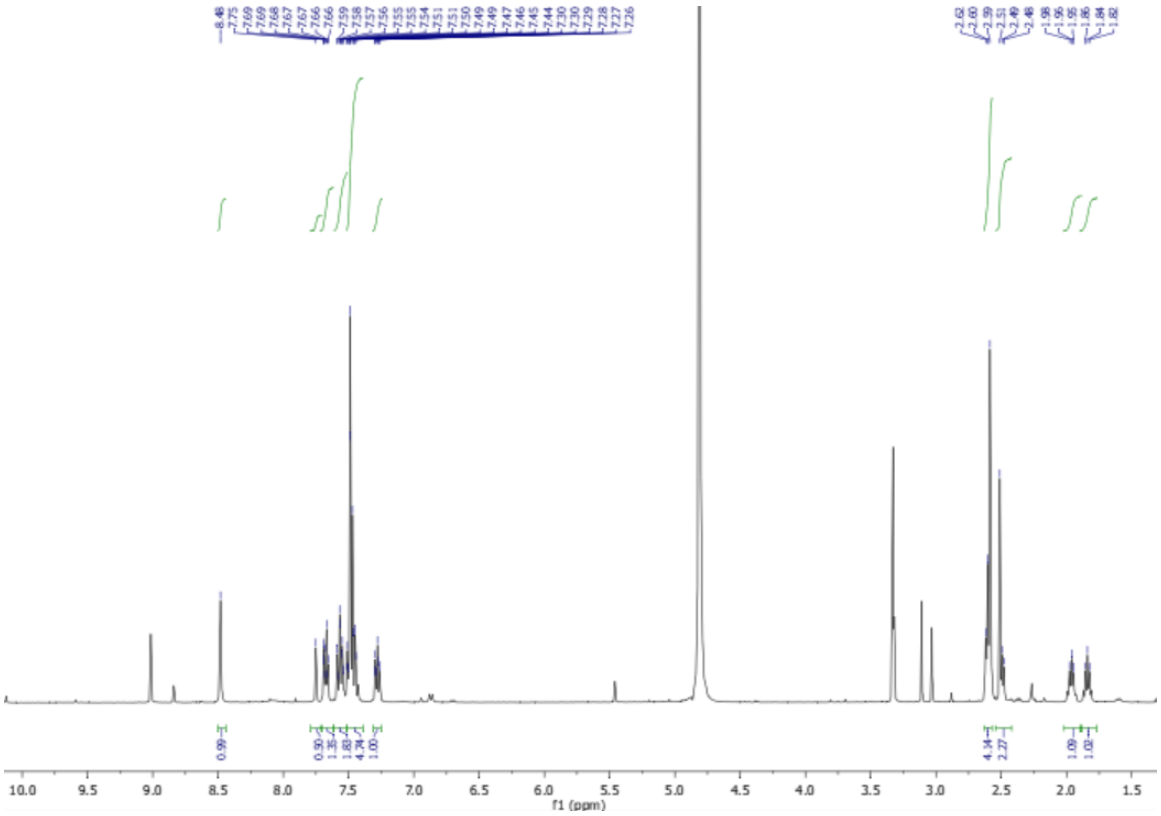

^{13}C

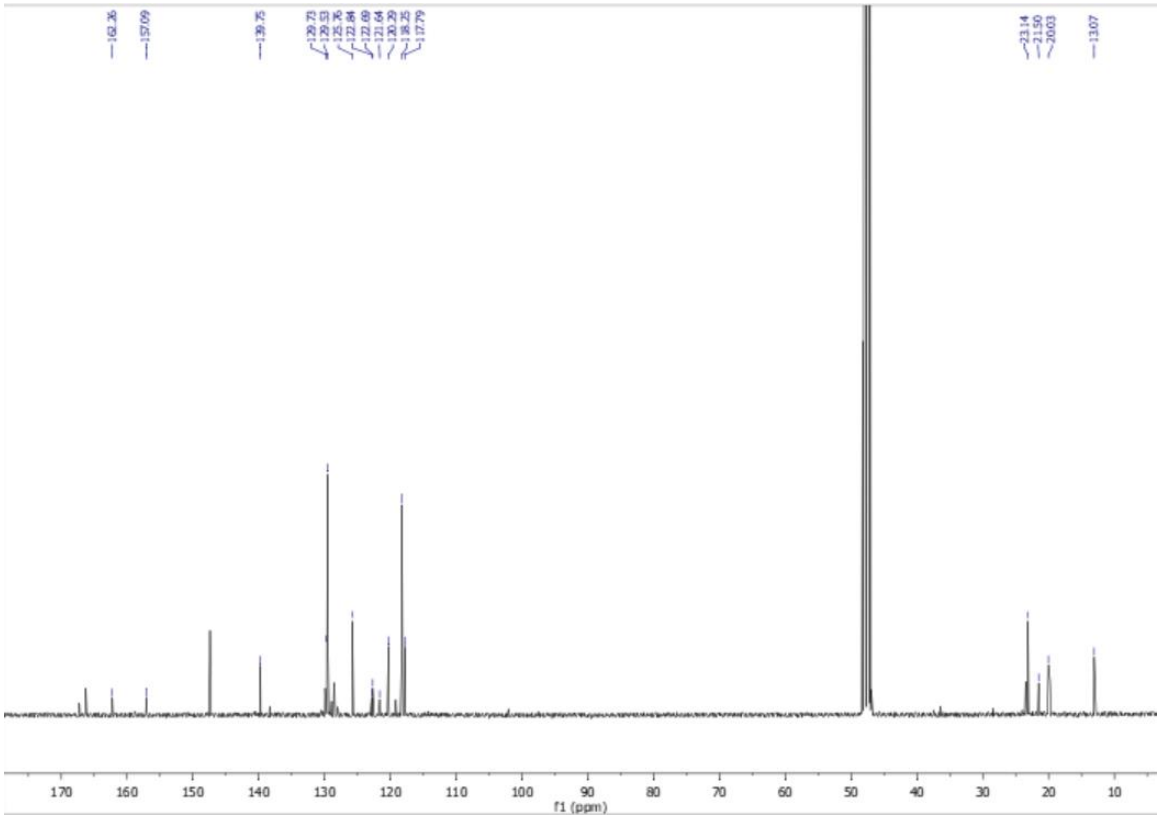
162.26
157.09
139.75
129.73
129.53
125.76
122.84
122.69
121.64
120.39
118.25
117.79
23.14
21.50
20.03
13.07
f1 (ppm)

HRMS

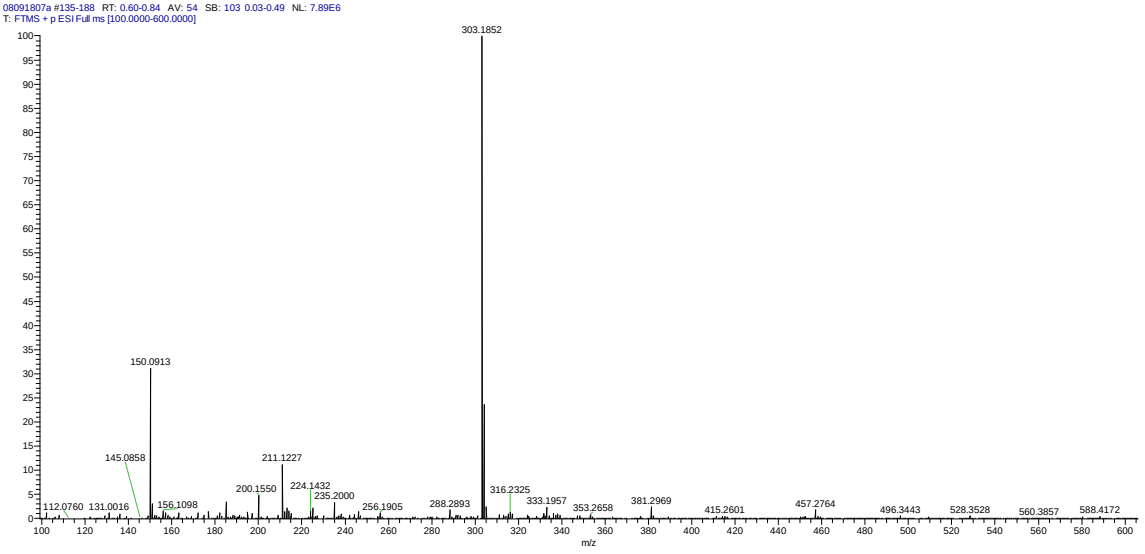
08091807a #135-188 RT: 0.60-0.84 AV: 54 SB: 103 0.03-0.49 NL: 7.89E6
T: FTMS + p ESI Full ms [100.0000-600.0000]
303.1852
150.0913
145.0858
211.1227
224.1432
235.2000
200.1550
316.2325
333.1957
381.2969
112.0760
131.0016
156.1098
256.1905
288.2893
353.2658
415.2601
457.2764
496.3443
528.3528
560.3857
588.4172
m/z

N-((E)-(6-((E)-(phenylimino)methyl)-4,5-dihydro-[1,1'-biphenyl]-2(3H) ylidene)methyl)aniline (Ph-V.H)

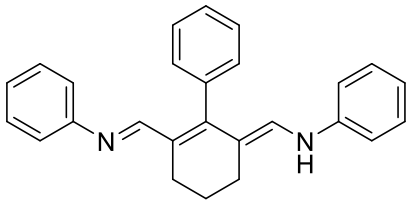

^{1}H

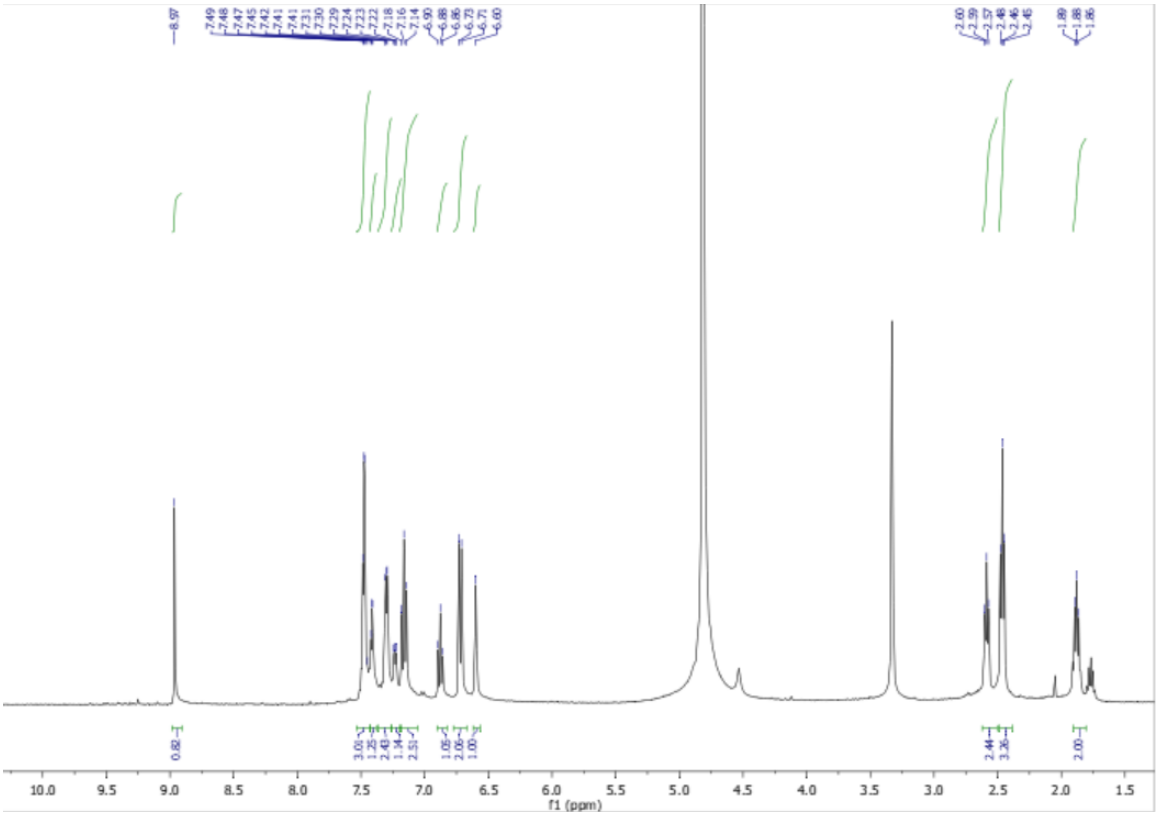

^{13}C

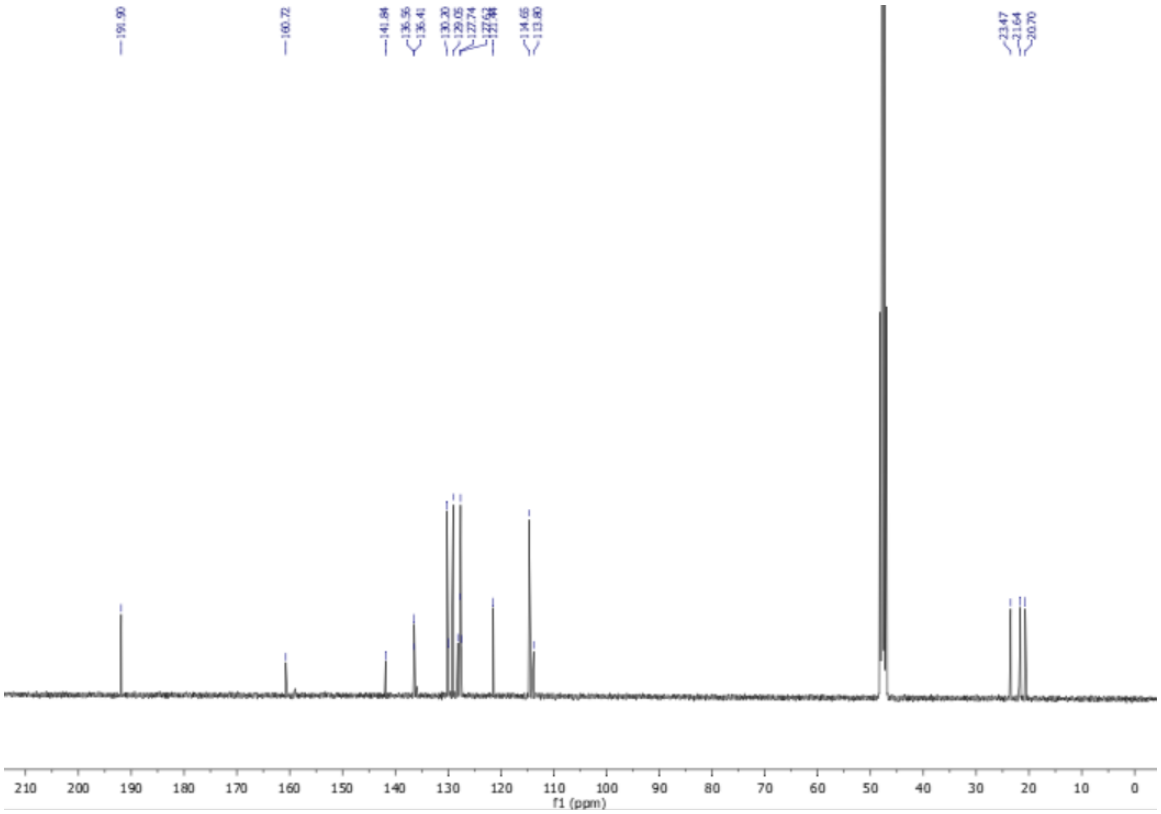
199.90
160.72
141.84
135.55
135.41
130.20
129.05
127.74
127.63
127.44
114.65
113.80
23.47
21.64
20.70
f1 (ppm)

HRMS

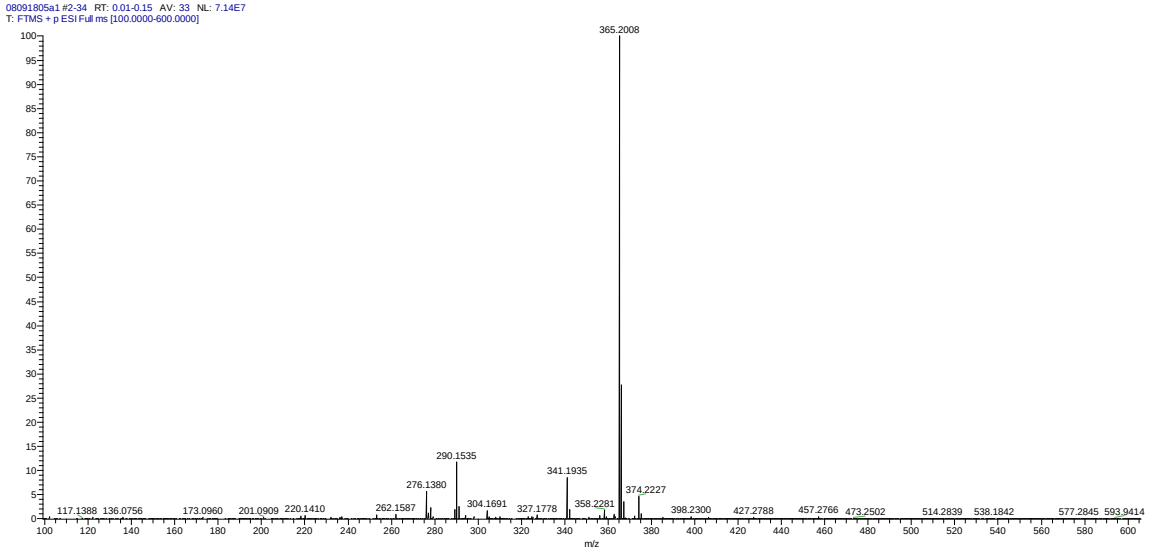
08091805a1 #2-34 RT: 0.01-0.15 AV: 33 NL: 7.14E7
T: FTMS + p ESI Full ms [100.0000-600.0000]
365.2008
290.1535
276.1380
341.1935
374.2227
304.1691
358.2281
327.1778
262.1587
220.1410
201.0909
173.0960
136.0756
117.1388
398.2300
427.2788
457.2766
473.2502
514.2839
538.1842
577.2845
593.9414
m/z

1-(5-carboxypentyl)-2,3,3-trimethyl-3H-indol-1-ium (2)

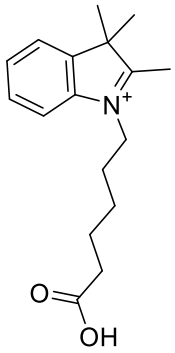

^{1}H

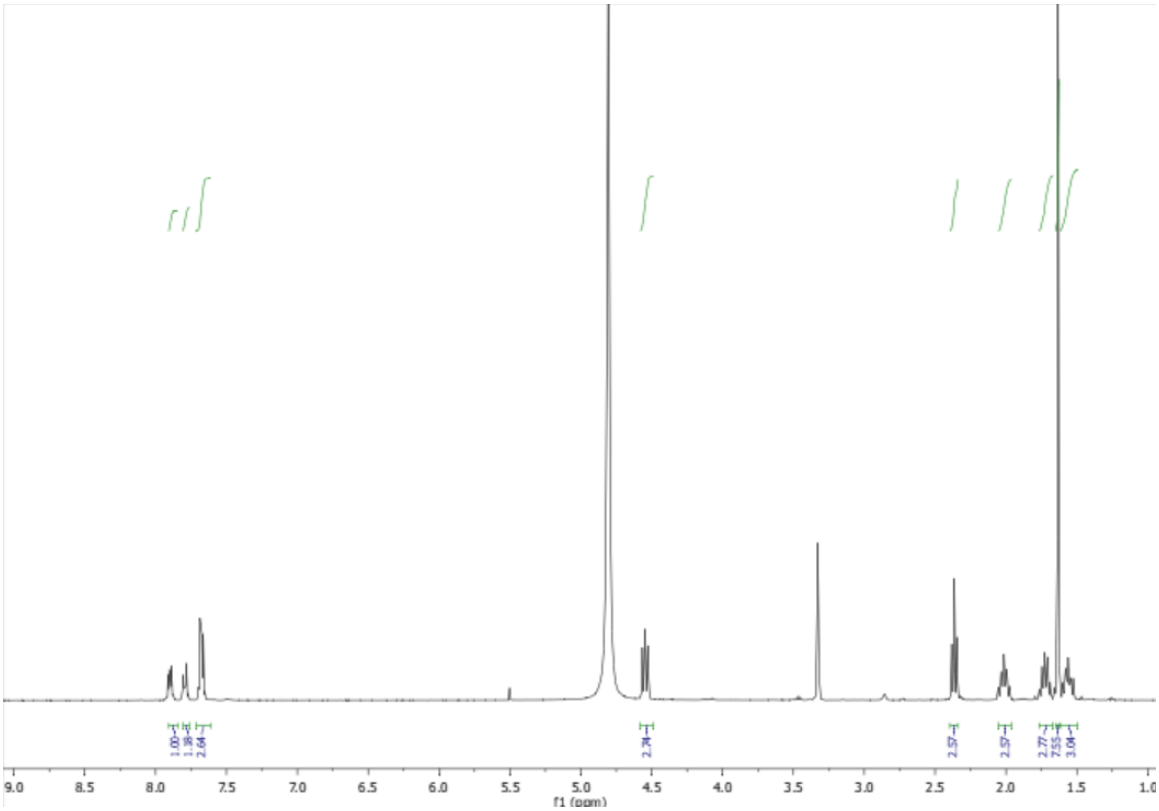

^{13}C

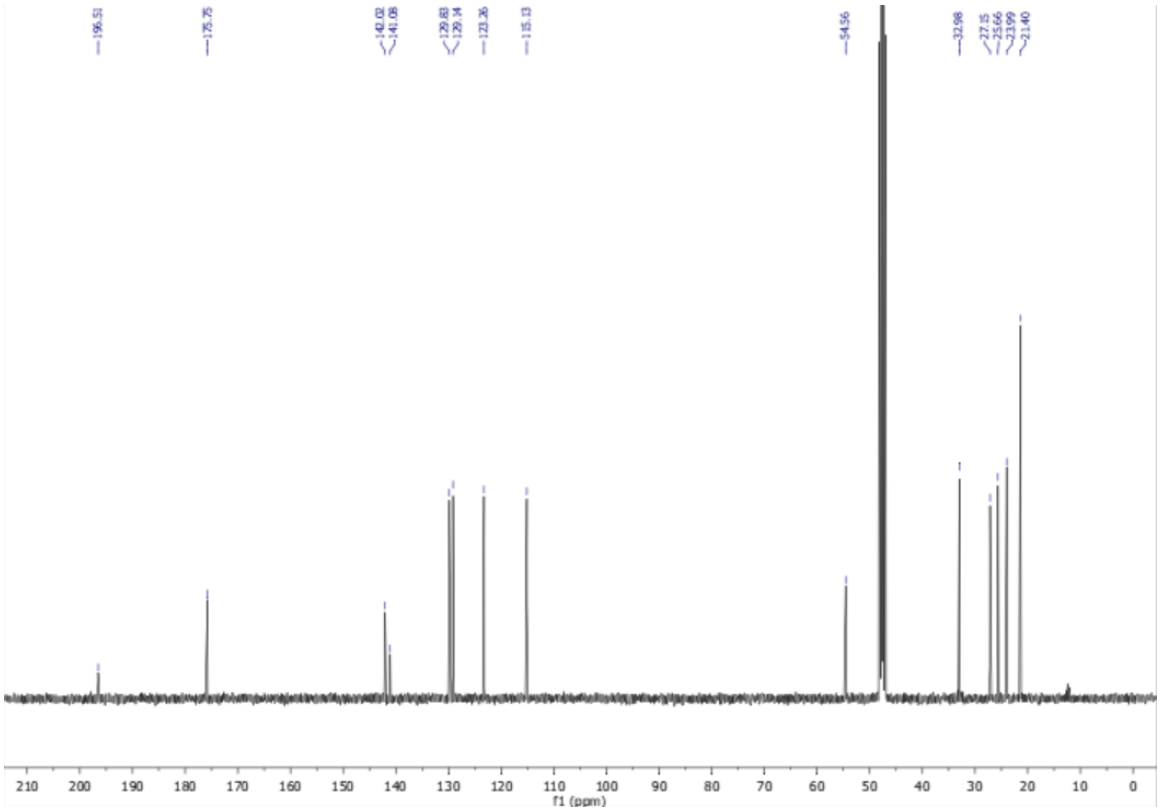
196.51
175.75
140.02
141.08
129.83
129.14
123.36
115.13
54.56
32.98
27.15
25.66
23.99
21.40
210 200 190 180 170 160 150 140 130 120 110 100 90 80 70 60 50 40 30 20 10 0
f1 (ppm)

1-(5-carboxypentyl)-2-((E)-2-((E)-3-(2-((E)-1-(5-carboxypentyl)-3,3-dimethylindolin-2-ylidene)ethylidene)-2-chlorocyclohex-1-en-1-yl)vinyl)-3,3-dimethyl-3H-indol-1-ium (1-Cl)

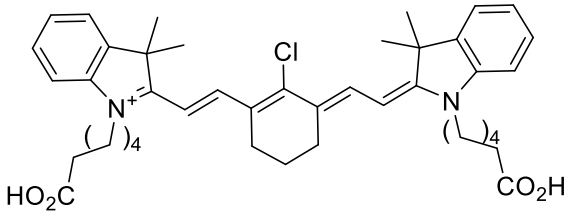

^{1}H

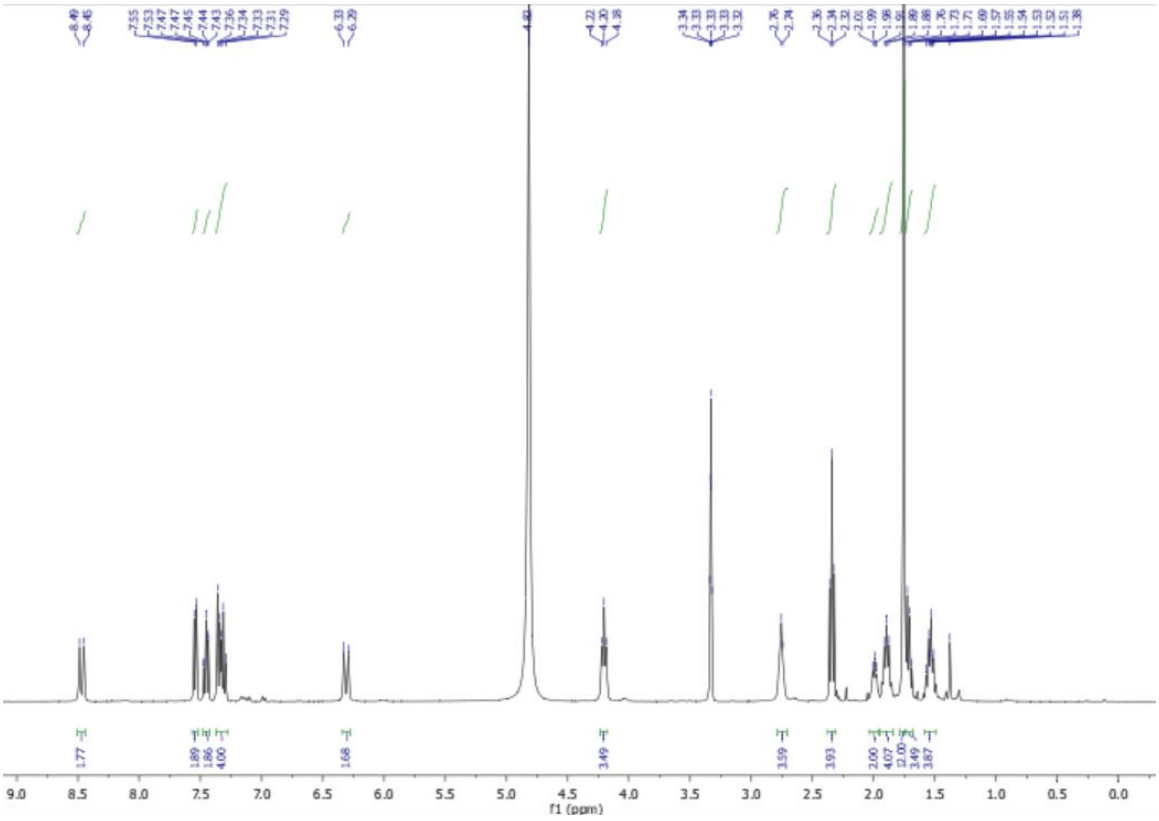

^{13}C

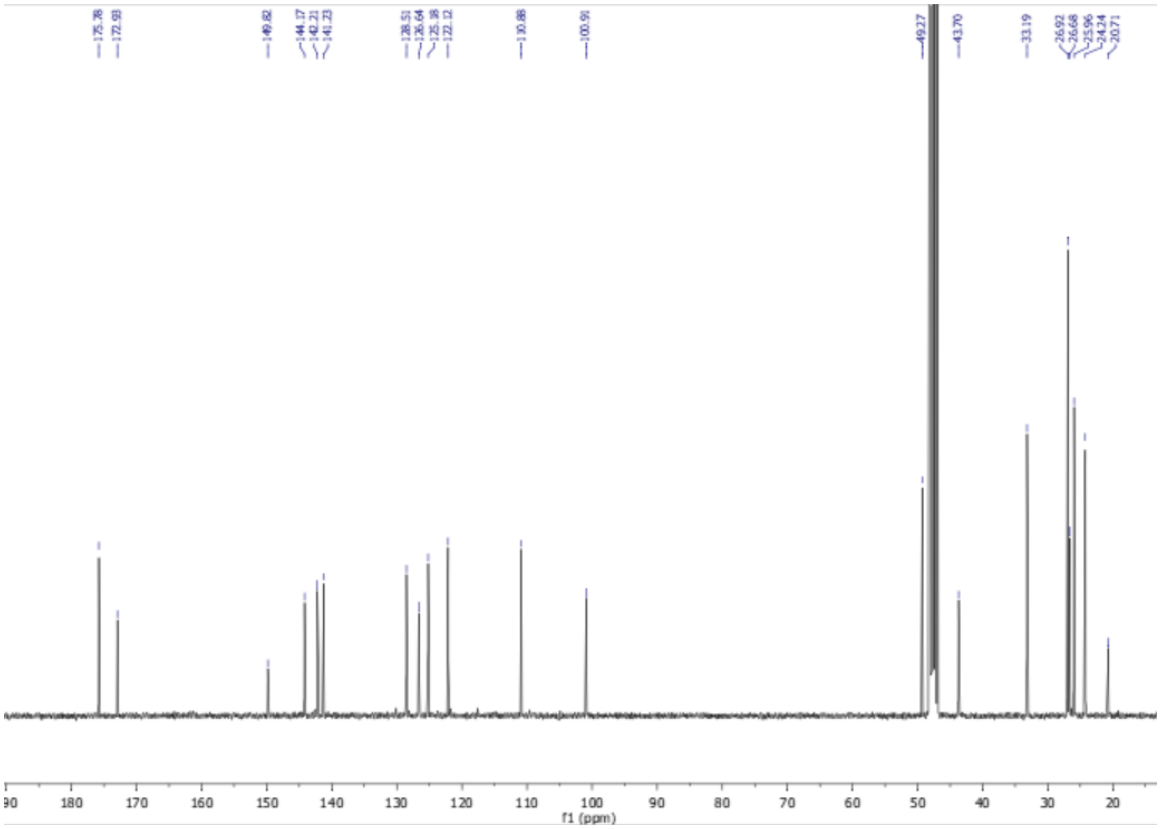
175.28
172.93
149.82
144.17
142.21
141.23
128.51
126.64
125.36
122.12
110.88
100.91
49.27
43.70
33.19
26.92
26.68
25.96
24.24
20.71
f1 (ppm)

1-(5-carboxypentyl)-2-((E)-2-((E)-3-(2-((E)-1-(5-carboxypentyl)-3,3-dimethylindolin-2-ylidene)ethylidene)cyclohex-1-en-1-yl)vinyl)-3,3-dimethyl-3H-indol-1-ium (1-H)

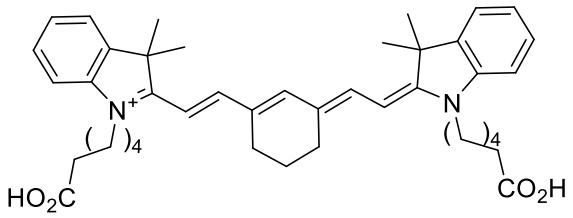

^{1}H

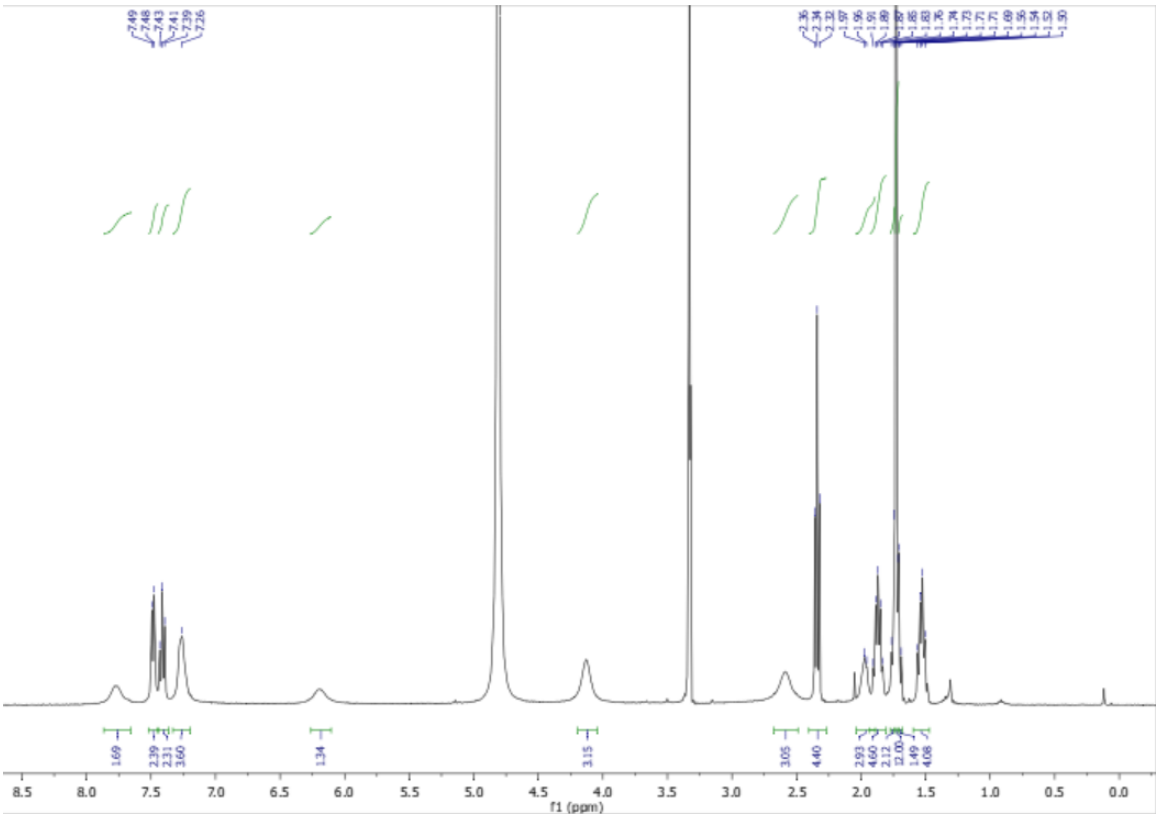

^{13}C

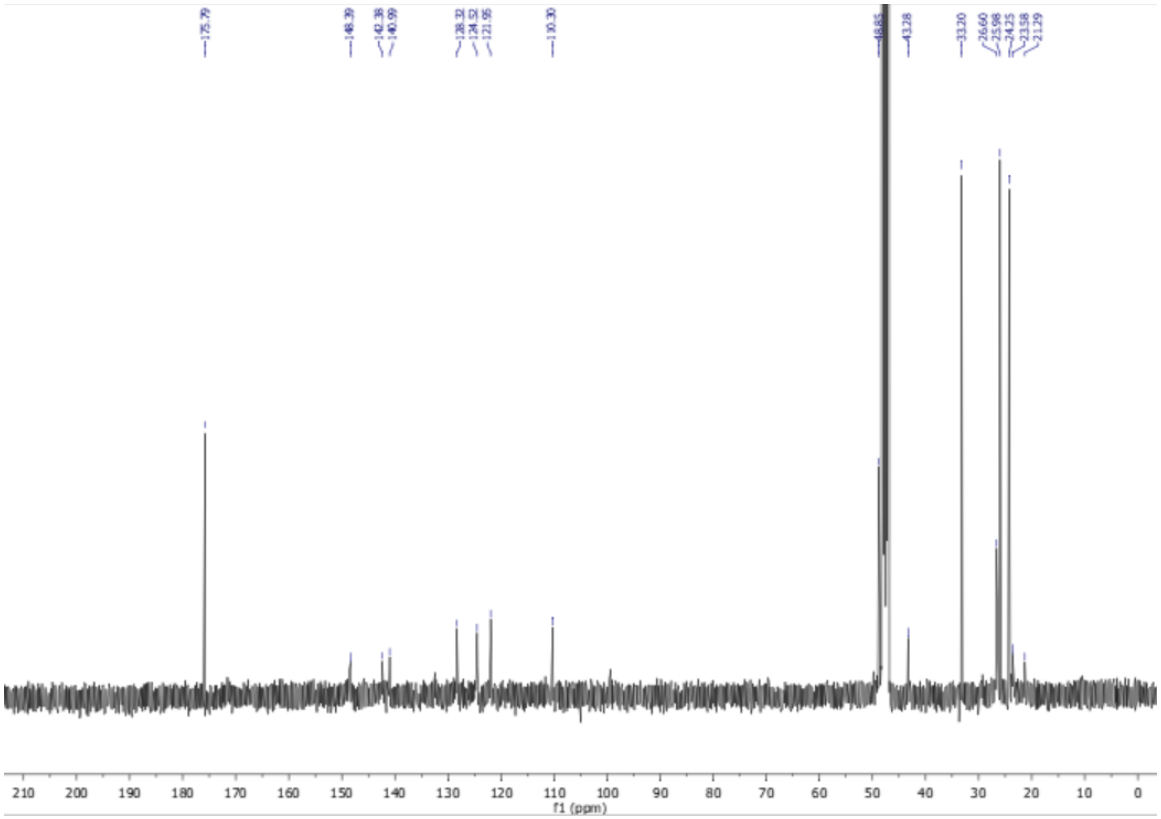
175.79
148.39
142.38
140.99
128.32
124.52
121.95
110.30
48.85
43.28
33.20
26.60
25.98
24.25
23.58
21.29
210 200 190 180 170 160 150 140 130 120 110 100 90 80 70 60 50 40 30 20 10 0
f1 (ppm)

HRMS

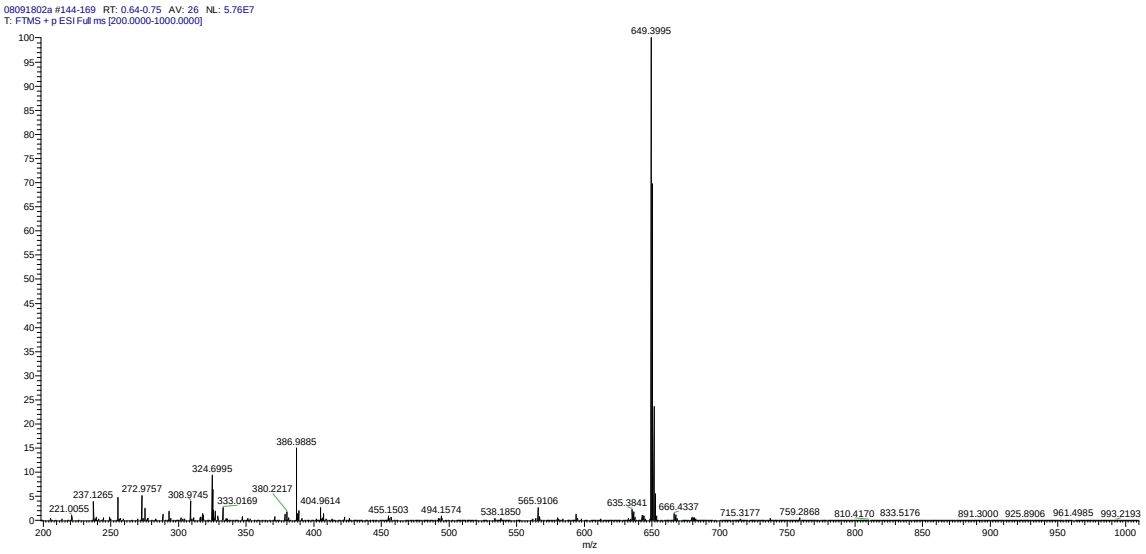
08091802a #144-169 RT: 0.64-0.75 AV: 26 NL: 5.76E7
T: FTMS + p ESI Full ms [200.0000-1000.0000]
649.3995
386.9885
324.6995
237.1265
272.9757
308.9745
333.0169
380.2217
404.9614
221.0055
455.1503
494.1574
538.1850
565.9106
635.3841
666.4337
715.3177
759.2868
810.4170
833.5176
891.3000
925.8906
961.4985
993.2193
m/z

1-(5-carboxypentyl)-2-(€-2-(€-3-(2-(€-1-(5-carboxypentyl)-3,3-dimethylindolin-2-ylidene)ethylidene)-2-methylcyclohex-1-en-1-yl)vinyl)-3,3-dimethyl-3H-indol-1-ium (1-Me)

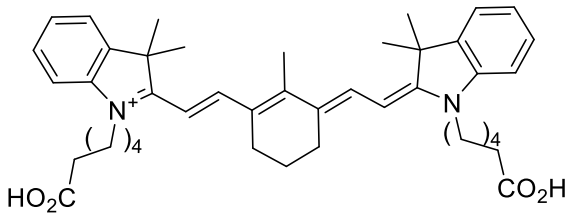

^{1}H

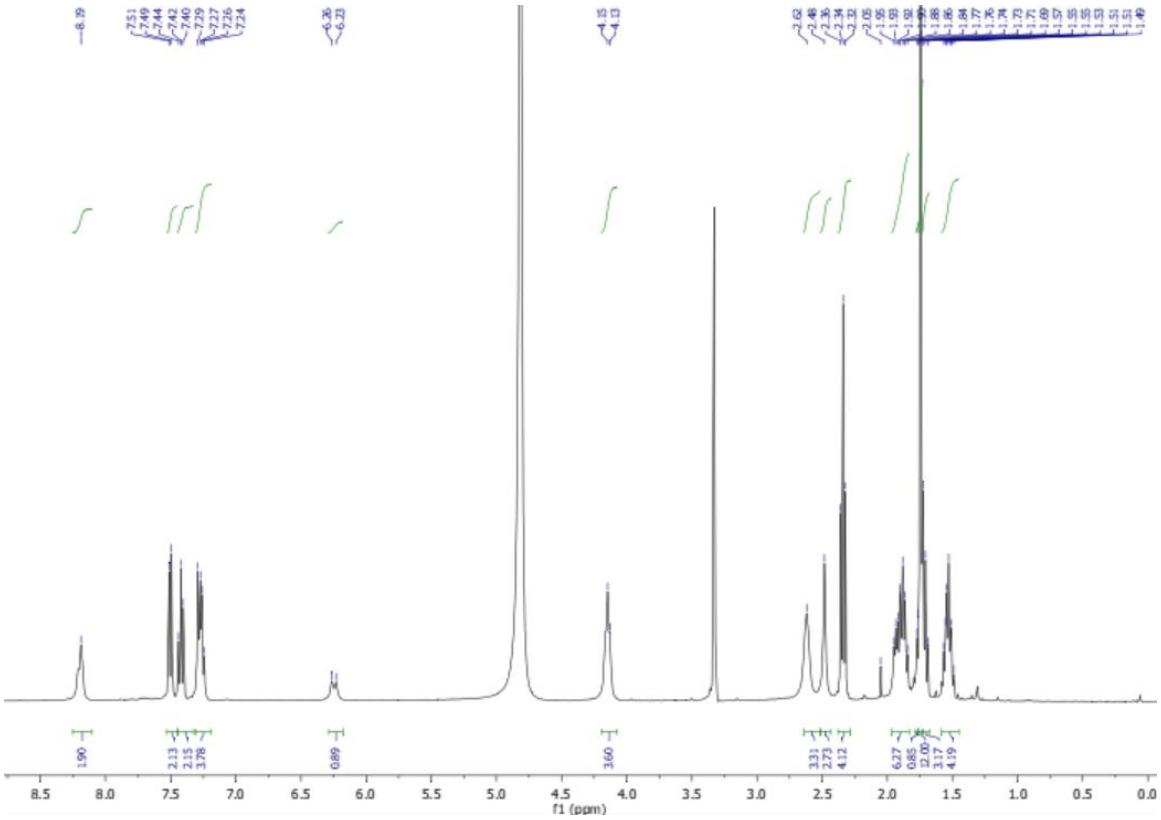

^{13}C

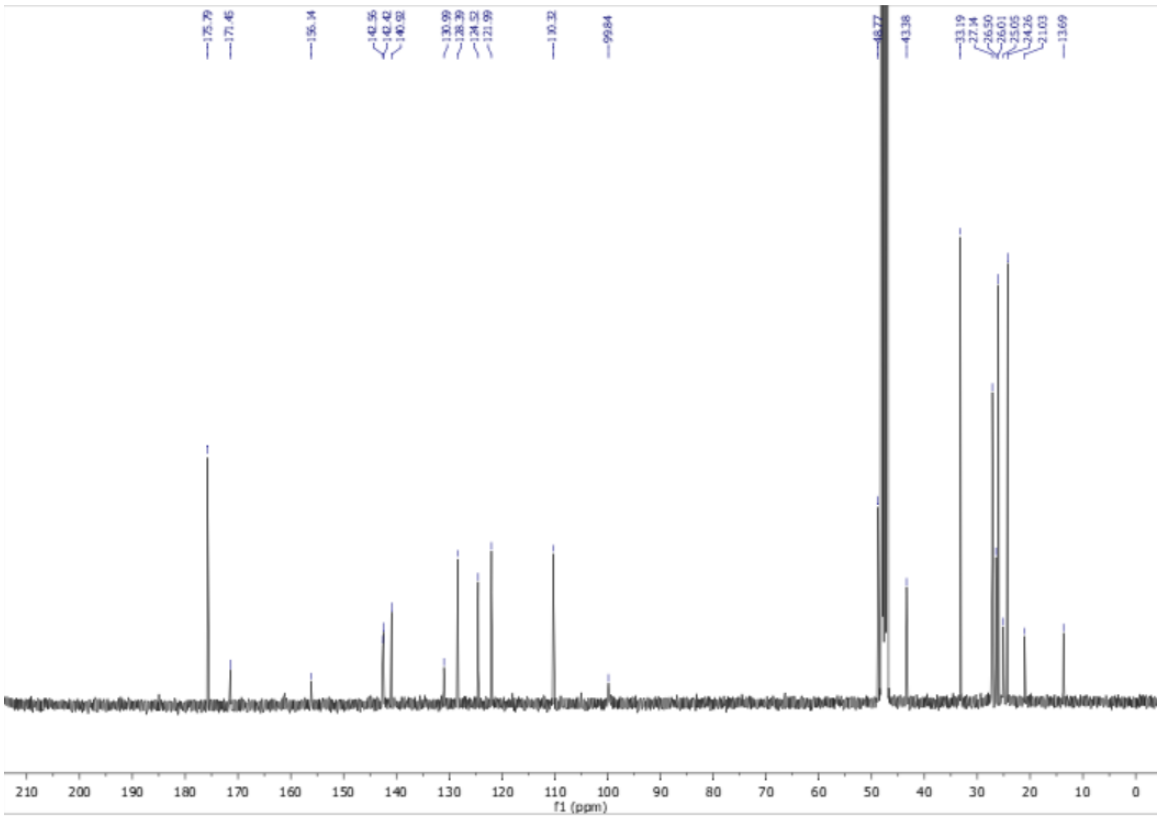
175.79
171.45
150.14
142.55
142.42
140.92
130.99
128.39
124.52
121.99
110.32
99.84
68.77
43.38
33.19
27.14
26.50
26.01
25.05
24.26
21.03
13.69
f1 (ppm)

HRMS

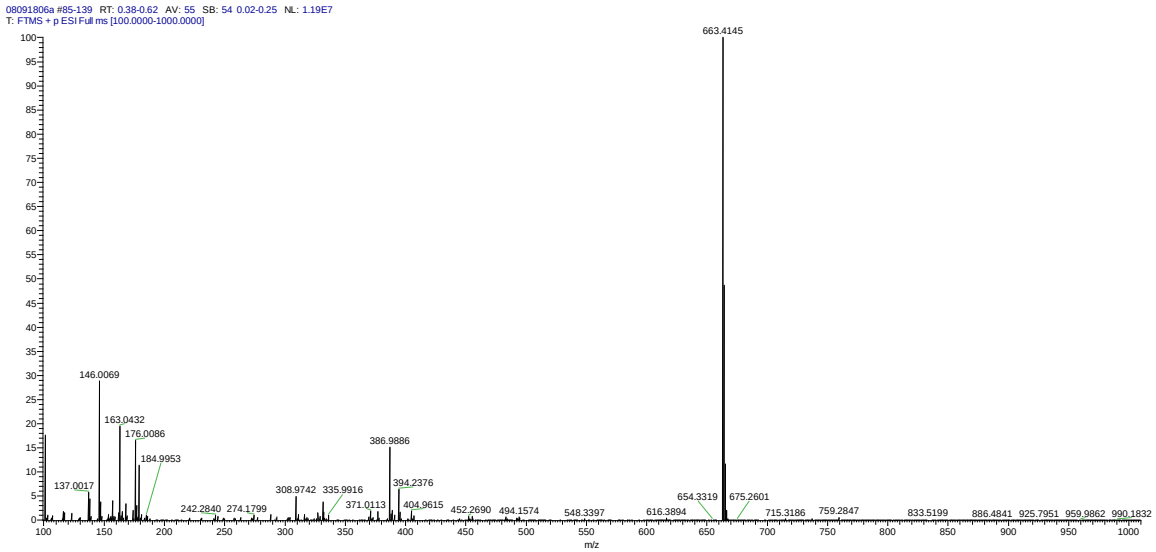
08091806a #85-139 RT: 0.38-0.62 AV: 55 SB: 54 0.02-0.25 NL: 1.19E7
T: FTMS + p ESI Full ms [100.0000-1000.0000]
663.4145
146.0069
163.0432
176.0086
184.9953
137.0017
386.9886
394.2376
308.9742
335.9916
371.0113
404.9615
654.3319
675.2601
242.2840
274.1799
452.2690
494.1574
548.3397
616.3894
715.3186
759.2847
833.5199
886.4841
925.7951
959.9862
990.1832
m/z

1-(5-carboxypentyl)-2-((E)-2-((E)-6-(2-((E)-1-(5-carboxypentyl)-3,3-dimethylindolin-2-ylidene)ethylidene)-3,4,5,6-tetrahydro-[1,1'-biphenyl]-2-yl)vinyl)-3,3-dimethyl-3H-indol-1-ium (1-Ph)

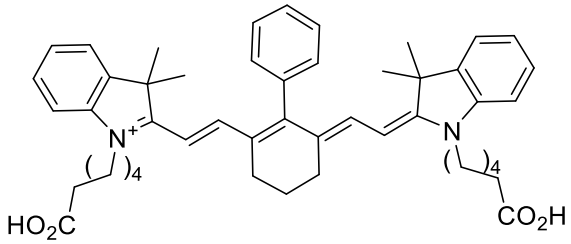

^{1}H

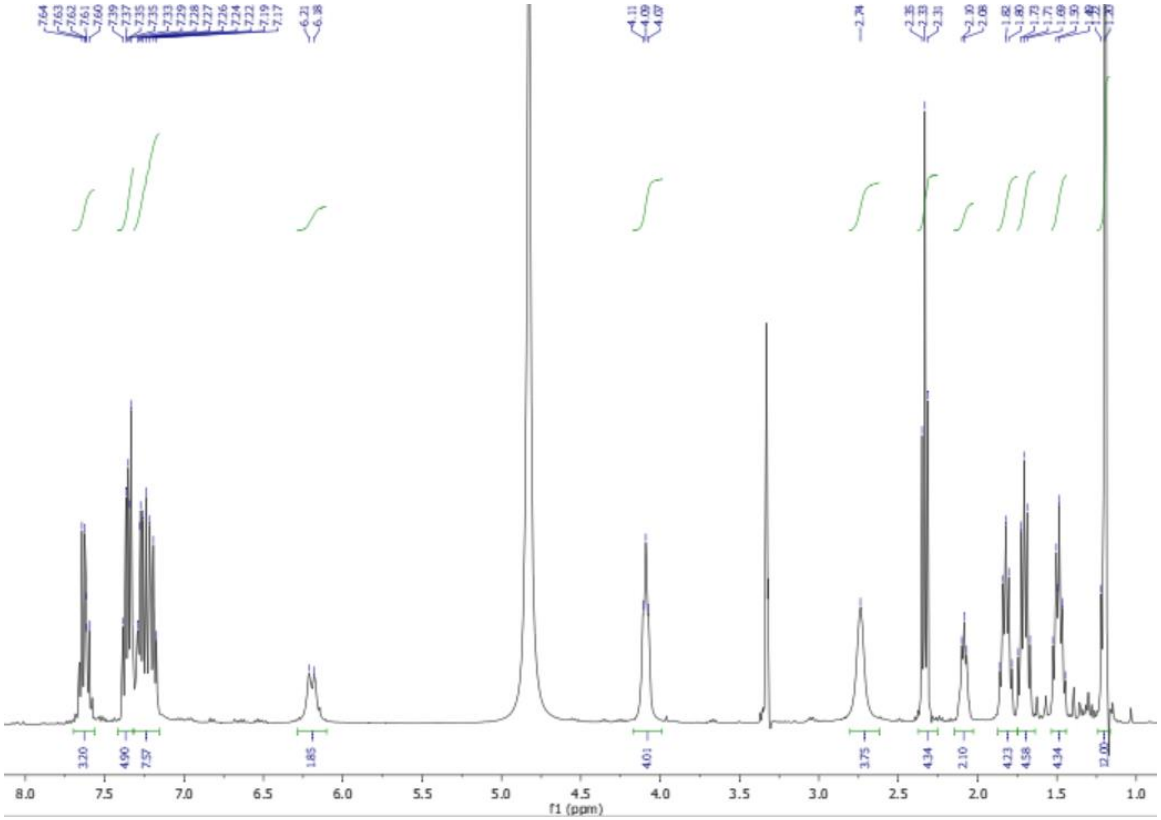

^{13}C

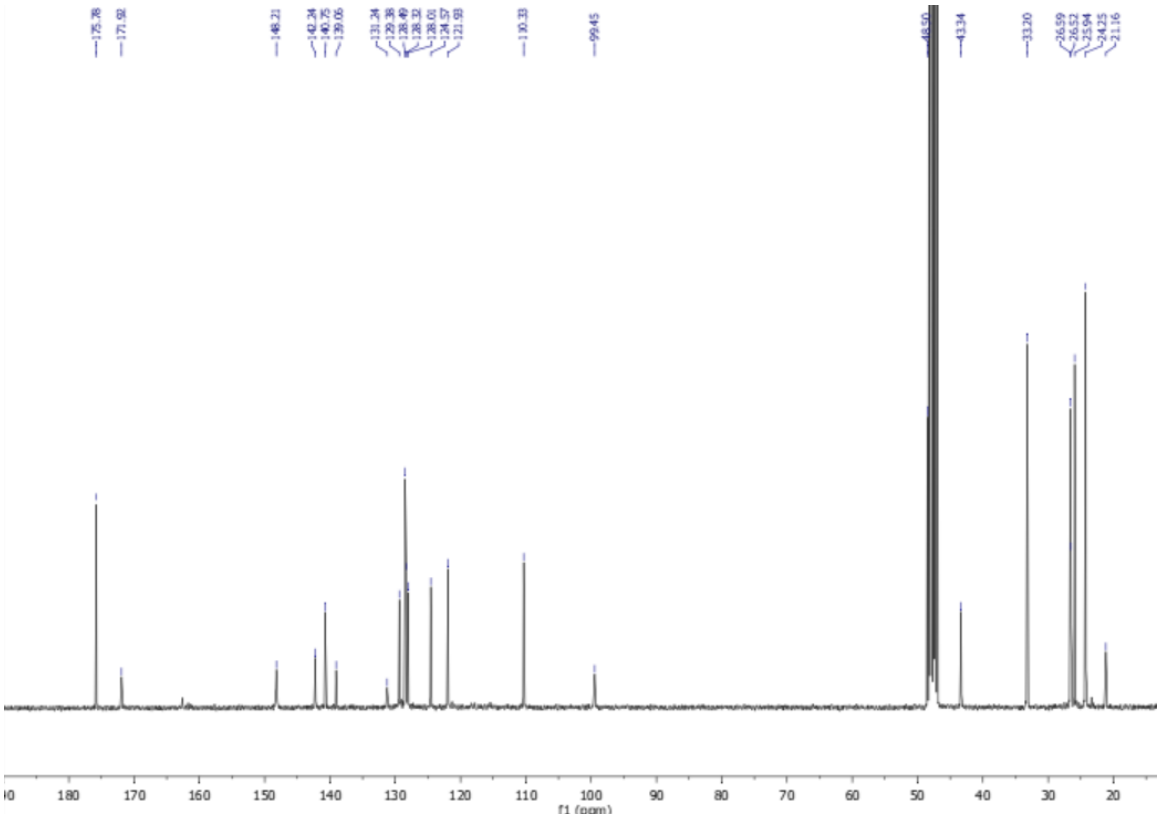
175.38
171.92
146.21
140.24
140.75
139.06
131.24
129.38
128.49
128.32
128.01
124.57
121.93
110.33
99.45
48.60
43.34
33.20
26.59
26.52
25.94
24.25
21.16
f1 (ppm)

HRMS

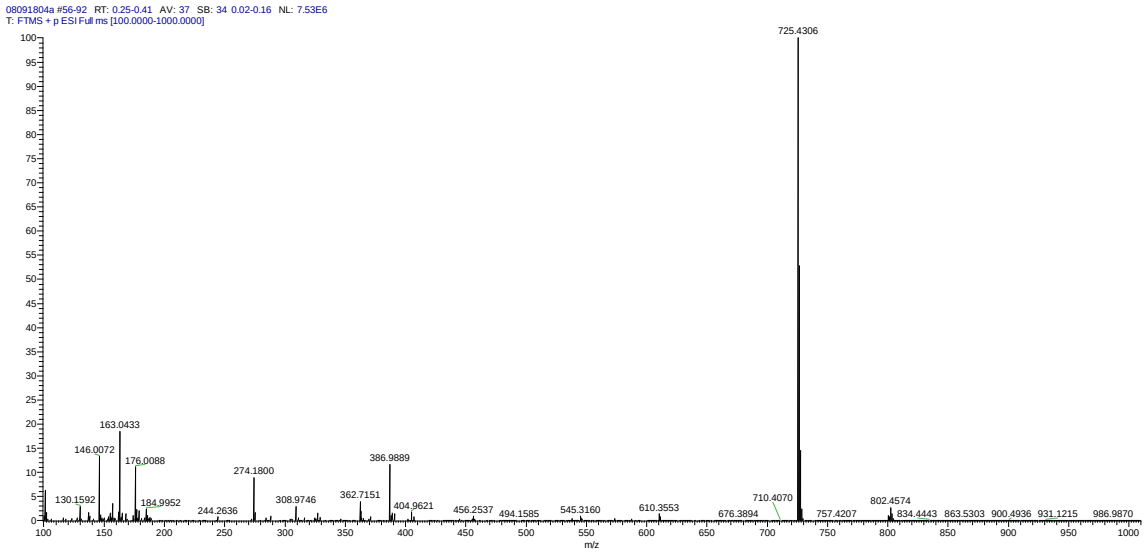
08091804a #56-92 RT: 0.25-0.41 AV: 37 SB: 34 0.02-0.16 NL: 7.53E6
T: FTMS + p ESI Full ms [100.0000-1000.0000]
725.4306
163.0433
146.0072
176.0088
130.1592
184.9952
244.2636
274.1800
308.9746
362.7151
386.9889
404.9621
456.2537
494.1585
545.3160
610.3553
676.3894
710.4070
757.4207
802.4574
834.4443
863.5303
900.4936
931.1215
986.9870
m/z

Supporting Figures

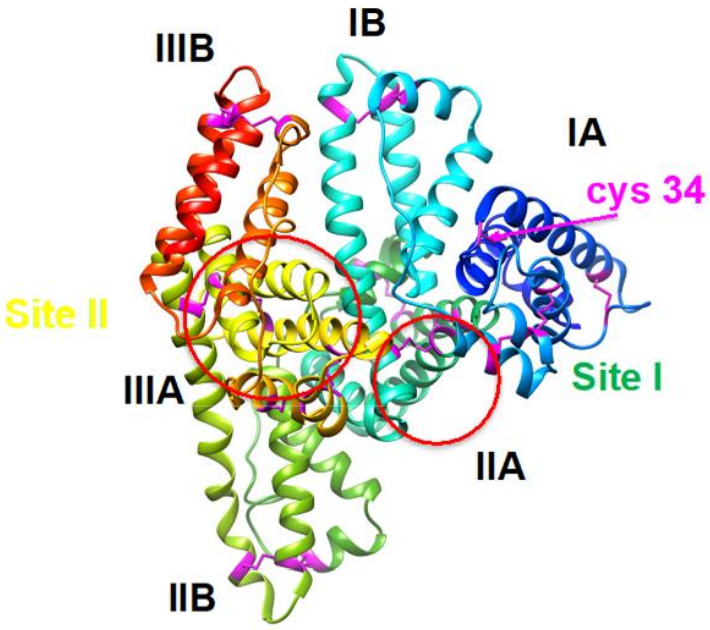

Figure C-S1. HSA with its different helices and binding sites (PDB 1AO6). Cysteines are colored in pink.

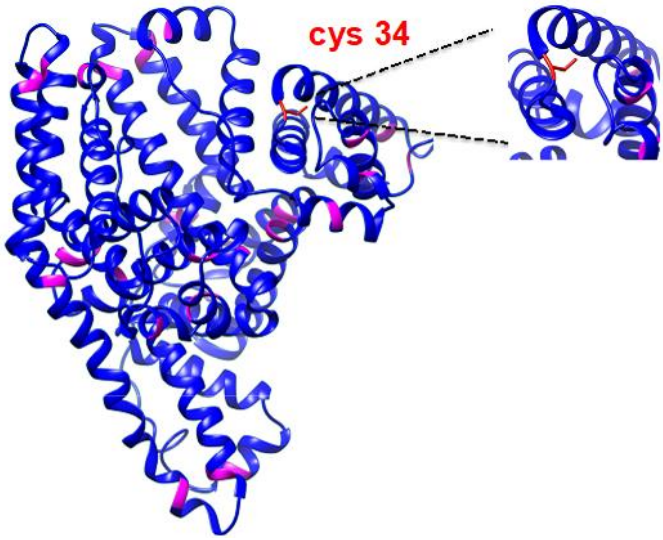

Figure C-S2. HSA with its different helices and binding sites (PDB 1AO6). Cysteines are colored in pink.

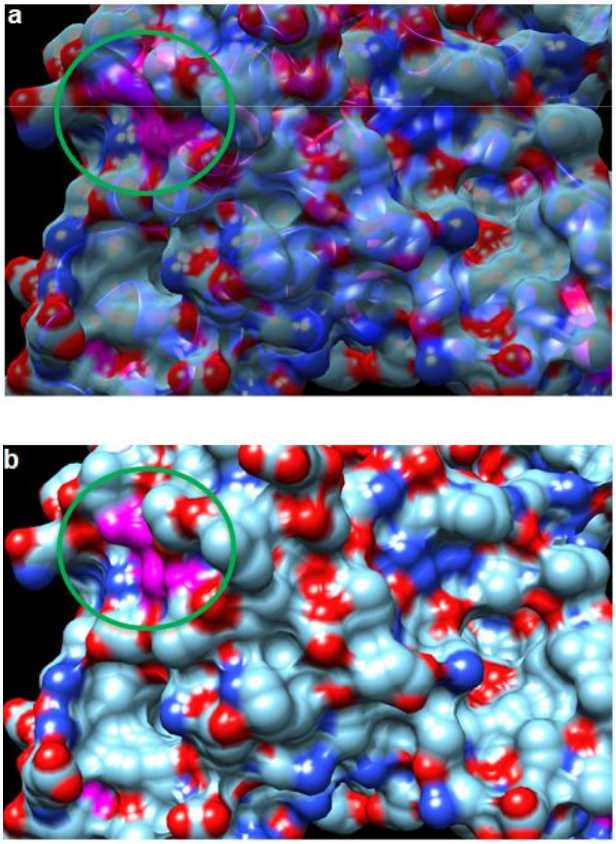

Figure C-S3. cysteine 34 binding site at **a,** 0% transparency and **b,** 50% transparency

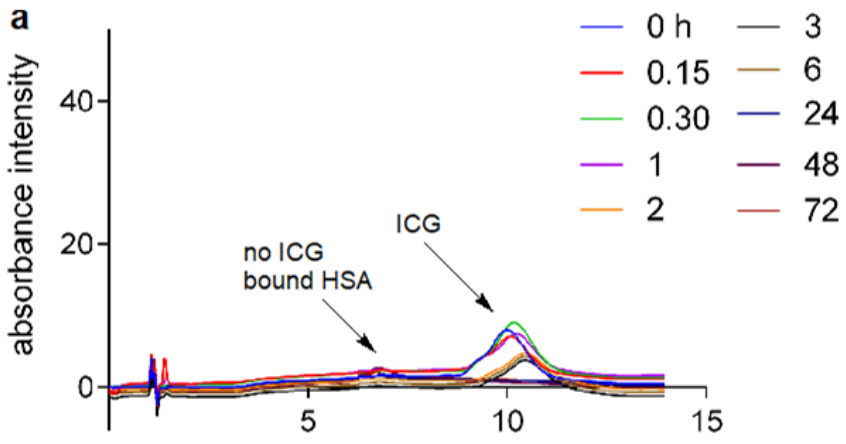

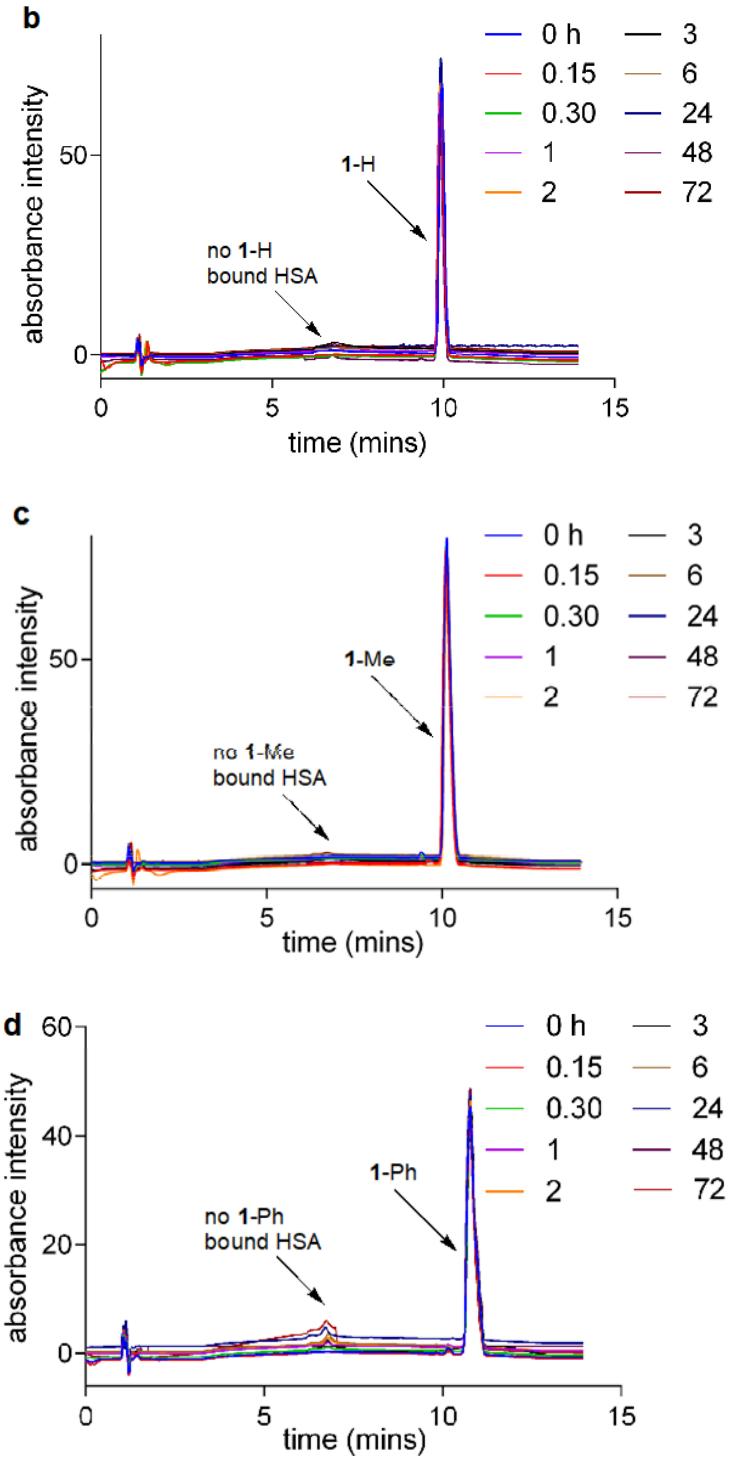
b
absorbance intensity
50
0
0
5
10
15
time (mins)
1-H
no 1-H
bound HSA
0 h
0.15
0.30
1
2
3
6
24
48
72
c
absorbance intensity
50
0
0
5
10
15
time (mins)
1-Me
no 1-Me
bound HSA
0 h
0.15
0.30
1
2
3
6
24
48
72
d
absorbance intensity
60
40
20
0
0
5
10
15
time (mins)
1-Ph
no 1-Ph
bound HSA
0 h
0.15
0.30
1
2
3
6
24
48
72

Figure C-S4. Kinetics of **a,** ICG, **b, 1**-H, **c, 1**-Me; **d, 1**-Ph in 1 M HEPES buffer pH 7.4. Only **1**-Cl showed an increase in peak with HSA. The kinetics was examined on C18 column using Agilent 1200 series LC/MS at 600 nm.

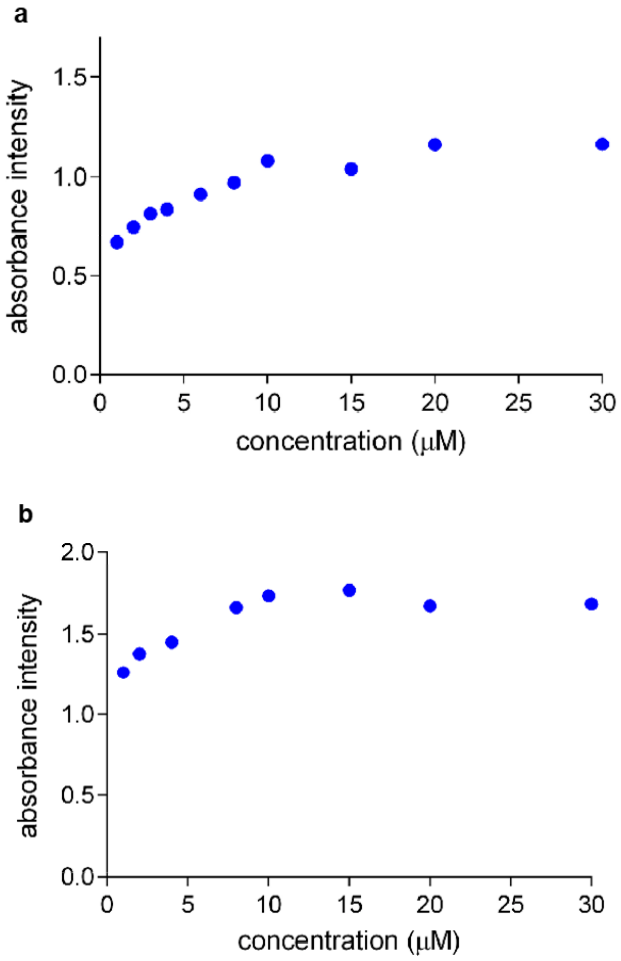

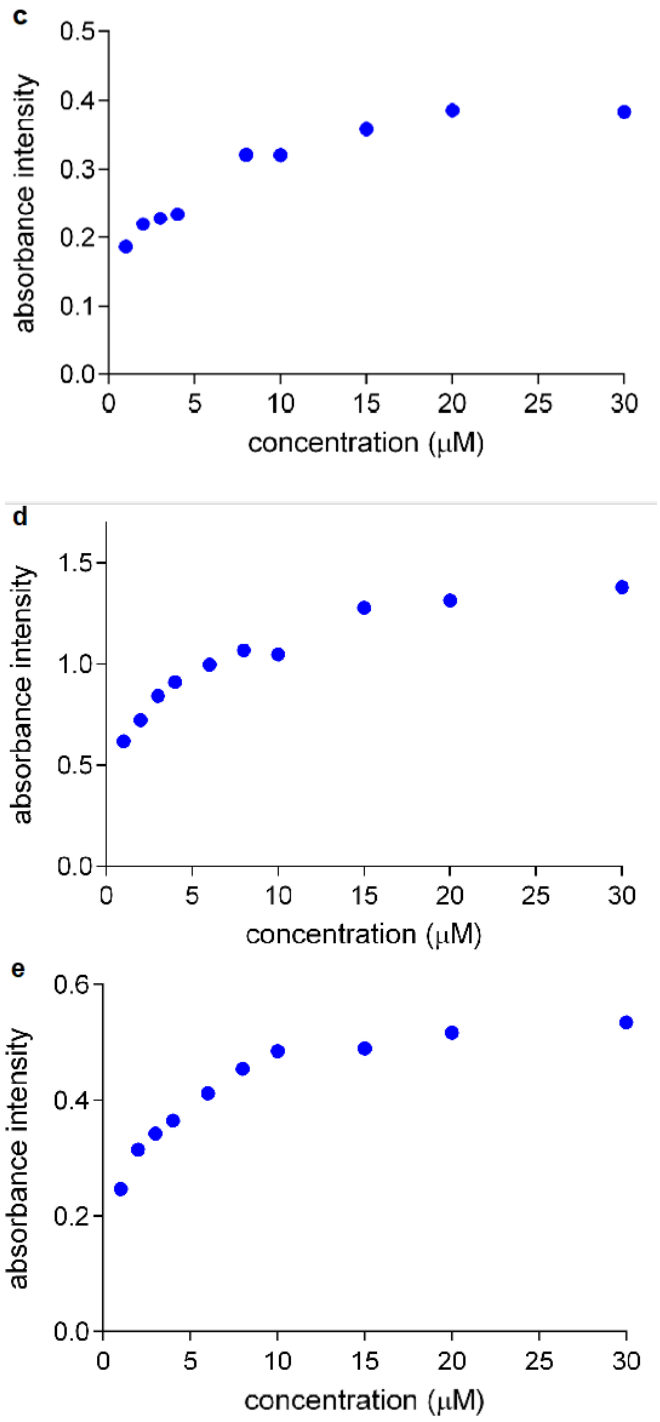

Figure C-S5. Absorbance with varied amount of HSA bound at 10 uM of **a,** ICG, **b, 1**-Cl; **c, 1**-H; **d, 1**-Me; **e, 1**-Ph in 10 mM PBS buffer pH 7.4. Ratio of binding is calculated

at the point where the dye concentration is saturated. ICG bound to 1.5 equivalents of HSA[218] whereas **1**-Cl binds to 1 equivalent of HSA.[211]

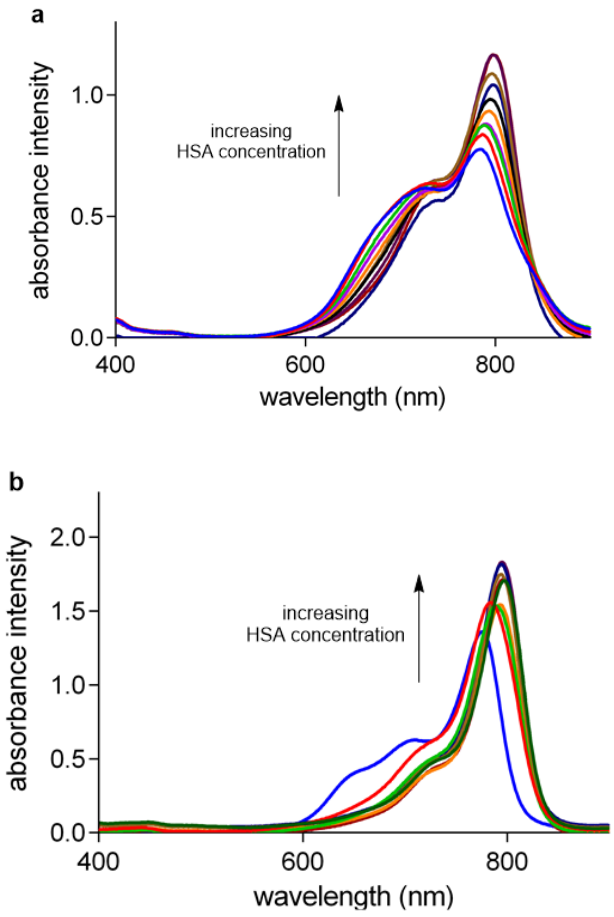

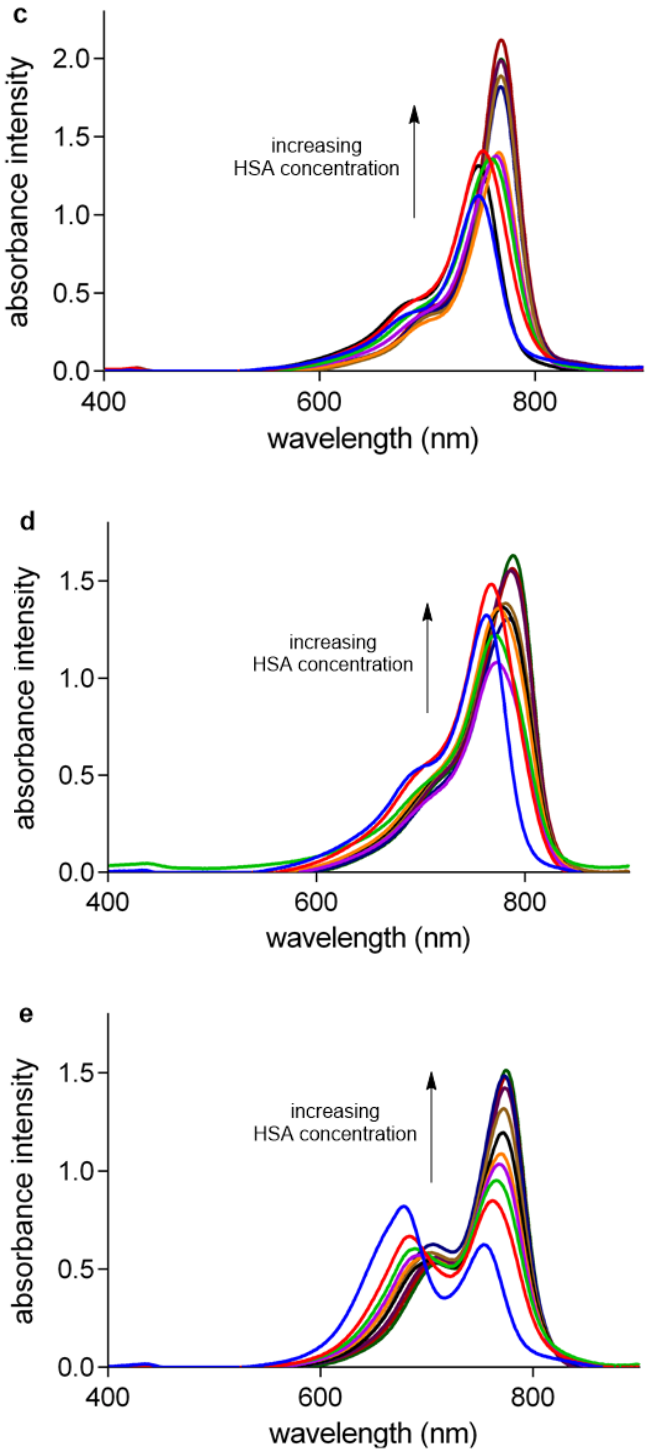

Figure C-S6. Absorbance with varied amount (0 – 30 □M) of HSA bound at 10 uM of **a,** ICG, **b, 1**-Cl; **c, 1**-H; **d, 1**-Me and **e**, **1**-Ph in 10 mM PBS buffer pH 7.4.

a

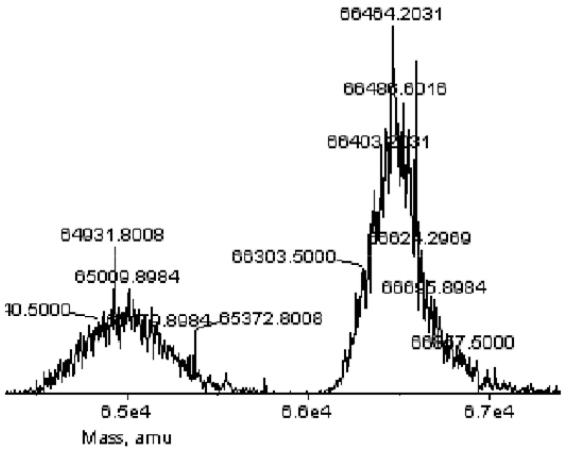
66464.2031
66486.6016
64931.8008
65009.8984
66303.5000
66695.8984
65372.8008
6.5e4
6.6e4
6.7e4
Mass, amu

b

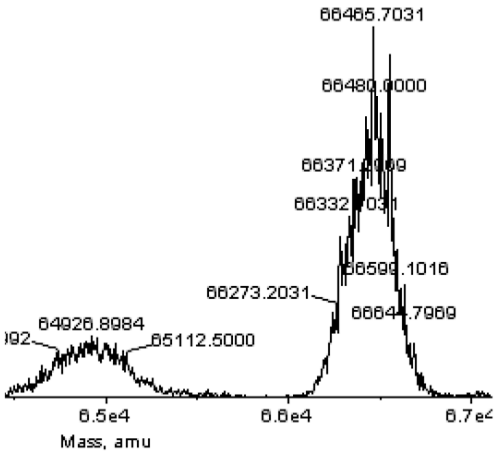
66465.7031
66480.6000
66273.2031
64926.8984
65112.5000
6.5e4
6.6e4
Mass, amu

c

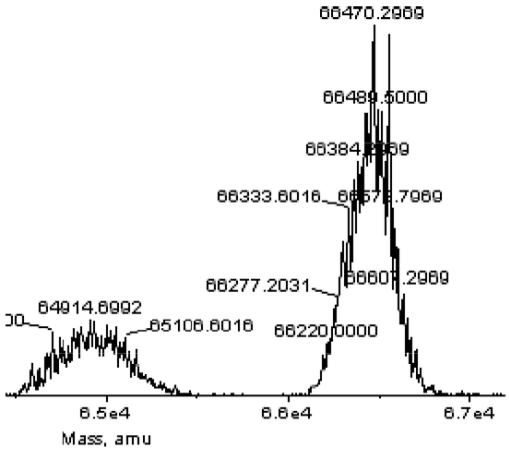
66470.2969
66489.5000
66333.6016
66277.2031
64914.6992
65106.6016
66220.0000
6.5e4
6.6e4
6.7e4
Mass, amu

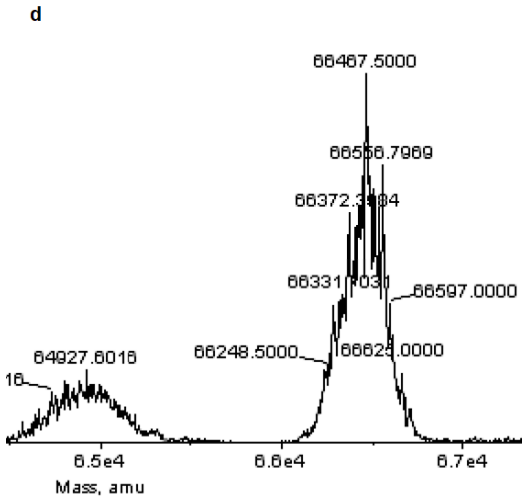

Figure C-S7. Mass Spec of **a,** ICG, **b, 1**-H; **c, 1**-Me; **d, 1**-Ph in 1 M HEPES buffer pH 7.4. Only the peaks of free HSA peak without any covalent binding was observed.

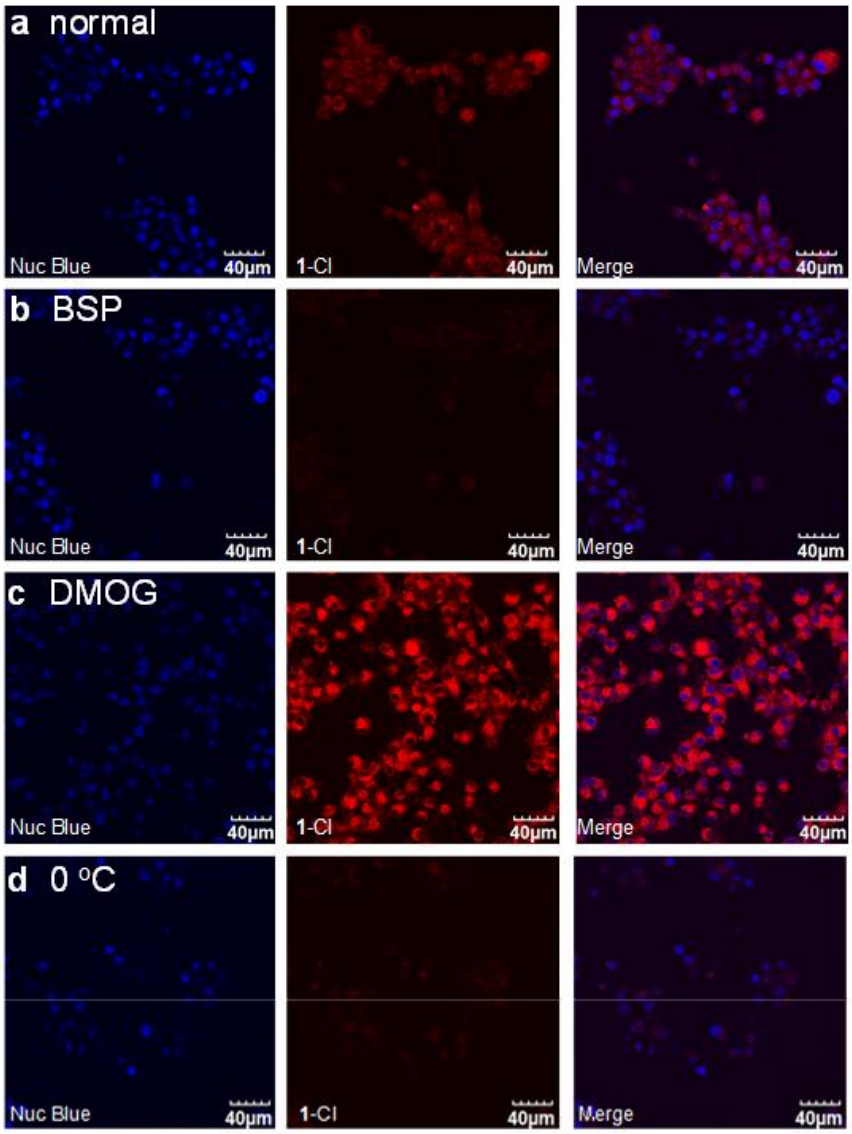

Figure C-S8. Experiments to test *uptake of **1**-Cl* (20 μM) into U87-MG cells (grown in DMEM media supplemented with 10% FBS, *i.e.* containing approximately 0.038 mM BSA). **a** Without any blocking agents or abnormal conditions; **b**, pre-blocked with 250 μM BSP to block OATPs for 10 mins; **c**, after the cells were pretreated with 1mM DMOG for 24 h to induce hypoxia; and **d**, when the cells were maintained at 0 °C for 30

mins to stop active transport. All images were collected using an Olympus confocal microscope at 20x magnification.

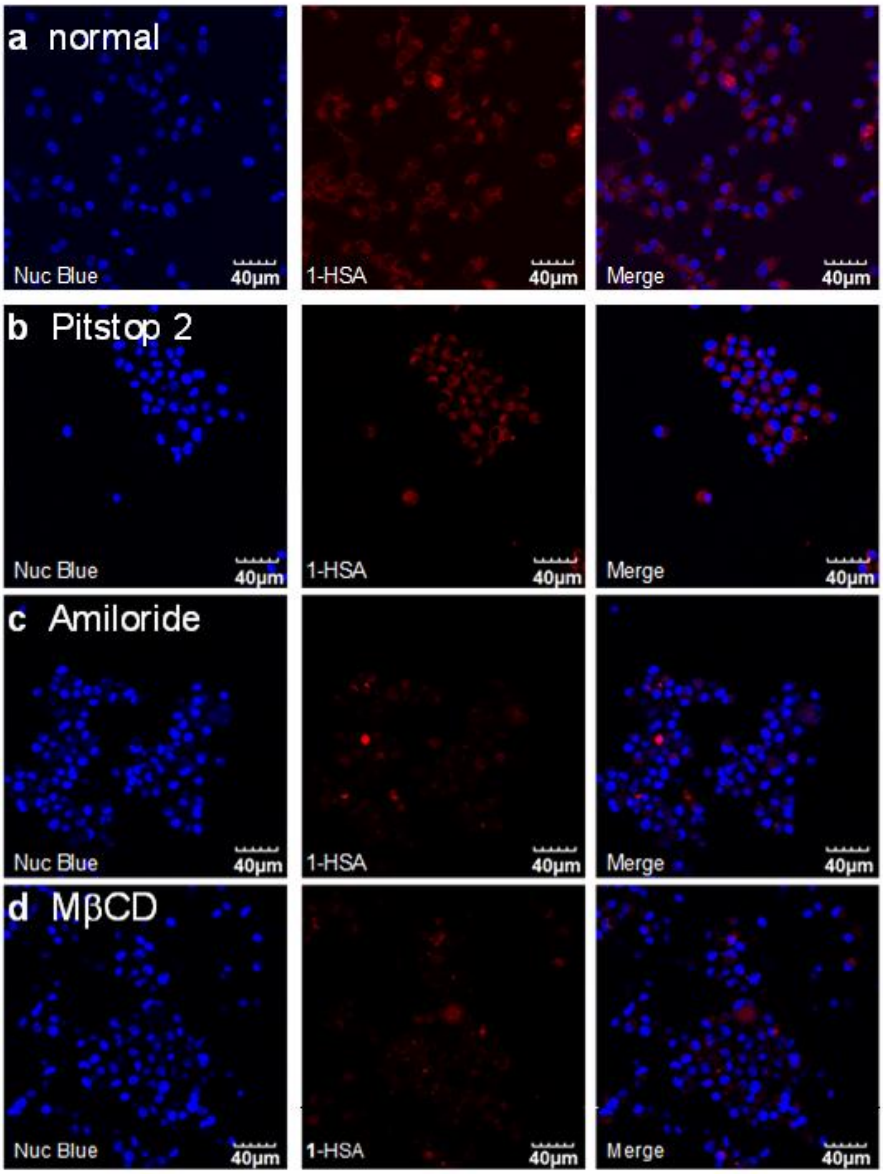

Figure C-S9. Experiments to test for uptake of **1**-HSA (20 µM) via endocytosis. All the experiments feature U87-MG cells incubated in serum free media for 16 h at 37 °C. Cells pretreated with the following agents before addition of **1**-HSA (20 µM): **a** no blocking agents or abnormal conditions; **b**, PitStop2 (20 µM) for 15 min to inhibit clathrin

mediated endocytosis; **c**, amiloride (1 mM) to inhibit micropinocytosis; and **d**, MβCD (Methyl-β-cyclodextrin, 15 μM) to inhibit lipid raft endocytosis. All images were collected using a Zeiss confocal microscope at 20x magnification.

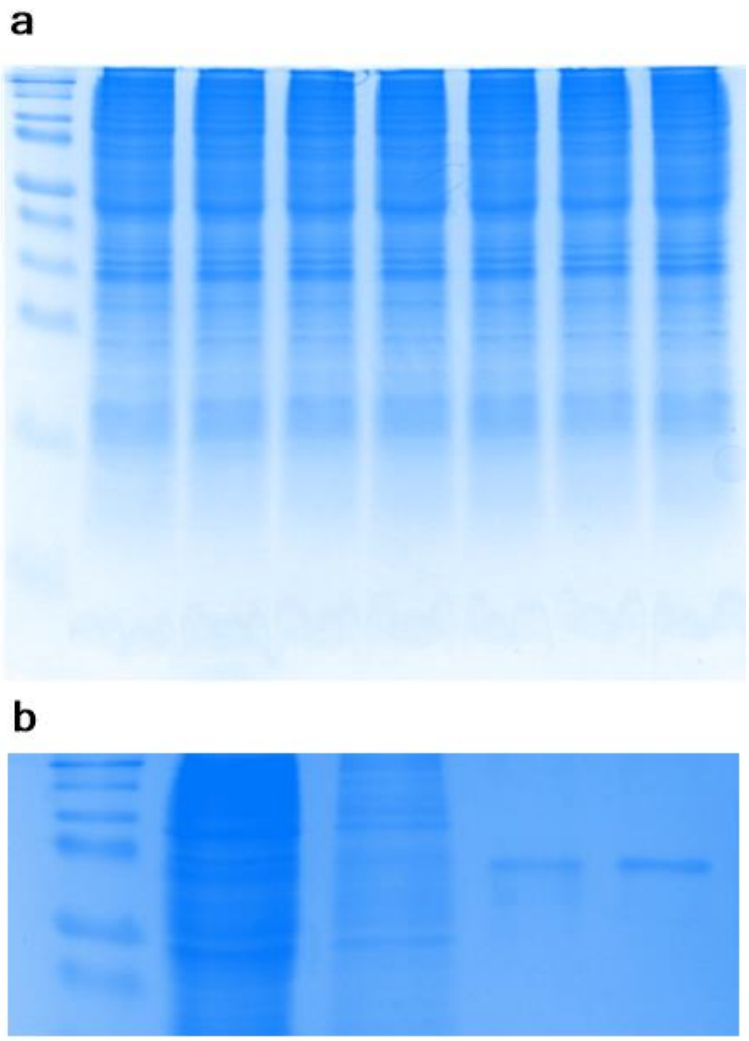

Figure C-S10. CBB G250 staining of gel referred to **a.** Figure 1a and **b.** Figure 1b.

APPENDIX D

SUPPORTING INFORMATION FOR CHAPTER V

General Experimental Procedures

All reactions were carried out under an argon atmosphere. Reagents were purchased at a high commercial quality (typically 97 % or higher) and used without further purification, unless otherwise stated. Dasatinib was purchased from AK Scientific. High field NMR spectra were recorded with Bruker Avance III at 400 MHz for ^{1}H, and 100 MHz for ^{13}C and were calibrated using residual non-deuterated solvent as an internal reference ($CDCl_3$: ^{1}H NMR = 7.24, ^{13}C NMR = 77.0, MeOD: ^{1}H NMR = 3.30, ^{13}C NMR = 49.0, DMSO-d_6: ^{1}H NMR = 2.50, ^{13}C NMR = 39.5). The following abbreviations were used to explain the multiplicities: s = singlet, d = doublet, t = triplet, q = quartet, quint = quintet, dd = double doublet, dt = double triplet, dq = double quartet, m = multiplet, br = broad. Electrospray ionization mass spectrometry (ESI-MS) data were collected on triple-stage quadrupole instrument in a positive mode. Flash chromatography was performed using silica gel (230-400 mesh). LC-MS analyses were collected from Agilent 1260 Infinity Quaternary LC and Agilent 6120 Quadrupole LC/MS modules using Poroshell 120 EC-C18 2.7 µM (4.6 x 50 mm) column in 5-95% CH_3CN/water gradient with 0.1% formic acid over 10 minutes. Prep HPLC was performed on Agilent 1260 Infinity in 50-90 CH_3CN/water gradient with 0.1% TFA over 20 mins. All statistical analyses were carried out by Graphpad Prism version 6.0 (Graphpad Software).

Synthesis Scheme

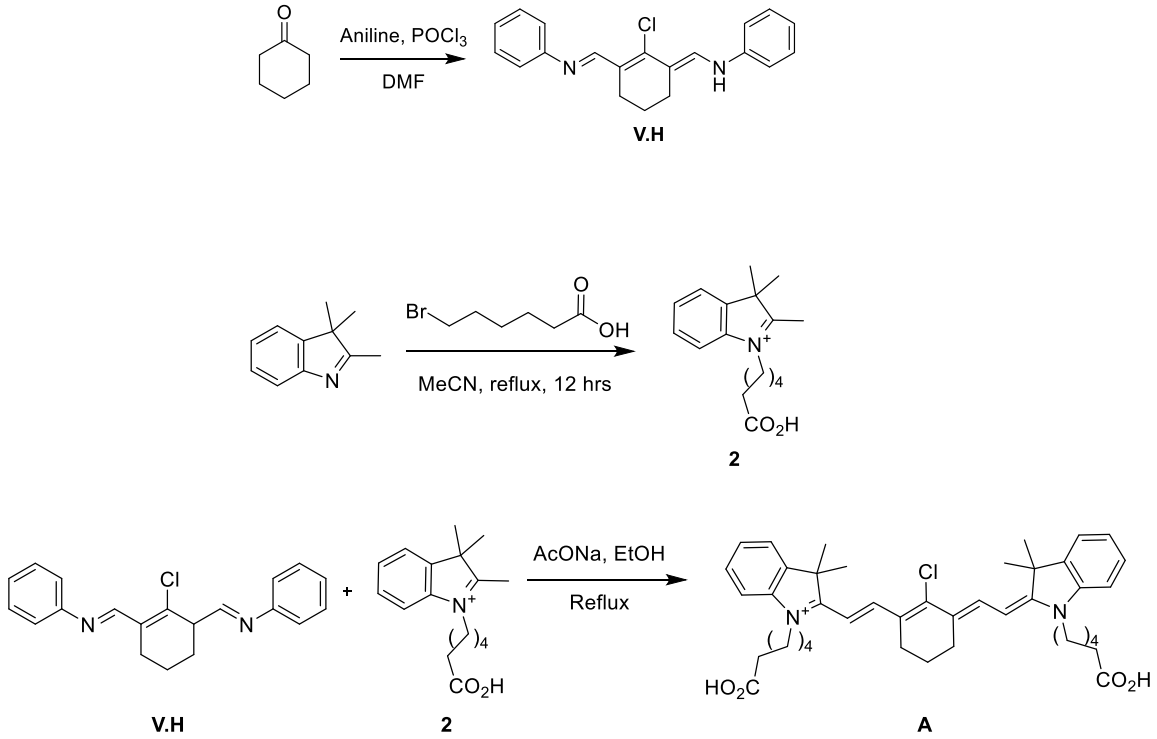

Scheme D-S1: Synthesis scheme for **A**

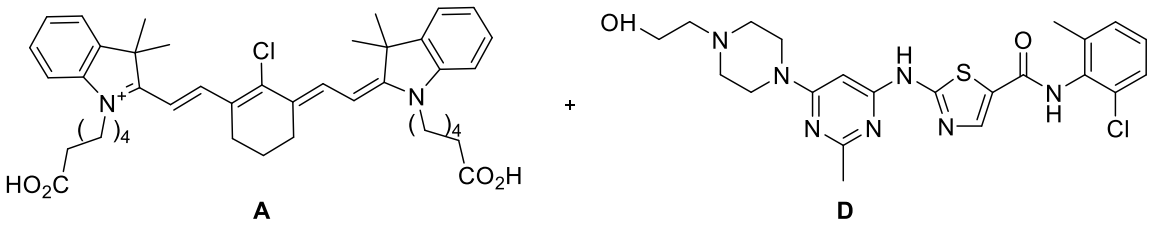

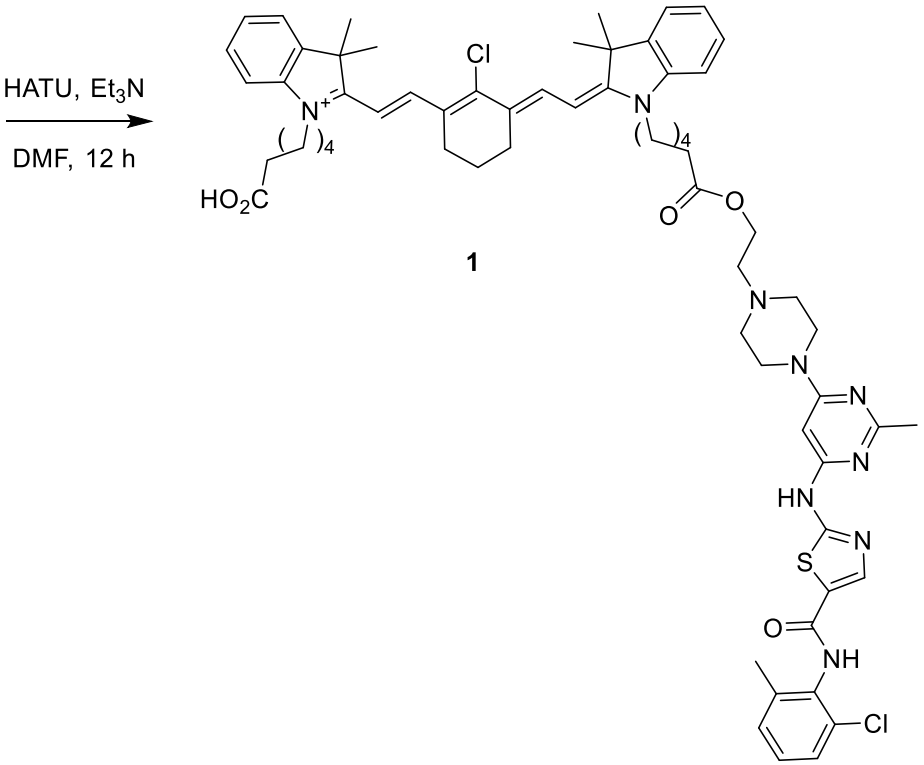

Scheme D-S2. Synthesis scheme of **1** by ester coupling between **A** and **D**.

Synthesis Procedure

Synthesis of (1E,1'E)-1,1'-(2-chlorocyclohex-1-ene-1,3-diyl)bis(N-phenylmethanimine) (V.H) [217]

DMF (65 mL, 0.85 mol) was added to a 500 mL round bottom flask and cooled in an ice bath. $POCl_3$ (55 mL, 0.6 mol) was added dropwise over 10 min and the mixture was stirred for 30 min. Cyclohexanone (27.5 mL, 0.265 mol) was added and the solution was refluxed at 100 ^oC for 1 h. Subsequently, the heating was stopped and the reaction was cooled down by placing on ice bath. While the mixture was cooling, aniline/EtOH

(1:1 v/v, 90 mL) was added, then the mixture was stirred for 1 h. The solution was poured to cold H_2O:conc. HCl (10:1, 110 mL) and allowed to stand for 2 h. The dark purple solid was collected by filtration and dissolved with methanol. The product was recrystallized using methyl *tert*-butyl ether:hexane (1:1) to give purple crystals (45.78 g, 86%).

^{1}H NMR (400 MHz, MeOD) δ 8.66 (s, 2H), 7.50 (s, 3H), 7.49 (d, *J* = 2.0 Hz, 3H), 7.31 (ddd, *J* = 8.4, 5.6, 3.0 Hz, 2H), 3.37 (s, 1H), 2.74 (t, *J* = 6.2 Hz, 4H), 2.00 (s, 2H).

^{13}C NMR (100 MHz, MeOD) δ 157.52, 149.00, 139.25, 129.70, 126.59, 118.47, 114.99, 24.19, 19.66.

Synthesis of 1-(5-carboxypentyl)-2,3,3-trimethyl-3H-indol-1-ium (2) [86]

In 500 mL round bottom flask, 2,3,3-trimethylindolenine (5 g, 31.4 mol) and 6-bromohexanoic acid (12.3 g, 62.8 mmol) were added to 200 mL of acetonitrile. The mixture was refluxed for 12 h. Subsequently, the mixture was cooled to room temperature and acetonitrile was removed by rotavap. Subsequently, the flask was placed in an ice bath, the solid residue was dissolved in 100 mL dichloromethane, then 300 mL diethyl ether was added to precipitate the product. That product was collected by filtration and washed with diethyl ether to afford pink crystals (6.4 g, 72%).

^{1}H NMR (400 MHz, MeOD) δ 7.91 – 7.84 (m, 1H), 7.79 (dt, *J* = 7.5, 3.8 Hz, 1H), 7.71 – 7.61 (m, 3H), 4.58 – 4.49 (m, 3H), 2.36 (t, *J* = 7.2 Hz, 3H), 2.05 – 1.96 (m, 3H), 1.77 – 1.67 (m, 3H), 1.63 (s, 8H), 1.62 – 1.49 (m, 3H).

^{13}C NMR (100 MHz, MeOD) δ 196.51, 175.75, 142.02, 141.08, 129.83, 129.14, 123.26, 115.13, 54.56, 32.98, 27.15, 25.66, 23.99, 21.40.

Synthesis of 1-(5-carboxypentyl)-2-((E)-2-((E)-3-(2-((E)-1-(5-carboxypentyl)-3,3-dimethylindolin-2-ylidene)ethylidene)-2-chlorocyclohex-1-en-1-yl)vinyl)-3,3-dimethyl-3H-indol-1-ium (A) [86]

Vilsmeir Haack Reagent **V.H** (1.27 g, 3.64 mmol), **2** (2.00 g, 7.28 mmol) and NaOAc (597 mg, 7.28 mmol) were dissolved in 100 mL of absolute ethanol in 250 mL round bottom flask. The mixture was refluxed for 6 h. The solvent was removed and the crude was purified by normal phase flash chromatography with MeOH:CH_2Cl_2 (1:25 v/v) to obtain green solid (0.98 g, 48%).

^{1}H NMR (400 MHz, MeOD) δ 8.47 (d, *J* = 14.1 Hz, 2H), 7.54 (d, *J* = 7.3 Hz, 2H), 7.48 – 7.42 (m, 2H), 7.37 – 7.28 (m, 4H), 6.31 (d, *J* = 14.1 Hz, 2H), 4.20 (t, *J* = 7.3 Hz, 3H), 2.75 (d, *J* = 5.5 Hz, 4H), 2.34 (t, *J* = 7.2 Hz, 4H), 2.04 – 1.96 (m, 2H), 1.95 – 1.84 (m, 4H), 1.76 (s, 12H), 1.74 – 1.68 (m, 3H), 1.59 – 1.49 (m, 4H).

^{13}C NMR (101 MHz, MeOD) δ 175.78, 172.93, 149.82, 144.17, 142.21, 141.23, 128.51, 126.64, 125.18, 122.12, 110.88, 100.91, 49.27, 43.70, 33.19, 26.92, 26.68, 25.96, 24.24, 20.71.

Synthesis of -(5-carboxypentyl)-2-((E)-2-((E)-2-chloro-3-(2-((E)-1-(6-(2-(4-(6-((5-((2-chloro-6-methylphenyl)carbamoyl)thiazol-2-yl)amino)-2-methylpyrimidin-4-

yl)piperazin-1-yl)ethoxy)-6-oxohexyl)-3,3-dimethylindolin-2-ylidene)ethylidene)cyclohex-1-en-1-yl)vinyl)-3,3-dimethyl-3H-indol-1-ium (1)

Cyanine dye **A** (200.0 mg, 0.29 mmol), triethylamine (48.50 uL, 0.34 mmol) and HATU (110.2 mg, 0.29 mmol) were added in 2 mL DMF and stirred for 15 min. Dasatinib (141.52 mg, 0.29 mmol) was added afterwards and stirred for 12 h under argon balloon. Solvent was removed and the crude was purified by reverse phase column on prep-HPLC {50% MeCN/50%H_2O – 90%MeCN/10%H_2O (containing 0.1% TFA) in 20 mins} to get the desired product as amorphous green solid (32 mg, 9.6%).

^{1}H NMR (400 MHz, MeOD) δ 8.46 (dd, *J* = 13.9, 9.9 Hz, 2H), 8.17 – 8.15 (m, 1H), 7.54 (d, *J* = 7.6 Hz, 2H), 7.45 (dd, *J* = 13.6, 7.5 Hz, 2H), 7.29 (dt, *J* = 14.8, 7.0 Hz, 6H), 6.30 (t, *J* = 13.8 Hz, 2H), 6.16 (s, 1H), 5.50 (s, 3H), 4.51 – 4.43 (m, 2H), 4.20 (dd, *J* = 12.0, 7.1 Hz, 4H), 3.98 (s, 3H), 3.53 – 3.40 (m, 5H), 3.37 (s, 1H), 2.74 (d, *J* = 5.9 Hz, 4H), 2.48 (dd, *J* = 16.6, 9.2 Hz, 6H), 2.37 – 2.28 (m, 6H), 2.01 – 1.94 (m, 2H), 1.89 (s, 4H), 1.75 (d, *J* = 2.1 Hz, 12H), 1.69 (dd, *J* = 14.3, 6.9 Hz, 5H), 1.53 (q, *J* = 14.7 Hz, 5H).

^{13}C NMR (101 MHz, MeOD) δ 175.83, 172.91, 172.56, 162.37, 157.49, 149.80, 144.53, 143.83, 142.27, 142.10, 141.30, 141.15, 128.76, 128.56, 126.93, 126.66, 126.46, 125.40, 125.05, 122.15, 111.04, 110.70, 101.24, 100.53, 83.20, 57.76, 55.32, 53.37, 51.60, 49.39, 49.17, 43.61, 41.02, 33.19, 32.97, 26.96, 26.89, 26.71, 25.99, 25.95, 24.22, 24.04, 20.72, 17.30.

HRMS (calculated): 1152.5062; found 1152.5067

(1E,1'E)-1,1'-(2-chlorocyclohex-1-ene-1,3-diyl)bis(N-phenylmethanimine) (V.H)

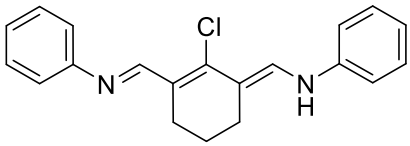

^{1}H

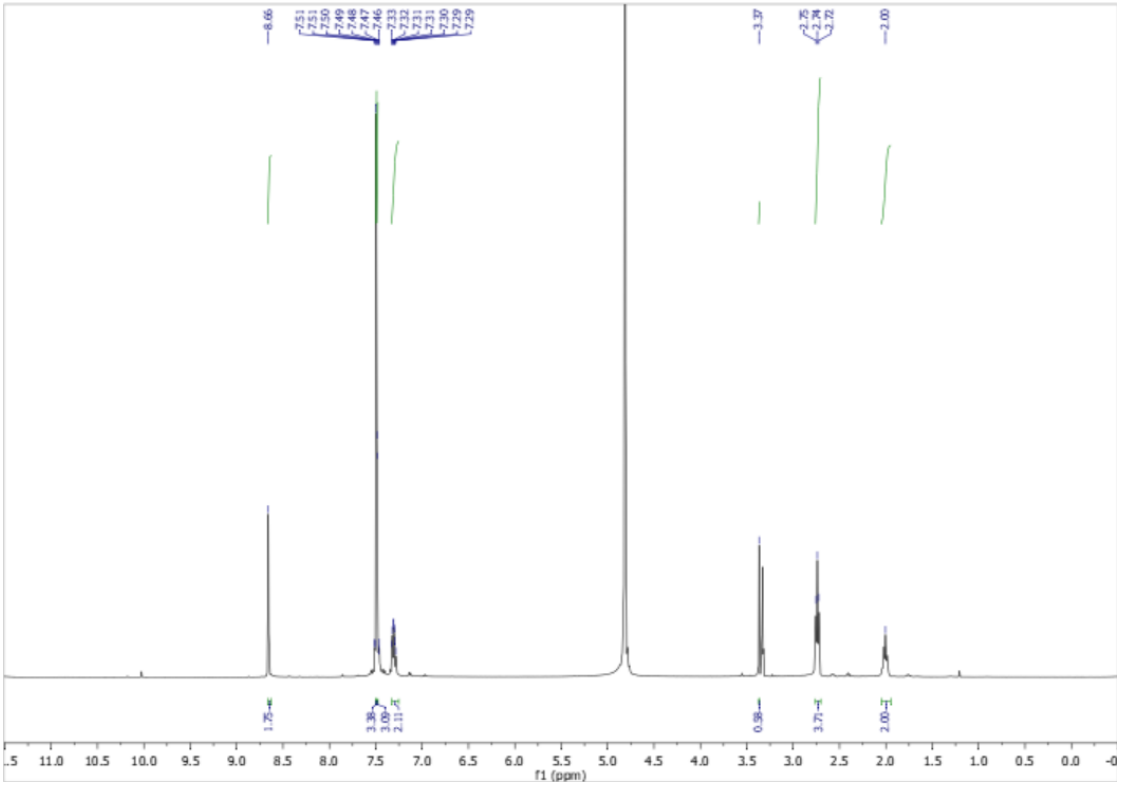

^{13}C

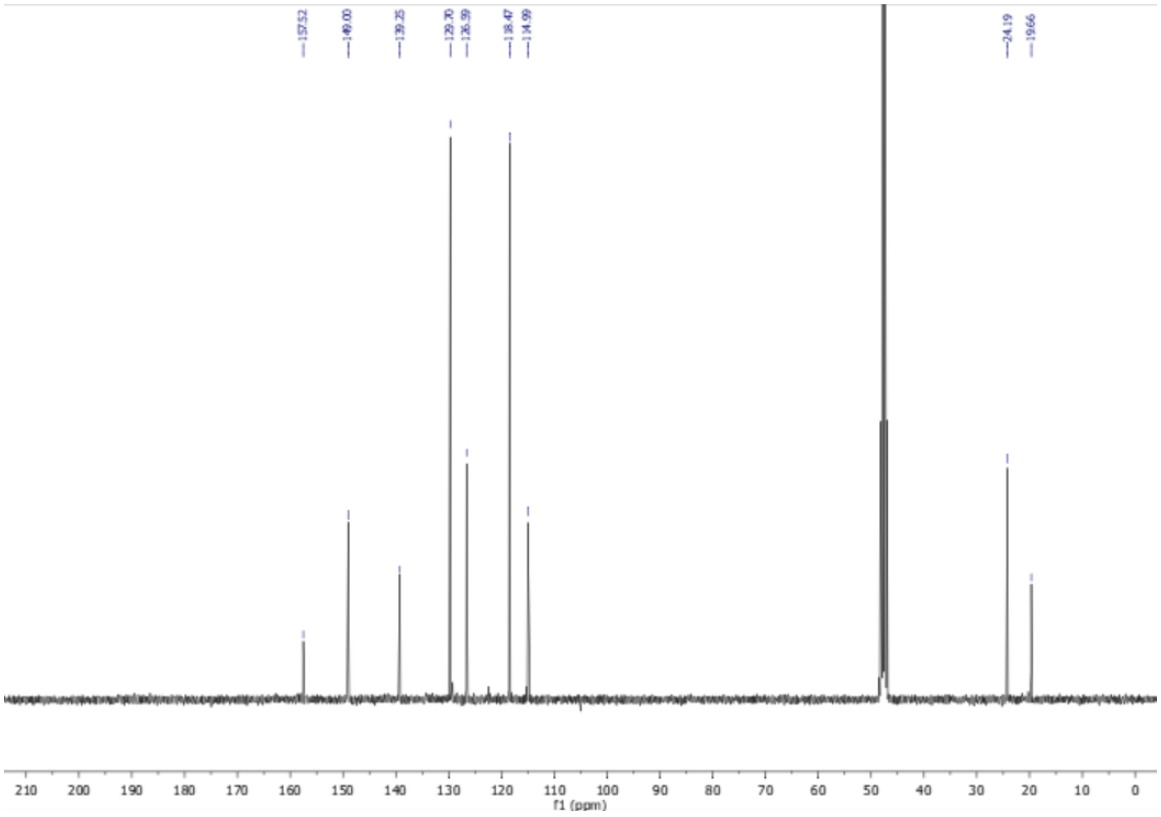
157.52
149.00
139.25
129.70
126.99
118.47
114.99
34.19
19.66
210 200 190 180 170 160 150 140 130 120 110 100 90 80 70 60 50 40 30 20 10 0
f1 (ppm)

1-(5-carboxypentyl)-2,3,3-trimethyl-3H-indol-1-ium (2)

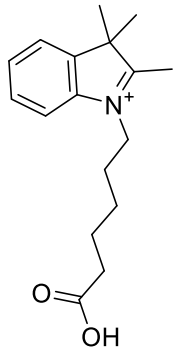

^{1}H

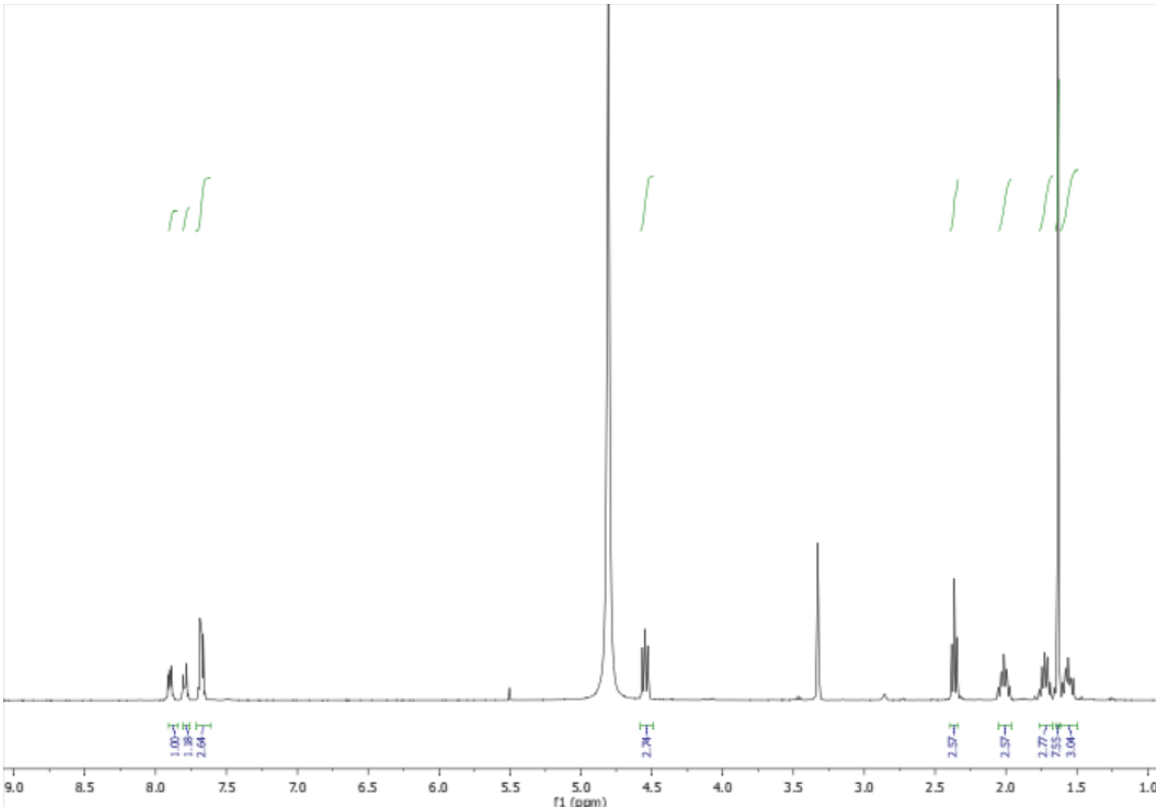

^{13}C

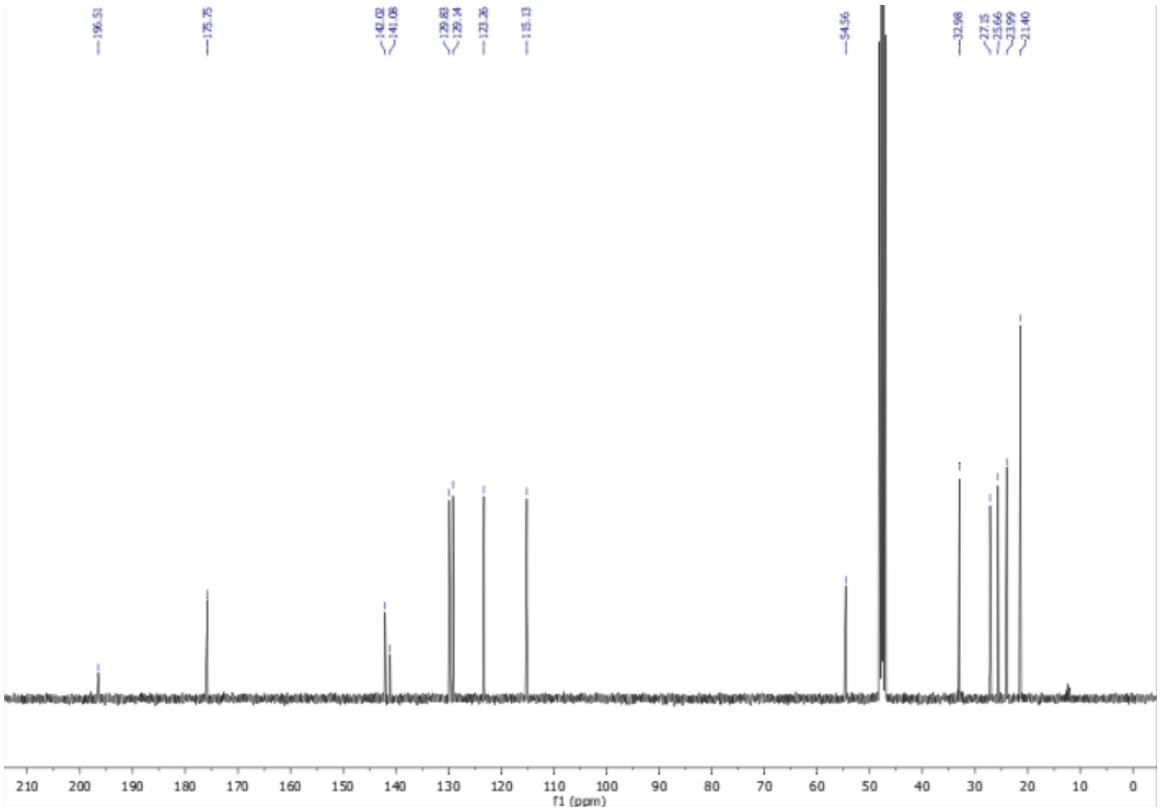
196.51
175.75
140.02
141.08
129.83
129.14
123.36
115.13
54.56
32.98
27.15
25.66
23.99
21.40
210 200 190 180 170 160 150 140 130 120 110 100 90 80 70 60 50 40 30 20 10 0
f1 (ppm)

1-(5-carboxypentyl)-2-((E)-2-((E)-3-(2-((E)-1-(5-carboxypentyl)-3,3-dimethylindolin-2-ylidene)ethylidene)-2-chlorocyclohex-1-en-1-yl)vinyl)-3,3-dimethyl-3H-indol-1-ium (A)

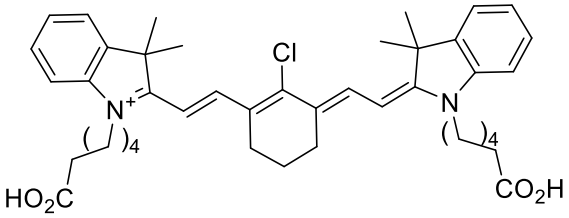

^{1}H

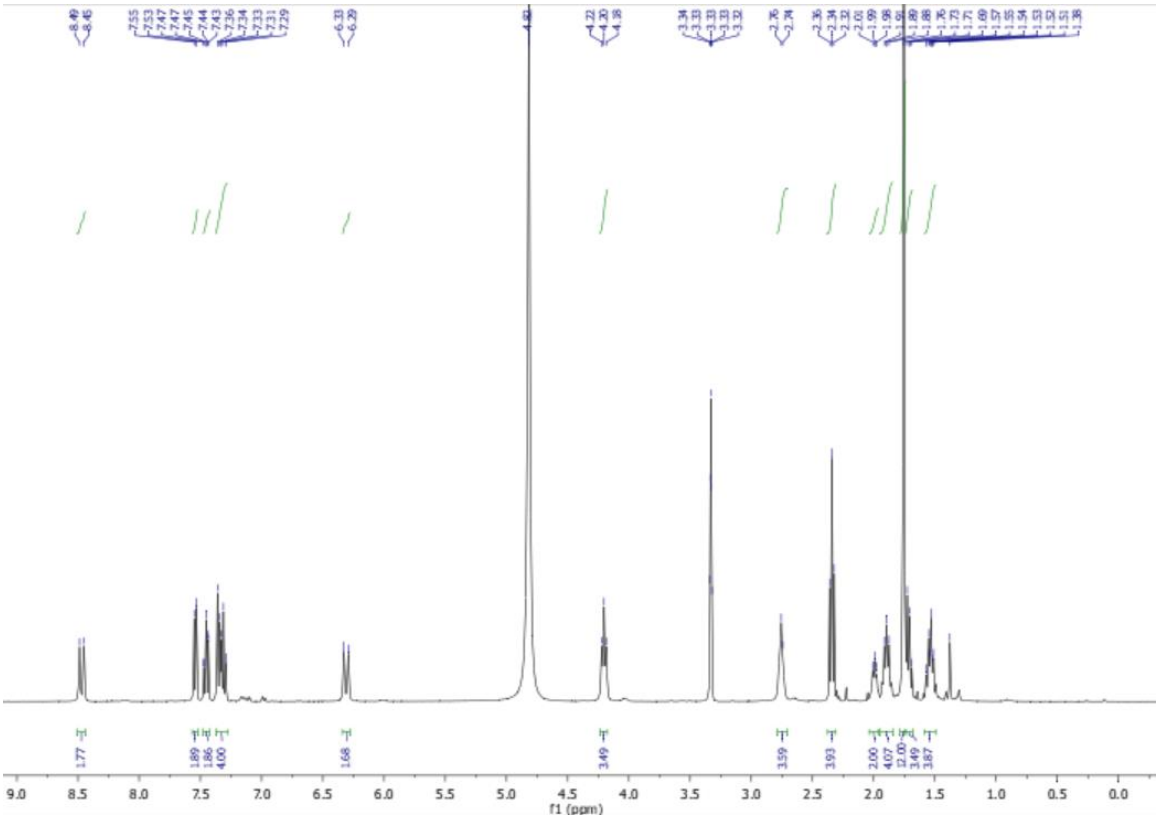

^{13}C

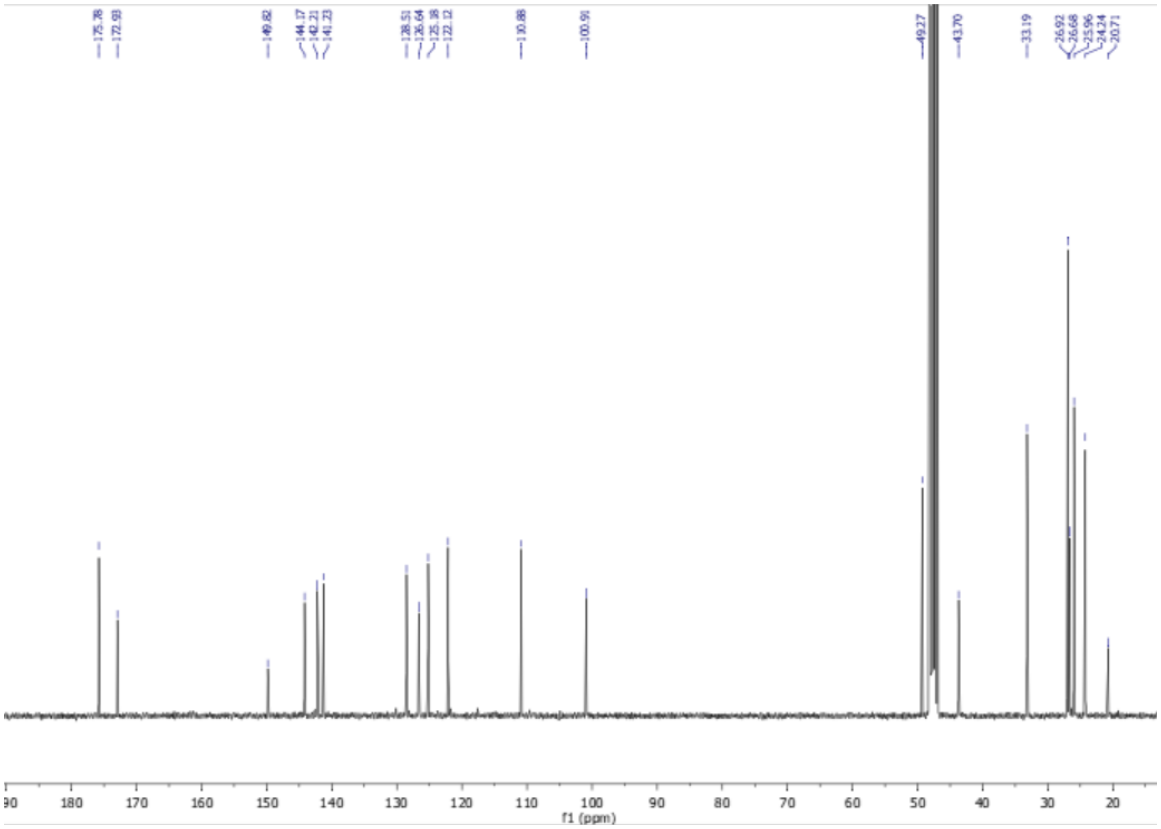
175.28
172.93
149.82
144.17
142.21
141.23
128.51
126.64
125.36
122.12
110.88
100.91
49.27
43.70
33.19
26.92
26.68
25.96
24.24
20.71
f1 (ppm)

1-(5-carboxypentyl)-2-((E)-2-((E)-2-chloro-3-(2-((E)-1-(6-(2-(4-(6-((5-((2-chloro-6-methylphenyl)carbamoyl)thiazol-2-yl)amino)-2-methylpyrimidin-4-yl)piperazin-1-yl)ethoxy)-6-oxohexyl)-3,3-dimethylindolin-2-ylidene)ethylidene)cyclohex-1-en-1-yl)vinyl)-3,3-dimethyl-3H-indol-1-ium (1)

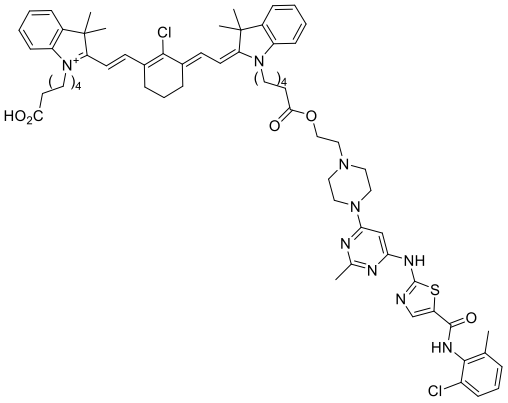

^{1}H

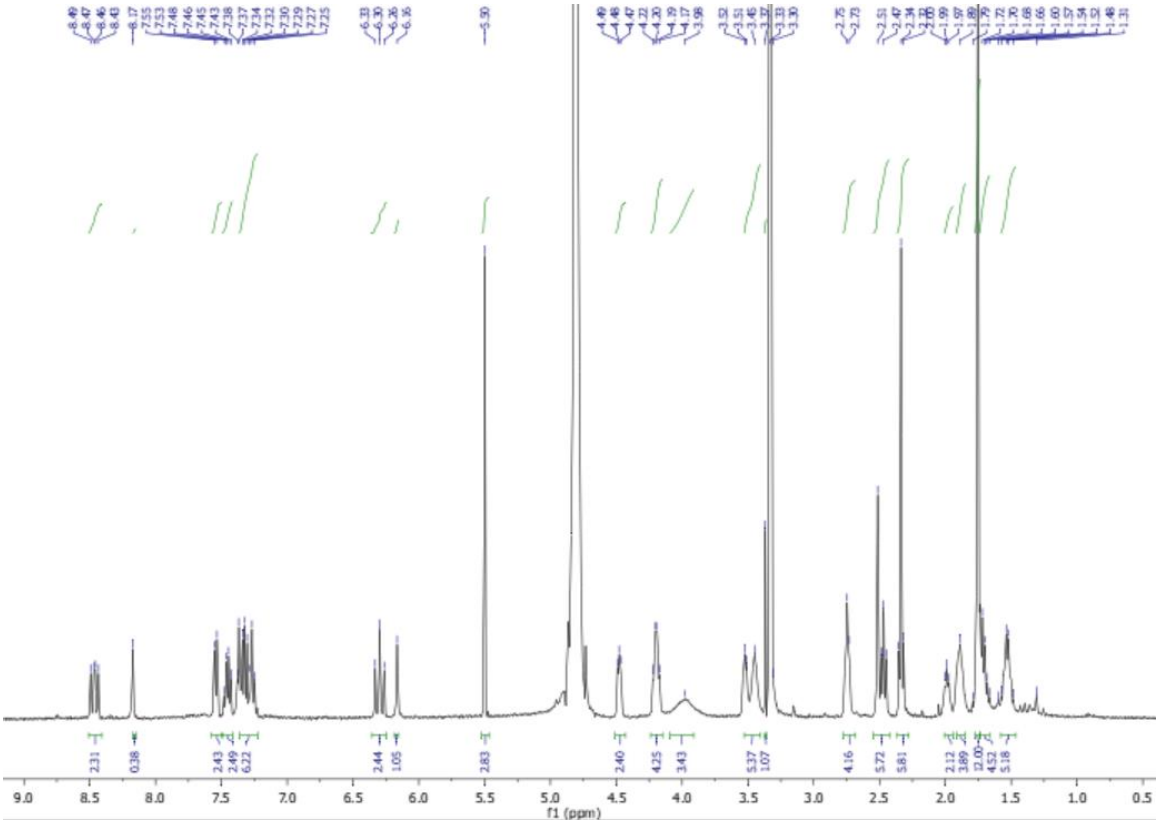

^{13}C

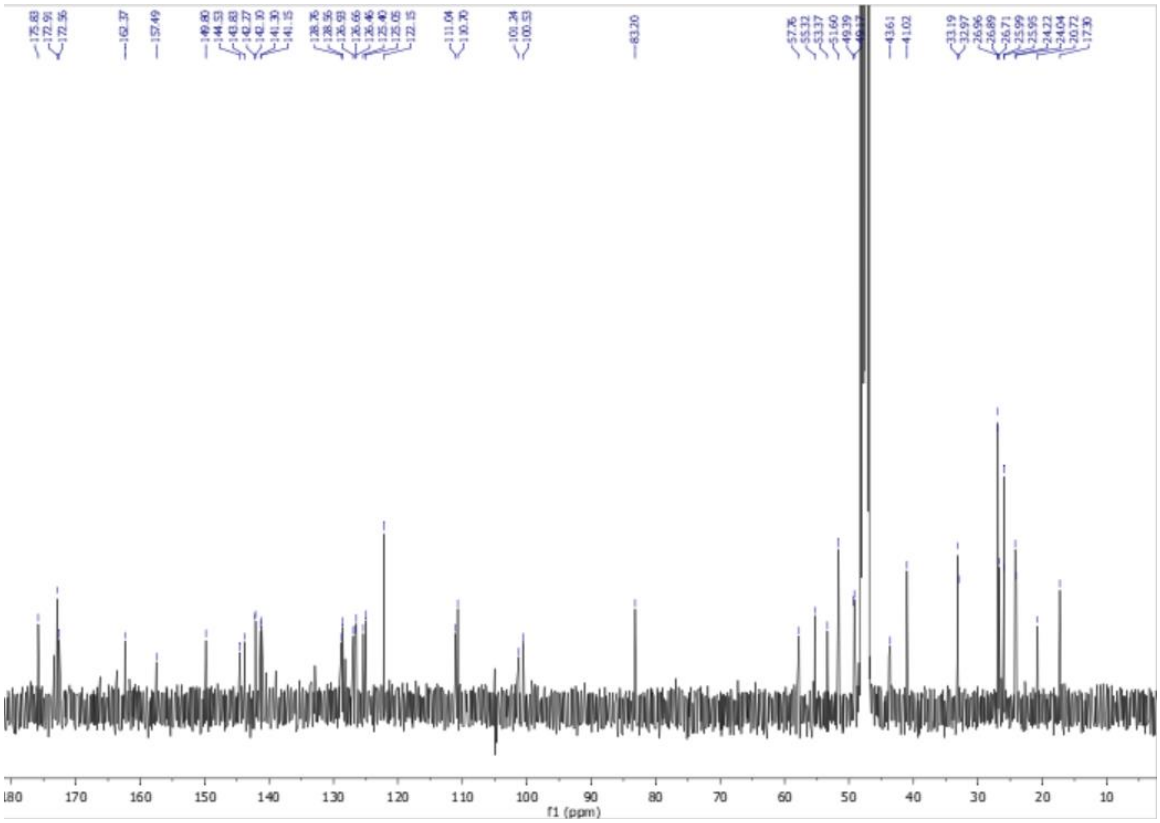
f1 (ppm)

HRMS

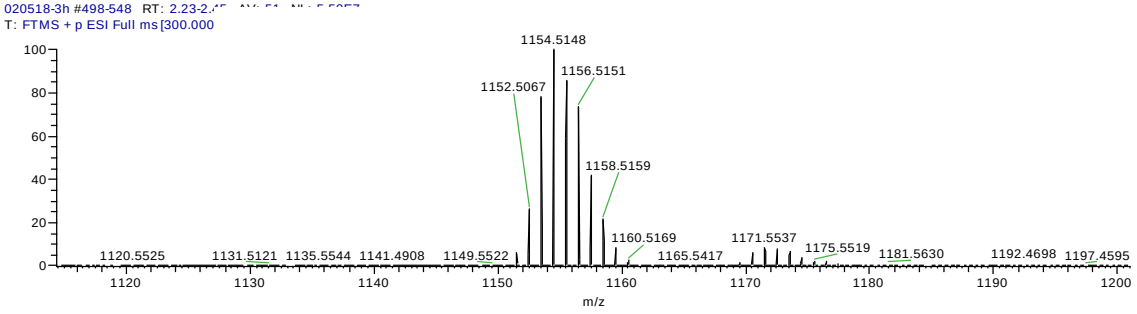
020518-3h #498-548 RT:
T: FTMS + p ESI Full ms [300.000
1154.5148
1156.5151
1152.5067
1158.5159
1160.5169
1171.5537
1175.5519
1120.5525
1131.5121
1135.5544
1141.4908
1149.5522
1165.5417
1181.5630
1192.4698
1197.4595
m/z

Photophysical Properties

Fluorescence Quantum Yield Calculation: Fluorescence quantum yield was determined according to previous literature procedure.[219] The fluorescence emission spectra of **1** were determined in PBS 7.4 (0.1% CrEL) using Cary-Varian 100 UV-Vis NIR spectrophotometer. Samples in PBS were excited in 1 cm path length cuvettes at 750 nm and integrated emission (760-900 nm) was quantified, keeping maximum absorbance below 0.1. ICG in DMSO (Q.Y=0.13) was used as internal standard to do the calculations. Briefly, the integrated fluorescence intensity was plotted against absorbance at different concentrations to generate gradient, which is proportional to the quantum yield of the samples.

$$\Phi_x = \Phi_{st} (Grad_x/Grad_{st})(\eta^2{}_x/\eta^2{}_{st})$$

Φ_{st} represents the quantum yield of the standard, and Φ_x represents the quantum yield of the unknown, Grad is the slope of the best linear fit, η is the refractive index of the solvent used and subscript x and st denote unknown and the standard respectively.

In Vitro Assays: HepG2 cells were grown in Dulbecco's Modified Eagle's medium (DMEM) containing 10% fetal bovine serum (FBS). Cells were grown in an incubator at 37°C, humidified atmosphere containing 5% CO_2. Cells were grown in T-75 culture flask till 70% confluency before splitting into next passage.

Live Cell Staining: Intracellular localization of dyes with the HEPG2 cells was measured using Olympus Fluoview FV1000. The images were taken at 60x/1.20 water immersed objective. Lysosome, Mitochondria and Nucleus were stained using Lysotracker Green DND 26, Mitotracker Green FM and, NucBlue respectively were bought from Life Technologies. 488 nm laser was used for green channel, 405 nm laser was used for nucleus and 633 nm laser was used for compound 1.

Briefly, 50,000 cells were seeded on 4 well chambers (Nunc Lab-Tek) and allowed to adhere overnight. The cells were incubated with 20 μM of compound **2** for 30 mins, washed twice with PBS, incubated with organelle stains according to manufacturer's instructions. The cells were washed twice again and stained with Nuc Blue for 10 mins. Mode of uptake of **1** was determined on Evos FL Imaging System (Thermofisher). The images were taken at 10x/0.4. Briefly, cells were either pre-blocked with 250 μM BSP for 10 mins or treated with 1 mM DMOG for 24 h before treating with the dye. After 30 mins incubation, cells were washed twice with PBS and stained with NucBlue for 10 mins and taken for imaging.

Cytotoxicity Assay: Approximately 5000 HepG2 cells/well were seeded on 96 well plate containing 10% fetal bovine serum (FBS). Cells were allowed to adhere overnight before test compounds were added. Stock solutions of **1, A, D** and **A+D** (0.02 M in DMSO) were diluted with protein-free medium (PFHM-II) to make desired final concentrations varying from 0.01 to 80 μM. The cells were incubated with the desired concentration for 48h. The cell viabilities were calculated using alamarBlue assay. Briefly, 10 μL of alamarBlue Reagent was incubated for an additional 2 h and

fluorescence was measured with excitation at 560 nm and emission wavelength at 590 nm with a BioTek Synergy 4 Microplate Reader. The viability of each cell line in response to the treatment with tested compounds was calculated as: % dead cells = 100 − (OD treated/OD control) × 100.

Cell Proliferation Assay: Approximately 2000 HepG2 cells/well were seeded on 96 well plate containing 10% fetal bovine serum (FBS). Cells were allowed to adhere overnight before test compounds were added. Stock solutions of **1, A, D** and **A+D** (0.02 M in DMSO) were diluted with protein-free medium (PFHM-II) to make final concentration of 5 μM. The media was change after every 3 days and MTT assay was performed to quantitate the proliferation of cells. For MTT assay, 5 mg was dissolved in 1 mL of Hank's Balanced Salt Solution

(HBBS) and 20 μL of solution was added to each well. After 2 hrs, entire media was removed and formazan crystals were dissolved in 100 μL of DMSO. The plate is shaken at 300 rpm for 5 mins to dissolve the formazan crystals. Afterwards, the absorbance of formazan dye is observed at 570 nm using BioTek Synergy 4 Microplate Reader.

Wound Healing Assay: HepG2 cells were seeded in 3-well silicone inserts (Ibidi, with two defined cell-free gaps) on a 6-well plate at a density of 5 $x10^5$ cells/mL (70 μL applied in each small well) in DMEM medium containing 10% fetal bovine serum and were allowed to adhere overnight. 3-well inserts were then removed and cells were washed carefully with PBS to help remove non-adherent cells or cell debris. Compounds were premixed with DMEM medium containing 10% FBS (DMSO = 0.1%) and added to the 6-well plate. Time-lapse images were obtained via EVOS Auto Fl 2 microscope

automated program every 20 min for a total of 28 h. Time-lapse videos were generated by ImageJ software. Quantification of wound healing assay was done by the "ACAS" online software (available from Ibidi website).

Western Blot: HepG2 cells were seeded in a 24-well plate (1 x10^5 cells/well) in DMEM medium containing 10% fetal bovine serum and were allowed to adhere overnight. Medium was replaced with fresh DMEM medium containing 10% FBS premixed with compounds (DMSO = 0.1%) and incubated for 24 h. Cells were washed twice with cold PBS and

lysed by RIPA buffer (Pierce) according to manufacturer's instructions to obtain the cell lysate. The total protein concentrations of all lysate samples were calibrated by BCA protein assay (Pierce). SDS-buffer was added to samples and boiled at 100 °C for 10 min. SDS-PAGE was performed using a handcast 10% polyacrylamide gel (50 µg total protein loaded). The gel was washed with distilled water twice and was transferred to PVDF membrane by Pierce Power Station according to manufacturer's instructions. The membrane was blocked with SuperBlock T20 (ThermoFisher) for 2 h at room temperature, incubated with anti-p-Src (Cell Signaling Technology, 1:1000) at 4 °C overnight, washed with TBST (TBS + 0.05% Tween 20) twice, incubated with HRP-conjugated anti-rabbit IgG (H+L) (ThermoFisher, 1:2000) for 1 h at room temperature and washed again with TBST 3-5 times. Afterwards, blots were treated with ECL Western Blotting Substrate (Pierce) and scanned by ChemiDoc XRS (BioRad) imaging system.

Flow Cytometry: Cellular uptake of **1** was quantified by using BD FACSAria II. Briefly, 100,000 cells were seeded on 24 well plate and allowed to adhere for 24 h. For hypoxia 1 mM DMOG was added for 24 h, for OATPs blocking 250 µM BSP was added for 10 mins and for ATP blocking cells were placed at 0 ^{o}C for 30 min prior to experiment. The cells were incubated with the dye for 30 min. After incubation, the cells were washed thrice with PBS, dissociated from the plate using 200 µM of Cell Dissociation Buffer, enzyme free (Thermofisher) and suspended in PBS. The fluorescence of the samples was measured by 633 nm excitation source and 750/45 emission filter.

Figures:

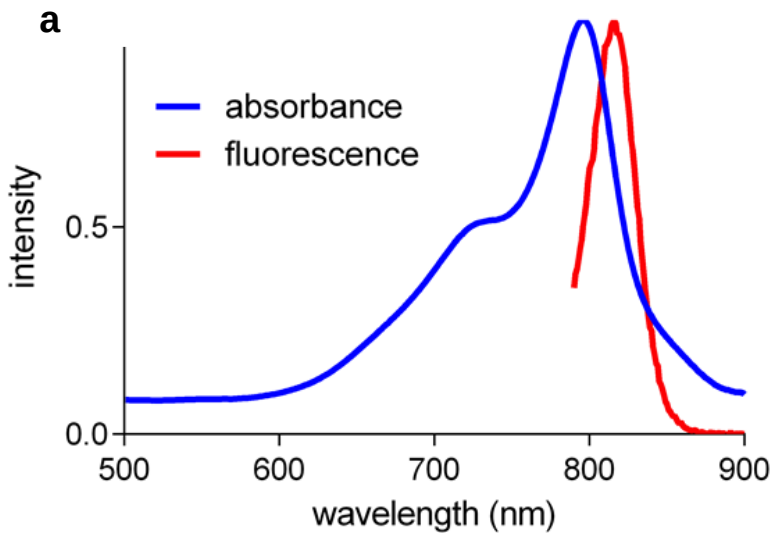

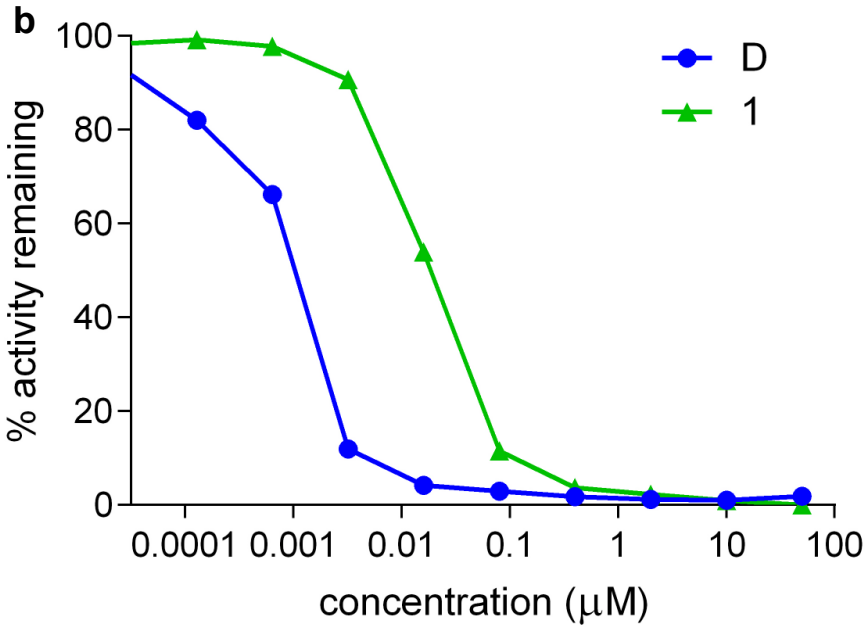
b
100
80
60
40
20
0
% activity remaining
D
1
0.0001
0.001
0.01
0.1
1
10
100
concentration (μM)

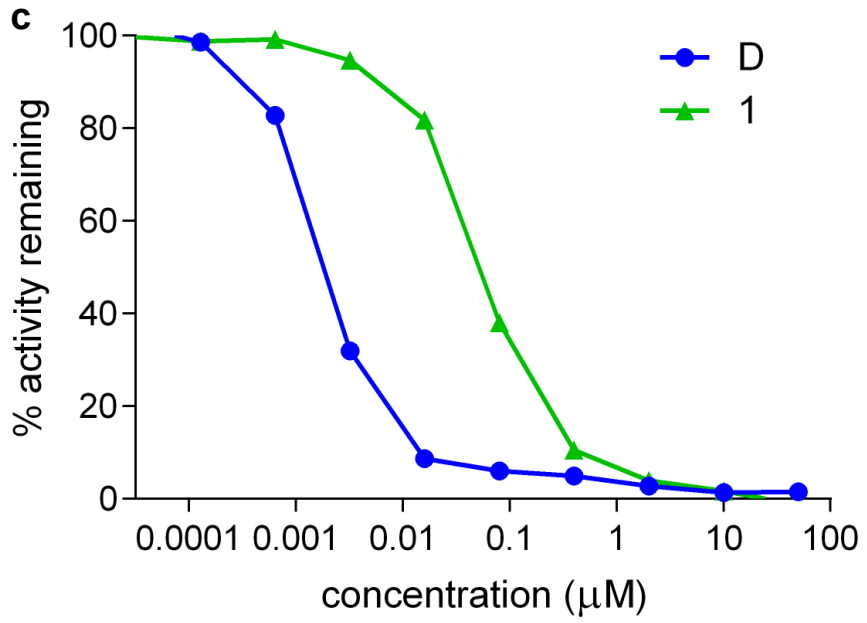
c
100
80
60
40
20
0
% activity remaining
D
1
0.0001
0.001
0.01
0.1
1
10
100
concentration (μM)

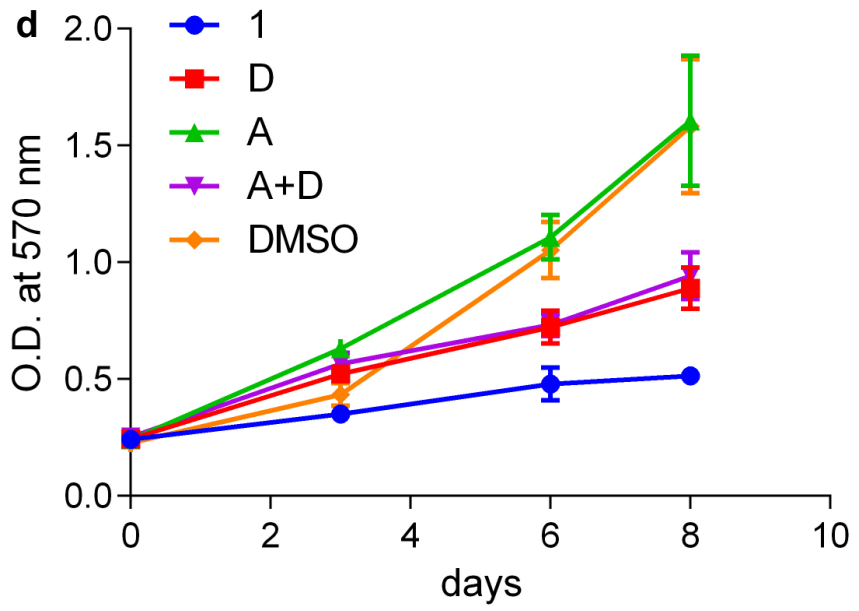

Figure D-S1. a Absorbance and fluorescence of compounds in compound **1** in PBS (pH 7.4) in 0.1% CrEL. IC_{50} determination of compound **1** and **D** with **b** Src, and **c** Lyn. **d** Proliferation assay was carried out for 8 days at 5 μM of **1**, **D**, **A**, equimolar concentration of **A**+**D** and DMSO (control).

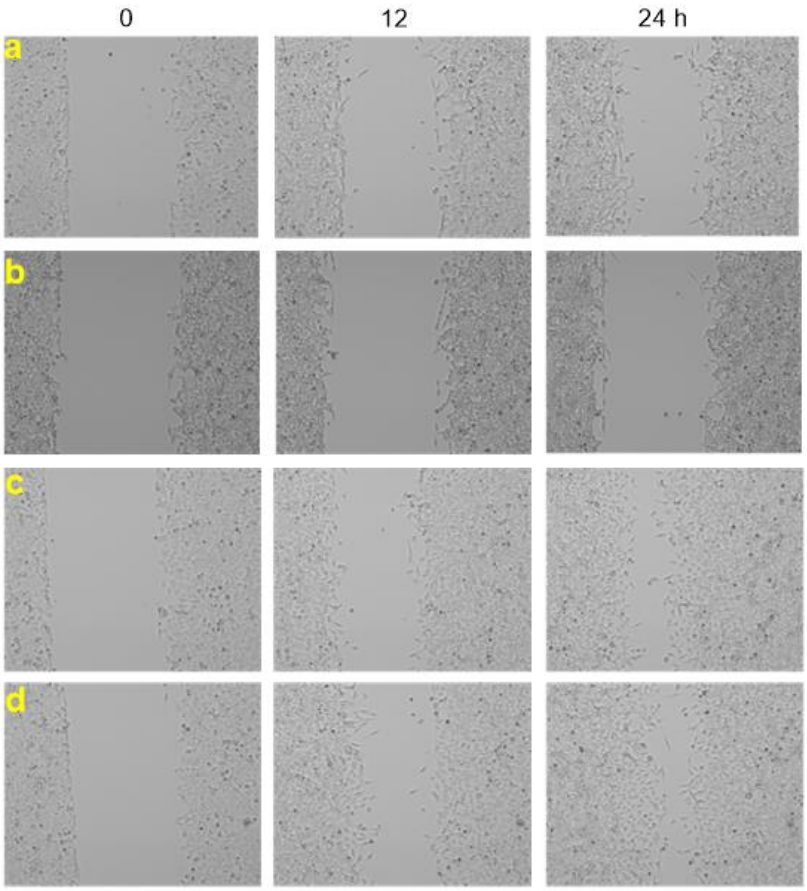

Figure D-S2. Wound healing assay at 1 μM of **a**, **1**; **b**, **D**; **c**, **A**; and **d**, DMSO at 0, 12 and 24 h.

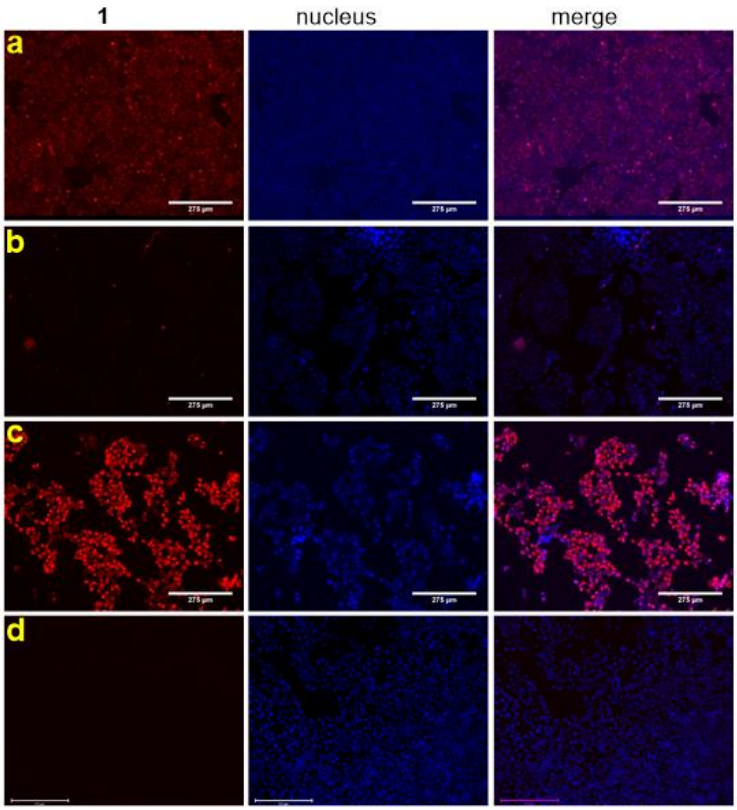

Figure D-S3. Uptake of **2ac** in **a**, normal conditions; **b**, blocked by BSP (OATPs inhibitors) and **c**, DMOG (hypoxia inducers) and **d**, 0 ºC (ATPs blocked). Magnification 10x. Scale bar 275 μM.

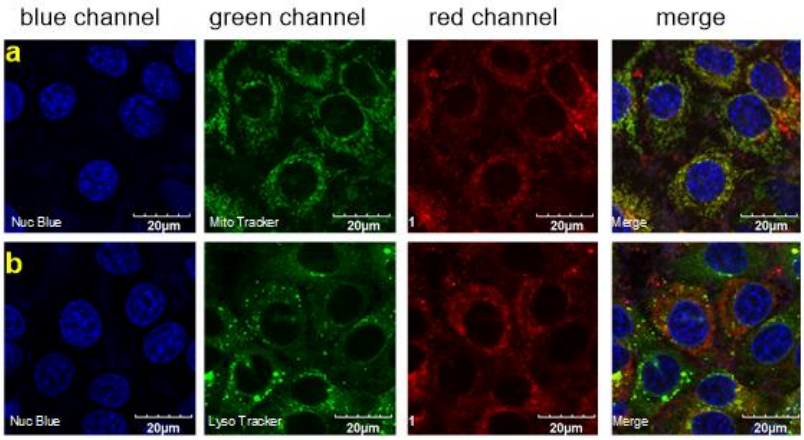

Figure D-S4. Organelle colocalization study of **1** with **a,** MitoTracker Green; and **b,** LysoTracker

APPENDIX E

SUPPORTING INFORMATION FOR CHAPTER VI

General Experimental Procedures

All reactions were carried out under an argon atmosphere. Reagents were purchased at a high commercial quality (typically 97 % or higher) and used without further purification, unless otherwise stated. High field NMR spectra were recorded with Bruker Avance III at 400 MHz for ^{1}H, and 100 MHz for ^{13}C and were calibrated using residual non-deuterated solvent as an internal reference ($CDCl_3$: ^{1}H NMR = 7.24, ^{13}C NMR = 77.0, MeOD: ^{1}H NMR = 3.30, ^{13}C NMR = 49.0, DMSO-d_6: ^{1}H NMR = 2.50, ^{13}C NMR = 39.5). The following abbreviations were used to explain the multiplicities: s = singlet, d = doublet, t = triplet, q = quartet, quint = quintet, dd = double doublet, dt = double triplet, dq = double quartet, m = multiplet, br = broad. Electrospray ionization mass spectrometry (ESI-MS) data were collected on triple-stage quadrupole instrument in a positive mode. Flash chromatography was performed using silica gel (230-400 mesh). LC-MS analyses were collected from Agilent 1260 Infinity Quaternary LC and Agilent 6120 Quadrupole LC/MS modules using Poroshell 120 EC-C18 2.7 µM (4.6 x 50 mm) column in 5-95% CH_3CN/water gradient with 0.1% formic acid over 10 minutes. Prep HPLC was performed on Agilent 1260 Infinity in 50-90 CH_3CN/water gradient with 0.1% TFA over 20 mins. All statistical analyses were carried out by Graphpad Prism version 6.0 (Graphpad Software).

General Synthesis Procedure: Reagents were purchased at a high commercial quality (typically 97 % or higher) and used without further purification, unless otherwise stated.

Compounds **0bb** and **0cc** were purchased from Sigma Aldrich and abcr GmbH respectively. General synthesis of **3a-d** and **compounds 1 – 2** are described below. Detailed synthesis and characterization are described in supporting.

Hemicyanine Synthesis (3a-d): Compound **A** (1 eq), **4a-b** or **5a-b** (1 eq) and NaOAc (1 eq) were dissolved in 100 mL of absolute ethanol in 250 mL round bottom flask. The mixture was heated at 50 ºC for 2 h. The solvent was removed and the crude material was purified by normal phase flash chromatography with MeOH:CH_2Cl_2 (1:25 v/v) for **3a**, **c** and MeOH:$CHCl_3$ (1:3) for **3b**, **d** to afford blue solid.

Unsymmetric and Symmetric cyanine synthesis (1 – 2): Compound **3a-d** (1 eq), **4a-c** or **5a-b** (1 eq) and NaOAc (1 eq) were dissolved in 50 mL of absolute ethanol in 100 mL round bottom flask. The mixture was refluxed for 3 h. The solvent was removed and the crude was purified by reverse phase prep HPLC.

HepG2 cells were grown in Dulbecco's Modified Eagle's medium (DMEM) containing 10% fetal bovine serum (FBS). Cells were grown in an incubator at 37°C, humidified atmosphere containing 5% CO_2. Cells were grown in T-75 culture flask till 70% confluency before splitting into next passage.

Fluorescence Quantum Yield Measurements: Fluorescence quantum yield was determined according to previous literature procedure. [219] The fluorescence emission spectra of compounds **0-2** were determined in PBS 7.4 (0.1% CrEL) using Cary-Varian 100 UV-Vis NIR spectrophotometer. Samples in PBS were excited in 1 cm path length cuvettes at 750 nm and integrated emission (760-900) was quantified, keeping maximum absorbance below 0.1. ICG in DMSO (Q.Y 0.13) was used as internal standard to do the

calculations. Briefly, the integrated fluorescence intensity was plotted against absorbance at different concentrations to generate gradient, which is proportional to the quantum yield of the samples.

$$\Phi_x = \Phi_{st} (Grad_x/Grad_{st})(\eta^2{}_x/\eta^2{}_{st})$$

Φ_{st} represents the quantum yield of the standard, and Φ_x represents the quantum yield of the unknown, Grad is the slope of the best linear fit, η is the refractive index of the solvent used and subscript x and st denote unknown and the standard respectively.

Singlet Oxygen Detection[220]**:** Singlet oxygen generation of compounds **0-2** was determined using 780 nm LEDs (Thor Lab, LED780E) embedded on 24 well plate holder. Sample solutions were prepared in PBS 7.4 (0.1% CrEL) at a concentration of 5 µM in 24 well plate. DPBP (1 mM) was prepared in DMSO and diluted to 80 µM in PBS 7.4 (0.1% CrEL). The decrease in absorbance was measured at 418 nm every one minute for 10 mins by BioTek Synergy 4 Microplate Reader. Rate of change of absorbance is plotted against irradiation time.

$$\Phi_x = \Phi_{st} (Grad_x/Grad_{st})(F_{st}/F_x)$$

Φ_{st} represents the quantum yield of the standard, and Φ_x represents the quantum yield of the unknown, Grad is the slope of the best linear fit, F stands for the absorption correction factor ($F = 1 - 10^{-abs}$; abs represent absorbance) and subscript x and st denote unknown and the standard respectively.

Photostability: Photostability of compounds **0-2** were compared by irradiating samples under 780 nm LEDs (Thor Lab, LED780E). The compounds were dissolved in PBS 7.4 (0.1% CrEL) to give a concentration of 10 µM. The decrease in absorbance at 780 nm

was measured every 2 mins for 10 mins and then every 10 mins interval for 60 mins by BioTek Synergy 4 Microplate Reader. Decrease in absorbance was plotted against time.

Live cell Staining: Intracellular localization of dyes with the HepG2 cells was measured using Olympus Fluoview FV1000. The images were taken at 60x/1.20 water immersed objective. Lysosome, Mitochondria and Nucleus were stained using Lysotracker Green DND 26, Mitotracker Green FM and, NucBlue respectively were bought from Life Technologies. 488 nm laser was used for green channel, 405 nm laser was used for nucleus and 633 nm laser was used for compound **2**.

Briefly, 50,000 cells were seeded on 4 well chambers (Nunc Lab-Tek) and allowed to adhere overnight. The cells were incubated with 20 μM of compound **2** for 30 mins, washed twice with PBS, incubated with organelle stains according to manufacturer's instructions. The cells were washed twice again and stained with Nuc Blue for 10 mins. The localization of **2ac** and **2bc** in organelles was quantified using ImageJ (coloc2 plug in).

Blocking Study: Mode of uptake of **2ac** was determined on Evos FL Imaging System (Thermofisher). The images were taken at 10x/0.4. Briefly, cells were either pre-blocked with 250 μM BSP for 10 mins or treated with 1 mM DMOG for 24 h before treating with the dye. After 30 mins incubation, cells were washed twice with PBS and stained with NucBlue for 10 mins and taken for imaging. The amount of uptake was quantified by using Image Studio Lite (Ver 5.2).

Cytotoxicity Assays: Approximately 5000 HepG2 cells/well were seeded on 96 well plate containing 10% fetal bovine serum. Cells were allowed to adhere overnight before

test compounds were added. Stock solutions of **2** (0.02 M in DMSO) were diluted with protein-free medium (PFHM-II) to make desired final concentrations varying from 0.01 to 80 μM. The cells were incubated with the desired concentration for 48h. The cell viabilities were calculated using AlamarBlue assay. Briefly, 10 μL of alamarBlue Reagent was incubated for an additional 2 h and fluorescence was measured with excitation at 560 nm and Emission wavelength at 590 nm with a BioTek Synergy 4 Microplate Reader. The viability of each cell line in response to the treatment with tested compounds was calculated as: % dead cells = 100 − (OD treated/OD control) × 100.

Photocytotoxicity Assays: Approximately 5000 cells in DMEM/F12 containing 10% FBS were seeded in 96 well plate. Cells were allowed to adhere overnight before test compounds were added. Stock solutions of **2** (0.02 M in DMSO) were diluted with protein-free medium (PFHM-II) to make desired final concentrations varying from 1 to 10 μM. The cells were treated with desired concentrations of compound for 1 h. Afterwards, cells were washed with PBS twice and culture media was changed to ACAS. LED light (3.8 mW/cm^2) was irridiated on the cells for 10 mins and the cells were incubated in dark for 24 h. Cell viabilities were determined by alamarBlue Assay as mentioned above.

Synthesis Scheme

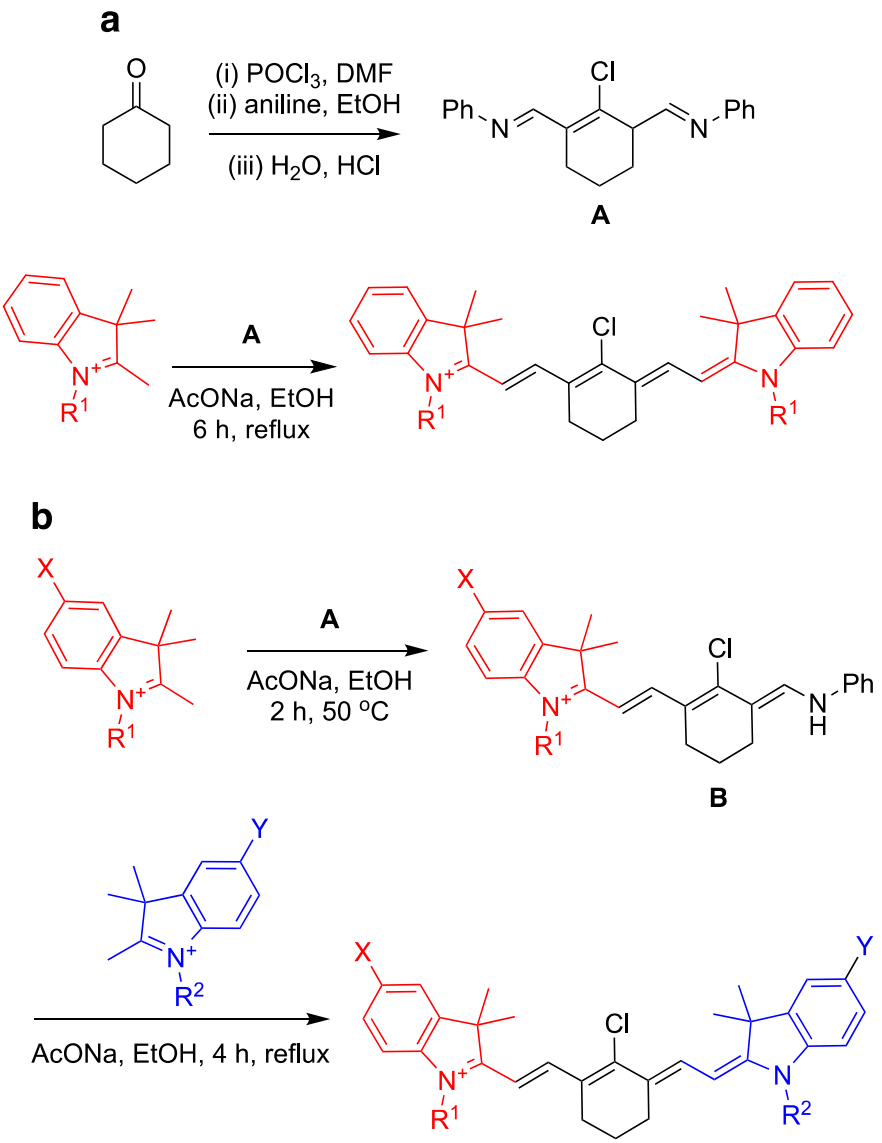

Scheme E-S1. General synthesis scheme for **a,** symmetric and **b,** unsymmetric cyanine dyes

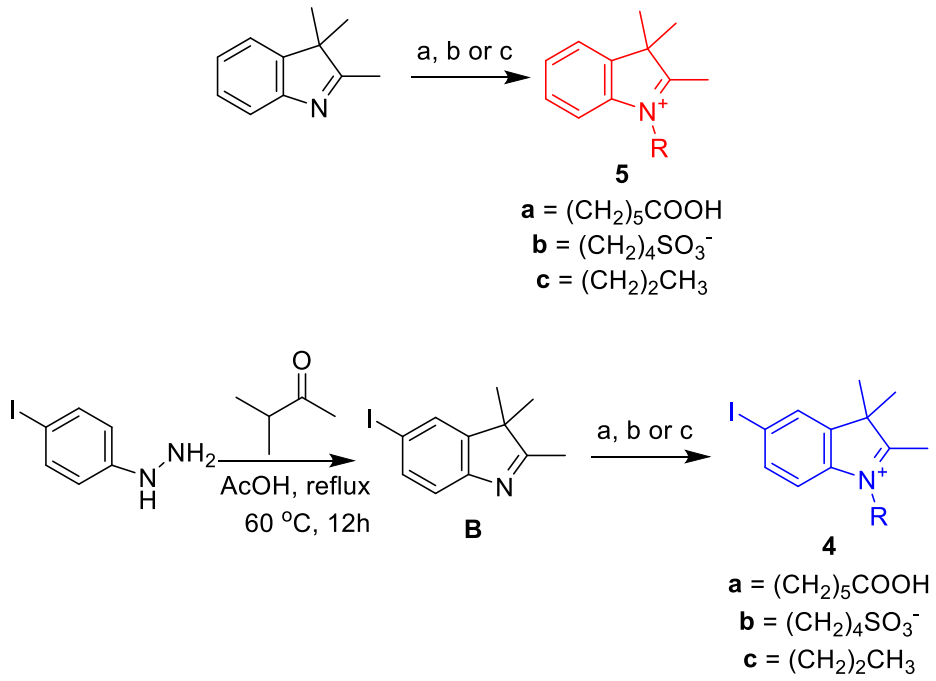

Scheme E-S2. Synthesis of iodinated and non-iodinated indoles. **a,** 6-bromohexanoic acid, CH_3CN, reflux 18h; **b,** 1,4-butane sultone, 1,2-dichlorobenzene, reflux, 18h; and **c,** propyl iodide, reflux, 18h

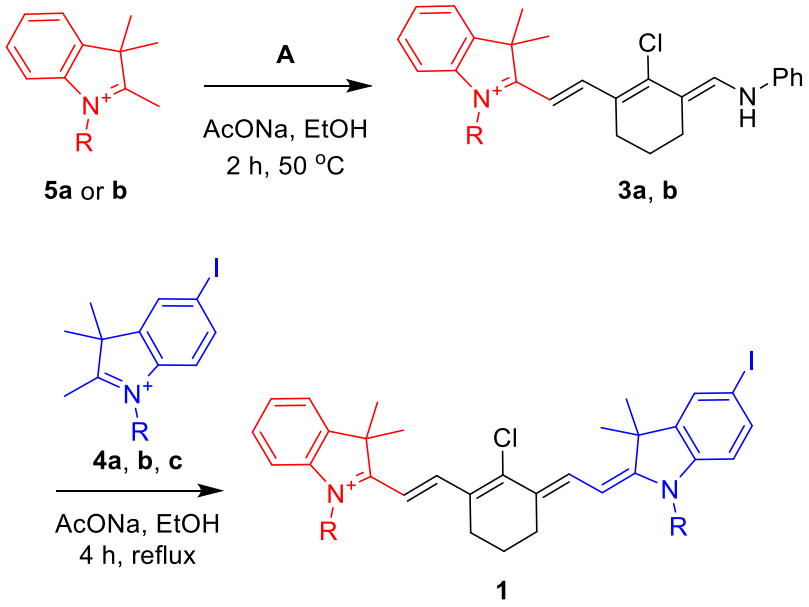

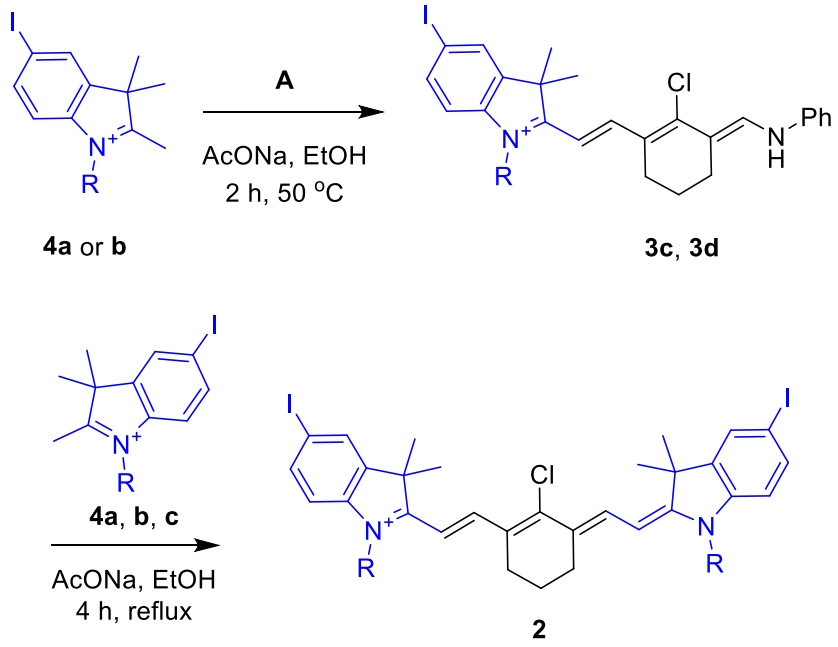

Scheme E-S3. General synthesis procedure for compounds **0** - **2**

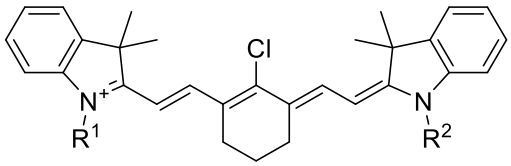

0
aa, **bb**, **cc**

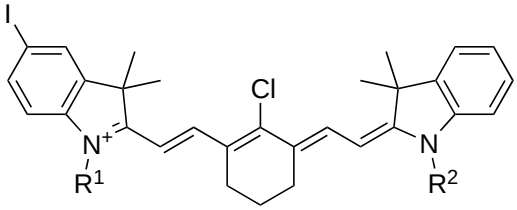

1
aa, **bb**, **ab**, **ac**, **bc**

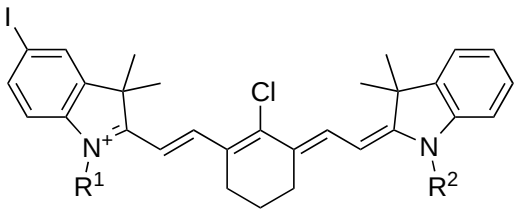

1
aa, **bb**, **ab**, **ac**, **bc**

where R^1 and R^2 are

a = 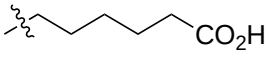 **b** = 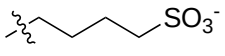 **c** = 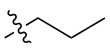

Scheme E-S4. General structures of the compounds synthesized or used in this study. Compound **0aa** was synthesized according to literature procedure[1], **0bb** and **0cc** were purchased from Sigma Aldrich and abcr GmbH.

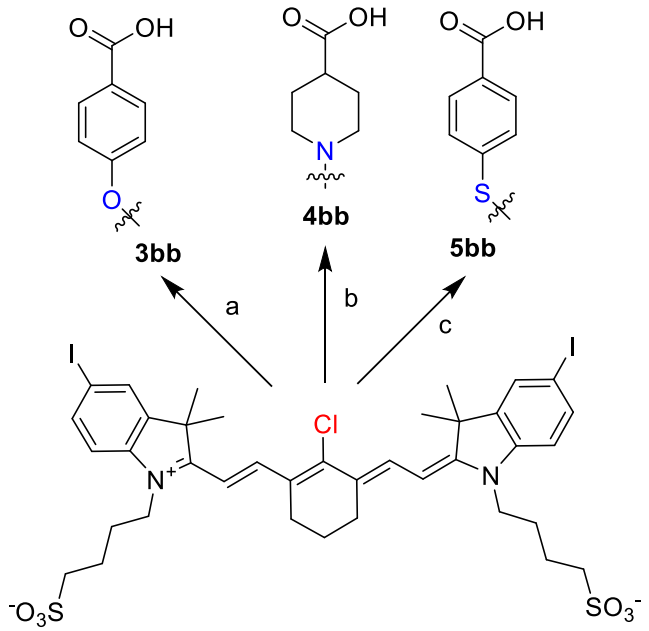

Scheme E-S5. Synthesis of **a,** NaH, 4 hydroxybenzoic acid, DMF, 25 ^{o}C, 18h, **b,** isonipecotic acid, 60 ^{o}C, 12h DMF **c,** 4-mercaptobenzoic acid, DMSO, 25^{o}C, 18h

Synthesis Procedure

Synthesis of (1E,1'E)-1,1'-(2-chlorocyclohex-1-ene-1,3-diyl)bis(N-phenylmethanimine) (A)

DMF (65 mL, 0.85 mol) was added to a 500 mL round bottom flask and cooled in an ice bath. Dropwise, $POCl_3$ (55 mL, 0.6 mol) was added and the mixture was stirred for 30 min. Cyclohexanone (27.5 mL, 0.265 mol) was added and the solution was refluxed at 100 ^oC for 1 h. Subsequently, the heating was stopped and the reaction was cooled down by placing on ice bath. While the mixture was cooling, aniline/EtOH (1:1 v/v, 90 mL) was added, then the mixture was stirred for 1 h. The solution was poured to cold H_2O:conc. HCl (10:1, 110 mL) and allowed to stand for 2 hours. The dark purple solid was collected by filtration and dissolved with methanol. The product was recrystallized using methyl *tert*-butylether:hexane (1:1) as purple crystals (45.78 g, 86%).

^1H NMR (400 MHz, MeOD) δ 8.66 (s, 2H), 7.50 (s, 3H), 7.49 (d, *J* = 2.0 Hz, 3H), 7.31 (ddd, *J* = 8.4, 5.6, 3.0 Hz, 2H), 3.37 (s, 1H), 2.74 (t, *J* = 6.2 Hz, 4H), 2.00 (s, 2H).

^{13}C NMR (100 MHz, MeOD) δ 157.52, 149.00, 139.25, 129.70, 126.59, 118.47, 114.99, 24.19, 19.66.

Synthesis of 5-iodo-2,3,3-trimethyl-3H-indole (B)[2]

(4-iodophenyl)-hydrazine (25 g, 106.8 mmol) was added to 3-methyl-2-butanone (14.1 mL, 162.3 mmol) and refluxed in glacial acetic acid (200 mL) for 12 h. Afterwards, glacial acetic acid was removed under reduced pressure and the crude was dissolved in diethyl ether. The insoluble solid residues were filtered and the clear ether solution was

washed twice with conc. NaOH, conc. $Na_2S_2O_3$ and water. The organic layer was dried using $MgSO_4$ and evaporated to afford thick red-brown liquid which was carried forward without further purification. (18.1 g, 60%).

^{1}H NMR (400 MHz, MeOD) δ 7.72 (d, *J* = 1.6 Hz, 1H), 7.63 (dd, *J* = 8.1, 1.7 Hz, 1H), 7.23 (d, *J* = 8.1 Hz, 1H), 2.26 (s, 3H), 1.28 (s, 6H).

^{13}C NMR (100 MHz, MeOD) δ 189.89, 152.22, 148.20, 136.63, 130.88, 120.88, 89.90, 53.96, 21.83, 13.97.

Synthesis of 1-(5-carboxypentyl)-2,3,3-trimethyl-3H-indol-1-ium (5a) [3]

In 500 mL round bottom flask, 2,3,3-trimethylindolenine (5 g, 31.4 mol) and 6-bromohexanoic acid (12.3 g, 62.8 mmol) were added to 200 mL of acetonitrile. The mixture was refluxed for 12 h. Subsequently, the mixture was cooled to room temperature and acetonitrile was removed by rotavap. Subsequently, the flask was placed in an ice bath, the solid residue was dissolved in 100 mL dichloromethane, then 300 mL diethyl ether was added to precipitate the product. That product was collected by filtration and washed with diethyl ether to afford pink crystals (6.4 g, 72%).

^{1}H NMR (400 MHz, MeOD) δ 7.91 – 7.84 (m, 1H), 7.79 (dt, *J* = 7.5, 3.8 Hz, 1H), 7.71 – 7.61 (m, 3H), 4.58 – 4.49 (m, 3H), 2.36 (t, *J* = 7.2 Hz, 3H), 2.05 – 1.96 (m, 3H), 1.77 – 1.67 (m, 3H), 1.63 (s, 8H), 1.62 – 1.49 (m, 3H).

^{13}C NMR (100 MHz, MeOD) δ 196.51, 175.75, 142.02, 141.08, 129.83, 129.14, 123.26, 115.13, 54.56, 32.98, 27.15, 25.66, 23.99, 21.40.

Synthesis of 1-(5-carboxypentyl)-5-iodo-2,3,3-trimethyl-3H-indol-1-ium (4a) was carried out as above to afford grey solid (4.3 g, 58%).

^{1}H NMR (400 MHz, MeOD) δ 8.22 (d, *J* = 1.5 Hz, 1H), 8.04 (dd, *J* = 8.5, 1.6 Hz, 1H), 7.70 (d, *J* = 8.5 Hz, 1H), 4.57 – 4.46 (m, 2H), 2.36 (t, *J* = 7.2 Hz, 2H), 1.99 (s, 2H), 1.71 (d, *J* = 7.6 Hz, 2H), 1.63 (s, 6H), 1.52 (d, *J* = 21.3 Hz, 3H).

^{13}C NMR (100 MHz, MeOD) δ 175.75, 144.05, 138.36, 132.76, 116.82, 95.22, 54.61, 32.96, 27.06, 25.63, 23.97, 21.21.

Synthesis of 4-(2,3,3-trimethyl-3H-indol-1-ium-1-yl)butane-1-sulfonate (5b)[4]

In 500 mL round bottom flask, 2,3,3-trimethylindolenine (5 g, 31.4 mmol) and 1,4-butane sultone (8.55 g, 62.8 mmol) were added to 50 mL of 1,2-dichlorobenzene. The mixture was refluxed for 12 h. Subsequently, the mixture was cooled to room temperature and acetonitrile was removed by rotavap. Subsequently, the flask was placed in an ice bath, the solid residue was precipitated from 2-propanol and collected by filtration. The precipitate was washed several times with isopropanol to afford red crystals. (5.4 g, 52%).

^{1}H NMR (400 MHz, MeOD) δ 7.94 (s, 1H), 7.77 (d, *J* = 3.1 Hz, 1H), 7.69 – 7.63 (m, 2H), 4.62 – 4.53 (m, 2H), 2.91 (t, *J* = 7.1 Hz, 2H), 2.18 (s, 2H), 1.98 (d, *J* = 7.6 Hz, 2H), 1.63 (s, 6H).

^{13}C NMR (100 MHz, MeOD) δ 7.94, 7.77, 7.77, 7.68, 7.67, 7.67, 7.66, 7.66, 7.65, 4.60, 4.58, 4.56, 2.93, 2.91, 2.90, 2.18, 1.99, 1.97, 1.63.

Synthesis of 4-(5-iodo-2,3,3-trimethyl-3H-indol-1-ium-1-yl)butane-1-sulfonate (4b) was carried out as above to afford red solid (4.1 g, 55%).

^{1}H NMR (400 MHz, MeOD) δ 8.20 (s, 1H), 8.03 (dd, *J* = 8.5, 1.6 Hz, 1H), 7.76 (d, *J* = 8.5 Hz, 1H), 4.58 – 4.49 (m, 2H), 2.90 (t, *J* = 7.1 Hz, 2H), 2.16 (dd, *J* = 9.1, 6.5 Hz, 2H), 1.98 – 1.91 (m, 2H), 1.62 (s, 6H).

^{13}C NMR (100 MHz, MeOD) δ 196.84, 144.04, 141.02, 138.39, 132.65, 117.03, 95.14, 63.35, 54.61, 49.72, 25.91, 23.89, 21.83, 21.23.

Synthesis of 2,3,3-trimethyl-1-propyl-3H-indol-1-ium (5c)

In 250 mL round bottom flask, 2,3,3-trimethylindolenine (10.5 g, 65.9 mmol) and 1-Iodo propane (57 mL, 0.19 mol) were added to 50 mL of acetonitrile. The mixture was refluxed for 12 h. The mixture was cooled to room temperature and then the acetonitrile was removed. Subsequently, acetone (150 mL) was added into the solid residue. The product was collected by filtration and washed with acetone to provide brown solid (13.0 g, 98%).

^{1}H NMR (400 MHz, $CDCl_3$) δ 7.73 – 7.65 (m, 1H), 7.54 (d, *J* = 3.0 Hz, 3H), 4.64 (t, *J* = 7.5 Hz, 2H), 3.10 (s, 3H), 2.00 (dd, *J* = 15.0, 7.5 Hz, 2H), 1.62 (s, 6H), 1.05 (t, *J* = 7.4 Hz, 3H).

^{13}C NMR (100 MHz, $CDCl_3$) δ 195.88, 141.67, 141.00, 130.16, 129.55, 123.38, 115.55, 54.72, 51.41, 23.28, 21.55, 17.24, 11.38.

Synthesis of 5-iodo-2,3,3-trimethyl-1-propyl-3H-indol-1-ium (4c)

In 250 mL round bottom flask, 5-iodo-2,3,3-trimethyl-3H-indole **(B)** (10.0 g, 35.1 mmol) and 1-Iodo propane (60 mL, 0.61 mol) were added to 100 mL of acetonitrile. The mixture was refluxed for 12 h. Subsequently, the mixture was cooled to room temperature and the flask was placed in an ice bath. The solid residue was precipitated and collected by filtration, washed with cold acetonitrile to provide brown solid (10.0 g, 87%).

^{1}H NMR (400 MHz, MeOD) δ 8.23 (d, *J* = 1.1 Hz, 1H), 8.03 (dd, *J* = 8.5, 1.3 Hz, 1H), 7.72 (d, *J* = 8.5 Hz, 1H), 4.53 – 4.46 (m, 2H), 2.07 – 1.95 (m, 2H), 1.64 (s, 6H), 1.11 (t, *J* = 7.4 Hz, 3H).

^{13}C NMR (100 MHz, MeOD) δ 196.59, 144.04, 140.97, 138.33, 132.74, 116.95, 95.26, 54.61, 49.52, 21.32, 20.97, 9.88.

Synthesis of hemicyanine dyes

General Procedure

Compound **A** (1 eq), **4a-b** or **5a-b** (1 eq) and NaOAc (1 eq) were dissolved in 100 mL of absolute ethanol in 250 mL round bottom flask. The mixture was heated at 50 ^{o}C for 2 h. The solvent was removed and the crude material was purified by normal phase flash chromatography with MeOH:CH_2Cl_2 (1:25 v/v) for **3a**, **c** and MeOH:$CHCl_3$ (1:3) for **3b**, **d** to afford blue solid.

1-(5-carboxypentyl)-2-((E)-2-((E)-2-chloro-3-((phenylamino)methylene)cyclohex-1-en-1-yl)vinyl)-3,3-dimethyl-3H-indol-1-ium (3a)

(2.2 g, 61%).

^{1}H NMR (400 MHz, MeOD) δ 8.66 (d, *J* = 14.7 Hz, 1H), 8.38 (s, 1H), 7.63 (d, *J* = 7.4 Hz, 1H), 7.56 – 7.50 (m, 2H), 7.47 – 7.41 (m, 3H), 7.37 (d, *J* = 7.7 Hz, 2H), 7.21 (t, *J* = 7.3 Hz, 1H), 6.49 (d, *J* = 14.6 Hz, 1H), 4.34 (t, *J* = 7.4 Hz, 2H), 2.78 – 2.69 (m, 4H), 2.34 (t, *J* = 7.2 Hz, 2H), 2.04 – 1.96 (m, 3H), 1.93 (s, 2H), 1.78 (s, 6H), 1.76 – 1.68 (m, 2H), 1.55 (d, *J* = 7.1 Hz, 2H).

^{13}C NMR (100 MHz, MeOD) δ 177.07, 175.76, 151.53, 148.19, 143.04, 141.96, 141.61, 140.28, 129.55, 128.79, 126.74, 125.42, 124.83, 122.36, 117.20, 114.12, 112.21, 103.07, 50.34, 44.46, 33.12, 26.98, 26.72, 25.87, 25.48, 24.51, 24.17, 20.28.

4-(2-((E)-2-((E)-2-chloro-3-((phenylamino)methylene)cyclohex-1-en-1-yl)vinyl)-3,3-dimethyl-3H-indol-1-ium-1-yl)butane-1-sulfonate (3b)

(1.8 g, 51%).

^{1}H NMR (400 MHz, DMSO) δ 8.44 (d, *J* = 14.6 Hz, 1H), 8.20 (s, 1H), 7.71 (dd, *J* = 12.5, 7.8 Hz, 2H), 7.50 (d, *J* = 7.7 Hz, 1H), 7.47 – 7.40 (m, 5H), 7.20 – 7.12 (m, 1H), 6.62 (d, *J* = 14.7 Hz, 1H), 4.44 – 4.34 (m, 2H), 2.72 (dt, *J* = 22.2, 6.0 Hz, 5H), 1.88 (d, *J* = 6.2 Hz, 4H), 1.75 (dd, *J* = 13.8, 6.2 Hz, 4H), 1.70 (s, 6H).

^{13}C NMR (100 MHz, DMSO) δ 149.79, 142.41, 141.98, 130.18, 129.34, 127.24, 125.84, 124.95, 123.13, 117.94, 113.60, 104.97, 50.97, 50.57, 45.14, 27.76, 26.86, 25.93, 25.42, 22.91, 20.46.

1-(5-carboxypentyl)-2-((E)-2-((E)-2-chloro-3-((phenylamino)methylene)cyclohex-1-en-1-yl)vinyl)-5-iodo-3,3-dimethyl-3H-indol-1-ium (3c)

(1.7 g, 37%).

^{1}H NMR (400 MHz, MeOD) δ 8.61 – 8.54 (m, 1H), 8.48 (s, 1H), 7.90 (s, 1H), 7.81 (d, *J* = 8.4 Hz, 1H), 7.48 – 7.43 (m, 2H), 7.39 (d, *J* = 8.0 Hz, 2H), 7.26 – 7.16 (m, 2H), 6.33 (d, *J* = 12.1 Hz, 1H), 4.22 (s, 2H), 2.73 (t, *J* = 5.7 Hz, 4H), 2.34 (t, *J* = 7.2 Hz, 2H), 2.06 – 1.95 (m, 2H), 1.93 – 1.82 (m, 2H), 1.79 – 1.73 (m, 6H), 1.73 – 1.67 (m, 2H), 1.51 (dd, *J* = 10.4, 4.8 Hz, 2H).

^{13}C NMR (100 MHz, MeOD) δ 175.81, 174.94, 153.16, 147.62, 147.55, 143.68, 141.64, 139.88, 137.88, 131.59, 129.70, 125.79, 125.68, 117.80, 115.40, 113.49, 101.75, 89.74, 49.84, 44.32, 33.28, 27.09, 26.85, 25.95, 25.57, 24.62, 24.22, 20.22.

Synthesis of 4-(2-((E)-2-((E)-2-chloro-3-((phenylamino)methylene)cyclohex-1-en-1-yl)vinyl)-5-iodo-3,3-dimethyl-3H-indol-1-ium-1-yl)butane-1-sulfonate (3d)

(1.2 g, 37%).

^{1}H NMR (400 MHz, DMSO) δ 8.32 (s, 2H), 8.07 (s, 1H), 7.80 (dd, *J* = 8.4, 1.2 Hz, 1H), 7.44 (q, *J* = 8.3 Hz, 5H), 6.46 (d, *J* = 14.4 Hz, 1H), 4.27 (t, *J* = 6.9 Hz, 2H), 2.72 (d, *J* = 6.5 Hz, 4H), 1.85 (dd, *J* = 12.9, 6.4 Hz, 4H), 1.74 (d, *J* = 7.0 Hz, 2H), 1.68 (s, 6H), 1.06 (t, *J* = 7.0 Hz, 3H).

^{13}C NMR (101 MHz, DMSO) δ 189.73, 144.32, 142.13, 137.80, 131.76, 130.16, 129.94, 128.43, 125.96, 125.49, 118.51, 115.03, 79.66, 56.49, 51.47, 51.00, 50.06, 49.06, 46.58, 44.78, 28.28, 27.70, 26.58, 25.94, 25.57, 23.09, 22.87, 20.48, 19.01.

Synthesis of symmetric and unsymmetric cyanine dyes

General Procedure: Compound **3a-d** (1 eq), **4a-c** or **5a-b** (1 eq) and NaOAc (1 eq) were dissolved in 50 mL of absolute ethanol in 100 mL round bottom flask. The mixture was refluxed for 3 h. The solvent was removed and the crude was purified by reverse phase prep HPLC.

1-(5-carboxypentyl)-2-((E)-2-((E)-3-(2-((E)-1-(5-carboxypentyl)-5-iodo-3,3-dimethylindolin-2-ylidene)ethylidene)-2-chlorocyclohex-1-en-1-yl)vinyl)-3,3-dimethyl-3H-indol-1-ium (1aa) , (114 mg, 70%)

^{1}H NMR (400 MHz, MeOD) δ 8.58 – 8.51 (m, 1H), 8.36 – 8.28 (m, 1H), 7.81 (d, *J* = 1.5 Hz, 1H), 7.72 (dd, *J* = 8.3, 1.6 Hz, 1H), 7.59 (d, *J* = 7.3 Hz, 1H), 7.48 (ddd, *J* = 15.8, 11.5, 4.2 Hz, 2H), 7.38 (t, *J* = 7.3 Hz, 1H), 7.05 (d, *J* = 8.4 Hz, 1H), 6.45 (d, *J* = 14.4 Hz, 1H), 6.16 (d, *J* = 13.8 Hz, 1H), 4.29 (t, *J* = 7.3 Hz, 2H), 4.08 (t, *J* = 7.3 Hz, 2H), 2.74 (d, *J* = 5.8 Hz, 4H), 2.34 (td, *J* = 7.2, 2.2 Hz, 4H), 2.00 – 1.95 (m, 2H), 1.90 (dd, *J* = 19.0, 11.6 Hz, 3H), 1.83 (d, *J* = 7.2 Hz, 1H), 1.75 (d, *J* = 9.3 Hz, 6H), 1.71 (s, 7H), 1.69 (s, 2H), 1.58 – 1.46 (m, 4H).

^{13}C NMR (101 MHz, MeOD) δ 175.83, 175.80, 175.01, 169.84, 149.81, 146.03, 143.12, 142.47, 141.86, 141.74, 137.39, 131.20, 128.73, 127.53, 126.82, 126.19, 122.29, 112.04, 111.73, 103.01, 99.38, 86.81, 49.92, 48.52, 44.24, 43.35, 33.24, 33.19, 26.99, 26.93, 26.81, 26.38, 25.97, 25.92, 24.27, 24.21, 20.67.

HRMS calculated for $C_{42}H_{51}ClIN_2O_4^+$ calculated: 809.2577; found 809.2508

4-((E)-2-((E)-2-(2-chloro-3-((E)-2-(3,3-dimethyl-1-(4-sulfonatobutyl)-3H-indol-1-ium-2-yl)vinyl)cyclohex-2-en-1-ylidene)ethylidene)-5-iodo-3,3-dimethylindolin-1-yl)butane-1-sulfonate (1bb), (80 mg, 50%)

^{1}H NMR (400 MHz, DMSO) δ 8.34 (d, *J* = 14.4 Hz, 1H), 8.16 (d, *J* = 13.8 Hz, 1H), 7.95 (d, *J* = 1.5 Hz, 1H), 7.74 – 7.65 (m, 2H), 7.59 (d, *J* = 8.0 Hz, 1H), 7.46 (dd, *J* = 11.5, 4.1 Hz, 1H), 7.35 (t, *J* = 7.5 Hz, 1H), 7.23 (d, *J* = 8.4 Hz, 1H), 6.52 (d, *J* = 14.4 Hz, 1H), 6.23 (d, *J* = 13.9 Hz, 1H), 4.34 – 4.27 (m, 2H), 4.11 (t, *J* = 6.6 Hz, 2H), 2.74 (d, *J* = 6.3 Hz, 4H), 2.56 (dd, *J* = 13.5, 6.6 Hz, 4H), 1.90 – 1.81 (m, 4H), 1.76 (dd, *J* = 9.5, 5.2 Hz, 6H), 1.69 (s, 6H), 1.65 (s, 6H).

^{13}C NMR (100 MHz, DMSO) δ 174.45, 169.95, 148.50, 145.15, 143.59, 142.76, 142.31, 142.03, 141.76, 137.50, 131.47, 129.22, 127.60, 126.89, 126.40, 123.02, 113.60, 112.84, 104.11, 100.70, 88.61, 51.17, 51.07, 49.99, 48.88, 44.68, 43.83, 27.92, 27.82, 26.69, 26.39, 26.30, 26.21, 22.82, 20.90.

HRMS calculated for $C_{38}H_{45}ClIN_2O_6S_2^-$calculated: 851.1458; found 851.1484

4-(2-((E)-2-((E)-3-(2-((E)-1-(5-carboxypentyl)-3,3-dimethylindolin-2-ylidene)ethylidene)-2-chlorocyclohex-1-en-1-yl)vinyl)-5-iodo-3,3-dimethyl-3H-indol-1-ium-1-yl)butane-1-sulfonate (1ab), (100 mg, 63%)

^{1}H NMR (400 MHz, DMSO) δ 8.36 (d, *J* = 14.5 Hz, 1H), 8.13 (d, *J* = 13.8 Hz, 1H), 7.94 (d, *J* = 1.6 Hz, 1H), 7.72 – 7.66 (m, 2H), 7.62 (d, *J* = 8.0 Hz, 1H), 7.52 – 7.45 (m, 1H), 7.37 (t, *J* = 7.5 Hz, 1H), 7.16 (d, *J* = 8.4 Hz, 1H), 6.57 (d, *J* = 14.5 Hz, 1H), 6.15 (d, *J* = 13.8 Hz, 1H), 4.40 – 4.28 (m, 2H), 4.14 – 4.04 (m, 4H), 2.73 (dt, *J* = 21.3, 5.7 Hz, 4H),

2.21 (t, *J* = 7.3 Hz, 2H), 1.87 (d, *J* = 6.3 Hz, 4H), 1.82 – 1.72 (m, 3H), 1.70 (s, 6H), 1.65 (s, 6H), 1.60 – 1.50 (m, 2H), 1.39 (d, *J* = 6.8 Hz, 2H).

^{13}C NMR (101 MHz, DMSO) δ 174.99, 174.73, 169.38, 158.87, 158.49, 148.39, 145.58, 143.47, 142.82, 142.21, 141.04, 137.44, 131.49, 129.27, 127.80, 126.68, 123.05, 113.25, 113.07, 104.73, 100.08, 88.27, 50.99, 50.15, 48.73, 44.87, 43.60, 33.96, 27.96, 27.77, 26.82, 26.75, 26.37, 26.29, 26.11, 24.66, 22.93, 20.89.

HRMS calculated for $C_{40}H_{48}ClIN_2O_5S$ calculated: 830.2017; found 830.2017

2-((E)-2-((E)-3-(2-((E)-1-(5-carboxypentyl)-5-iodo-3,3-dimethylindolin-2-ylidene)ethylidene)-2-chlorocyclohex-1-en-1-yl)vinyl)-3,3-dimethyl-1-propyl-3H-indol-1-ium (1ac), (85 mg, 72%)

^{1}H NMR (400 MHz, MeOD) δ 8.54 (d, *J* = 14.3 Hz, 1H), 8.29 (d, *J* = 13.5 Hz, 1H), 7.78 (d, *J* = 1.4 Hz, 1H), 7.69 (dd, *J* = 8.3, 1.5 Hz, 1H), 7.59 (d, *J* = 7.4 Hz, 1H), 7.51 – 7.43 (m, 2H), 7.38 (t, *J* = 7.1 Hz, 1H), 7.03 (d, *J* = 8.4 Hz, 1H), 6.46 (d, *J* = 13.5 Hz, 1H), 6.13 (d, *J* = 12.6 Hz, 1H), 4.26 (t, *J* = 7.1 Hz, 2H), 4.06 (t, *J* = 7.1 Hz, 2H), 2.73 (s, 4H), 2.33 (t, *J* = 7.2 Hz, 2H), 1.93 (dd, *J* = 14.3, 7.2 Hz, 4H), 1.87 – 1.78 (m, 3H), 1.76 (s, 6H), 1.73 (d, *J* = 3.7 Hz, 2H), 1.69 (s, 6H), 1.55 – 1.45 (m, 2H), 1.08 (t, *J* = 7.4 Hz, 3H).

^{13}C NMR (101 MHz, MeOD) δ 175.77, 175.27, 174.28, 169.50, 149.71, 146.10, 143.07, 142.51, 141.95, 141.75, 137.38, 131.17, 129.64, 128.74, 127.54, 126.76, 126.28, 122.29, 111.98, 111.89, 103.24, 99.21, 86.71, 49.99, 49.96, 48.45, 48.42, 45.89, 43.34, 33.28, 27.07, 26.87, 26.39, 25.98, 24.29, 20.79, 20.66, 10.28.

HRMS calculated for $C_{39}H_{47}ClIN_2O_2^+$ calculated: 737.2365; found 737.2334

4-((E)-2-((E)-2-(2-chloro-3-((E)-2-(3,3-dimethyl-1-propyl-3H-indol-1-ium-2-yl)vinyl)cyclohex-2-en-1-ylidene)ethylidene)-5-iodo-3,3-dimethylindolin-1-yl)butane-1-sulfonate (1bc), (95 mg, 80%)

^{1}H NMR (400 MHz, MeOD) δ 8.51 (s, 1H), 8.32 (s, 1H), 7.71 (dd, *J* = 8.3, 1.5 Hz, 1H), 7.56 (d, *J* = 7.4 Hz, 1H), 7.51 – 7.44 (m, 1H), 7.38 (dd, *J* = 14.3, 7.7 Hz, 2H), 7.09 (d, *J* = 8.4 Hz, 1H), 6.29 (d, *J* = 75.4 Hz, 1H), 4.17 (d, *J* = 44.5 Hz, 4H), 2.90 (t, *J* = 6.9 Hz, 2H), 2.74 (s, 3H), 1.95 (dt, *J* = 14.6, 6.8 Hz, 9H), 1.76 (s, 6H), 1.73 (d, *J* = 6.5 Hz, 1H), 1.71 (s, 6H), 1.08 (t, *J* = 7.4 Hz, 3H).

^{13}C NMR (100 MHz, MeOD) δ 174.59, 170.20, 150.13, 145.75, 143.13, 142.68, 142.36, 142.05, 141.56, 137.52, 131.16, 128.71, 127.42, 126.00, 122.27, 112.33, 111.59, 102.53, 99.88, 87.17, 50.41, 49.80, 49.78, 45.78, 43.52, 27.20, 27.09, 26.04, 25.69, 22.25, 20.76, 20.68, 10.46.

HRMS calculated for $C_{37}H_{44}ClIN_2O_3S$ calculated: 758.1806; found 758.1819

1-(5-carboxypentyl)-2-((E)-2-((E)-3-(2-((E)-1-(5-carboxypentyl)-5-iodo-3,3-dimethylindolin-2-ylidene)ethylidene)-2-chlorocyclohex-1-en-1-yl)vinyl)-5-iodo-3,3-dimethyl-3H-indol-1-ium (2aa), (98 mg, 65%)

^{1}H NMR (400 MHz, MeOD) δ 8.44 (d, *J* = 14.1 Hz, 2H), 7.89 (d, *J* = 1.5 Hz, 2H), 7.78 (dd, *J* = 8.4, 1.5 Hz, 2H), 7.16 (d, *J* = 8.4 Hz, 2H), 6.30 (d, *J* = 14.1 Hz, 2H), 4.17 (t, *J* = 7.3 Hz, 4H), 2.75 (t, *J* = 5.9 Hz, 4H), 2.34 (t, *J* = 7.2 Hz, 4H), 1.97 (d, *J* = 5.8 Hz, 2H), 1.91 – 1.82 (m, 4H), 1.74 (s, 12H), 1.72 – 1.67 (m, 4H), 1.51 (dd, *J* = 10.5, 4.9 Hz, 4H).

^{13}C NMR (100 MHz, MeOD) δ 175.83, 172.17, 150.25, 144.28, 143.53, 142.11, 137.60, 131.40, 127.54, 112.81, 101.28, 88.22, 49.18, 43.81, 33.18, 26.82, 26.60, 25.92, 24.22.

HRMS calculated for $C_{42}H_{50}ClI_2N_2O_4^+$ calculated: 935.1543; found 935.1545

4-((E)-2-((E)-2-(2-chloro-3-((E)-2-(5-iodo-3,3-dimethyl-1-(4-sulfonatobutyl)-3H-indol-1-ium-2-yl)vinyl)cyclohex-2-en-1-ylidene)ethylidene)-5-iodo-3,3-dimethylindolin-1-yl)butane-1-sulfonate (2bb), (120 mg, 77%)

^{1}H NMR (400 MHz, DMSO) δ 8.26 – 8.18 (m, 2H), 8.02 (d, *J* = 1.2 Hz, 2H), 7.76 (dd, *J* = 8.4, 1.3 Hz, 2H), 7.33 (d, *J* = 8.4 Hz, 2H), 6.37 (d, *J* = 14.1 Hz, 1H), 4.20 (s, 4H), 2.73 (s, 4H), 2.59 (t, *J* = 7.0 Hz, 4H), 1.83 (dd, *J* = 13.6, 6.6 Hz, 5H), 1.75 (dd, *J* = 14.1, 7.4 Hz, 4H), 1.67 (s, 12H), 1.26 (dd, *J* = 13.3, 6.8 Hz, 2H).

^{13}C NMR (100 MHz, DMSO) δ 171.93, 148.81, 143.98, 143.61, 142.46, 137.66, 131.64, 127.57, 123.77, 114.30, 102.51, 89.89, 54.08, 51.10, 49.45, 44.26, 27.80, 26.38, 22.74, 20.88, 18.53, 17.20.

HRMS calculated for $C_{38}H_{44}ClI_2N_2O_6S_2^-$ calculated: 977.0424; found 977.6188

2-((E)-2-((E)-2-chloro-3-(2-((E)-5-iodo-3,3-dimethyl-1-propylindolin-2-ylidene)ethylidene)cyclohex-1-en-1-yl)vinyl)-5-iodo-3,3-dimethyl-1-propyl-3H-indol-1-ium (2cc), (37 mg, 15%)

^{1}H NMR (400 MHz, $CDCl_3$) δ 8.31 (d, *J* = 14.1 Hz, 2H), 7.68 (dd, *J* = 8.3, 1.5 Hz, 2H), 7.63 (d, *J* = 1.5 Hz, 2H), 6.89 (d, *J* = 8.4 Hz, 2H), 6.16 (d, *J* = 14.1 Hz, 2H), 4.02 (t, *J* =

7.2 Hz, 4H), 2.64 (t, *J* = 5.9 Hz, 4H), 1.93 (m, 2H), 1.84 (dd, *J* = 14.5, 7.3 Hz, 4H), 1.70 (d, *J* = 9.4 Hz, 12H), 1.01 (t, *J* = 7.4 Hz, 6H).

^{13}C NMR (100 MHz, $CDCl_3$) δ 171.71, 151.11, 144.52, 143.22, 142.18, 137.74, 131.37, 128.36, 112.66, 101.61, 88.67, 49.23, 46.04, 28.09, 26.28, 20.74, 11.39.

HRMS calculated for $C_{36}H_{42}ClI_2N_2^+$ calculated: 791.1120; found 791.1152

2-((E)-2-((E)-3-(2-((E)-1-(5-carboxypentyl)-5-iodo-3,3-dimethylindolin-2-ylidene)ethylidene)-2-chlorocyclohex-1-en-1-yl)vinyl)-5-iodo-3,3-dimethyl-1-propyl-3H-indol-1-ium (2ac), (98 mg, 68%)

^{1}H NMR (400 MHz, MeOD) δ 8.43 (dd, *J* = 13.2, 7.1 Hz, 2H), 7.88 (dd, *J* = 4.8, 1.5 Hz, 2H), 7.78 – 7.73 (m, 2H), 7.16 (t, *J* = 8.0 Hz, 2H), 6.30 (t, *J* = 12.6 Hz, 1H), 4.15 (d, *J* = 7.1 Hz, 4H), 2.74 (s, 4H), 2.33 (t, *J* = 7.2 Hz, 2H), 1.97 (m, 2H), 1.92 – 1.80 (m, 4H), 1.73 (d, *J* = 2.0 Hz, 12H), 1.70 (d, *J* = 7.9 Hz, 2H), 1.51 (s, 2H), 1.06 (t, *J* = 7.4 Hz, 3H).

^{13}C NMR (100 MHz, MeOD) δ 175.79, 172.40, 171.96, 150.19, 144.38, 144.09, 143.54, 143.50, 142.22, 142.13, 137.61, 131.39, 127.50, 112.95, 112.78, 101.45, 101.17, 88.33, 88.17, 49.23, 49.13, 49.11, 45.47, 43.81, 33.22, 26.87, 26.61, 25.93, 24.24, 20.43, 10.25.

HRMS calculated for $C_{39}H_{46}ClI_2N_2O_2^+$ calculated: 863.1332; found 863.1348

4-(2-((E)-2-((E)-3-(2-((E)-1-(5-carboxypentyl)-5-iodo-3,3-dimethylindolin-2-ylidene)ethylidene)-2-chlorocyclohex-1-en-1-yl)vinyl)-5-iodo-3,3-dimethyl-3H-indol-1-ium-1-yl)butane-1-sulfonate (2ab), (110 mg, 77%)

^{1}H NMR (400 MHz, MeOD/$CDCl_3$) δ 8.40 (d, *J* = 14.3 Hz, 1H), 8.28 (d, *J* = 13.9 Hz, 1H), 7.72 (dd, *J* = 8.4, 1.5 Hz, 1H), 7.68 – 7.60 (m, 3H), 7.09 (d, *J* = 8.4 Hz, 1H), 6.86 (d, *J* = 8.4 Hz, 1H), 6.30 (d, *J* = 14.3 Hz, 1H), 5.99 (d, *J* = 13.9 Hz, 1H), 4.12 (s, 2H), 2.90 (t, *J* = 6.6 Hz, 2H), 2.69 (d, *J* = 6.0 Hz, 2H), 2.62 (t, *J* = 6.0 Hz, 2H), 2.30 (t, *J* = 7.3 Hz, 2H), 2.02 – 1.89 (m, 6H), 1.80 (m, 2H), 1.70 (d, *J* = 6.4 Hz, 7H), 1.68 (s, 6H), 1.65 (s, 1H), 1.47 (d, *J* = 7.2 Hz, 2H).

^{13}C NMR (100 MHz, MeOD/$CDCl_3$) δ 175.52, 173.10, 170.21, 151.50, 146.35, 143.37, 143.35, 142.90, 142.07, 141.63, 138.04, 137.64, 131.36, 128.71, 127.78, 113.36, 111.99, 102.61, 99.84, 89.69, 87.94, 44.66, 43.94, 33.57, 28.03, 27.87, 26.68, 26.24, 25.95, 24.31, 22.41.

HRMS calculated for $C_{40}H_{47}ClI_2N_2O_5S$ calculated: 956.0984; found 956.0984

4-((E)-2-((E)-2-(2-chloro-3-((E)-2-(5-iodo-3,3-dimethyl-1-propyl-3H-indol-1-ium-2-yl)vinyl)cyclohex-2-en-1-ylidene)ethylidene)-5-iodo-3,3-dimethylindolin-1-yl)butane-1-sulfonate (2bc), (70 mg, 52%)

^{1}H NMR (400 MHz, DMSO) δ 8.30 – 8.18 (m, 2H), 8.02 (dd, *J* = 12.0, 1.2 Hz, 2H), 7.79 – 7.72 (m, 2H), 7.36 (d, *J* = 8.4 Hz, 1H), 7.27 (d, *J* = 8.4 Hz, 1H), 6.42 (d, *J* = 14.3 Hz, 1H), 6.30 (d, *J* = 14.1 Hz, 1H), 4.22 (t, *J* = 7.1 Hz, 2H), 4.14 (t, *J* = 7.0 Hz, 2H), 2.72 (dd, *J* = 11.8, 5.9 Hz, 4H), 1.83 (dd, *J* = 13.6, 6.8 Hz, 4H), 1.75 (dd, *J* = 13.2, 6.1 Hz, 4H), 1.67 (s, 12H), 0.95 (t, *J* = 7.4 Hz, 3H).

^{13}C NMR (100 MHz, DMSO) δ 172.56, 172.53, 171.53, 171.50, 148.79, 144.11, 143.83, 142.97, 142.68, 142.36, 137.71, 137.58, 131.65, 127.72, 127.29, 114.52, 114.00, 103.10,

101.85, 90.30, 89.52, 51.03, 49.62, 49.31, 45.51, 44.47, 31.13, 27.86, 27.73, 26.46, 26.32, 22.92, 20.85, 20.80, 11.50.

HRMS calculated for $C_{37}H_{43}ClI_2N_2O_3S$ calculated: 884.0772; found 884.0770

4-((E)-2-((E)-2-(2-(4-carboxyphenoxy)-3-((E)-2-(5-iodo-3,3-dimethyl-1-(4-sulfonatobutyl)-3H-indol-1-ium-2-yl)vinyl)cyclohex-2-en-1-ylidene)ethylidene)-5-iodo-3,3-dimethylindolin-1-yl)butane-1-sulfonate (3bb)

4-hydroxybenzoic acid (34.2 mg, 0.248 mmol) and NaH (5.9 mg, 0.248 mmol) were added to 2 mL of dry DMF and stirred for 15 mins. Afterwards, **2bb** (30 mg, 0.031 mmol) was added and the reaction mixture was stirred at room temperature for 18 h. The solvent was dried and purified by reverse phase prep HPLC. green solid (24.1 mg, 72%)

^{1}H NMR (400 MHz, DMSO) δ 8.01 (d, *J* = 8.9 Hz, 2H), 7.88 (d, *J* = 1.6 Hz, 2H), 7.75 (s, 1H), 7.73 – 7.69 (m, 2H), 7.68 (d, *J* = 1.6 Hz, 1H), 7.25 (t, *J* = 9.1 Hz, 4H), 6.25 (d, *J* = 14.3 Hz, 2H), 4.11 (d, *J* = 6.6 Hz, 4H), 2.75 (d, *J* = 5.9 Hz, 4H), 2.55 (t, *J* = 7.0 Hz, 4H), 1.95 (m, 2H), 1.79 – 1.62 (m, 9H), 1.25 (s, 12H).

^{13}C NMR (100 MHz, DMSO) δ 171.35, 167.01, 162.96, 162.25, 143.86, 142.35, 140.93, 137.54, 132.66, 131.54, 125.38, 122.45, 115.02, 114.06, 101.36, 89.52, 51.09, 49.03, 44.08, 27.43, 26.30, 24.18, 22.75, 21.11.

HRMS calculated for $C_{45}H_{49}I_2N_2O_9S_2^-$ calculated: 1079.0974; found 1079.0961

4-((E)-2-((E)-2-(2-(4-carboxypiperidin-1-yl)-3-((E)-2-(5-iodo-3,3-dimethyl-1-(4-sulfonatobutyl)-3H-indol-1-ium-2-yl)vinyl)cyclohex-2-en-1-ylidene)ethylidene)-5-iodo-3,3-dimethylindolin-1-yl)butane-1-sulfonate (4bb)

Isonipecotic acid (4.01 mg, 0.031 mmol) and **2bb** (30 mg, 0.031 mmol) were added together in DMF and heated at 60 ^{o}C for 18 h. The solvent was dried and purified by reverse phase prep HPLC. blue solid (58.2 mg, 58%)

^{1}H NMR (400 MHz, DMSO) δ 7.81 (d, *J* = 1.6 Hz, 2H), 7.61 (dd, *J* = 8.3, 1.6 Hz, 2H), 7.41 (d, *J* = 13.0 Hz, 2H), 7.04 (d, *J* = 8.4 Hz, 2H), 5.84 (d, *J* = 12.3 Hz, 2H), 4.06 – 3.86 (m, 7H), 3.71 (t, *J* = 11.0 Hz, 2H), 2.82 (dd, *J* = 12.6, 8.9 Hz, 1H), 2.54 (d, *J* = 7.1 Hz, 4H), 2.13 (d, *J* = 10.3 Hz, 2H), 1.87 (dd, *J* = 21.3, 10.6 Hz, 2H), 1.80 – 1.61 (m, 12H), 1.58 (s, 12H).

^{13}C NMR (100 MHz, DMSO) δ 175.56, 166.46, 158.56, 143.33, 142.96, 138.91, 137.15, 131.07, 124.33, 112.19, 95.54, 86.00, 54.17, 51.33, 47.60, 42.99, 30.03, 28.68, 25.79, 22.92, 21.74.

HRMS calculated for $C_{44}H_{54}I_2N_3O_8S_2^-$ calculated: 1070.1447; found 1070.1471

4-((E)-2-((E)-2-(2-((4-carboxyphenyl)thio)-3-((E)-2-(5-iodo-3,3-dimethyl-1-(4-sulfonatobutyl)-3H-indol-1-ium-2-yl)vinyl)cyclohex-2-en-1-ylidene)ethylidene)-5-iodo-3,3-dimethylindolin-1-yl)butane-1-sulfonate (5bb)

4-mercaptobenzoic acid (4.81 mg, 0.031 mmol) and **2bb** (30 mg, 0.031 mmol) were added together in DMSO and stirred at room temperature for 18 h. The solvent was dried and purified by reverse phase prep HPLC. green solid (26.4 mg, 78%)

^{1}H NMR (400 MHz, DMSO) δ 8.52 (d, *J* = 14.1 Hz, 2H), 7.89 (dd, *J* = 17.2, 5.1 Hz, 5H), 7.71 (dd, *J* = 8.4, 1.6 Hz, 2H), 7.37 (d, *J* = 8.6 Hz, 2H), 7.28 (d, *J* = 8.5 Hz, 3H), 6.39 (d, *J* = 14.2 Hz, 2H), 4.14 (d, *J* = 7.1 Hz, 5H), 2.81 (t, *J* = 5.4 Hz, 4H), 2.54 (t, *J* = 7.1 Hz, 4H), 2.00 – 1.91 (m, 2H), 1.81 – 1.68 (m, 9H), 1.38 (s, 12H).

^{13}C NMR (100 MHz, DMSO) δ 171.73, 167.12, 148.03, 145.11, 143.99, 143.28, 142.40, 137.58, 134.55, 131.54, 130.91, 130.78, 128.36, 126.65, 125.88, 114.22, 102.80, 89.77, 51.09, 49.24, 44.25, 31.14, 27.43, 26.41, 26.34, 22.81, 20.86.

HRMS calculated for $C_{45}H_{49}I_2N_2O_8S_3^-$ calculated: 1095.0746; found 1095.0708

Compound 0 Series

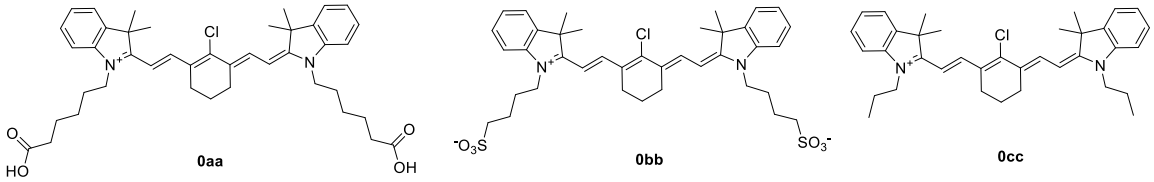

0aa 0bb 0cc

Compound 1 Series

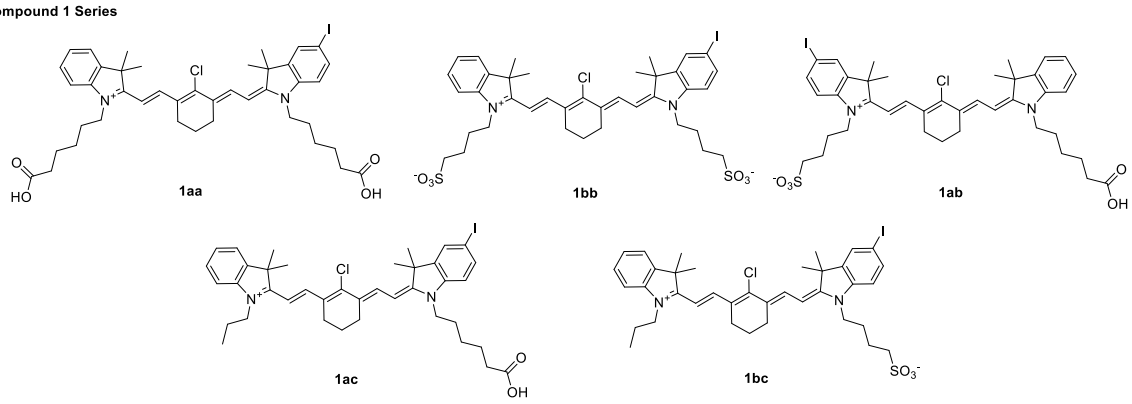

1aa 1bb 1ab 1ac 1bc

Compound 2 Series

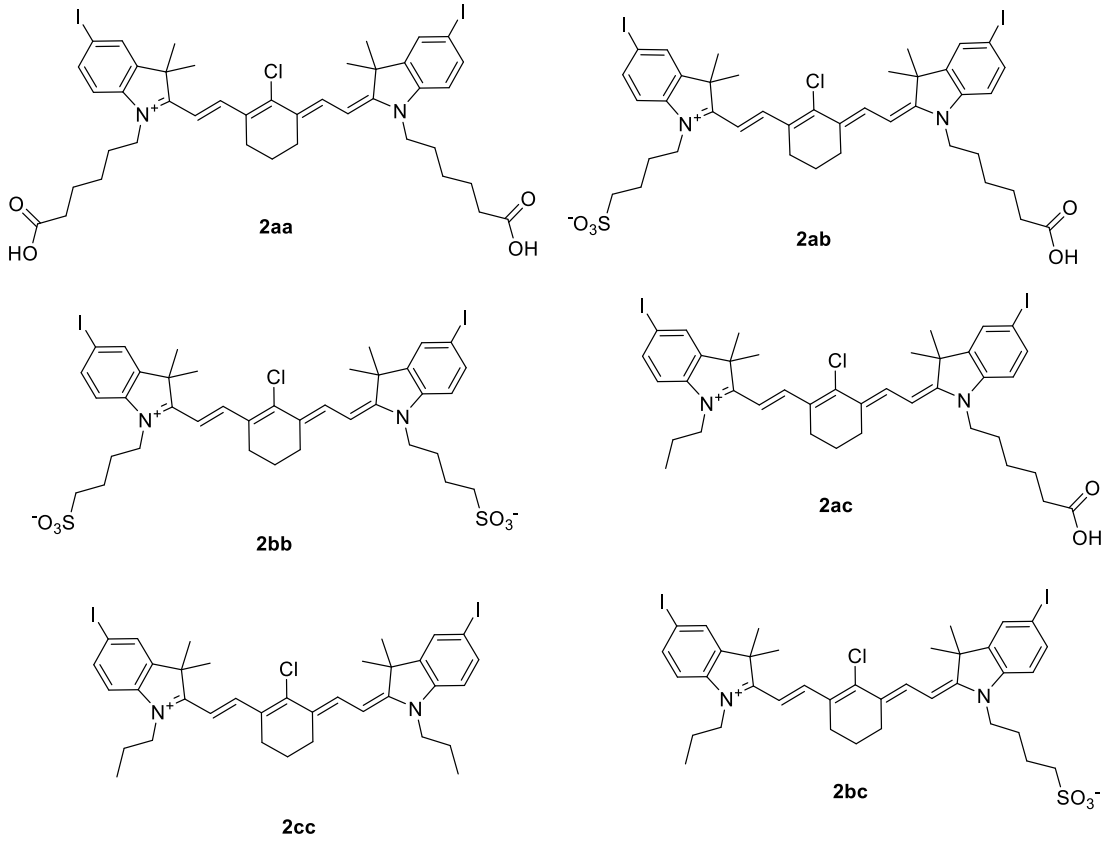

Scheme E-S6. Chemical structures of the compound **0 – 2**

Supporting Tables

Table E-S1. Calculated structural properties i.e. logP, logD, Polar surface area and hydrogen bond donors and acceptors were calculated using ChemAxon's Marvin and JChem plugins. These values were calculated at pH 7.4.

	Compound	logP	logD	polarizibility	polar surface area (Å)	hydrogen bond donor/acceptor
	aa	6.57	4.48	77.05	87.71	2 / 5
0	**bb**	3.98	3.63	77.89	121.85	1 / 6
	cc	6.55	6.55	65.29	7.45	1 / 0
	aa	7.5	5.39	81.99	87.71	1 / 4
	bb	4.91	4.56	82.94	121.85	1 / 6
1	**ab**	6.21	5.22	82.46	104.78	1 / 5
	ac	7.49	8.26	76.03	47.58	1 / 2
	bc	6.19	8.22	76.49	64.65	1 / 3
	aa	8.43	6.27	87.1	87.71	1 / 4
	bb	5.84	5.49	88.12	121.85	1 / 6
2	**cc**	8.41	8.41	75.12	7.45	1 / 0
	ab	7.14	6.09	87.60	104.78	1 / 5
	ac	8.42	9.19	81.11	47.58	1 / 2
	bc	7.12	9.15	81.6	64.65	1 / 3

Table E-S2. Calculated brightness (brightness = quantum yield x extinction coefficient)

	Compound	ε_{max} ($M^{-1}cm^{-1}$)	Φ	Brightness (ε x Φ)
	aa	($M^{-1}cm^{-1}$)	0.076	17869
0	**bb**	340920	0.095	32387
	cc	100080	0.077	7706
	aa	209480	0.071	14873
	bb	208600	0.072	15019
1	**ab**	211800	0.069	14614
	ac	199960	0.077	15397
	bc	200240	0.071	14217
	aa	229200	0.044	10085
	bb	252000	0.065	16380
2	**cc**	148360	0.047	6973
	ab	268560	0.063	16919
	ac	180680	0.069	12467
	bc	248960	0.062	15436

Supporting Figures

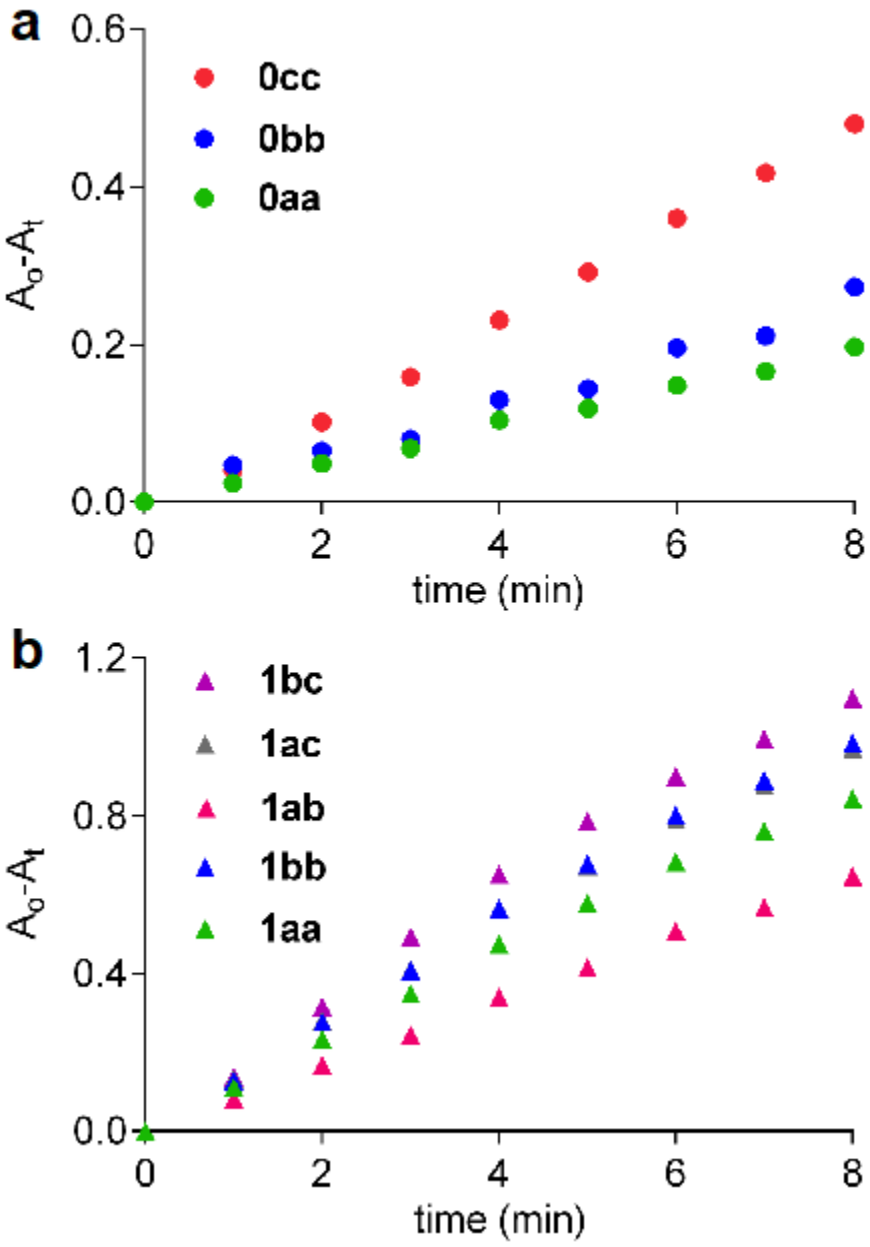

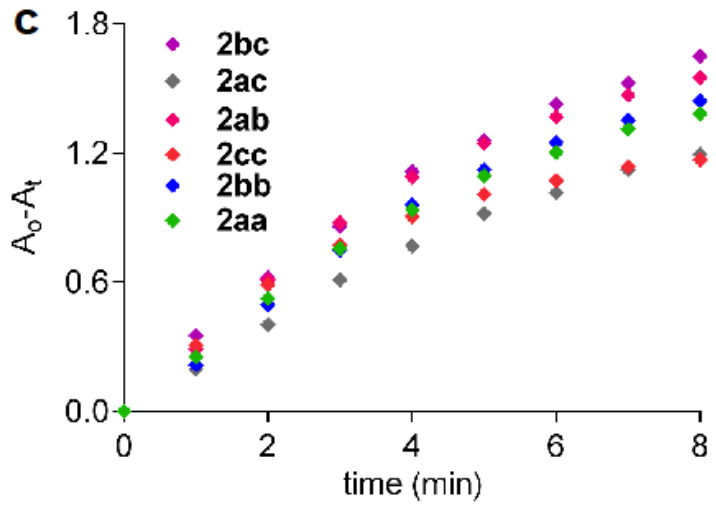

Figure E-S1. Singlet oxygen ($^1O_2$) generation assay as deduced by of change in absorbance of DPBF (1,3-diphenylisobenzofuran; added *in situ*) at 418 nm. **a** Compounds **0**; **b 1**; and **c 2**.

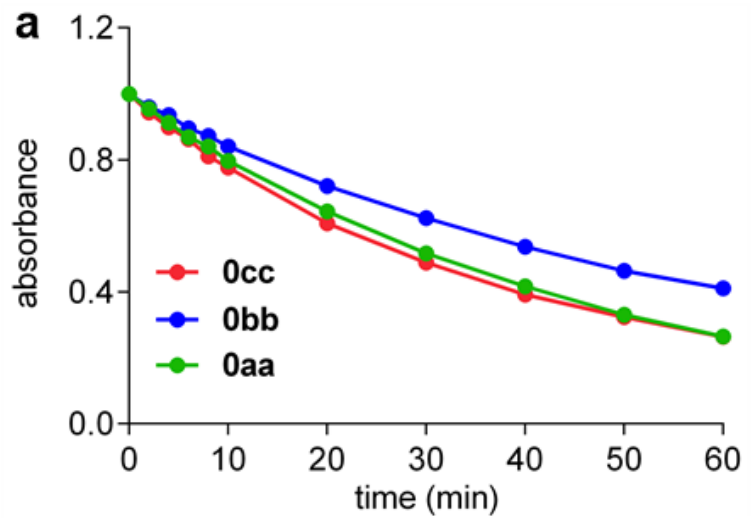

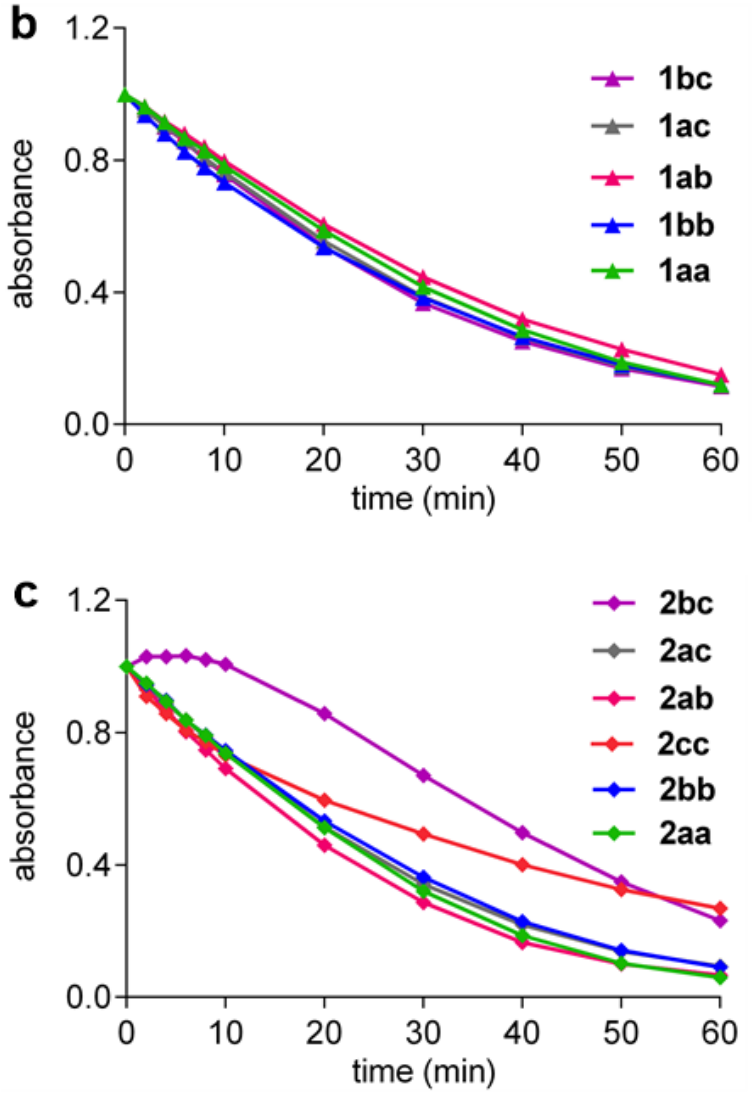

Figure E-S2. Photostability of **a**, compound **0**; **b**, **1** and **c**, **2** under LED irradiation of 780 nm. Compounds were dissolved in PBS buffer (pH 7.4) containing 1% CrEL to a 10 µM final concentration

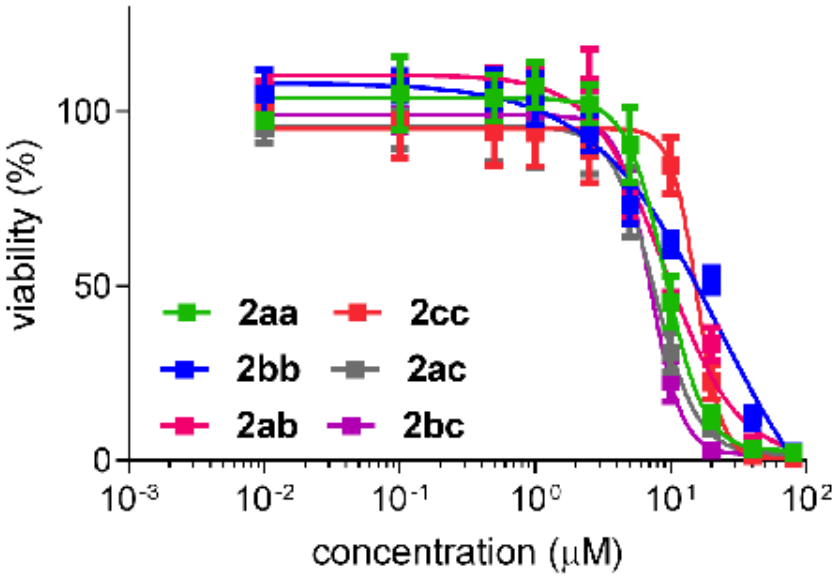

IC_{50} of **2aa** = 9.11 ± 0.42 μM
2bb = 23.33 ± 9.80 μM
2ab = 8.90 ± 0.85 μM
2cc = 15.51 ± 0.85 μM
2ac = 7.60 ± 0.45 μM
2bc = 7.05 ± 0.23 μM

Figure E-S3. Cytotoxicity of the compounds were determined on HEPG2 cells by incubating them for 48 h without washing before doing Alamar Blue Assay for cell viability. The samples were *not* illuminated at their λ_{max} in these experiments. IC_{50} of **2aa**, **bb**, **ab**, **cc**, **ac**, **bc** was determined as shown.

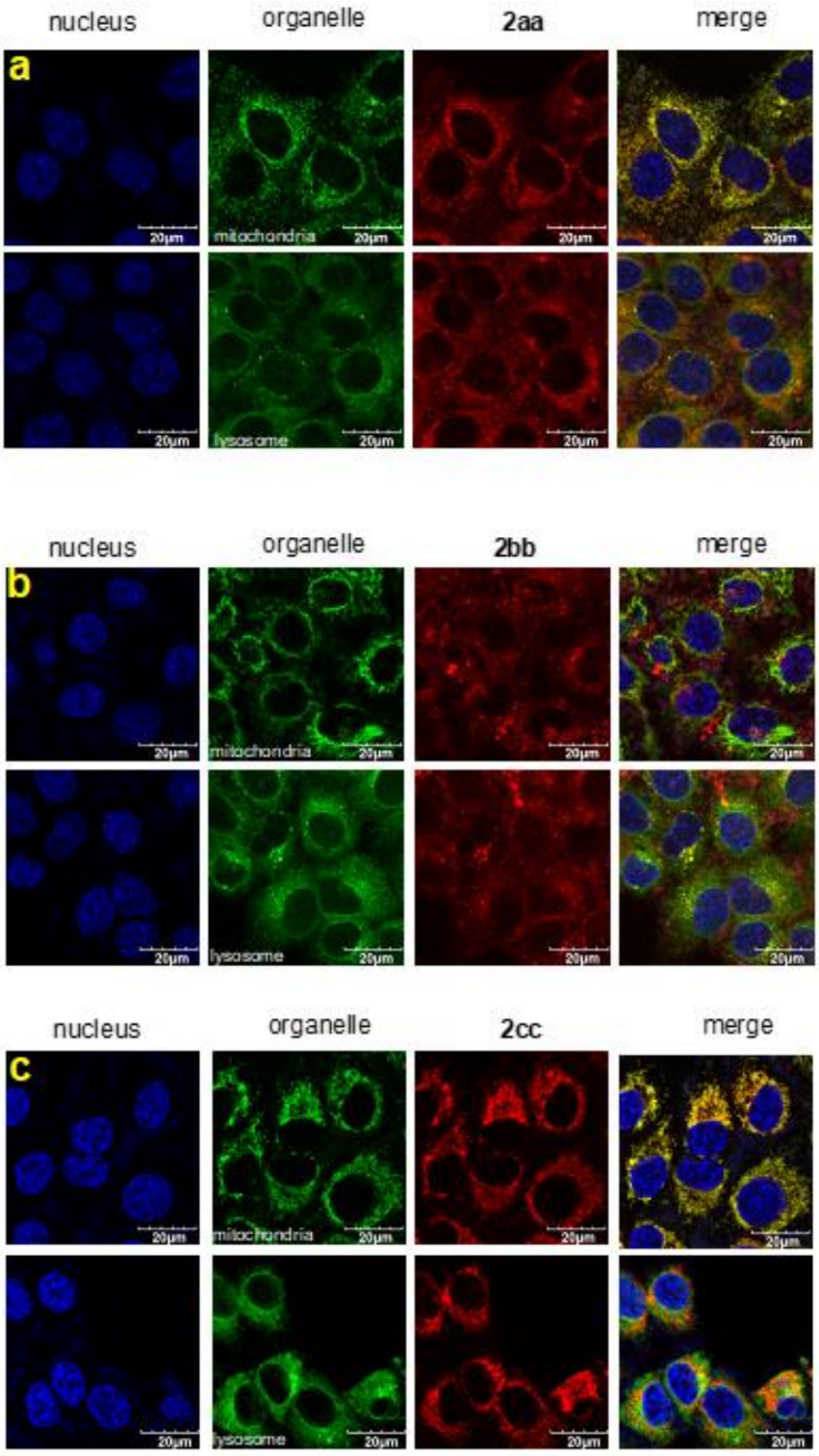
nucleus
organelle
2aa
merge
a
mitochondria
lysosome
20μm
nucleus
organelle
2bb
merge
b
mitochondria
lysosome
20μm
nucleus
organelle
2cc
merge
c
mitochondria
lysosome
20μm

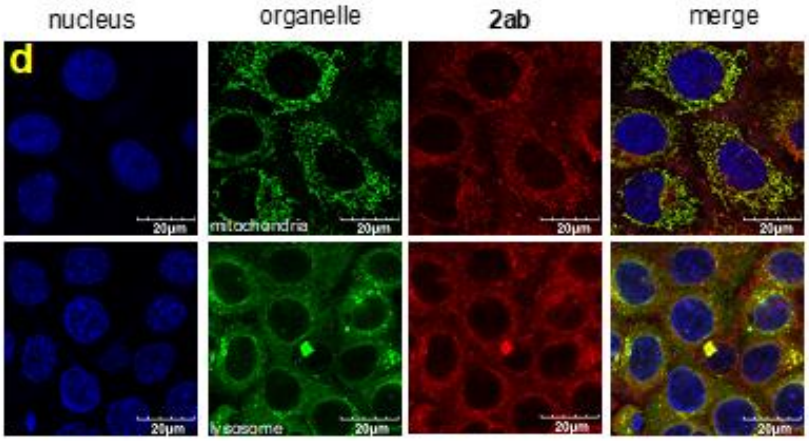

Figure E-S4. Organelle colocalization study in **a, 2aa**; **b, 2bb**; **c, 2cc** and **d, 2ab** with LysoTracker and MitoTracker Green.

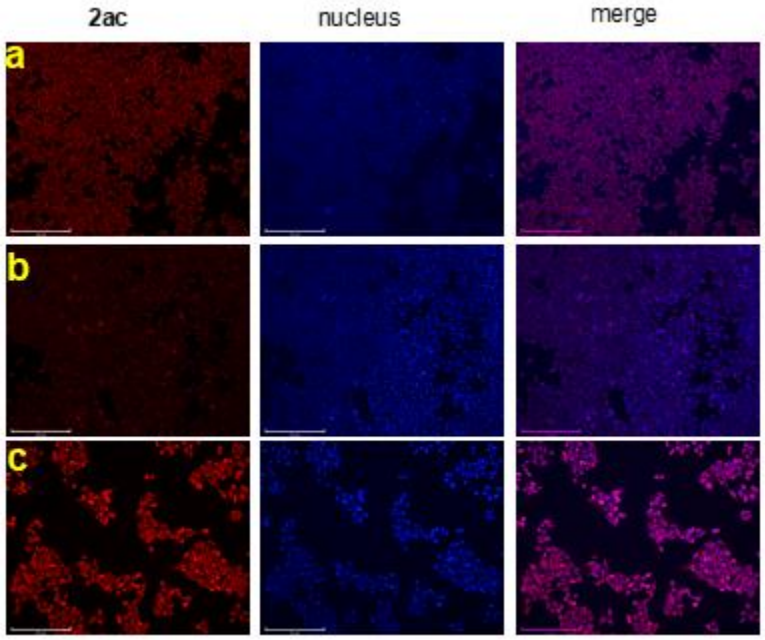

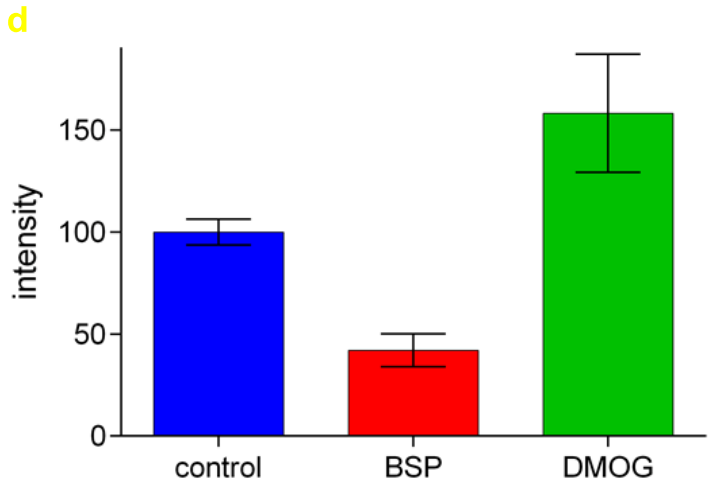

Figure E-S5. Uptake of **2ac** in **a,** normal (control) conditions; **b,** blocked by BSP (OATPs inhibitors) **c,** DMOG (hypoxia inducers) and **d,** quantification of uptake. Magnification 10x. Scale bar 250 µM.

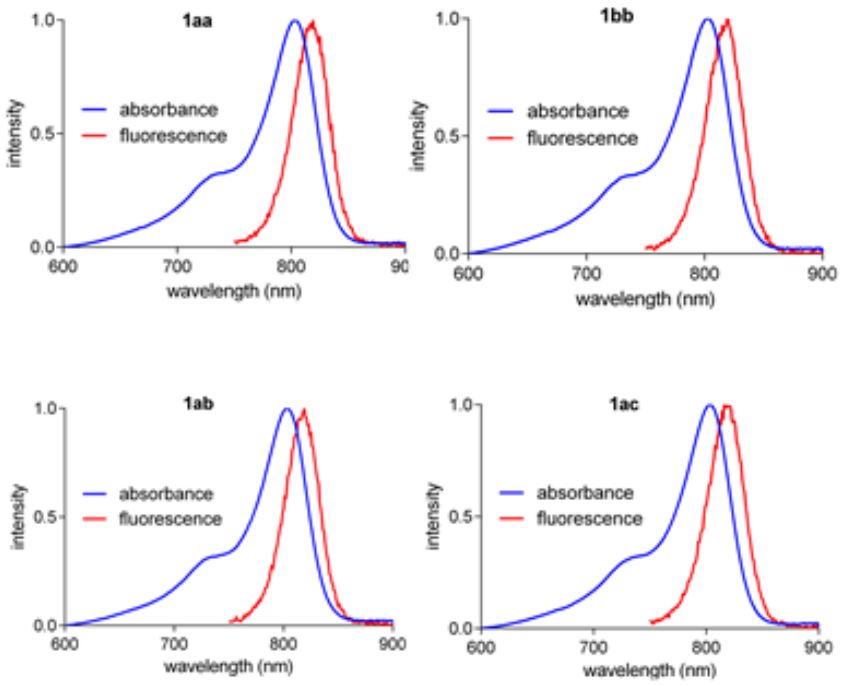

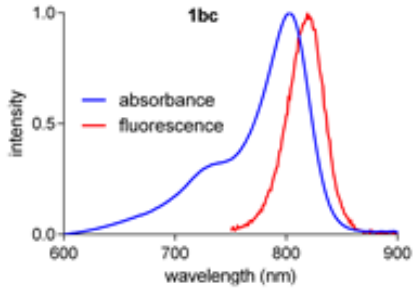
1bc
absorbance
fluorescence
intensity
1.0
0.5
0.0
600
700
800
900
wavelength (nm)

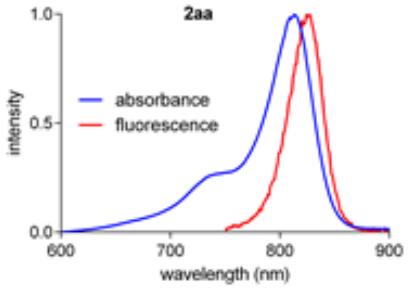
2aa
absorbance
fluorescence
intensity
1.0
0.5
0.0
600
700
800
900
wavelength (nm)

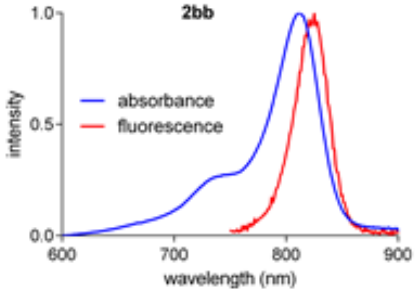
2bb
absorbance
fluorescence
intensity
1.0
0.5
0.0
600
700
800
900
wavelength (nm)

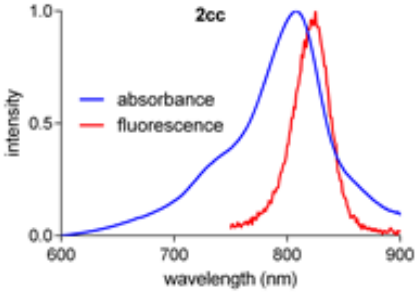
2cc
absorbance
fluorescence
intensity
1.0
0.5
0.0
600
700
800
900
wavelength (nm)

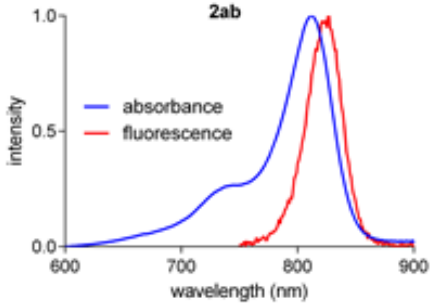
2ab
absorbance
fluorescence
intensity
1.0
0.5
0.0
600
700
800
900
wavelength (nm)

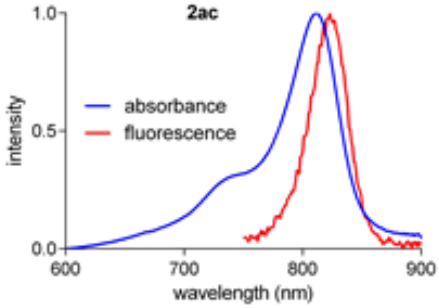
2ac
absorbance
fluorescence
intensity
1.0
0.5
0.0
600
700
800
900
wavelength (nm)

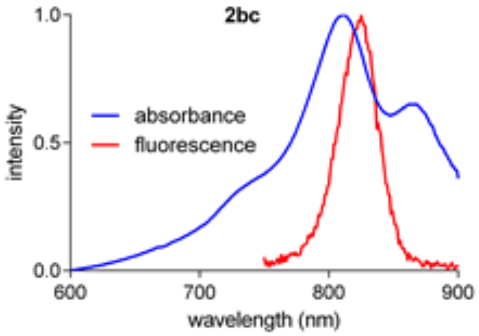
2bc
absorbance
fluorescence
intensity
1.0
0.5
0.0
600
700
800
900
wavelength (nm)

Figure E-S6. Absorbance and fluorescence of compounds in compound in series **1 (1aa, 1bb,1ab, 1ac, 1bc)** and **2** (**2aa, 2bb, 2cc, 2ab, 2ac, 2bc)** in PBS (pH 7.4) in 0.1% CrEL.

NMR Spectra And HRMS

(1E,1'E)-1,1'-(2-chlorocyclohex-1-ene-1,3-diyl)bis(N-phenylmethanimine) (A)

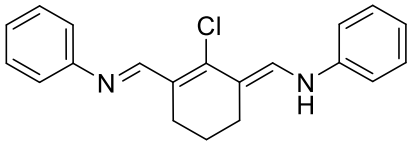

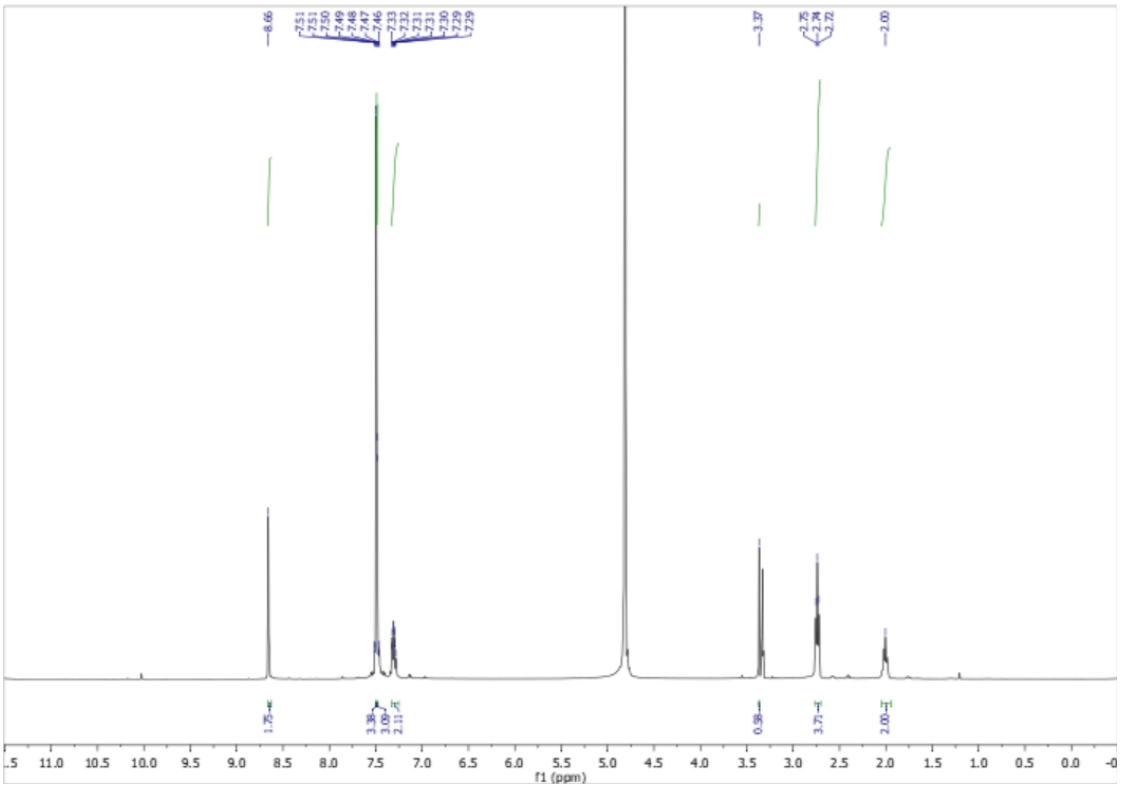

Figure E-S7. ^{1}H NMR spectrum of compound **A**

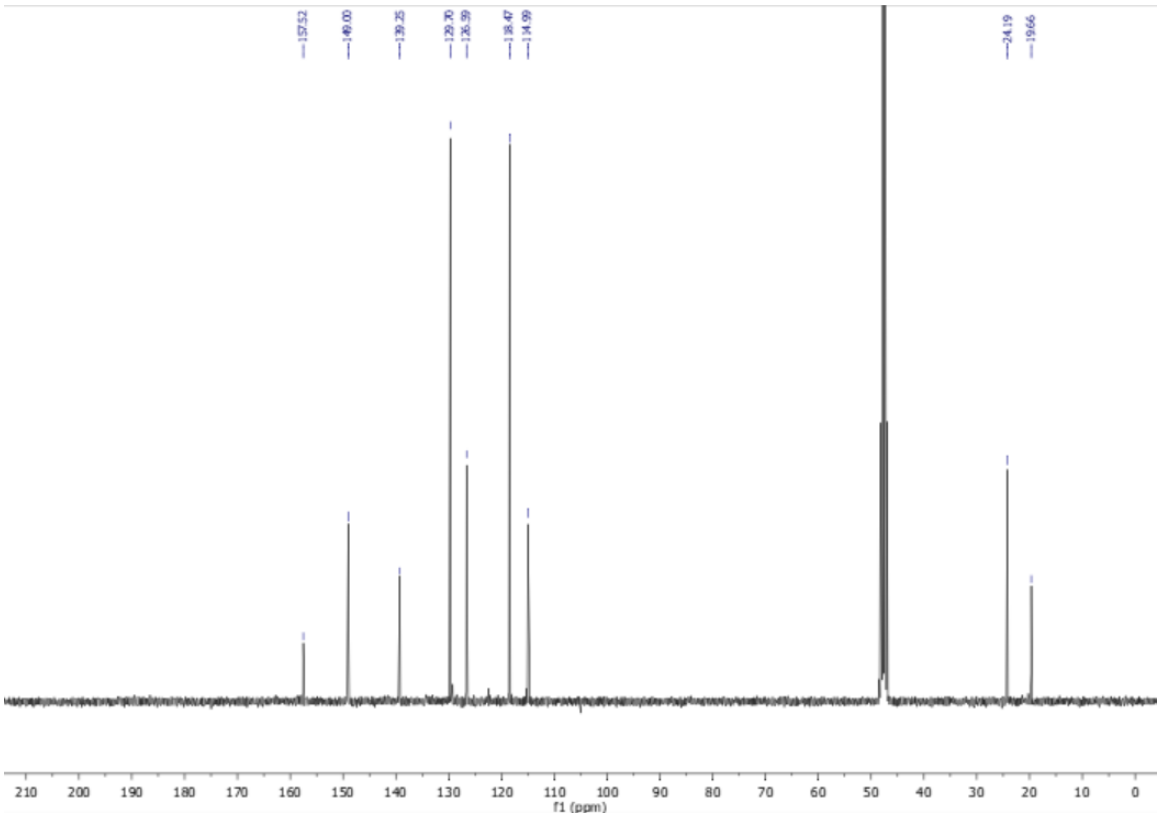

Figure E-S8. ^{13}C NMR spectrum of compound **A**

5-iodo-2,3,3-trimethyl-3H-indole (B)

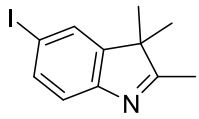

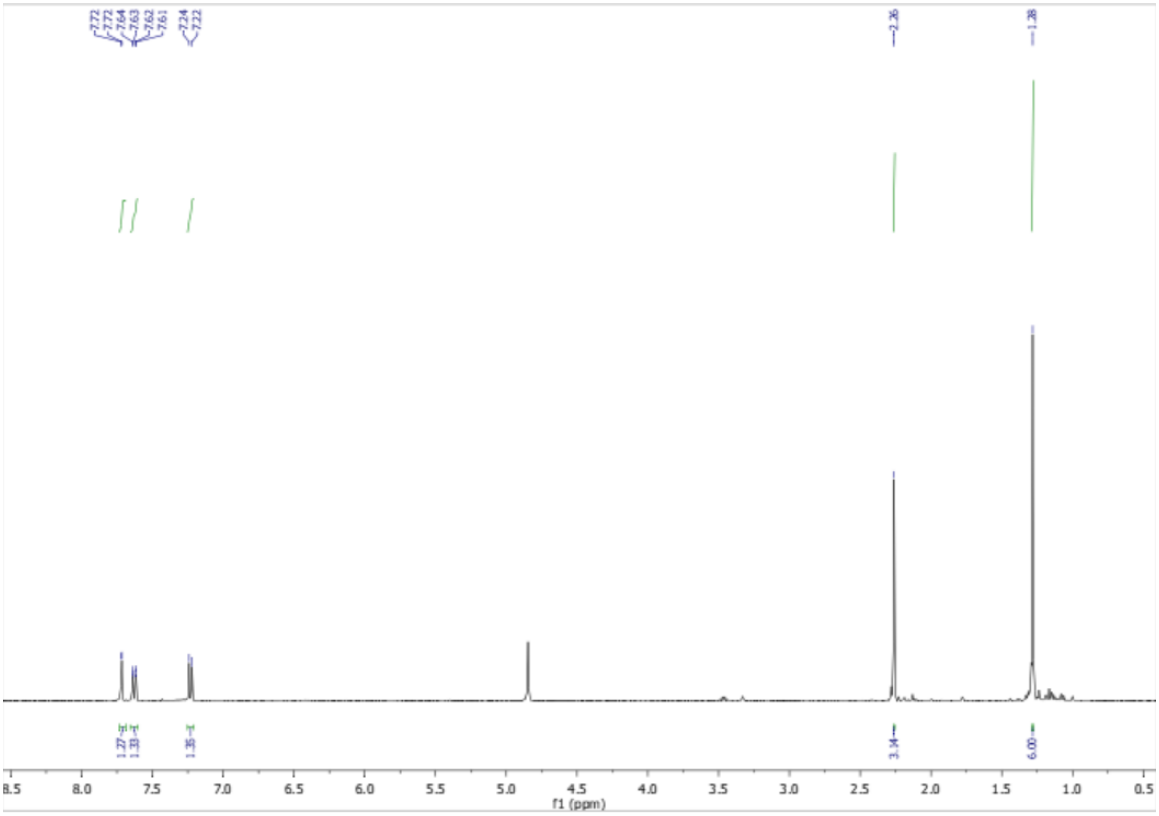

Figure E-S9. ^{1}H NMR spectrum of compound **B**

^{13}C

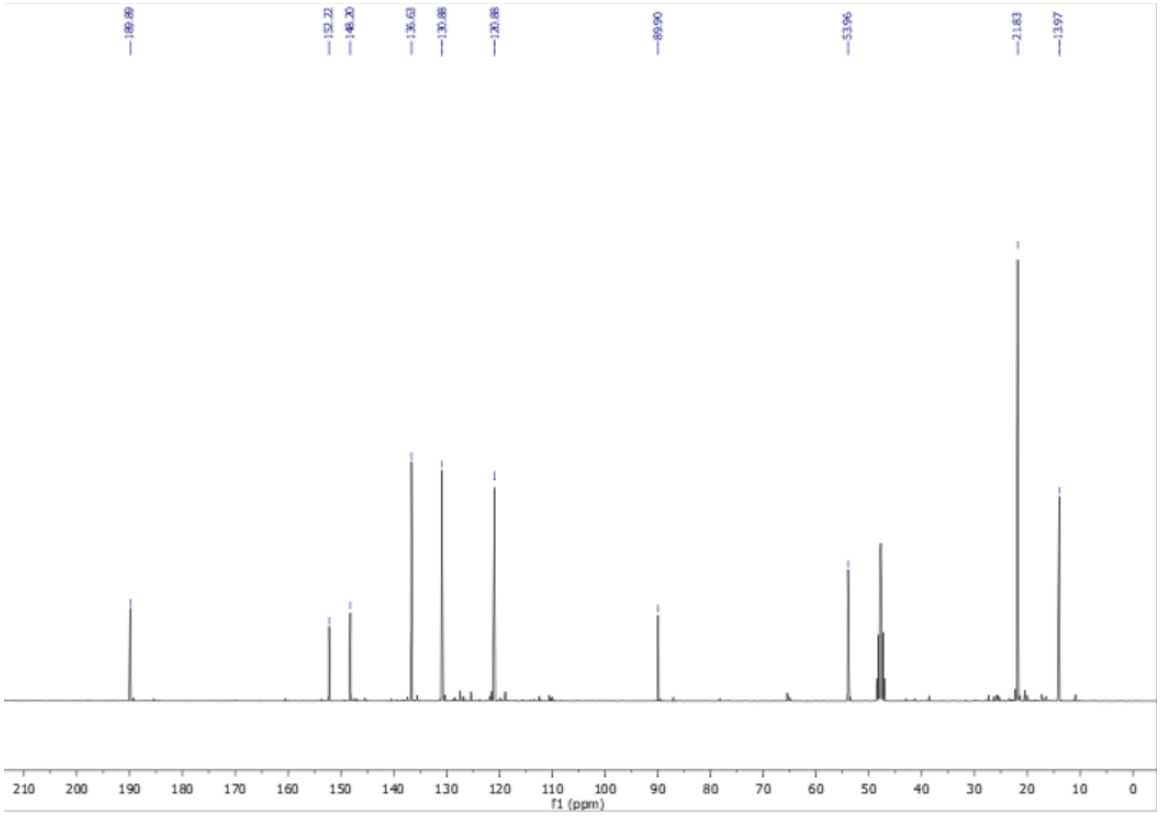

Figure E-S10. ^{13}C NMR spectrum of compound **B**

1-(5-carboxypentyl)-2,3,3-trimethyl-3H-indol-1-ium (5a)

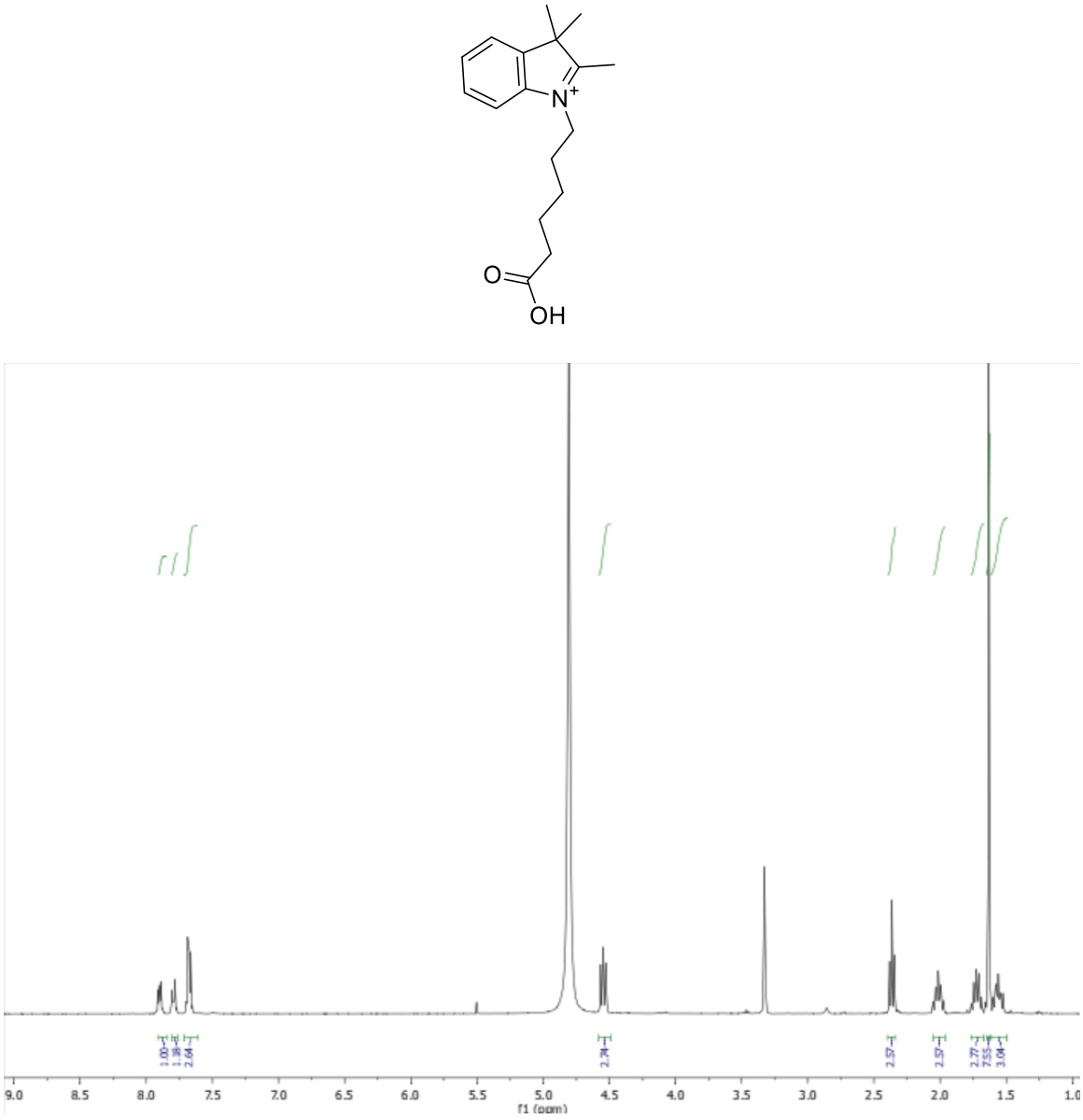

Figure E-S11. ^{1}H NMR spectrum of compound **5a**

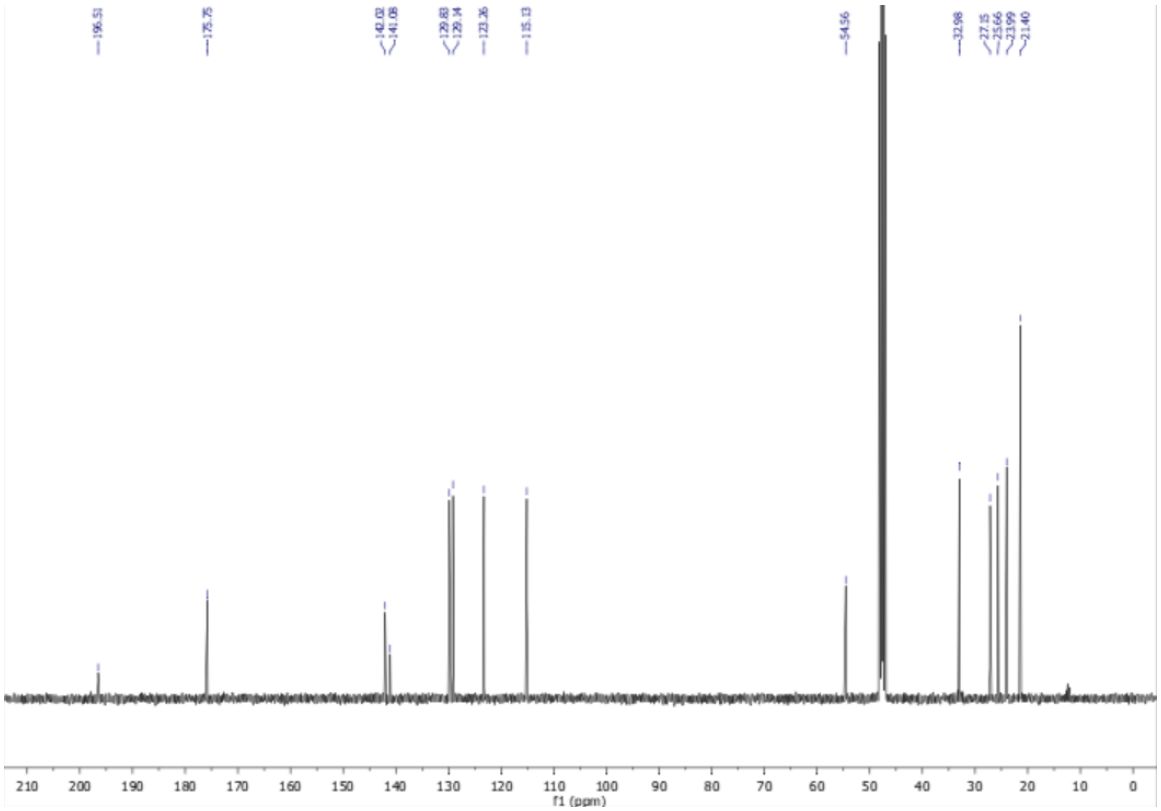

Figure E-S12. ^{13}C NMR spectrum of compound **5a**

1-(5-carboxypentyl)-5-iodo-2,3,3-trimethyl-3H-indol-1-ium (4a)

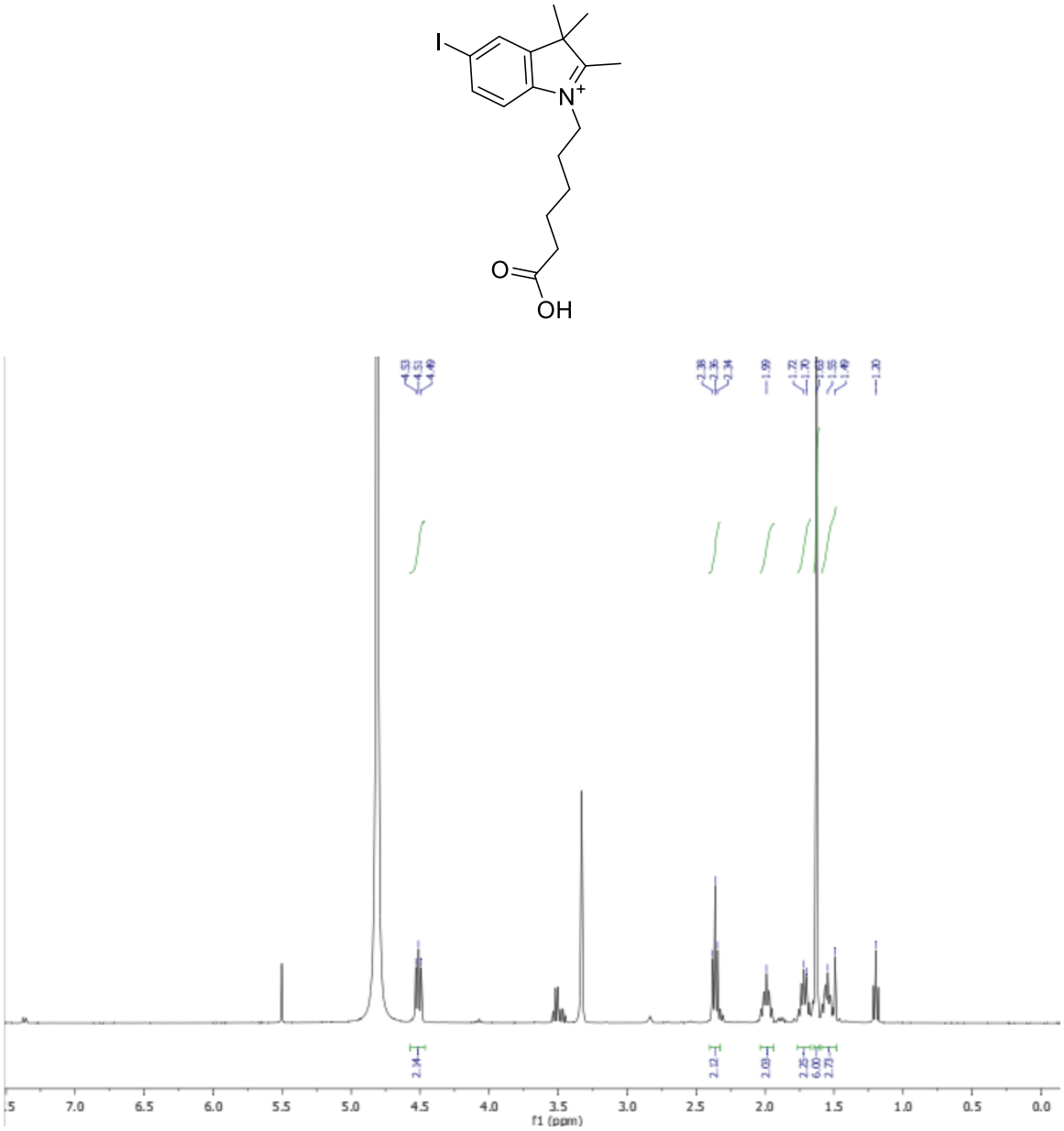

Figure E-S13. ^{1}H NMR spectrum of compound **4a**

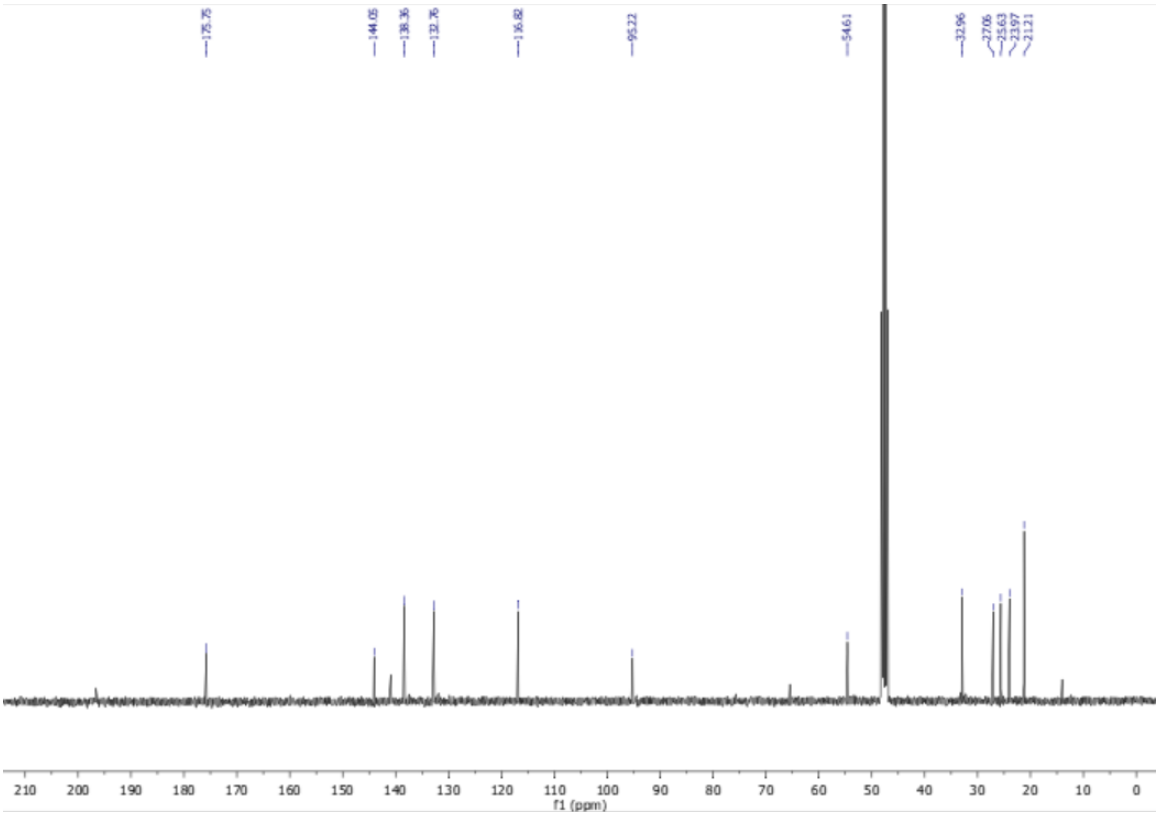

Figure E-S14. ^{13}C NMR spectrum of compound **4a**

4-(2,3,3-trimethyl-3H-indol-1-ium-1-yl)butane-1-sulfonate (5b)

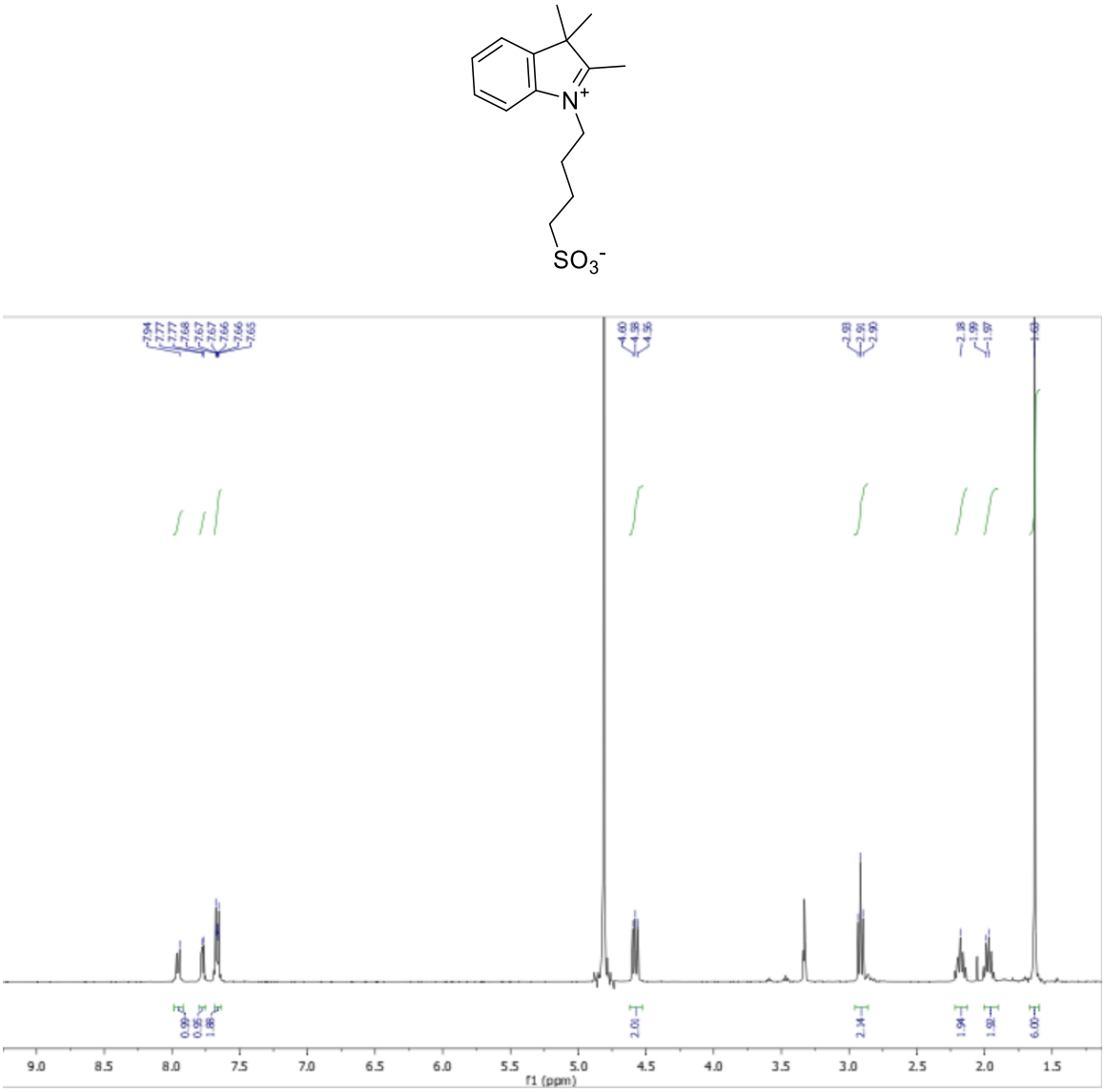

Figure E-S15. ^{1}H NMR spectrum of compound **5b**

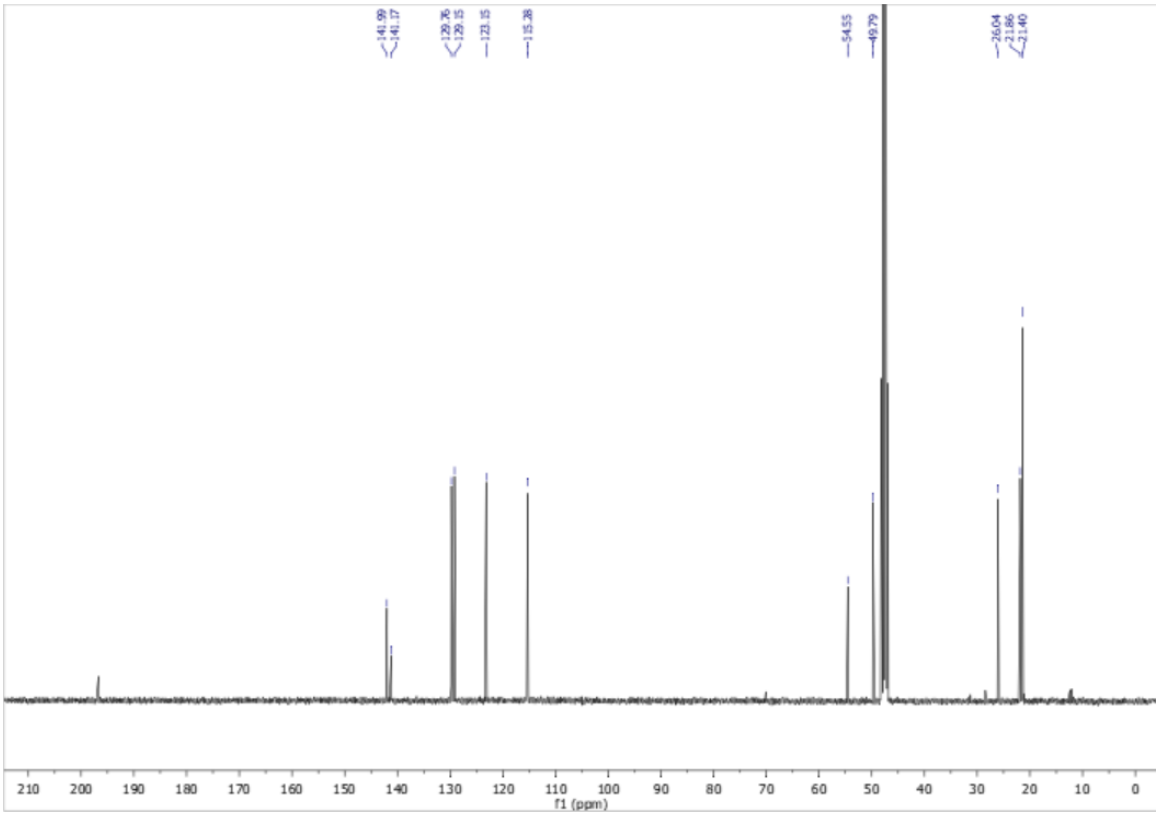

Figure E-S16. ^{13}C NMR spectrum of compound **5b**

4-(5-iodo-2,3,3-trimethyl-3H-indol-1-ium-1-yl)butane-1-sulfonate (4b)

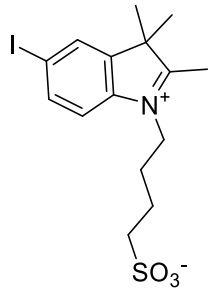

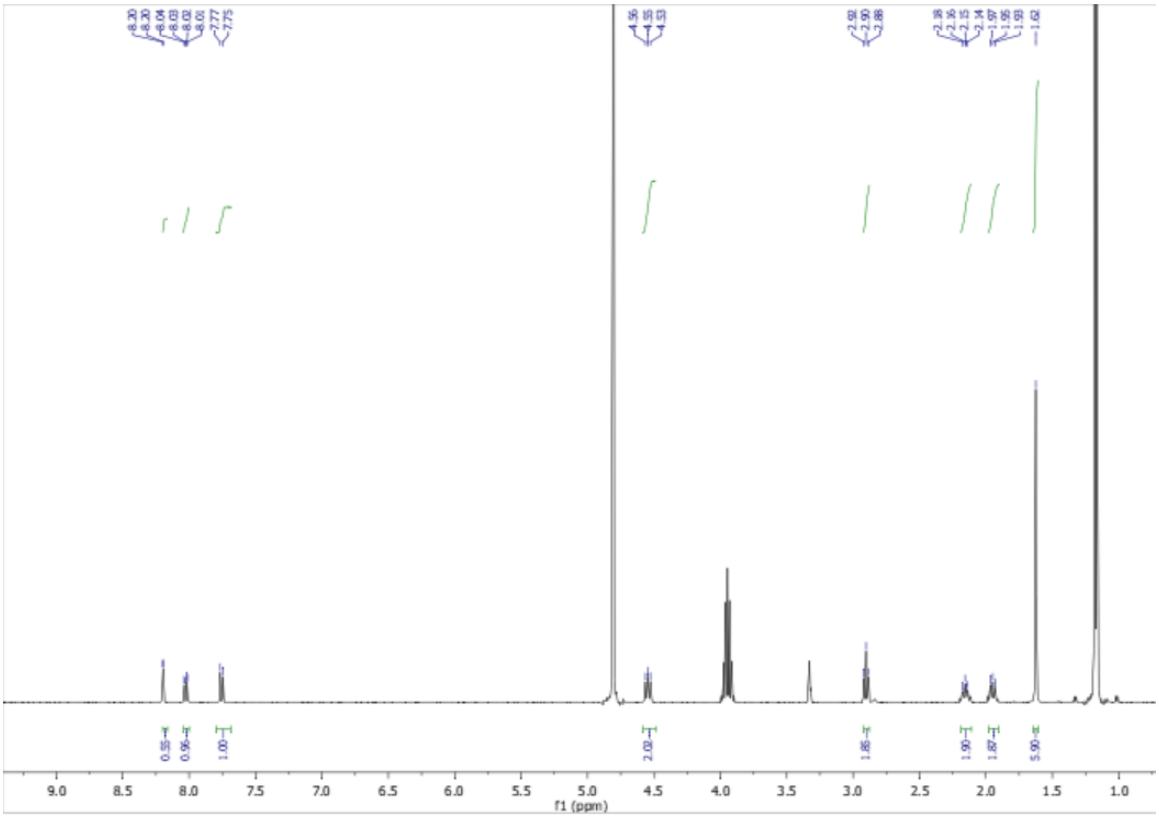

Figure E-S17. ^{1}H NMR spectrum of compound **4b**

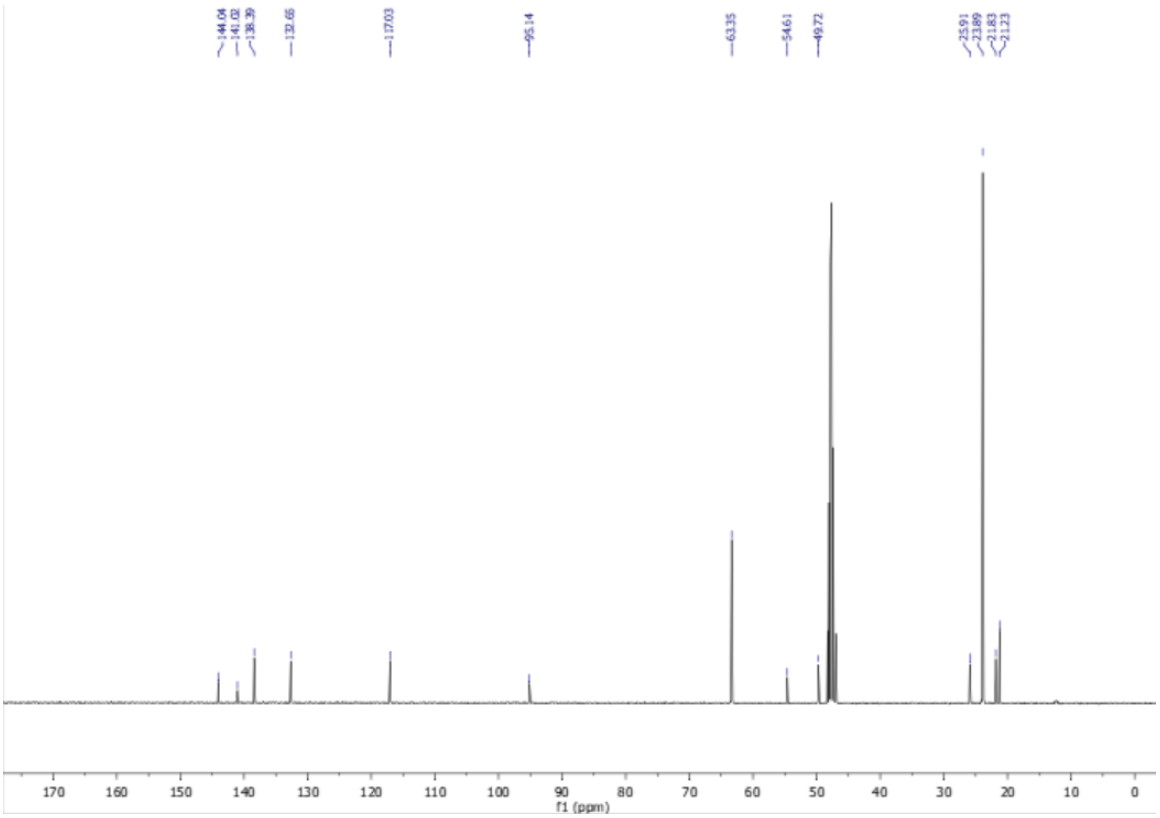

Figure E-S18. ^{13}C NMR spectrum of compound **4b**

2,3,3-trimethyl-1-propyl-3H-indol-1-ium (5c)

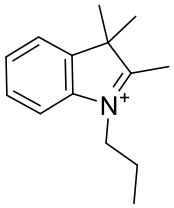

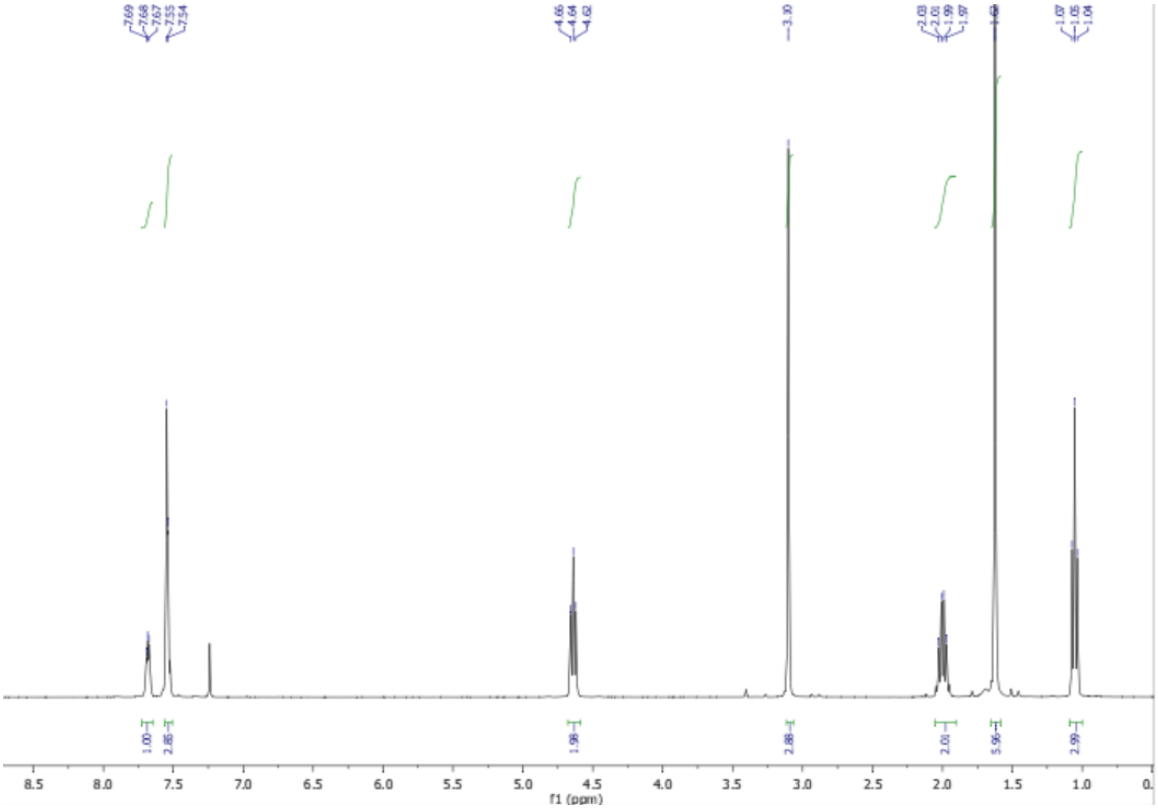

Figure E-S19. ^{1}H NMR spectrum of compound **5c**

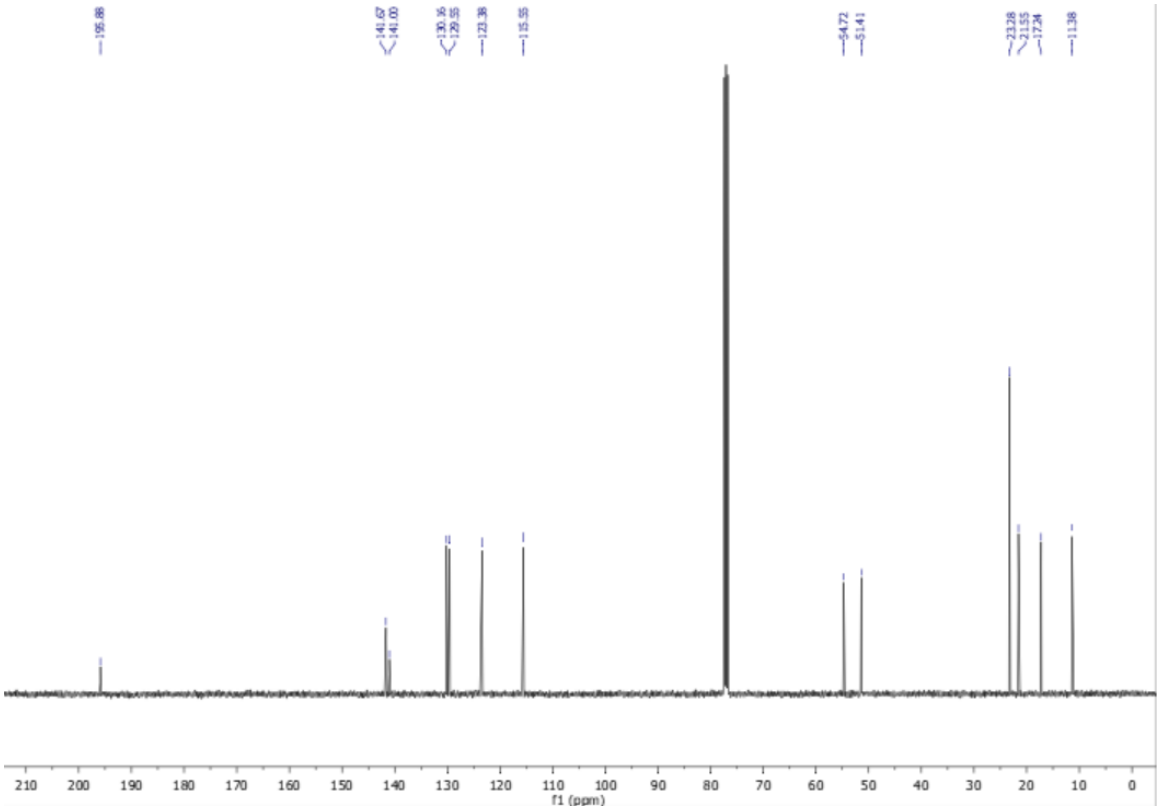

Figure E-S20. ^{13}C NMR spectrum of compound **5c**

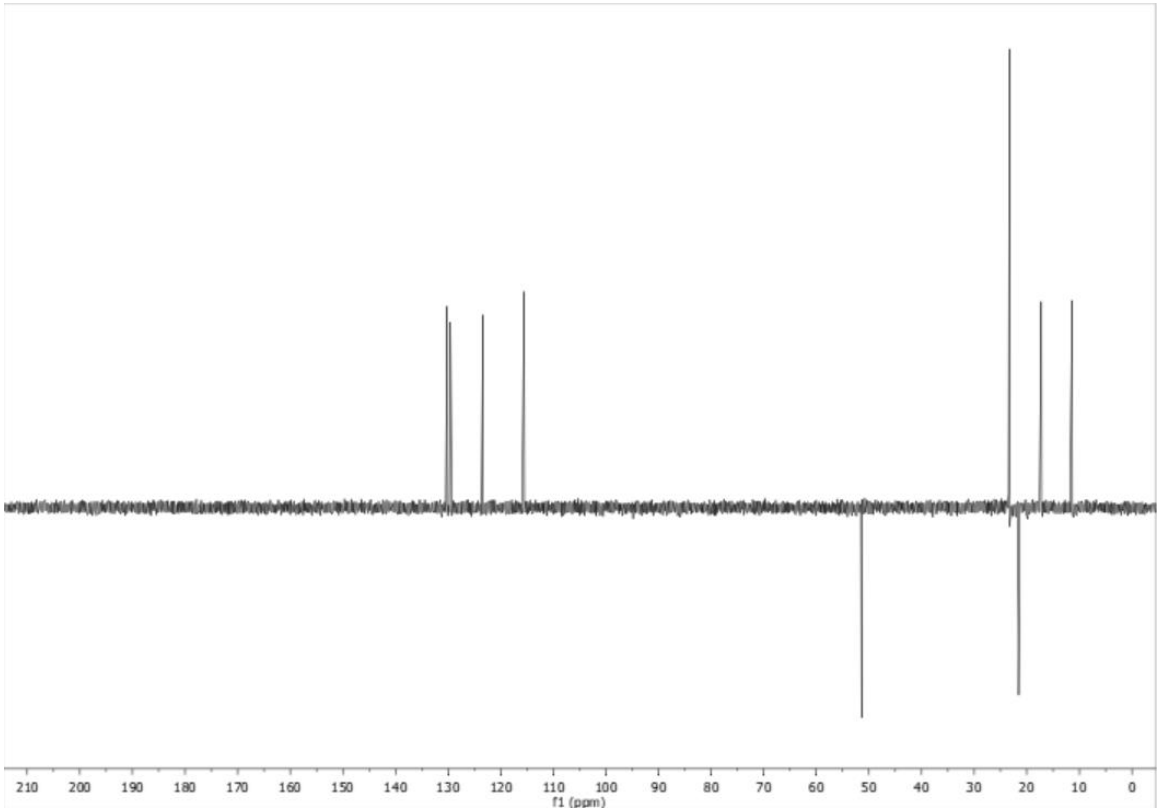

Figure E-S21. DEPT135 NMR spectrum of compound **5c**

5-iodo-2,3,3-trimethyl-1-propyl-3H-indol-1-ium (4c)

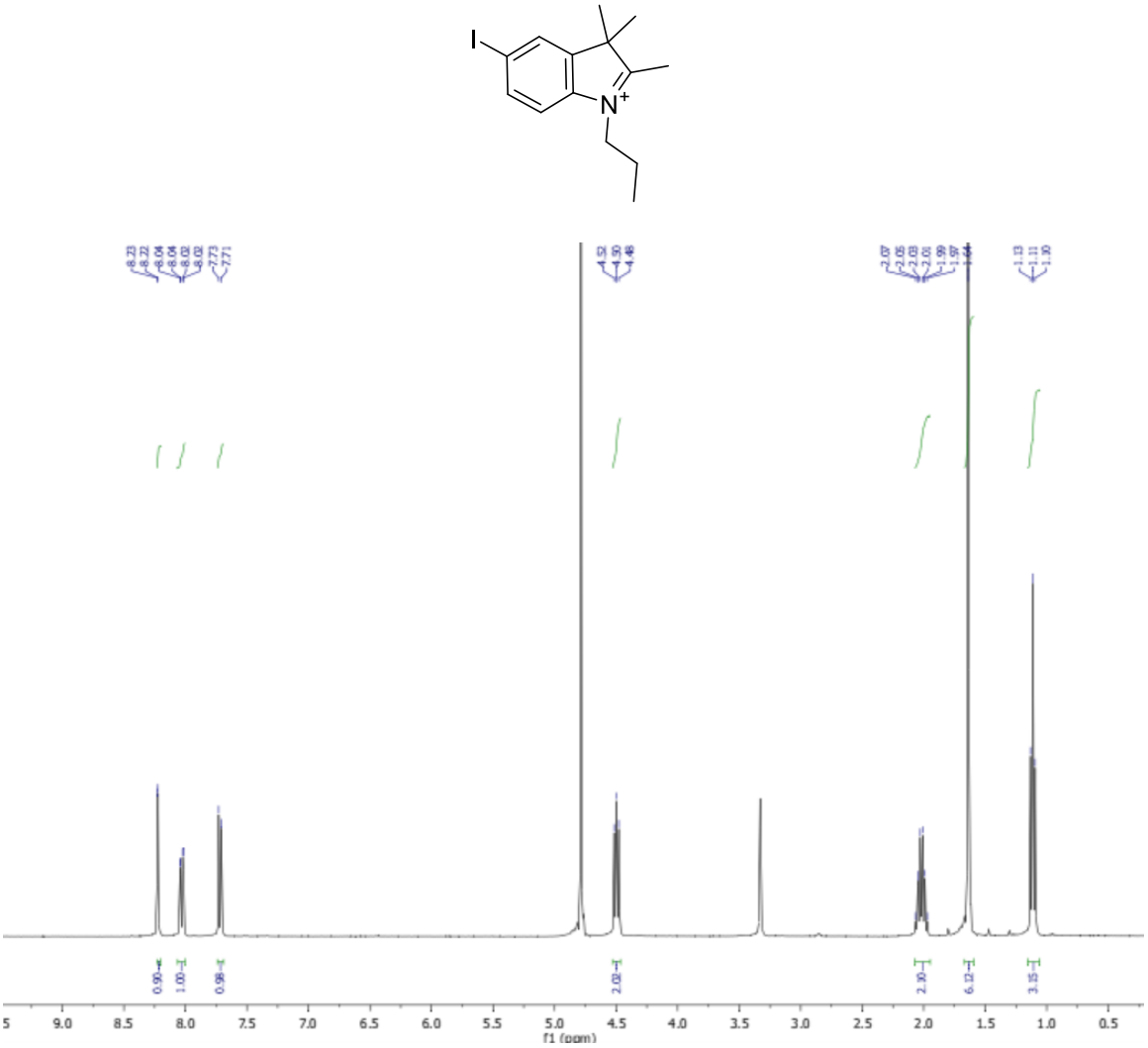

Figure E-S22. ^{1}H NMR spectrum of compound **4c**

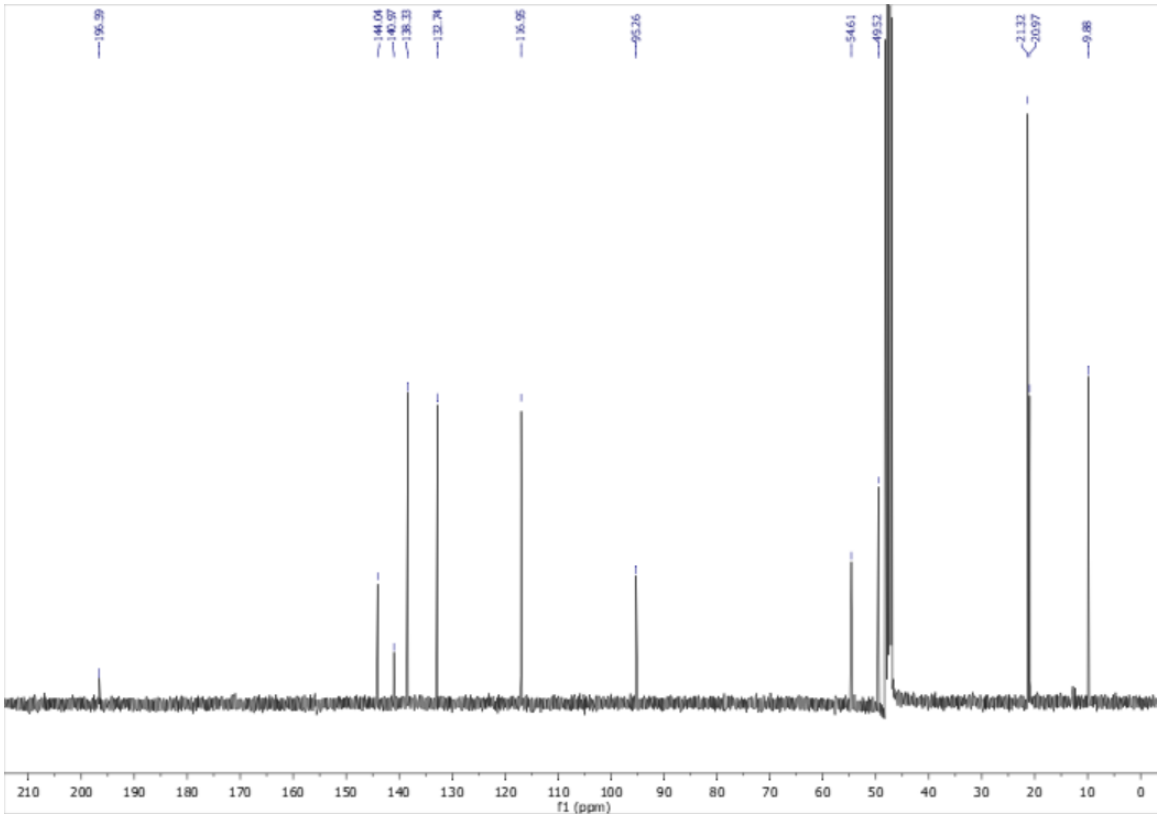

Figure E-S23. ^{13}C NMR spectrum of compound **4c**

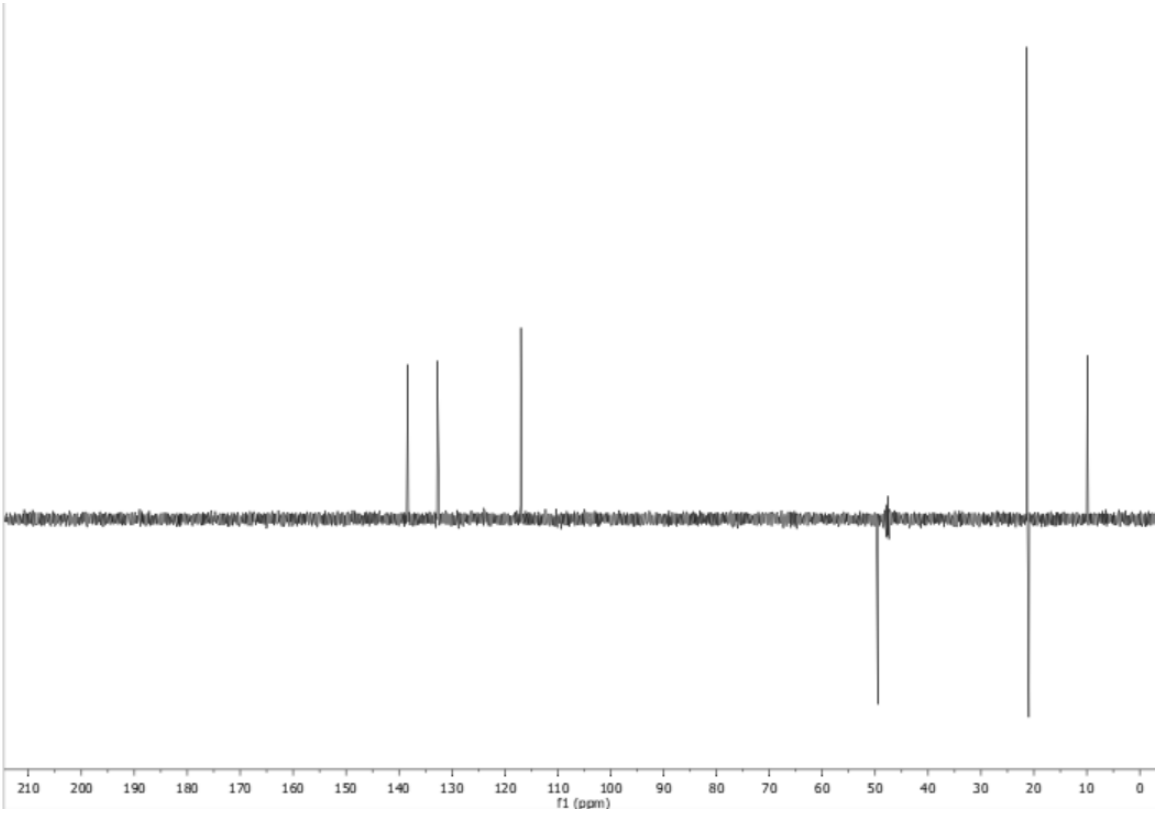

Figure E--S24. DEPT135 NMR spectrum of compound **4c**

1-(5-carboxypentyl)-2-((E)-2-((E)-2-chloro-3-((phenylamino)methylene)cyclohex-1-en-1-yl)vinyl)-3,3-dimethyl-3H-indol-1-ium (3a)

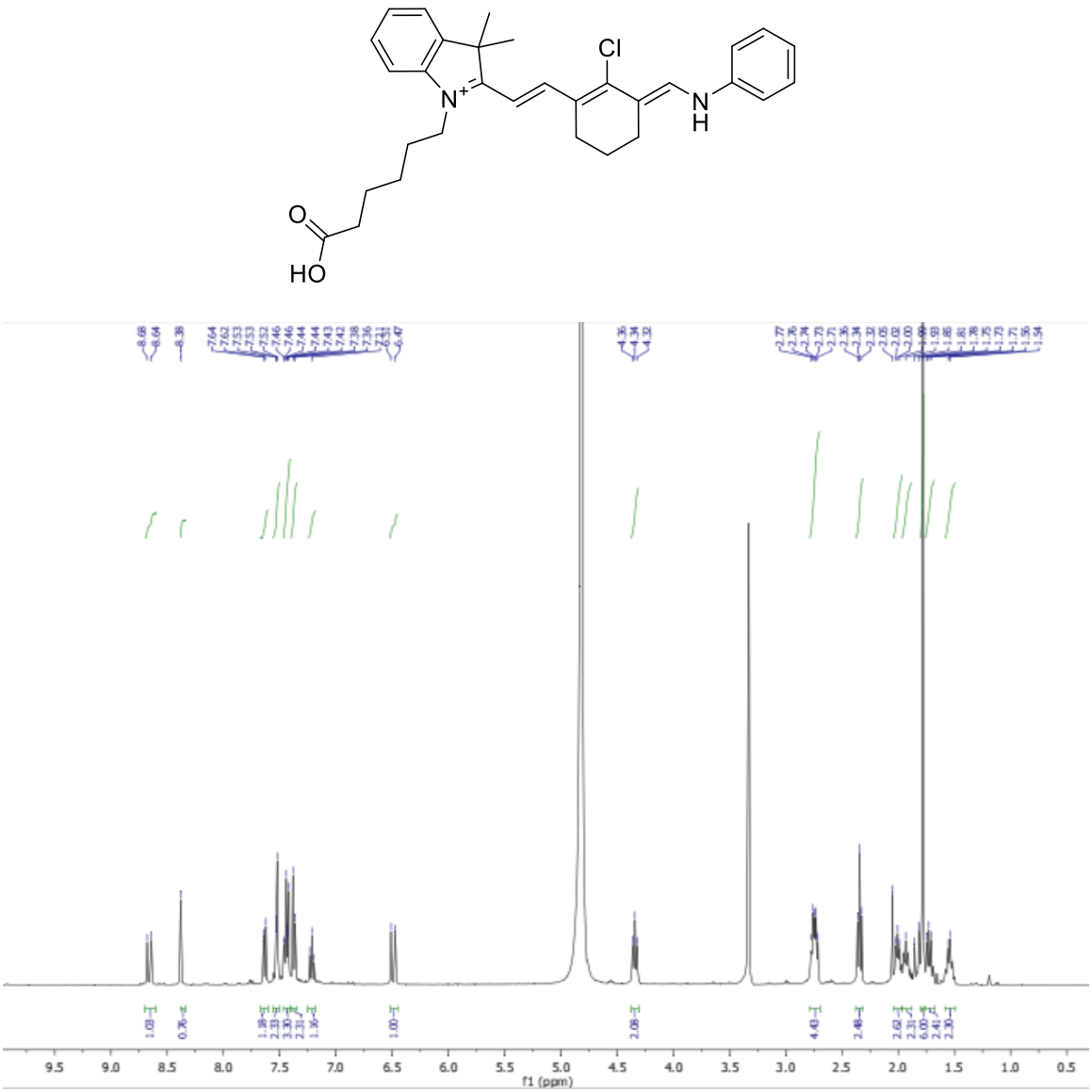

Figure E-S25. ^{1}H NMR spectrum of compound **3a**

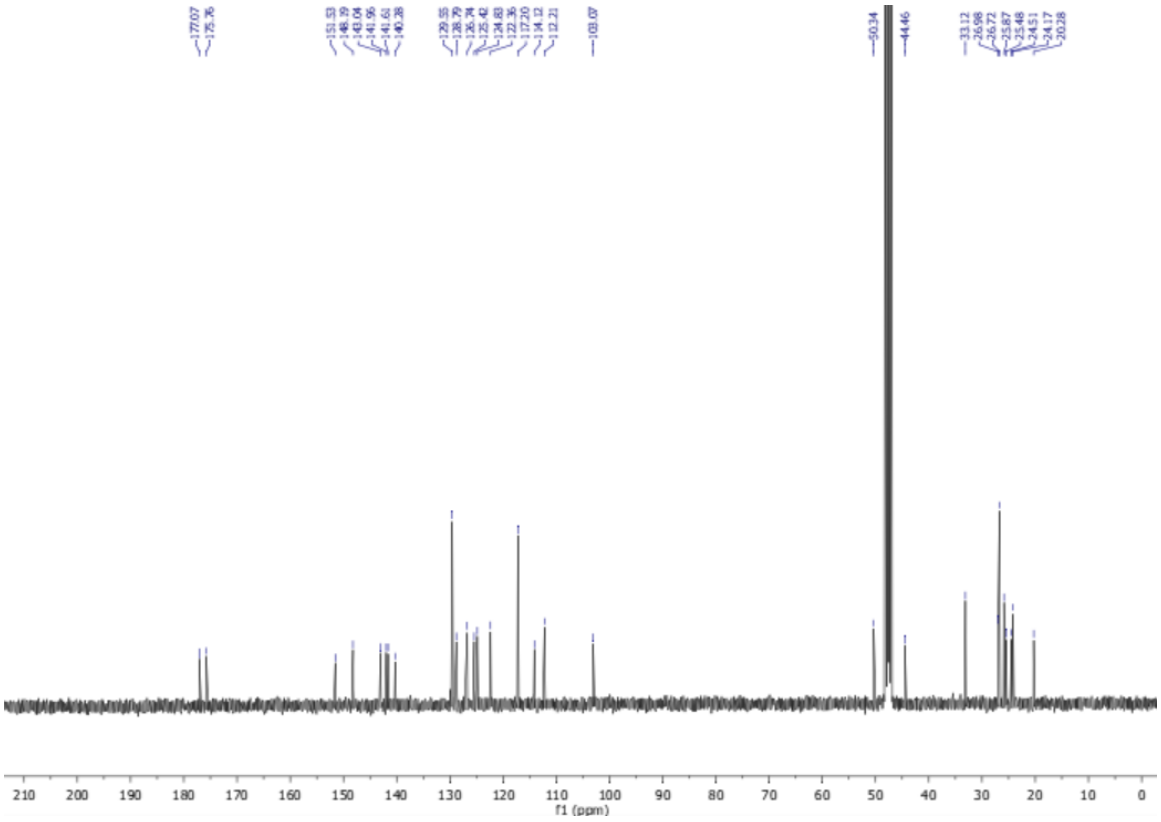

Figure E-S26. ^{13}C NMR spectrum of compound **3a**

4-(2-((E)-2-((E)-2-chloro-3-((phenylamino)methylene)cyclohex-1-en-1-yl)vinyl)-3,3-dimethyl-3H-indol-1-ium-1-yl)butane-1-sulfonate (3b)

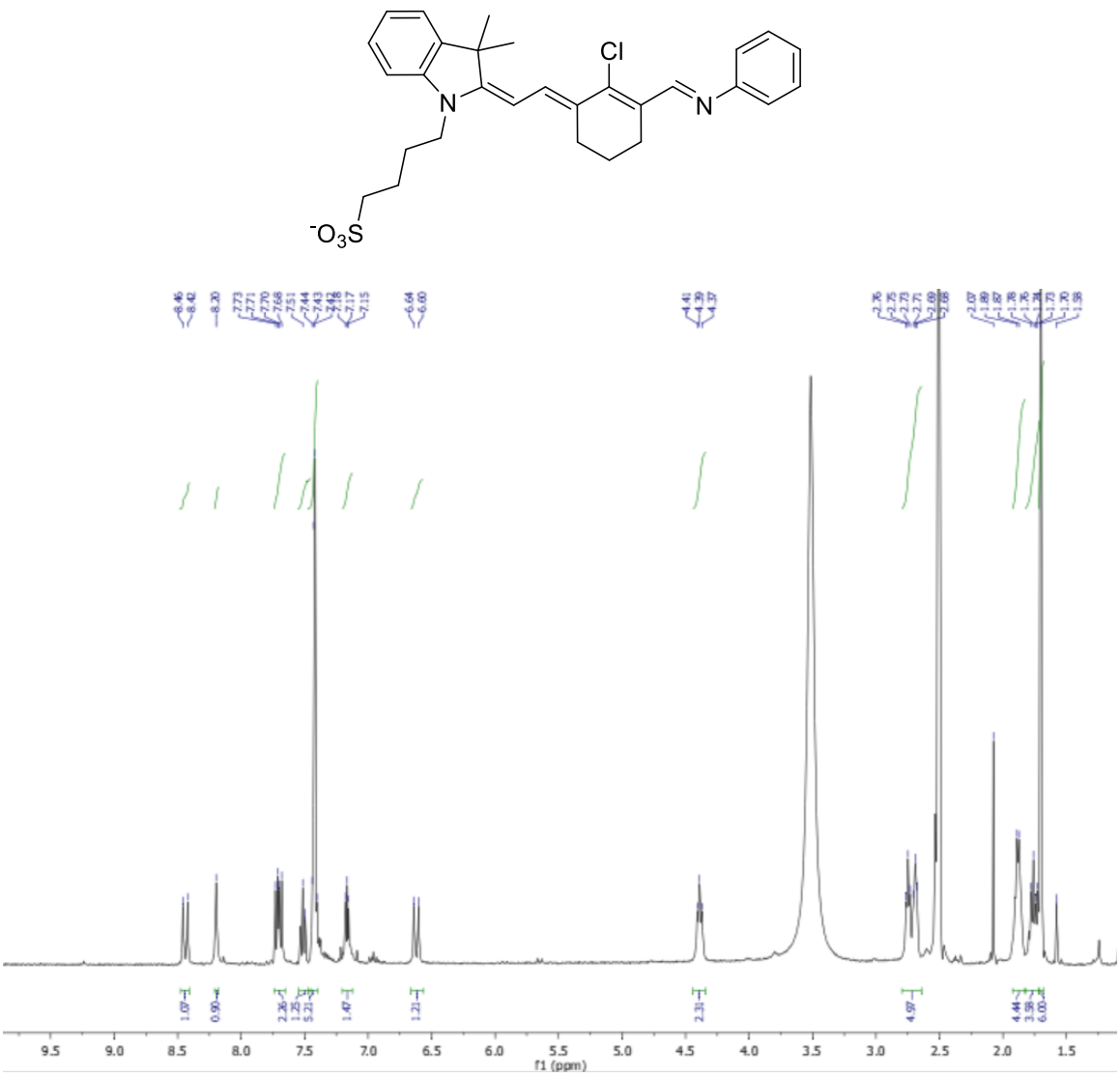

Figure E-S27. ^{1}H NMR spectrum of compound **3b**

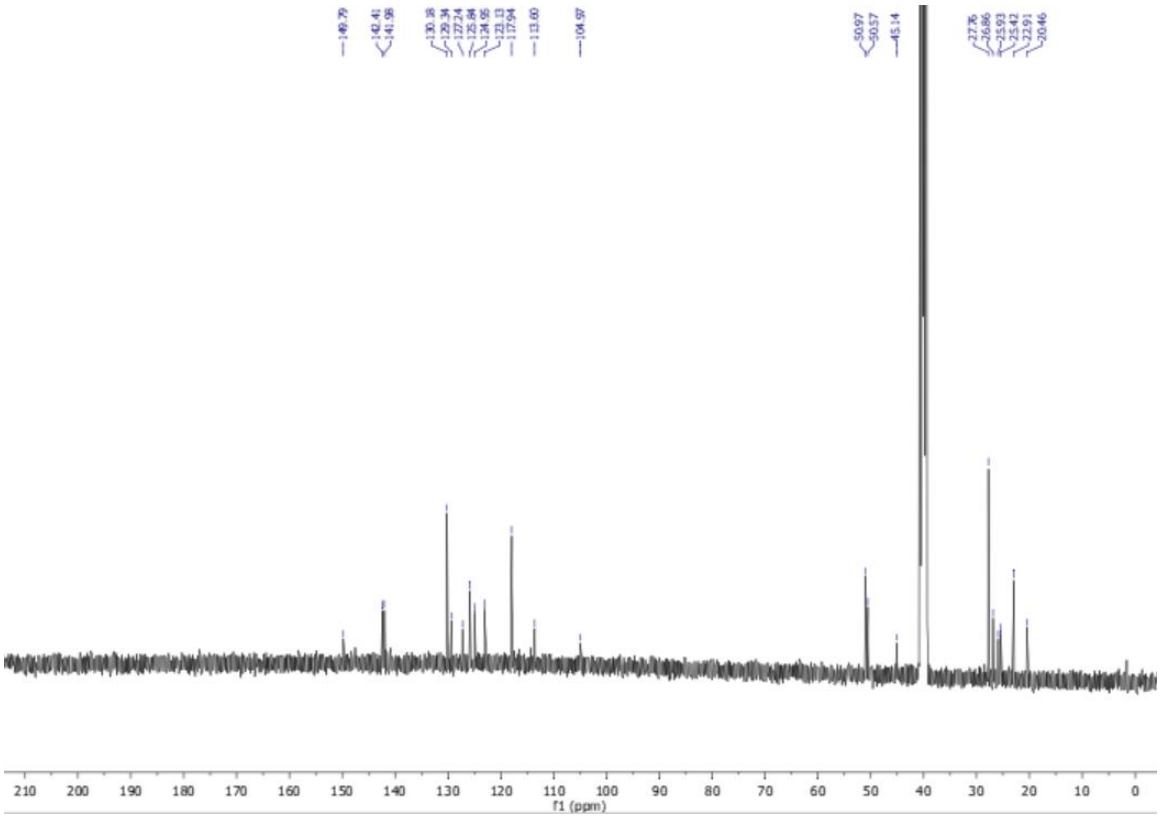

Figure E-S28. ^{13}C NMR spectrum of compound **3b**

1-(5-carboxypentyl)-2-((E)-2-((E)-2-chloro-3-((phenylamino)methylene)cyclohex-1-en-1-yl)vinyl)-5-iodo-3,3-dimethyl-3H-indol-1-ium (3c)

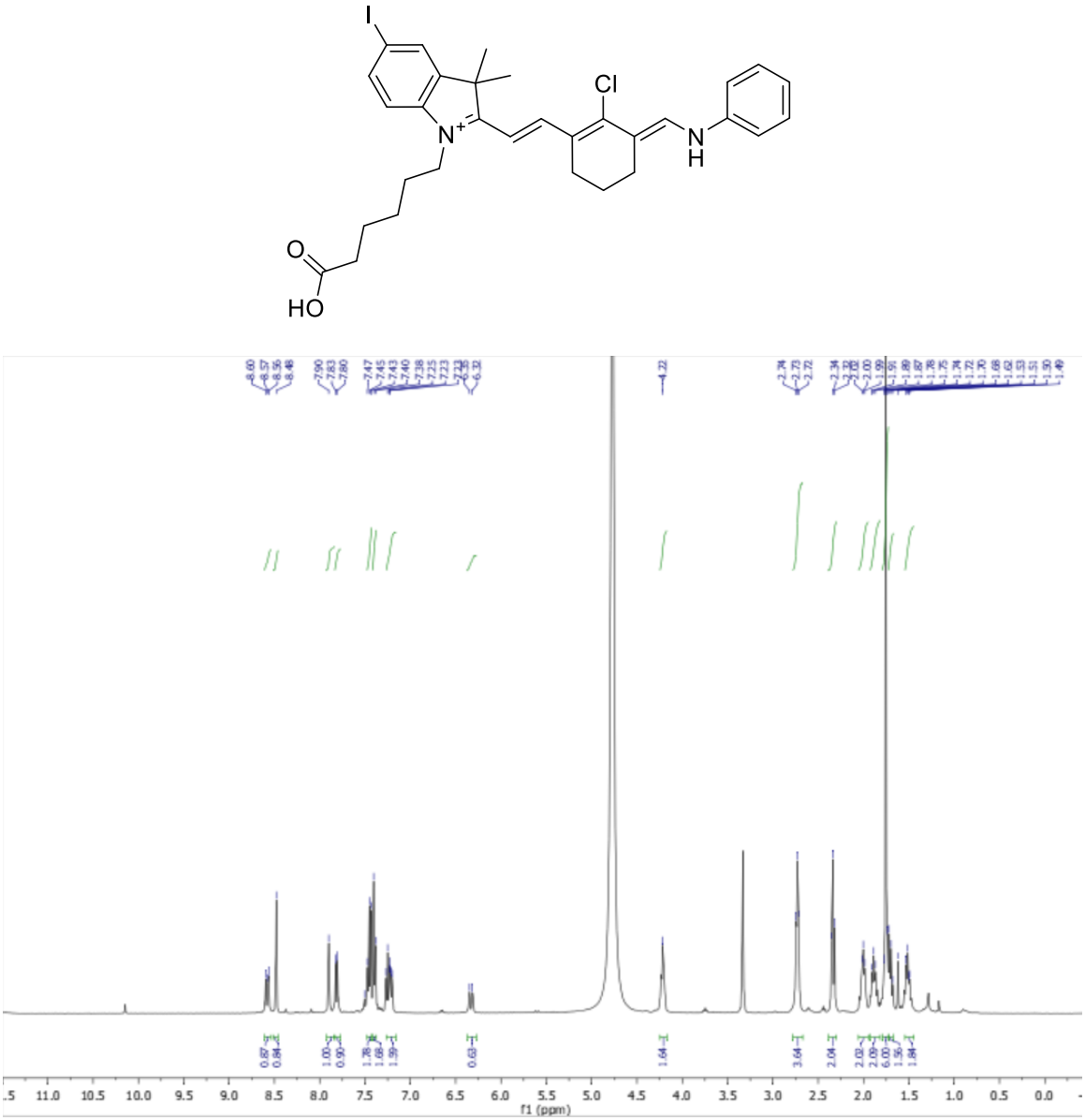

Figure E-S29. ^{1}H NMR spectrum of compound **3c**

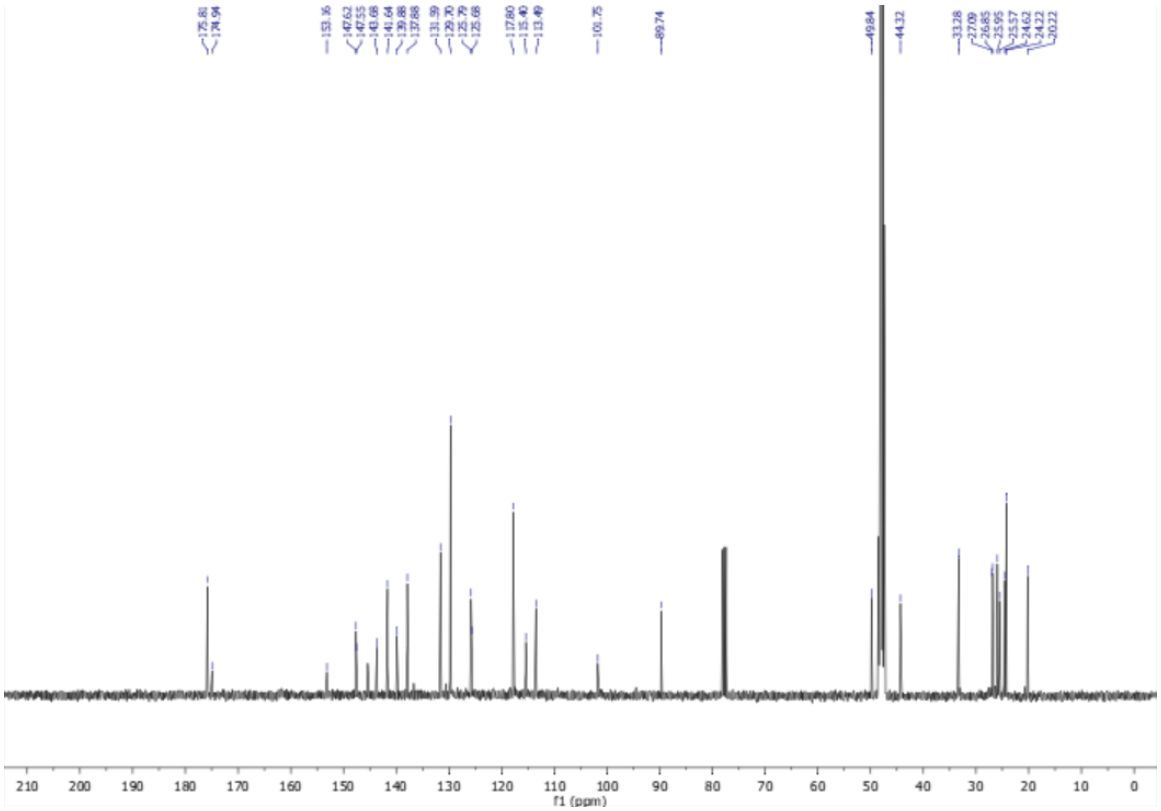

Figure E-S30. ^{13}C NMR spectrum of compound **3c**

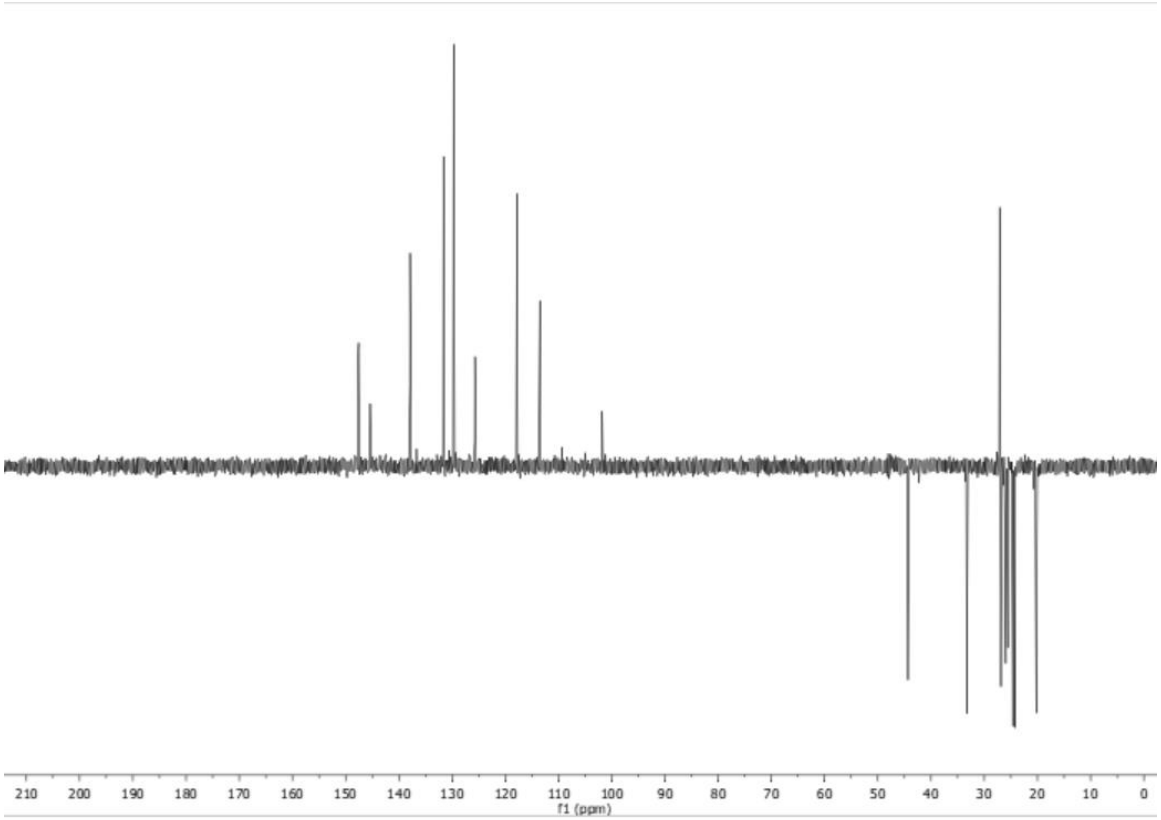

Figure E-S31. DEPT135 NMR spectrum of compound **3c**

4-(2-((E)-2-((E)-2-chloro-3-((phenylamino)methylene)cyclohex-1-en-1-yl)vinyl)-5-iodo-3,3-dimethyl-3H-indol-1-ium-1-yl)butane-1-sulfonate (3d)

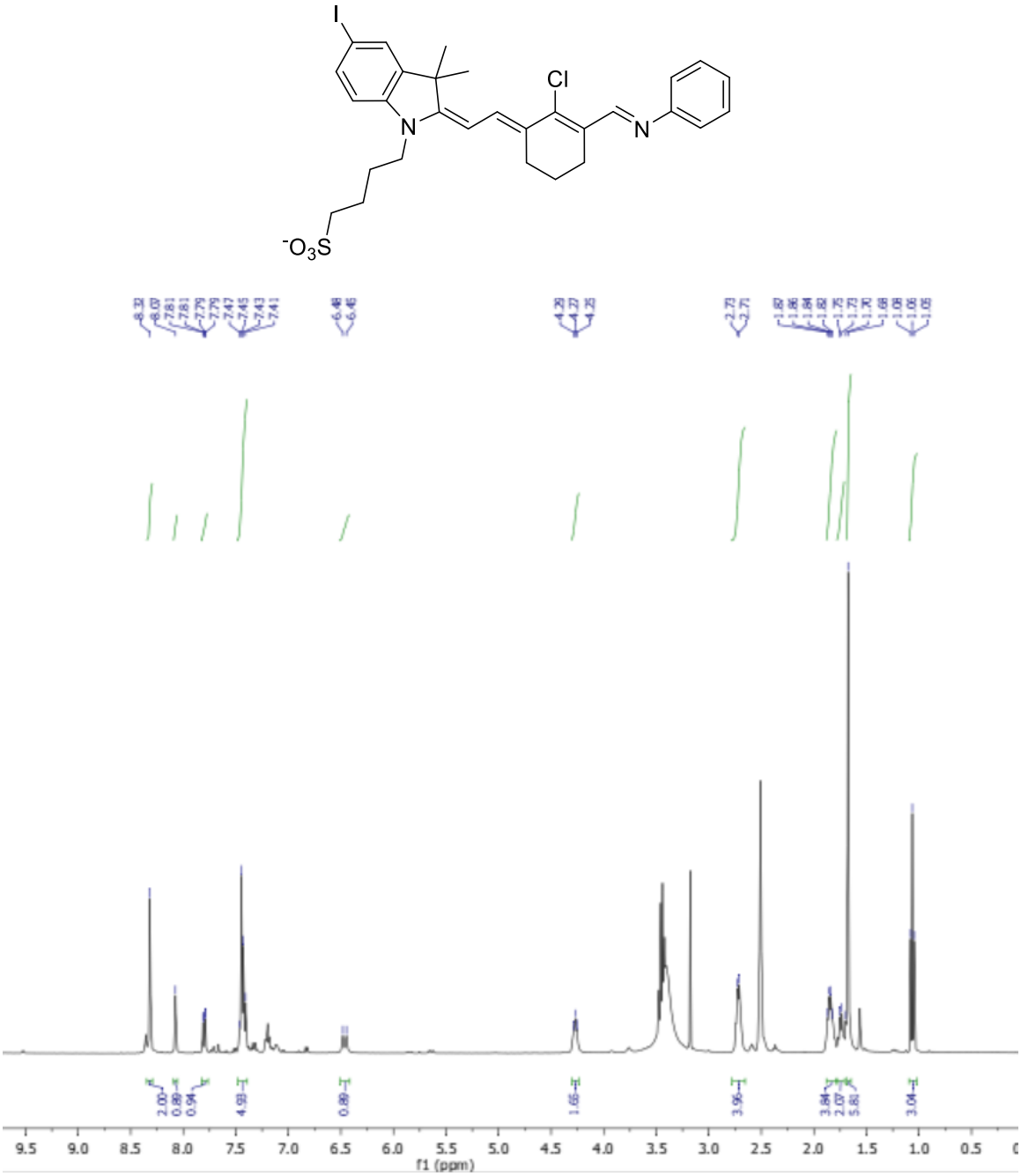

Figure E-S32. ^{1}H NMR spectrum of compound **3d**

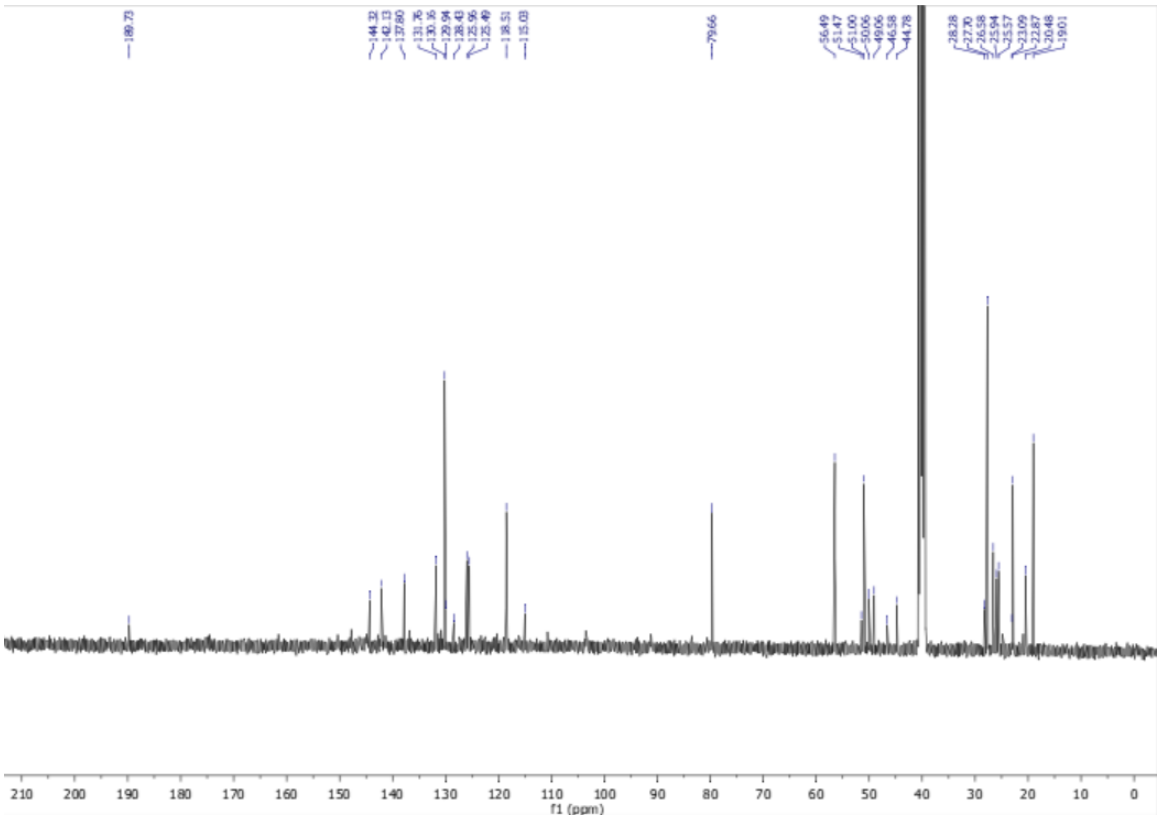

Figure E-S33. ^{13}C NMR spectrum of compound **3d**

1-(5-carboxypentyl)-2-((E)-2-((E)-3-(2-((E)-1-(5-carboxypentyl)-5-iodo-3,3-dimethylindolin-2-ylidene)ethylidene)-2-chlorocyclohex-1-en-1-yl)vinyl)-3,3-dimethyl-3H-indol-1-ium (1aa)

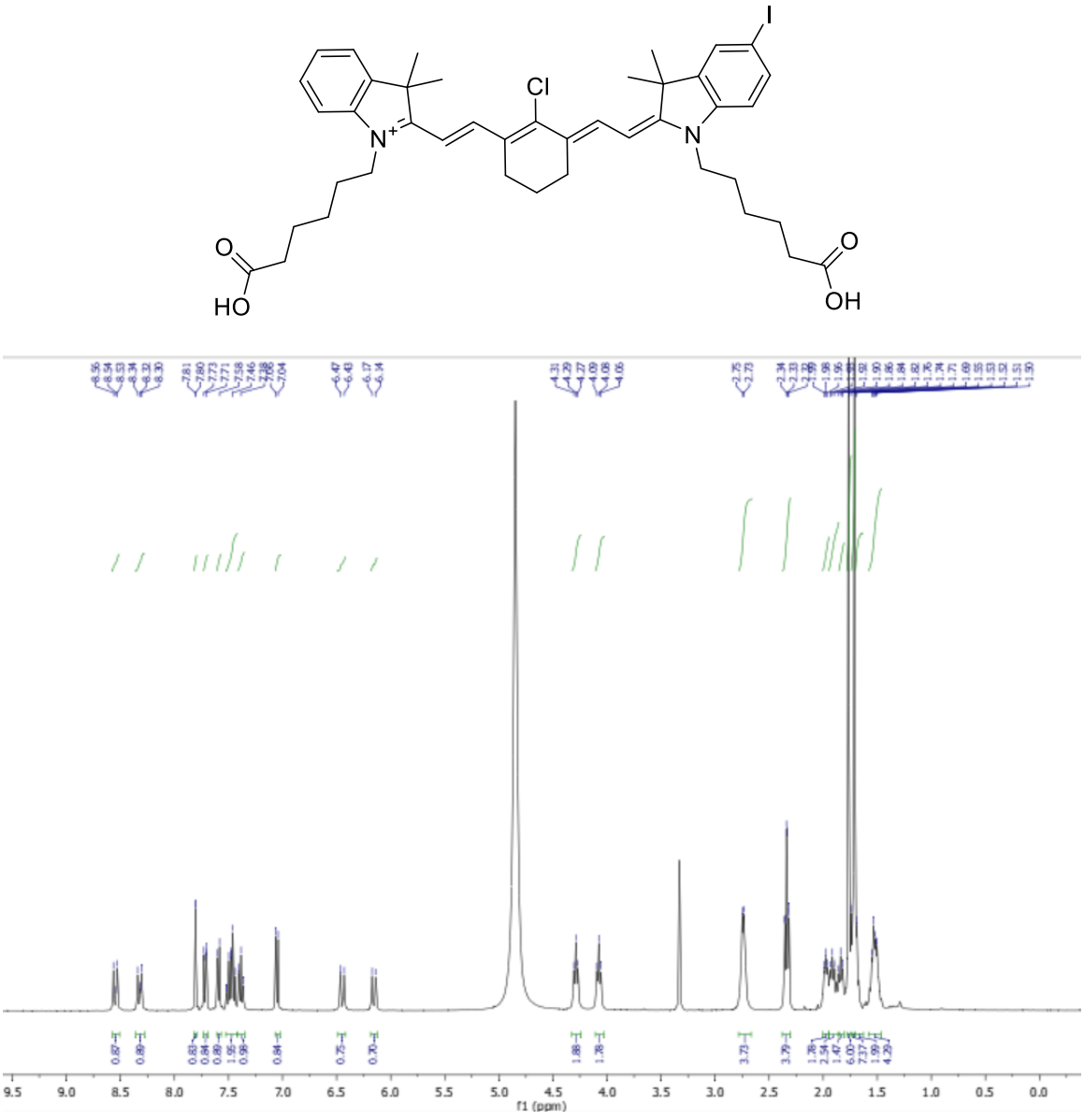

Figure E-S34. ^{1}H NMR spectrum of compound **1aa**

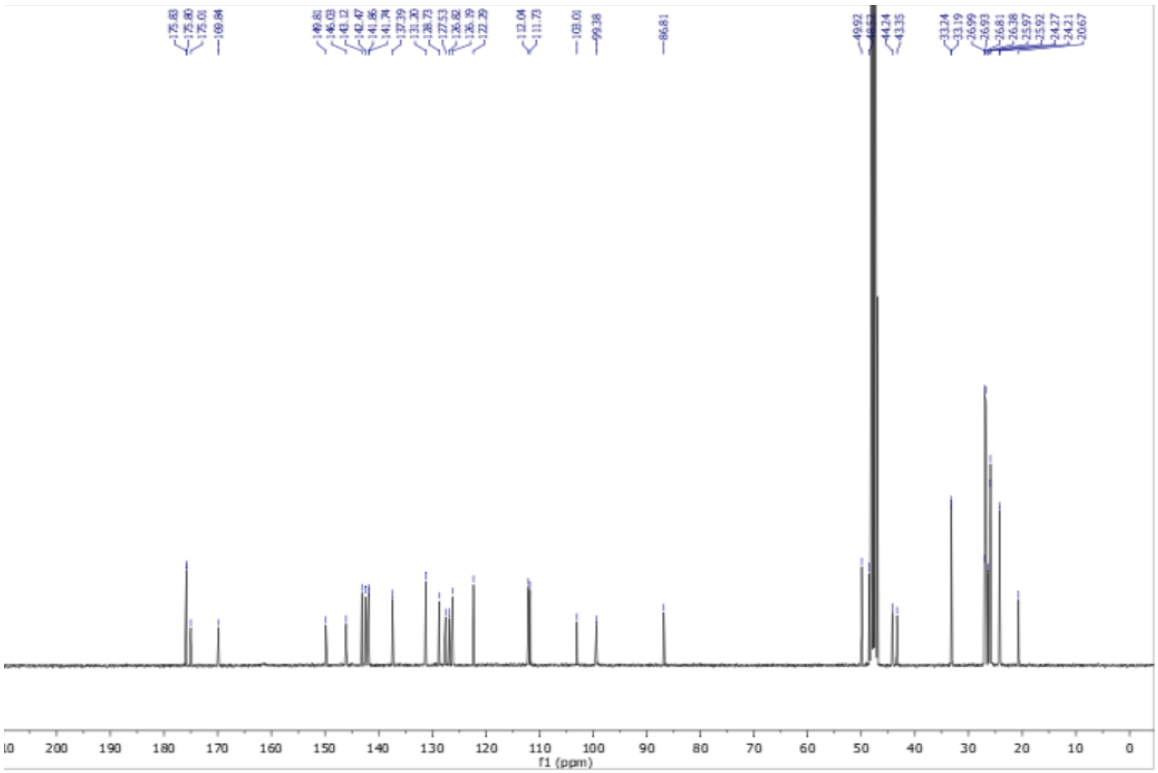

Figure E-S35. ^{13}C NMR spectrum of compound **1aa**

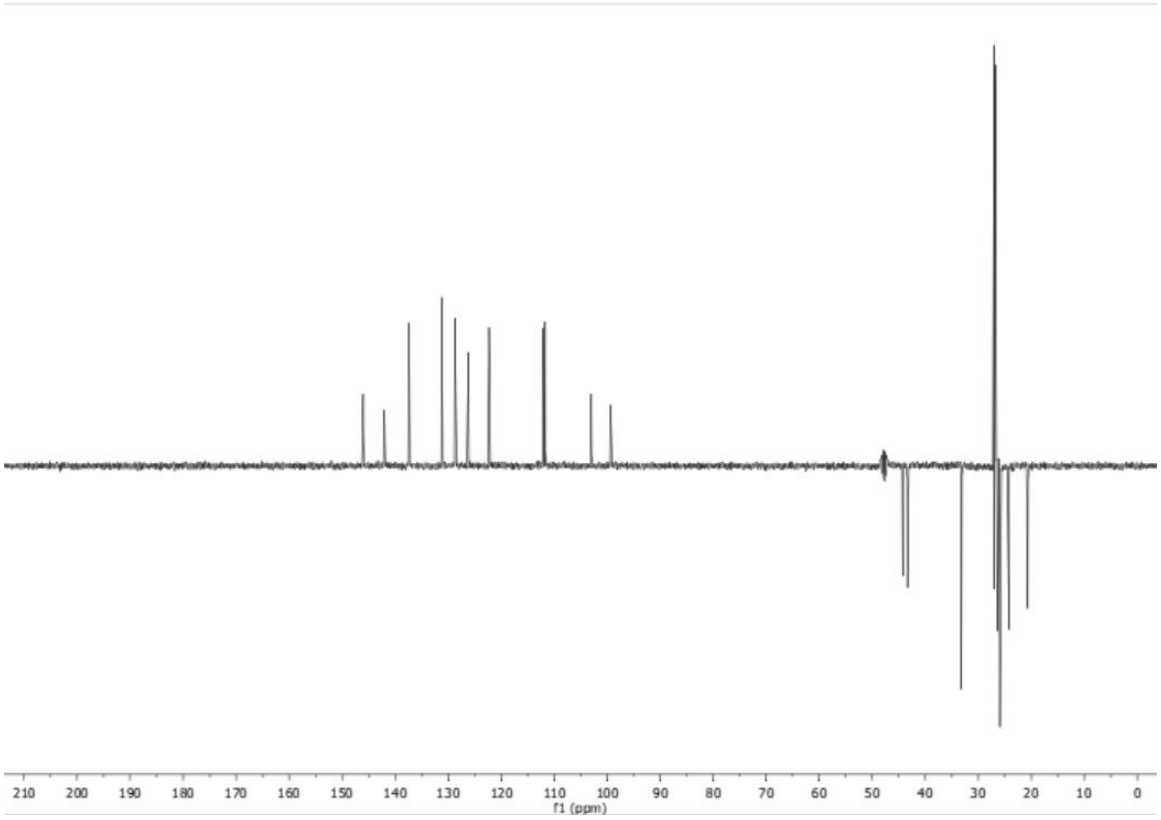

Figure E-S36. DEPT135 NMR spectrum of compound **1aa**

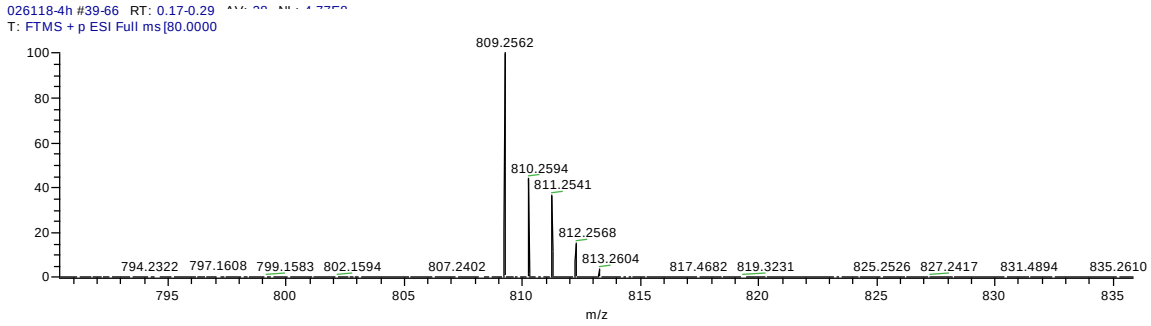

Figure E-S37. HRMS spectrum of compound **1aa**

4-((E)-2-((E)-2-(2-chloro-3-((E)-2-(3,3-dimethyl-1-(4-sulfonatobutyl)-3H-indol-1-ium-2-yl)vinyl)cyclohex-2-en-1-ylidene)ethylidene)-5-iodo-3,3-dimethylindolin-1-yl)butane-1-sulfonate (1bb)

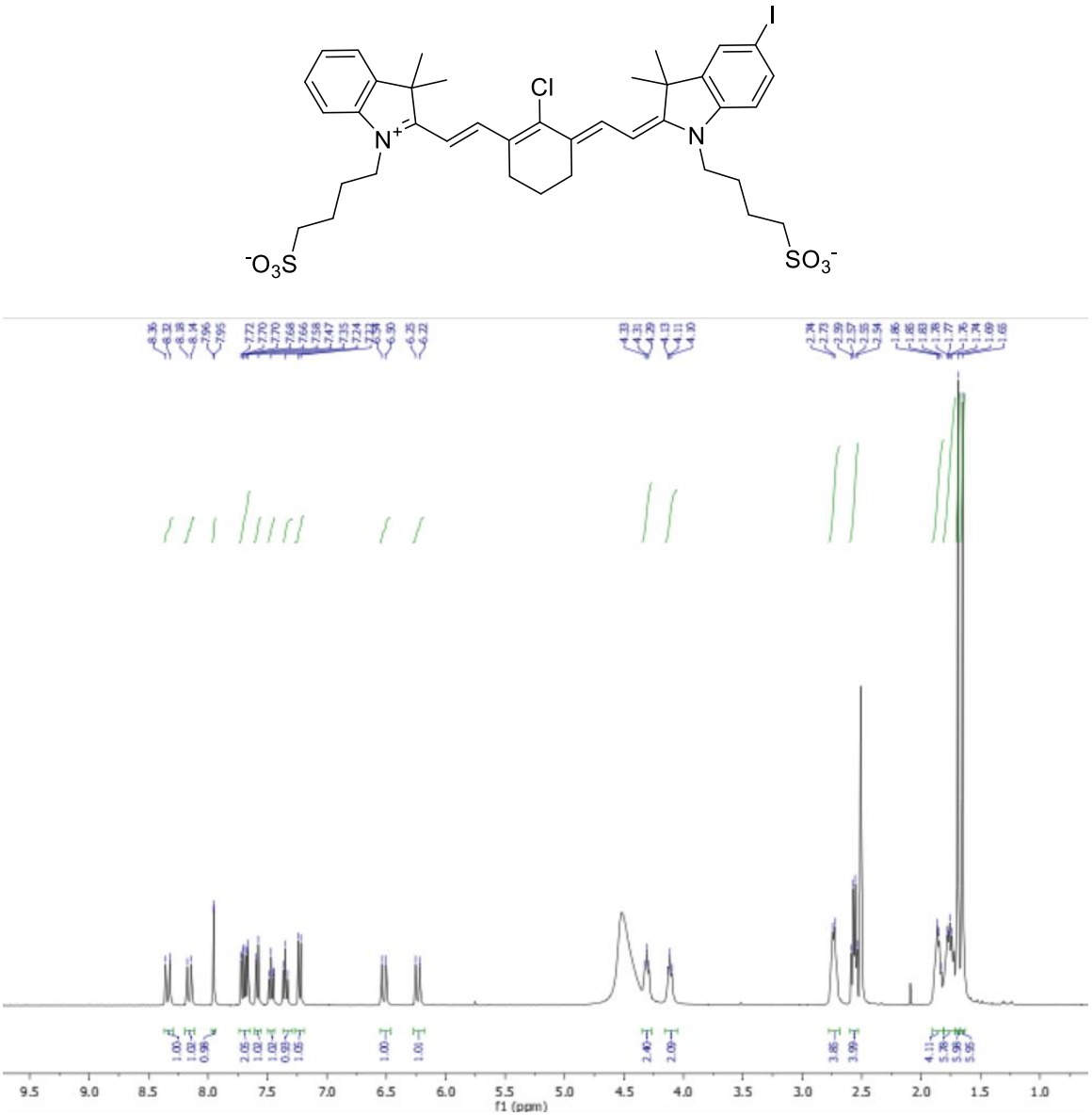

Figure E-S38. ^{1}H NMR spectrum of compound **1bb**

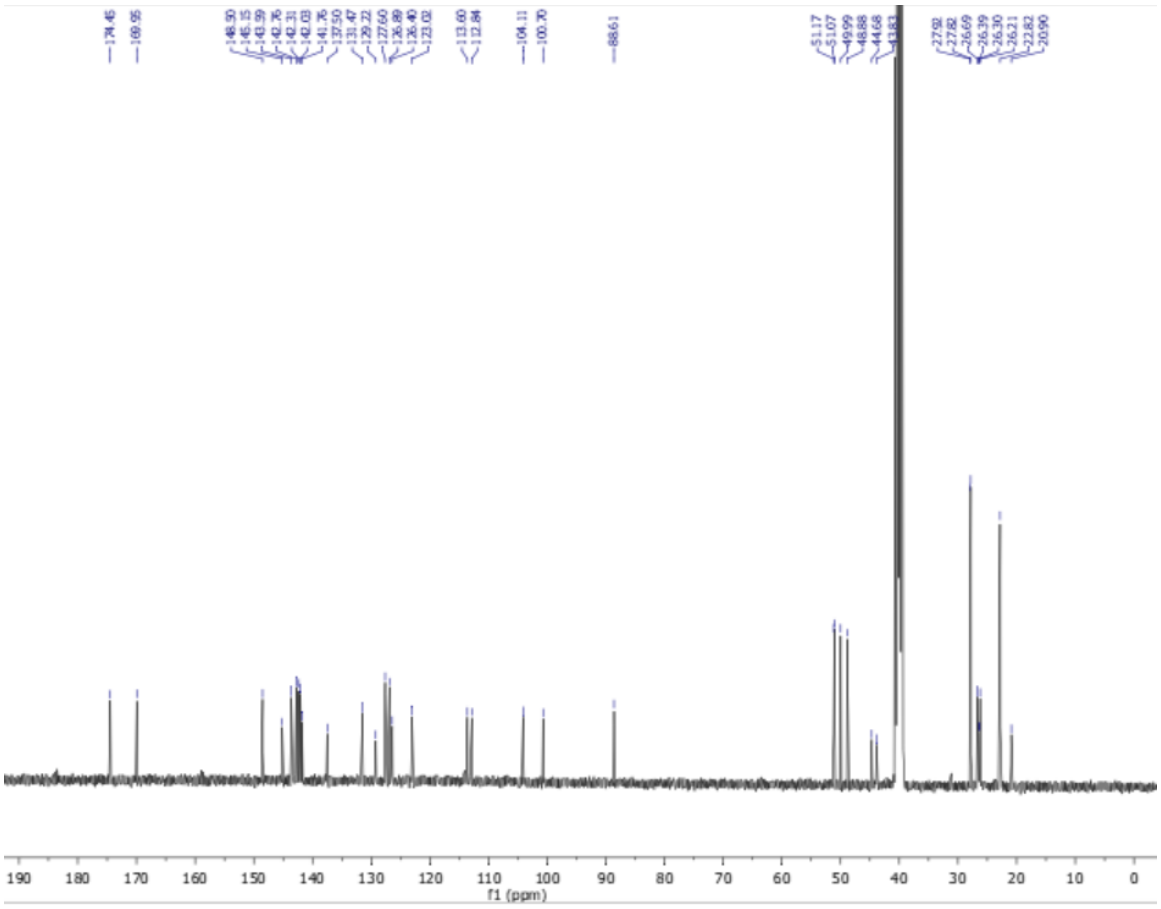

Figure E-S39. ^{13}C NMR spectrum of compound **1bb**

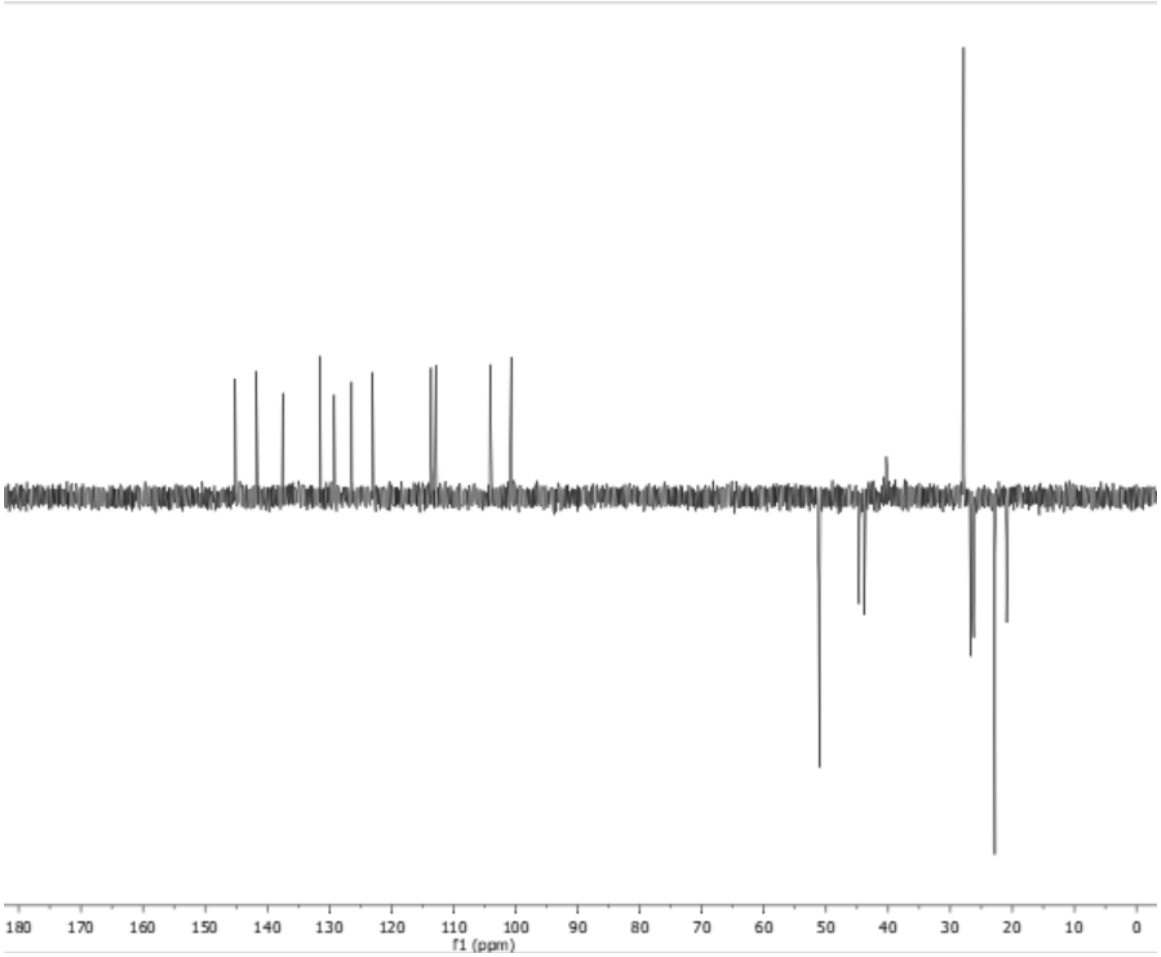

Figure E-S40. DEPT135 NMR spectrum of compound **1bb**

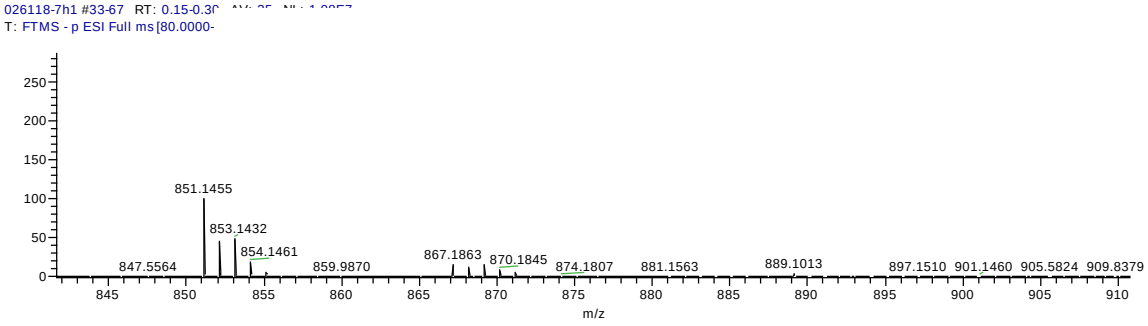

Figure E-S41. HRMS spectrum of compound **1bb**

4-(2-((E)-2-((E)-3-(2-((E)-1-(5-carboxypentyl)-3,3-dimethylindolin-2-ylidene)ethylidene)-2-chlorocyclohex-1-en-1-yl)vinyl)-5-iodo-3,3-dimethyl-3H-indol-1-ium-1-yl)butane-1-sulfonate (1ab)

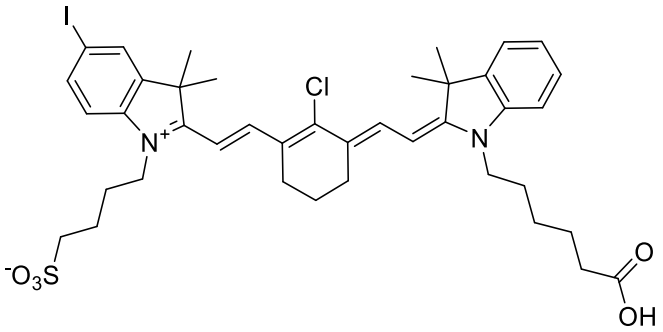

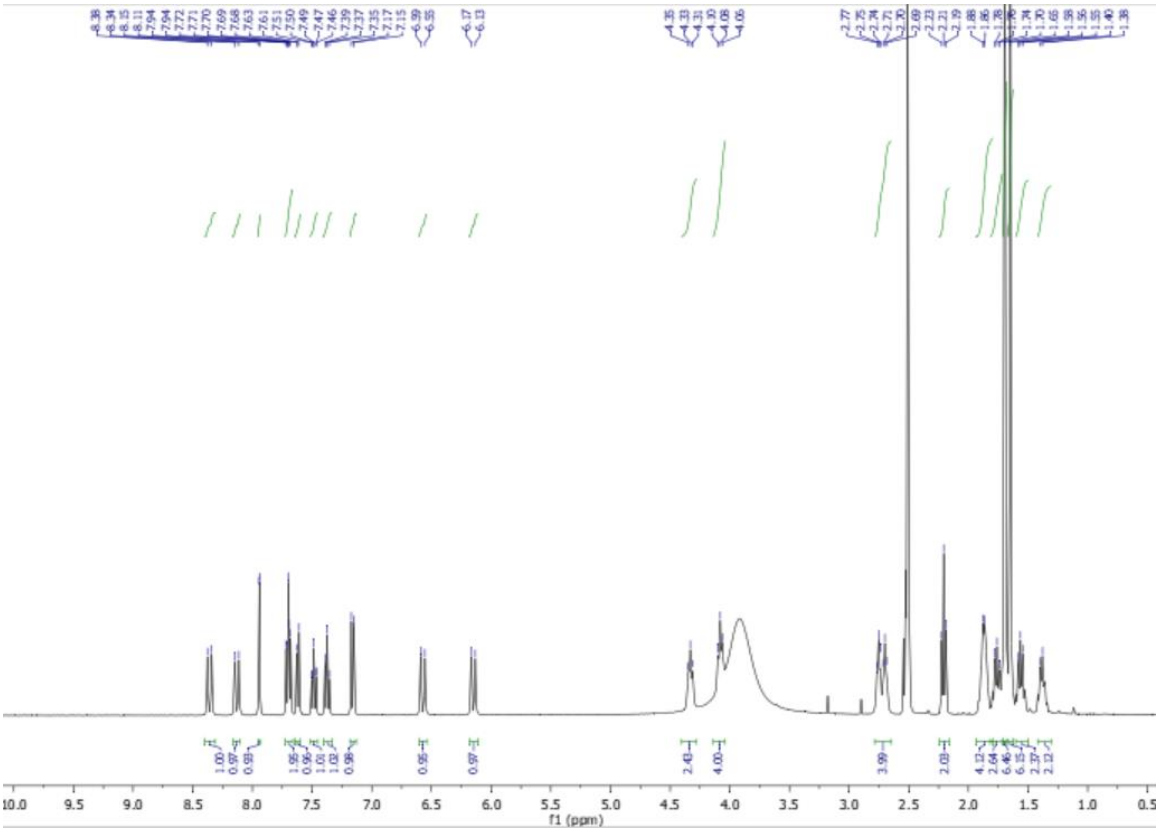

Figure E-S42. ^{1}H spectrum of compound **1ab**

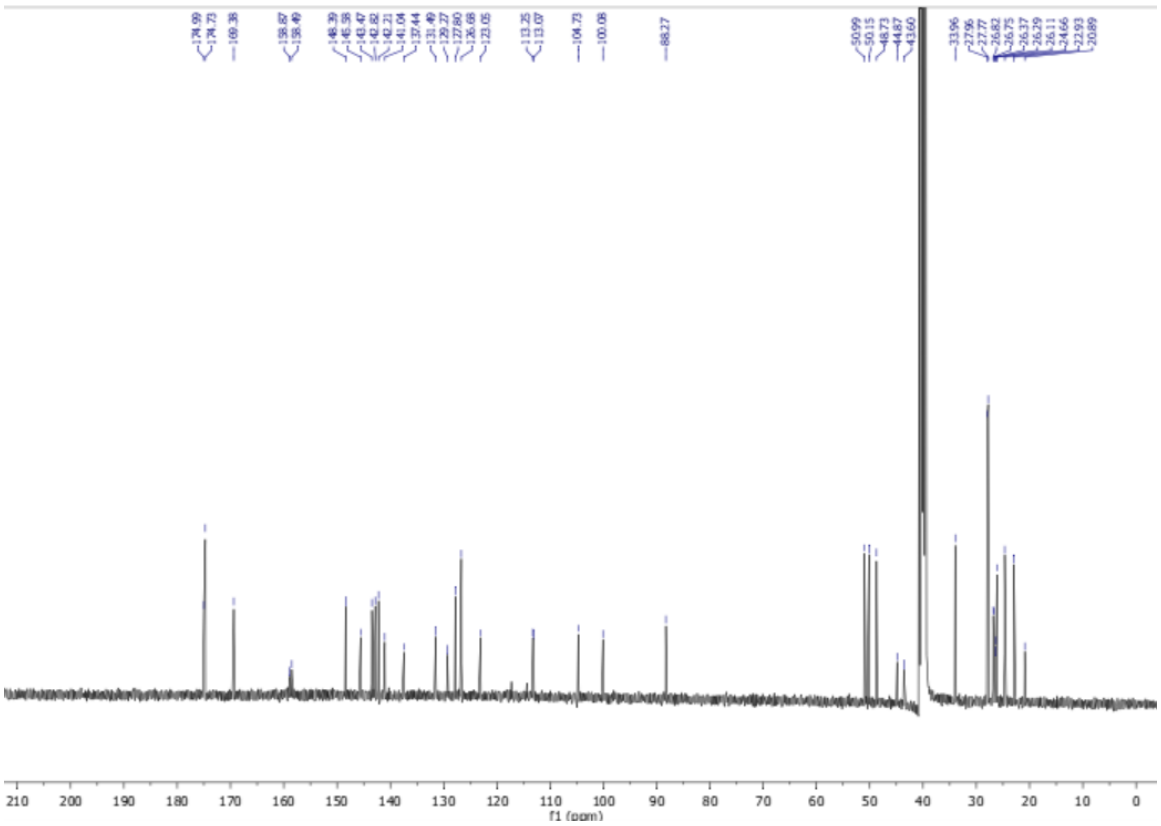

Figure E-S43. ^{13}C spectrum of compound **1ab**

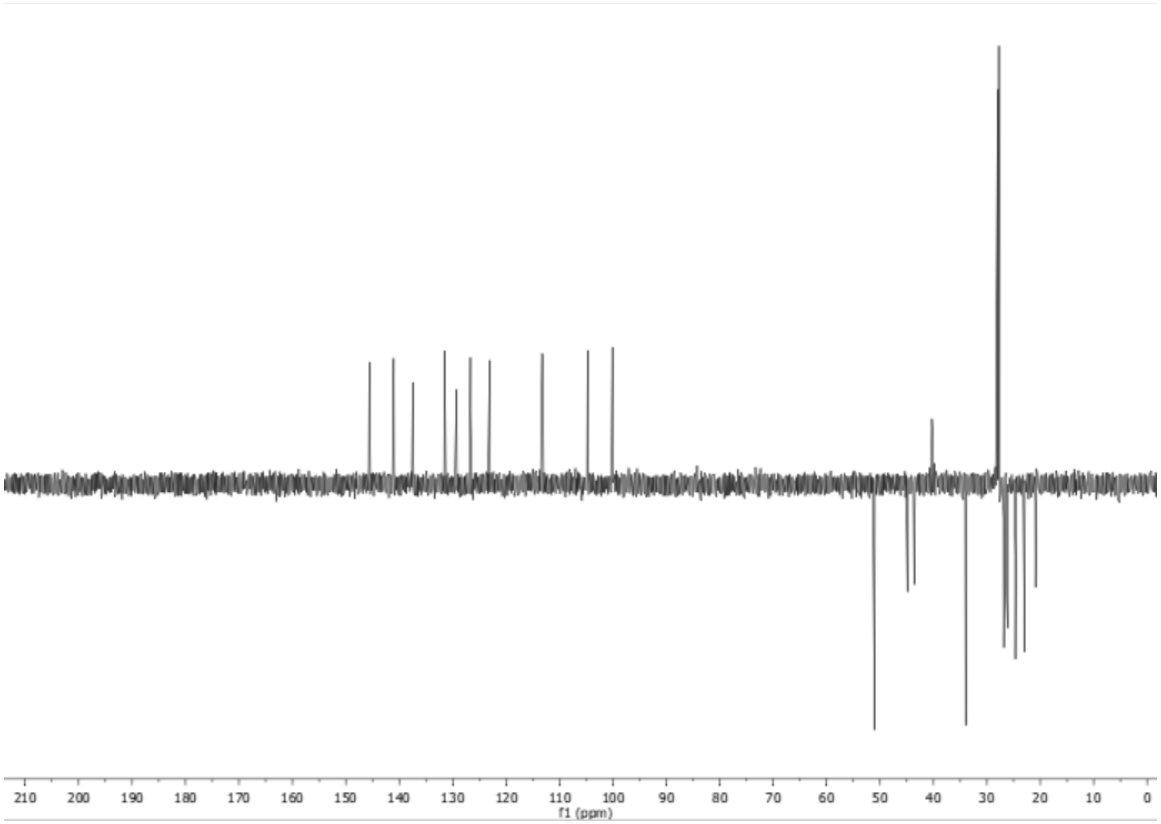

Figure E-S44. DEPT135 spectrum of compound **1ab**

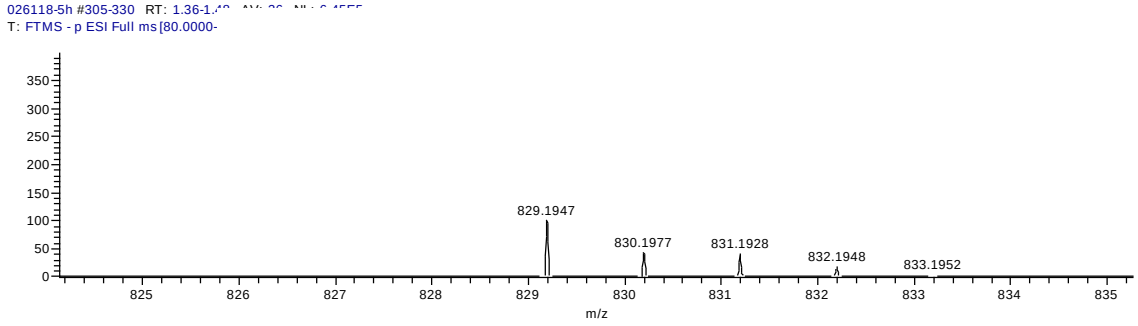

Figure E-S45. MRMS spectrum of compound **1ab**

2-((E)-2-((E)-3-(2-((E)-1-(5-carboxypentyl)-5-iodo-3,3-dimethylindolin-2-ylidene)ethylidene)-2-chlorocyclohex-1-en-1-yl)vinyl)-3,3-dimethyl-1-propyl-3H-indol-1-ium (1ac)

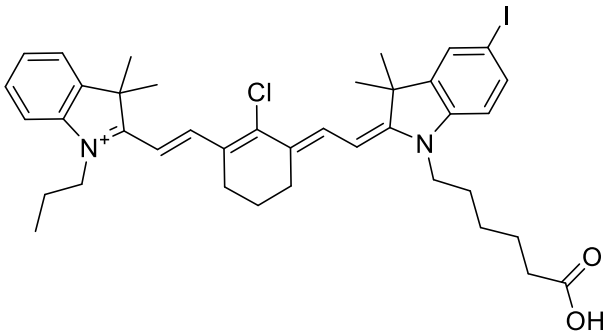

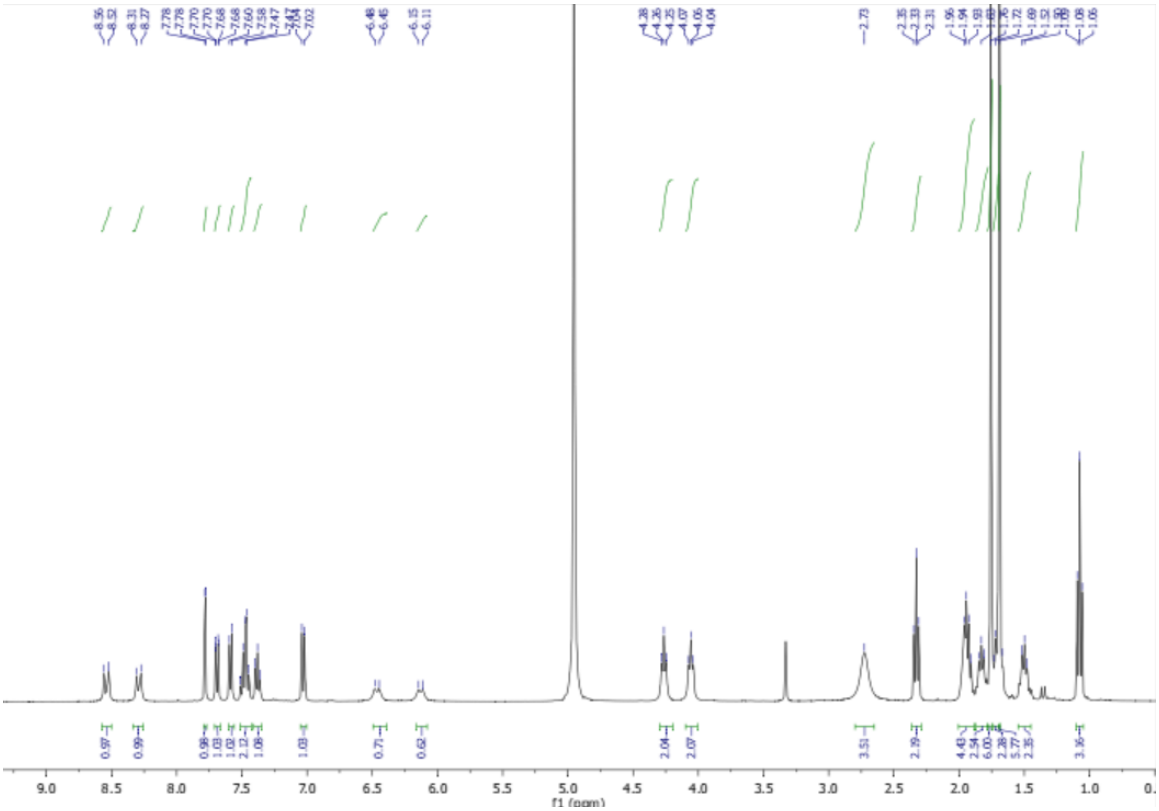

Figure E-S46. ^{1}H spectrum of compound **1ac**

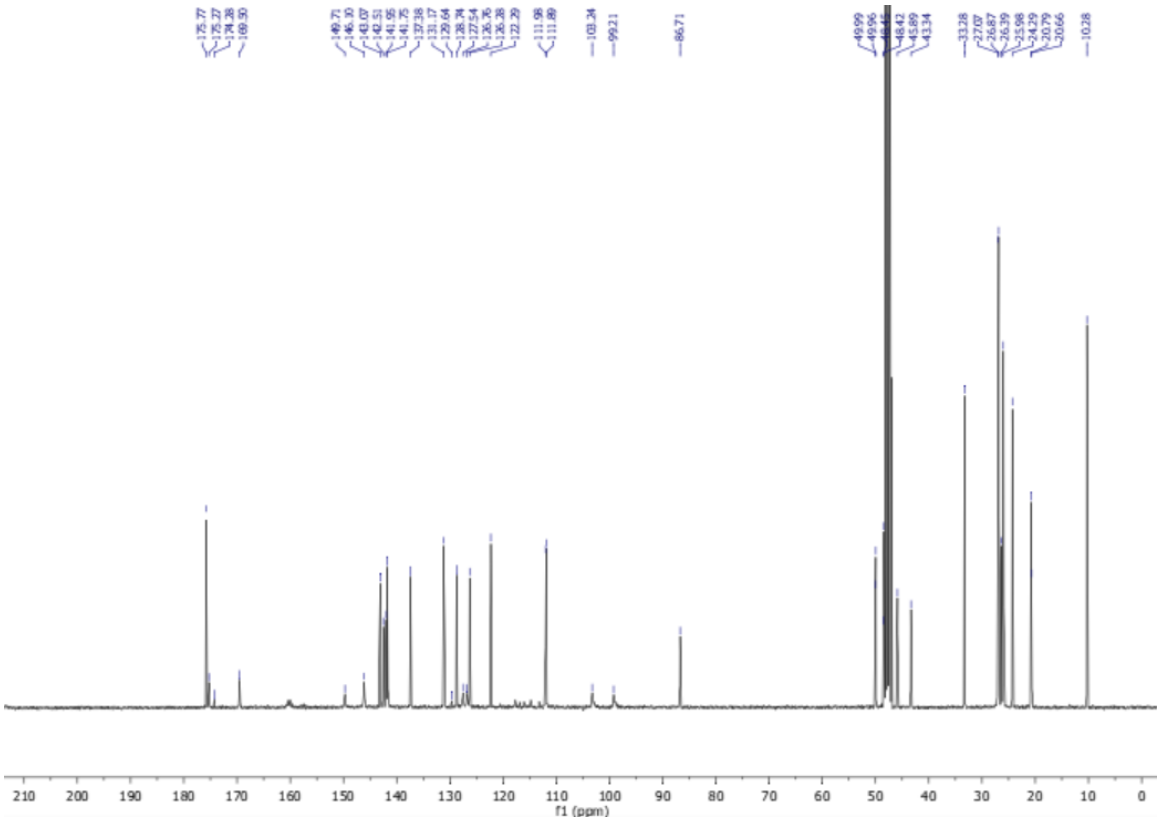

Figure E-S47. ^{13}C spectrum of compound **1ac**

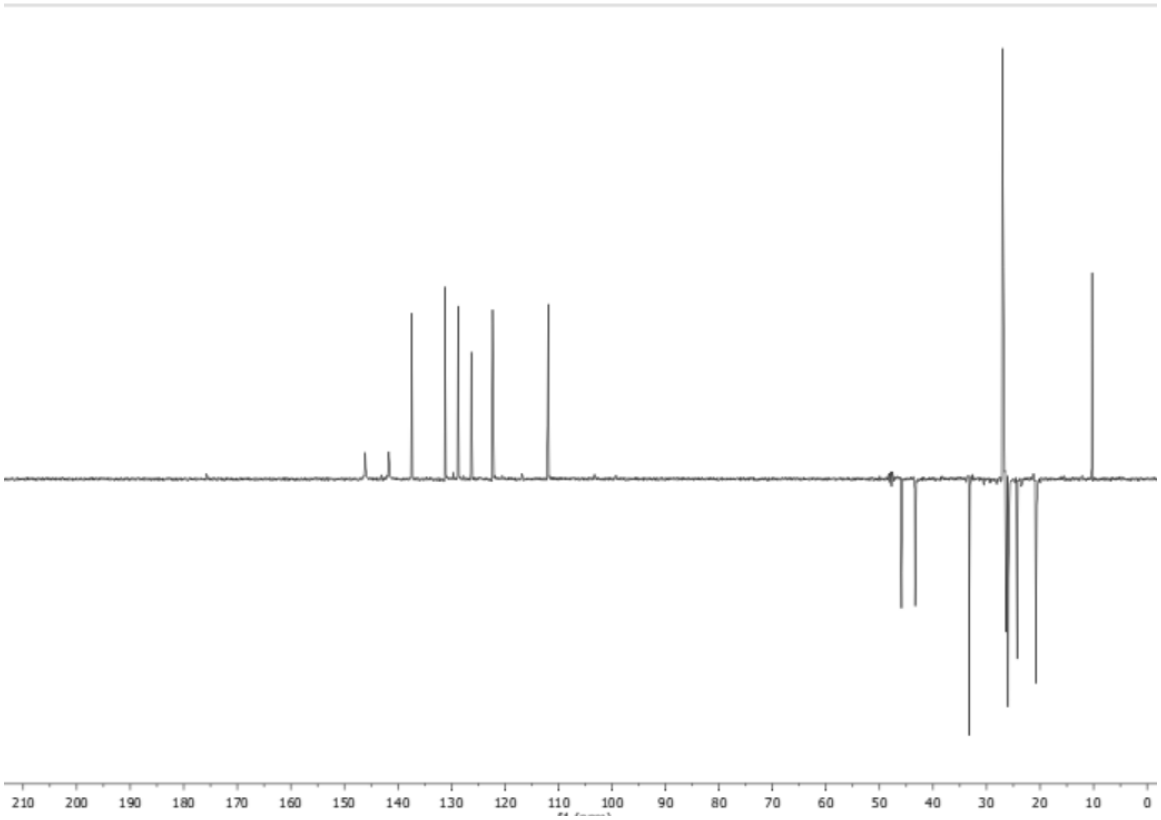

Figure E-S48. DEPT135 spectrum of compound **1ac**

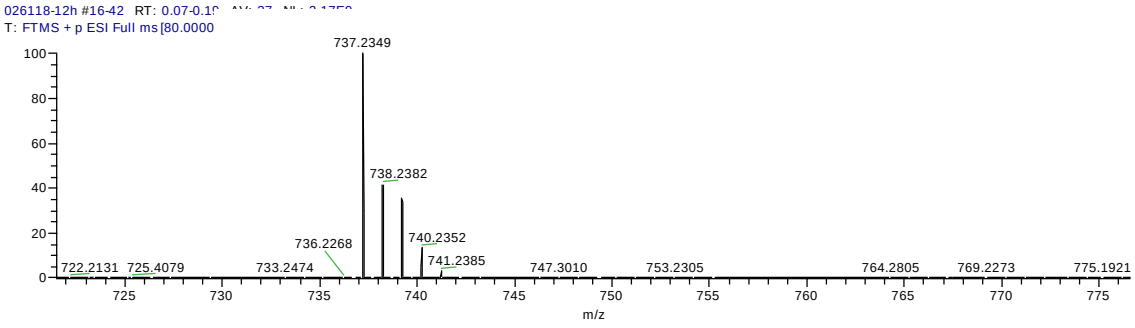

Figure E-S49. HRMS spectrum of compound **1ac**

4-((E)-2-((E)-2-(2-chloro-3-((E)-2-(3,3-dimethyl-1-propyl-3H-indol-1-ium-2-yl)vinyl)cyclohex-2-en-1-ylidene)ethylidene)-5-iodo-3,3-dimethylindolin-1-yl)butane-1-sulfonate (1bc)

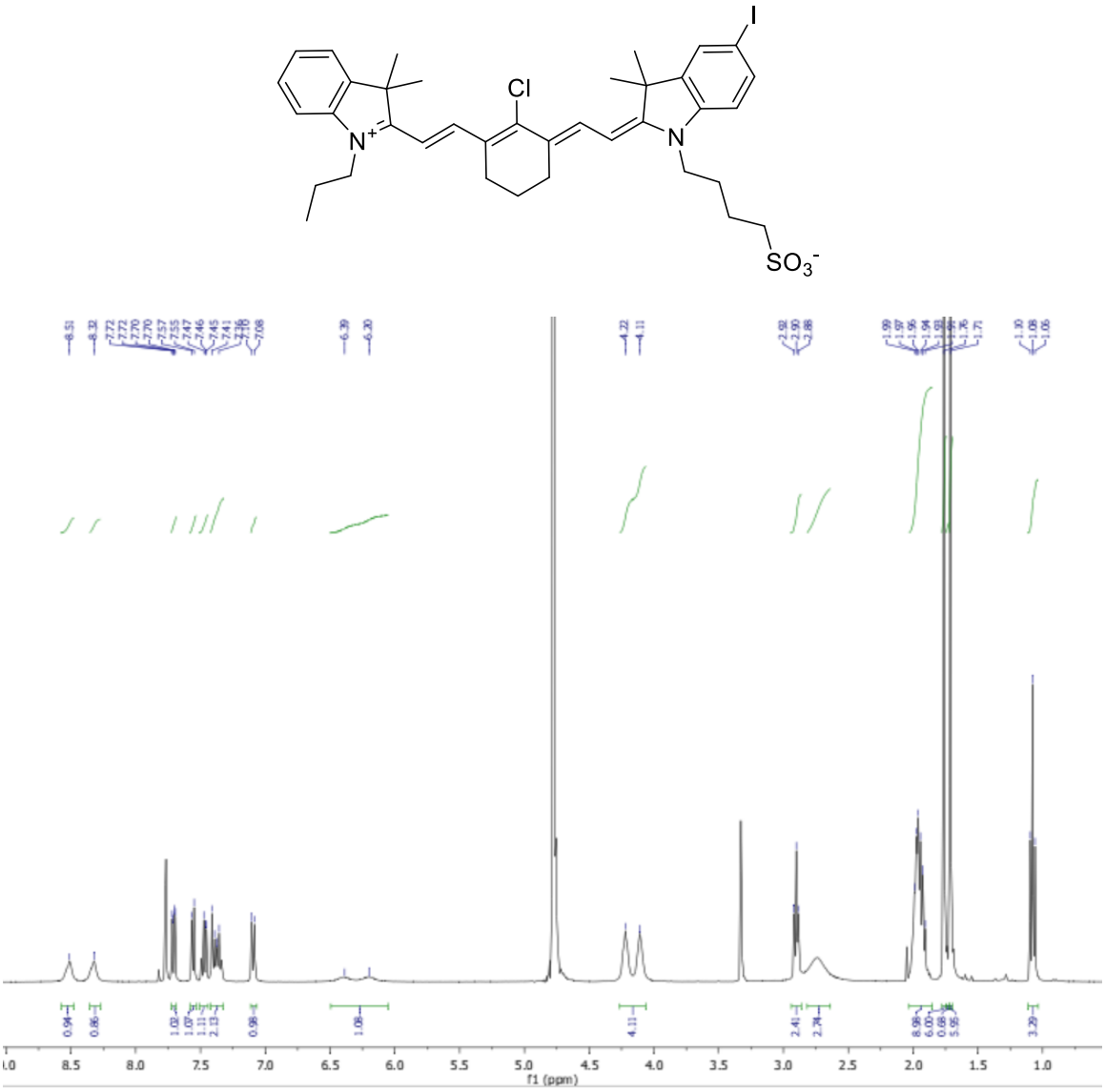

Figure E-S50. ^{1}H spectrum of compound **1bc**

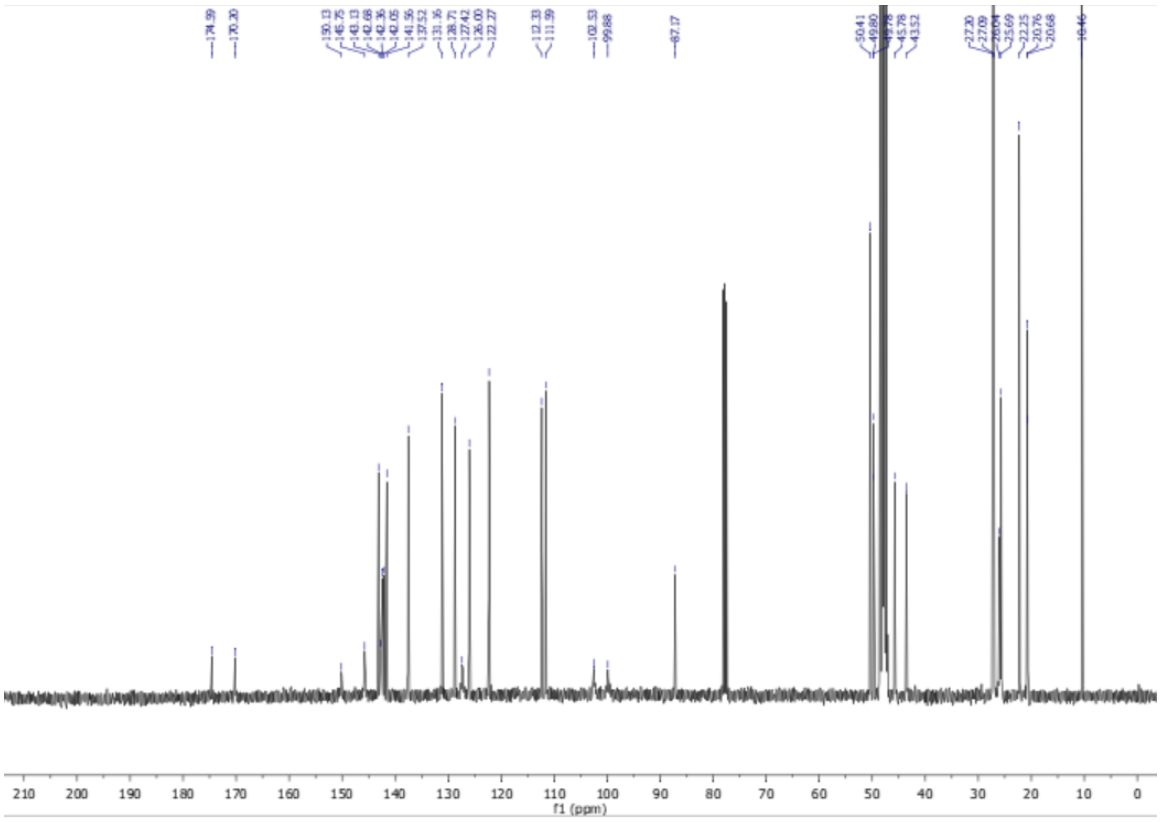

Figure E-S51. ^{13}C spectrum of compound **1bc**

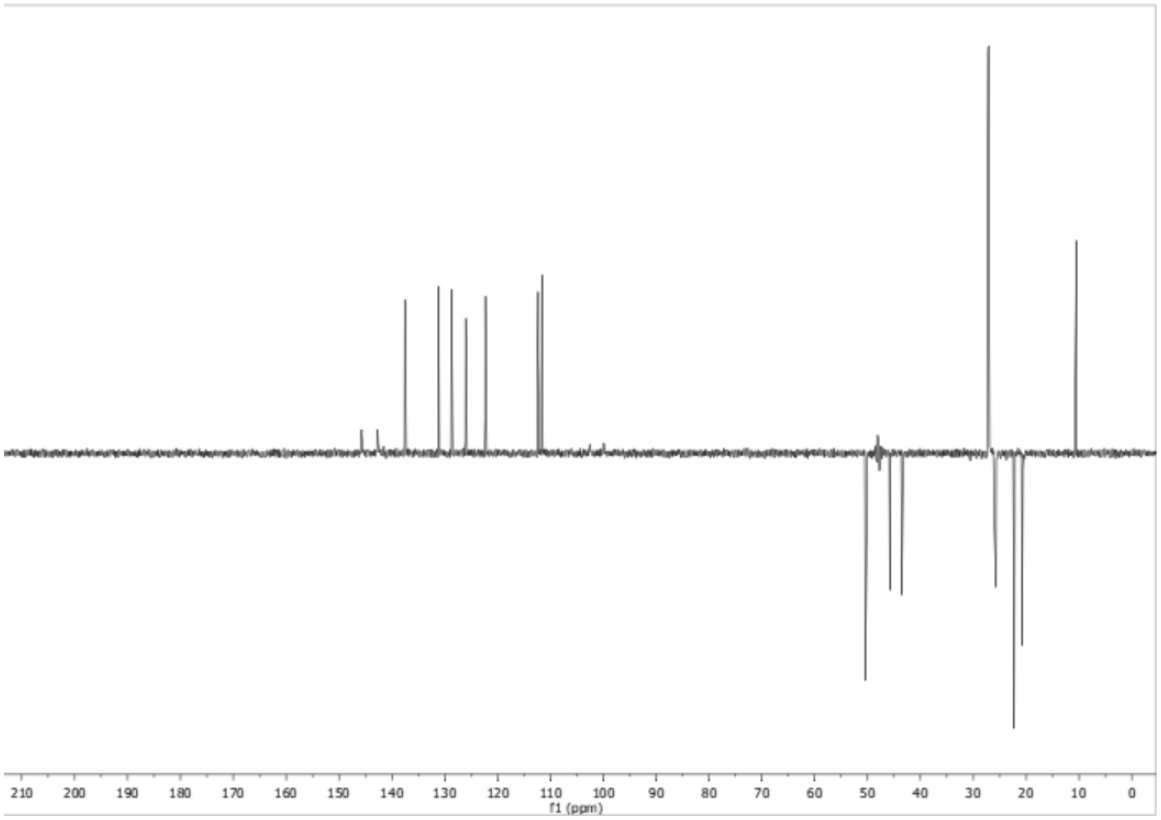

Figure E-S52. DEPT135 spectrum of compound **1bc**

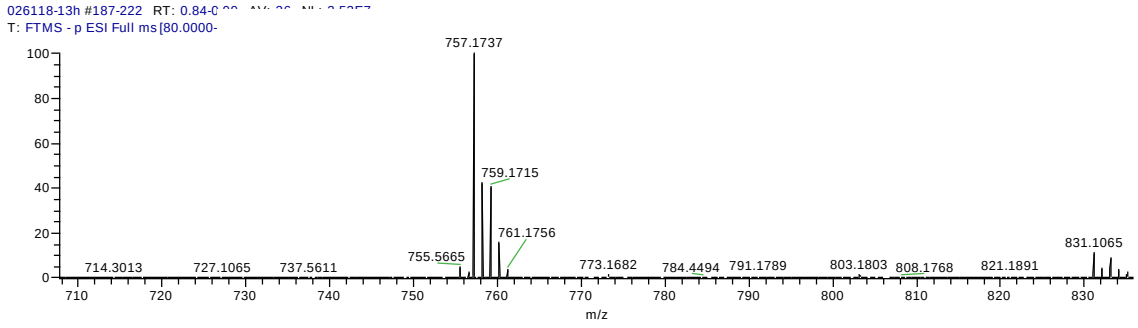

Figure E-S53. HRMS spectrum of compound **1bc**

1-(5-carboxypentyl)-2-((E)-2-((E)-3-(2-((E)-1-(5-carboxypentyl)-5-iodo-3,3-dimethylindolin-2-ylidene)ethylidene)-2-chlorocyclohex-1-en-1-yl)vinyl)-5-iodo-3,3-dimethyl-3H-indol-1-ium (2aa)

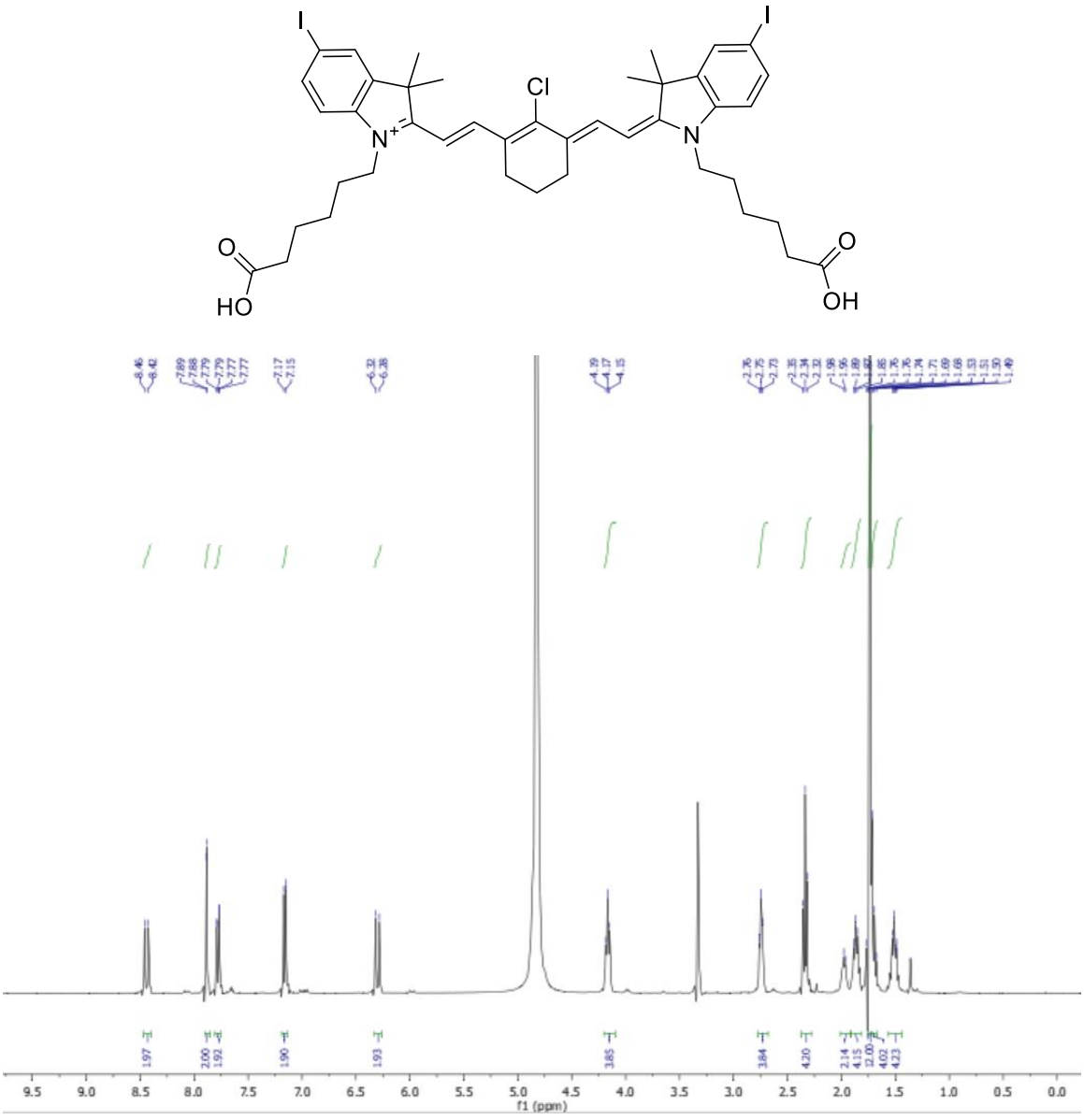

Figure E-S54. ^{1}H spectrum of compound **2aa**

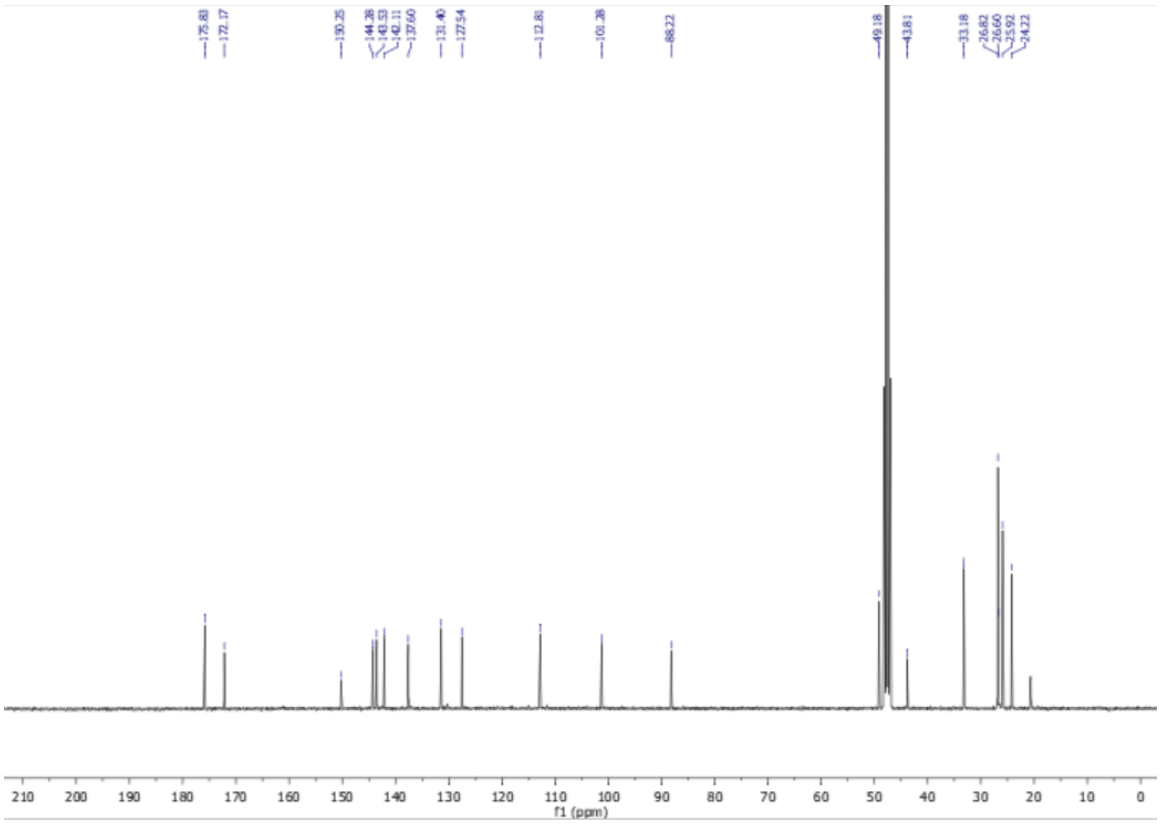

Figure E-S55. ^{13}C spectrum of compound **2aa**

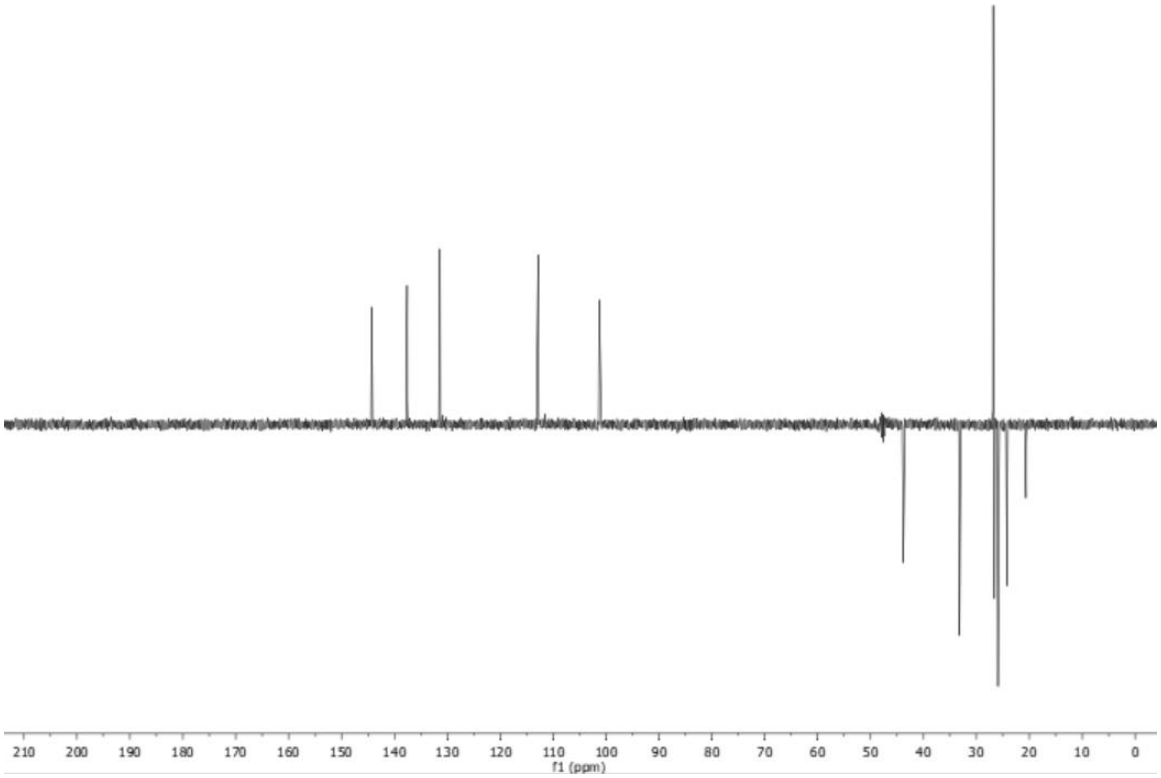

Figure E-S56. DEPT135 spectrum of compound **2aa**

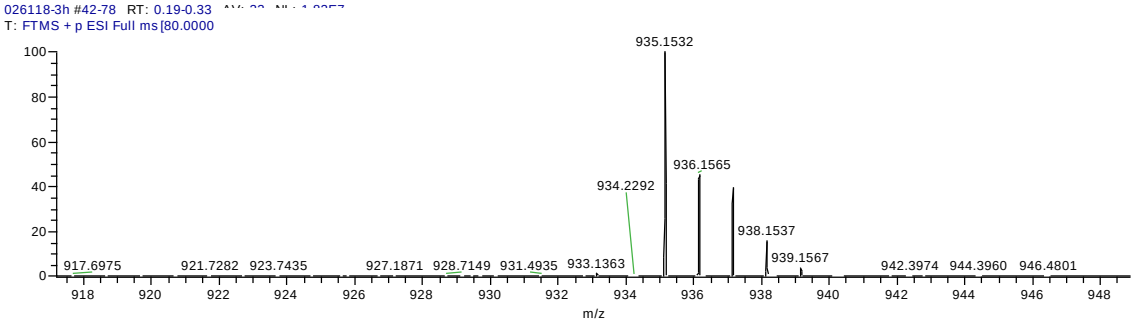

Figure E-S57. HRMS spectrum of compound **2aa**

4-((E)-2-((E)-2-(2-chloro-3-((E)-2-(5-iodo-3,3-dimethyl-1-(4-sulfonatobutyl)-3H-indol-1-ium-2-yl)vinyl)cyclohex-2-en-1-ylidene)ethylidene)-5-iodo-3,3-dimethylindolin-1-yl)butane-1-sulfonate (2bb)

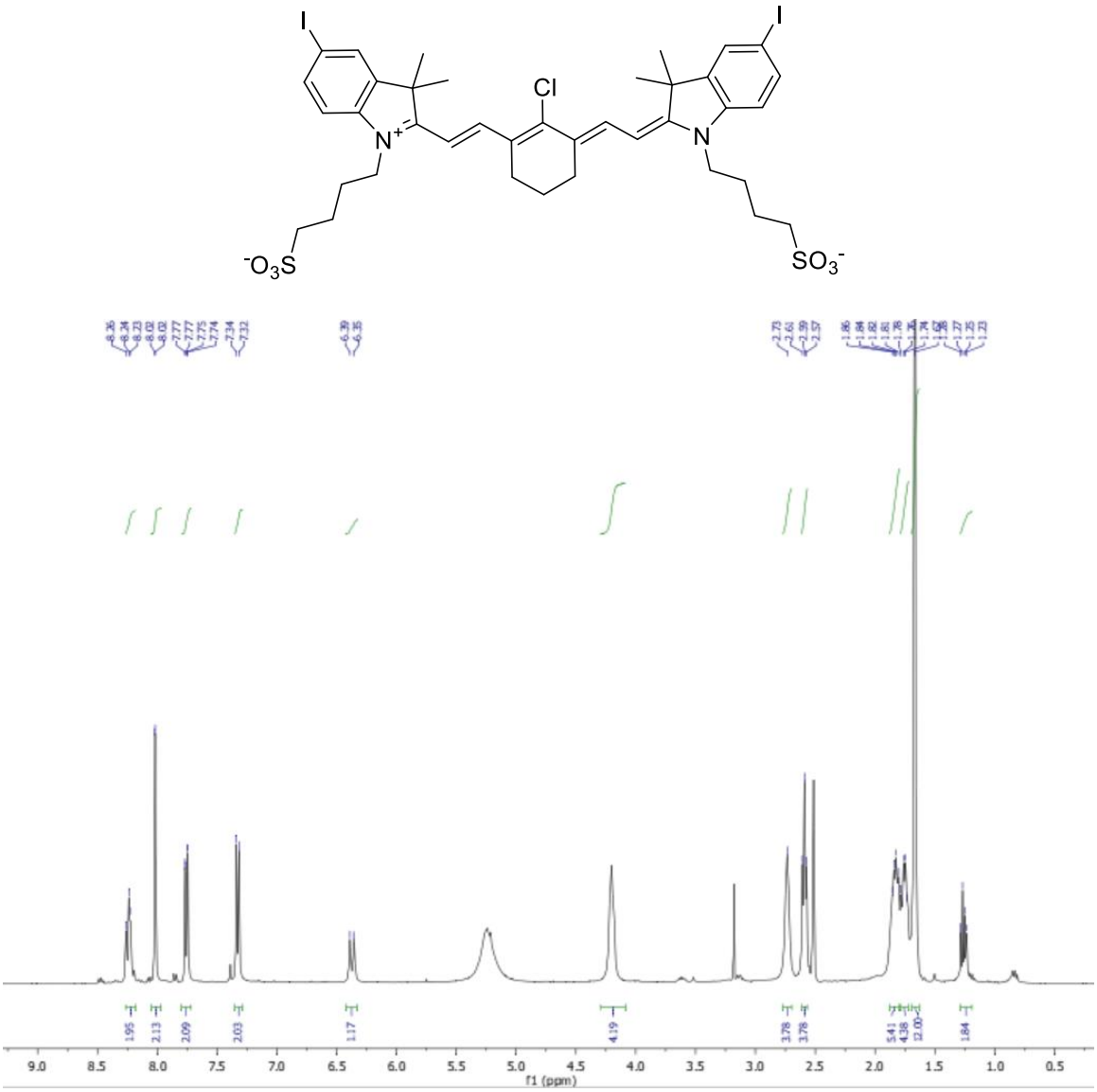

Figure E-S58. ^{1}H spectrum of compound **2bb**

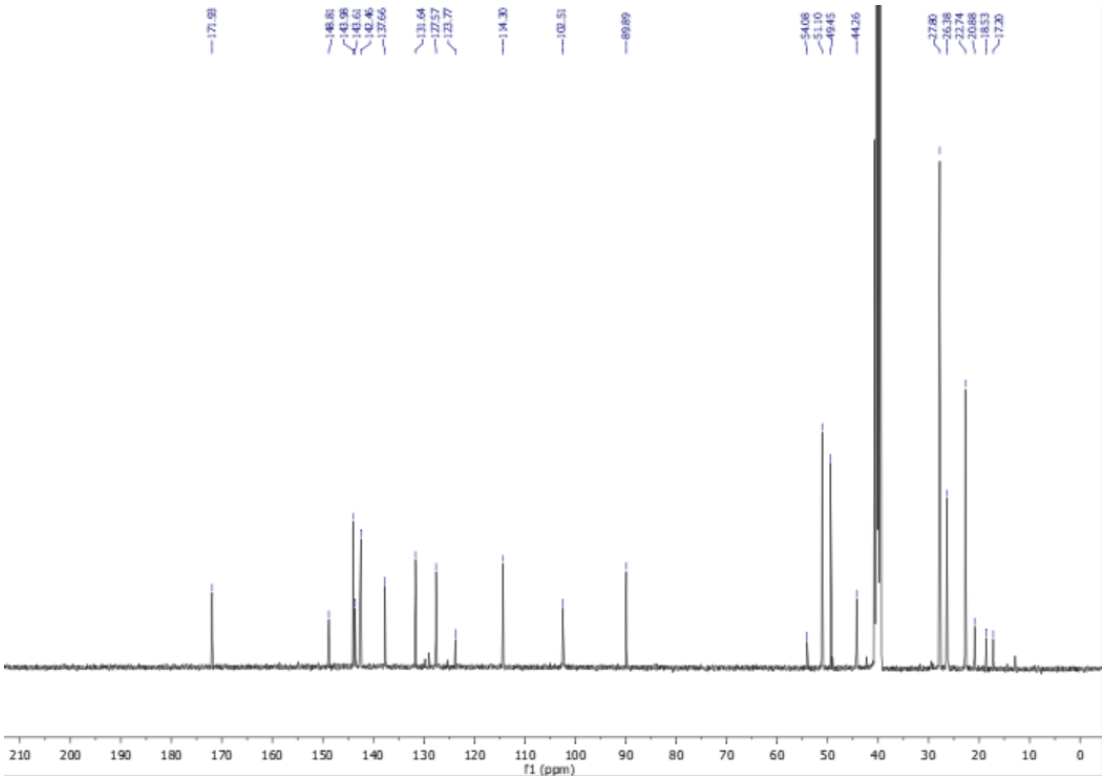

Figure E-S59. ^{13}C spectrum of compound **2bb**

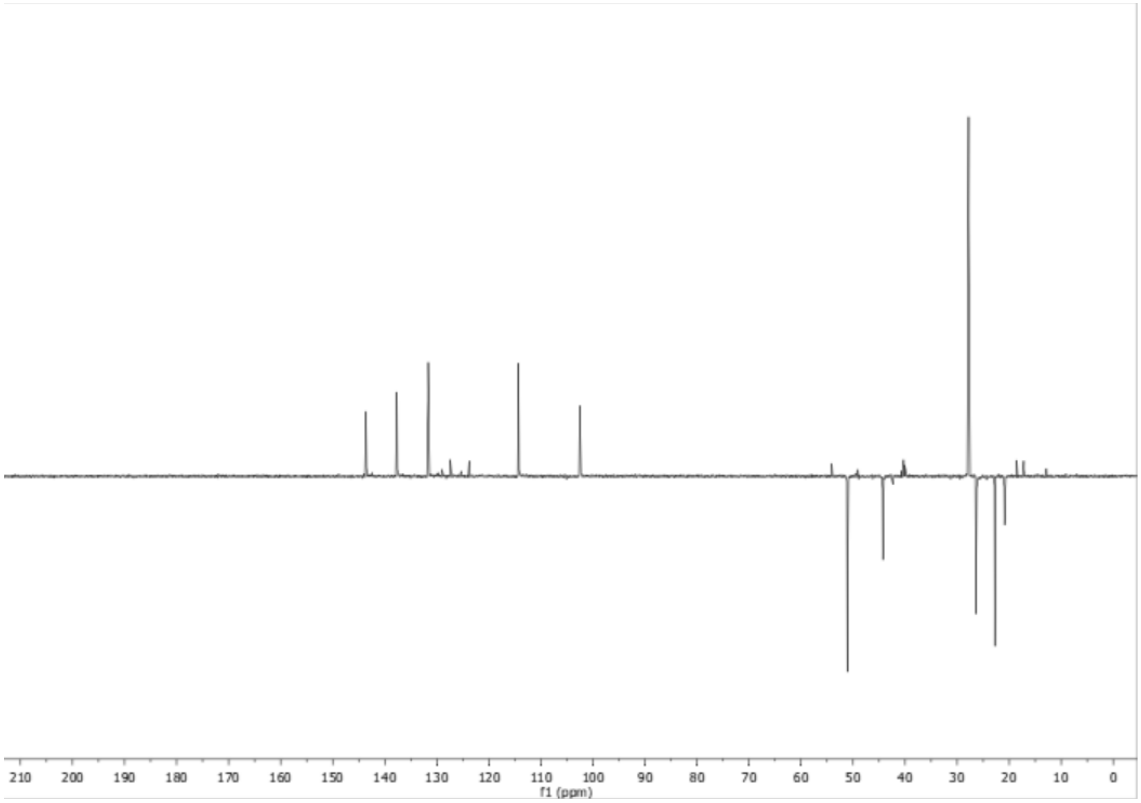

Figure E-S60. DEPT135 spectrum of compound **2bb**

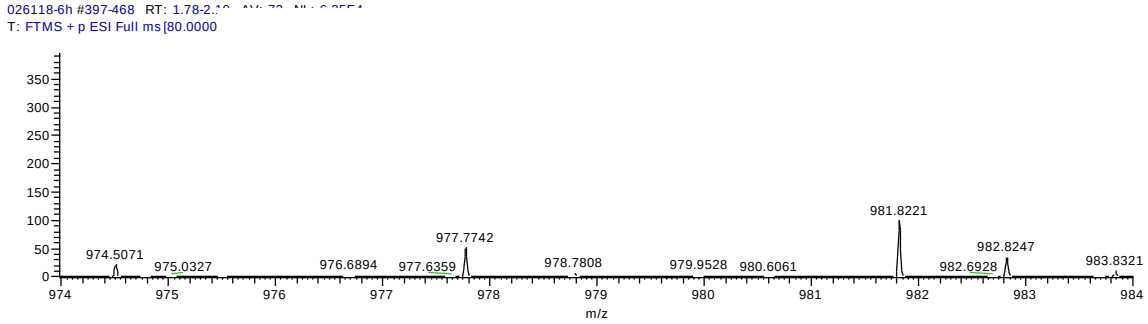

Figure S61. HRMS spectrum of compound **2bb**

2-((E)-2-((E)-2-chloro-3-(2-((E)-5-iodo-3,3-dimethyl-1-propylindolin-2-ylidene)ethylidene)cyclohex-1-en-1-yl)vinyl)-5-iodo-3,3-dimethyl-1-propyl-3H-indol-1-ium **(2cc)**

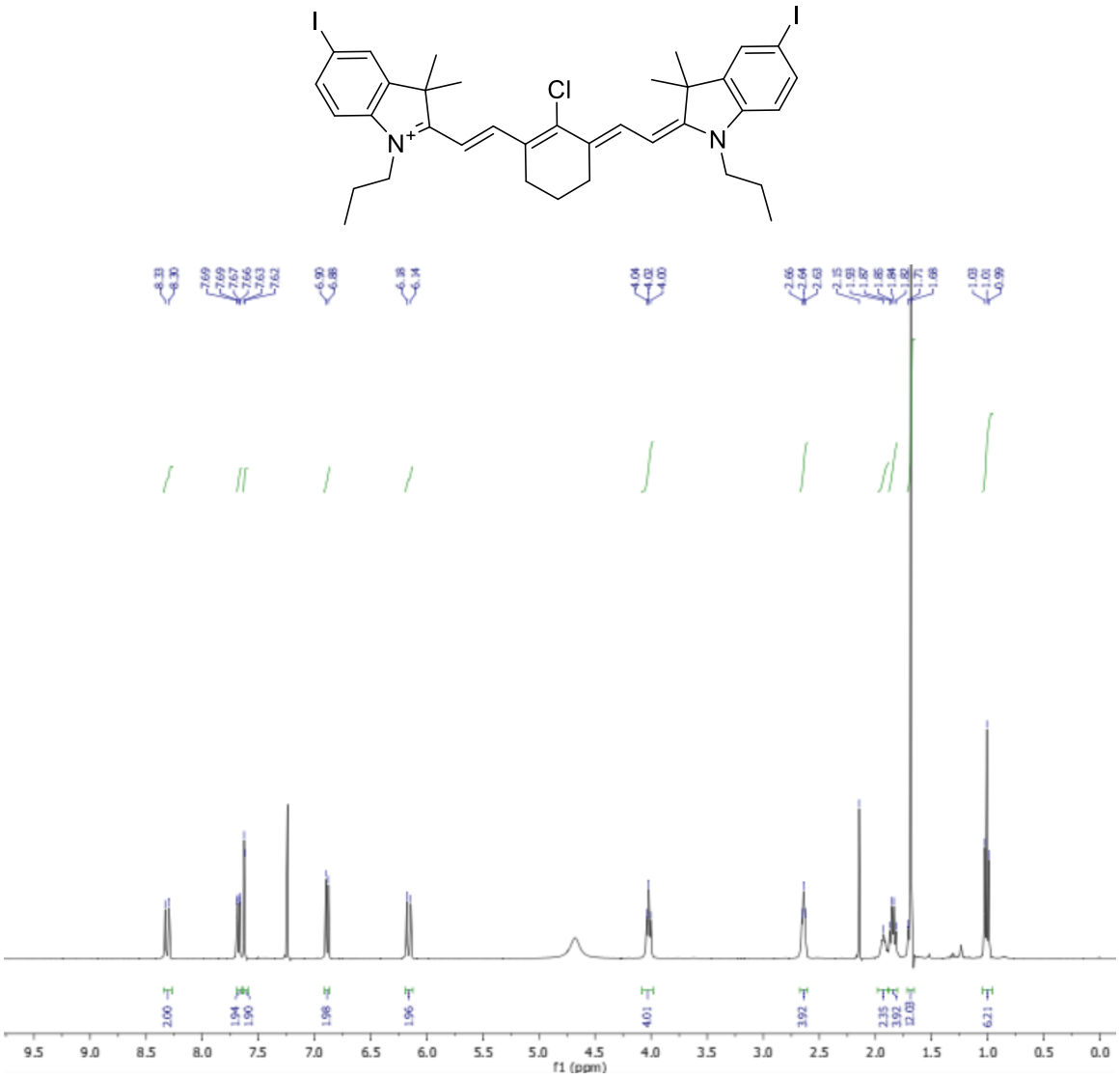

Figure E-S62. [1]H spectrum of compound **2cc**

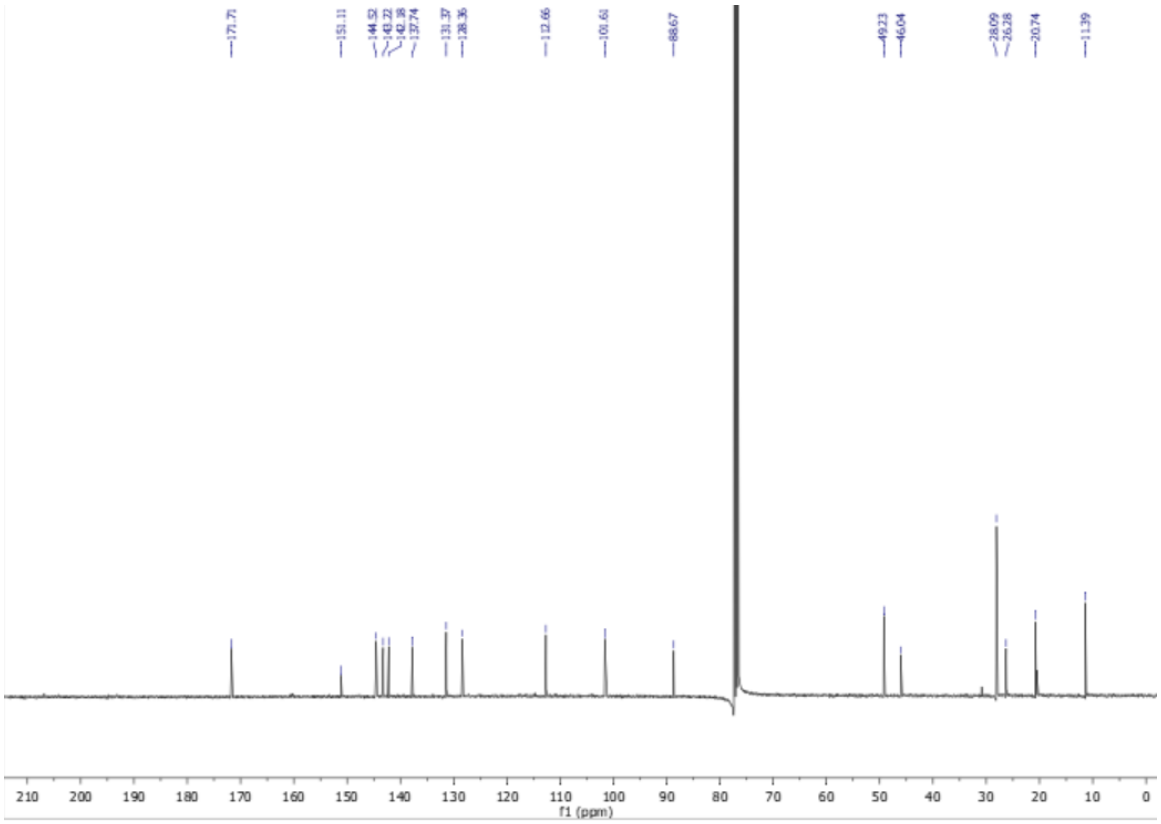

Figure E-S63. ^{13}C spectrum of compound **2cc**

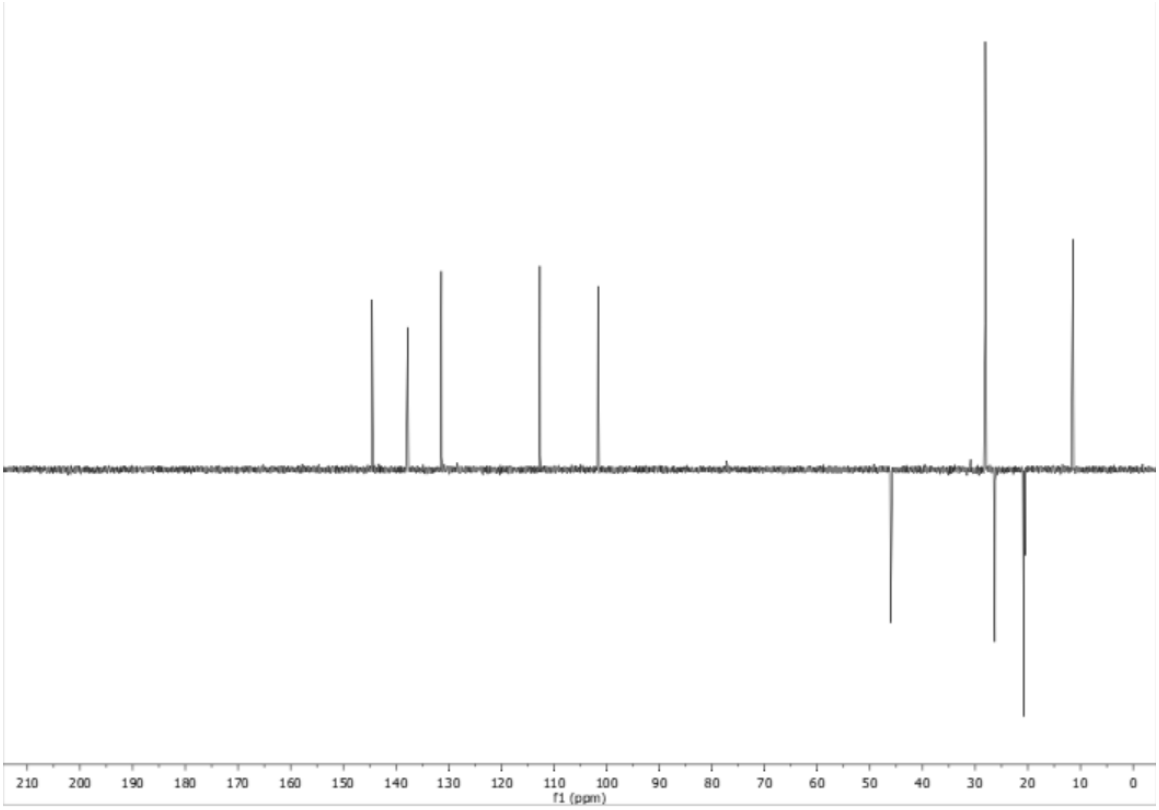

Figure E-S64. DEPT135 spectrum of compound **2cc**

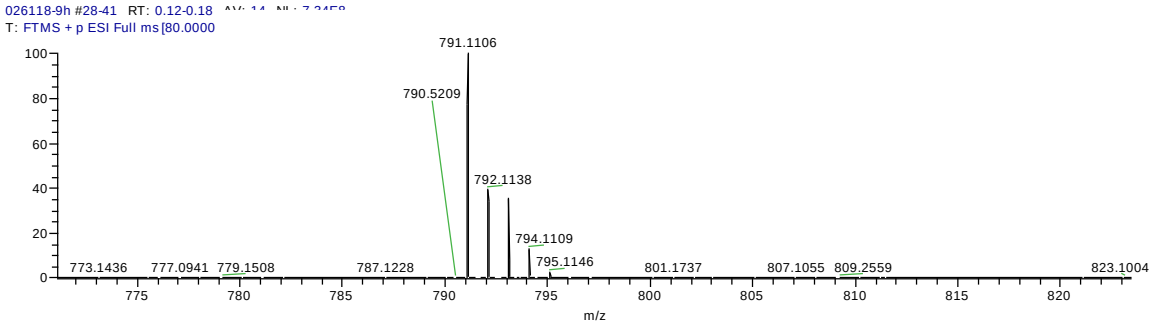

Figure E-S65. HRMS spectrum of compound **2cc**

4-(2-((E)-2-((E)-3-(2-((E)-1-(5-carboxypentyl)-5-iodo-3,3-dimethylindolin-2-ylidene)ethylidene)-2-chlorocyclohex-1-en-1-yl)vinyl)-5-iodo-3,3-dimethyl-3H-indol-1-ium-1-yl)butane-1-sulfonate (2ab)

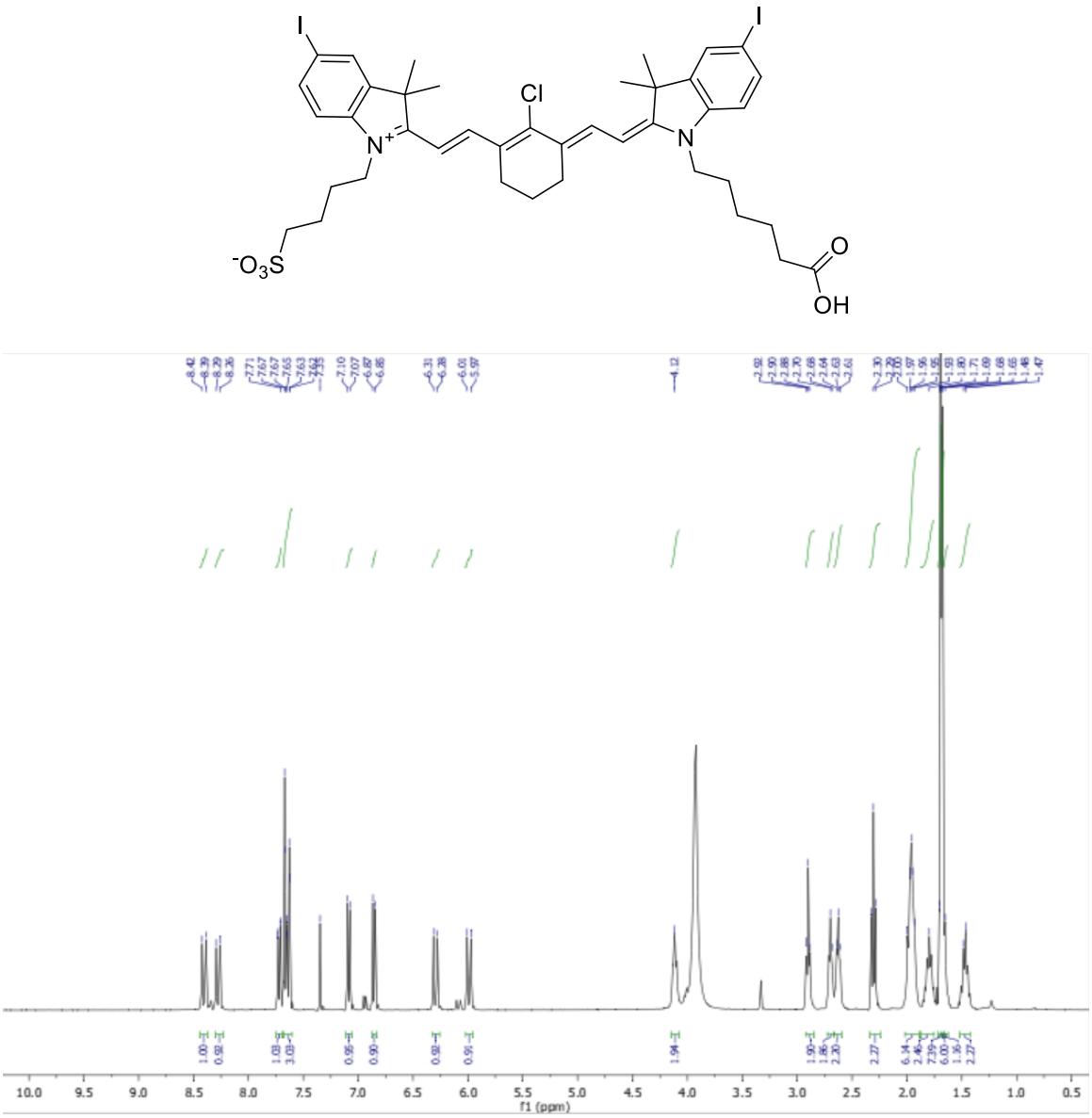

Figure E-S66. ^{1}H spectrum of compound **2ab**

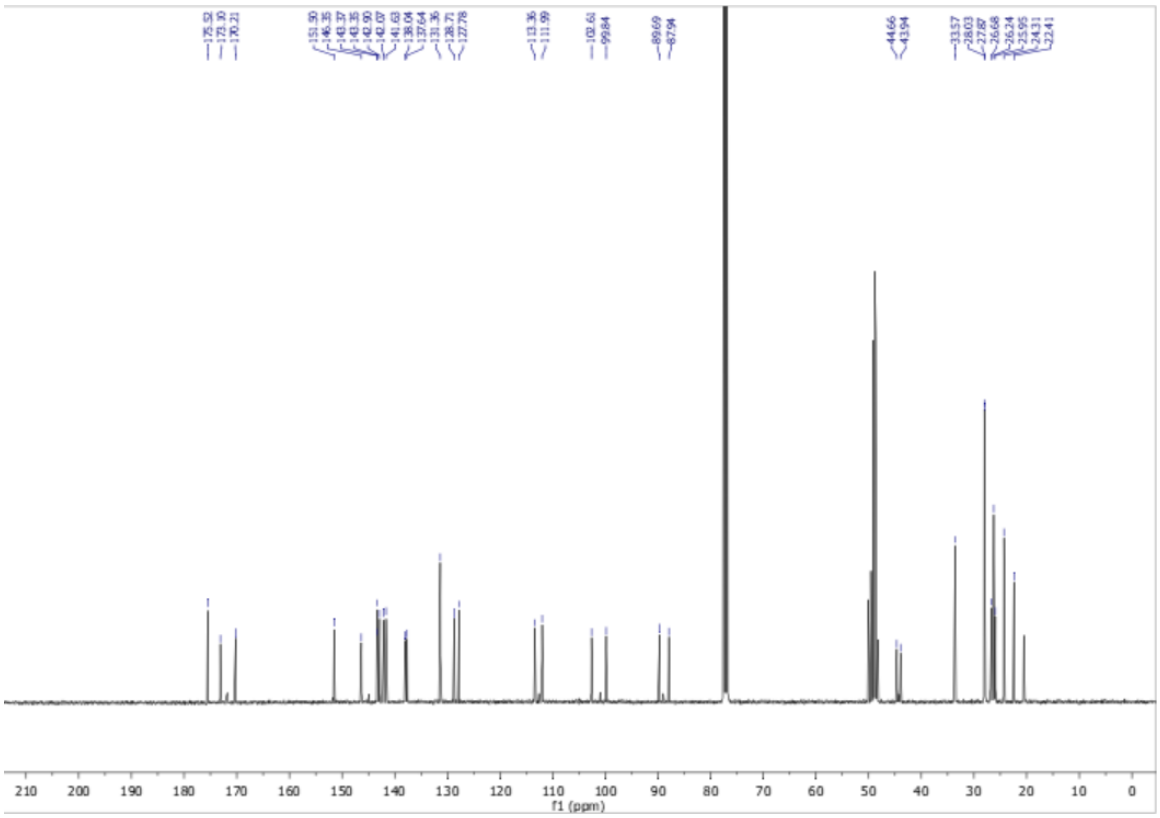

Figure E-S67. ^{13}C spectrum of compound **2ab**

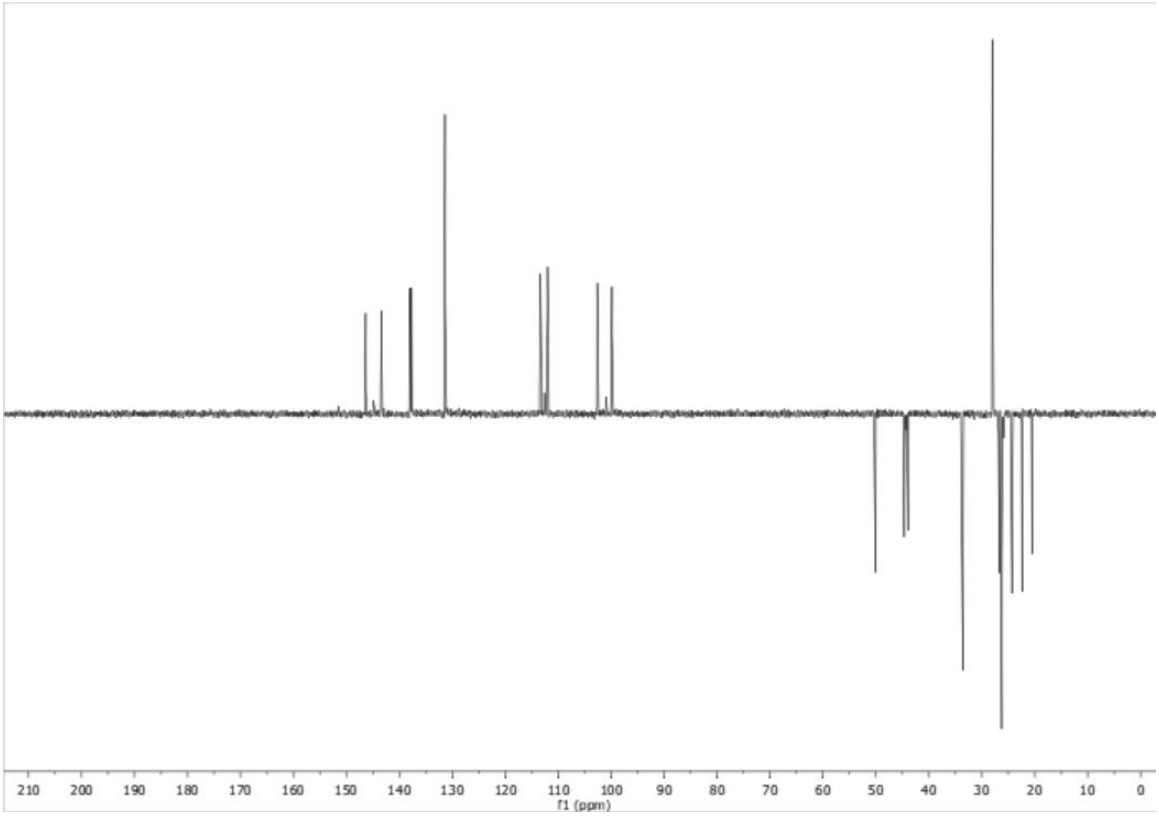

Figure E-S68. DEPT135 spectrum of compound **2ab**

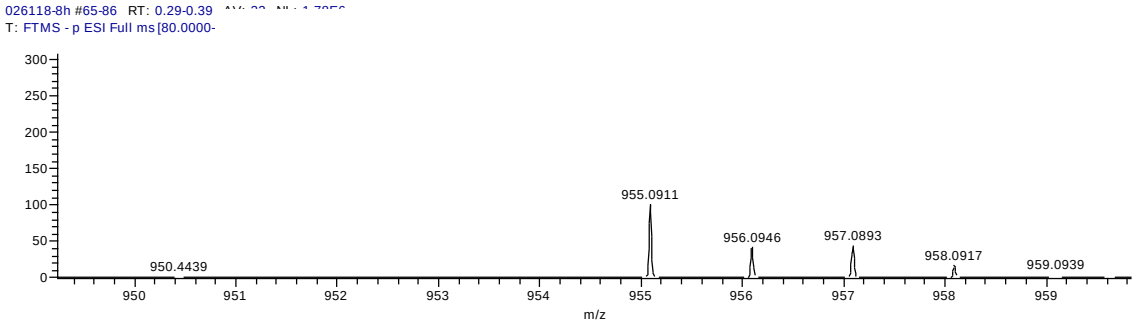

Figure E-S69. HRMS spectrum of compound **2ab**

2-((E)-2-((E)-3-(2-((E)-1-(5-carboxypentyl)-5-iodo-3,3-dimethylindolin-2-ylidene)ethylidene)-2-chlorocyclohex-1-en-1-yl)vinyl)-5-iodo-3,3-dimethyl-1-propyl-3H-indol-1-ium (2ac)

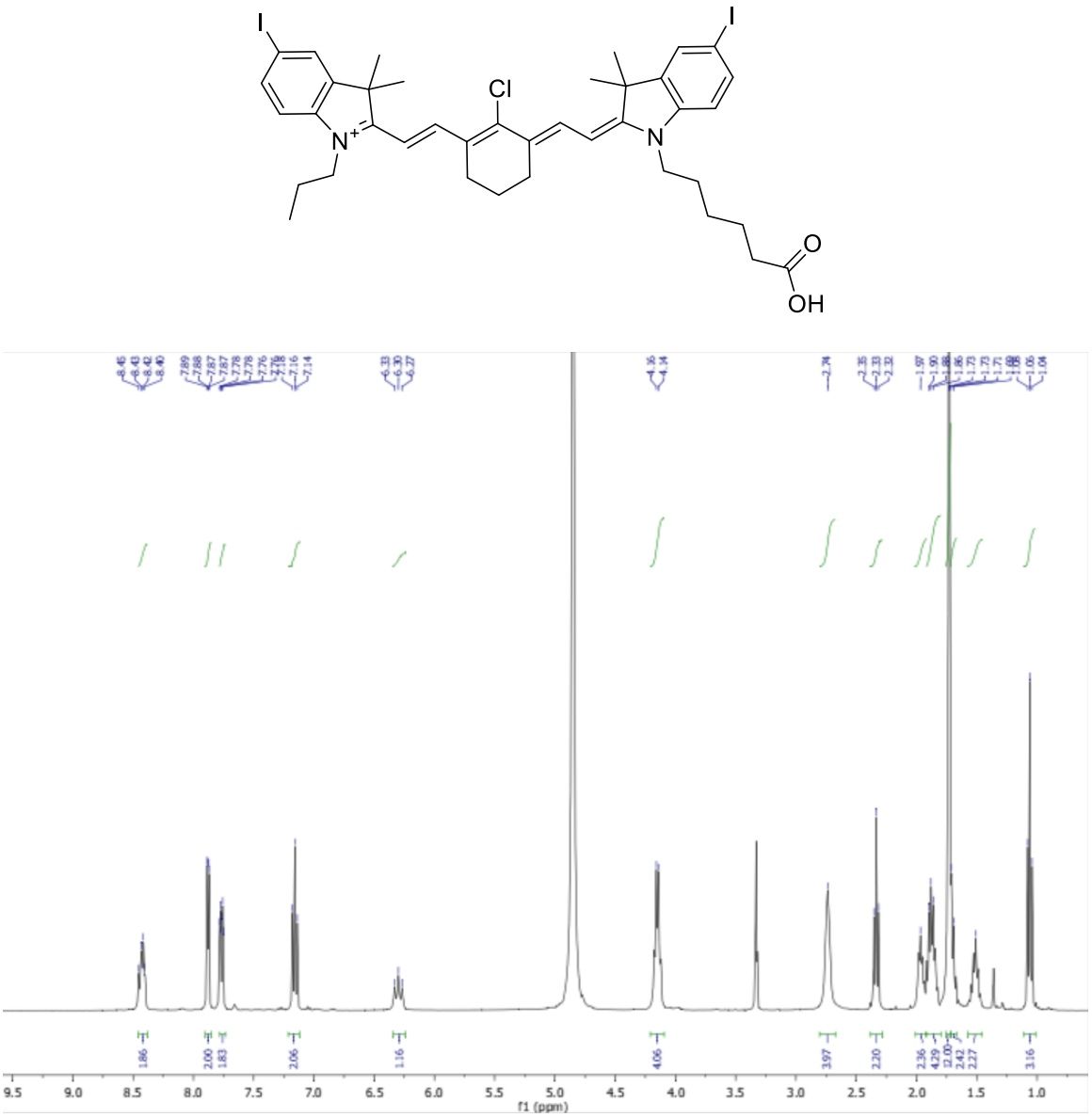

Figure E-S70. ^{1}H spectrum of compound **2ac**

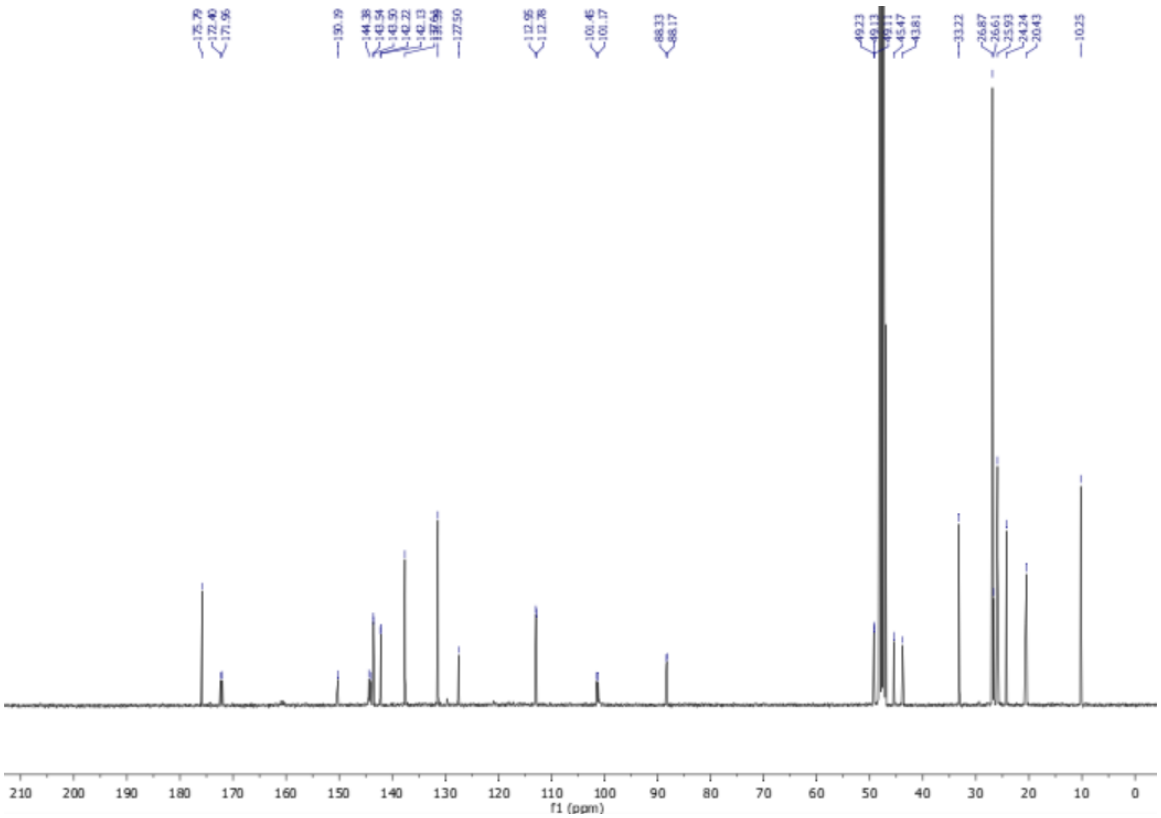

Figure E-S71. ^{13}C spectrum of compound **2ac**

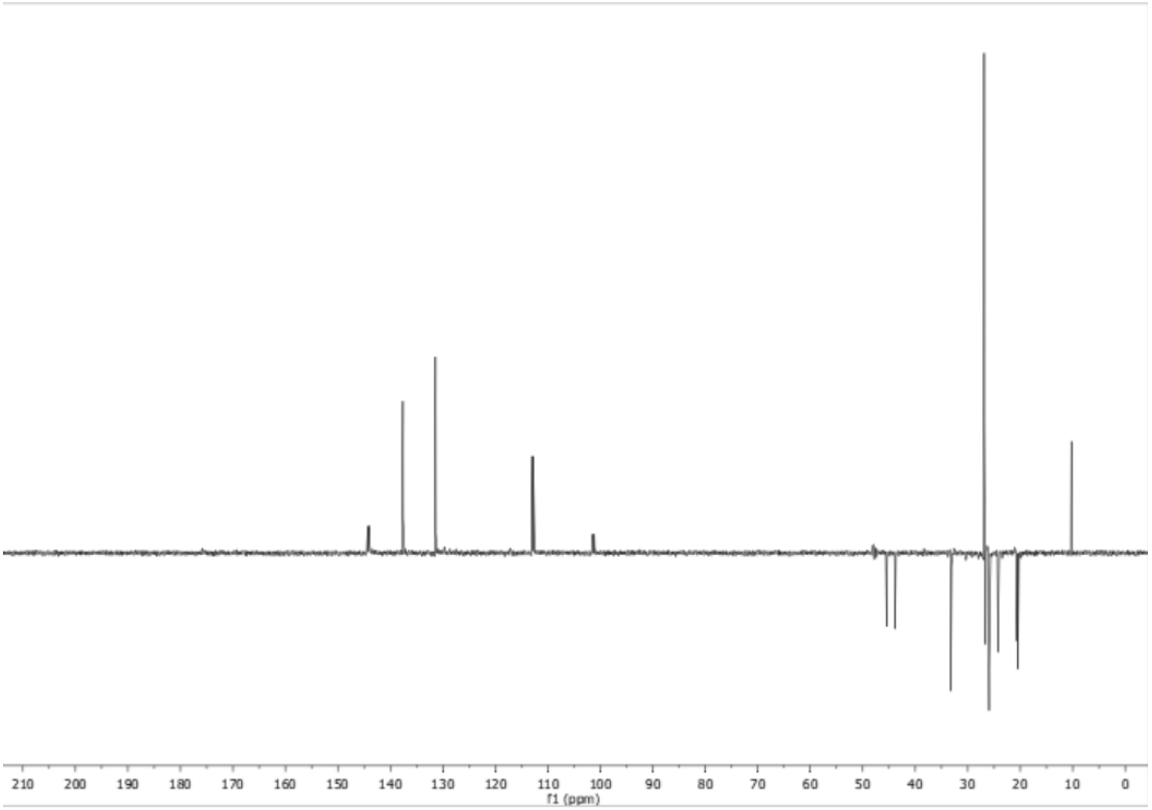

Figure E-S72. DEPT135 spectrum of compound **2ac**

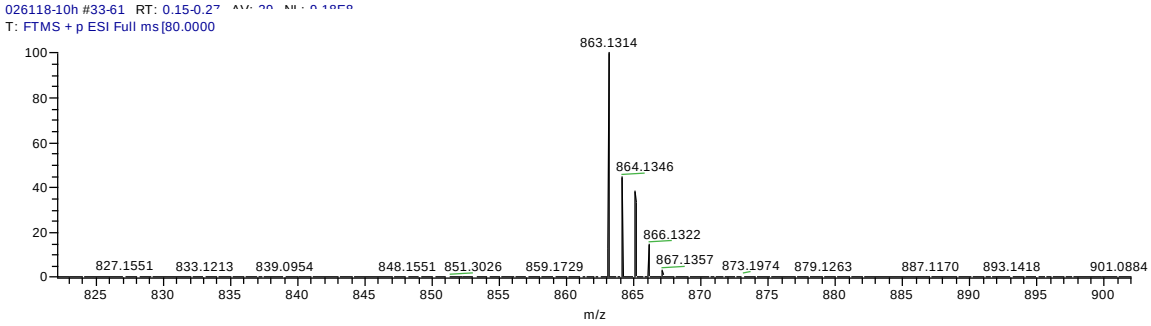

Figure E-S73. HRMS spectrum of compound **2ac**

4-((E)-2-((E)-2-(2-chloro-3-((E)-2-(5-iodo-3,3-dimethyl-1-propyl-3H-indol-1-ium-2-yl)vinyl)cyclohex-2-en-1-ylidene)ethylidene)-5-iodo-3,3-dimethylindolin-1-yl)butane-1-sulfonate (2bc)

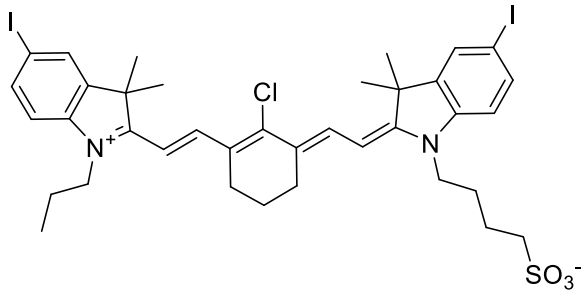

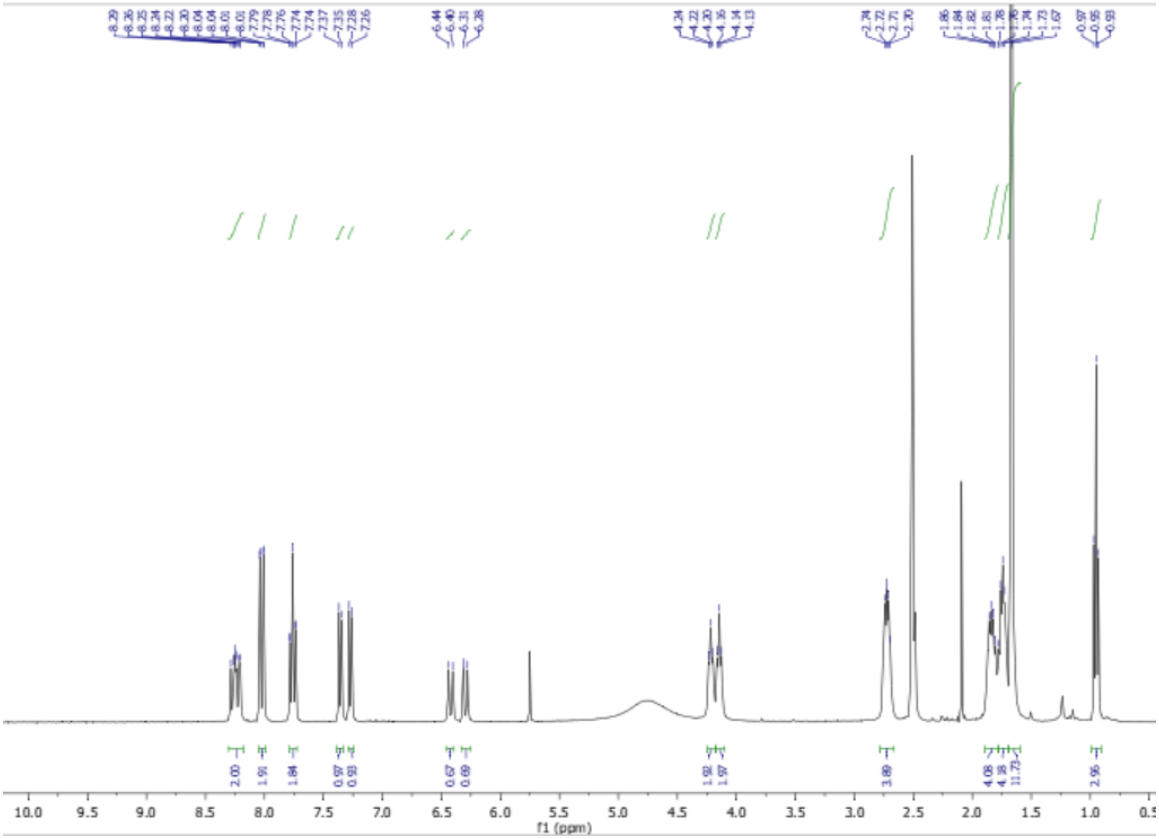

Figure E-S74. ^{1}H spectrum of compound **2bc**

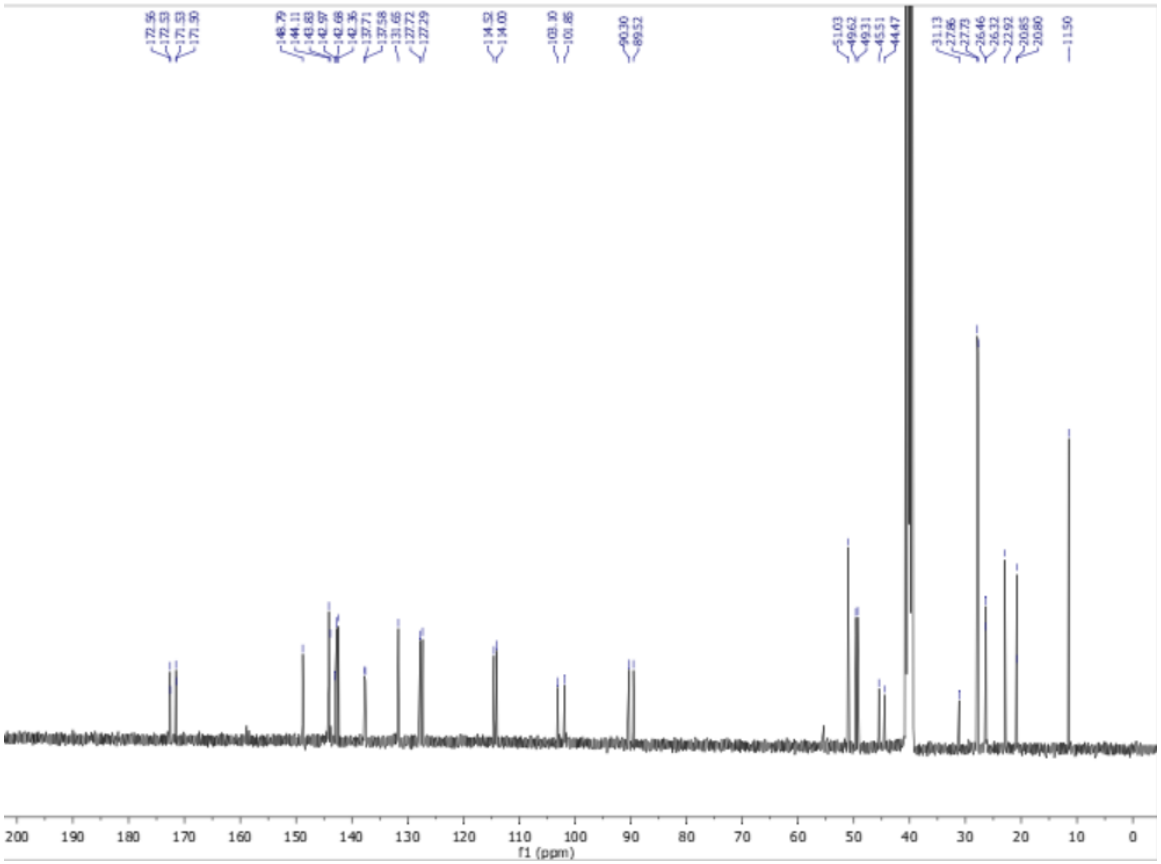

Figure E-S75. ^{13}C spectrum of compound **2bc**

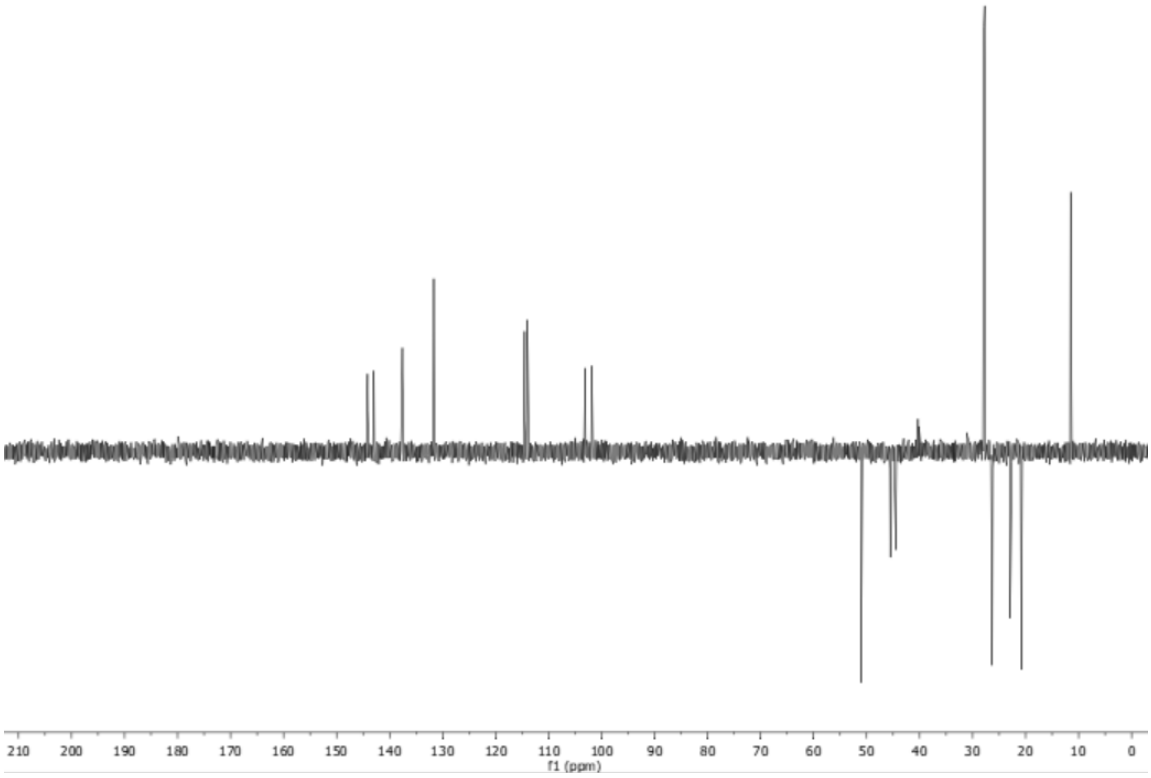

Figure E-S76. DEPT135 spectrum of compound **2bc**

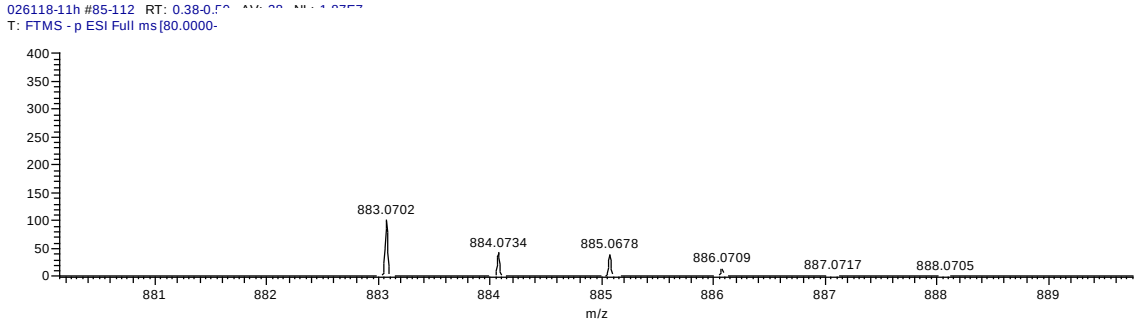

Figure E-S77. HRMS spectrum of compound **2bc**

4-((E)-2-((E)-2-(2-(4-carboxyphenoxy)-3-((E)-2-(5-iodo-3,3-dimethyl-1-(4-sulfonatobutyl)-3H-indol-1-ium-2-yl)vinyl)cyclohex-2-en-1-ylidene)ethylidene)-5-iodo-3,3-dimethylindolin-1-yl)butane-1-sulfonate (3bb)

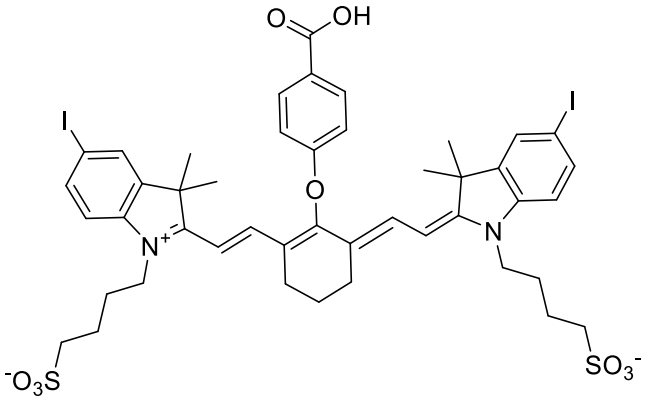

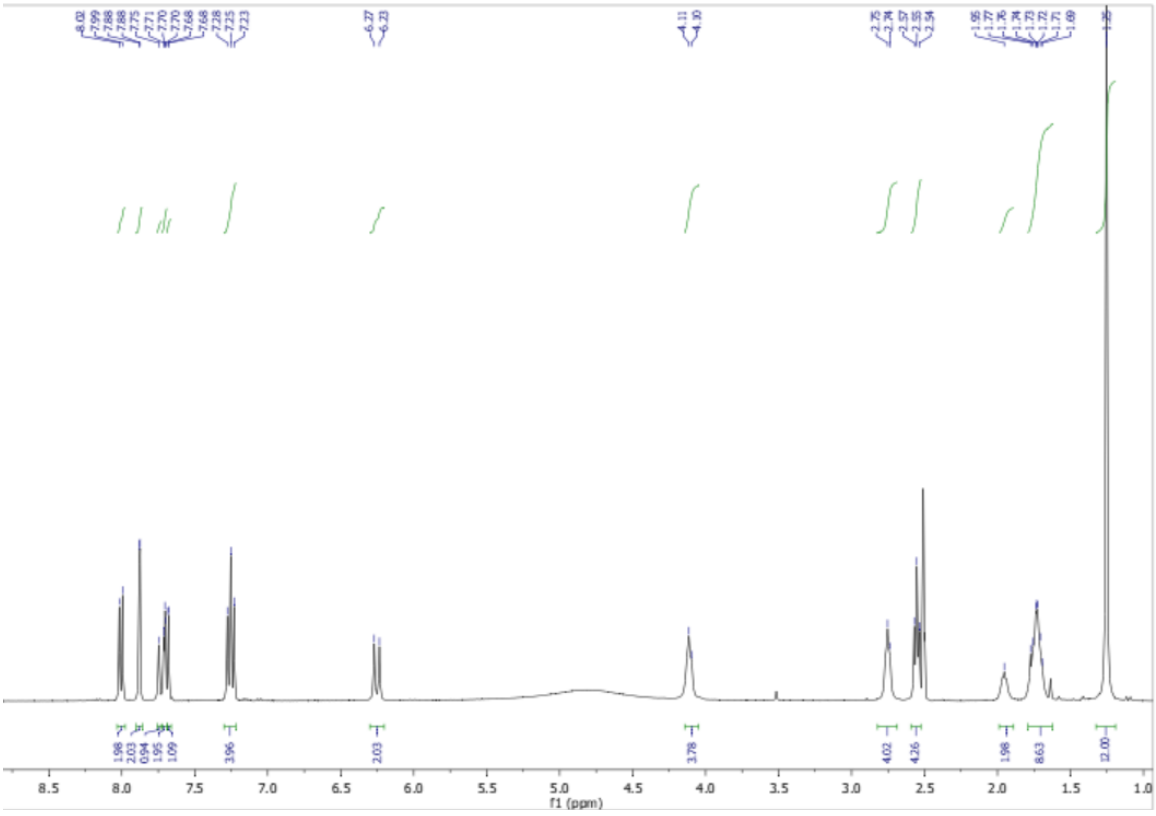

Figure E-S78. ^{1}H spectrum of compound **3bb**

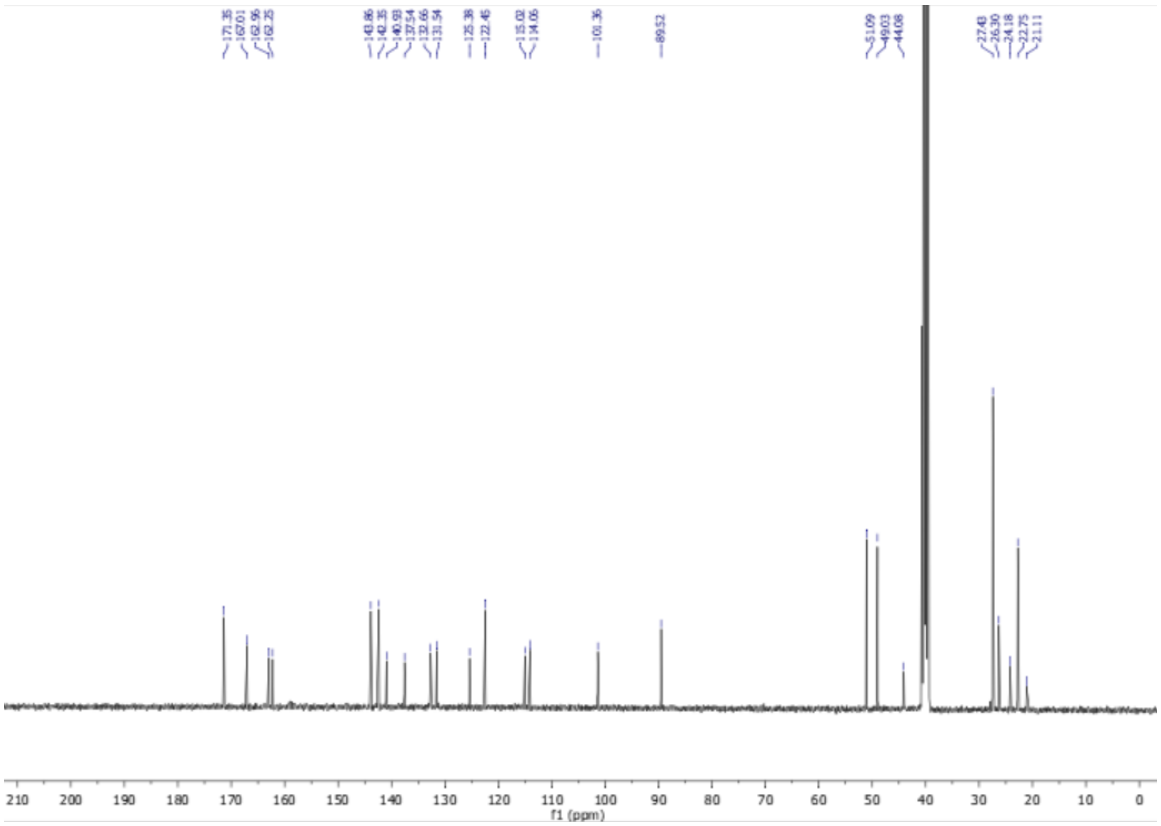

Figure E-S79. ^{13}C spectrum of compound **3bb**

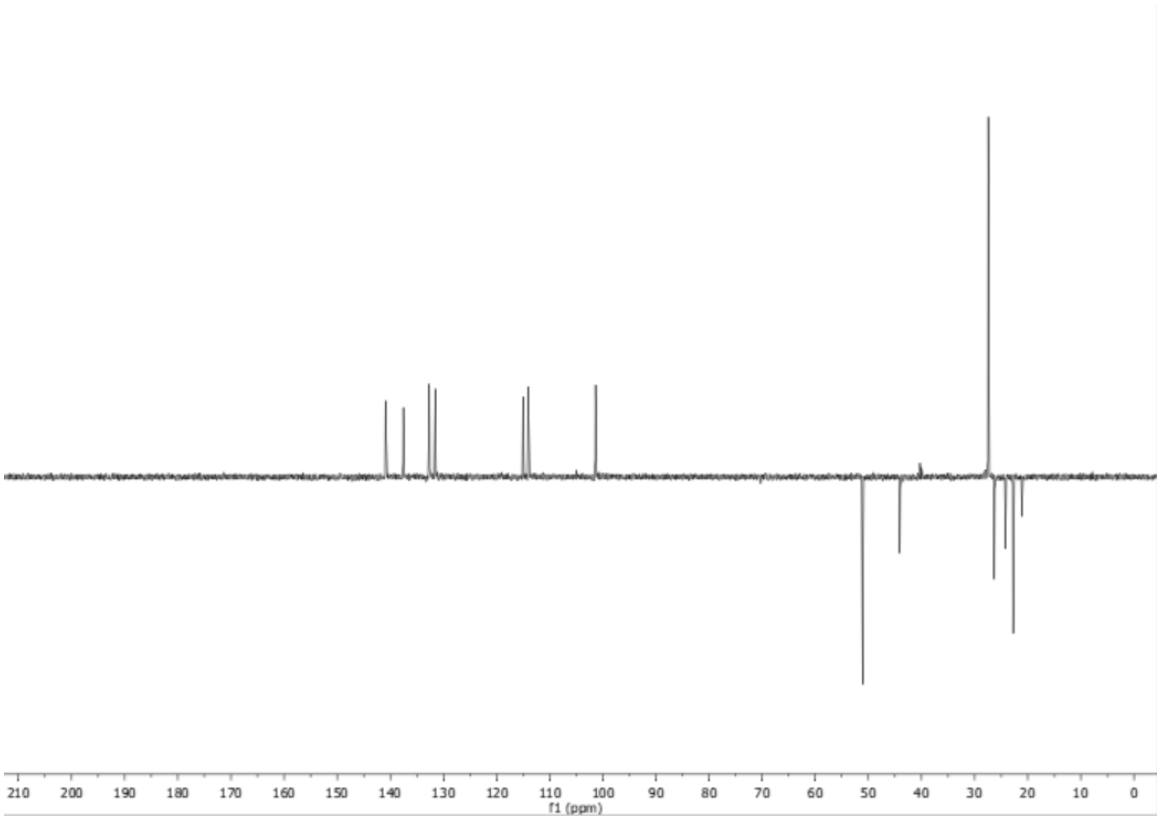

Figure E-S80. DEPT135 spectrum of compound **3bb**

4-((E)-2-((E)-2-(2-(4-carboxypiperidin-1-yl)-3-((E)-2-(5-iodo-3,3-dimethyl-1-(4-sulfonatobutyl)-3H-indol-1-ium-2-yl)vinyl)cyclohex-2-en-1-ylidene)ethylidene)-5-iodo-3,3-dimethylindolin-1-yl)butane-1-sulfonate (4bb)

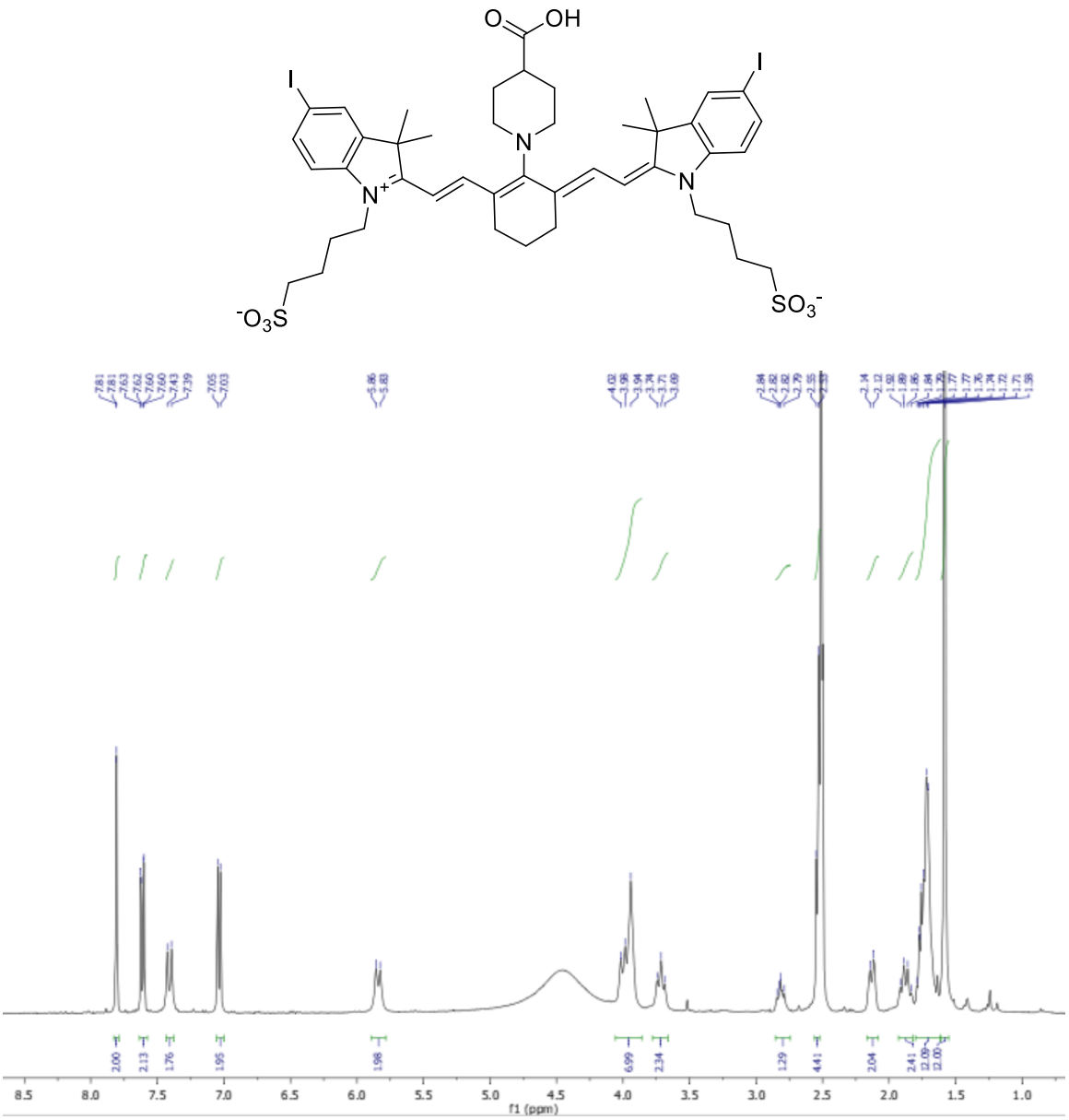

Figure E-S81. ^{1}H spectrum of compound **4bb**

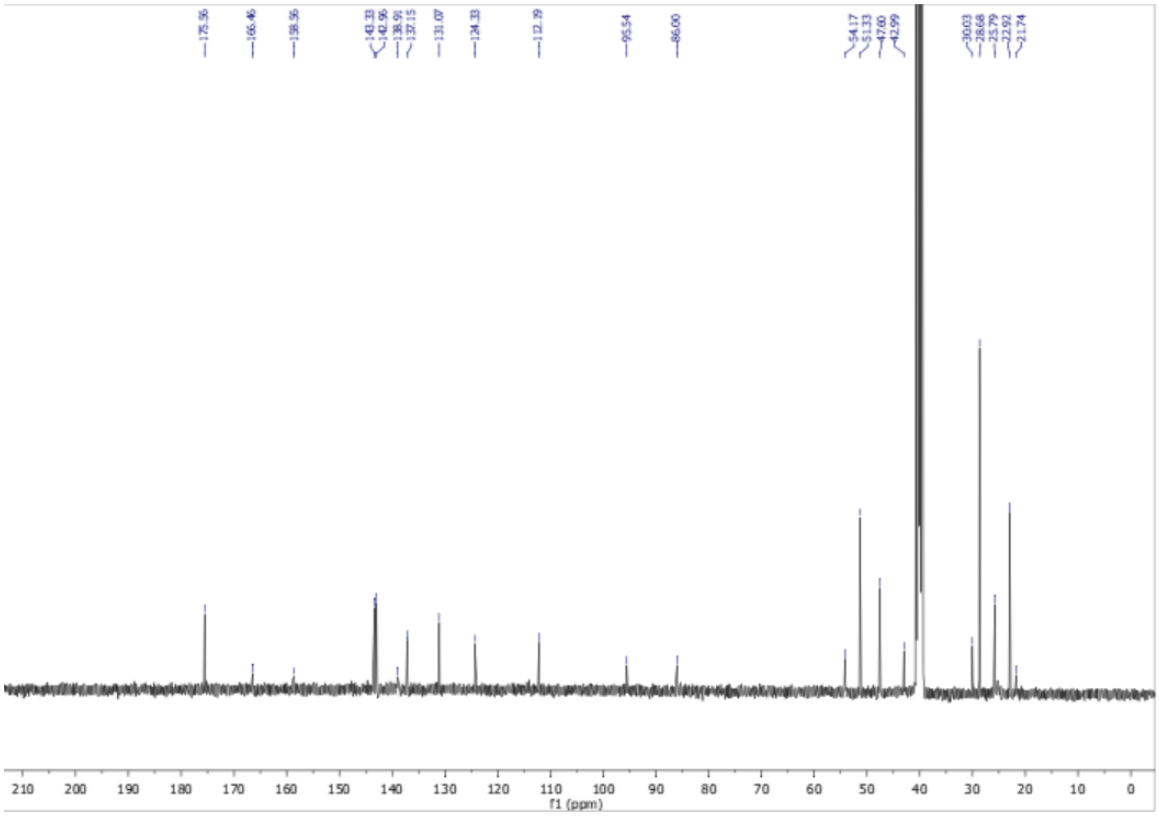

Figure E-S82. ^{13}C spectrum of compound **4bb**

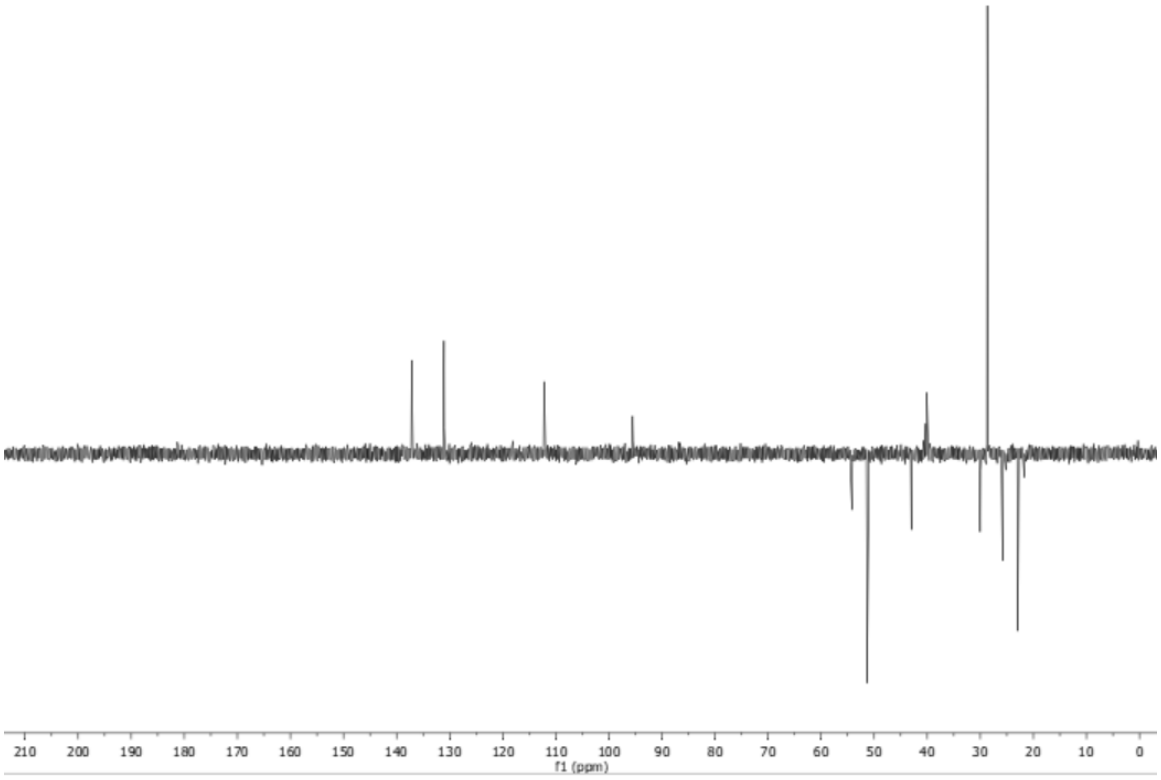

Figure E-S83. DEPT135 spectrum of compound **4bb**

4-((E)-2-((E)-2-(2-((4-carboxyphenyl)thio)-3-((E)-2-(5-iodo-3,3-dimethyl-1-(4-sulfonatobutyl)-3H-indol-1-ium-2-yl)vinyl)cyclohex-2-en-1-ylidene)ethylidene)-5-iodo-3,3-dimethylindolin-1-yl)butane-1-sulfonate (5bb)

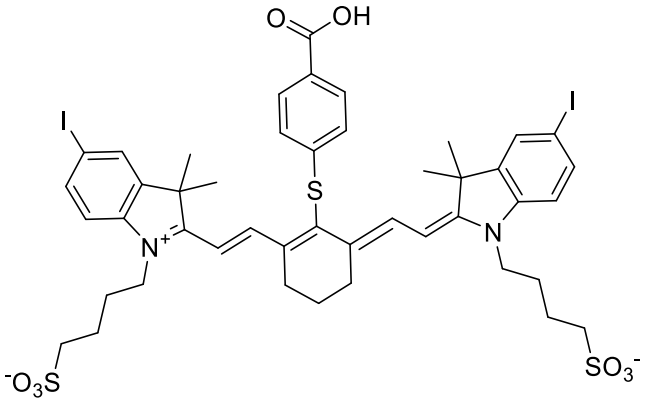

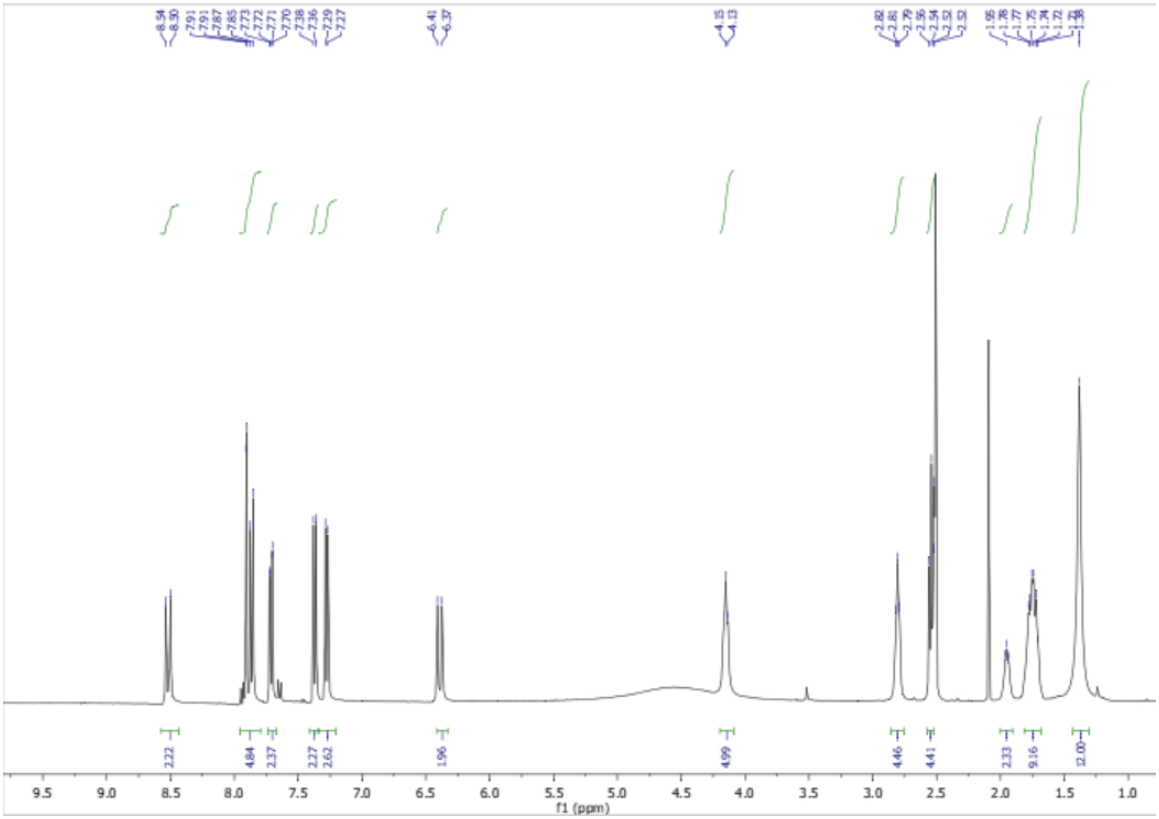

Figure E-S84. ^{1}H spectrum of compound **5bb**

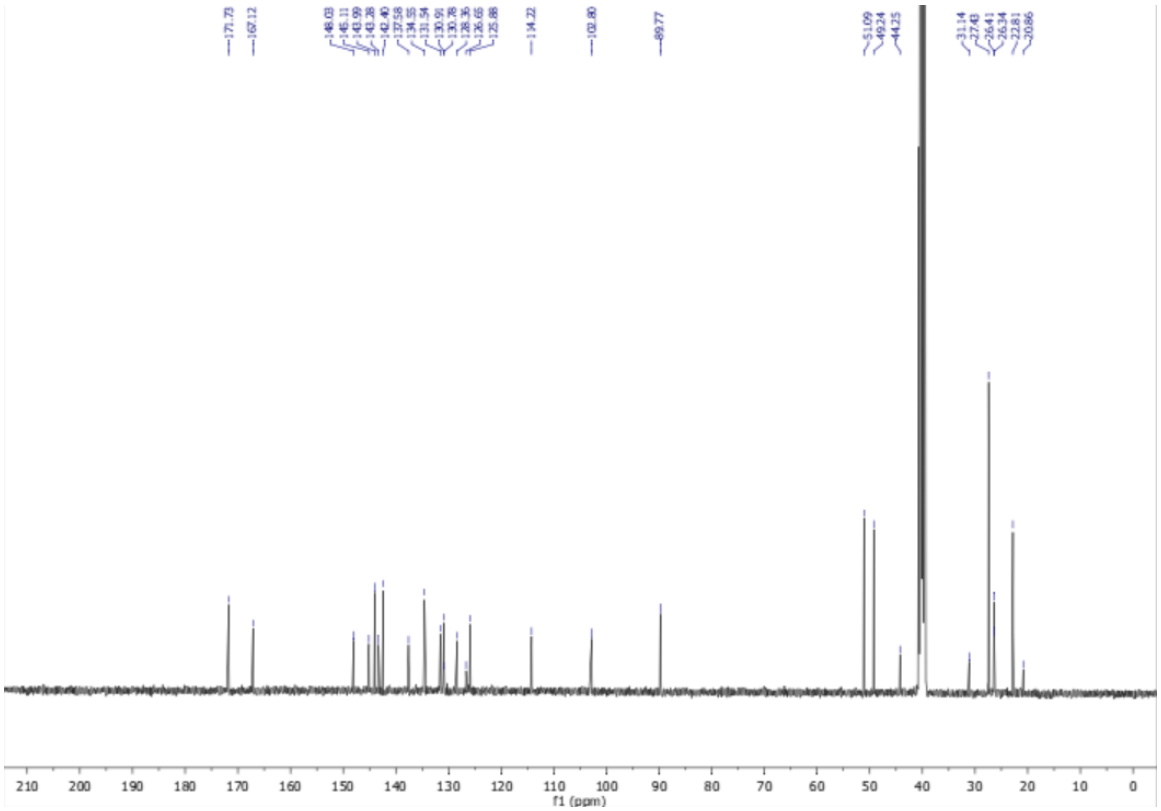

Figure E-S85. ^{13}C spectrum of compound **5bb**

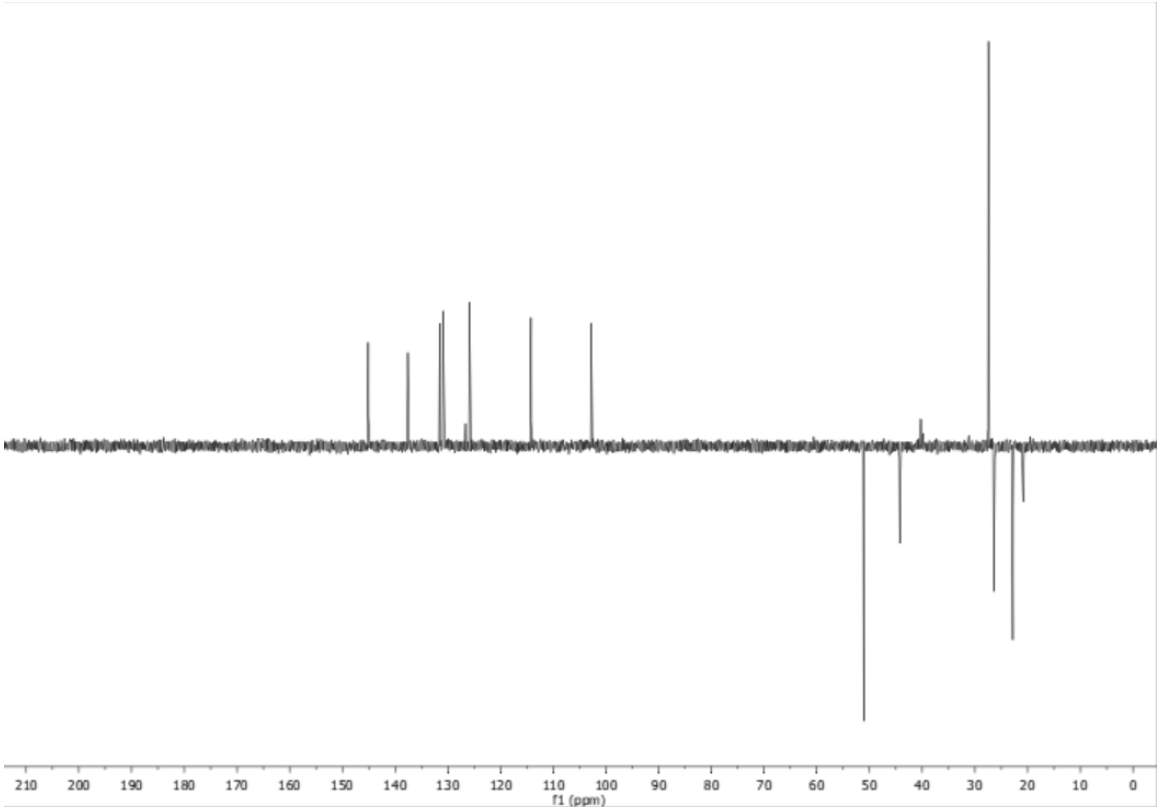

Figure E-S86. DEPT135 spectrum of compound **5bb**

APPENDIX F

ARE OATP RECEPTORS IMPORTANT FOR UPTAKE OF TUMOR-SEEKING CYANINE DYES?

Introduction:

Some cyanine-7 dyes have the remarkable characteristic of localizing in any type of human solid tumor implanted into mice, with no published exceptions, and they have excellent characteristics for optical imaging *in vivo*.[44-47] This means that they have potential as *clinical* agents for optical imaging. Moreover, their tumor-seeking properties can be exploited in drug conjugates for active targeting.[221,51,53,57-61,170] Therapeutic applications of the dyes may be assisted by retention in tumors; in some cases near-IR fluorescence can be observed 3 – 4 days after *iv* injection. This provides a means to substantially alter the pharmacokinetics of substances conjugated to the dyes.

Fluorophore **1**-Cl localizes in many different types of cancer lines and in solid tumors (*e.g.* prostate,[48] gastric,[49] kidney,[50]) but not in normal cells and tissue.[69,86-88,94] Cyanine **2**-Cl is similar to **1**-Cl except the chains are one methylene group shorter and terminated with sulfonic acid groups. Like **1**-Cl, the disulfonic acid **2**-Cl selectively localizes in tumors over healthy tissue,[94] *e.g.* in hepatocytes,[51] kidney,[50] lung,[52] and intracranial human glioblastoma cells (U87).[53] Cyanine **3**-Cl, is a hybrid of **1**-Cl and **2**-Cl but, unlike **2**-Cl, it has a carboxylic acid that can be used for convenient functionalization. There is evidence that **3**-Cl also accumulates in solid tumors (*e.g.* hepatocytes,[96] glioblastoma,[53] Burkitt Lymphoma,[222] breast cancer[60]). Cyanine **4**-Cl has

two propyl group on indoles and has been reported to localize in lung and breast cancer[88] and stem cells.[223]

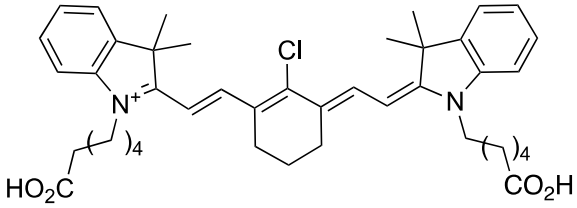

1-Cl

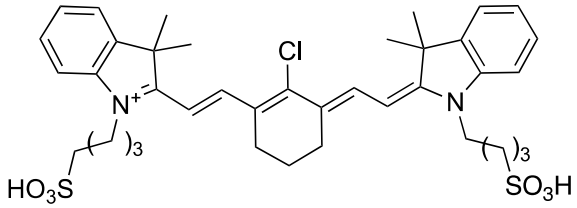

2-Cl

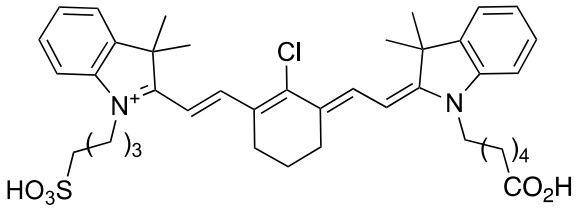

3-Cl
DZ-1

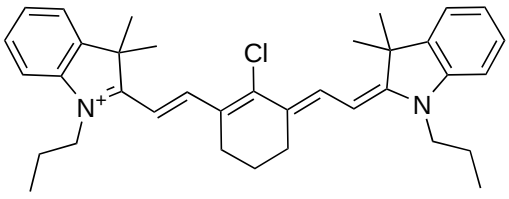

4-Cl
IR-780

Several publications,[48-50,54-56,59,94,222-228] latterly including one of ours,[113] has stated or implied preferential uptake of tumor seeking dyes like **1**-Cl - **4**-Cl is mediated by Organic Anion Transporting Polypeptides (OATPs). This assertion is reasonable because hypoxia triggers activation of HIF1α, which promotes OATPs expression.[49,56] Further, it is known that OATP receptors influx organic anions including bile salts, steroids, bilirubin, and thyroid hormones and efflux OATPs efflux bicarbonate, glutathione, and glutathione-adducts to balance the charge. However, to our minds, the hypothesis that OATP receptors are responsible for uptake of tumor-seeking dyes is unproven, and it does not explain a structural feature they all share: the *meso*-chloride. To the best of our knowledge, there is nothing in the literature to connect OATP-mediated transport with this functionality.

Recently we discovered the *meso*-chloride of **1**-Cl is displaced by *S*-nucleophiles under physiological conditions,[97] including the free Cys residue in serum albumins (Cys^{34} in human serum albumin, HSA). Thus in serum, where there is an extremely high concentration of albumin (around 35-50 g/L or 0.53-0.73 mM in humans),[149] **1**-Cl may form a covalent adduct with a half-life of just over 30 min.[113] Similar data on the reaction of **1**-Cl with nucleophiles, including albumin, was simultaneously collected by Conovas *et al* in an independent study.[229]

Two issues need to be explained regarding tumor-seeking dyes, *ie* why they accumulate in tumors, and why they persist there. This manuscript considers interactions of OATP receptors with tumor-seeking dyes, and evaluates the evidence that these are involved in the uptake.

Results and Conclusions:

Compounds considered: Four key compounds in this study are **1**-Cl, **1**-Ph, **5**-Cl, and **5**-Ph. Central to these is MHI-148, **1**-Cl, which reacts relatively rapidly via displacement of the *meso*-chloride with the free ^{34}Cys thiol of albumin (*vide supra*).[97,113] By comparision, the reaction of QuatCy[230] with albumin is extremely slow under physiological conditions, but it will form an analogous covalent adduct. This difference may be related to the extra positive charge on the QuatCy core **5** one relative to the MHI-148 framework **1**; this difference impacts the affinity of the two dyes towards proteins, their water solubilities, logP (reflecting partitioning of ions) and logD (partitioning of all neutral species and ions) values. *Meso*-substituted derivatives of MHI-148 and QuatCy, *i.e.* **1**-Ph, and **5**-Ph, are included in this study because they have no *meso*-chloride to be displaced by nucleophiles, they cannot form the same type of albumin adduct that MHI-148 does, but they are otherwise physiochemically similar to **1**-Cl and **5**-Cl, respectively.

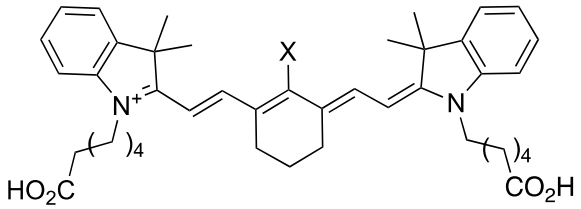

1

X = Cl, MHI-148, **1**-Cl, *reacts quickly with albumin*, logP= 6.57, logD= 3.82
= Ph, **1**-Ph, *cannot react with albumin*, 7.85, 5.09

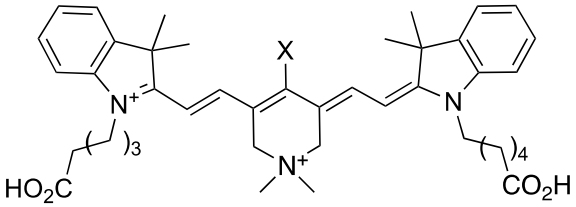

5

X = Cl, QuatCy, **5**-Cl, *reacts slowly with albumin*,1.10, 2.64
= Ph, **5**-Ph, *cannot react with albumin*, 2.38, 3.92

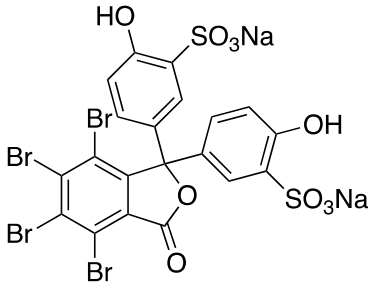

BSP
bromosulphthalein, or
phenoltetrabromophthalein
sodium sulphonate

BSP Blocks Cellular Uptake Of MHI-148 In Serum Free Media: Bromosulphthalein (BSP) is a pan-OATP receptor inhibitor.[130] The most compelling evidence for involvement of OATP receptors in the uptake of tumor-seeking dyes into cancer cells comes from the influence of BSP on this process. Specifically, a set of experiments featuring BSP has become standard when testing tumor-seeking near-IR dyes in tissue culture; these experiments are conducted in the following way.[48-50,54-56,59,94,222-225,231] Incubation of the fluorophore with the cells then observation via microscopy reveals a baseline level of uptake, as shown in Figure F-S1a for **1**-Cl. Treatment of the cells with BSP *suppresses* this uptake, implying inhibition of the OATP receptor. Conversely, pretreatment of the cells with a compound that induces hypoxia (DMOG),[49,56] and which

promotes OATP receptor expression, *enhances* the uptake. Hypoxia has been reported to promote expression of OATP receptors, so uptake suppression into normoxic cancer cells treated with BSP, and enhancement of uptake into hypoxic cancer cells (in the absence of BSP) is consistent with involvement of OATP receptors.

Figure F-1 shows the data collected for **1**-Ph under the standard conditions outlined above, but they are not materially distinguishable to that accumulated for **1**-Cl (Figure S1; data for the chloride is placed in the supporting because this particular experiment has been performed by others for **1**-Cl, but it has not for **1**-Ph). Baseline uptake of **1**-Ph (Figure F-1a) was suppressed by BSP (F-1b), and enhanced under hypoxic conditions (F-1c). This comparison shows that removal of the possibility for substitution of the *meso*-Cl has no impact on the uptake in SFM. Consequently, *the possibility of meso-Cl substitution is inconsequential to uptake in SFM* because **1**-Cl and **1**-Ph (vulnerable and invulnerable to *meso*-substitution, respectively) follow the same trend.

MDA-MB-231 breast cancer cells were selected as a model line throughout this study because they are derived from an aggressive metastatic tumor. However, HepG2 liver cancer cells were also tested because a key probe in this study, bromosulphthalein (BSP) has special relevance to the liver cells hence might be expected to behave differently to MDA-MB-231. However, the data collected (summarized at the end of this section) is nearly identical. There appears to be nothing unique to the observations we report for MDA-MB-231 cells.

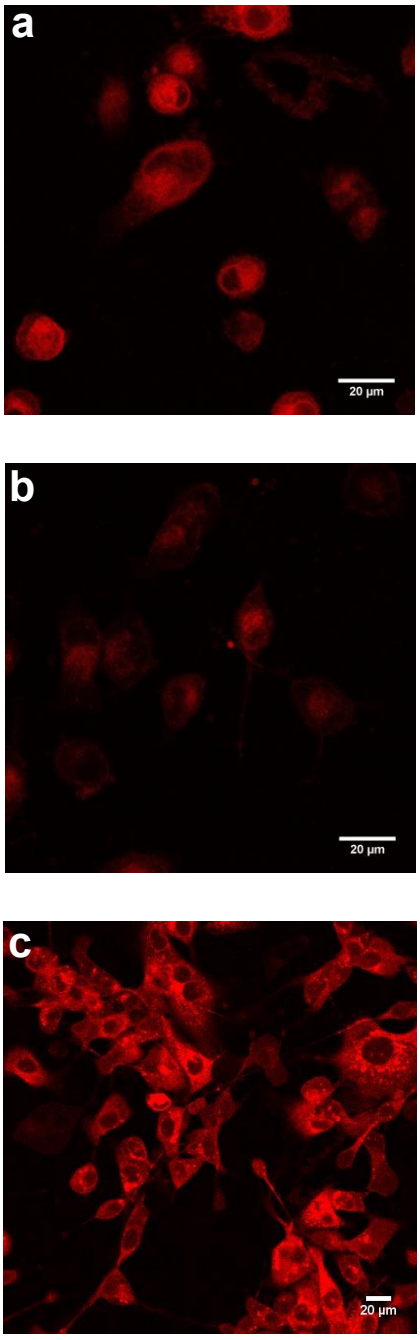

Figure F-1. **a** MDA-MB-231 cells incubated with **1**-Ph (20 µM) in serum free media; **b** same experiment but pre-blocked with by incubating with 250 µM BSP for 5 mins; **c** same as **a**, but cells pre-blocked with 1mM DMOG to induce hypoxia. Fig S1 shows

data from identical experiments but using **1**-Cl. Throughout, images were taken at by Leica Confocal Microscope at 20X/0.75 NA.

Effects Of Albumin Outweigh Those Of BSP In Serum-containing Media: In media that contains serum ("serum" in these tissue culture experiments) the outcome of these uptake experiments is *not* the same (Figure F-2 for **1**-Cl) as without serum (Figure F-1). Compared to uptake in SFM (Figure F-2a), *uptake of **1**-Cl and **1**-Ph is suppressed in serum-containing media that does not contain BSP* (Figure F-2b). A combination of BSP in serum gives approximately the same degree of suppression as serum alone (this is hard to deduce by comparing Figures F-2b and F-2d, but the quantitation data in F-2e shows this to be true).

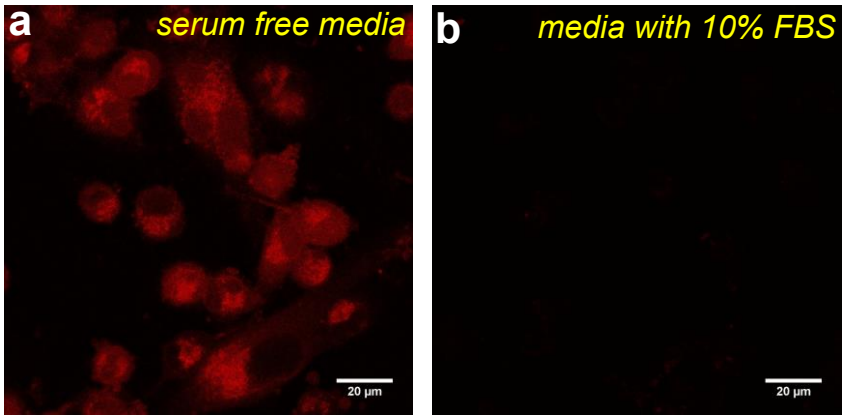

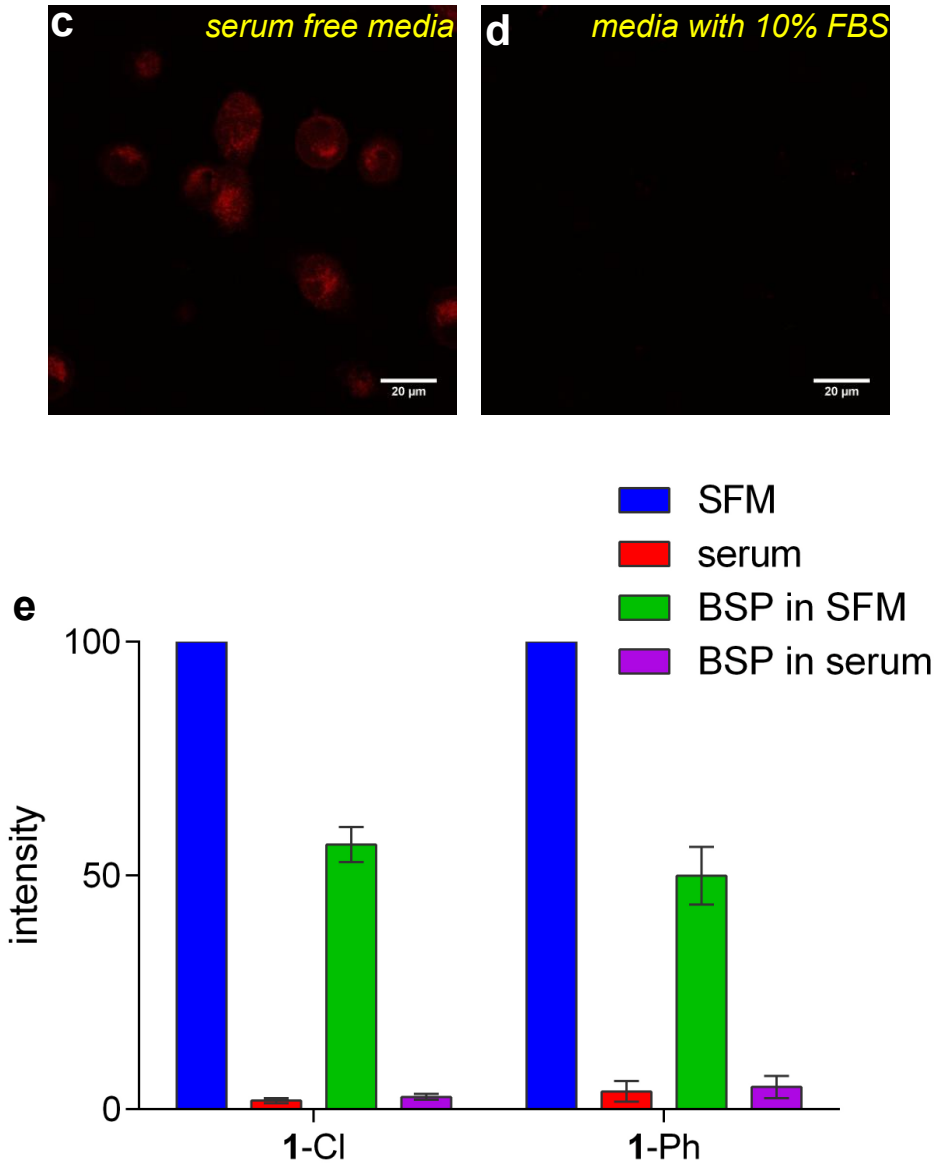

Figure F-2. **1**-Cl (20 µM) in **a** serum free media, **b** media with 10% FBS **c** 250 µM BSP serum free, and **d** 250 µM BSP with media containing 10%FBS and **e** quantification of above mentioned results by FACS.

Levels of cellular uptake in Figure F-2 were quantitated using FACS (summarized in Fig 2e). As expected, uptake of **1**-Cl and **1**-Ph were significantly (~40 -

50 %) decreased by BSP in SFM. Figure F-2e shows uptake of **1**-Cl under these conditions is marginally less than for **1**-Ph, perhaps because it is less hydrophobic, but the difference is small. Several other aspects of these experiments, however, are extremely revealing. First, *serum had a greater negative impact on uptake of **1**-Cl and of **1**-Ph than BSP*. Second, *uptake of the QuatCy derivatives **5**-Cl and **5**-Ph were significantly enhanced by BSP in serum free media*. A caveat here is that the degree of uptake of **5**-Cl and **5**-Ph in SFM is low anyway with respect to **1**-Cl and **1**-Ph (Figure F-S3), so measurements of differences in uptake are less accurate. Third, *uptake of both QuatCy derivatives **5**-Cl and **5**-Ph were unaffected by serum, and only marginally depressed by BSP in serum* (Figure F-S2).

Figure F-S2 shows data for uptake of all four featured compounds (**1**-Cl, **1**-Ph, **5**-Cl and **5**-Cl) using BSA added to serum free media. The outcome of these experiments were almost identical to those in serum, again supporting the assertion that interactions of the dyes with albumin dominate uptake in media.

Albumin is the predominant serum-protein.[125-127] Our previous work[97,113] had already established **1**-Cl combines with albumin under physiological conditions. A series of UV and fluorescence spectra were also used to confirm that the determinant feature of serum is its albumin content. First, reactions of **1**-Cl with HSA and with serum (*i.e.* 10 % FBS in DMEM buffer) were compared; the red shift in DMEM containing 10% FBS was similar to that observed for **1**-Cl combined with HSA (Figure F-3a and F-S4a). UV spectra of **1**-Ph with HSA, and serum, showed the same instantaneous red-shifts of the absorption maxima, attributed to non-covalent binding of

1-Cl. Unsurprisingly, unlike **1**-Cl, **1**-Ph in these experiments did *not* give UV spectra that revert formation of a covalent adduct, because there it has no *meso*-Cl to displace (Figures F-3b and F-S4b). On the basis of these observations, other data we have collected,[97,113] and the work of Conovas *et al*,[229] we assume that the prevailing reaction of MHI-148 derivatives (having a *meso*-Cl) in serum is with albumin. Thus, that there is a complicated interplay of three components: the fluorophore, BSP, and albumin); consequently, UV and fluorescence studies were initiated to ascertain how these entities interact with each other.

BSP Cannot Displace MHI-derivatives 1 From Their Non-covalent Complexes With Albumin: Figure F-3 shows UV absorbance data for **1**-Cl (a) and **1**-Ph (b) in PBS with 50 equivalents of HSA incubated for 0 - 5 h at 37°C. At 0.05 h (first data point), the absorbance maxima for the mixture featuring **1**-Cl was completely red shifted to 805 nm. After 5 h, however, a new UV spectrum formed corresponding to a species with an intermediately red-shifted absorption maxima at 791 nm. This instantaneous red-shifted absorbance maxima, followed slower formation of a relatively blue-shifted peak, can be explained in the following way. *Albumin rapidly forms a non-covalent adduct with MHI-148, **1**-Cl, followed by transformation into a ^{34}Cys-bound covalent adduct*. Support for this assertion comes from the corresponding experiment with the *meso*-blocked dye **1**-Ph (Figure F-3b). For **1**-Ph, Figure F-3a shows addition of albumin led to instantaneous formation to a new UV spectrum with a red-shifted absorption maximum, which is invariant over 5 h, the time span of the experiment. Thus ***1**-Ph with albumin*

forms only the non-covalent adduct; no covalent adduct was formed because there was no possibility of displacement of chloride from the *meso*-position because that site is blocked by the phenyl group.

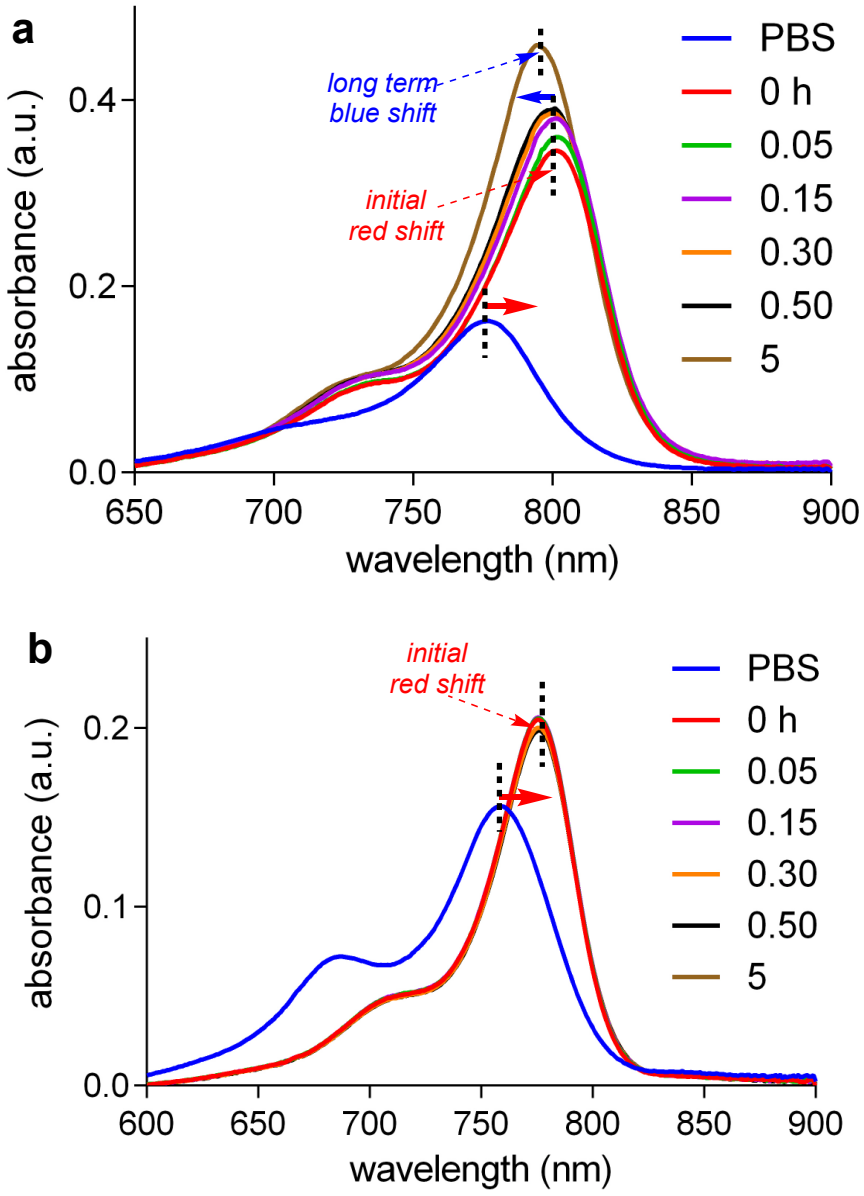

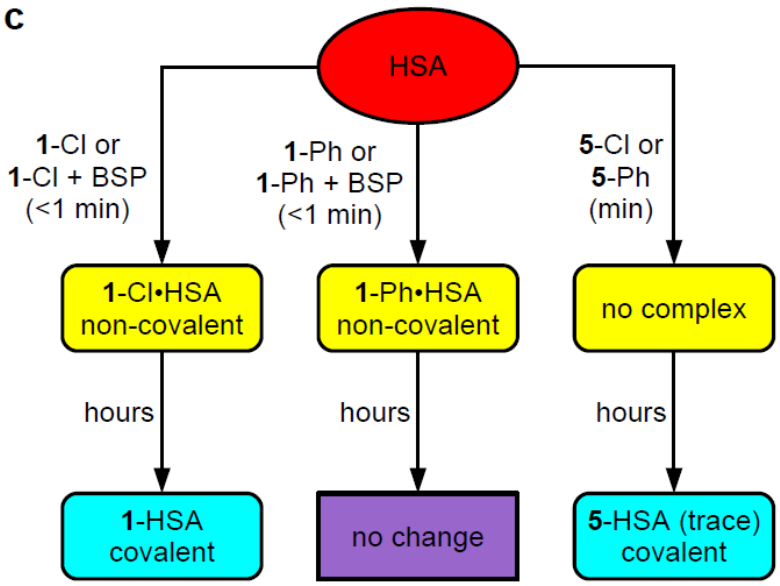

Figure F-3. Interaction of **a** **1**-Cl, and **b** **1**-Ph (1 μM) with HSA (50 μM) at pH 7.4 in PBS buffer at 37 ^{o}C observed via UV Vis spectroscopy, **c** summary of key UV experiments for albumin interactions with **1**, **5**, and BSP.

Interactions of albumin with **5**-Cl and with **5**-Ph have already been studied in our laboratory. Neither of these compounds appears to form a non-covalent adduct on mixing with albumin; their UV absorbance maxima wavelengths and intensities were unperturbed on mixing with HSA. Only the *meso*-chloride, **5**-Cl shows any signs of forming a covalent adduct with albumin under physiological conditions, but this process largely incomplete after several hours; this observation is consistent with the hypothesis that relatively rapid formation of a non-covalent adduct from albumin and **1**-Cl facilitates the evolution of this into a covalent one.

BSP has a high affinity for albumin, such that according to one estimate more than 99% of BSP is bound to albumin after injection in body.[232] According to one report, equimolar concentrations of BSP and albumin afforded less than 0.1% of unbound BSP.[233] Consequently, experiments were performed to ascertain if BSP in its non-covalent adduct with albumin could be displaced by **1**-Cl. Thus, HSA and increasing concentrations of BSP (up to 50 equivalents) were mixed then **1**-Cl added, but there was no shift in the UV absorption maxima of the dye (Figure F-S6c) and that UV which was observed to corresponded to the non-covalent complex. This experiment was repeated in the reverse way (Figure F-S6d), *i.e.* HSA and **1**-Cl were mixed then increasing concentrations of BSP (up to 50 equivalents) were then added; the outcome was essentially the same. In both experiments, the UV absorbance intensity was somewhat reduced by addition of BSP, implying some interaction of BSP with the non-covalent albumin•**1**-Cl complex that does not replace the cyanine. Fluorescence spectra for were also recorded, and similar shifts were observed (Figure F-S7). These data do not prove the binding of the dye to albumin is stronger than albumin•BSP, because BSP binds multiple binding sites on albumin.[234] However, these experiments do prove ***1****-Cl is not displaced from albumin by BSP*. In an interesting control, the intensity of the MHI alone was shown to be decreased by about 30 % when BSP was added, but without a blue shift (Figure F-S6b).

Out of necessity, experiments described above to probe interactions of albumin, BSP and **1**-Cl were performed within approximately 30 min after mixing at room temperature, because very little of the *covalent* adduct **1**-HSA forms under these

conditions over that time. There was an unlikely possibility that both **1**-Cl and BSP bound to albumin have extremely slow k_{off} rates, hence dissociation of either species could not be forced by introducing the other into solution. To probe for this possibility, the similar experiments were repeated but using a derivative that cannot form the covalent adduct, **1**-Ph, hence the duration of the experiment then could be extended to 5 h to allow for equilibration; the outcome was essentially the same (Figure F-S8).

BSP had no impact on the absorption maximum of **5**-Cl mixed with albumin. This observation is consistent with the assertion that the dye does not bind albumin to form a non-covalent adduct (Figure F-S9).

A series of experiments was carried out to attempt to determine the HSA binding pocket that **1**-Cl occupies in the non-covalent complex (Figure F-S10). Warfarin, ibuprofen, and digoxin are known to bind three different sites on albumin. [235,236] Of these three binders, preincubation with ibuprofen had the most effect on the fluorescence spectra of **1**-Cl mixed with BSA, relative to no added inhibitor (blank), but the differences were modest hence these experiments were inconclusive.

Reactions of dyes **2**-Cl – **4**-Cl with HSA were shown to also give non-covalent adducts, that morphed into covalent ones (Figure FS11). Relative rates for the formation of covalent adducts were (at 37 °C with 2 equiv of HSA): **4**-Cl (IR780; $t_{1/2}$ 2 min) > **1**-Cl (6 h) > **3**-Cl (24 h) > **2**-Cl (72 h).

On The Uptake Of Other Tumor-seeking Dyes, And Import Into Other Cells: Figures F-S14 and F-S15 summarize key data for **2**-Cl (IR-783, having two sulfonate

chains) and ICG (also having two sulfonate chains) in experiments similar to those outlined above. Dye **2**-Cl does not react with albumin in the time course of these experiments (see above). Both these dyes display red-shifted absorbance maxima when mixed with albumin (with decreased absorbance). Thus, IR-783 and ICG both appear to interact with albumin to form non-covalent adducts. Dependence on the dye was also considered. Investigation (FACS) of uptake of **2**-Cl (IR783) and ICG into the MDA-MB-231 breast cancer cells in SFM showed both dyes was suppressed by serum, BSP, and BSA, just as for **1**-Cl (Figures F-S14b,c and F-S15b,c).

Uptake of **1**-Cl, **1**-Ph, **5**-Cl and **5**-Ph into HegG2 liver cancer cells was explored to test if there was something particular to MDA-MB-231 breast cancer cells, but the data (Figure F-S16 and F-S17) followed the same trends as identified above.

MHI-148 And Albumin-FITC In Media Are Uptaken Into Cells And Colocalize: In a key confocal microscopy experiment, **1**-Cl and fluorescein-labeled BSA (FITC-BSA) incubated with MBA-MD-231 cells colocalized (Figure F-4a; Pearson coefficient 0.65). This experiment shows *the non-covalent adduct is influxed and does not dissociate significantly in the cells*. Images of uptaken, preformed **1**-BSA-FITC appear similar (Figure F-4b; Pearson coefficient 0.54), supporting the assertion that the covalent adduct does not dissociate. When **1**-Cl was preincubated with Cys^{34}-blocked HSA this gave the same result (Figure F-4c; Pearson coefficient 0.56), and **1**-Ph and HSA-FITC also colocalized (Figure F-4d Pearson coefficient 0.63); these data are highly indicative that **1**-Cl is imported as a non-covalent complex that persists in cells.

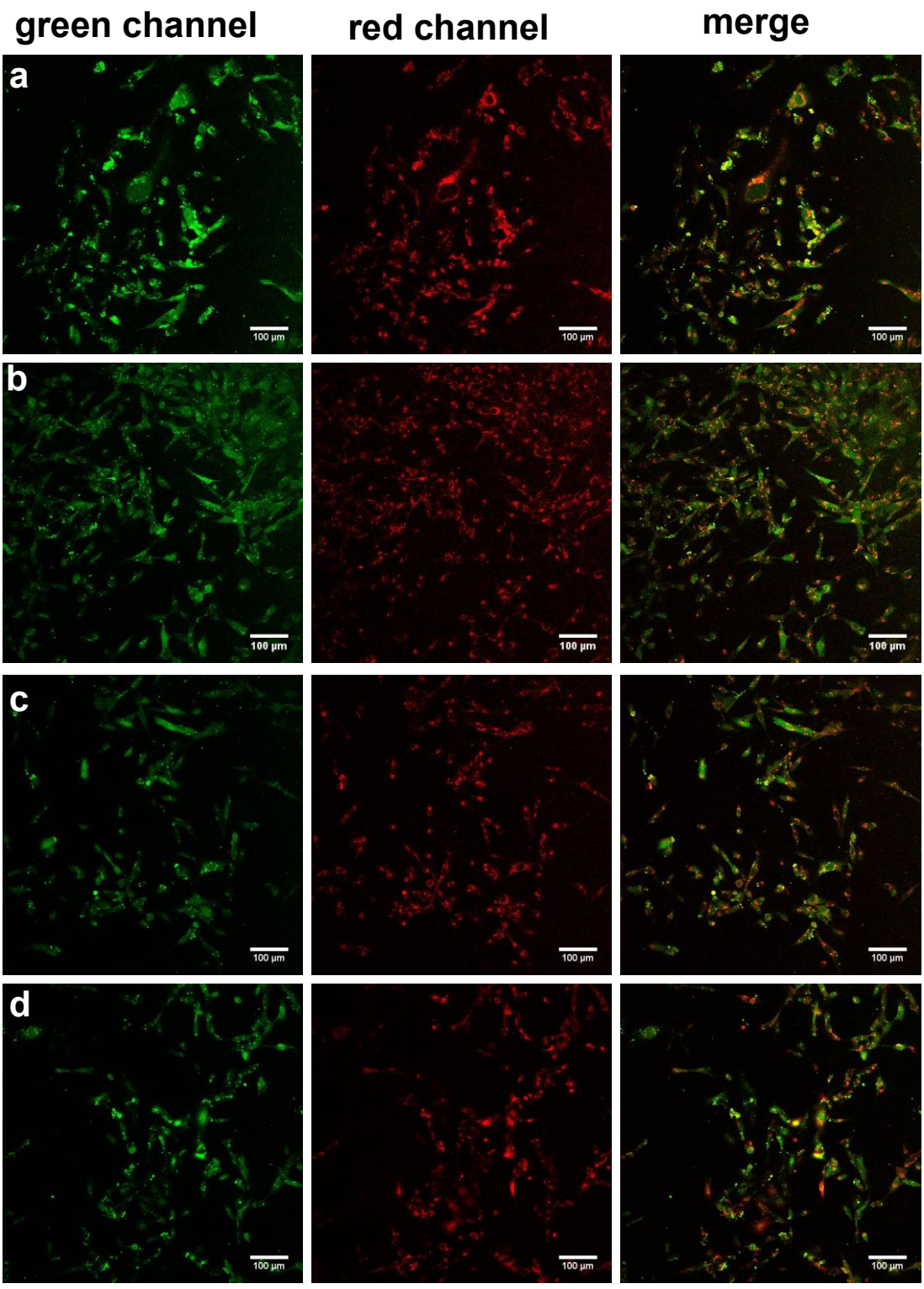
green channel
red channel
merge
a
b
c
d
100 µm

Figure F-4. MDA-MB-231 cells incubated with the following. **a** **1**-Cl (10 μM throughout) and ~1 equiv BSA-FITC (mixed then used as a non-covalent adduct, *ie* before a covalent adduct could form). **b** **1**-Cl preincubated with ~1 equiv of BSA-FITC for 24 h to form covalent adduct. **c** **1**-Cl with BSA-FITC preincubated with 6-maleimidohexanoic acid for 24 h to block Cys[34]. **d** **1**-Ph (10 μM) and ~1 equiv BSA-FITC. Throughout the incubation conditions were 37 ºC, 5% CO_2, 2 h unless otherwise indicated. Images at 20x magnification.

Evidence accumulated above facilitated predictions regarding the clearance and tumor accumulation of **1**-Ph relative to known parameters for **1**-Cl. It is known that MHI-148 accumulates in solid tumors but also to a significant extent in the liver and kidneys[59,225] Since **1**-Ph binds albumin, but cannot form a covalent adduct, we predicted it would be uptaken into tumors *in vivo* just as **1**-Cl, but not persist there for as long. The QuatCy derivatives **5**-Cl and **5**-Ph do not form even non-covalent albumin adducts, hence we suspected their uptake into tumors would be slower than for **1**-Cl and **1**-Ph if tight adducts with albumin were required. In the long term, however, **5**-Cl will slowly form a covalent adduct with albumin under physiological conditions, so dye this was predicted to persist in tumor tissue longer than **5**-Ph. The following *in vivo* experiments were performed to test those predictions.

Conclusions:

It emerges from the observations summarized above that the dyes featured in this study (**1**-Cl, **1**-Ph, **5**-Cl, and **5**-Ph) have complementary properties. Both MHI-148 derivatives **1** form non-covalent adducts with albumin, but only **1**-Cl can form a covalent adduct. Conversely, the QuatCy derivatives **5** do not form non-covalent adducts with albumin; **5**-Cl can form a covalent one, but much more slowly than **1**-Cl.

Data summarized above demonstrates cellular uptake experiments in the absence of serum are *not* indicative of physiological environments because the albumin is present under those conditions and this protein has important effects on the uptake of tumor-seeking dyes. Dyes **1**-Cl and -Ph immediately form non-covalent complexes with albumin on mixing, and this complex formation retards cellular uptake. Nevertheless, these two compounds, **1**-Cl and **1**-Ph, are both uptaken into cells in tissue culture experiments, hence *removal of the meso-Cl has no impact under these conditions*. Uptake of the QuatCy derivatives **5** in tissue culture experiments is significantly slower than import of **1**-Cl consistent with slow formation of a covalent adduct then uptake, implying *uptake of the tumor seeking dyes **1** under physiological conditions is mediated by albumin receptors*. The fact that **1**-Ph is imported indicates covalent albumin complex formation is *not* required for uptake. These conclusions are consistent with import of **1**-Cl, **1**-Ph by FITC-labeled albumin *and colocalization* (*cf* under these conditions QuatCy derivatives that do not form non-covalent adducts are *not* imported).

Supporting Information:

General Experimental Procedures: All reactions were carried out under an argon atmosphere. Reagents were purchased at a high commercial quality (typically 97 % or higher) and used without further purification, unless otherwise stated. High field NMR spectra were recorded with Bruker Avance III at 400 MHz for ^{1}H, and 100 MHz for ^{13}C and were calibrated using residual non-deuterated solvent as an internal reference ($CDCl_3$: ^{1}H NMR = 7.24, ^{13}C NMR = 77.0, MeOD: ^{1}H NMR = 3.30, ^{13}C NMR = 49.0, DMSO-d_6: ^{1}H NMR = 2.50, ^{13}C NMR = 39.5). The following abbreviations were used to explain the multiplicities: s = singlet, d = doublet, t = triplet, q = quartet, quint = quintet, dd = double doublet, dt = double triplet, dq = double quartet, m = multiplet, br = broad. Electrospray ionization mass spectrometry (ESI-MS) data were collected on triple-stage quadrupole instrument in a positive mode. Flash chromatography was performed using silica gel (230-400 mesh). LC-MS analyses were collected from Agilent 1260 Infinity Quaternary LC and Agilent 6120 Quadrupole LC/MS modules using Poroshell 120 EC-C18 2.7 µM (4.6 x 50 mm) column in 5-95% CH_3CN/water gradient with 0.1% formic acid over 10 minutes. Prep HPLC was performed on Agilent 1260 Infinity in 50-90 CH_3CN/water gradient with 0.1% TFA over 20 mins. All statistical analyses were carried out by Graphpad Prism version 6.0 (Graphpad Software).

Synthesis Schemes and Procedures

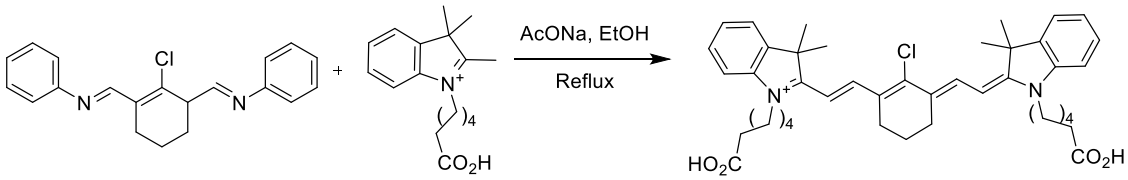

1-Cl

Scheme F-1. Synthesis of **1**-Cl was carried out according to literature procedure. [113]

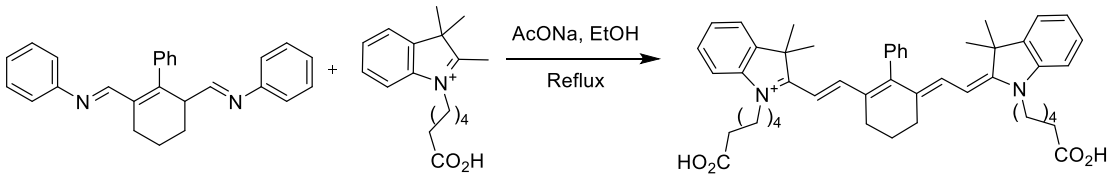

1-Ph

Scheme F-2. Synthesis of **1**-Ph was carried out according to literature procedure.[113]

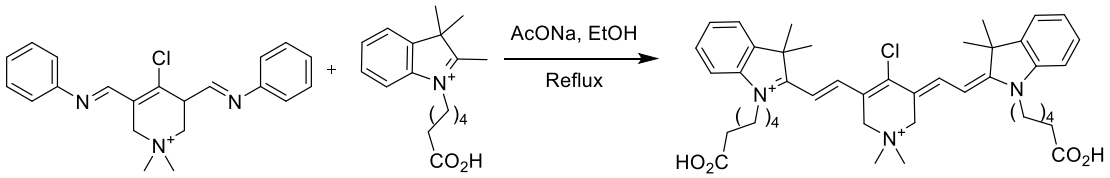

5-Cl

Scheme F-3. Synthesis of **5**-Cl was carried out according to literature procedure.[230]

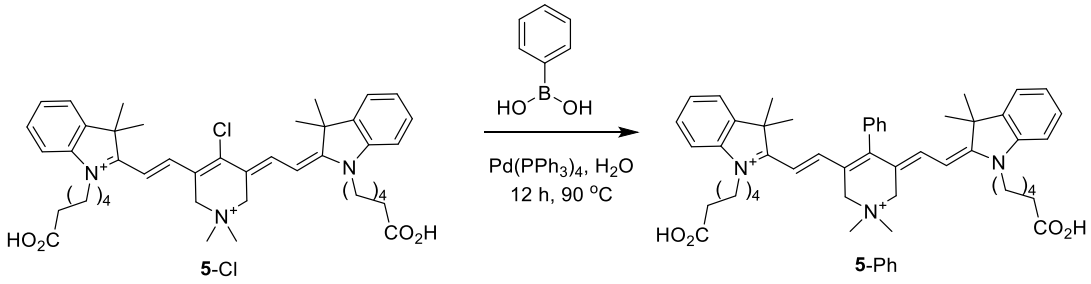

5-Cl **5**-Ph

Scheme F-4. Synthesis of **5**-Ph was carried out according to literature procedure. [237]

Photophysical Properties

ICG and IR783 were bought from Ark Pharm and Sigma respectively. Human serum albumin (HSA), Bovine Serum Albumin (BSA) and BSA labeled with FITC were bought from Sigma Aldrich. HSA and BSA were stored in -20 ^{o}C and fresh 0.5 mM (33 mg in 1 mL) solution was prepared for experiments.

UV Absorbance experiments: Compounds **1**-Cl, **1**-Ph, **5**-Cl, **5**-Ph, **2**-Cl and ICG were dissolved in PBS (pH 7.4) with HSA and the spectra were taken at different time intervals.

Compounds **1**-Cl, **1**-Ph (5 μM) were incubated increasing concentrations of BSP (5, 50 or 250 μM). For blocking experiment the dyes were either incubated with HSA (5 μM) prior to adding BSP (5, 50 or 250 μM) or increasing concentration of BSP was added to HSA before adding the dyes. The absorbance and fluorescence spectra were determined by Cary-Varian 100 UV-Vis NIR spectrophotometer.

UV Absorbance with DMEM: 5 μM of **1**-Cl, **1**-Ph, **5**-Cl and **5**-Ph were dissolved FluoroBrite DMEM with or without 10%FBS. The absorbance was determined using Cary-Varian 100 UV-Vis NIR spectrophotometer.

Kinetics Experiment[97]**:** 200 μM of **1**-Cl, **1**-Ph, **2**-Cl, **3**-Cl, **4**-Cl, **5**-Cl and **5**-Ph were dissolved with HSA (500 μM) in PBS pH 7.4. The reaction mixture was kept in incubator at 37 ^{o}C for up to 72 h. The formation of conjugate was observed at 780 nm at different time points using C4 column on Agilent 1200 Infinity II.

Binding Pocket Determination: Determination of binding pocket of **1**-Cl was carried out as reported in literature.[235,236] Briefly, 5 μM of BSA was pre-blocked with 50X

excess of known binders of pocket I (warfarin), pocket II (ibuprofen) and pocket III (digoxin) for 1 h before adding 5 μM of **1**-Cl. The fluorescence was measured using spectrometer.

In-Vitro Assays: MDA-MB-231 and HepG2 cells were grown in Dulbecco's Modified Eagle's medium (DMEM) containing 10% fetal bovine serum (FBS). Cells were grown in an incubator at 37°C, humidified atmosphere containing 5% CO_2. Cells were grown in T-75 culture flask till 70% confluency before splitting into next passage.

Live Cell Staining: Uptake of dyes with the MDA-MB-231 and HepG2 cells was measured using Leica SP8 Confocal Microscope. The images were taken at 20x/0.75 water immersed objective. The NIR dye samples were excited at 670 nm laser (PMT detectors; 716-789 nm) and FITC samples were excited at 490 nm (HyD detectors; 500 – 589 nm).

BSA-FITC and 1-Cl colocalization: Briefly, 50,000 MDA-MB-231 cells divided into 4 groups. 1. **1**-Cl was incubated with BSA-FITC and used immediately. 2. **1**-Cl was preincubated with BSA-FITC for 24 h. 3. **1**-Cl was incubated with BSA that had Cys34 blocked. 4. **1**-Ph was incubated with BSA-FITC. Equimolar concentrations of dyes and BSA-FITC was used in each experiment. After 2 h of incubation, the cells were washed twice and PBS and imaged using Leica SP8 Confocal Microscope as mentioned above.

Blocking Experiment: The cells were divided in 4 groups; 1. control (no serum), 2. with serum, 3. BSP with serum, and 4. BSP without serum. Briefly, 50,000 cells were seeded using media containing serum on 4 well chambers (Nunc Lab-Tek) and allowed to adhere overnight. The cells were starved for 4 h in serum free media before the

experiment. Group 1 was used as a standard for other groups. Group 3 and 4 were pre-blocked for 5 mins with 250 μM of BSP with or without serum containing media respectively. The cells were incubated with **1**-Cl, **1**-Ph, **2**-Cl, **5**-Cl, **5**-Ph and ICG for 30 mins, washed twice with PBS imaged using Leica SP8 Confocal Microscope.

DMOG was added to the chambers 24 h prior to experiment to induce hypoxia in cells. Dyes were added to the chambers for 30 mins, washed and imaged using Leica Microscope.

Cellular uptake of **1**-Cl, **1**-Ph, **2**-Cl, **5**-Cl, **5**-Ph and ICG was quantified by using BD FACSAria II. The cells were again divided into 4 groups and treated as mentioned above. After incubation, the cells were washed thrice with PBS, dissociated from the plate using 200 μM of Cell Dissociation Buffer, enzyme free (Thermofisher) and suspended in PBS. The fluorescence of the samples was measured by 633 nm excitation source and 750/45 emission filter.

Cellular uptake of **1**-Cl, **1**-Ph, **2**-Cl, **5**-Cl, **5**-Ph and ICG was also quantified using BSA only in the media. MDA-MB-231 cells were seeded on 4 well chamber and starved for 4 h. Dyes were added to the chambers with or without BSA in the solution. Sample without BSA was considered as control and quantified using BD FACSAria II.

Supporting Figures:

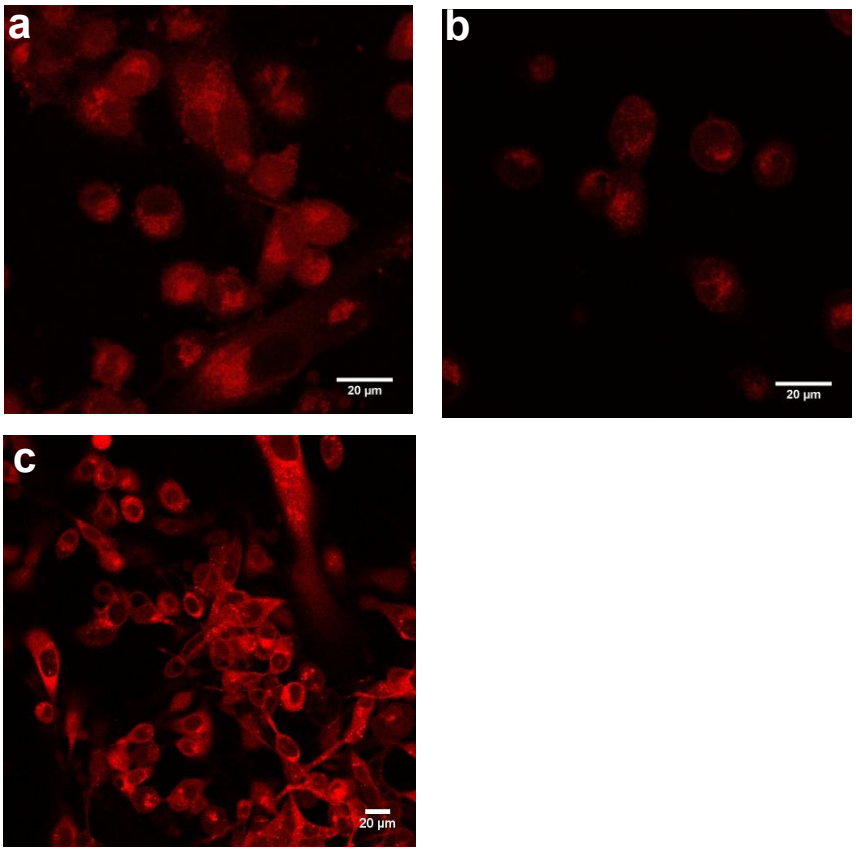

Figure F-S1. 1-Cl (20 µM) in serum free media **a** control, **b** blocked with BSP for 5 mins (250 µM) **c** DMOG (1mM). Throughout the experiments, images were taken at by Leica Confocal Microscope at 20X/0.75 NA

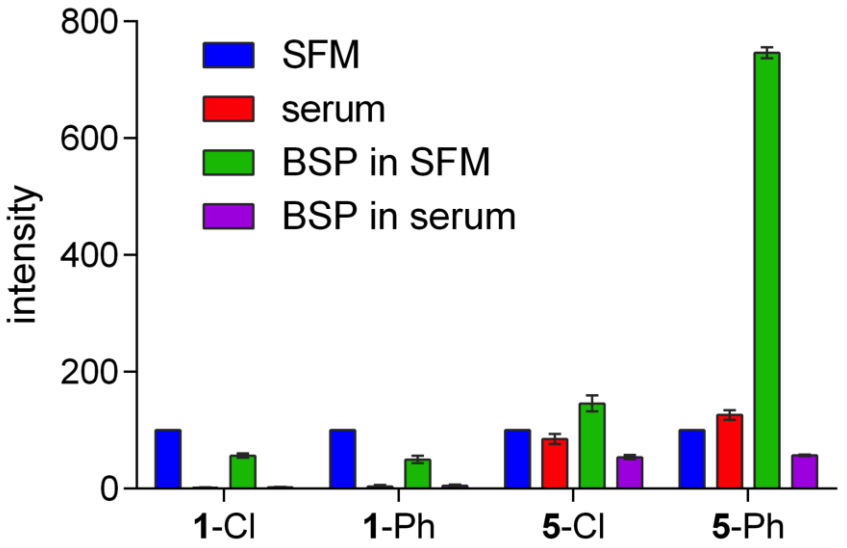

Figure F-S2. uptake of dye in serum free (blue) and serum media (red) and BSP blocking in serum free media (green) and serum media (purple) was quantified of **1**-Cl, **1**-Ph, **5**-Cl, and **5**-Ph. Uptake of dye into cells were quantified by FACS.

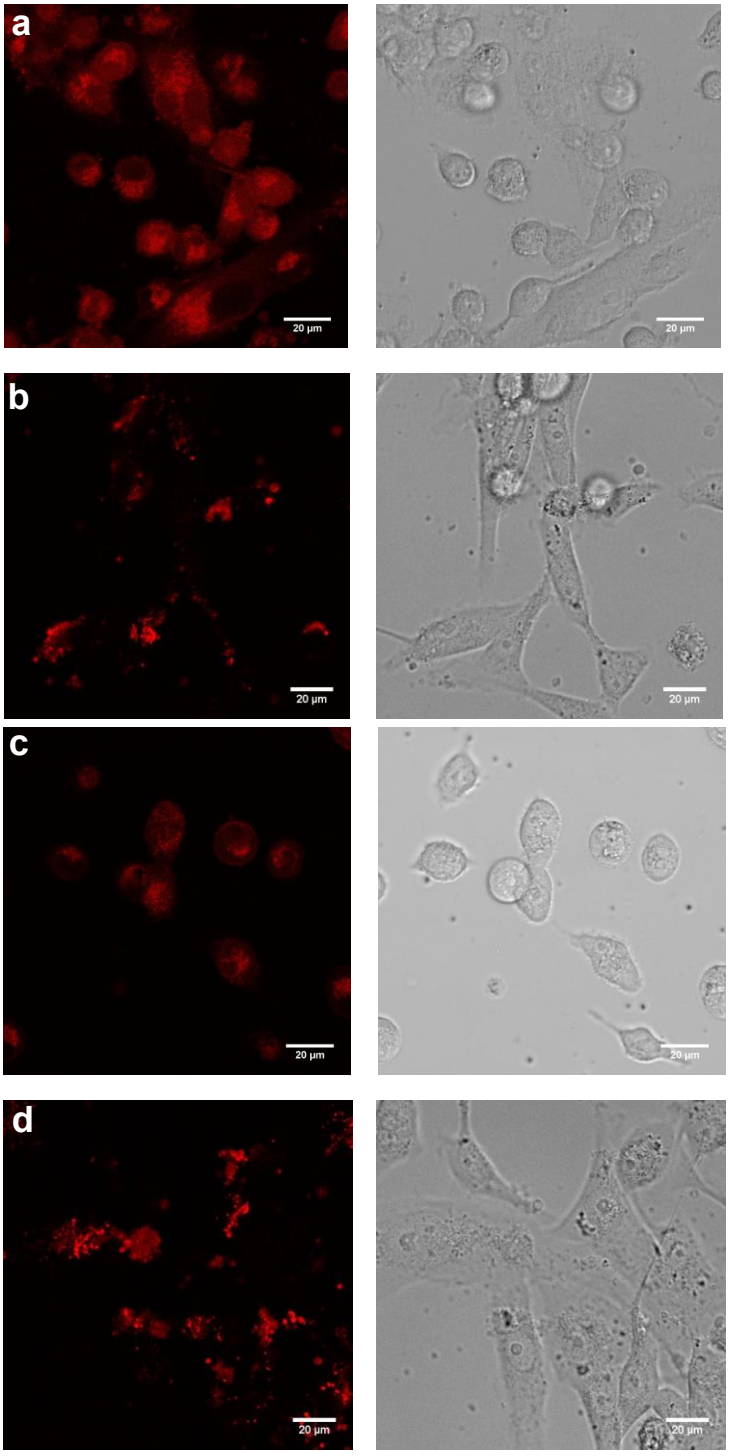

Figure F-S3. qualitative uptake comparison of **a 1**-Cl with **b 5**-Cl, and **c 1**-Ph with **5**-Ph

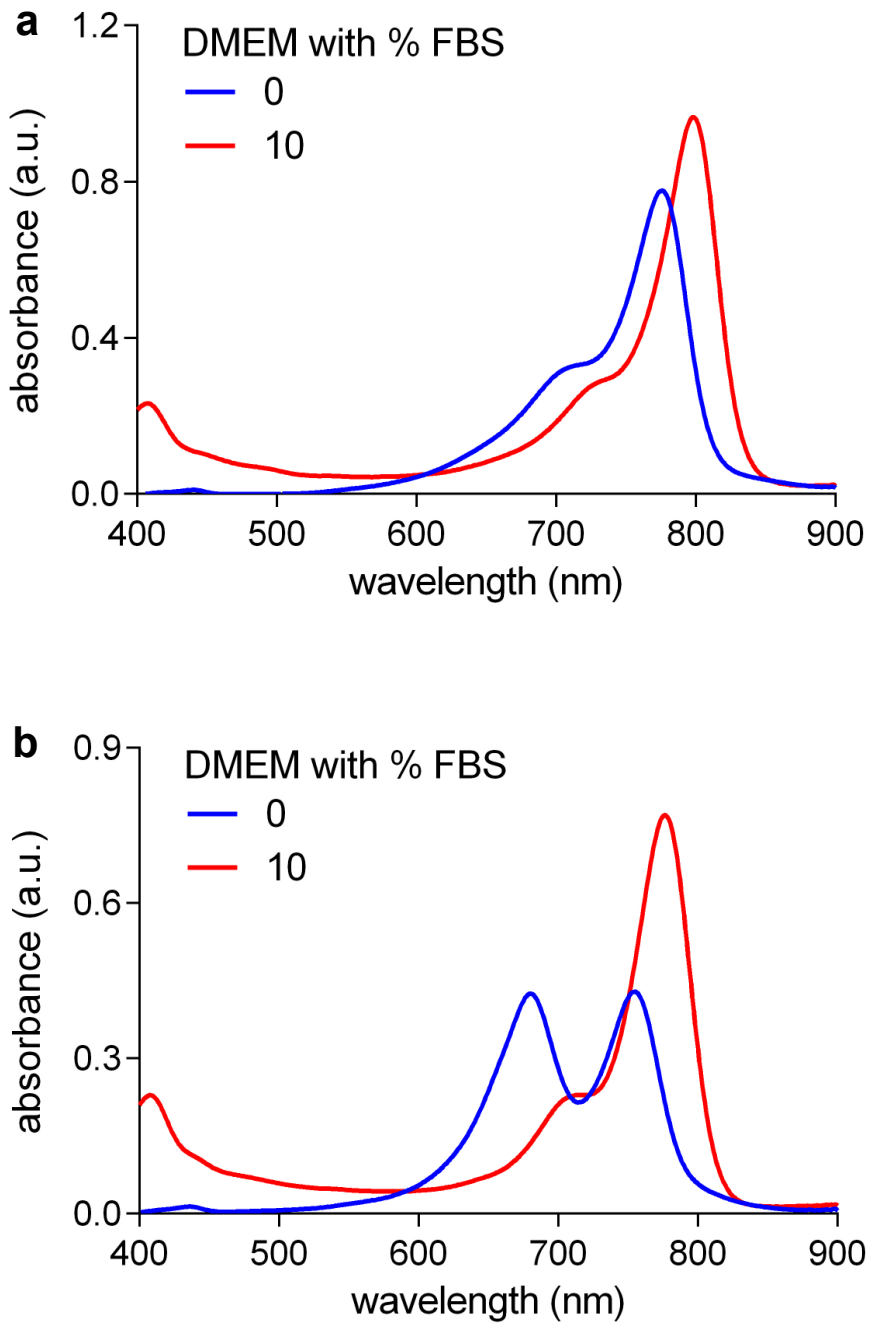

Figure F-S4. Absorbance spectra at 5 μM of **a 1**-Cl, and **b 1**-Ph in presence and absence of FBS in DMEM media. Absorbance was observed by UV Vis spectrometer.

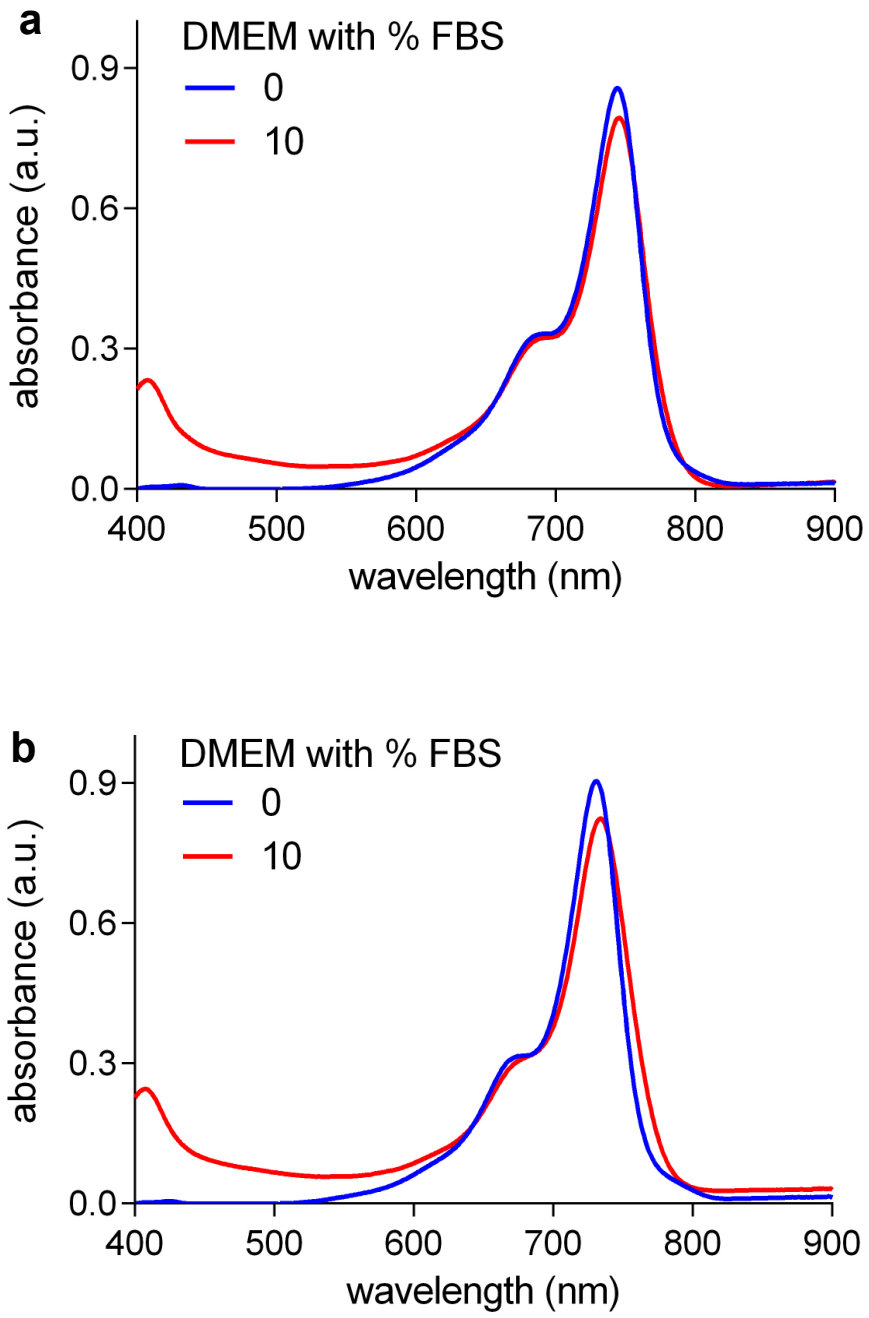

Figure F-S5. Absorbance spectra at 5 μM of **a 5**-Cl, and **b 5**-Ph in presence and absence of FBS in DMEM media. Absorbance was observed by UV Vis spectrometer.

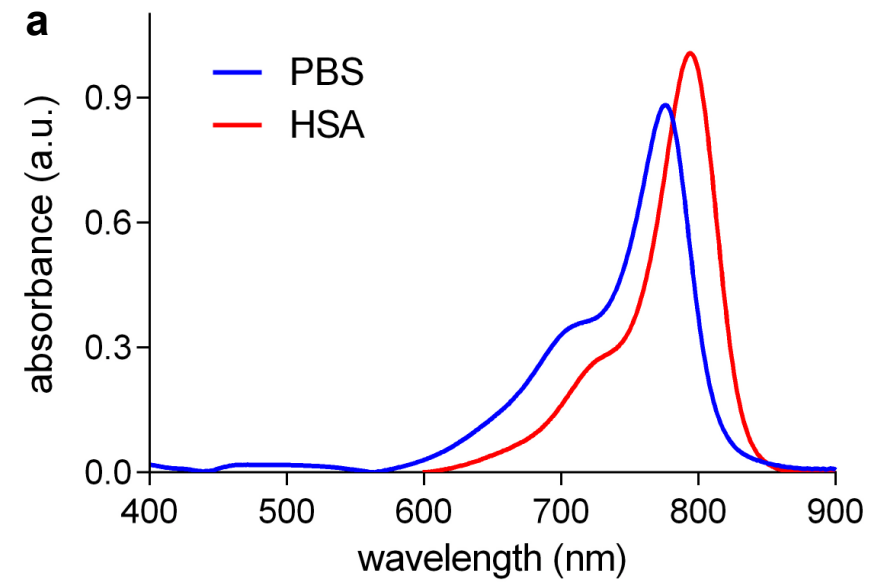
a
PBS
HSA
absorbance (a.u.)
0.0
0.3
0.6
0.9
400
500
600
700
800
900
wavelength (nm)

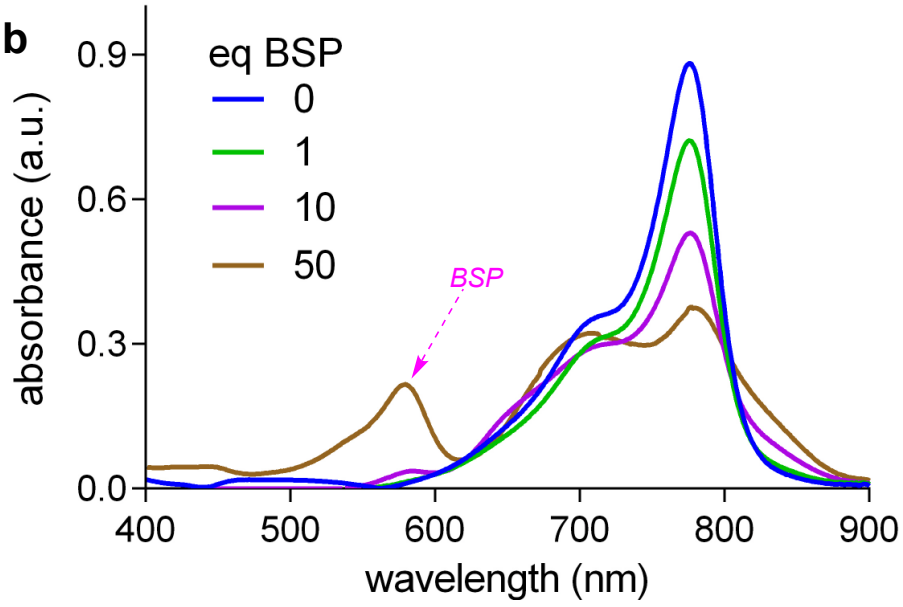
b
eq BSP
0
1
10
50
BSP
absorbance (a.u.)
0.0
0.3
0.6
0.9
400
500
600
700
800
900
wavelength (nm)

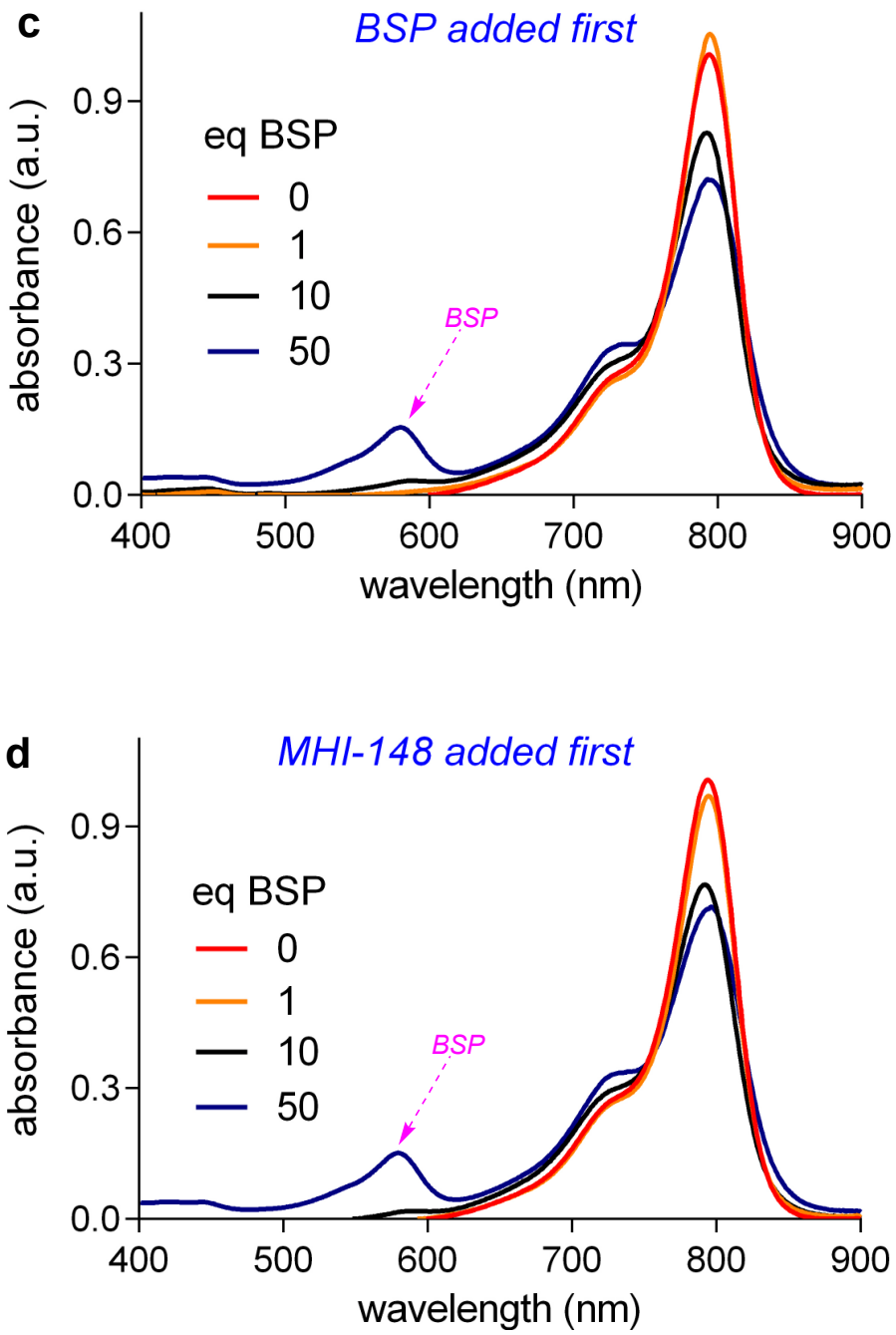

Figure F-S6. Absorbance spectra of Interaction of **1**-Cl (5 μM) **a** in presence and absence of HSA (5 μM), and **b** increasing concentration of BSP, **c** addition of **1**-Cl in presence of HSA-BSP complex, and **d** addition of BSP in presence of **1**-Cl-HSA

noncovalent complex. The experiments were carried out at pH 7.4 in PBS buffer at 37 ºC and were observed by UV Vis spectrometer.

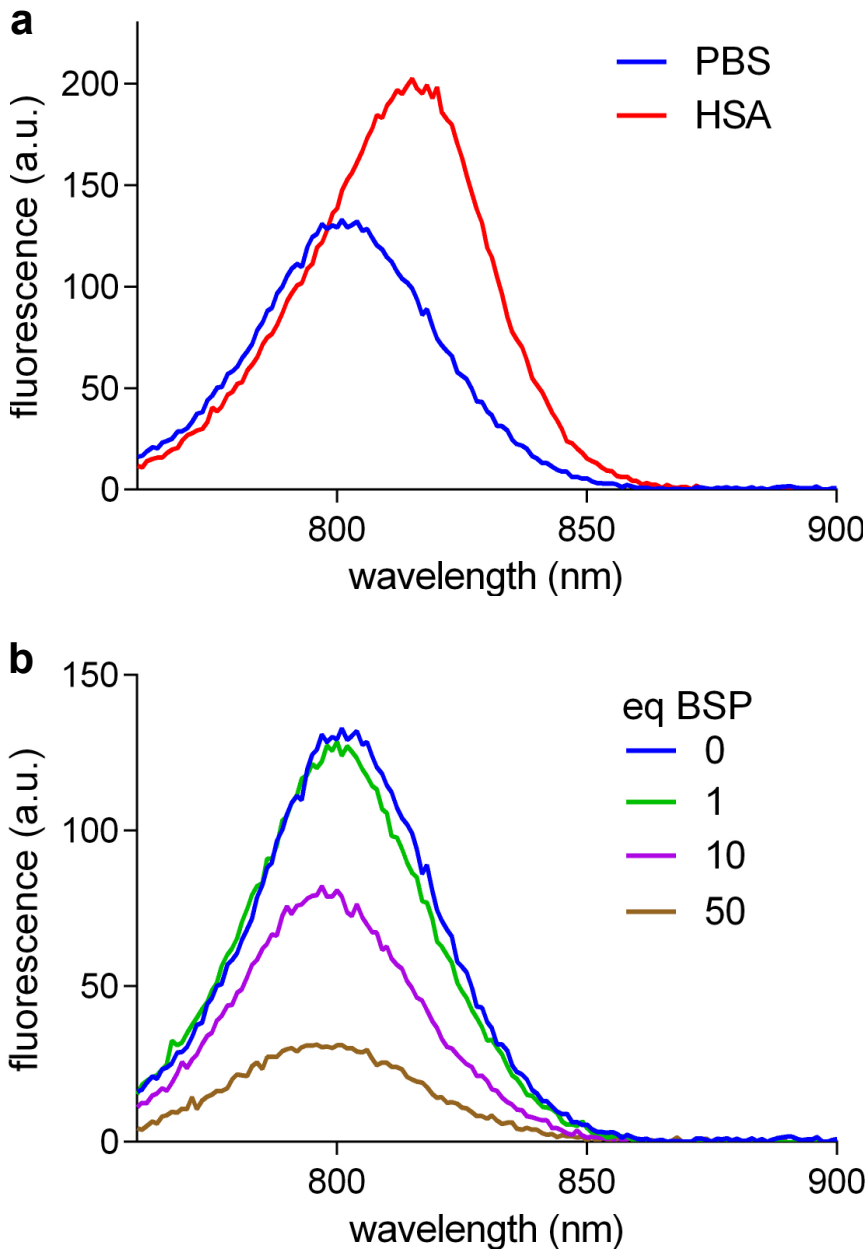

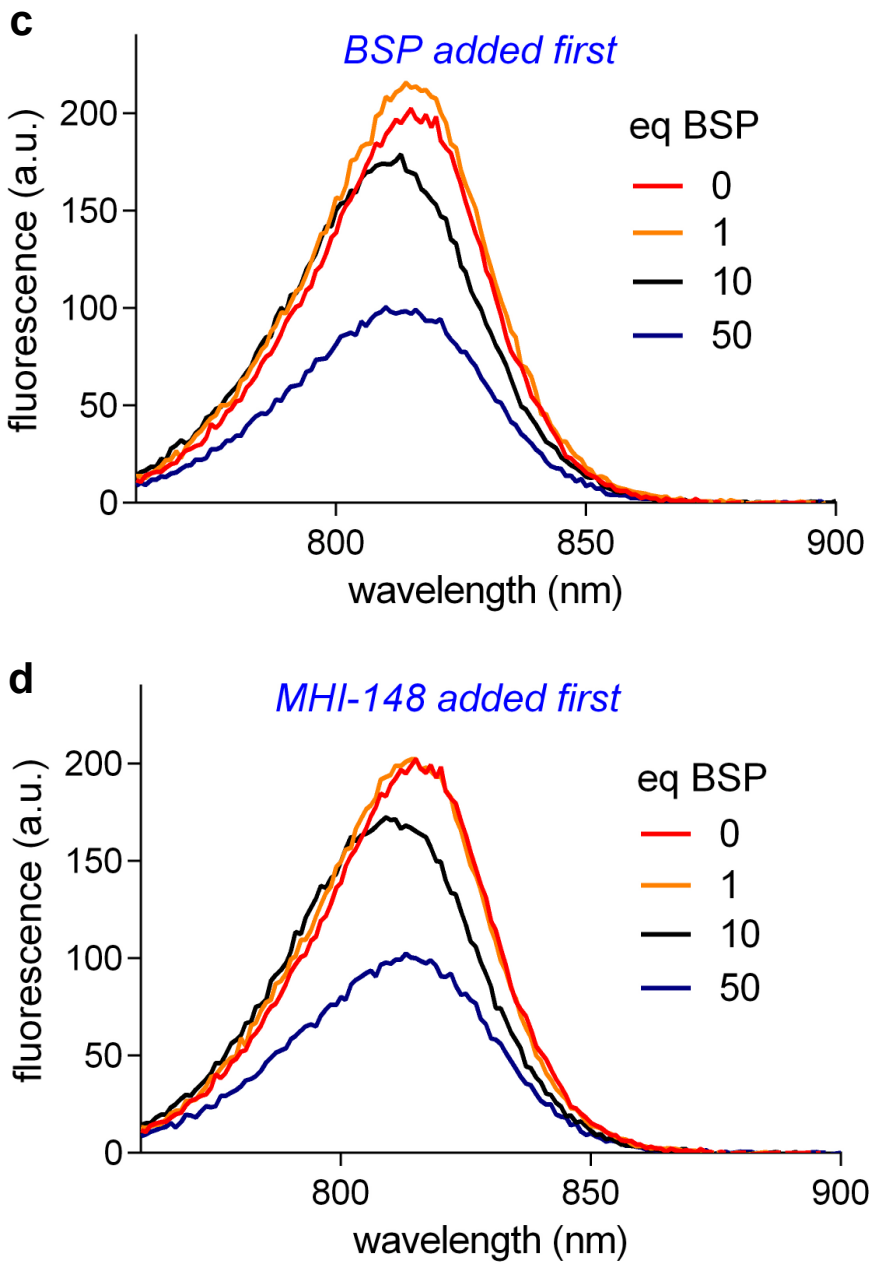

Figure F-S7. Fluorescence spectra of Interaction of **1**-Cl (5 μM) **a** in presence and absence of HSA (5 μM), and **b** increasing concentration of BSP, **c** addition of **1**-Cl in presence of HSA-BSP complex, and **d** addition of BSP in presence of **1**-Cl-HSA

noncovalent complex. The experiments were carried out at pH 7.4 in PBS buffer at 37 ºC and were observed by UV Vis spectrometer.

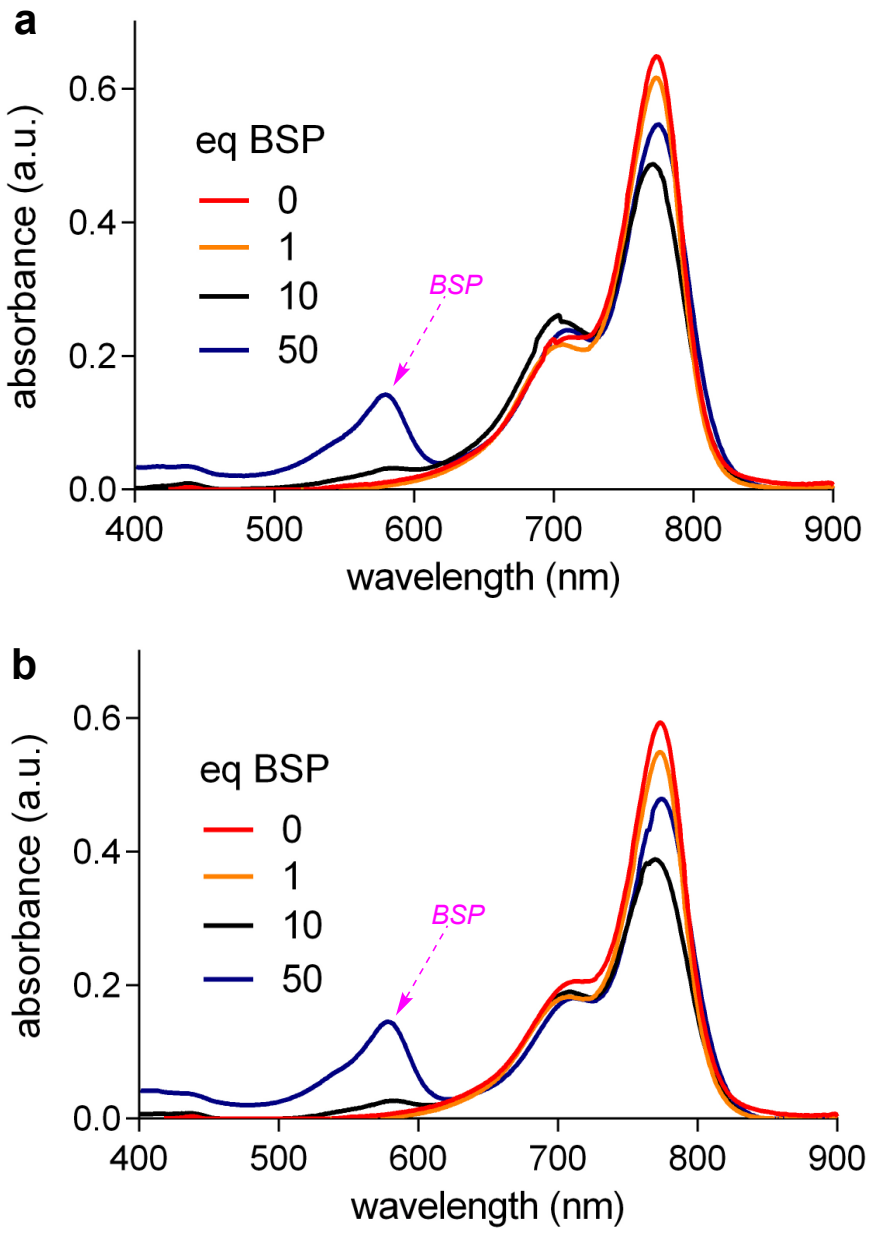

Figure F-S8. Interaction of **1**-Ph (5μM) at 0, 1, 10 and 50 eq of BSP after **a** 0 h; **b** 5 h. The experiments were carried out at pH 7.4 in PBS buffer at 37 ^{o}C and were observed by UV Vis spectrometer.

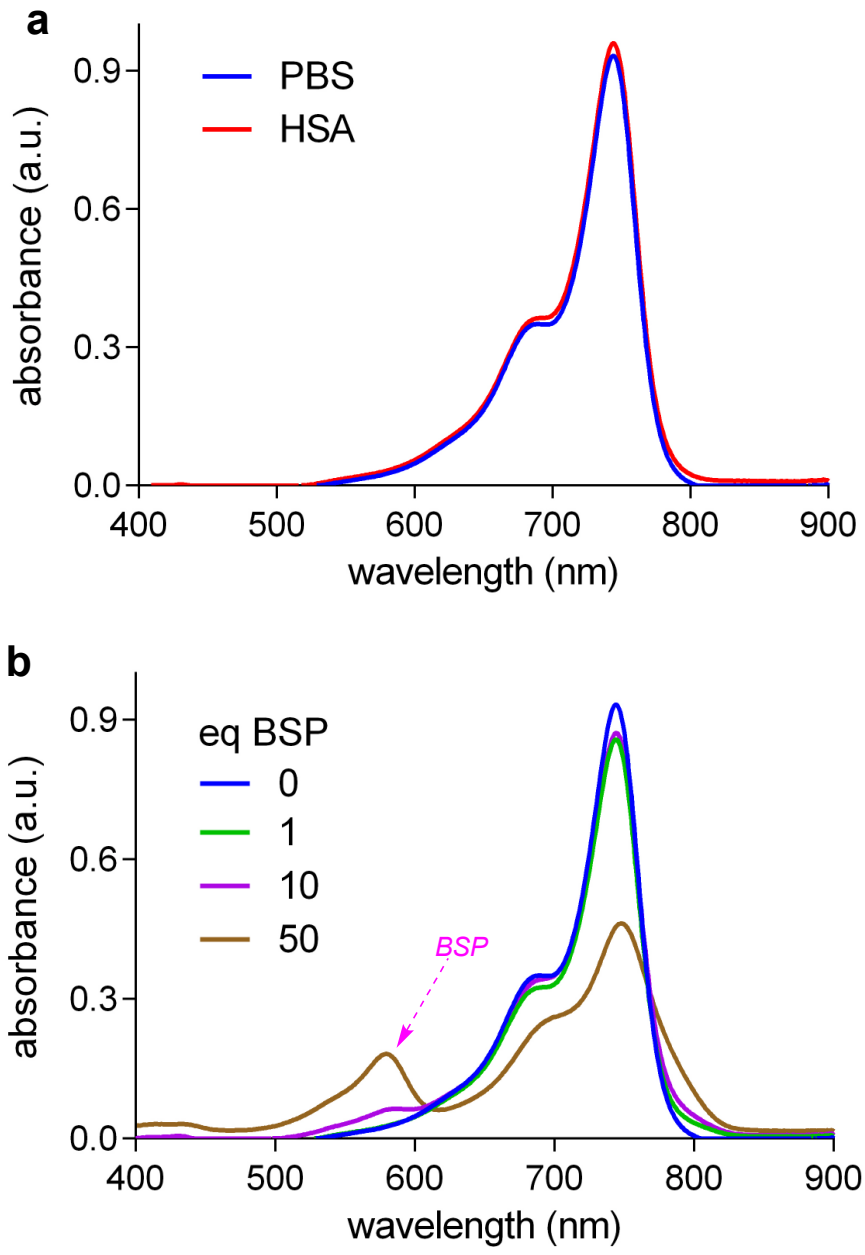

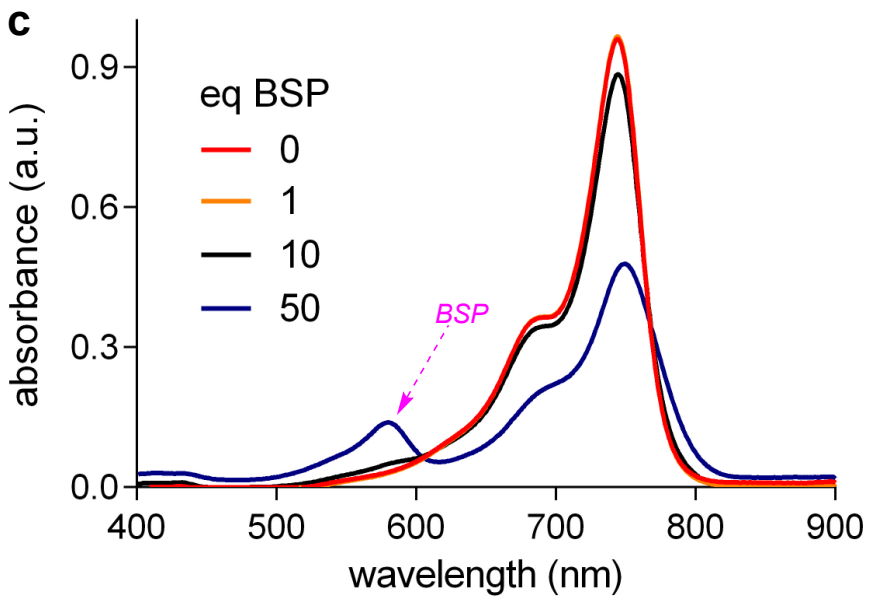

Figure F-S9. UV spectra to monitor interaction of **5**-Cl (5 μM) **a** in presence and absence of HSA (μM); and, **b** with increasing concentrations of BSP. **c** Addition of BSP to the **5**-Cl-HSA complex. The experiments were carried out at pH 7.4 in PBS buffer at 37 ^{o}C.

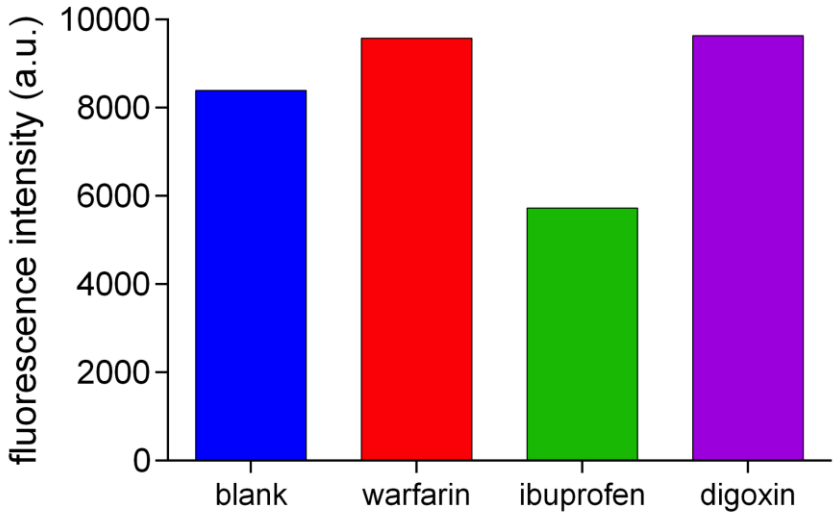

Figure F-S10. Determination of binding pocket of **1**-Cl by competitive binding with other known binders of pocket I (warfarin), pocket II (ibuprofen) and pocket III (digoxin). 5 μM of BSA was pre-blocked with the known binders for 1 h before adding 5 μM of **1**-Cl. The fluorescence was measured after 1 h using spectrometer.

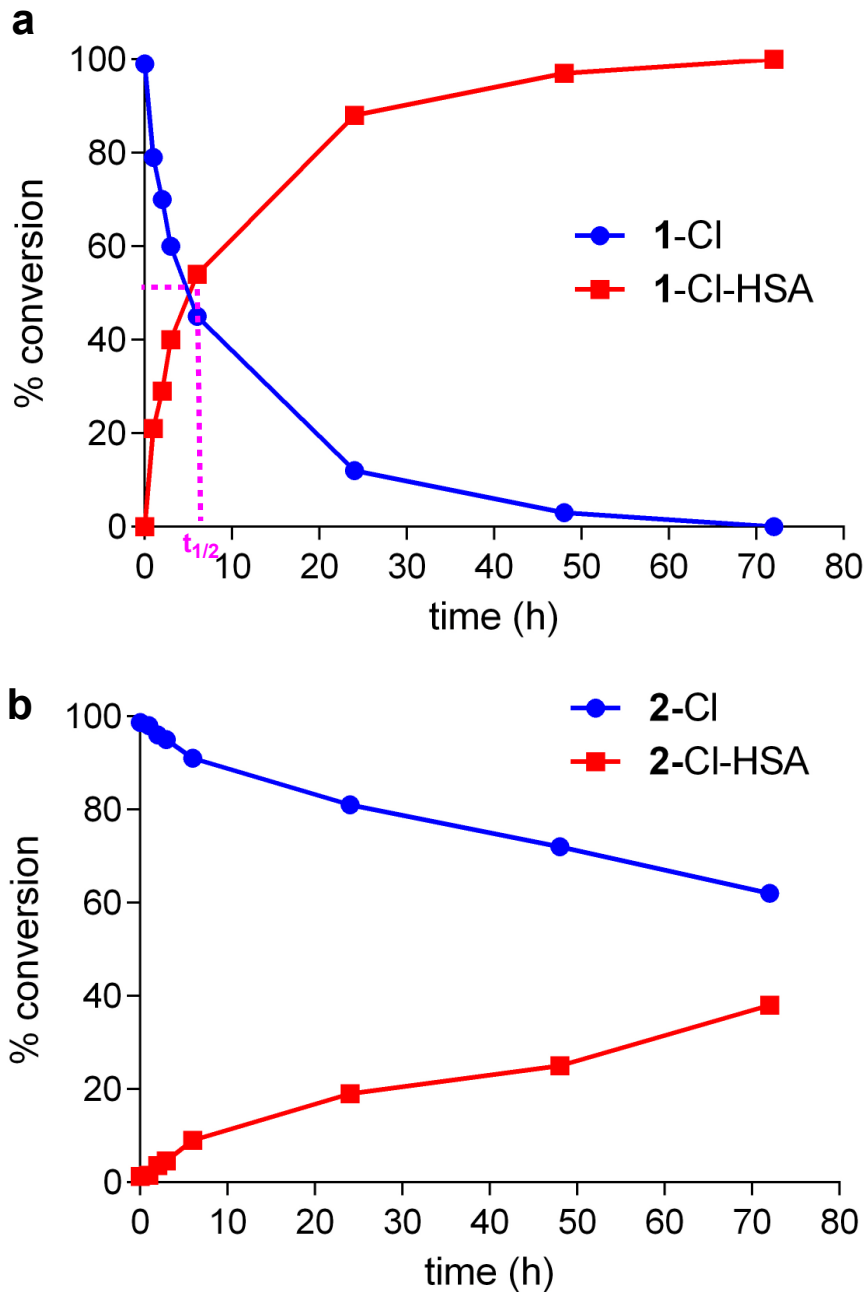

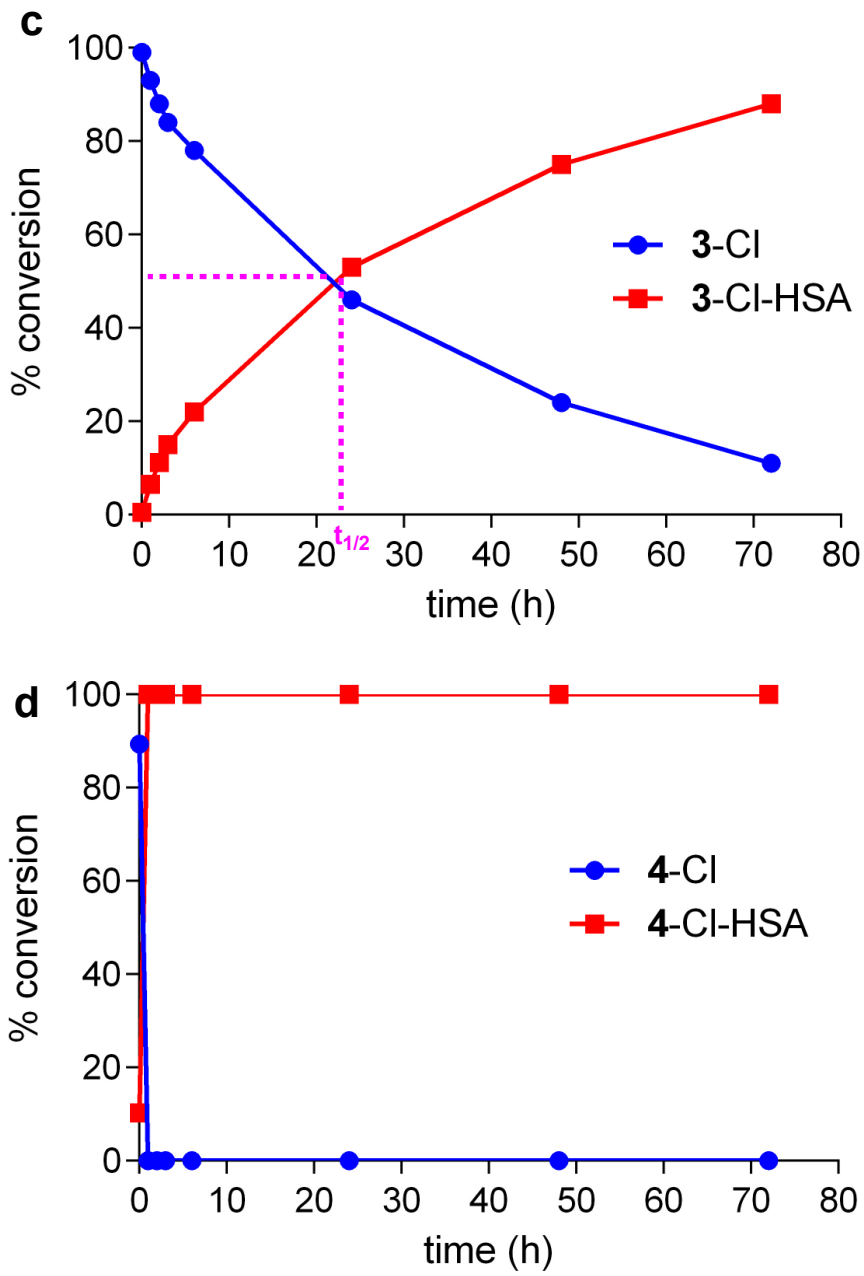

Figure F-S11. Reactivity of 1 eq of **a 1**-Cl, **b 2**-Cl, **c 3**-Cl and **d 4**-Cl was tested with HSA (2 eq) at pH 7.4 in PBS buffer at 37 ºC.

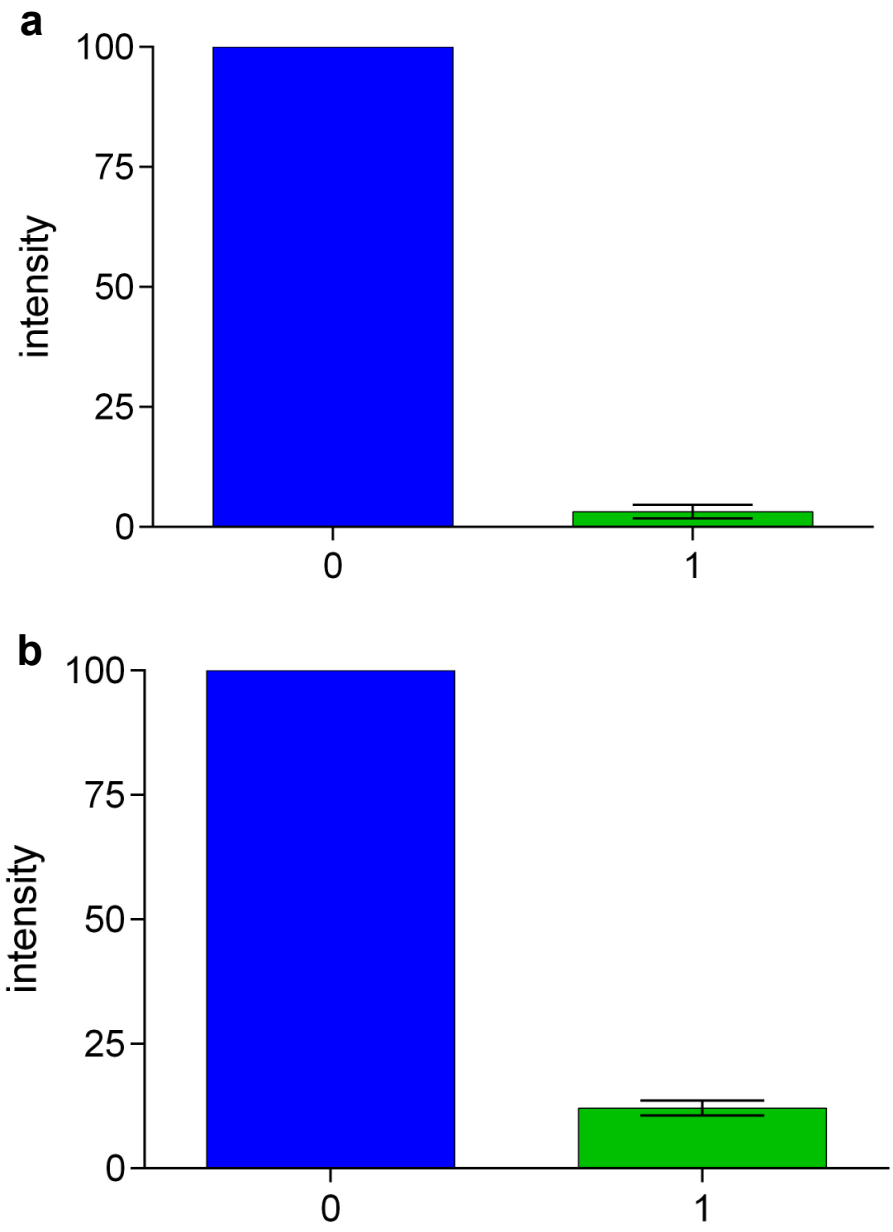

Figure F-S12. MDA-MB-231 cells were incubated with **a 1**-Cl and **b 1**-Ph at 20 μM with 0 and 1 eq of BSA at 37 ºC for 20 mins. Relative uptake of dyes was quantified by FACS.

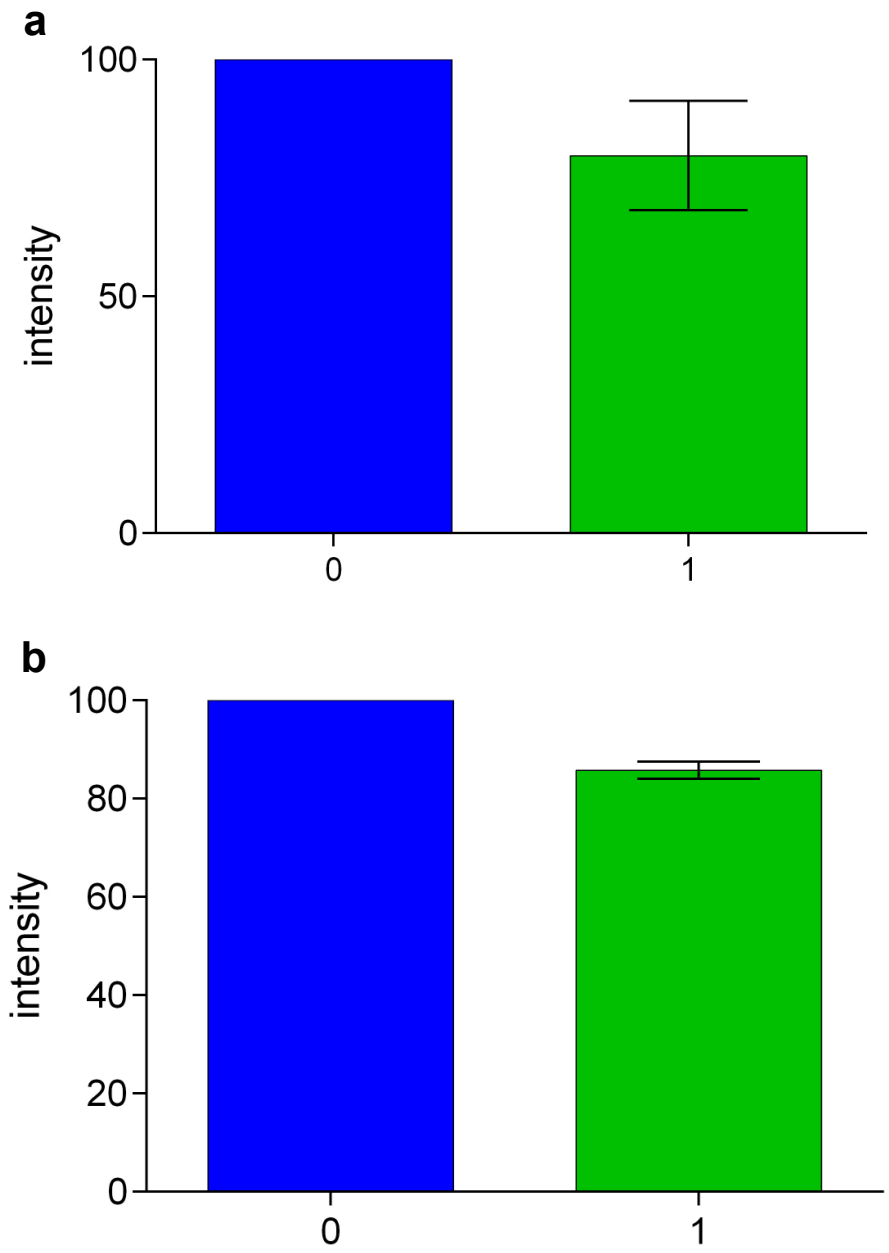

Figure F-S13. MDA-MB-231 cells were incubated with **a 5**-Cl and **b 5**-Ph at 20 μM with 0, 0.5 and 1 eq of BSA at 37 ºC for 20 mins. Uptake of dye into cells were quantified by a FACS.

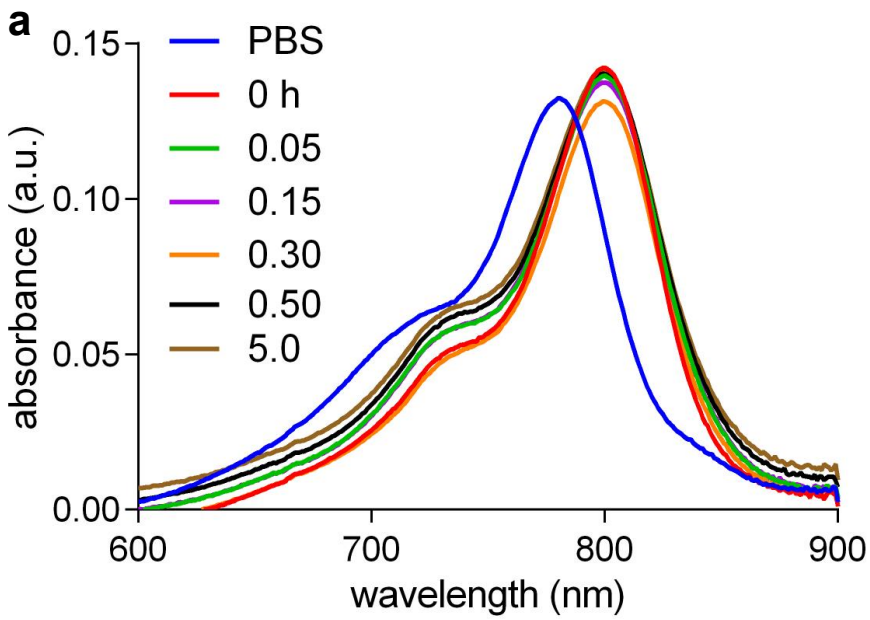
a
0.15
0.10
0.05
0.00
absorbance (a.u.)
PBS
0 h
0.05
0.15
0.30
0.50
5.0
600
700
800
900
wavelength (nm)

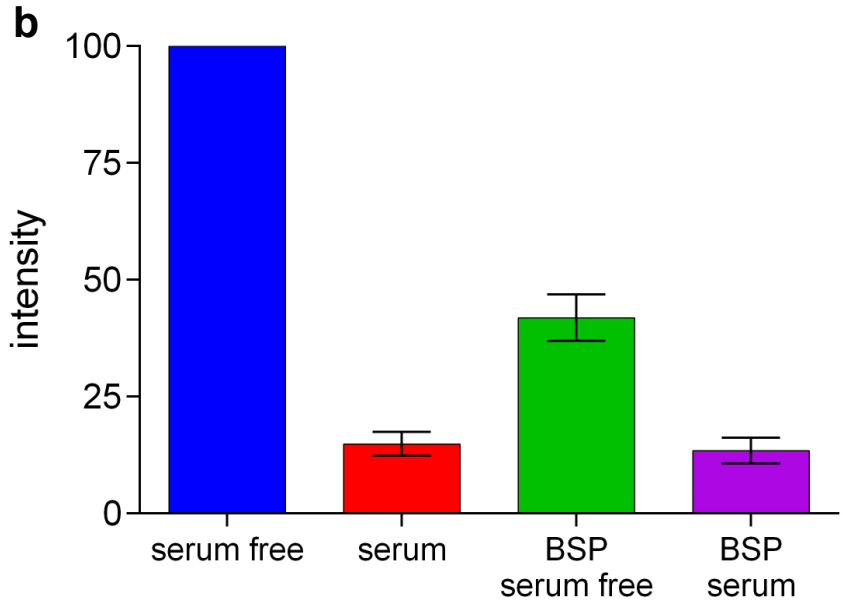
b
100
75
50
25
0
intensity
serum free
serum
BSP
serum free
BSP
serum

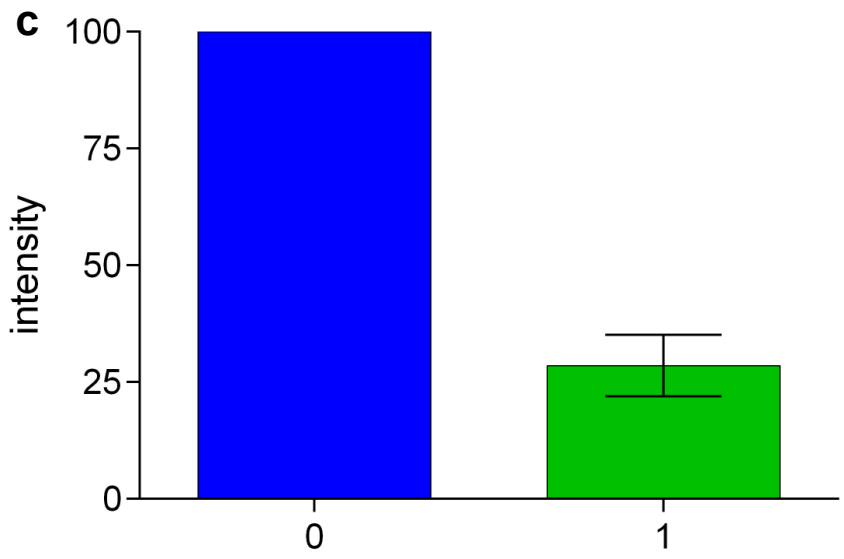

Figure F-S14. **a** Absorbance spectra of **2**-Cl in PBS and after addition of 50 eq of HSA. Uptake of **2**-Cl by MDA-MB-231 cells (as measured by FACS): **b** with and without BSP and serum; and, **c** in presence of 1 eq of BSA.

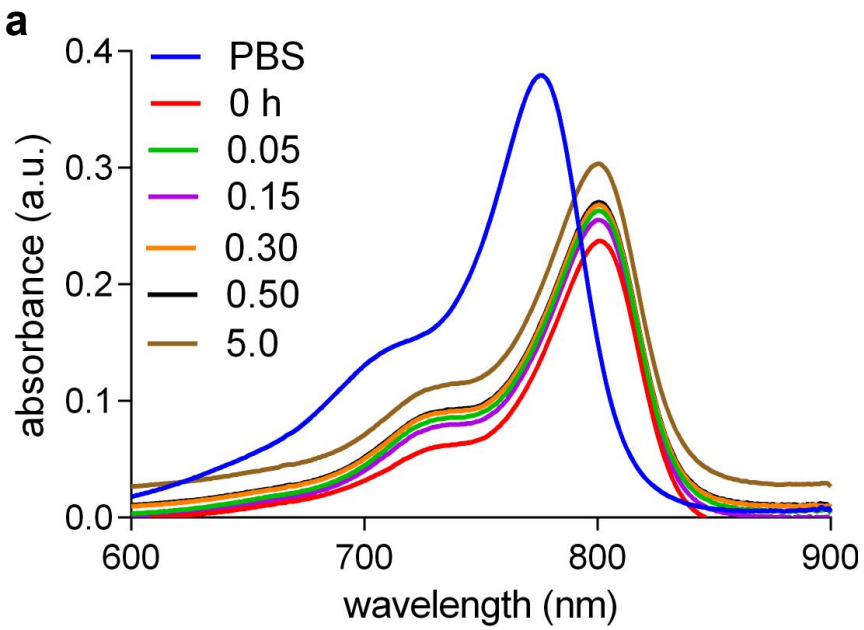

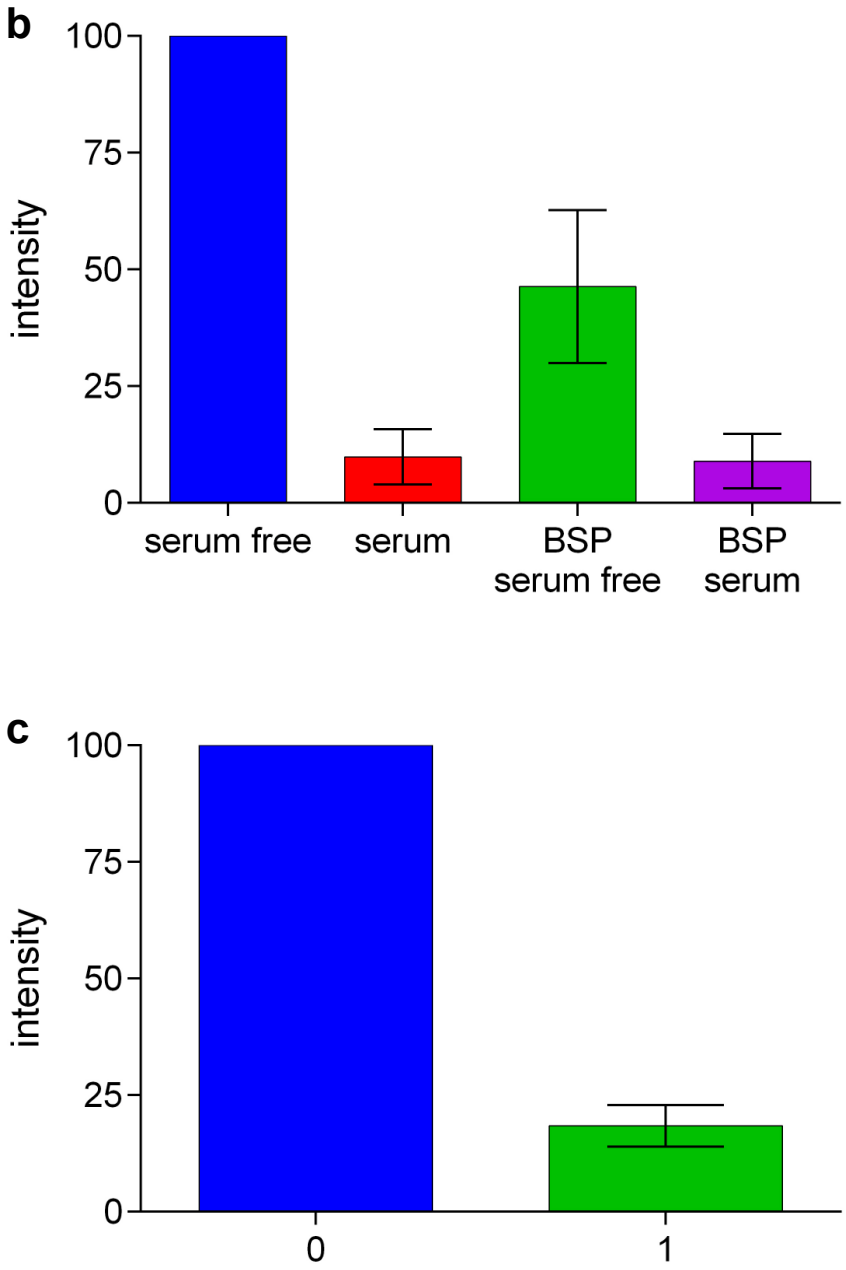

Figure F-S15. a Absorbance spectra of ICG in PBS and after addition of 50 eq of HSA. Uptake of **2**-Cl by MDA-MB-231 cells (as measured by FACS): **b** with and without BSP and serum; and, **c** in presence of 1 eq of BSA.

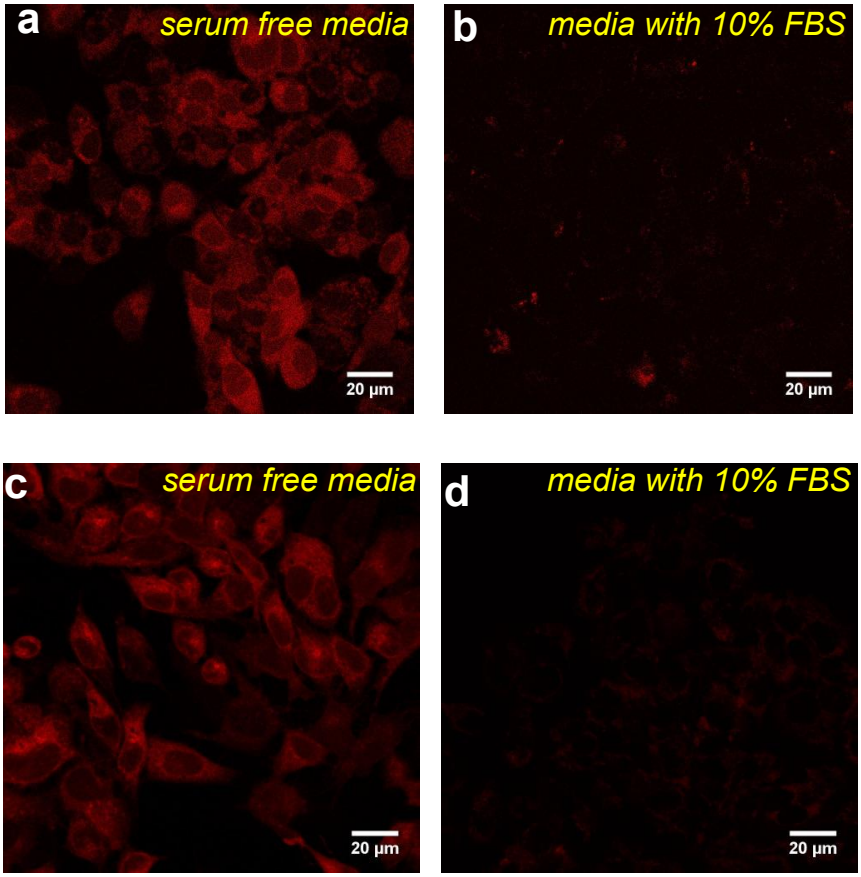

Figure F-S16. HepG2 cells were incubated with **1**-Cl in **a** serum free media and **b** serum with 10% FBS and **1**-Ph in **a** serum free media and **b** serum with 10% FBS at 20 μM for 20 mins.

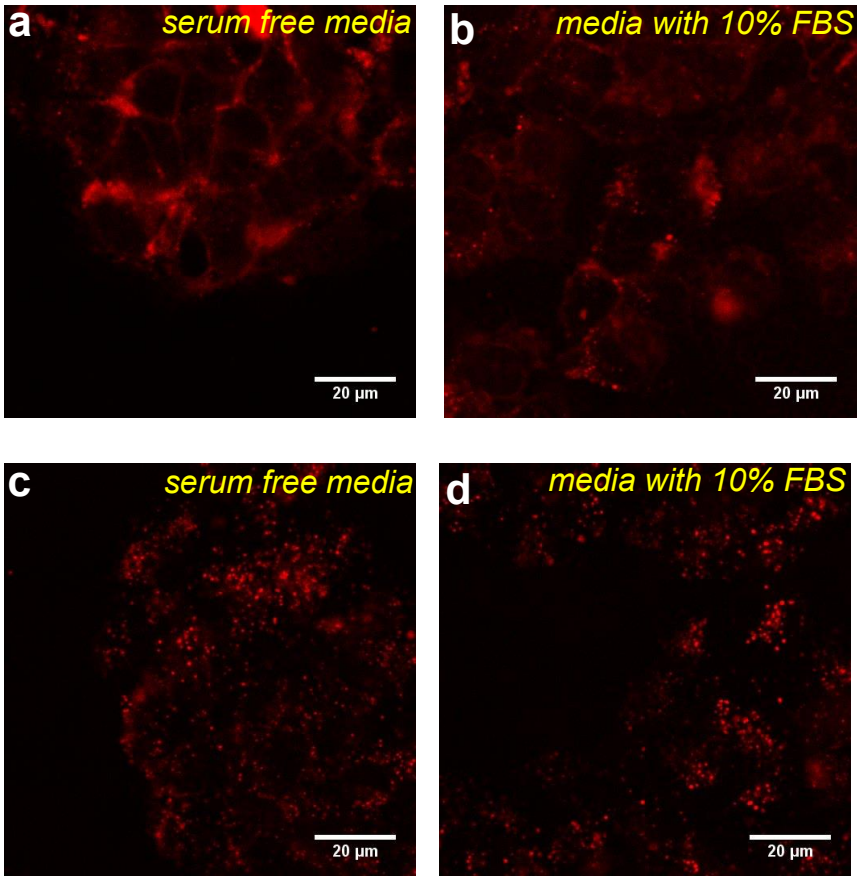

Figure F-S17. HepG2 cells were incubated with **5**-Cl in **a** serum free media and **b** serum with 10% FBS and **5**-Ph in **a** serum free media and **b** serum with 10% FBS at 20 µM for 20 mins.

APPENDIX G

UNPUBLISHED DATA OF OTHER CYANINE-KINASE INHIBITORS

CONJUGATES

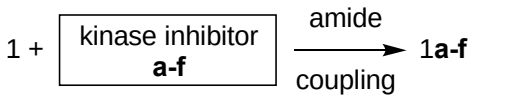

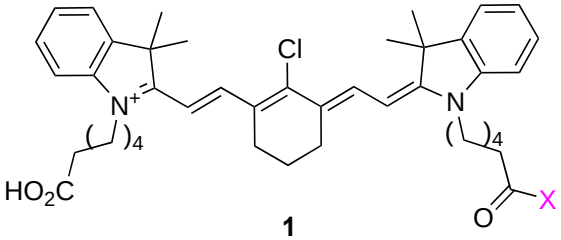

1

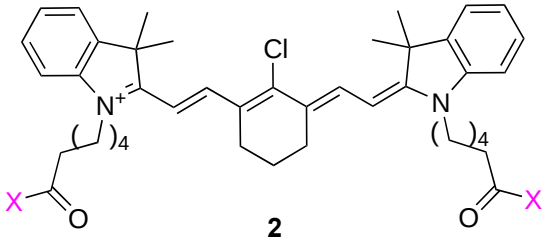

2

X =

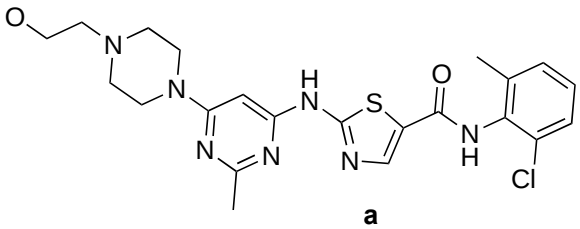

a

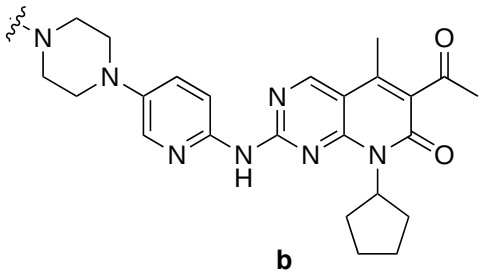

b

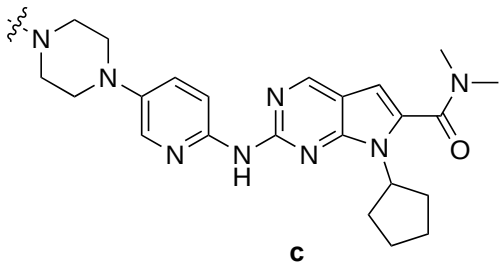

c

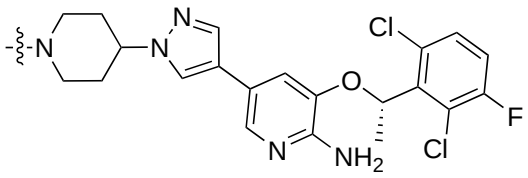

d

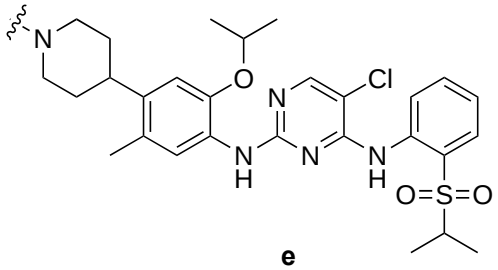

e

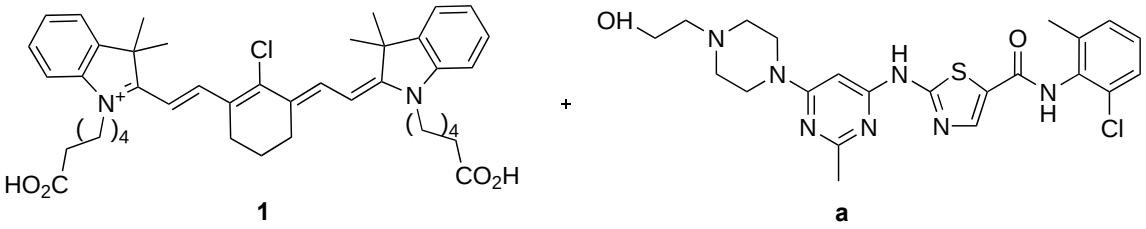

1 **a**

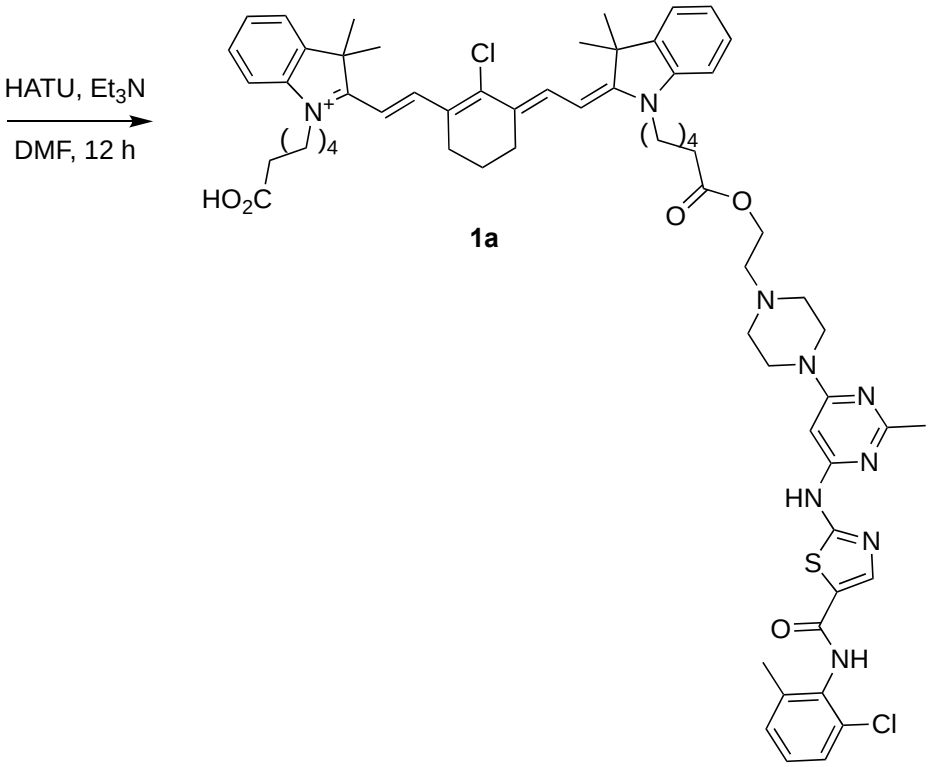

Scheme G-1. Synthesis scheme for **1a**

Synthesis of **1a**

Cyanine dye **1** (200.0 mg, 0.29 mmol), triethylamine (48.50 uL, 0.34 mmol) and HATU (110.2 mg, 0.29 mmol) were added in 2 mL DMF and stirred for 15 mins followed by **a** (141.52 mg, 0.29 mmol) was added afterwards and stirred for 12 h under argon balloon. Solvent was removed and the crude was purified by reverse phase column on prep-HPLC {50% MeCN/50%H_2O – 90%MeCN/10%H_2O (containing 0.1% TFA) in 20 mins} to get the desired product as amorphous green solid (32 mg, 9.6%).

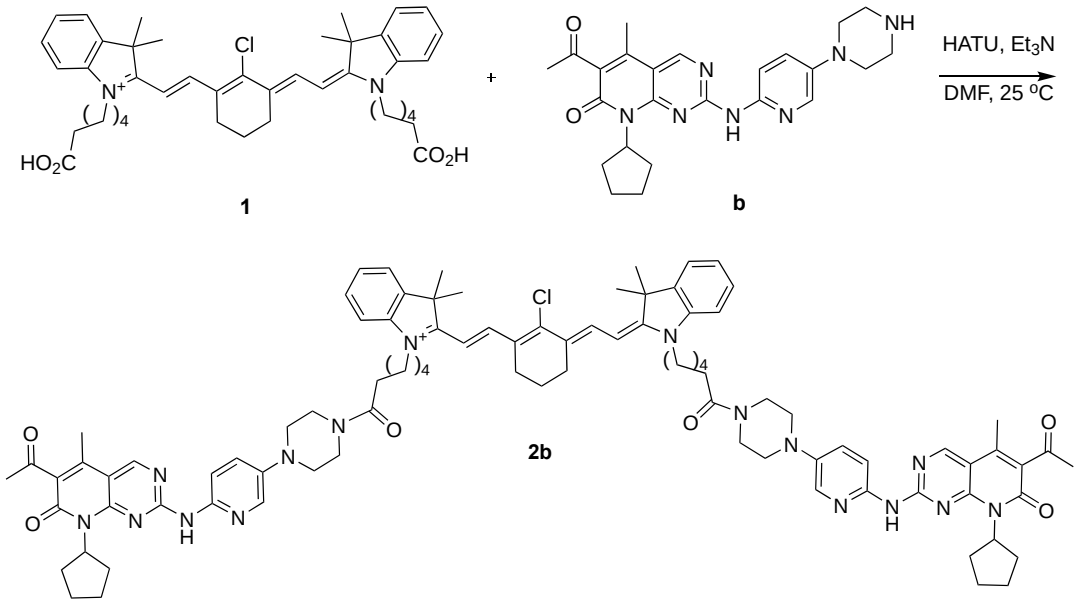

Scheme G-2. Synthesis scheme for **2b**

Synthesis of **2b**

Cyanine dye **1** (200.0 mg, 0.29 mmol), triethylamine (48.50 uL, 0.34 mmol) and HATU (110.2 mg, 0.29 mmol) were added in 2 mL DMF and stirred for 15 mins followed by **b** (130.5 mg, 0.58 mmol) and stirred for 12 h under argon balloon. Solvent was removed and the crude was purified by reverse phase column on prep-HPLC {50% MeCN/50%H_2O – 90%MeCN/10%H_2O (containing 0.1% TFA) in 20 mins} to get the desired product as amorphous green solid (143.4 mg, 32%).

Characterization of 1a, b, c, d, e, f and 2b

1a

^{1}H NMR (400 MHz, MeOD) δ 8.46 (dd, *J* = 13.9, 9.9 Hz, 2H), 8.17 – 8.15 (m, 1H), 7.54 (d, *J* = 7.6 Hz, 2H), 7.45 (dd, *J* = 13.6, 7.5 Hz, 2H), 7.29 (dt, *J* = 14.8, 7.0 Hz, 6H), 6.30 (t, *J* = 13.8 Hz, 2H), 6.16 (s, 1H), 5.50 (s, 3H), 4.51 – 4.43 (m, 2H), 4.20 (dd, *J* = 12.0, 7.1 Hz, 4H), 3.98 (s, 3H), 3.53 – 3.40 (m, 5H), 3.37 (s, 1H), 2.74 (d, *J* = 5.9 Hz, 4H), 2.48 (dd, *J* = 16.6, 9.2 Hz, 6H), 2.37 – 2.28 (m, 6H), 2.01 – 1.94 (m, 2H), 1.89 (s, 4H), 1.75 (d, *J* = 2.1 Hz, 12H), 1.69 (dd, *J* = 14.3, 6.9 Hz, 5H), 1.53 (q, *J* = 14.7 Hz, 5H).

^{13}C NMR (101 MHz, MeOD) δ 175.83, 172.91, 172.56, 162.37, 149.80, 143.83, 142.27, 142.10, 141.30, 141.15, 128.76, 128.56, 126.93, 126.66, 126.46, 125.40, 125.05, 122.15, 111.04, 110.70, 100.53, 83.20, 57.76, 55.32, 53.37, 51.60, 49.39, 49.17, 48.30, 41.02, 33.19, 32.97, 26.96, 26.89, 26.71, 25.99, 25.95, 24.22, 24.04, 20.72, 17.30.

HRMS: calculated 1152.5062 found 1152.5067

^{1}H

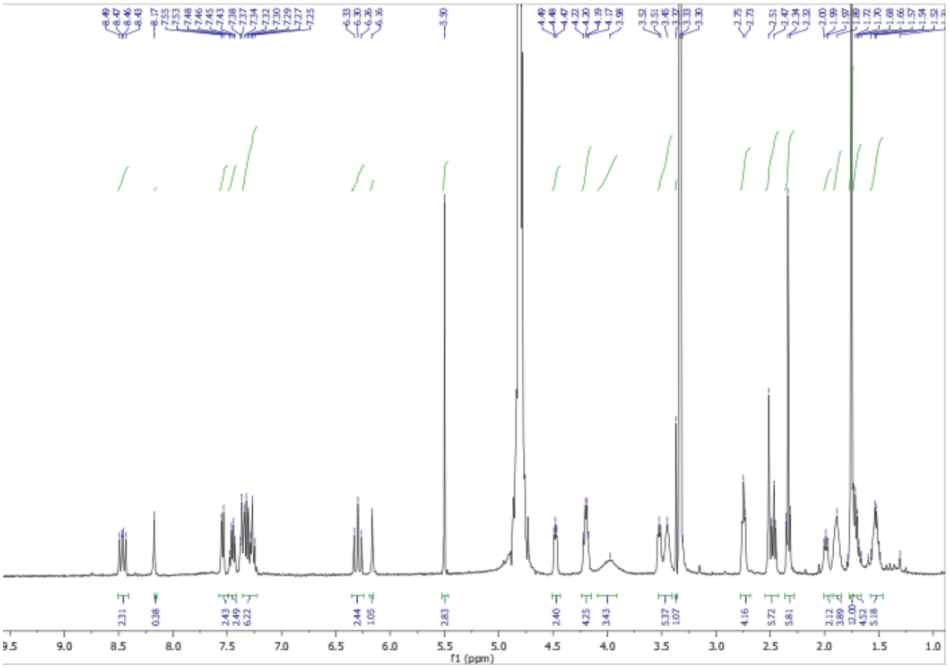

^{13}C

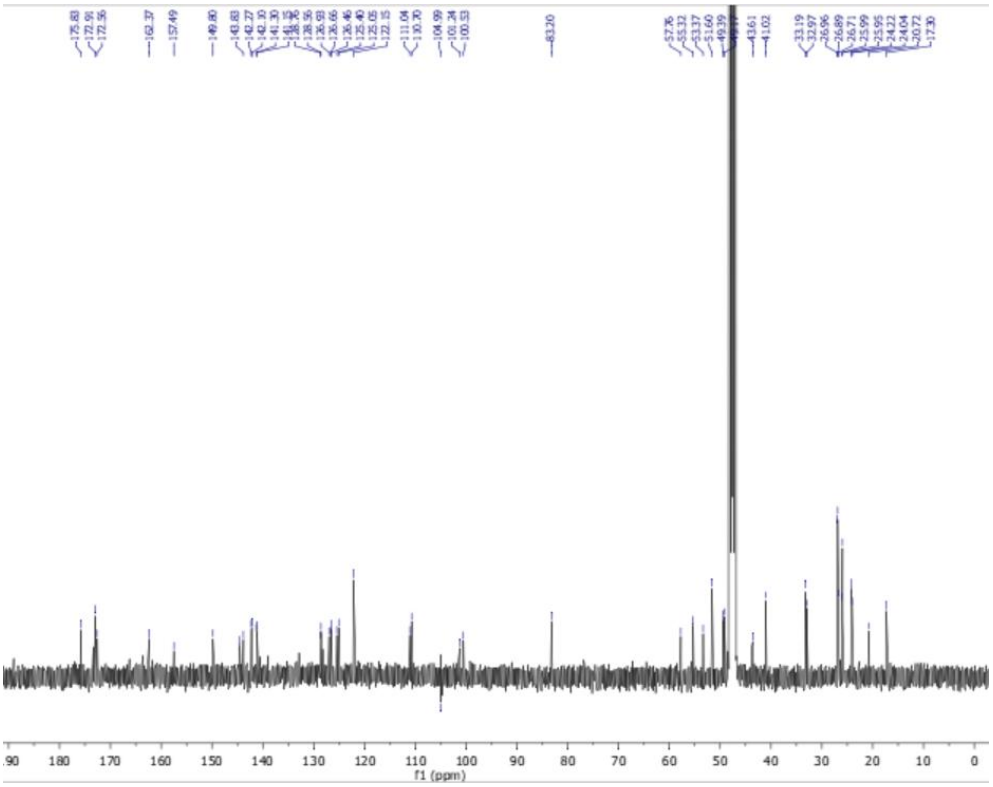

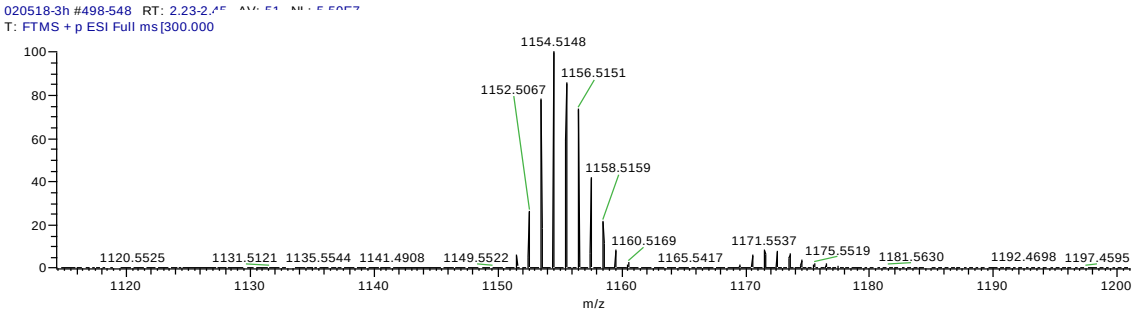

1b

^{1}H NMR (400 MHz, MeOD) δ 8.97 (d, *J* = 4.4 Hz, 1H), 8.47 (d, *J* = 14.2 Hz, 1H), 8.37 (s, 1H), 7.94 (d, *J* = 8.2 Hz, 2H), 7.72 (d, *J* = 10.0 Hz, 1H), 7.55 (d, *J* = 7.2 Hz, 1H), 7.50 (d, *J* = 7.5 Hz, 1H), 7.47 (s, 1H), 7.46 – 7.45 (m, 1H), 7.44 (s, 1H), 7.41 (s, 1H), 7.38 (d, *J* = 7.5 Hz, 2H), 7.34 – 7.23 (m, 3H), 6.34 (d, *J* = 14.1 Hz, 1H), 6.20 (d, *J* = 14.1 Hz, 1H), 6.03 – 5.88 (m, 1H), 4.25 (t, *J* = 6.9 Hz, 2H), 4.15 (t, *J* = 7.3 Hz, 2H), 3.80 – 3.68 (m, 4H), 3.25 (dd, *J* = 8.6, 5.0 Hz, 4H), 2.72 (dt, *J* = 11.8, 6.1 Hz, 4H), 2.54 – 2.43 (m, 5H), 2.39 (d, *J* = 3.2 Hz, 3H), 2.33 (dd, *J* = 15.8, 8.5 Hz, 4H), 2.08 (s, 2H), 2.01 – 1.81 (m, 8H), 1.77 (s, 6H), 1.73 (s, 1H), 1.72 (s, 6H), 1.69 (d, *J* = 7.3 Hz, 2H), 1.56 – 1.45 (m, 4H), 1.31 (s, 1H).

^{13}C NMR (101 MHz, MeOD) δ 202.73, 175.82, 173.27, 172.73, 172.47, 161.22, 157.37, 156.11, 155.59, 149.73, 144.19, 144.00, 143.34, 143.19, 142.20, 142.03, 141.79, 141.30, 141.13, 131.92, 128.53, 128.44, 126.48, 126.43, 125.27, 125.14, 122.17, 122.09, 115.85, 111.05, 110.74, 109.31, 101.13, 100.75, 54.07, 49.36, 49.23, 48.31, 48.24, 48.09, 48.02, 44.98, 43.69, 40.97, 33.18, 31.76, 30.07, 27.68, 26.97, 26.93, 26.58, 25.94, 25.32, 24.68, 24.20, 20.71, 12.72.

^{1}H

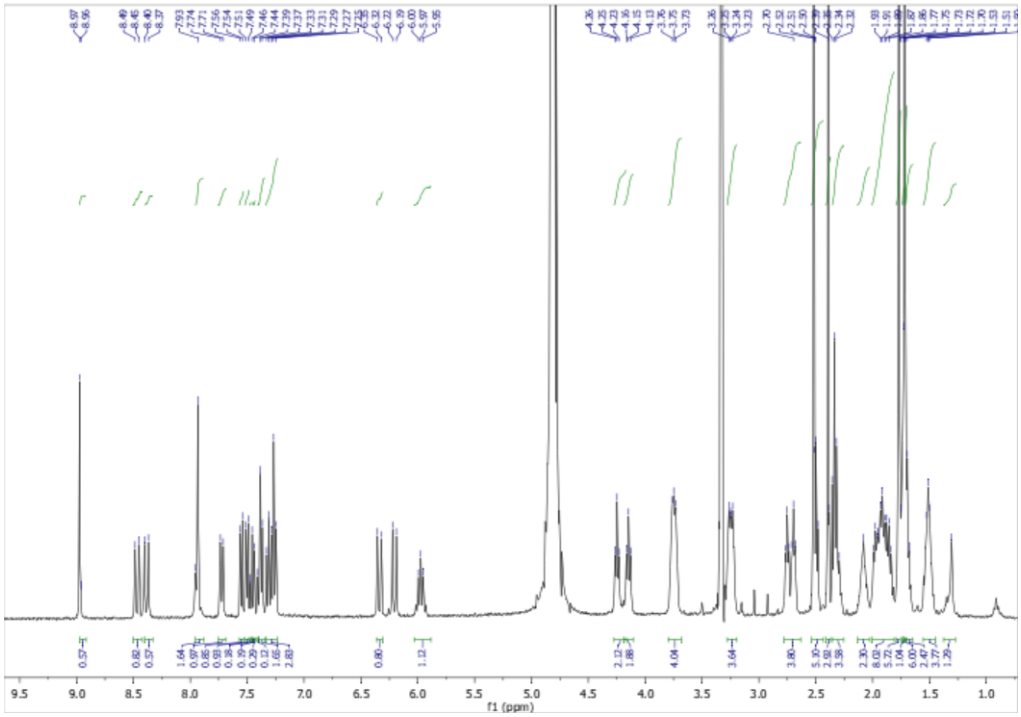

^{13}C

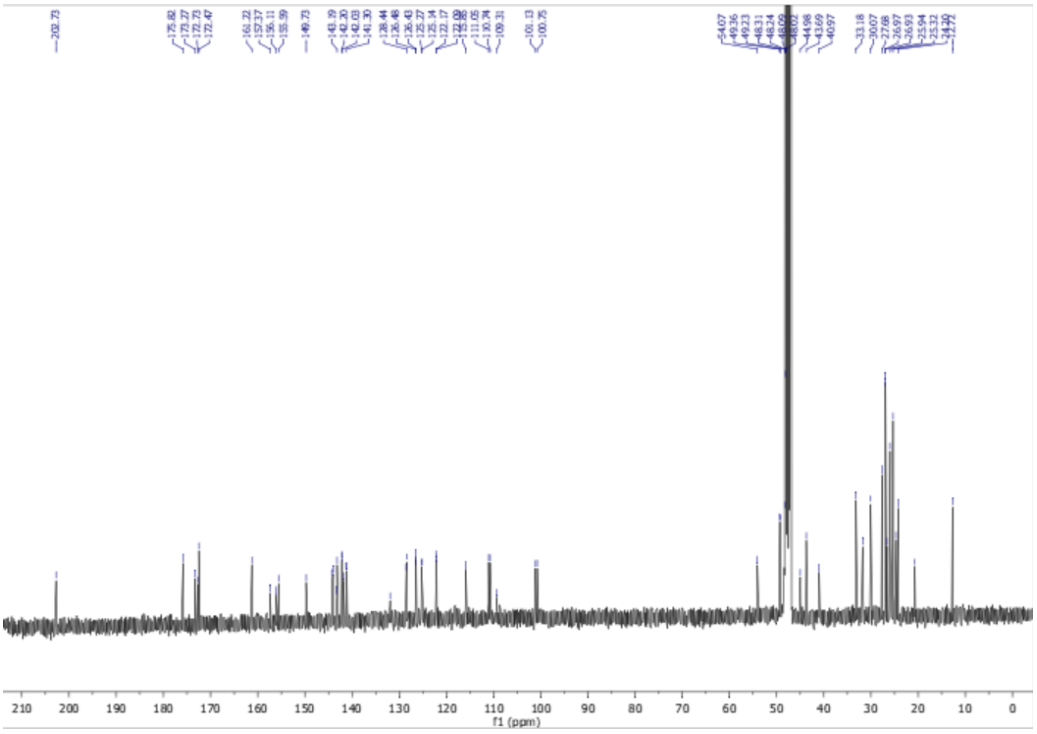

1c

^{1}H NMR (400 MHz, MeOD) δ 8.95 (s, 1H), 8.49 (s, 1H), 8.46 (d, *J* = 4.6 Hz, 1H), 8.43 (s, 1H), 8.40 (d, *J* = 4.8 Hz, 1H), 8.07 (d, *J* = 2.9 Hz, 1H), 8.05 (d, *J* = 2.9 Hz, 1H), 7.87 (d, *J* = 2.8 Hz, 1H), 7.53 (dd, *J* = 13.3, 7.2 Hz, 2H), 7.48 – 7.42 (m, 2H), 7.42 – 7.36 (m, 2H), 7.34 – 7.26 (m, 3H), 6.80 (s, 1H), 6.34 (d, *J* = 14.1 Hz, 1H), 6.24 (d, *J* = 14.1 Hz, 1H), 4.24 (t, *J* = 7.0 Hz, 2H), 4.13 (t, *J* = 7.3 Hz, 2H), 3.78 – 3.70 (m, 3H), 3.26 – 3.12 (m, 9H), 2.74 (dd, *J* = 12.0, 6.0 Hz, 3H), 2.50 (t, *J* = 7.2 Hz, 4H), 2.34 (t, *J* = 7.2 Hz, 2H), 2.14 – 2.04 (m, 4H), 2.00 (s, 2H), 1.92 (d, *J* = 7.6 Hz, 2H), 1.85 (s, 2H), 1.77 (s, 5H), 1.75 (s, 2H), 1.73 (s, 6H), 1.69 (dd, *J* = 12.4, 7.8 Hz, 3H), 1.56 – 1.47 (m, 4H).

^{13}C NMR (101 MHz, MeOD) δ 175.74, 173.16, 172.81, 172.41, 163.54, 152.17, 151.74, 149.74, 147.05, 144.29, 144.03, 142.35, 142.24, 142.09, 141.29, 141.16, 136.16, 134.28, 128.52, 126.50, 125.24, 125.17, 122.40, 122.16, 122.09, 115.22, 114.99, 111.01, 110.83, 100.94, 100.74, 58.20, 49.33, 49.24, 44.92, 43.73, 43.64, 40.95, 38.24, 33.97, 33.17, 31.85, 30.08, 26.94, 26.91, 26.60, 26.03, 25.93, 24.64, 24.20, 24.17, 20.72.

HRMS: calculated 1099.6047 found 1099.6035

^{1}H

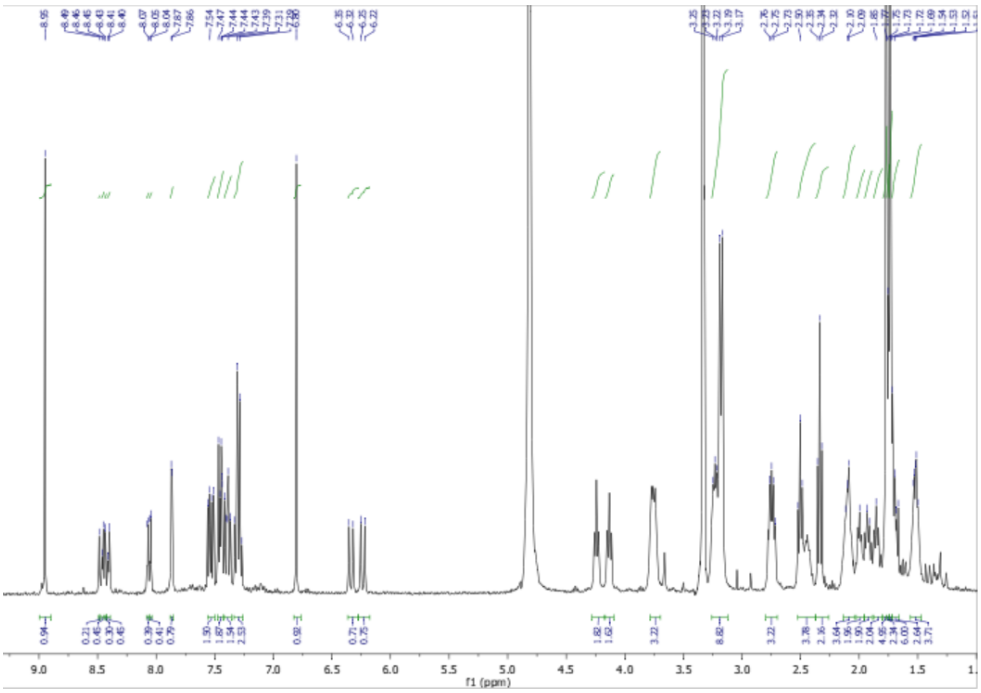

^{13}C

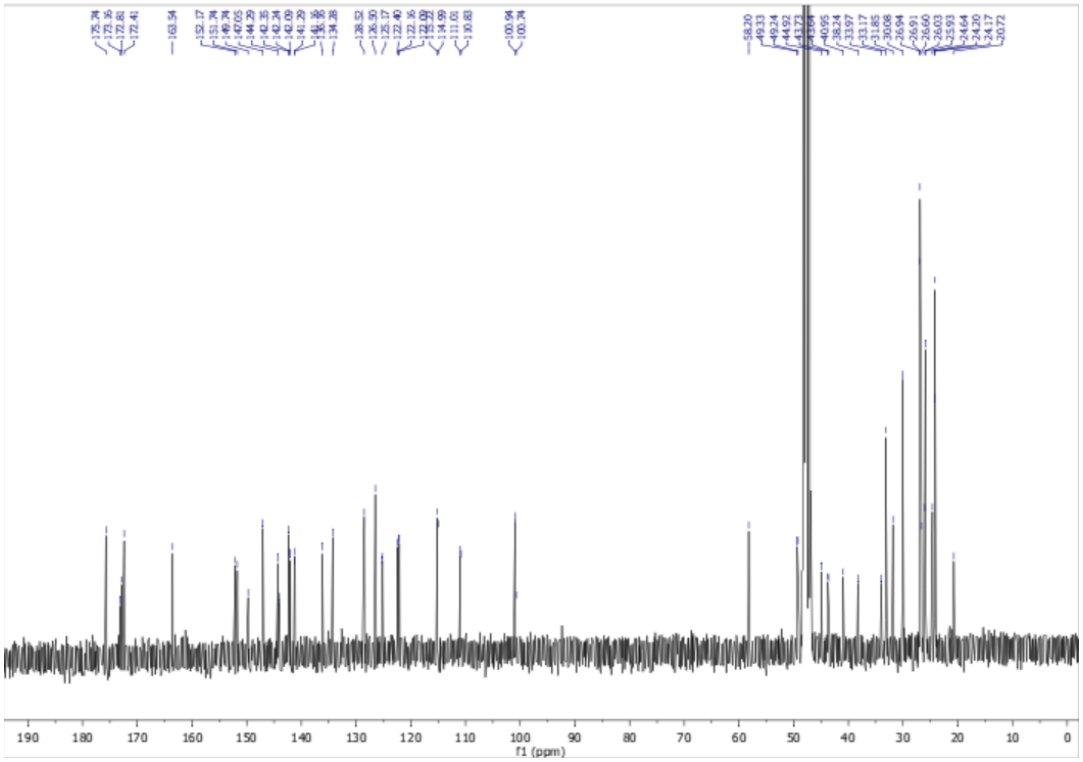

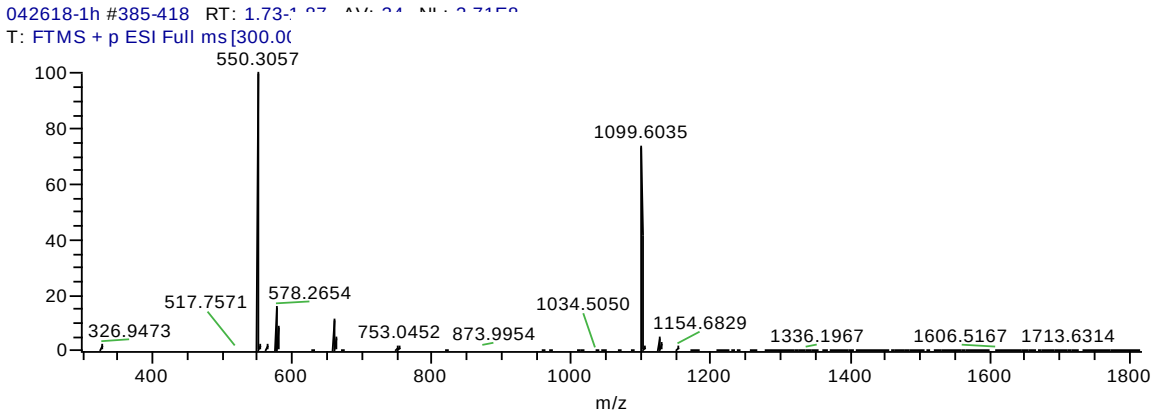

1d

^{1}H NMR (400 MHz, MeOD) δ 8.46 (dd, *J* = 14.1, 5.0 Hz, 2H), 7.93 (s, 1H), 7.66 – 7.59 (m, 2H), 7.54 (dd, *J* = 7.6, 2.3 Hz, 2H), 7.52 – 7.46 (m, 2H), 7.46 – 7.41 (m, 2H), 7.37 (d, *J* = 7.5 Hz, 1H), 7.35 – 7.32 (m, 1H), 7.32 – 7.26 (m, 2H), 7.16 (d, *J* = 1.2 Hz, 1H), 6.38 – 6.26 (m, 3H), 4.64 (d, *J* = 14.5 Hz, 1H), 4.51 – 4.39 (m, 1H), 4.28 – 4.15 (m, 4H), 4.10 (d, *J* = 13.7 Hz, 1H), 2.79 (dd, *J* = 26.1, 8.7 Hz, 5H), 2.50 (t, *J* = 7.3 Hz, 2H), 2.34 (t, *J* = 7.2 Hz, 2H), 2.13 (d, *J* = 13.9 Hz, 3H), 2.01 – 1.79 (m, 13H), 1.76 (s, 7H), 1.74 (s, 6H), 1.69 (dd, *J* = 14.1, 6.6 Hz, 2H), 1.55 (dt, *J* = 15.2, 7.6 Hz, 4H).

^{13}C NMR (101 MHz, MeOD) δ 175.74, 172.94, 172.27, 146.88, 144.14, 142.26, 142.19, 141.73, 141.22, 135.61, 135.18, 129.02, 128.52, 126.58, 125.20, 125.08, 122.14, 121.52, 121.24, 118.41, 118.29, 117.49, 117.26, 116.78, 110.89, 100.95, 74.34, 58.89, 49.29, 44.22, 43.76, 40.35, 33.17, 32.44, 32.20, 31.69, 26.92, 26.68, 26.16, 25.95, 24.74, 24.23, 20.73, 17.55.

HRMS: calculated 1114.4690 found 1114.4678

^{1}H

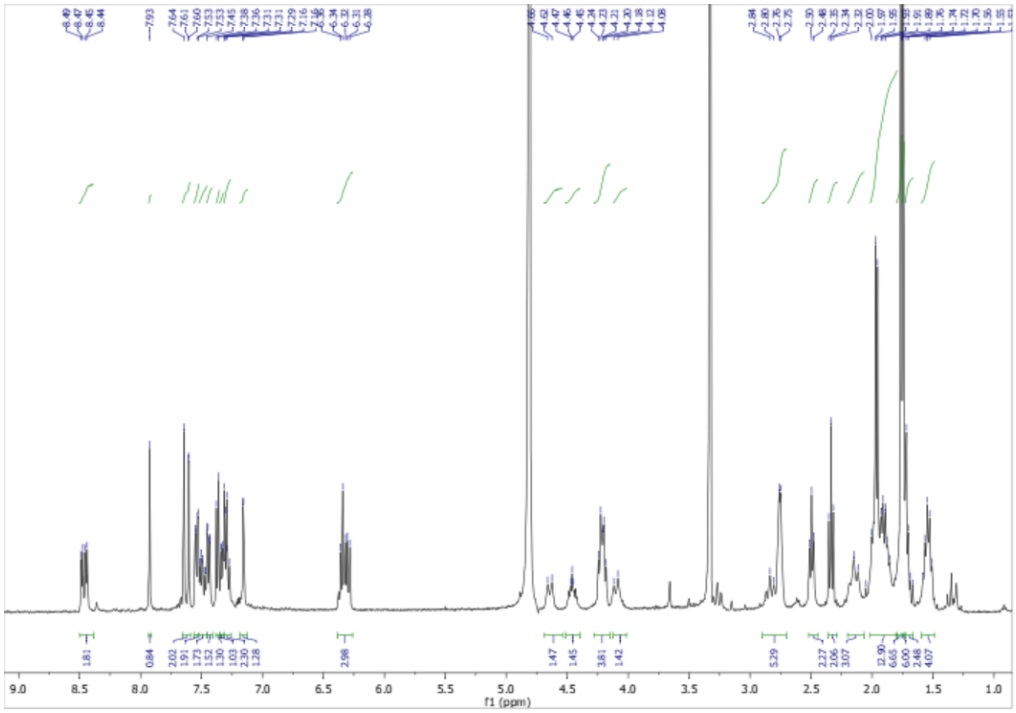

^{13}C

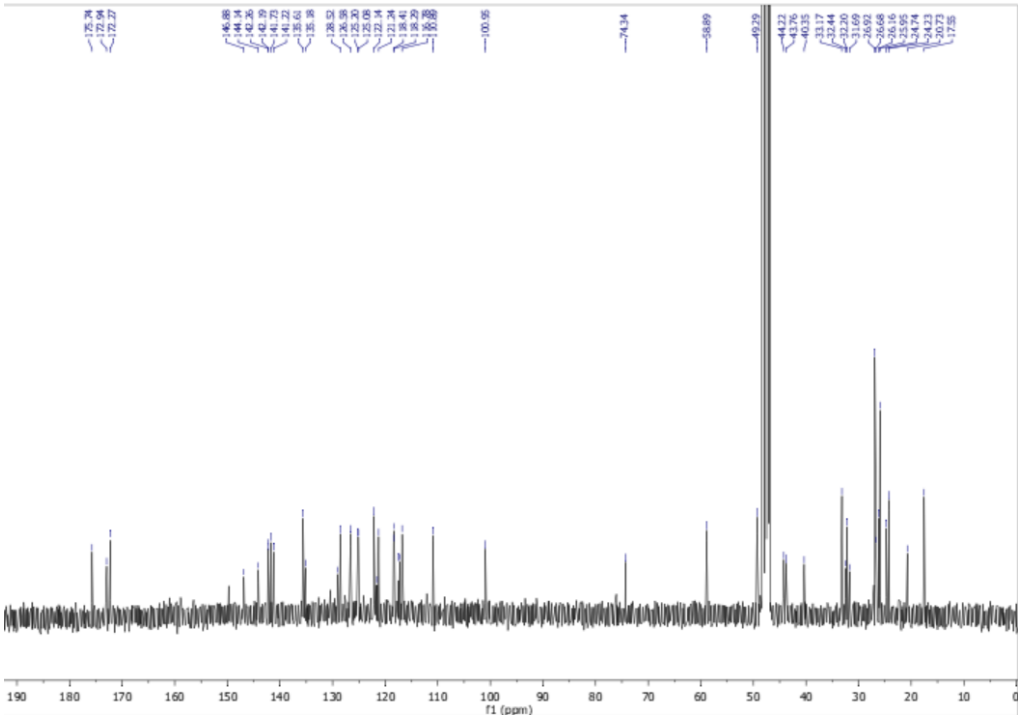

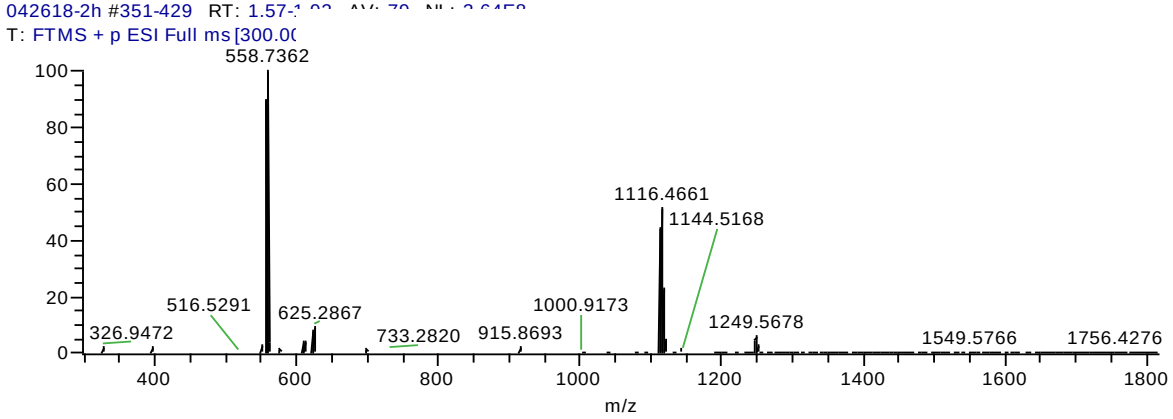

1e

^{1}H NMR (400 MHz, MeOD) δ 8.48 (s, 1H), 8.45 (d, *J* = 4.7 Hz, 1H), 8.42 (s, 1H), 8.40 (s, 1H), 8.14 (s, 1H), 7.95 (dd, *J* = 8.0, 1.5 Hz, 1H), 7.70 – 7.64 (m, 2H), 7.53 (dd, *J* = 10.5, 7.3 Hz, 2H), 7.49 – 7.41 (m, 2H), 7.41 (s, 1H), 7.38 (s, 1H), 7.36 (s, 1H), 7.35 – 7.26 (m, 3H), 6.81 (s, 1H), 6.33 – 6.22 (m, 2H), 4.70 (s, 1H), 4.57 (dt, *J* = 12.3, 6.1 Hz, 1H), 4.23 (t, *J* = 7.2 Hz, 2H), 4.17 (t, *J* = 7.4 Hz, 2H), 4.10 (d, *J* = 13.8 Hz, 1H), 3.20 (s, 1H), 3.00 (s, 1H), 2.81 – 2.64 (m, 5H), 2.49 (td, *J* = 7.2, 3.0 Hz, 2H), 2.32 (t, *J* = 7.3 Hz, 2H), 2.17 (d, *J* = 10.0 Hz, 3H), 1.94 (td, *J* = 13.3, 5.9 Hz, 4H), 1.90 – 1.78 (m, 5H), 1.76 (s, 6H), 1.73 (s, 6H), 1.71 – 1.66 (m, 2H), 1.56 (ddd, *J* = 23.4, 17.2, 10.7 Hz, 6H), 1.28 (dd, *J* = 12.8, 6.5 Hz, 14H).

^{13}C NMR (101 MHz, MeOD) δ 175.70, 173.02, 172.18, 156.06, 149.73, 146.41, 144.25, 143.99, 142.27, 142.13, 141.22, 138.85, 134.65, 131.06, 128.52, 127.25, 126.58, 125.24, 125.16, 124.48, 124.11, 123.08, 122.11, 111.65, 110.91, 105.19, 101.00, 100.89, 71.62,

55.48, 49.28, 46.37, 43.72, 42.37, 38.11, 33.16, 32.93, 32.30, 32.16, 29.33, 26.92, 26.81, 26.65, 26.13, 25.95, 24.82, 24.21, 21.03, 20.74, 17.67, 14.08.

^{1}H

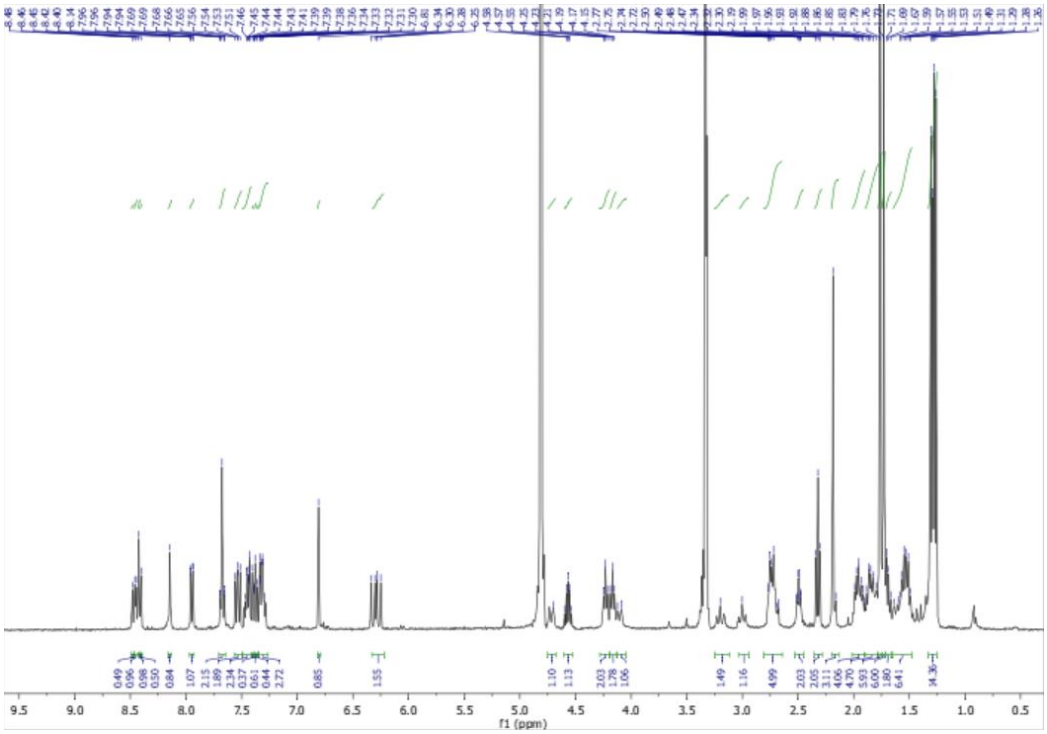

^{13}C

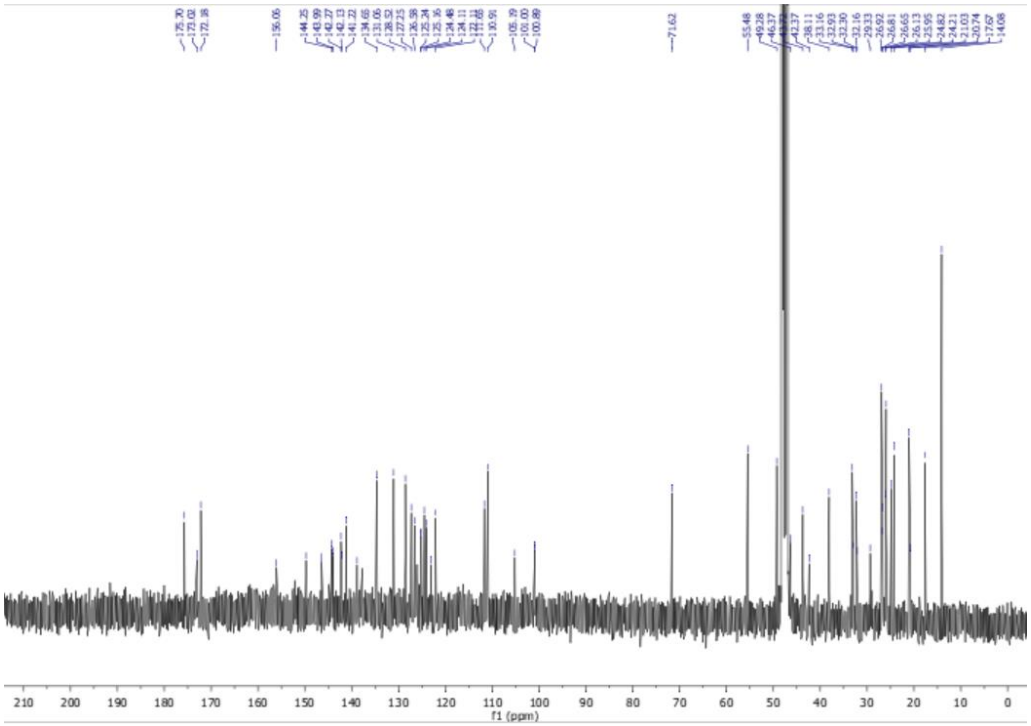

2b

^{1}H NMR (400 MHz, MeOD) δ 9.00 (s, 2H), 8.40 (d, *J* = 14.1 Hz, 2H), 8.03 (dd, *J* = 9.5, 2.7 Hz, 2H), 7.92 (d, *J* = 2.8 Hz, 2H), 7.67 (d, *J* = 9.5 Hz, 2H), 7.52 (d, *J* = 7.4 Hz, 2H), 7.40 (t, *J* = 7.6 Hz, 2H), 7.33 – 7.25 (m, 3H), 6.26 (d, *J* = 14.1 Hz, 2H), 6.04 – 5.92 (m, 2H), 4.19 (t, *J* = 7.0 Hz, 3H), 3.81 – 3.68 (m, 7H), 3.30 – 3.20 (m, 7H), 2.71 (t, *J* = 5.9 Hz, 3H), 2.51 (s, 6H), 2.49 (d, *J* = 7.1 Hz, 3H), 2.40 (s, 5H), 2.32 (dd, *J* = 11.6, 7.9 Hz, 4H), 2.09 (s, 4H), 2.00 – 1.82 (m, 9H), 1.77 (s, 1H), 1.74 (s, 12H), 1.69 (dd, *J* = 13.3, 6.9 Hz, 5H), 1.53 – 1.44 (m, 4H).

^{13}C NMR (101 MHz, MeOD) δ 202.51, 173.03, 172.40, 161.15, 157.16, 155.82, 155.66, 149.65, 144.03, 143.12, 143.01, 142.08, 141.62, 141.22, 132.27, 128.46, 126.38, 125.22, 122.13, 116.00, 110.92, 109.65, 100.98, 54.11, 49.31,

44.88, 43.71, 40.90, 31.81, 30.03, 27.67, 26.97, 26.86, 25.98, 25.93, 25.31, 24.62, 20.73, 12.73.

HRMS: calculated 1541.8164 found 1541.8180

^{1}H

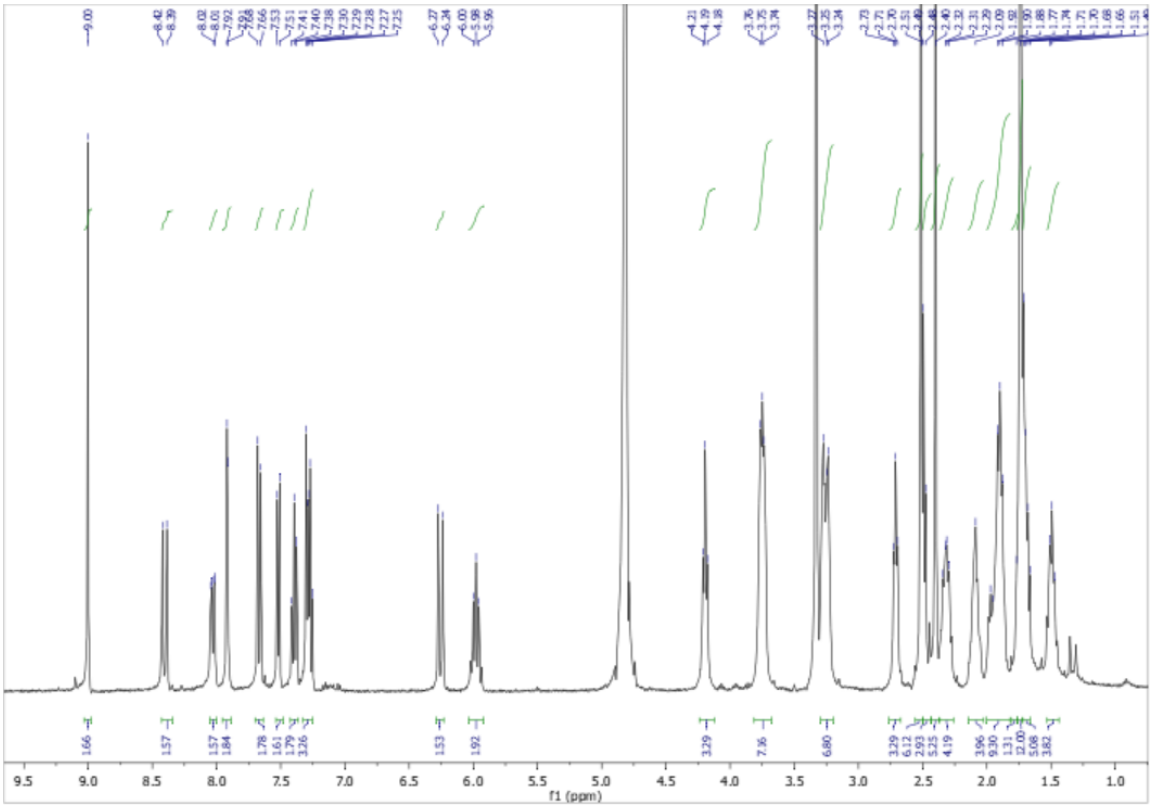

^{13}C

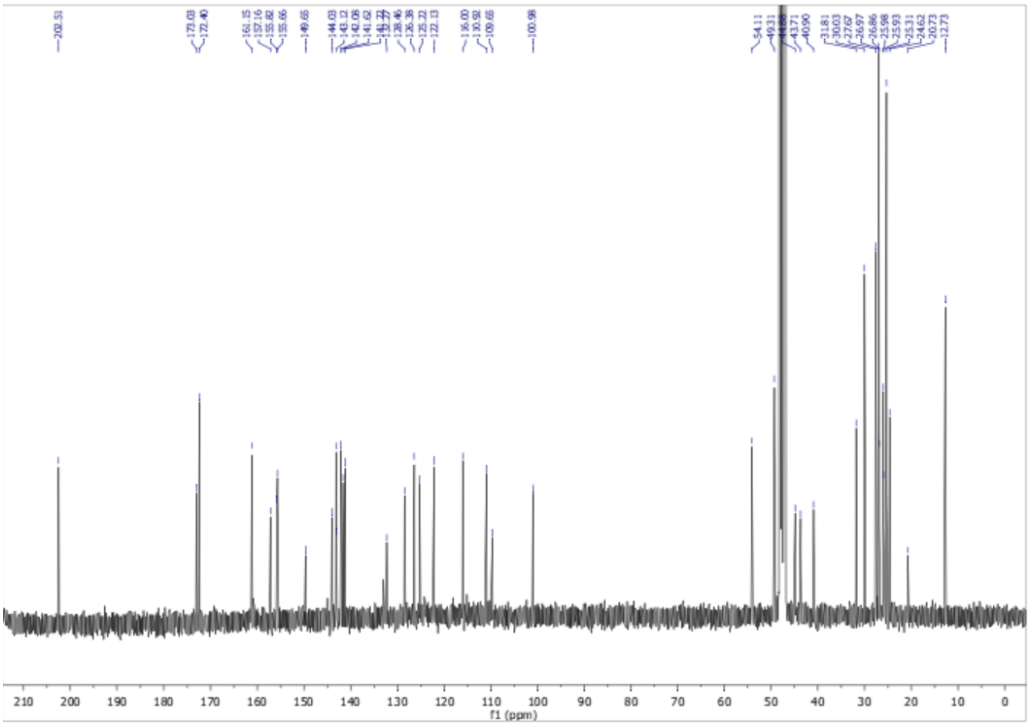

042618-3h #428-442 RT: 1.92-

T: FTMS + p ESI Full ms [500.0(

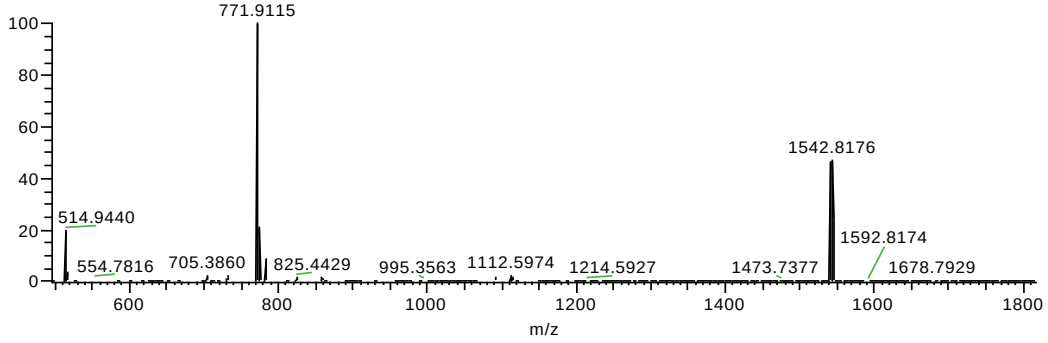

Dasatinib (Kinase Inhibitor "a") Conjugates

Figure G-1 shows that the conjugate **1a** is significantly more toxic than the parent dye (red line), the parent kinase inhibitor (red line), or a mixture of the dye and kinase inhibitor (purple line) on HEPG2 liver cancer cells (a) and (b) U87MG glioblastoma cells.

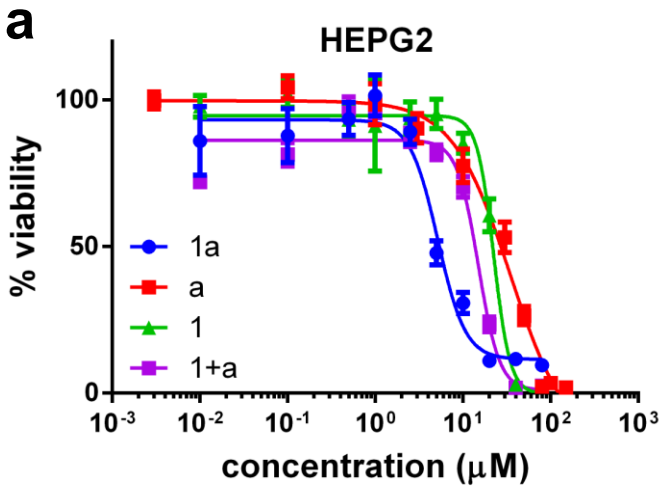

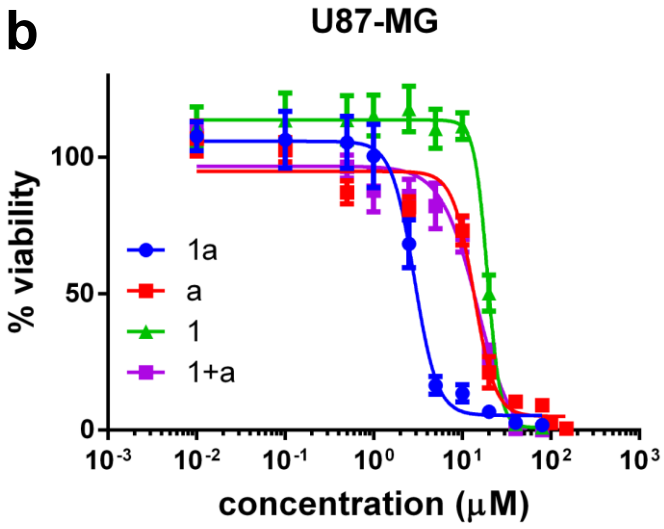

Figure G-1. Cell viability assay of **1a** on: **a** HepG2 cells (liver cancer); and **b** U87-MG cells (glioblastoma). **1a** was more found to be toxic than individual **1**, **a** or a combination of **1**+**a**.

Figure G-2a visualizes some of the data from Figure 1 (that on HEPG2 cells). Compound **1a** has a much stronger influence on the cell morphology after 24 and 48 h when compared the parent kinase inhibitor dasatinib **a**.

Localization of compounds in mitochondria tends to give more pronounced cytotoxicity effects than accumulation in most organelles. Figure G-2b shows **1a** localizes preferentially in mitochondria, though some colocalized with a dye that tracks lysosomes.

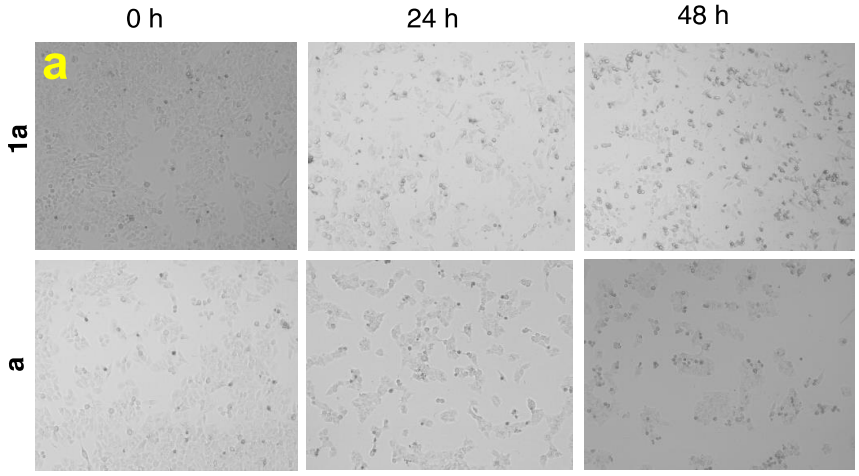

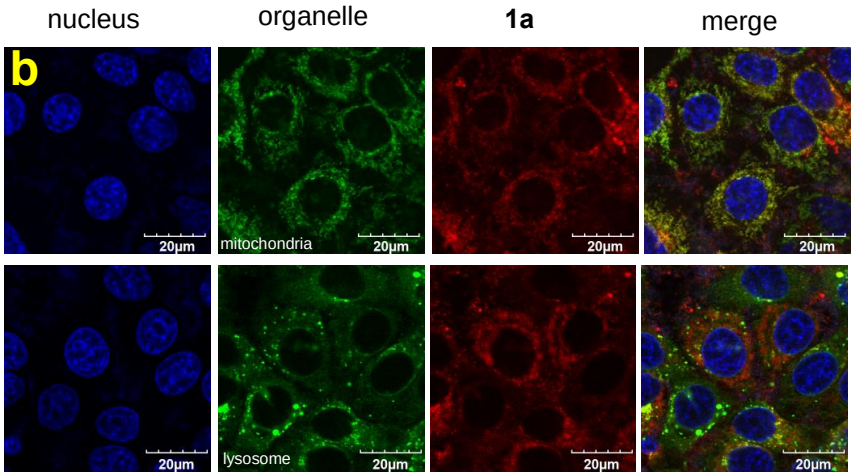

Figure G-2. 1a in HepG2 cells **a** morphology change; **b** co-localization study in organelles showed it localizes more in mitochondria than lysosomes.

Palbociclib (Kinase Inhibitor "b") Conjugates

Figure G-3 shows that the conjugate **1b** is significantly more toxic than the parent dye (red line), the parent kinase inhibitor (red line), or a mixture of the dye and kinase inhibitor (purple line) on HepG2 liver cancer cells (a), U87MG glioblastoma cells (b) and K562 leukemia cells (c).

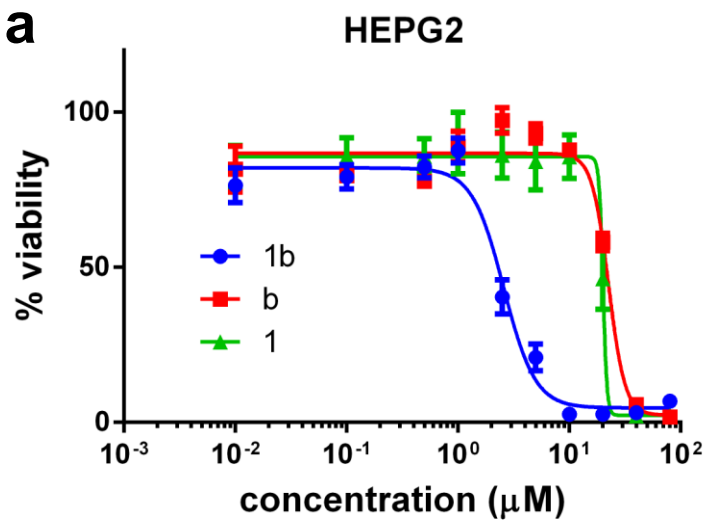

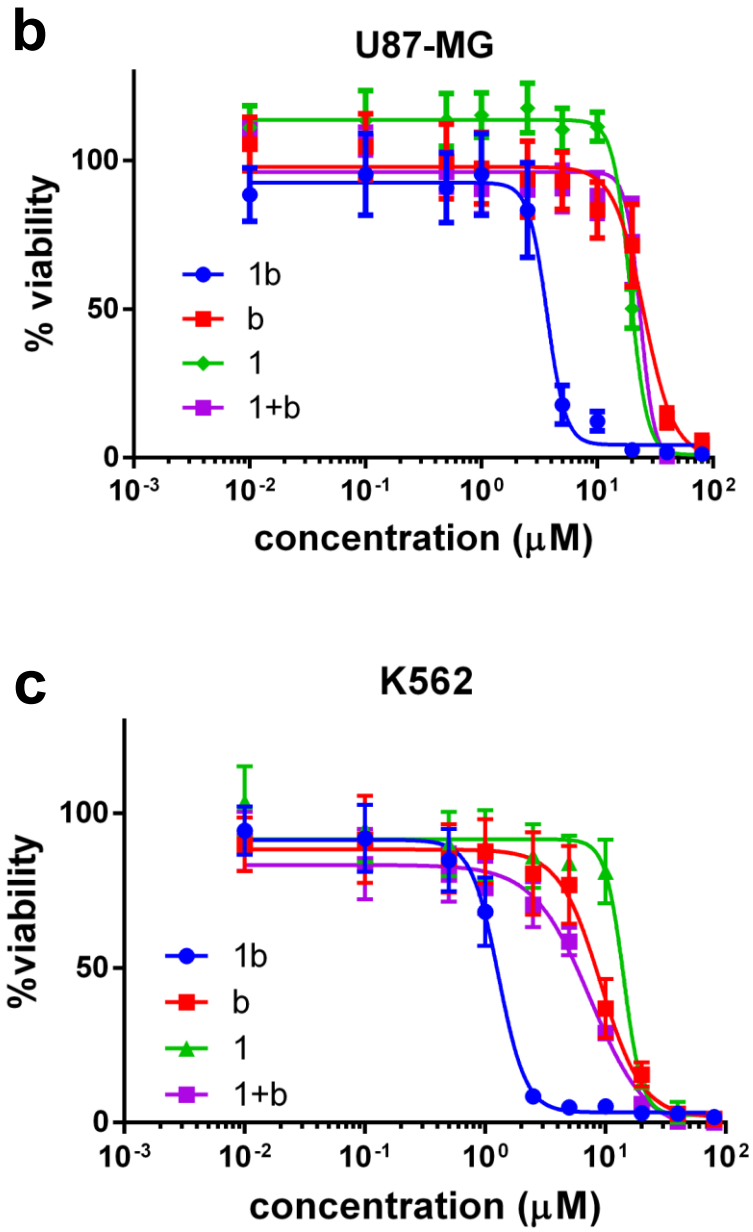

Figure G-3. Cell viability assay of **1b** on **a**. HepG2 cells (liver cancer); **b.** U87-MG cells (glioblastoma cancer) and **c**. K562 (leukemia cancer). **1b** was more found to be toxic than individual **1**, **b** or a combination of **1+b**.

Ribociclib (Kinase Inhibitor "c") Conjugates

Figure G-4 shows that the conjugate **1c** is significantly more toxic than the parent dye (red line), the parent kinase inhibitor (red line), or a mixture of the dye and kinase inhibitor (purple line) on MDA-MB-231 "triple negative" breast cancer cells.

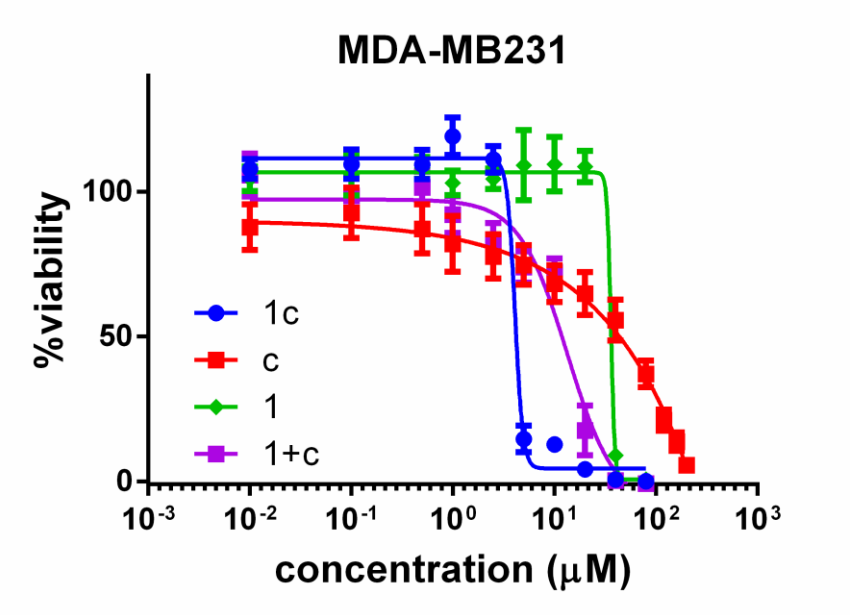

Figure G-4. Cell viability assay of **1c** on MBA-MB-231 (breast cancer cells). **1c** was more found to be toxic than individual **1**, **c** or a combination of **1+c**.

Crizotinib (Kinase Inhibitor "d") Conjugates

Figure G-5 shows that the conjugate **1d** is significantly more toxic than the parent dye (red line), the parent kinase inhibitor (red line), or a mixture of the dye and kinase inhibitor (purple line) on MDA-MB-231 "triple negative" breast cancer cells.

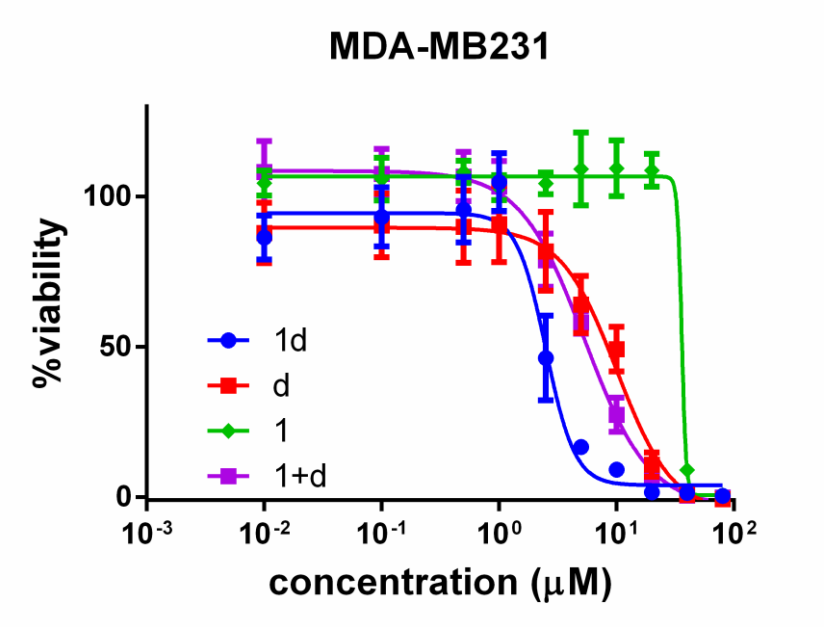

Figure G-5. Cell viability assay of **1d** on MDA-MB-231 (breast cancer cells). **1d** was more found to be toxic than individual **1**, **d** or a combination of **1+d**.